UNIVERSITY OF CALIFORNIA,
IRVINE

Tissue engineering of temporomandibular joint disc implants toward clinical translation

DISSERTATION

Submitted in partial satisfaction of the requirements
for the degree of

DOCTOR OF PHILOSOPHY

in Biomedical Engineering

by

Ryan Patrick Donahue

Dissertation Committee:
Distinguished Professor Kyriacos A. Athanasiou, Chair
Professor Boaz Arzi
Professor Wendy F. Liu
Assistant Professor Dean Wang
Program Manager Jerry C. Hu

2022

To my fiancée, Holly Patrick,

who has been a constant source of support and encouragement during my PhD work.

I am forever thankful to have you in my life.

To my parents, Kent and Kelly Donahue,

for cultivating in me the drive to pursue my dreams, no matter how big.

To those suffering intractable pain from temporomandibular joint disorders.

I hope this dissertation brings the necessary research closer

to alleviating pain and improving function.

Table of Contents

List of Figures xv

List of Tables xx

List of Supplementary Figures xxi

List of Supplementary Tables xxii

Acknowledgements xxiv

Curriculum Vitae xxviii

Abstract xxxi

Introduction 1

Chapter 1: Considerations for Translation of Tissue Engineered Fibrocartilage from Bench to Bedside 8

Abstract 8

Introduction 8

Fibrocartilage Types, Epidemiology, Pathology, and Clinical Treatments 10

The knee meniscus and TMJ disc 10

Epidemiology and pathology 12

Current clinical treatments 14

Using tissue engineering for fibrocartilage 16

Characterization Studies of Fibrocartilages 17

Histomorphological properties 18

Biochemical properties 20

Mechanical properties 22

Tissue Engineering of Fibrocartilage 24

Cell sources 24

Scaffold and scaffold-free methods 30

Biochemical stimuli 31

Mechanical stimuli 33

Toward tissue engineering the fibrocartilage spectrum 35

Evaluation of tissue engineered fibrocartilage 35

Toward Translation of Tissue Engineering 37

The FDA paradigm 37

Preclinical animal models 40

Clinical trials 42

Future directions 43

Conclusion 45

Chapter 2: Remaining Hurdles for Tissue-Engineering the Temporomandibular Joint Disc 46

Abstract 46

Highlights 46

Motivation for Tissue-Engineering of the Temporomandibular Joint Disc 47

Recent Tissue-Engineering Efforts 50

Novel scaffold-based and scaffold-free approaches 52

Cell sources 55

Improvement of mechanical properties of TMJ disc fibrocartilage 57

Current animal models 59

The Path to Translation 60

Application of proper tissue-engineering parameters for tuning of TMJ disc constructs to the TMJ mechanical environment 62

Tailoring of tissue-engineered TMJ discs to human discal pathologies and size 62

Novel and cogent translational studies 64

Overcoming additional clinical and regulatory hurdles 65

Concluding Remarks 66

Outstanding Questions 67

Chapter 3: Knee Orthopaedics as a Template for the Temporomandibular Joint 68

Abstract 68

Highlights 68

Introduction 69

Pathology 73

The TMJ requires improved diagnostic modalities despite similarities in osteoarthritis progression 73

TMJ disorders are more prevalent in women 74

The anatomical challenge of sensory structures near the TMJ versus the knee 75

Current Clinical Practices 76

Divergence of end-stage treatment strategies for osteoarthritis of the knee and TMJ 76

Training disparities between knee and TMJ surgeons 77

From incidence to clinic: Gender imbalances in physician populations and clinical trials 78

Commercial Products 80

Joint prostheses: Successes in the knee and catastrophic setbacks in the TMJ 80

The TMJ field trails the progress of tissue engineering in the knee 81

Future Directions 82

The vicious cycle of translating TMJ research 82

Increasing the quantity of rigorous TMJ research 83

Bolstering training opportunities for researchers and physicians 85

Narrowing and specifying indications for TMDs toward establishing the commercial landscape for TMJ cartilage products 87

Implementing industry guidance for treatment of TMJ cartilages 88

Conclusion 89

Chapter 4: Long-term Safety and Efficacy of Temporomandibular Joint Disc Regeneration in the Yucatan Minipig 91

Abstract 91

Introduction 92

Results 95

Tissue-engineered implants approached native tissue values, and the intralaminar perforation surgical technique secured tissue-engineered implants in the Yucatan minipig TMJ disc 95

Perforation defects in the TMJ disc healed with tissue-engineered implants 98

Tissue-engineered implants facilitated regeneration of mechanically robust repair tissue that reached native TMJ disc tensile properties 101

Repair tissue of implant-treated discs mimicked the native TMJ disc biochemical content 102

Implantation of tissue-engineered neocartilages resulted in no abnormal systemic effects 103

Tissue-engineered implants were well-tolerated immunologically 106

Tissue-engineered implants remodeled to a native-like tissue 108

Discussion 110

Materials and Methods 116

Tissue engineering of implants 116

In vivo experiments 118

Presurgical medication and anesthesia 118

Surgical implantation and defect creation 119

Postoperative medication and animal care 120

Animal euthanasia 121

TMJ sample preparation 121

In vitro sample preparation.....122
Histology and immunohistochemistry.....122
Mechanical testing.....122
Biochemical testing.....123
Mass spectrometry analyses for crosslinks quantification and bottom-up proteomics.....124
ICRS scoring.....124
Statistical analyses.....125
Supplementary Materials.....126
Chapter 5: The Effect of Neonatal, Juvenile, and Adult Donors on Rejuvenated Neocartilage Functional Properties.....141
Abstract.....141
Impact Statement.....142
Introduction.....142
Materials and Methods.....146
Costal cartilage harvest and isolation.....146
Chondrocyte expansion and aggregate rejuvenation.....148
Neocartilage self-assembly.....149
Sample processing and photometric biochemical analysis.....149
Pyridinoline mass spectrometry analysis.....150
Bottom-up mass spectrometry proteomic analysis.....150
Mechanical testing and analysis.....151
Histological processing and staining.....151
Statistical analyses.....152
Results.....152
Gross morphology and histology.....152
Biochemical and proteomic properties.....153

Mechanical properties 155

Discussion 157

Conclusion 161

Supplementary Materials 163

Chapter 6: Proteomic, Mechanical, and Biochemical Development of Tissue-Engineered Neocartilage 173

Abstract 173

Introduction 173

Methods 176

Costal cartilage harvest and isolation 176

Costal chondrocyte expansion and aggregate rejuvenation 176

Neocartilage self-assembly and bioactive factor treatment 178

Sample preparation 178

Histology 179

Mechanical testing 179

Collagen, GAG, and DNA assays 179

Fluorophore assisted carbohydrate electrophoresis (FACE) 180

Collagen crosslink quantification 180

Bottom-up proteomics 181

Statistical analysis 181

Results 181

Neocartilage histology 181

Mechanical properties 182

Biochemical properties 183

Crosslink quantification 186

Bottom-up proteomic analysis 186

Discussion 189

Supplementary Materials 195

Chapter 7: Proteomic, Mechanical, and Biochemical Characterization of Cartilage Development 198

Abstract 198

Introduction 199

Methods 201

Sample collection 201

Histology 202

Mechanical testing 203

Photometric biochemical assays for total collagen, GAG, and DNA content 204

Fluorophore assisted carbohydrate electrophoresis (FACE) 204

Crosslink quantification and bottom-up proteomics 204

Statistical analysis 205

Results 205

Histology 205

Mechanical testing 206

Biochemical content 208

Crosslinks analysis 208

Bottom-up proteomics 212

Discussion 212

Supplementary Materials 218

Chapter 8: The Functionality and Translatability of Neocartilage Constructs are Improved with the Combination of Fluid-induced Shear Stress and Bioactive Factors 220

Abstract 220

Introduction 221

Methods 226
Overview of experimental phases 226
Isolation of bovine articular chondrocytes 227
Isolation of minipig costal chondrocytes 227
Passaging and aggregate rejuvenation of minipig costal chondrocytes 228
Self-assembly of neocartilage constructs 229
FIS stress stimulation and devices 230
Bioactive factor treatment 232
Analysis of mechanical properties 232
Analysis of biochemical properties 233
Histology 233
Statistics 234
Results 234
Phase I: FIS stress stimulation during the maturation stage yields the largest functional increases over nonstimulated controls 234
Phase II: FIS stress yields similar neocartilage functional increases using expanded and rejuvenated minipig costal chondrocytes 236
Phase III: Bioactive factors in conjunction with FIS stress yield further functional improvements over bioactive factors alone 238
Phase IV: Large constructs derived from highly passaged cells are mechanically robust and flat 241
Discussion 243
Chapter 9: Isolation and Characterization of Porcine Macrophages and their Inflammatory and Fusion Responses in Different Stiffness Environments 249
Abstract 249
Introduction 250

Results 252
Isolation of porcine bone marrow- and peripheral blood-derived macrophages 252
Porcine macrophages express F4/80 and CD68 on the cell surface 255
Porcine macrophages respond to LPS and increase the expression of inflammatory genes. 257
Substrate stiffness influences porcine macrophage inflammatory activation and fusion ...260
Discussion 261
Methods 264
Isolation of bone marrow- and peripheral blood derived-macrophages and differentiation 264
Flow cytometry 264
Assessment of cytokine secretion by ELISA and immunofluorescence staining of the cells 265
Polyacrylamide hydrogel synthesis 266
RNA isolation, cDNA preparation, and qRT-PCR analysis 266
Statistical analysis 266
Supplementary Materials 268
Chapter 10: Stiffness- and Bioactive Factor-Mediated Protection of Self-assembled Cartilage against Macrophage Challenge in a Novel Co-culture System 269
Abstract 269
Introduction 270
Materials and Methods 274
Isolation, expansion, and aggregate rejuvenation of chondrocytes 274
Isolation of bone marrow-derived monocytes and differentiation into macrophages 276
Formation of self-assembled cartilage constructs 276
Co-culture of macrophages and self-assembled cartilage constructs 277

Sample processing and biochemical analyses 278
Mechanical testing 279
Histology 279
Enzyme linked immunosorbent assays for cytokine analysis 279
Statistical analysis 280
Results 280
Study 1 280
C-ABC$_{comp.}$ modulates compressive stiffness in CHG-treated constructs 280
Stiff, CHG-treated constructs are protected from macrophage inflammatory challenge even in the presence of an elevated proinflammatory response 283
Study 2 286
C-ABC$_{comp.}$ modulates compressive stiffness in TCL-treated constructs 286
TCL-treated constructs better withstand macrophage challenge 289
Co-culture with TCL-treated constructs suppress LPS-induced TNF-α production, and increased stiffness enhances the anti-inflammatory effect of IL-10-stimulated macrophages 292
Study 1 and Study 2 Comparison 293
TCL-treated constructs maintain or increase aggregate modulus compared to CHG-treated constructs after 2 weeks of co-culture 293
Discussion 294
Chapter 11: Tissue-Engineered Implants Regenerate Large Perforations in the Yucatan Minipig Temporomandibular Joint Disc 300
Abstract 300
Introduction 301
Results 303
Tissue-engineered implants were suitable for implantation 303

The intralaminar perforation surgical technique was successful in securing implants in large perforation defects 304
Implants achieved tissue regeneration after 8 weeks; controls did not heal 307
Regenerated tissue, only present in implant-treated discs, displayed robust tensile properties....310
Regenerated tissue biochemical and proteomic composition was reminiscent of native TMJ discs 311
Tissue adjacent to perforations in controls deviated from native TMJ disc composition ...312
Implants remodeled, exhibiting biochemical and proteomic contents similar to native TMJ discs 315
Implants exhibited safety, as shown by no adverse systemic response and minimal local response....319
Discussion 322
Materials and Methods 327
Tissue engineering of implants 327
In vivo experiments....329
Presurgical medication and anesthesia....329
Surgical implantation and defect creation....330
Postoperative medication and animal care....331
Animal euthanasia 331
Sample preparation....331
Histology....332
Mechanical testing 332
Biochemical testing....333
Mass spectrometry analyses for crosslinks quantification and bottom-up proteomics 333
Statistical analyses 334

Supplementary Materials 335

Conclusions and Future Directions 341

References 348

List of Figures

Figure 1-1: Anatomy of the knee meniscus and TMJ disc. 11

Figure 1-2: Clinical indications of the knee meniscus and TMJ disc. 13

Figure 1-3: Tissue engineering of fibrocartilage.....17

Figure 1-4: The FDA paradigm. 18

Figure 1-5: Cell morphology and collagen alignment of the knee meniscus and TMJ disc. 20

Figure 2-1: TMJ disc anatomy.....49

Figure 2-2: Internal derangement of the TMJ disc. 50

Figure 2-3: Tissue-engineering paradigm of TMJ disc constructs. 54

Figure 2-4: Toward the path to translation. 61

Figure 2-5: The intralaminar fenestration surgical technique.....63

Figure 3-1: Knee and TMJ anatomy and proximity to crucial sensory structures.....70

Figure 3-2: Clinical practices for the knee and TMJ. 79

Figure 3-3: The vicious cycle of TMJ translational research. 83

Figure 4-1: Neocartilages were fabricated using the self-assembling process and exhibited robust matrix content for implantation into the TMJ disc. 96

Figure 4-2: The intralaminar perforation surgical technique secured tissue-engineered implants in perforation defects. 97

Figure 4-3: Gross morphology and histological cross sections of TMJ discs showed lack of complete healing in controls and repair tissue in implant-treated groups.....100

Figure 4-4: Tensile properties of repair tissue of implant-treated discs were higher compared to fill tissue of controls. 101

Figure 4-5: Collagens in the matrix of repair tissue was reminiscent of native TMJ disc content. 103

Figure 4-6: Heatmap of normalized complete blood count and comprehensive metabolic panel parameters show no abnormal systemic effects.....104
Figure 4-7: Immunohistochemical staining for T cells, B cells, and macrophages showed immunogenic tolerance to tissue-engineered implants.....105
Figure 4-8: Histological and biochemical properties of neocartilages after implantation showed remodeling toward native TMJ discs.....107
Figure 4-9: Bottom-up proteomic analysis of neocartilages after implantation also showed remodeling toward native TMJ disc content.....110
Figure 5-1: Costal cartilage harvest and isolation and the tissue engineering process..147
Figure 5-2: Gross morphology and histology of neocartilage constructs.....153
Figure 5-3: Biochemical properties of neocartilage constructs. 154
Figure 5-4: Proteomic analysis of neocartilage constructs. 155
Figure 5-5: Mechanical properties of neocartilage constructs. 156
Figure 6-1: The tissue-engineering process using costal chondrocytes and neocartilage sample preparation.....177
Figure 6-2: Histology and gross morphology of neocartilage constructs. 182
Figure 6-3: Mechanical properties of neocartilage constructs. 184
Figure 6-4: Biochemical composition of neocartilage constructs.....185
Figure 6-5: Collagen crosslink composition of neocartilage constructs. 187
Figure 6-6: Bottom-up proteomics analysis of neocartilage constructs.....188
Figure 7-1: Sample collection diagram.....203
Figure 7-2: Representative histology and gross morphology images for porcine articular cartilage of different developmental ages.....206
Figure 7-3: Mechanical results for porcine articular cartilage of different developmental ages. 207

Figure 7-4: Biochemical results for porcine articular cartilage of different developmental ages. 209
Figure 7-5: Crosslink quantification results for porcine articular cartilage of different developmental ages.....210
Figure 7-6: Bottom-up proteomic results for porcine articular cartilage of different developmental ages.....211
Figure 8-1: Maturation dependency and modes of action.....222
Figure 8-2: The two FIS stress devices used for stimulation of circular and rectangular neocartilage constructs.....231
Figure 8-3: Identifying the best time of application for FIS stress. 235
Figure 8-4: Translating FIS stress stimulation to costal chondrocytes from the Yucatan minipig.....237
Figure 8-5: Combining bioactive factors and FIS stress to further improve the functional properties of neocartilage constructs. 239
Figure 8-6: Scaling-up the size of neocartilage constructs created from highly passaged chondrocytes using FIS stress and bioactive factors.....240
Figure 8-7: Combining bioactive factors and FIS stress increases intensity for glycosaminoglycan staining. 242
Figure 9-1: Schematic representation of the protocol used to isolate and differentiate bone marrow- and peripheral blood-derived macrophages.....254
Figure 9-2: Bone marrow- and peripheral blood derived-macrophages express CD68 and F4/80 upon differentiation. 256
Figure 9-3: Differentiated bone marrow- and peripheral blood-derived macrophages are activated upon LPS stimulation. 258
Figure 9-4: Substrate stiffness enhances inflammatory activation and fusion of macrophages.....259

Figure 10-1: Stiffness is modulated via C-ABC$_{comp.}$, and macrophages are adhered and stimulated in a direct co-culture system. 278

Figure 10-2: C-ABC$_{comp.}$ modulates the compressive stiffness of CHG-treated constructs. 281

Figure 10-3: CHG-treated constructs of soft and medium stiffness differ in staining intensity. 284

Figure 10-4: Soft and medium stiffness CHG-treated constructs suffer losses in aggregate modulus values despite no increases in TNF-α production. 285

Figure 10-5: C-ABC$_{comp.}$ modulates the compressive stiffness of TCL-treated constructs. 287

Figure 10-6: Saf-O staining after 2 weeks of macrophage co-culture shows donor-related variation, with diminished staining among LPS-stimulated co-cultures. 290

Figure 10-7: Aggregate modulus values of TCL-treated constructs only decrease in soft construct, LPS-stimulated co-cultures. 291

Figure 10-8: TNF-α secretion of TCL-treated construct co-cultures increases with stiffness, decreases with construct co-culture, and diminishes when macrophages are stimulated toward an anti-inflammatory phenotype. 292

Figure 11-1: Tissue-engineered implants were suitable for nonhomologous usage in the TMJ disc. 305

Figure 11-2: The intralaminar perforation technique secured implants in place toward regeneration of large perforation defects. 306

Figure 11-3: Control discs and condyles showed degenerative changes compared to implant-treated discs and condyles after 8 weeks. 308

Figure 11-4: Implant-treated discs exhibited regeneration in the centrolateral region of the TMJ disc, and controls displayed lack of healing. 309

Figure 11-5: Defect perimeter and area after 8 weeks of implantation were higher in controls.....310
Figure 11-6: Regenerated tissue tensile properties approached native tissue values. ...311
Figure 11-7: Biochemical and crosslink content of regenerated tissue recapitulated native TMJ disc content.....313
Figure 11-8: Adjacent tissue to control perforations deviated from native tissue in biochemical and crosslink content.....314
Figure 11-9: Histology of neocartilage implanted for 8 weeks displayed similarities to native TMJ discs. 316
Figure 11-10: Biochemical properties of implants after 8 weeks remodeled toward native tissue values. 317
Figure 11-11: Crosslink content after 8 weeks remodeled toward native tissue values. .318
Figure 11-12: Proteomic analytes after 8 weeks of implantation further approached native tissue values. 319
Figure 11-13: Heatmap of normalized complete blood count and comprehensive metabolic panel parameters showed no abnormal systemic effects due to implants. 321
Figure 11-14: H&E revealed moderate cellular response to TMJ disc implants. 322

List of Tables

Table 1-1: Selected list of key publications for fibrocartilage tissue engineering. 25

Table 2-1: Recent tissue-engineering studies of the TMJ disc published since 2013. 51

Table 3-1: Comparison of the knee and TMJ fields. 73

Table 5-1: Morphological properties of neocartilage constructs.....152

Table 8-1: Timeline of FIS stress and bioactive factor application.....230

Table 10-1: Additional properties of CHG-treated constructs.....282

Table 10-2: Additional properties of TCL-treated constructs.....288

Table 10-3: CHG-treated constructs decrease aggregate modulus values compared to TCL-treated constructs which maintain or increase aggregate modulus values after 2 weeks of macrophage co-culture.....293

List of Supplementary Figures

Supplementary Figure 4-1: Depiction of the surgical placement of the incision, defect, and implant.....126

Supplementary Figure 4-2: Short-term gross morphology of implant-treated TMJ discs. 126

Supplementary Figure 4-3: Gross morphology of all discs in the long-term study. 127

Supplementary Figure 4-4: Gross morphology and mediolateral histological cross sections of condyles.....128

Supplementary Figure 4-5: The synovium of empty defect and implant-treated TMJs....137

Supplementary Figure 4-6: Controls for immunohistochemical staining. 138

Supplementary Figure 4-7: TMJ disc sample preparation and excision. 140

Supplementary Figure 9-1: Comparison of anti-coagulants. 268

Supplementary Figure 9-2: Immunofluorescence confocal images of secondary antibodies stained for 1h in bone marrow-derived macrophages. 268

List of Supplementary Tables

Supplementary Table 4-1: Osteoarthritis scores of condyles.....129

Supplementary Table 4-2: Tensile properties of intralaminar fusion. 129

Supplementary Table 4-3: Crosslinks in the fill and repair tissues. 129

Supplementary Table 4-4: Bottom-up proteomics data for all tissues. 130

Supplementary Table 4-5: Raw values for the complete blood count and comprehensive metabolic panel parameters. 133

Supplementary Table 4-6: Crosslinks in the implants after extended culture or implantation.....139

Supplementary Table 4-7: Compressive properties of neocartilage. 139

Supplementary Table 4-8: Immunohistochemistry parameters. 139

Supplementary Table 5-1: Full list of proteins returned from bottom-up mass spectrometry analysis. 163

Supplementary Table 6-1: Additional mechanical outcomes of neocartilage constructs. 195

Supplementary Table 6-2: Bottom-up proteomics analytes of neocartilage constructs..195

Supplementary Table 7-1: Bottom-up proteomics results on porcine knee cartilage.....218

Supplementary Table 9-1: List of primers used in this study for qRT-PCR analysis. 268

Supplementary Table 11-1: Intralaminar fusion metrics. 335

Supplementary Table 11-2: Bottom-up proteomics raw data.....336

Supplementary Table 11-3: Dry weight crosslink normalizations and biochemical data for regenerated tissue. 338

Supplementary Table 11-4: Dry weight crosslink normalizations and biochemical data for adjacent tissue. 338

Supplementary Table 11-5: Compressive properties of implants cultured *in vitro*. 338

Supplementary Table 11-6: Raw complete blood count and complete metabolic panel data. 339

Acknowledgements

Graduate school has been an immensely awarding experience that has culminated in this dissertation. During my time as a doctoral student in Driving Engineering and Life-science Translational Advances at Irvine (DELTA*i*), I have expanded the boundaries of my knowledge while substantially developing as a biomedical engineer and scientist. Many of the professional, ethical, and moral lessons learned during my graduate program have gone on to influence me individually as well; as a direct result, I've also grown personally during my graduate career. I will be forever appreciative for those individuals, experiences, and entities who have helped me to this point, from my parents raising me, to my high school and college experiences, to the committee members who have advised me on this dissertation.

Firstly, my parents, Kent and Kelly Donahue, and siblings, Jillian and Brady Donahue, have always been and will continue to be a great source of encouragement and motivation. It is them who I've learned my most important life lessons from, and they continue to support me throughout my academic and professional journey.

Without my outstanding high school experience at Biotechnology High School, I would have never considered biomedical engineering as a profession. The teachers and administrators bred a passion for excellence, as our motto was, "Excellence is in our DNA." In addition to the administrators and teachers, I would like to thank my friends, Nitish Sardana, Richard Thornton, and Rebecca Barresi, who continued to provide friendship from across the country during graduate school. Their ability to make me smile no matter how long it had been since we last spoke will never be taken for granted.

Long before I attended UC Irvine, my research career began at the University of Miami. I was lucky to have found many passionate mentors in the regenerative medicine space, including Dr. Daniel Pelaez, my primary research advisor. His ability to take a complicated topic and break it down was outstanding. As his first undergraduate research student as a principal investigator, I was afforded a number of fantastic opportunities that propelled me to apply for

graduate school. Also during my time at the “U,” teammates, coworkers, fellow students, and, most importantly, friends, further motivated and inspired me to pursue excellence in everything I do. Connor Walsh, Nathan Bates, Victoria Marks, Ivan Traczuk, Coleman Reardon, Morgan Parees, and many others, to you all, I say thank you for your remarkable friendship over the years.

My early graduate career was filled with fond memories of “Butter Baes” dinners and game nights with cohort-mates Austin Lefebvre, Christopher Toh, and Benjamin Bielajew. Thank you for being diligent classmates and steadfast friends. The Graduate Association of Biomedical Engineering Students members, past and present, also filled my entire graduate career with great memories of hanging out after the work day and outside of the lab. And to all others at UC Irvine, who have supported or encouraged me in any way, thank you.

To the lab members, past and present, of DELTA*i*: Thank you for providing me with the training, guidance, friendship, humor, and mental sanity it took to complete a PhD. As they say, “it takes a village.” That village consisted of many, including: 1) Dr. Jarrett Link, Dr. Evelia Salinas, Dr. Erik Gonzalez-Leon, and Gaston Otarola, all who were senior graduate students that acted in a dual capacity as role models and outstanding friends when I first joined the group, 2) Drs. Wendy Brown and Heenam Kwon, who have proven to be excellent scientific mentors on a daily basis, 3) Drs. Rachel Nordberg, Gabriela Espinosa, and Nathan Castro, all who have been key collaborators during my PhD work, 4) Dr. Natalia Vapniarsky and all those who trailblazed the path before me on the temporomandibular joint disc project, and 5) Dr. Benjamin Bielajew, who is a cohort-mate, a lab-mate, a crucial collaborator on much of the work described here, and a close friend. I would also like to acknowledge the National Institutes of Health, more specifically the National Institute of Dental and Craniofacial Research (NIDCR) and National Institute of Arthritis and Musculoskeletal and Skin Diseases (NIAMS), for funding the work described here through multiple R01s to Dr. Kyriacos Athanasiou (R01 DE015038, R01 AR071457, R01 AR078389, and R01 AR067821).

In addition to my colleagues in DELTA*i*, there has been a large supporting cast that has provided crucial contributions to the work here. Chrisoula Toupadakis Skouritakis has provided excellent medical illustrations throughout this work. Linda Talken, Amy Lesneski, and Kirstie Tully have been instrumental in facilitating the animal surgeries and immediate post-operative care at UC Davis. Campus Veterinary Services at UC Davis also provided day-to-day animal care after surgeries. Drs. Clinton Yu and Lan Huang at the UCI High-end Mass Spectrometry Facility helped to run samples on the Orbitrap mass spectrometer and performed MaxQuant analysis.

I am lucky to have my committee members as collaborators and mentors. Dr. Boaz Arzi, who I have worked with extensively at UC Davis to complete the *in vivo* portions of this work, has been an outstanding scientific mentor who is also a phenomenal human being. His passion in veterinary research and life alike shines through whenever I speak to him. Dr. Wendy Liu has also been a collaborator on the immunology work presented here and one of the core faculty members who I looked to for mentorship outside DELTA*i*. She was crucial in developing my early scientific thinking while at UC Irvine through taking her courses. Dr. Vijaykumar Meli, who works under Dr. Liu, has also been instrumental in facilitating the immunology collaboration and a source of immunology expertise. I've also had the pleasure of interacting with Dr. Dean Wang on a regular basis to learn further about the orthopaedics field and juxtapose it to the oral and maxillofacial field. His knowledge of the musculoskeletal system is phenomenal, and, thus, he has offered crucial insights into the treatments we at DELTA*i* are developing for cartilage ailments.

Dr. Jerry Hu has been an invaluable and irreplaceable mentor. He has challenged me to ask the hard questions and dig up the evidence to answer such questions. Without him, much of the work in this dissertation would not be possible. He has provided the historical context and the answers to many of my simple questions that would otherwise leave me searching for hours. Without his unwavering energy and humor, graduate school would have been much more bland.

Of all my mentors, Dr. Kyriacos Athanasiou has been the one who has shaped me the most into the biomedical engineer, scientist, and person I am today. Dr. Athanasiou's wisdom, in both life and science, is unparalleled. Many times I have had a conversation that started with scientific discussion and ended with a moral or ethical lesson. He recognizes that, while science is important, the way you go about it and life lessons you learn along the way are of the utmost importance. Dr. Athanasiou, thank you for everything you have done for me professionally and personally. It is an honor to rub shoulders with someone of your stature.

Lastly and most importantly, thank you to my wonderful fiancée and soon-to-be wife, Holly Patrick, who has seen the worst and the best of me during graduate school and provides all her love and support no matter what. Without her, I would not be a man worthy of receiving a PhD or a man worth anything.

Curriculum Vitae

Ryan Patrick Donahue

Education

2022, PhD in Biomedical Engineering, University of California Irvine

2020, MS in Biomedical Engineering, University of California, Irvine

2017, BS in Biomedical Engineering (Magna Cum Laude), University of Miami

Appointments

January 2018 to March 2022, Graduate Student Researcher, Driving Engineering and Life-science Translational Advances at Irvine (DELTA*i*), University of California, Irvine, Advisor: Kyriacos Athanasiou

September 2017 to December 2017, Rotating Student, Zhao Lab, Sue and Bill Gross Stem Cell Research Center, University of California, Irvine, Advisor: Weian Zhao

March 2015 to May 2017, Undergraduate Research Assistant, Dr. Nasser Ibrahim Al-Rashid Orbital Vision Research Center, Bascom Palmer Eye Institute, University of Miami, Advisor: Daniel Pelaez

May 2013 to July 2013, Student Assistant, Reproductive Science Center of New Jersey, Advisor: Scott Kratka

Publications

1. **Donahue, R.P.**, Bielajew, B.J., Vapniarsky, N., Heney, C.M., Arzi, B., Hu, J.C., Athanasiou, K.A. Long-term safety and efficacy of temporomandibular joint disc regeneration in the Yucatan minipig. In preparation for submission in *Nature Biomedical Engineering*.

2. **Donahue, R.P.**,* Bielajew, B.J.,* Vapniarsky, N., Heney, C.M., Arzi, B., Hu, J.C., Athanasiou, K.A. Tissue-engineered implants regenerate large perforations in the Yucatan minipig temporomandibular joint disc. In preparation for submission in *Nature Medicine* (* These authors contributed equally.)

3. Bielajew, B.J.,* **Donahue, R.P.**,* Lamkin, E.K., Hu, J.C., Hascall, V.C., Athanasiou, K.A. Proteomic, mechanical, and biochemical development of tissue-engineered neocartilage. Submitted to *Biomaterials*. (* These authors contributed equally.)

4. Salinas, E.Y.,* **Donahue, R.P.**,* Herrera, J.M.,* Hu, J.C., Athanasiou, K.A. The functionality and translatability of neocartilage constructs are improved with the combination of fluid-induced shear stress and bioactive factors. *The FASEB Journal*, April 2022, 36(4): e22225. (* These authors contributed equally.)

5. Bielajew, B.J.,* **Donahue, R.P.**,* Lamkin, E.K., Hu, J.C., Hascall, V.C., Athanasiou, K.A. Proteomic, mechanical, and biochemical characterization of cartilage development. *Acta Biomaterialia*. February 2022, online ahead of print. (* These authors contributed equally.)

6. **Donahue, R.P.**,* Link, J.M.,* Meli, V.S., Hu, J.C., Liu, W.F., Athanasiou, K.A. Stiffness- and bioactive factor-mediated protection of self-assembled cartilage against macrophage challenge in a novel co-culture system. *Cartilage*, January 2022, 13(1): 19476035221081466. (* These authors contributed equally.)

7. **Donahue, R.P.**,* Nordberg, R.C.,* Bielajew, B.J., Hu, J.C., Athanasiou, K.A. The effect of neonatal, juvenile, and adult donors on rejuvenated neocartilage functional properties. *Tissue Engineering Part A*. January 2022, online ahead of print. (* These authors contributed equally.)

8. Meli, V.S., **Donahue, R.P.**, Link, J.M., Hu, J.C., Athanasiou, K.A., Liu, W.F. Isolation and characterization of porcine macrophages and their inflammatory and fusion responses in different stiffness environments. *Biomaterials Science*, November 2021, 9(23): 7851-7861.

9. Bielajew, B.J.,* **Donahue, R.P.**,* Espinosa, M.G.,*, Arzi, B., Wang, D., Hatcher, D.C., Paschos, N.K., Wong, M.E.K., Hu, J.C., Athanasiou, K.A. Knee orthopaedics as a template for the temporomandibular joint. *Cell Reports Medicine*, April 2021, 2(5): 100241. (* These authors contributed equally.)

10. Young, S., Kasper, F.K., Melville, J., **Donahue, R.P.**, Athanasiou, K.A., Mikos, A.G., Wong, M.E.K. Tissue engineering in Oral and Maxillofacial Surgery. In: Principles of Tissue Engineering, 5th ed. Cambridge, MA: Academic Press; 2020, p1201-1220.

11. **Donahue, R.P.**,* Gonzalez-Leon, E.A.,* Hu, J.C., Athanasiou, K.A. Considerations for translation of tissue engineered fibrocartilage from bench to bedside. *Journal of Biomechanical Engineering*, July 2019, 141(7): 070802. (* These authors contributed equally.)

12. **Donahue, R.P.**, Hu, J.C., Athanasiou, K.A. Remaining hurdles for tissue-engineering the temporomandibular joint disc. *Trends in Molecular Medicine*, March 2019, 25(3): 241-256.

Abstracts and Presentations

1. **Donahue, R.P.**, Bielajew, B.J., Vapniarsky, N., Heney, C.M., Arzi, B., Hu, J.C., Athanasiou, K.A. Treating small perforations of the temporomandibular joint disc using tissue-engineered implants. 2022 TMJ Bioengineering Conference, Pittsburgh, PA, May 2022.

2. **Donahue, R.P.**,* Bielajew, B.J.,* Vapniarsky, N., Heney, C.M., Arzi, B., Hu, J.C., Athanasiou, K.A. Treatment of large perforation defects of the temporomandibular joint disc using tissue-engineered implants. 2022 TMJ Bioengineering Conference, Pittsburgh, PA, May 2022. (* These authors contributed equally.)

3. **Donahue, R.P.**, Bielajew, B.J., Vapniarsky, N., Heney, C.M., Arzi, B., Hu, J.C., Athanasiou, K.A. Regeneration of TMJ disc perforations using self-assembled, tissue-engineered implants in the Yucatan minipig. 2022 American Society of Temporomandibular Joint Surgeons Annual Meeting, Del Mar, CA, March 2022.

4. **Donahue, R.P.**, Link, J.M., Meli, V.S., Hu, J.C., Liu, W.F., Athanasiou, K.A. The effect of stiffness on macrophage-mediated inflammation in TMJ implants. 2020 TMJ Bioengineering Conference, Pittsburgh, PA, June 2020.

In the Media

1. **"UCI biomedical engineers spotlight disparities in knee and jaw joint treatments,"** in UCI News, May, 2021. Available from https://news.uci.edu/2021/05/05/uci-biomedical-engineers-spotlight-disparities-in-knee-and-jaw-joint-treatments/.

2. **"UCI engineers aim to pioneer tissue-engineering approach to TMJ disorders,"** in UCI News, March, 2019. Available from https://news.uci.edu/2019/03/20/uci-engineers-aim-to-pioneer-tissue-engineering-approach-to-tmj-disorders/.

3. **"Remaining Hurdles for Tissue Engineering the Temporomandibular Joint Disc,"** in TMJ News Bites by TMJ Association, Issue 2, 2019. Available from http://tmj.org/wp-content/uploads/2020/08/TMJNewsBites_Issue2_2019.pdf.

Leadership and Outreach Activities

Graduate Association of Biomedical Engineering Students, UC Irvine	2018-2021
Housing and Residential Life, University of Miami	2014-2017
Homecoming Executive Committee, University of Miami	2014-2016
Student Government, University of Miami	2013-2017

Honors and Distinctions

Who's Who Among Students in American Universities and Colleges	2017
Mortar Board National College Honor Society	2016
Alpha Eta Mu Beta, National Biomedical Engineering Honor Society	2016
Omicron Delta Kappa: The National Leadership Honor Society	2015
Tau Beta Pi: The Engineering Honor Society	2015
Alpha Lambda Delta National Honor Society	2013

Abstract

Tissue engineering of temporomandibular joint disc implants toward clinical translation

by

Ryan Patrick Donahue

Doctor of Philosophy in Biomedical Engineering

University of California, Irvine, 2022

Distinguished Professor Kyriacos A. Athanasiou, Chair

Temporomandibular joint (TMJ) disorders (TMDs) are a group of painful and debilitating conditions, affecting 5-25% of the general US population. While generally an outdated umbrella term, recent work has delineated TMDs into those of myogenous (associated with the muscles) and arthrogenous (associated with the joint) etiologies. Specifically, in the arthrogenous category, the fibrocartilaginous TMJ disc, situated between the temporal bone of the skull and the mandible, is central to TMDs; up to 70% of all TMD cases include a pathology called disc displacement, which is an abnormal positioning of the disc. As a result of this, a condition known as disc perforation can also develop. Current treatments for discal TMDs quickly progress to end-stage surgical techniques because non-surgical approaches are only palliative and do not induce reparative effects. Recently, tissue engineering has been proposed as an intermediate solution that may be able to regenerate TMJ disc defects. However, prior to translation of tissue-engineered therapeutics, 1) tissue engineering methodologies must be optimized to create mechanically robust constructs for implantation in the orthotopic environment, 2) given that neocartilage surgical implantation causes an immune response, immune challenge of tissue-engineered implants must be investigated *in vitro* toward implant survivability *in vivo*, and 3) implants must be tested for safety and efficacy in a suitable large animal model. Toward overcoming these three hurdles, the global objectives of this dissertation are 1) to engineer

neocartilage implants that can withstand the demanding environment of the TMJ disc, both mechanically and immunogenically, and 2) to expand treatable indications of tissue-engineered TMJ disc implants to perforation defects via preclinical investigations in a suitable large animal model.

Toward expanding indications for discal TMDs, this work first examined focal perforation defects in the Yucatan minipig TMJ disc in tandem with allogeneic, self-assembled implants derived from costal chondrocytes. Across 24 weeks, implant treatment was safe and efficacious in healing focal (i.e., 3 mm diameter) perforation TMJ disc defects. For safety, full body necropsy, blood work, and local joint responses indicated that implants were well-tolerated immunogenically. In terms of efficacy, repair tissues of implant-treated discs were 6.2-times tougher, 8.9-times more resilient, 3.4-times stronger, and had a 2.5-times higher strain at failure, compared to fill tissues of empty defect controls. This represented significantly improved healing of TMJ disc perforation defects in the Yucatan minipig.

Prior to scaling-up to larger defects, the tissue engineering process and immune response to constructs were examined. Across three studies examining the tissue engineering processes, 1) juvenile costal chondrocytes from the minipig were selected as the ideal tissue donor source, 2) 56 days of culture in the self-assembling process, which mimics native porcine knee cartilage development, resulted in the greatest tensile properties, and 3) large (i.e., 11x17 mm) implants derived from highly passaged (i.e., passage 6) cells were mechanically robust and flat. In another two studies assessing the immune response to implants, 1) minipig macrophages from the blood and bone marrow were harvested and characterized, and 2) macrophage co-culture revealed constructs were protected from macrophage inflammatory challenge and resulting degradation via their robust matrix content and bioactive factor application during the self-assembling process.

Using the information generated from the *in vitro* studies described, a second *in vivo* study was performed examining regeneration of large (i.e., 6 mm diameter) TMJ disc perforation

defects when treated with self-assembled implants. Implant-treated discs exhibited complete closure of defects with regenerated tissue after only 8 weeks, recapitulating between 64.4% and 81.2% of native disc tensile properties. Controls remained perforated after 8 weeks. Ultimately, this study further bolstered the safety and efficacy of self-assembled implants toward future use in human discal TMDs, such as disc displacement and perforation. This dissertation establishes the translational pathway for tissue-engineered implants to clinical use in humans, potentially providing long-term relief of pain and improved function for the millions of people suffering from discal TMDs.

Introduction

The temporomandibular joint (TMJ) is a ginglymoarthrodial joint involved in everyday activities such as chewing, speaking, and breathing. A group of ailments, called TMJ disorders (TMDs), affect between 5-25% of the general population according to epidemiological reports [1-5], and cost the US economy up to $4 billion per year [6]. Generally, the “TMD” term is outdated and has caused much confusion in the TMJ field, but recent work has sufficiently delineated this umbrella term into the conditions of myogenous (those affecting the muscles) and arthrogenous (those affecting the joint) origins. Specifically, in the arthrogenous category, the TMJ disc is central to TMDs, and, in up to 70% of TMD cases [7], pathologies of the disc include the medical condition of disc displacement (also known as internal derangement or anterior disc displacement), an abnormal positioning of the interpositional fibrocartilaginous tissue situated between the mandible and temporal bone of the skull. Concurrent with disc displacement, another medical condition, known as disc perforation, can occur in up to 15% of cases, but there are also independent cases of disc perforation [8-10]. Based on these prevalences, it is estimated that there are up to 9 million people in the US alone living with disc perforations. While a large proportion of these do not require medical intervention, disc perforations remain a significant clinical indication, causing intractable pain and dysfunction in the day-to-day lives of TMD patients.

Cartilage afflictions in the knee have established algorithms for treatment, but cartilage-associated TMDs, such as the conditions of disc displacement and disc perforation, do not currently have well-defined, well-accepted treatment pathways [11]. Generally, the treatment of discal TMDs is approached based on severity [12]. Non-invasive interventions such as analgesics, mechanical stabilizers (e.g., orthodontic and prosthodontic devices), and physical therapy may be suitable for early-stage cases [11]. Surgical procedures are reserved for more severe cases, with only 5-10% of TMD cases being subjected to open joint surgery [13, 14]. These procedures include discectomy and total joint replacements, but these interventions are

plagued with revision surgeries due to joint degradation after disc removal and the young patient age (i.e., 20-40 years old) coupled with average total joint implant lifetimes (i.e., 20 years) [11]. There is no effective intermediate solution for addressing discal TMDs currently, and, thus, the field would benefit from new interventions that can significantly halt or slow progression of TMJ disc pathologies or regenerate damaged discs.

Tissue engineering has been proposed as a potential long-term, regenerative solution to TMJ disc pathologies [15, 16]. By implanting tissue-engineered therapeutics in injured TMJ discs, they are envisioned to heal and regenerate defects present within the fibrocartilage. Specifically, the self-assembling process has been developed over the last two decades toward addressing various types of cartilage pathologies [17], including those of the TMJ disc. Since costal cartilage has been previously used as an interpositional material after discectomy [18], costal chondrocytes of the rib have been proposed as a potential cell source for self-assembled TMJ disc implants [19-22]. Most recently, self-assembled implants derived from allogeneic costal chondrocytes have been shown to be safe and efficacious in healing partial thickness defects in the Yucatan minipig TMJ disc [23], a suitable large animal model for TMJ disc pathologies [24]. However, there are still a number of hurdles that need to be overcome prior to translating neocartilage therapeutics for TMJ disc pathologies.

In recent years, there have been a number of advances in the self-assembling process, including methods to serially expand chondrocytes and then rejuvenate the cells back toward a chondrogenic phenotype [25]. These techniques allow many TMJ disc implants to be made from few chondrocytes, even at relatively low passages (e.g., passage 3). However, as defects progress in both area and thickness, implants will require more cells and, thus, more passaging of the costal chondrocytes used in the implants. As defects increase in size, implants will also be exposed to higher mechanical stresses *in situ* when placed in the TMJ disc. Given that TMJ disc implants derived from highly passaged costal chondrocytes in large formats required for increasing defect size have not been previously investigated, it is important to revisit the tissue

engineering process toward examining the efficacy and functionality of implants intended to be used in an *in vivo* setting.

Another obstacle to *in vivo* survival of implants is the potential immune response as a result of surgery. Since tissue-engineered implants proposed here are allogeneic, they have the potential to exacerbate the immune response in the TMJ disc as a result of implantation. Even though various cartilages have been shown to be immunoprivileged [26], surgical implantation of TMJ disc implants would still result in the accumulation of immune cells [23], such as T cells, B cells, and macrophages, which could potentially hamper regeneration of discal defects. Specifically, macrophages have been known to be a key initial mediator of the immune response [27] and are sensitive to both biochemical and biophysical cues [28]. In particular, substrate stiffness has been shown to positively correlate with macrophage-mediated inflammation [29]. Given that it is the goal of tissue-engineered implants to be robust for *in vivo* loading, this stiffness-mediated macrophage response is in direct contrast to engineering stiff implants; the inflammatory response has the potential to cause catabolic degradation of implants. However, the immune response is also well known to switch to a resolution response after an initial inflammatory cascade, inducing healing of tissues. Thus, further investigation into the macrophage-mediated immune response to TMJ disc implants is necessary toward ensuring implant survivability and eventual tissue healing.

Ultimately, to progress along the translational pathway, tissue-engineered implants must be proven safe and efficacious prior to widespread human use. A critical step along this pathway is the use of preclinical animal models toward examining initial safety and efficacy. The Yucatan minipig has emerged as the gold-standard for modeling TMJ disc pathologies due to its similarities to humans in diet, joint biomechanics, and disc biochemical and mechanical properties [24]. Preliminary studies examining disc thinning (i.e., partial thickness) defects have proven initial safety and efficacy [23], but more clinically relevant indications, such as disc perforations, should be examined toward translation of neocartilage therapeutics.

Considering the desire for translation of TMJ disc implants, this work aims to examine the safety and efficacy of self-assembled implants derived from allogeneic costal chondrocytes in TMJ disc perforation defects in the Yucatan minipig model. The global objectives of this work are two-fold: 1) To engineer neocartilage implants that can withstand the demanding environment of the TMJ disc, both mechanically and immunogenically, and 2) to expand treatable indications of tissue-engineered TMJ disc implants to perforation defects via preclinical investigations in a suitable large animal model. These objectives were examined across four aims:

Specific Aim 1: To assess the long-term safety and efficacy of small neocartilage implants in a focal perforation defect in the TMJ disc. Encouraged by the success of previous studies [23], this aim seeks to extend existing tissue engineering methods of self-assembled implants to focal (3 mm diameter) perforation defects. It was hypothesized that implant-treated discs would have more mechanically robust repair tissue compared to fill tissue of empty defect controls as a result of less scar tissue-like formation and more native tissue-like regeneration.

Specific Aim 2: To examine, optimize, and scale-up the tissue engineering process toward generation of large neocartilage constructs. Toward addressing larger perforations, this aim sought to examine the age of donors for generation of neocartilage constructs, optimize the time of self-assembly to maximize tensile properties, and scale-up to 11x17 mm constructs using highly passaged chondrocytes. It was hypothesized that 11x17 mm constructs could be generated using highly passaged costal chondrocytes from young donors in the self-assembling process to maximize tensile properties toward mimicry of the TMJ disc.

Specific Aim 3: To evaluate the stiffness mediated-macrophage response to neocartilage constructs. Since it has been previously shown that macrophages may mount an attack against stiff neocartilages, this aim examined macrophage-neocartilage coculture. It was hypothesized that stiffer constructs would elicit a proinflammatory macrophage response that would result in catabolic breakdown of the neocartilage. Furthermore, it was expected that neocartilage would

be protected from deleterious macrophage effects in the presence of neocartilage bioactive factors.

Specific Aim 4: To assess the safety and efficacy of large neocartilage implants in a large perforation defect in the TMJ disc. Toward expanding the treatable indications for patients suffering from disc perforations, this aim assessed regeneration of large (6 mm diameter) perforation defects toward improved healing using the information derived from earlier aims. It was hypothesized that empty defect controls would not heal while implant-treated discs would have robust regenerated tissue fill after 8 weeks.

These four aims have been completed fully, and this dissertation describes all the work that contributed to their completion. Chapters 1, 2, and 3 establish the background and techniques used in tissue-engineering of TMJ disc implants within this work. Chapter 1 describes considerations for translation of various types of tissue-engineered fibrocartilages, including the TMJ disc. Chapter 2 focuses more specifically on the TMJ disc and explains the current state of tissue-engineering and the remaining hurdles necessary to overcome prior to clinical translation. Chapter 3 compares the field which the TMJ is under, oral and maxillofacial surgery, to the orthopaedics field; given the well-established orthopaedics field, the oral and maxillofacial field should consider modeling their treatments, training, and products after those found in orthopaedics. Together, these three chapters guided the execution of the specific aims as presented below.

Toward achieving Aim 1, Chapter 4 examines healing in the Yucatan minipig using self-assembled neocartilage implants. Using a focal (3 mm diameter) full thickness defect, disc perforation is modeled for 24 weeks, representing a long-term study. Local and systemic safety is examined, as well as efficacy. For safety, immunohistochemical staining for T cells, B cells, and macrophages reveal an immune response that dampens after 8 weeks, and systemic safety is established through full body necropsy and blood work. Repair tissue mechanical outcomes are improved when treated with an implant compared to empty defect controls, which exhibit

scar-like fill tissue in terms of biochemical content. This study established the feasibility of treating TMJ disc perforations with self-assembled implants.

Aim 2 consists of Chapters 5, 6, 7, and 8. In Chapter 5, donor age is investigated using costal chondrocytes as the cell source. Given that it has been previously shown that donor age greatly affects functional outcomes of tissue-engineered constructs [30, 31], this study examines neonatal, juvenile, and adult cells in conjunction with the self-assembling process. However, it is shown here that donor age minimally affects functional outcomes of constructs, and, thus, juvenile costal chondrocytes are used as the cell source in the remaining chapters. In Chapter 6, the development of self-assembled constructs is examined over time, given the self-assembling process has aspects reminiscent of native tissue developmental processes. Toward establishing theses similarities between native tissue development and the self-assembling process, Chapter 7 characterizes the proteomic, mechanical, and biochemical development of porcine knee cartilage. In the self-assembling process, which mimics the trends seen in native tissue development, tensile properties are highest after 8 weeks of culture, and, to balance with previous optimizations which state that 4 weeks of culture is optimal, 6 weeks of culture is carried forward since the TMJ disc operates under high tensile strains [32]. Finally, Chapter 8 examines the use of fluid-induced shear stress toward further enhancing construct functionality and translatability of large 11x17 mm constructs derived from highly passaged costal chondrocytes. Flat, robust constructs are fabricated using the fluid-induced shear stress regimen developed in this chapter, and this methodology is used as the basis for generation of mechanically robust constructs for implantation in Aim 4.

For Aim 3, Chapters 9 and 10 describe the isolation and characterization of various minipig macrophage sources and co-culture of constructs with macrophages. In Chapter 9, the methodology to isolate blood- and bone marrow-derived macrophages from the minipig is detailed. These macrophages are then used in a novel co-culture system with neocartilage constructs in Chapter 10. It is discovered that stiffer constructs elicit an inflammatory response

from macrophages but are sufficiently protected by their robust matrix content and further by addition of neocartilage bioactive factors. Thus, neocartilage constructs are shown to have immunoprotective effects, further bolstering their potential *in vivo* use in the TMJ disc.

Finally, toward accomplishing Aim 4, Chapter 11 examines the healing of large perforation defects using the methods, models, and implants developed in earlier aims. In the Yucatan minipig disc, it is shown that large defects ultimately do not heal if left untreated. However, the TMJ discs treated with a self-assembled implant heal phenomenally, with the regenerated tissue approaching native TMJ disc functional properties. Together with Chapter 4, this is a significant body of preclinical animal work that proves the safety and efficacy of tissue-engineered implants for addressing TMJ disc perforations.

In conclusion, the body of work here furthers the translation of tissue-engineered implants for addressing TMJ disc perforations. A significant portion of this work is performed in preclinical animal models, which may be applied toward eventual regulatory approval for future self-assembled therapeutics meant to address discal TMDs.

Chapter 1: Considerations for Translation of Tissue Engineered Fibrocartilage from Bench to Bedside[1]

Abstract

Fibrocartilage is found in the knee meniscus, the temporomandibular joint (TMJ) disc, the pubic symphysis, the annulus fibrosus of intervertebral disc, tendons, and ligaments. These tissues are notoriously difficult to repair due to their avascularity, and limited clinical repair and replacement options exist. Tissue engineering has been proposed as a route to repair and replace fibrocartilages. Using the knee meniscus and TMJ disc as examples, this review describes how fibrocartilages can be engineered toward translation to clinical use. Presented are fibrocartilage anatomy, function, epidemiology, pathology, and current clinical treatments because they inform design criteria for tissue engineered fibrocartilages. Methods for how native tissues are characterized histomorphologically, biochemically, and mechanically to set gold standards are described. Then, provided is a review of fibrocartilage-specific tissue engineering strategies, including the selection of cell sources, scaffold or scaffold-free methods, and biochemical and mechanical stimuli. In closing, the Food and Drug Administration paradigm is discussed to inform researchers of both the guidance that exists and the questions that remain to be answered with regard to bringing a tissue engineered fibrocartilage product to the clinic.

Introduction

Cartilage is a connective tissue that is classified by its biochemical properties into hyaline, elastic, and fibrous cartilage (also referred to as fibrocartilage). Of these, fibrocartilage is marked by the presence of type I collagen and traces of type II collagen. Glycosaminoglycans (GAGs) are present in fibrocartilage, albeit in lower amounts than in hyaline articular cartilage

[1] **Chapter published as:** Donahue, R.P.,* Gonzalez-Leon, E.A.,* Hu, J.C., Athanasiou, K.A. Considerations for translation of tissue engineered fibrocartilage from bench to bedside. *Journal of Biomechanical Engineering*, July 2019, 141(7): 070802. (* These authors contributed equally.)

[33]. Areas in the body containing fibrocartilage include the knee meniscus [34], the temporomandibular joint (TMJ) disc [35], the pubic symphysis, the annulus fibrosus of the intervertebral disc, tendons, and ligaments. Fibrocartilage undergoes a range of stresses including tension, compression, and shear in different areas of the body. Much like hyaline articular cartilage, fibrocartilage has a naturally low regenerative capacity due to its avascularity [33]. Fibrocartilages are notoriously difficult to repair with limited clinical options. Tissue engineering may be a route to provide novel clinical treatments, but the pathway for these products can be ill-defined due to the low number of FDA-approved cellular products. While Food and Drug Administration (FDA) guidance documents exist for human cells, tissues, and cellular and tissue-based products (HCT/Ps) in general [36] and, specifically, for products intended to repair or replace hyaline articular cartilage [37], an equivalent document for fibrocartilage does not exist. Formation of clinically relevant, tissue engineered fibrocartilages would require satisfying a variety of design criteria and regulatory requirements. This review uses the knee meniscus and TMJ disc fibrocartilages as two examples to discuss how tissue engineered fibrocartilages may be translated from the bench to bedside.

In the following sections, anatomy and structure-function relationships of the knee meniscus and TMJ disc will be presented. Epidemiology of these tissues and the causal pathologies that lead to specific indications for current clinical treatments will be provided. Assays for characterization for histomorphological, biochemical, and mechanical properties of fibrocartilages will be explained. Together, anatomy, function, epidemiology, pathology, current clinical treatments, and characterization studies inform design criteria for tissue engineered fibrocartilages. In context to these design criteria, current tissue engineering methods for fibrocartilage, specifically the meniscus and TMJ disc, will be discussed via subsections on the selection of cell source, a scaffolding or scaffold-free approach, biochemical stimuli, and mechanical stimuli. In addition, evaluation of tissue engineered fibrocartilages and discussion of engineering a fibrocartilage spectrum will be provided. The final section of this paper will look

toward the translation of tissue engineered fibrocartilage and how this type of product may be shepherded through the FDA paradigm. A focus will be considerations for preclinical animal models and clinical trials. Future directions will be recommended, motivation for FDA guidance will be discussed, and remaining questions or concerns will be presented.

Fibrocartilage Types, Epidemiology, Pathology, and Clinical Treatments

Fibrocartilage anatomy, function, epidemiology, and pathology all inform how tissue engineered fibrocartilage should be designed and made. Current clinical options and practices can inform how tissue engineered fibrocartilage may be deployed in the clinical setting and can, thus, inform design criteria as well. These are provided below.

The knee meniscus and TMJ disc

In 2005, more than 46 million adults incurred over $353 billion in direct healthcare costs related to different rheumatic conditions in the United States alone [38]. These conditions encompass those affecting fibrocartilages. Two fibrocartilages of high clinical relevance are the knee menisci and TMJ disc. Knee menisci are semi-circular, wedge-shaped fibrocartilaginous tissues, located between the distal femur and the tibial plateau (Figure 1-1), that protect articular cartilage via load distribution. The knee contains a medial and a lateral meniscus (Figure 1-1). Under compressive load, the menisci's wedge shape causes tension to develop, which is resisted by circumferentially aligned collagen. A gradient of healing capabilities in the knee meniscus correlates with the degree of vascularity, with the capacity for healing decreasing as one moves closer to the innermost, avascular region (Figure 1-1, white-white region).

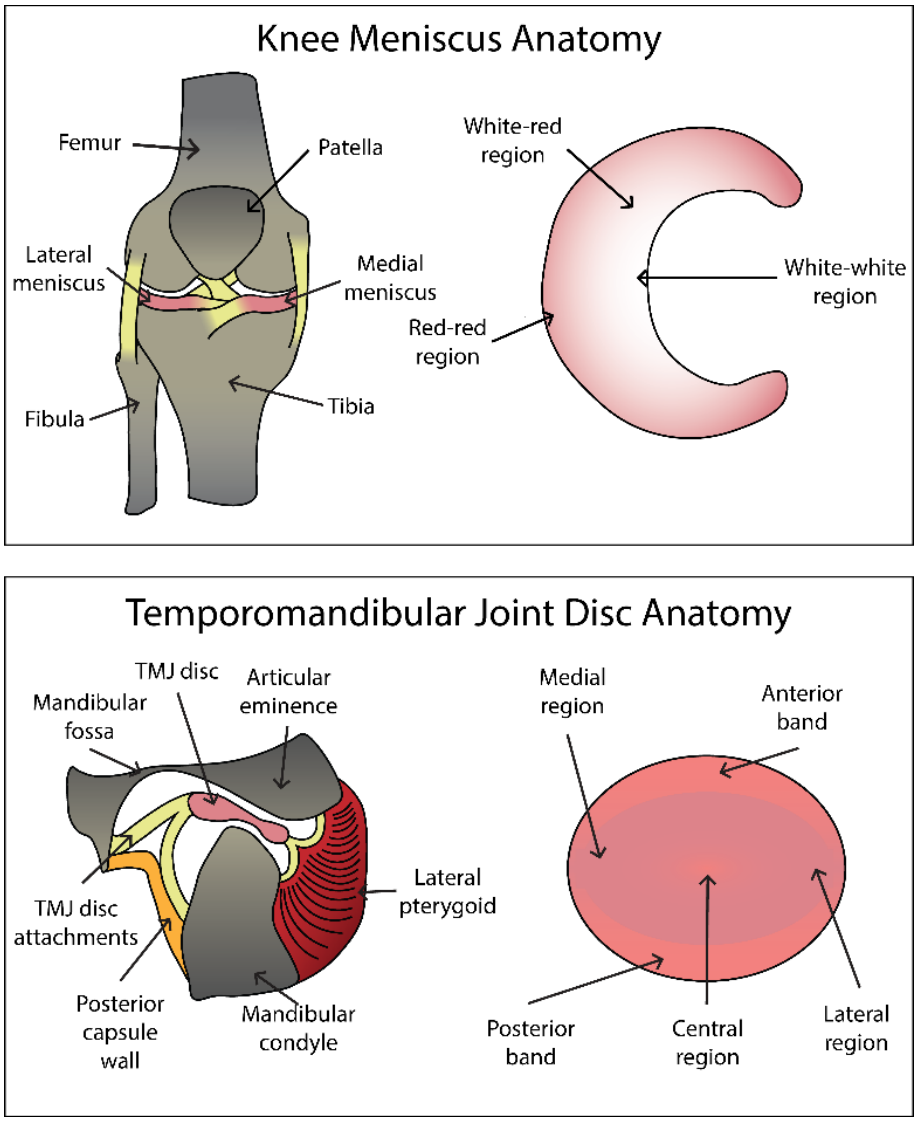

Figure 1-1: Anatomy of the knee meniscus and TMJ disc.
The anatomical structures of the knee are shown, with the menisci depicted between the femur and tibia. The transverse view is shown in the right panel, indicating the different vascular regions of each meniscus. The TMJ disc is shown from a sagittal view between the mandibular condyle and the articular eminence in an open jaw position. The disc from a transverse view is depicted in the right-hand panel.

The TMJ is a ginglymoarthrodial joint that contains a fibrocartilaginous disc situated between the mandibular condyle on the inferior side, and articular eminence and mandibular fossa on the superior side (Figure 1-1). The TMJ disc is biconcave and consists of the anterior and posterior bands as well as the lateral, central, and medial zones that are collectively referred to as the intermediate zone (Figure 1-1) [39]. The TMJ disc serves to increase

congruity between the eminence and fossa, to distribute load, and to aid in joint lubrication [40]. The movement of the TMJ disc serves the rotational motion of the joint primarily in the rotational axis during normal mastication and the translational motion of the joint when the mouth is opened wide. During typical movements of the joint, loading patterns in the anterior portion of the mandibular condyle and posterior portion of the articular eminence lead to complex shear, compressive, and tensile forces on the fibrocartilaginous disc.

Epidemiology and pathology

Meniscal lesions are the most common intra-articular knee injuries and most frequent cause of orthopedic surgical procedures in the U.S. [41]. This is reflected by the size of the meniscus repair market, which in 2008 was anticipated to increase at a compound annual growth rate of 10.6% to an estimated $318 million in 2015 [42]. Previously reported incidences of meniscal injury leading to meniscectomy were noted at 61 per 100,000 persons [43], but damage to the medial meniscus is significantly more prevalent than in the lateral meniscus (81% and 19%, respectively) [43-49]. Injury to the lateral meniscus, while less frequent, leads to the degeneration of knee function, lower Lysholm scale scores—a scale from 0-100 that measures patient-reported pain where 100 represents a better outcome with fewer symptoms or disability, and a higher rate of instability when treated via meniscectomy as compared to meniscectomy of the medial meniscus [45, 46].

Meniscal lesions are classified by their spatial alignment as vertical longitudinal (or longitudinal), radial, oblique, complex (or degenerative), and horizontal tears (Figure 1-2). Complex tears are more likely to arise with increasing age, while other tears are more commonly attributed to traumatic injury. Oblique and vertical longitudinal tears represent 81% of meniscal tears [50, 51]. Vertical longitudinal tears run parallel to the long axis of the meniscus and are perpendicular to the tibial plateau (Figure 1-2). These tears divide the circumferentially aligned collagen fibers and are categorized as either complete or incomplete vertical

longitudinal tears. The former is known as a bucket handle tear, which more commonly affects the medial meniscus. Bucket handle tears are often unstable and can cause mechanical symptoms or locking of the knee [51], and are more amenable to repair if found within a vascularized region of the meniscus [52].

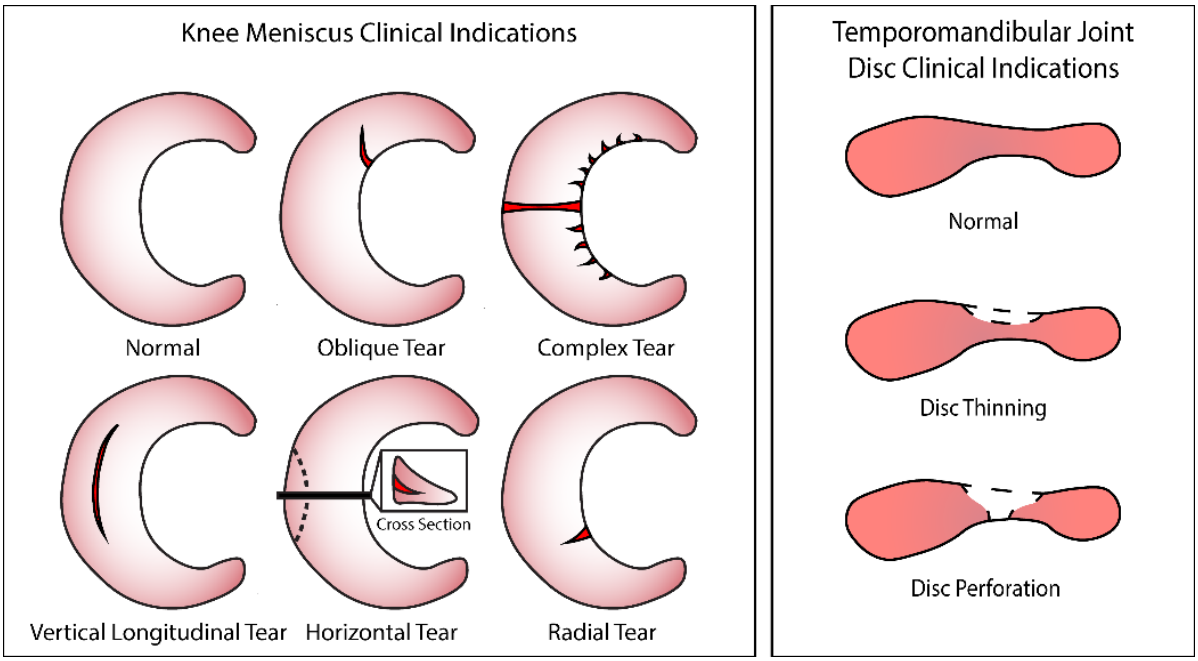

Figure 1-2: Clinical indications of the knee meniscus and TMJ disc.
Different clinical indications for the meniscus are shown including five different tears: oblique, complex, vertical longitudinal, horizontal, and radial tears. For the TMJ disc, disc thinning and disc perforation are the clinical indications presented.

TMJ disorders (TMDs) encompass any issue with the jaw and the muscles that control it. TMDs are the second most common musculoskeletal condition resulting in pain and disability [53] and cost an estimated $4 billion per annum in healthcare in the U.S. alone. TMDs may cause pain in 20-25% of adults worldwide [54]. A gender paradox exists with TMDs because a 3.5-fold higher prevalence is seen in women than men [55, 56]. This gender paradox has been well studied and has been hypothesized to occur due to hormone differences between genders [55]. TMD symptoms are wide-ranging, including clicking, restricted or deviating range of motions, and cranial and/or muscular pain [54].

Up to 70% of TMD patients suffer from internal derangement (ID) of the disc [7], where the TMJ disc is displaced from its normal anatomic position. Severe cases of ID are often presented with focal thinning of the disc, with eventual progression to larger areas of thinning or disc perforation (DP) (Figure 1-2) [9]. Osteoarthritis (OA) often accompanies TMDs [57], but there is conflicting evidence of a clear causal relationship between ID and OA [58].

Epidemiological and economic data make the knee meniscus and TMJ disc highly significant fibrocartilages for tissue engineering. When one considers the mechanical behaviors of the knee meniscus and TMJ disc, and how these functions fail due to pathology, many similarities begin to emerge. For example, both fibrocartilages function under large magnitudes of mechanical stress; engineered implants must be ready to bear similar loads. While specific pathological features may differ for the knee meniscus and TMJ disc (tears for the meniscus and thinning or perforation for the TMJ disc), late-stage pathologies of both fibrocartilages are often treated by tissue removal without long-term options for replacement, leading to joint degeneration. The similarities lead to comparable design criteria for the tissue engineering of these fibrocartilages.

Current clinical treatments

Fibrocartilage treatments usually follow a path of two stages: nonsurgical methods followed by surgical intervention that range from minimally to highly invasive procedures. Nonsurgical methods may include physical therapy, analgesics for pain management, and behavioral modification, and are indicated for early disease stages. If no improvement in symptoms is shown, surgery may be indicated. Surgical options for fibrocartilage are limited and progress rapidly to final stage options, such as arthroplasty, beyond which, even fewer options exist [59]. Tissue engineered fibrocartilage could potentially bridge the gap between the early and end stages of fibrocartilage pathology.

Initial diagnoses of knee meniscus injuries begin with clinical examination using a variety of tests [51]. If a meniscal tear is identified, the tear's severity is categorized to determine treatment which includes repair via arthroscopy, partial or full meniscectomy, and allograft transplantation [51]. Therapeutic efficacy varies by indication in part due to anatomy. For example, tears found in the red-white region of the meniscus are more amenable to repair than the white-white region due to the higher levels of vascularity in that region [52]. If possible, meniscectomy should be reserved for cases refractory to repair because meniscal repair tends to yield better clinical outcomes than meniscectomy [60].

Meniscectomy removes parts of the knee meniscus or cleans up degenerative debris, leading to immediate pain relief, although this is not always observed. Meniscectomy virtually guarantees the emergence of OA [61]. While some meniscectomy patients report pain relief, a statistically significant increase in quality of life after meniscectomy over alternatives such as physical therapy has not been observed, illustrating the limitations of fibrocartilage removal without replacement [62-64].

Diagnosis of TMDs follows patients' report of pain in the TMJ, headaches behind or around the eyes, and pain spreading to the temple, neck, ears, and shoulders [57]. Patients will often undergo a physical exam and multiple imaging modalities, such as MRI and/or computed tomography [54]. Although many TMJ symptoms can resolve themselves [53, 57], approximately 3-5% of TMD patients will require medical intervention in various forms.

Even in the most severe cases of TMDs, nonsurgical treatment is preferred [57]. Surgical options for TMDs are limited but include disc repositioning or discectomy with or without disc replacement [54, 65]. Hemiarthroplasty is replacement of the articulating joint surface [66], most commonly the superior side in the TMJ with a vitallium alloy in the mandibular fossa-articular eminence region [67]. For certain indications such as ID, the disc can be repositioned in the correct anatomic position. Another option is discectomy, where the TMJ disc is removed. Postoperative follow-up in 3 years shows that discectomy increases mandibular

motion [68] but is also associated with signs of degenerative changes including flattening of the articular surfaces and osteophytes [54, 69]. Alloplastic disc replacements have been studied including Teflon-Proplast- [70] and silicone-based [54] implants. Biologic materials such as fat have also been explored [71], but all have required follow-up intervention. When a substantial portion of the joint is lost due to degeneration from trauma or significant degeneration in the articulating surfaces, total joint reconstruction may be indicated [54]. Costochondral grafts are used to replace the condyle in autologous TMJ reconstruction [72]. Alloplastic materials have been used in three FDA approved products [40, 54] and often require secondary surgery due to the average patient age and resultant implant degradation [54].

As illustrated with the knee meniscus and TMJ disc, both nonsurgical and surgical options for fibrocartilage repair and replacement are lacking in long-term efficacy. Nonsurgical methods commonly treat symptoms and attempt to delay degeneration but are often unsuccessful in doing so. Surgical methods can cause degeneration in the joint space and commonly require additional surgical follow-ups. An important consideration for tissue engineers will be where and how engineered products might fit into existing treatment modalities, such as serving as a bridge between early- and late-stage surgical interventions.

Using tissue engineering for fibrocartilage

The need for interventions that can delay or arrest joint degeneration motivates the development of tissue engineered fibrocartilages. In early-to mid-stage pathologies, such as a partial vertical longitudinal tear in the knee meniscus or thinning of the TMJ disc, tissue engineered fibrocartilage implants may be used to bolster failing tissues to slow down or to arrest the degenerative process. Late-stage pathology where fibrocartilage removal by meniscectomy or discectomy is indicated may be combined with implantation of a tissue engineered fibrocartilage replacement. While there is hope for these strategies, there is currently a lack of tissue engineered fibrocartilage products on the market. Subsequent sections

outline the process of fibrocartilage tissue engineering (Figure 1-3) and examines the necessary steps for translating a tissue engineered fibrocartilage product to clinical use (Figure 1-4).

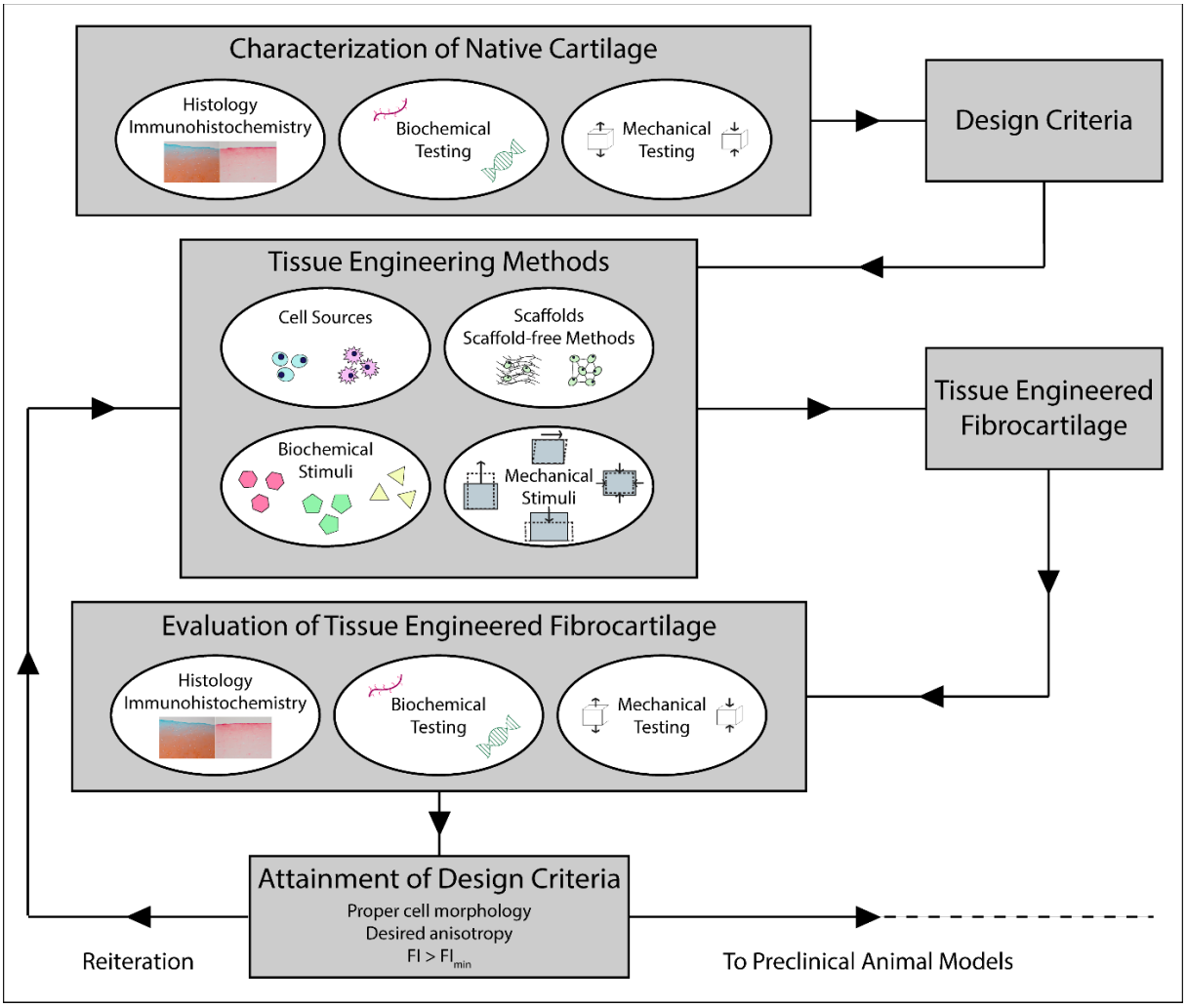

Figure 1-3: Tissue engineering of fibrocartilage.
Tissue engineering requires characterization of native cartilage from which design criteria can be specified. Tissue engineering parameters such as selection of a cell source, choice of scaffold or scaffold-free methodology, and use of biochemical or mechanical stimuli results in tissue engineered fibrocartilage which is subsequently tested for appropriate properties. If design criteria are met, the tissue engineered fibrocartilage and methodology used may move to preclinical animal models or the tissue engineering process might be reiterated to obtain improved tissue engineered fibrocartilage.

Characterization Studies of Fibrocartilages

Prior to carrying out tissue engineering studies, design criteria must be acquired. These are determined via characterization studies of the native fibrocartilage using histology, immunohistochemistry (IHC), biochemical testing, and mechanical testing (Figure 1-3). Various

animals commonly serve as models due to their anatomical, structural, and functional similarities to human tissues. Various reviews and comparative studies in the literature discuss different animal models and their similarities to human tissue for both the knee meniscus [73, 74] and TMJ disc [75, 76] and should be referenced to determine comparability. Test results establish the gold standards toward which tissue engineers aim for in terms of histomorphological, biochemical, and mechanical properties of the engineered tissue. This section will provide guidance for the aforementioned testing and will provide values for native knee meniscus and TMJ disc properties that are relevant to tissue engineering.

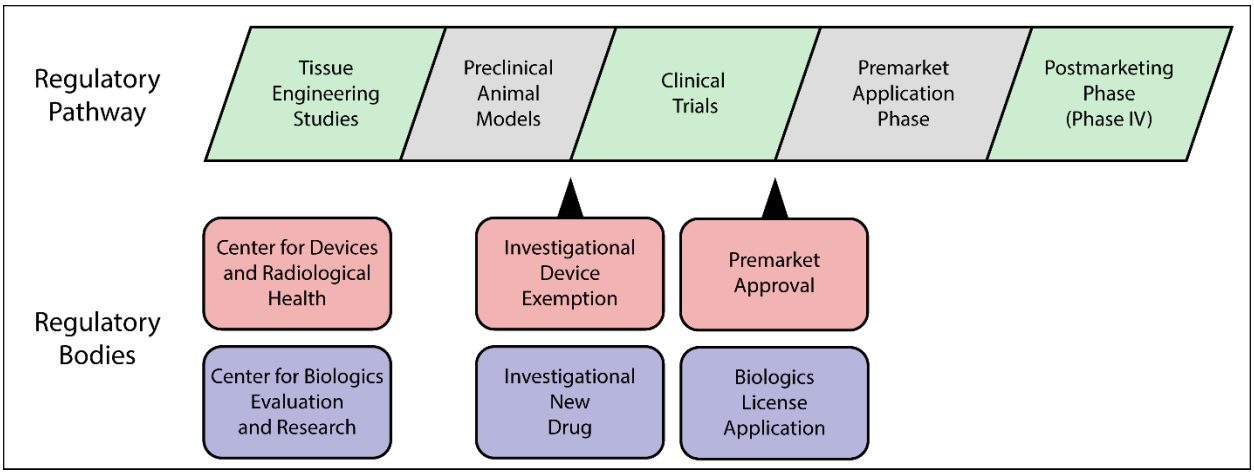

Figure 1-4: The FDA paradigm.
The FDA paradigm is outlined from tissue engineering studies to the postmarketing phase with appropriate milestones for CBER and CDRH depicted.

Histomorphological properties

Histology and IHC allows for examination of a tissue's microscopic organization. In fibrocartilage, the distribution of different cell types [24, 77-79], GAGs [24, 78, 80-83], and collagen [24, 78, 81-84] can be visualized using hematoxylin staining, Safranin O staining with a Fast Green counterstain, and Picrosirius Red staining, respectively. IHC uses antibodies for more specific visualization of the aforementioned items [81, 85, 86]. For example, multiple collagen types exist within fibrocartilages, and these can be discerned using IHC.

Histology, IHC, and microscopy techniques (e.g., polarized light, second harmonic generation) are used widely to elucidate fibrocartilage properties. For example, different cell types reside side-by-side in fibrocartilage, as seen in the meniscus where chondrocyte-like cells exist in its inner region and transition to a fibroblast-like phenotype in its outer region [87, 88] (Figure 1-5A). In the TMJ disc, the ratio of fibroblasts to chondrocyte-like cells varies by region as well, with the highest relative number of chondrocyte-like cells present in the intermediate zone [77] (Figure 1-5C). GAGs were evenly distributed throughout young equine menisci, whereas samples from older horses showed distinct positive and negative staining locations [89]. IHC determined the presence of hyaluronic acid backbone, keratan sulfate, and chondroitin sulfate in the primate TMJ disc [85]. In addition, collagen fibers in an equine knee meniscus model were shown to be randomly organized in the distal and proximal surface layers [89, 90] (B), while the innermost layer exhibited circumferentially aligned collagen fibers with parallel alignment in the red-red region [89]. Polarized light microscopy Gutman, Kim [91] and scanning electron microscopy [86] showed that collagen aligned primarily circumferentially of the human and porcine TMJ discs, with the intermediate zone showing alignment anteroposteriorly (Figure 1-5D). Finally, IHC showed greater type I collagen staining than type II collagen staining throughout the porcine TMJ disc [86].

Overall, histology and IHC are an adequate starting point for confirming presence and distribution of cells, GAGs, and collagen within fibrocartilage. While useful for the visualization of tissue organization, histology and IHC are qualitative assays and should be supported by sufficient sample sizes and quantitative assays, such as biochemical and mechanical testing.

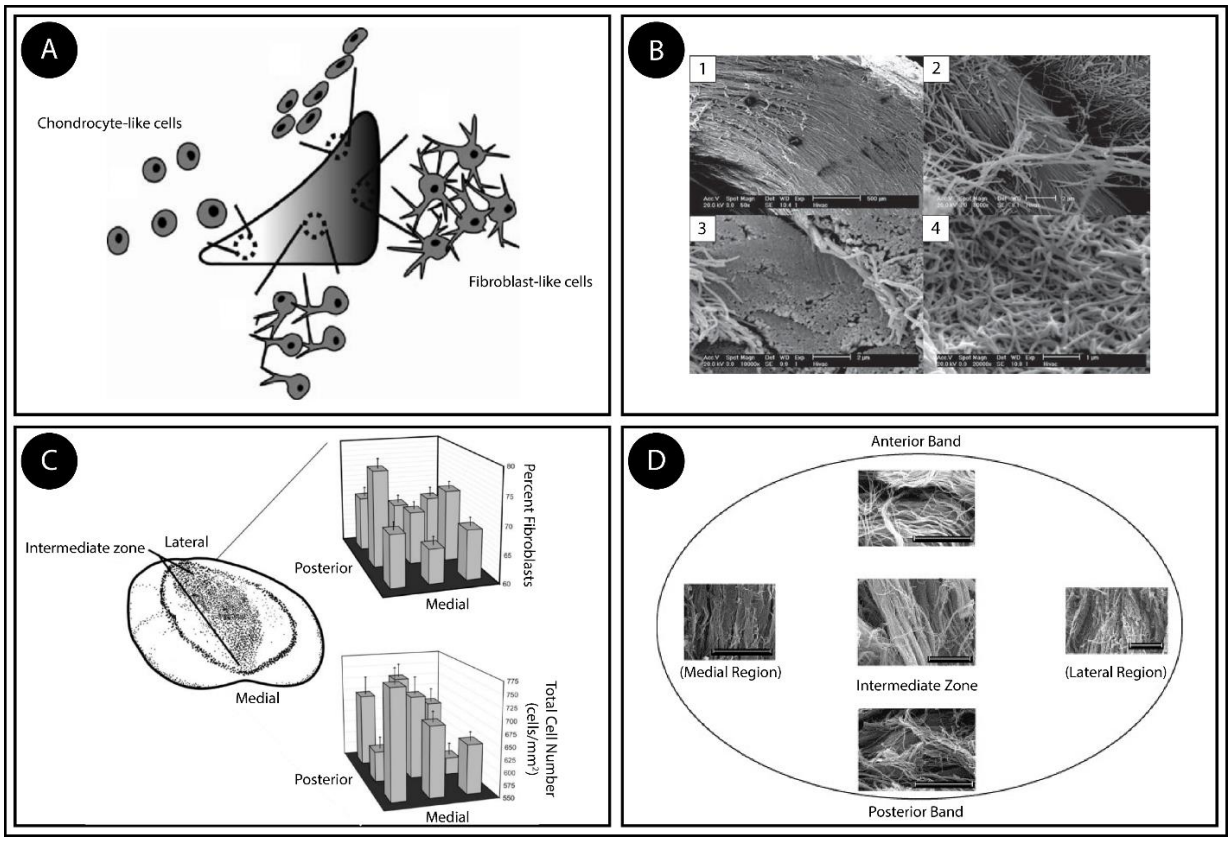

Figure 1-5: Cell morphology and collagen alignment of the knee meniscus and TMJ disc.
A) A representation of the wedge-shape of the meniscus is depicted with the innermost region showing rounded, chondrocyte-like cells transitioning to spindle-shaped, fibroblast-like cells toward the outermost region. Figure reused with permission from Springer Nature: Cellular and Molecular Bioengineering [88]. B) Scanning electron micrographs showing (1) the circumferential collagen alignment, (2) a close-up view depicting individual collagen fibers, (3) a cross section of a collagen bundle, and (4) the random collagen orientation on the outer surfaces of the meniscus. Figure reused with permission from SAGE Publications: Proceedings of the Institution of Mechanical Engineers, Part H: Journal of Engineering in Medicine [90]. C) Ratio between fibroblasts and chondrocyte-like cells, and overall cellularity in the TMJ disc are reported, showing the posterior and anterior bands have a higher proportion of fibroblasts when compared to the intermediate zone. Figure reused with permission from Elsevier: Journal of Oral and Maxillofacial Surgery [77]. D) Scanning electron micrographs of various regions of the TMJ disc showing primarily anteroposterior alignment in the intermediate zone, while the anterior and posterior bands show circumferential alignment. Scale bars are 10 microns except for the lateral region where the scale bar represents 200 microns. Figure reused with permission from Elsevier: Matrix Biology [86].

Biochemical properties

Biochemical assays yield quantitative data that allow one to determine how similar properties of tissue engineered fibrocartilage are when compared with those of native tissue. DNA content can be quantified using, for example, PicoGreen [24, 92]. Sulfated GAGs are often quantified using dimethyl methylene blue (DMMB) [24, 83]. Collagen content can be measured by assaying for hydroxyproline [24, 83, 93]; a modified version of this assay which excludes use of

perchloric acid to measure the collagen content has recently been published [93]. For quantification of specific types of collagen and GAG, enzyme-linked immunosorbent assay (ELISA) is used [81, 86]. Pyridinoline content, a measure of collagen crosslinking, can also be quantified with high performance liquid chromatographic assays [24, 83, 94]. Much like histology and IHC, many of these biochemical assays can be performed to determine regional variation.

The knee meniscus extracellular matrix (ECM) is composed of water, fibrillar components, proteoglycans, and adhesion glycoproteins. Water, collagen, and GAGs account for the majority of components by mass and has been shown to be 72%, 22%, and 0.8%, respectively in human menisci. The remainder of the tissue is made up of DNA (0.12%) and adhesion molecules. The distribution pattern of GAGs is as follows: 40% chondroitin 6-sulfate, 10-20% chondroitin 4-sulfate, 20-30% dermatan sulfate, and 15% keratan sulfate [95]. Collagen accounts for approximately 60-70% of the dry weight, and includes types I, II, III, V, and VI collagen [96]. Of these, type I collagen is by far the most predominant in the meniscus, accounting for more than 90% of total collagen [97]. The outer two-thirds of bovine menisci is composed primarily of type I collagen, whereas the inner one-third is 60% type II collagen and 40% type I collagen [98]. Pyridinoline collagen crosslinking has been shown to be highest in the inner region [99].

The biochemical composition of the TMJ disc is similar to the meniscus, being composed of primarily collagen and GAGs. Collagen is approximately 68.2% per dry weight in the porcine TMJ disc [100], while GAG content ranges from 0.273-0.936% per wet weight among species [80]. In a study on the structure-function relationship of the Yucatan minipig TMJ disc, the tissue showed regional variation in DNA content via PicoGreen assay ranging from 0.024%-0.041% per wet weight [24]. In a study on the porcine TMJ disc using ELISA to quantify GAGs, chondroitin sulfate was the most abundant GAG found, compromising 74% of the total GAG content [86]. For regional collagen variation, the intermediate zone had slightly more collagen per dry weight than the anterior and posterior bands of the disc, while in the mediolateral direction the central region contained significantly higher collagen than the lateral

region [100]. In the Yucatan minipig TMJ disc, pyridinoline content was found to be significantly lower in the anterior and posterior bands than in the lateral and medial regions of the disc [24].

Biochemically, the knee meniscus and TMJ disc are similar due to their fibrocartilaginous nature. Both have similar ranges for collagen, GAG, and DNA content, and vary regionally as discussed above. In addition, the meniscus and TMJ disc both are composed of primarily type I collagen in relation to other collagen types. Uniform biochemical characterization can be used for fibrocartilages and is a required quantitative step after performing histomorphological studies. Although biochemical assays may provide insight on structure, they should be supplemented by mechanical testing to yield an understanding into fibrocartilage function.

Mechanical properties

Inasmuch as fibrocartilages bear and distribute load, recapitulating the tissue's mechanical properties is a critical design criterion. Tension and compression tests are commonly used to derive target values. Uniaxial tensile testing provides tensile Young's modulus and ultimate tensile strength (UTS) [24, 82, 83, 92, 101]. For compression properties, creep indentation testing and incremental stress relaxation provide, among other properties, aggregate modulus [102-104] coefficient of viscosity [81, 92, 105], and instantaneous and relaxation moduli [24, 80, 83, 91, 92]. In addition to aggregate modulus, Poisson's ratio and permeability are also obtained from creep indentation testing [103, 104, 106]. These values can be derived from experimental data using different models based on linear elasticity, viscoelasticity including the standard linear solid model, poroelasticity, and mixture theories including the biphasic model. In-depth descriptions of these tests and their assumptions, performance, and mechanical models are available in the literature [33, 107-111]. While no one testing modality is the gold-standard for measuring mechanical properties, tissue structure-function relationships dictate which testing modality might be most informative when measuring characteristic properties of a native tissue. For example, the knee meniscus functions under compression, but its geometry causes

tensile forces to develop within the tissue, and, thus, the tensile properties of a tissue engineered meniscus may be more indicative of whether it will be effective in replacing diseased tissue. Similarly, an analogous argument can be made for the TMJ disc which though it functions primarily under compression, the end result is principally tensile strain fields in the ECM. Values derived from mechanical testing of the meniscus and TMJ disc are provided below.

Since both the knee meniscus and the TMJ disc exhibit anisotropy, the mechanical properties depend on testing direction. The knee meniscus exhibits more robust tensile mechanical properties in the circumferential orientation rather than the radial due to the generally circumferentially aligned collagen fibers; this holds true throughout the depth of the tissue for the tissue's Young's modulus [101]. The Young's modulus is approximately 100-300 MPa in the circumferential direction and 10-fold lower in the radial direction [34]. The meniscus has been shown to have an aggregate modulus of 100-150 kPa [104]. Incremental stress relaxation testing of porcine knee menisci in synovial fluid have yielded instantaneous and relaxation moduli for 20% strain of 2.37-6.75 MPa and 0.07-0.15 MPa, respectively [112]. Values of mechanical properties can vary from species to species, as well as different testing modalities [106, 113].

The mechanical properties of the TMJ disc display anisotropic, regional, and interspecies variations. Research on the Yucatan minipig TMJ disc revealed that UTS and tensile Young's modulus of the central region was highest in the anteroposterior direction, while the posterior band was stiffest and strongest in the mediolateral direction, when determined by uniaxial tensile testing [24]. Creep indentation testing shows that the medial region of the TMJ disc had the largest aggregate modulus at 28.9 ± 12.3 kPa and was found to be significantly higher than the anterior, posterior, central, and lateral regions [103]. Instantaneous and relaxation moduli for 20% strain in the Yucatan minipig TMJ disc were found to be 216-1,540

kPa and 20.5-57.5 kPa, respectively dependent on region [24]. Uniaxial tensile testing, creep indentation testing, and incremental stress relaxation all provide valuable design criteria.

As tissues that undergo constant mechanical loading, the gold standard for fibrocartilage functionality should accordingly be mechanical testing. Appropriate characterization of not only mechanical properties, but histomorphological and biochemical properties, defines the design criteria to be used in tissue engineering studies. By defining native tissue values, tissue engineers know what criteria they need to strive for and mimic within tissue engineered fibrocartilages.

Tissue Engineering of Fibrocartilage

The tools developed to address the design criteria for tissue engineering fall into the general category of cells, scaffolds, and signals. For fibrocartilage, of particular interest are the issues of finding an appropriate cell source, choosing a scaffold or scaffold-free approach, and identifying both biochemical and mechanical stimuli as depicted in Figure 1-3. A selection of the most impactful studies outlined in this section is summarized in Table 1-1. The following subsections will include information on each of the aforementioned components with a focus on approaches shown efficacious when applied with a scaffold-free, self-assembling process of tissue formation.

Cell sources

Cell sources used in tissue engineering of fibrocartilage vary from tissue-specific, terminally differentiated cells to various stem cell types. In terms of tissue-specific cells for tissue engineering of the knee meniscus, meniscus cells (MCs) and hyaline articular chondrocytes (ACs) [81, 92, 105, 114] have been explored. For engineering the TMJ disc, TMJ disc cells [20, 115-126], articular eminence cells [116], mandibular condyle cells [127], costal chondrocytes (CCs) [20, 21, 23, 128-130], ACs [21, 83, 131-133], MCs [83, 132, 133], and dermal fibroblasts [20] have been explored. Mesenchymal stem cells (MSCs) are the most heavily examined stem

cell population for tissue engineering of both fibrocartilages. Factors to take into account for all cells are an autologous versus allogeneic approach, coculture of cells, and various cell expansion technologies. For stem cells, additional considerations include their theoretically infinite ability to expand and suboptimal differentiation efficiency.

Table 1-1: Selected list of key publications for fibrocartilage tissue engineering.
Fibrocartilage tissue engineering studies were selected for their impact on the field. Authors, year of publication, cell source, scaffold or scaffold-free approach, biochemical stimuli, and mechanical stimuli are listed for these studies.

Authors, Year	Cell Source	Scaffold or Scaffold-free Approach	Biochemical Stimuli	Mechanical Stimuli	Tissue Engineered
Kasemkijwattana, *et al*., 2000 [134]	Leporine MCs	Monolayer	EGF, IGF-1, bFGF, PDGF, TGF-β1, transforming growth factor alpha, acidic fibroblast growth factor, and nerve growth factor	None	Knee Meniscus
Springer, *et al*., 2001 [116]	Human and Porcine TMJ disc cells and articular eminence cells	Polyamide, PTFE, and PGA scaffold	None	None	TMJ Disc
Detamore & Athanasiou, 2005 [123]	Porcine TMJ disc cells	PGA scaffold	IGF-1	Fluid-induced shear	TMJ Disc
Eifler, *et al*., 2006 [135]	Leporine MCs	Monolayer	None	Oscillatory fluid flow-induced shear	Knee Meniscus
Bean, *et al*., 2006 [125]	Porcine TMJ disc cells	PGA scaffold	Ascorbic acid	None	TMJ Disc
Almarza & Athanasiou, 2006 [126]	Porcine TMJ disc cells	Monolayer and PGA scaffolds	None	Hydrostatic pressure	TMJ Disc

Aufderheide & Athanasiou, 2007 [136]	Bovine ACs and MCs	Self-assembly	None	None	Knee Meniscus
Johns, *et al*., 2008 [20]	CCs, dermal fibroblasts, TMJ disc cells	Self-assembly	None	None	TMJ Disc
Gunja, *et al*., 2009 [137]	Leporine MCs	PLA scaffold	TGF-β1	Hydrostatic pressure	Knee Meniscus
Huey & Athanasiou, 2011 [81]	Bovine ACs and MCs	Self-assembly	TGF-β1, C-ABC	Tension and compression	Knee Meniscus
Huey & Athanasiou, 2011 [105]	Bovine ACs and MCs	Scaffold-Self-assembly	TGF-β1, C-ABC	None	Knee Meniscus
Kalpakci, *et al.*, 2011 [132]	Bovine ACs and MCs	Self-assembly	TGF-β1, IGF-1	None	TMJ Disc
Baker, *et al*., 2011 [138]	Bovine MSCs	PCL scaffold	TGF-β3	Cyclic tension	Fibrocartilage
Hagandora, *et al*., 2013 [129]	Caprine CCs	Poly (glycerol-sebacate) scaffold	None	None	TMJ Disc
Hadidi & Athanasiou *et al*., 2013 [92]	Bovine ACs and MCs	Self-assembly	LPA	None	Knee Meniscus
MacBarb, *et al*., 2013 [139]	Bovine ACs and MCs	Self-assembly	C-ABC, TGF-β1	None	Fibrocartilage
Ahtiainen, *et al*., 2013 [140]	Leporine adipose-derived MSCs	PLA scaffold	TGF-β1	None	TMJ Disc
Moriguchi, *et al*., 2013 [141]	Porcine synovium-derived MSCs	Cell sheet engineering	BMP-2	None	Knee Meniscus
Makris, *et al*., 2014 [83]	Bovine ACs and MCs	Self-assembly	TGF-β1, C-ABC, LOXL2	None	Fibrocartilage
Higashioka, *et al*., 2014 [142]	Bovine ACs and MCs	Self-assembly	None	None	Knee Meniscus
MacBarb, *et al*., 2014 [143]	Bovine ACs and MCs	Self-assembly	None	Passive axial compression	TMJ Disc

Murphy, *et al*., 2015 [130]	Porcine CCs	Self-assembly	C-ABC, TGF-β1, LOXL2	None	TMJ Disc
Murphy, *et al*., 2015 [144]	Porcine CCs	Self-assembly	TGF-β1, bFGF, PDGF	None	Fibrocartilage
Legemate, *et al*., 2016 [145]	Human bone marrow-derived MSCs	PCL scaffold	CTGF, TGF-β3	None	TMJ Disc
Warren, *et al*., 2017 [146]	None	PCL scaffold	None	None	Knee Meniscus
Wang, *et al*., 2018 [147]	Rabbit TMJ disc cells and synovium-derived MSCs	PLGA scaffold	TGF-β3	None	TMJ Disc

Autologous tissue-specific, terminally differentiated cells directly from native tissue, such as TMJ disc cells or MCs, offer the lowest risk of rejection, but sourcing can be a difficulty due to insufficient healthy tissue. Other cell sources that can potentially be derived in an autologous fashion for tissue engineered fibrocartilages include cells from hyaline articular cartilage [21, 83, 131-133], costal cartilage [20, 21, 23, 128-130], tendon, and ligament [148]. Autologous sources require two surgical procedures on the same patient: one for harvest of the donor tissue and another for implantation of engineered tissue. An allogeneic approach, which employs cells from a non-self donor, mitigates the issue of multiple surgeries for the patient and donor site morbidity but is limited by a possible immune response and rejection. Traditionally, articular cartilage has been considered to be an immunoprivileged tissue; immune response against cells within cartilage is rare due to the dense ECM [33]. A recent minipig study showed minimal to no T cells, B cells, and macrophages within allogeneic, tissue engineered fibrocartilage implants in the TMJ disc [23], providing evidence that fibrocartilage, like hyaline articular cartilage, may also be immunoprivileged.

Cocultures of cells have been explored to recreate the various fibrocartilages that naturally contain different cell types and ECM composition. For example, a one-to-one coculture ratio of ACs and MCs [81, 92, 105], in comparison to other ratios, has been shown to be optimal in reconstituting the native meniscal cross section as well in providing adequate strength and stiffness [136]. Menisci that exhibit a more hyaline articular cartilage-like inner region and a more fibrous outer region have been engineered by seeding 100% ACs in the inner region and a one-to-one mix of ACs to MCs in the outer region. This regionally variant meniscus exhibited significantly higher compressive properties as well as GAG per dry weight in the inner region, while the outer region exhibited significantly higher circumferential tensile modulus and collagen per dry weight [142]. These compositional and functional properties mimic the biochemical and mechanical differences seen in native meniscus regions (Figure 1-5B). For tissue engineering the TMJ disc, AC and MC cocultures [83, 132, 133], and CC and dermal fibroblast cocultures [20] have been examined. In AC and MC coculture, it was found that the presence of ACs is required to maintain a cylindrical shape by reducing contraction [132]. CC and dermal fibroblast coculture was inferior to CCs alone in terms of GAG content, total collagen, and type I collagen [20]. Coculture of multiple cell sources remains a viable option for creating more biomimetic tissue engineered fibrocartilages. Clinically, this may be more difficult to achieve using an autologous approach due to donor site morbidity and increasing number of surgeries as previously discussed, but an allogeneic approach might be appropriate if coculture were used.

Advances in cell expansion technologies that preserve cell phenotype, in combination with an allogeneic approach, have the potential to mitigate the concerns that repeat surgeries, donor site morbidity, and cell sourcing pose. For example, a combination of transforming growth factor beta 1 (TGF-β1), basic fibroblast growth factor (bFGF), and platelet-derived growth factor (PDGF) increases the post-expansion chondrogenic potential of CCs by increasing GAG content, altering the ratios of collagen types, and improving compressive properties engineered using treated cells [149]. After expansion, the phenotype of CCs can be preserved by culturing

them in three-dimensional (3D) aggregates [144]. During this aggregate redifferentiation process, application of TGF-β1, growth differentiation factor 5 (GDF-5), and bone morphogenetic protein 2 (BMP-2) also improves biochemical and mechanical properties of neocartilage using treated cells [150]. This process allows defined expansion of cells and preservation of phenotype by aggregate culture, and is extremely promising for allogeneic approaches, increasing the impact one donor can have.

Stem cells offer a solution to sourcing issues by having a theoretically infinite capability to expand. Synovial MSCs have been explored for the repair of the meniscus in scaffold-free culture methods [141] as well as via injection [151, 152]. TMJ disc engineering has used both MSCs from bone marrow [145] and adipose tissue [140]. The current limitation of stem cells for tissue engineered fibrocartilage formation lies in their suboptimal differentiation protocols, which often lack efficiency (i.e., only a low percentage of cells attain the target phenotype) and may result in “chondrocyte-like” cells [153] that may not form mechanically robust tissue engineered fibrocartilage. Additional concerns with stem cell use include tumorigenic potential and possible xenogeneic culture components. While stem cells for tissue engineered fibrocartilages have been used in research, their infinite expansion potential has yet to be realized clinically due to lack of efficiency.

To summarize, an autologous approach may be the ultimate goal because the cells are patient-specific, but not the most practical because the scarcity of healthy tissue remains an issue in these already diseased patients. An allogeneic approach may be the most translatable, especially with the advent of cell expansion technologies and evidence that suggests fibrocartilage as immunoprivileged. Allogeneic cells solve the issue of donor site morbidity and repeated surgeries from autologous approaches. Using stem cells may present the solution to the cell sourcing issue, but their translatability is not yet realized due to efficiency and possible tumorigenic potential. The selection of a cell source is among the most important choices a

tissue engineer can make and should be well-informed by how a tissue engineered fibrocartilage will be translated.

Scaffold and scaffold-free methods

For 3D cell culture of tissue engineered fibrocartilage, both scaffold and scaffold-free methods exist. Scaffolds can be used to direct cell behavior by engineering specific biochemical and mechanical cues into the biomaterial. In addition, scaffolds also allow immediate cell attachment and provide support to the cells. Tissues can also be engineered without scaffolds. Scaffold-free tissue engineering is particularly useful when one wants to avoid scaffold degradation products and stress shielding cells. With scaffold-free methods, degradation products and residual byproducts from fabrication and their associated toxicity to the cells do not need to be considered. Stress-shielding of cells via scaffolds is another consideration that is removed in scaffold-free approaches. While scaffolds retain the ability to directly alter cell behavior and support cells, for fibrocartilage tissue engineering, soluble and mechanical signals have both shown efficacy in directing cell performance in the absence of scaffolds.

A variety of scaffolding materials have been explored for tissue engineered fibrocartilages including alginate [119], polycaprolactone (PCL) [145], poly(glycolic acid) [116, 117, 119, 121-126, 131], decellularized matrix [154], polyamide [116], polytetrafluoroethylene (PTFE) [116], poly(glycerol sebacate) [129], type I collagen [115, 127], poly(lactic acid) (PLA) [117, 131, 140], and poly(lactic-co-glycolic acid) (PLGA) [118, 145]. Considerations for scaffold formulations include degradation rates and products, and fabrication methods and resulting residual byproducts. Also, a recently added consideration may be compatibility with 3D printing because the technology is conducive toward producing tissue engineered fibrocartilages that are anisotropic and regionally variant, characteristics important in the function of native fibrocartilages. For example, anisotropic collagen alignment has been produced in 3D printed menisci [146]. Similarly, a regionally variant TMJ disc has been produced using 3D printing with

PCL and spatiotemporal delivery of PLGA microspheres with connective tissue growth factor (CTGF) and transforming growth factor, beta 3 (TGF-β3) encapsulated [145]. The wide range of scaffolds available for knee meniscus and TMJ disc tissue engineering has been reviewed elsewhere [34, 75, 155].

Self-organization and the self-assembling process are techniques that generate 3D structures in a scaffold-free manner, but they are distinctly different. Self-organization is defined as any technique that produces biomimetic tissues with use of external forces or energy whereas the self-assembling process is defined as a spontaneous organization of cells that mimics native tissue structures without external forces or energy. Self-assembly occurs via the minimization of free energy through cell-cell interactions. Examples of self-organization includes cell sheet engineering and bioprinting of cells. Self-assembly is used across multiple tissue types, including fibrocartilage. Self-assembly addresses considerations of scaffold-based methods by the creation of robust tissue engineered fibrocartilages that can immediately bear load and do not shield the cells from various stresses present in the joint environment [156].

Biochemical stimuli

Biochemical stimuli are used to target cells and ECM molecules to improve mechanical properties. This can occur, for example, via increased production of ECM, improved collagen fiber alignment, or increased collagen crosslinking. For the production of scaffold-free, tissue engineered fibrocartilage, prior studies have applied a variety of growth factors including TGF-β1, small molecules such as ascorbic acid and phospholipid lysophosphatidic acid (LPA), and matrix modifying enzymes chondroitinase ABC (C-ABC) and lysyl oxidase-like 2 (LOXL2) separately and in combination.

Growth factors have been extensively studied for tissue engineered fibrocartilages. TGF-β1 [83, 105, 137, 139], TGF-β3 [117, 118, 145], CTGF [145], PDGF [22, 120, 134], bFGF [120, 121, 124, 134], insulin-like growth factor 1 (IGF-1) [22, 117, 120, 121, 124, 132, 157], and

epidermal growth factor (EGF) [22, 134] are examples of growth factors that have shown various levels of efficacy in enhancing tissue engineered fibrocartilage formation. For example, TGF-β1 has been shown by microarray analysis to promote AC synthesis of ECM [158] and has shown similar effects in fibrocartilage studies [83, 105, 137, 139]. Small molecules such as LPA and ascorbic acid have been studied as well. LPA increased values of tensile Young's modulus from 247 ± 89 kPa in control groups to 503 ± 159 kPa in stimulated groups, along with collagen fiber density and organization in meniscal tissue engineered fibrocartilage [92]. Ascorbic acid is a vital component to cell culture media and was found to be optimal at 25 μg/mL for cell concentration, collagen deposition, and aggregate modulus values in a TMJ disc model [125]. Enzymes such as the GAG-depleting enzyme C-ABC and the collagen crosslinking enzyme LOXL2 have been previously shown to have a positive effect on mechanical properties. Specifically in articular cartilage, C-ABC has been shown to increase tensile properties exhibiting an increase of 121% and 80% compared to untreated controls in UTS and Young's modulus, and allow for more type II collagen deposition as a result of GAG depletion [159]. For the native knee meniscus, LOXL2 has been shown to increase tensile properties approximately 1.9-fold during explant culture [160]. More thorough and extensive reviews of various biochemical stimuli and their effects on tissue engineered fibrocartilage are available in the literature [34, 161, 162].

Various growth factors and enzymes have also been used in combinations to create synergistic effects between increased ECM and more mature ECM. For example, increases in radial tensile moduli by 5-fold over untreated controls of meniscal tissue engineered fibrocartilage were observed over untreated controls when a combination of TGF-β1 and C-ABC was applied [105]. A TGF-β1 and C-ABC combination can be used to tissue engineer other fibrocartilages as well because it has been observed to increase both tensile Young's modulus and UTS over unstimulated controls, reaching the lower range of native values [139]. Combining TGF-β1, C-ABC, and LOXL2 treatments during the culture of tissue engineered fibrocartilage

led to further significant improvement of tensile Young's modulus and UTS by 245% and 186%, respectively [83]. This combination has also been used to enhance mechanical properties and integration of TMJ disc tissue engineered fibrocartilages, resulting in values of tensile Young's modulus of over 6 MPa and compressive instantaneous modulus of over 1200 kPa after 8 weeks in culture [130]. The biochemical stimuli that have been used and their varying efficacy might warrant additional research into novel, synergistic combinations of stimuli.

Mechanical stimuli

Mechanical forces exerted naturally on native fibrocartilage are critical in tissue development and homeostasis. Native fibrocartilages experience tension, compression, hydrostatic pressure, and shear, and each of these forces has been applied to tissue engineered fibrocartilage as well. Prior tissue engineering studies involving mechanical loading either alone or combined with biochemical stimuli have resulted in significant increases of mechanical properties and also anisotropy.

Tension and compression are two commonly applied mechanical stimuli for tissue engineered fibrocartilage. While typically applied as separate stimuli, in fibrocartilage they often work together. For example, in the meniscus when a compressive load is applied, tensile strains develop due to the meniscus' wedge shape [34]. Meniscal tissue engineered fibrocartilage comprised of a nanofibrous matrix seeded with MSCs was subjected to dynamic tensile loading, leading to an increase in tensile modulus by 16% [138]. Independently of tension, passive axial compression of 0.1 N in a TMJ disc model has been shown to increase collagen and GAG content significantly as well as increase relaxation and tensile Young's modulus by 96% and 255%, respectively, over controls [143]. Combining TGF-β1 and C-ABC treatments with direct tension-compression loading during culture significantly increased instantaneous modulus (3-fold), relaxation modulus (2-fold), and tensile Young's modulus in the radial (6-fold) and circumferential (4-fold) directions of self-assembled meniscal fibrocartilage. The direct

compression-tension bioreactor for menisci was fabricated such that the platens matched the curved surface and elliptical shape of the meniscal tissue engineered fibrocartilage, ensuring simultaneous compression and tension stimulation [81].

Although less often examined, hydrostatic pressure and shear also have been used to tissue engineer fibrocartilage. When subjected to a hydrostatic pressure loading regimen, PLA scaffolds seeded with MCs exhibited increases in ECM production exhibiting 3-fold higher GAG deposition and 4-fold higher collagen deposition [137]. In a study on TMJ disc cells on PLA scaffolds, hydrostatic pressure was applied at 10 MPa either intermittently at 1 Hz or continuously for 4 hours a day. Type I collagen was highest in the continuous stimulation group compared to the non-loaded and intermittent stimulation groups [126]. Fluid shear, while typically regarded as being a detrimental mechanical stimulus for the maintenance of a chondrocyte-like phenotype, may merit exploration for tissue engineered fibrocartilages. Exposing MCs to oscillatory fluid flow in parallel plate flow chambers has been shown to upregulate calcium signaling and GAG production [135]. Use of a rotating bioreactor in TMJ disc cell culture led to earlier and greater contraction compared to the control. This resulted in a denser ECM and cell composition; however, total ECM content and compressive stiffness were not significantly different [123]. Overall, there is currently not enough evidence to conclude whether fluid-induced shear is beneficial for tissue engineered fibrocartilages.

Using mechanical stimuli on tissue engineered fibrocartilages is an effective way to increase ECM production and organization, which subsequently results in more robust mechanical properties. This in conjunction with a biochemical stimulus regimen may also lead to synergistic effects, further enhancing tissue engineered fibrocartilage functionality. While there are limited studies using mechanical stimuli on tissue engineered fibrocartilage, many of the stimuli discussed here have been extensively studied for hyaline articular neocartilage in other reviews [163]. Further examination of mechanical stimulus regimens for tissue engineered

fibrocartilage is warranted because specific application times and load amounts can have either beneficial or detrimental effects.

Toward tissue engineering the fibrocartilage spectrum

Due to the spectrum of fibrocartilage structures in the body, each tissue engineering strategy will be slightly different. The outlined studies here provide insight into current tissue engineering methodology for the knee meniscus and the TMJ disc, but the approach to the pubic symphysis or annulus fibrosus of the intervertebral disc might require different methods. However, the concepts discussed in the prior sections can be used generally to approach tissue engineered fibrocartilages in a uniform manner. One way to tailor the tissue engineering approach used is application of multiple types of stimuli, varying the cell source, or using a different scaffolding or scaffold-free approach. Taking these considerations into account is critical when designing and carrying out tissue engineering studies. By properly considering these factors, a translational approach can be created and quickly shifted from basic research to preclinical animal models. This can eventually result in transition to clinical trials and a tangible product that can be put through the FDA paradigm (Figure 1-4).

Evaluation of tissue engineered fibrocartilage

Histomorphological, biochemical, and mechanical testing of tissue engineered fibrocartilage yields properties that can be compared with those of native tissue to determine whether the tissue engineering design criteria have been met. All evaluation methods outlined in the prior section can be applied to tissue engineered fibrocartilage (Figure 1-3). The quantitative values derived from these assays can be statistically compared to each other to determine whether one tissue engineering modality is more efficacious than another. Quantitative values can also be normalized to native tissue values in the form of a functionality index (FI), Eq. (1). The FI accounts for biochemical and mechanical properties found in native tissue and normalizes

tissue engineered values to those of native tissue. The FI provides a quantitative value that reflects the overall quality of tissue engineered constructs that can be compared to each other. For example, the TMJ disc FI accounts for GAG, total collagen, instantaneous modulus values, relaxation modulus values, tensile Young's modulus values, and UTS values. The FI in Equation 1 weighs each of the metrics equally [23, 164]. The FI varies between 0% and 100%, where 100% is the value of native fibrocartilage.

$$FI(TE|N) = \frac{1}{6}\left[\begin{array}{l}\left(1-\left|\frac{GAG_N - GAG_{TE}}{GAG_N}\right|\right)+\left(1-\left|\frac{Col_N - Col_{TE}}{Col_N}\right|\right)+\left(1-\left|\frac{E_N^{20i}-E_{TE}^{20i}}{E_{MC}^{r}}\right|\right)\\ +\left(1-\left|\frac{E_N^{20r}-E_{TE}^{20r}}{E_N^{r}}\right|\right)+\left(1-\left|\frac{E_N^{T}-E_{TE}^{T}}{E_N^{T}}\right|\right)+\left(1-\left|\frac{UTS_N - UTS_{TE}}{UTS_N}\right|\right)\end{array}\right] * 100\% \qquad (1)$$

Similarly, a knee meniscus FI might include similar components with the addition of radial tensile modulus to account for the tissue's anisotropy.

It is important to note that a perfect FI of 100% is not necessarily needed for proper functioning of tissue engineered fibrocartilage *in vivo*. For example, an FI of 42% was adequate for a TMJ disc thinning model in the Yucatan minipig, where the implanted disc exhibited mechanical robustness *in situ*, adaptively remodeled, and improved integration stiffness [23]. For specific models of fibrocartilage injury, appropriate FI values need to be established for the translation of tissue engineered fibrocartilages that researchers can aim for

It is important to note that the tissue engineering approach must meet established design criteria (Figure 1-3). As discussed, this can be measured by an index such as an FI, but other characteristics such as cell morphology and tissue anisotropy need to be evaluated qualitatively or using other measurements. If the tissue engineering approach does not meet design criteria in any of these categories, the process can be reiterated, and the approach can be modified to meet the target design criteria (Figure 1-3). Upon meeting design criteria for the tissue engineering phase, researchers still need to demonstrate safety and efficacy in preclinical animal models and approved by the FDA before a tissue engineered fibrocartilage can be marketed as a therapy.

Toward Translation of Tissue Engineering

Tissue engineered fibrocartilage safety and efficacy must first be reviewed and cleared by the FDA before it can be marketed for clinical use. After tissue engineering studies, tissue engineered fibrocartilages should be demonstrated as safe and effective in animal models before examining the products' effects in humans. This section will present the FDA paradigm (Figure 1-4), diving into preclinical animal models and clinical trials, and discussing considerations for both. Because there is lack of approved tissue engineered fibrocartilage products existing for repair or replacement, this section uses existing articular cartilage guidance as a way to infer how tissue engineered fibrocartilage products might be regulated. This section closes with a discussion on areas where additional guidance from the FDA is desired, for example, through the creation of a fibrocartilage guidance document analogous to that which exists for articular cartilage.

The FDA paradigm

Tissue engineered fibrocartilage products will be regulated as HCT/Ps, a category of products containing or consisting of human cells or tissues intended for implantation, transplantation, infusion, or transfer into humans [36]. Much like tissue engineered products for hyaline articular cartilage [37], tissue engineered fibrocartilage products will be regulated through two centers of the FDA: the Center for Biologics Evaluation and Research (CBER) and/or the Center for Devices and Radiological Health (CDRH). CBER and CDRH co-authored the FDA guidance document for products intended to repair or replace hyaline articular cartilage [37], and this document can give insight into how tissue engineered fibrocartilage products might be regulated given similarities between the two tissue types.

If an HCT/P is minimally manipulated, intended for homologous use, and uncombined with another object, then it is only subject to regulation under Section 361 of the Public Health Service (PHS) Act and Title 21 of the Code of Federal Regulations Section 1271.3(d)(1). These

HCT/Ps are referred to as 361 products and do not require premarket approval. Examples of 361 products include bone (including demineralized bone), ligaments, tendons, and cartilage, which may have been sourced from cadaveric tissues. In terms of specific fibrocartilage products, cadaveric fibrocartilaginous tissue to be used as an allograft such as the knee meniscus and TMJ disc would fall under the category of 361 products. Otherwise, HCT/Ps are regulated as drugs, and/or biological products under Section 351 of the PHS Act and/or the Federal Food, Drug, and Cosmetic (FD&C) Act and are referred to as 351 products. Examples as provided by the FDA include cultured cartilage cells, cultured nerve cells, and gene therapy products. For fibrocartilage, expanded TMJ disc cells or MCs might fall under this category as well as tissue engineered fibrocartilage cultured using the self-assembling process.

Under the CDRH, products are regulated as devices under the FD&C Act. Human collagen and preserved umbilical cord vein grafts are in this classification. Biomaterial scaffolds without combination of cells for fibrocartilage repair or replacement may fall into this category. In addition, certain HCT/Ps can be classified as combination products by the Office of Combination Products and assigned to CBER or CDRH for primary jurisdiction. One example is cultured cells on synthetic membranes or combined with collagen. This product has potential to be regulated as a device or biological product, but is currently under review and may be regulated by CBER under device or 351 product regulations [36]. Tissue engineered fibrocartilage with use of a scaffold and seeded chondrocytes may fit into this category. Due to the many ways and materials with which fibrocartilage can be engineered, the FDA's classification of tissue engineered fibrocartilage products can vary. Consultation with the FDA is recommended if there is confusion as to the categorization of a specific tissue engineered fibrocartilage product.

Following product classification, a sponsor seeking FDA approval may consult guidance documents and the regulation of other approved products to determine data that need to be collected and submitted to the FDA. Guidance documents specifically for tissue engineered fibrocartilage products have not been published, but a guidance document has been published

for products intended for repair or replacement of hyaline articular cartilage, which shares many similarities with fibrocartilage. In addition, autologous cultured chondrocytes on a porcine collagen membrane is an approved cellular and gene therapy product whose pathway to regulatory approval may offer insights for tissue engineered fibrocartilage products. The guidance document for articular cartilage products contains non-binding recommendations to the industry on preparation and submission of investigational device exemption (IDE) and/or an investigational new drug (IND) application. Recommendations for classification of products, preclinical data, biocompatibility testing, and clinical study protocols are described. For example, goats, sheep, and horses are listed as the most frequently used large animal models for testing biological response, durability, toxicology, dose response, lesion size and location, appropriate endpoints, and use of arthroscopic or MRI imaging evaluations for articular cartilage repair [37]. Fibrocartilage large animal models are similar to the ones employed for articular cartilage with the addition of the minipig, farm pig, and dog [24, 74, 76, 165]. For clinical trials, design, controls, study populations, endpoints, implantation procedures, and patient follow-up are all discussed as well [37]. Examples of measures that may be used to assess endpoints for articular cartilage products are the Knee Injury and Osteoarthritis Outcome Score (KOOS), IKDC Subjective Knee Evaluation Form-2000, and Western Ontario and McMaster Universities Osteoarthritis Index (WOMAC) [37]. For fibrocartilage within the knee such as the meniscus, these scoring systems might be adaptable while the TMJ disc fibrocartilage might need new indices created. This motivates the creation of a standardized scoring system for fibrocartilages throughout the body.

Guidance documents as well as meetings with the FDA help to provide clarity on the process by which a product receives FDA approval, and this process is briefly depicted in Figure 1-4. Tissue engineering studies yield a product candidate that is then tested in preclinical animal studies to generate data for submission of an IDE and/or IND application dependent on product classification. An IDE/IND is necessary for clinical trials. Clinical trials are conducted in phases, and considerations for clinical trials include defining and measuring endpoints, the surgical

procedures used, and patient follow-up. Upon completion, data from the trials are submitted via a premarket approval (PMA) and/or a biologics license application (BLA) to the FDA. These applications will be under review for a time-period known as the premarket application phase where the FDA reviews the data for safety and efficacy of the product. FDA approval allows the product to be marketed. Product safety and efficacy continues to be monitored in the post-marketing phase, sometimes referred to Phase IV clinical trials. For more information on the FDA paradigm and general translation of tissue engineering products, readers are directed to a recent review [166].

Preclinical animal models

Currently, there are limited approved fibrocartilage HCT/Ps or clinical trials. Putting this in context of Figure 1-4, the general state of fibrocartilage tissue engineering currently straddles the phases of tissue engineering studies (discussed in Section 4) and preclinical animal studies. Animal studies provide preclinical data that show how the product functions *in vivo*. Animal studies are used to assess biological responses, the durability of repair, toxicology, dose response, lesion size and location, appropriate endpoints mirroring those to be used in humans, and use of arthroscopic and/or MRI evaluations as has been previously outlined [37]. Aside from examining the host, testing modalities outlined in characterization section should also be applied to the tissue engineered fibrocartilage implant both before and after implantation. Data on how the implant's biochemical, mechanical, and cellular properties change or remain the same will inform the success of the tissue engineering process and implant performance *in vivo*. Similar to using the FI to optimize tissue engineering procedures, the FI can be for *in vivo* studies to determine, for example, implant properties that correlate with a durable repair response. It is worth noting that, unlike suggestions found in the hyaline articular cartilage product guidance document which only touches on compressive testing modalities [37], an appropriate FI for fibrocartilage should include both tensile and compressive properties due to the way

fibrocartilage functions. Correlation of the implant's FI to host response might further inform eventual release criteria for the manufacturing of tissue engineered fibrocartilage products. An index such as the FI for general fibrocartilage tissue engineering would be informative to the field and allow comparison of various tissue engineering strategies for different fibrocartilages.

Ideally, preclinical studies in animals would test a version of the product that is identical to that which will be used in clinical studies. Investigating a product that contains human cells in animal models could require immunosuppressive agents to avoid rejection upon implantation, and this can be difficult if not impossible to implement in certain animal models. Recently, a review on experimental immunosuppression and immunomodulation has been published and may help provide strategies by which these can be applied to xenogeneic or allogeneic animal models [167]. Alternatively, one can test an analogous cellular product in terms of cellular characteristics and biological activity, derived from the animal species used in studies in an allogeneic strategy.

Preclinical data can be obtained from a combination of small and large animal studies. Small animal models, such as rodent and leporine models, allow for larger, more economical studies. However, for fibrocartilage injuries, surgical procedures in small animals may become difficult due to small joints that provide little space for operating. Translational applications in humans for tissue engineered fibrocartilage are best modeled in large animals that replicate human biomechanics as much as possible. As noted above, goats, sheep, and horses are recommended for examining hyaline articular cartilage repair [37], but other species may suit fibrocartilage studies better. For example, menisci in pigs and sheep are most similar to humans' in terms of size and proportion [73], while ovine menisci are also similar to humans' in terms of composition and biomechanics [168]. For the TMJ disc, the Yucatan minipig has also been deemed a suitable comparative model to humans in terms of its structure-function relationships [24], and has seen success in a regeneration study by our group which used CCs to tissue engineer allogeneic TMJ disc fibrocartilage [23]. As such, the pig (including minipigs) and sheep

may prove useful as large animal models for fibrocartilage studies, especially in those regarding the knee meniscus and TMJ disc.

For each animal model, details such as the specific surgical procedure for implanting the fibrocartilage product, how that surgical procedure may translate to human studies, how the study models particular indications, and specialized recovery or post-operative care must all be considered. For example, in a recent study where a focal thinning defect model was used, there was careful consideration of the minipig's post-operative diet [23]. After TMJ surgery, a diet consisting of mainly soft foods or liquids as opposed to hard foods is more amenable to repair. Thus, even if an animal model displays anatomical and functional similarities to humans, it does not automatically mean that the model should be chosen if surgical, husbandry, or other aspects listed above cannot be adequately developed for the animal.

Clinical trials

After obtaining preclinical data and approval of an IDE and/or IND, clinical trials can commence. Phase I and II trials commonly contain small patient cohorts compared to Phase III trials. Phase I trials are meant to determine safety and dosage of the tissue engineered fibrocartilage product. Phase II trials determine product efficacy and possible side effects of fibrocartilage therapies. Phase III trials examine long-term safety and efficacy in larger patient cohorts.

While animal models may inform endpoints in humans, it is ultimately clinical trial data that will be used in final approval for market. Because explanting implanted tissue engineered fibrocartilages would impair function, it is oftentimes not possible to test human implant properties as done in preclinical animal models. Therefore, endpoints are often defined via subjective scales, such as pain and range of motion testing. Development of a standard fibrocartilage scoring system would be of great value to clinical trials of tissue engineered fibrocartilage products. Arthroscopic evaluation, histologic evaluation, serological assessments for inflammation, and imaging might also inform endpoints [37].

Considerations that ensure successful repair in animals should likewise be thought out in clinical trials. For example, surgical approaches such as technique and post-operative care must be standardized and inspected particularly in multi-center trials to minimize center-to-center variability. In addition, for the indication that a tissue engineered fibrocartilage product intends to treat, participants that undergo current gold standard treatment should also be enrolled to demonstrate the tissue engineered product's efficacy over standard of care. For example, for late-stage pathology of the TMJ disc such as perforation, either discectomy or total joint reconstruction is often indicated. These two clinical treatments will ultimately be two treatments that a tissue engineered TMJ disc may be compared to. Lastly, follow-up of treatment with tissue engineered fibrocartilage will be required in these patient populations. It is common for the FDA to require safety and efficacy data over a number of years to compare short-term results of the tissue engineered fibrocartilage to current clinical treatments. The FDA will also use these data to evaluate claims of the product. For successful execution of clinical trials, these considerations should be taken into account to gain FDA approval for commercialization.

Future directions

Tissue engineering approaches of fibrocartilage have improved markedly within the last decade, allowing for the fabrication of more mechanically robust tissue engineered fibrocartilages. However, as previously discussed, current clinical treatments that address indications such as meniscal tears and TMJ disc perforation require follow-up clinical procedures within a short time frame. In addition, there is a lack of tissue engineered fibrocartilage products on the market. This may be due, in part, to a dearth of clarity on how tissue engineered fibrocartilage products can be translated.

Outlined here is the FDA paradigm as seen through current documentation and resources with numerous specific considerations for preclinical animal models and clinical trials

of potential fibrocartilage products. The considerations discussed here are just an example of what must be taken into account when going through the FDA paradigm. Clarification of important considerations and guidelines must occur in order to allow translation of tissue engineered fibrocartilage products. As such, the field should gravitate toward studies that have translational implications and perhaps ask for the FDA to create a guidance document similar to the one that exists for articular cartilage products [37]. A guidance document would provide recommendations to researchers and streamline translational advances to tissue engineered fibrocartilage products used in the clinic.

There are a number of remaining questions and concerns surrounding the creation of such a guidance document. One concern is how such a document can be created when there are multiple types of fibrocartilaginous tissues in the body varying in function. As examined earlier, there are actually significant similarities between meniscus and TMJ disc pathologies and current clinical treatments that allow for similar tissue engineering approaches to be used for both. These tissues are just two fibrocartilage examples. Hence, discussion and exploration of other fibrocartilaginous tissues like the pubic symphysis and annulus fibrosus of the intervertebral disc is warranted. Along those same lines, critics might question the inclusion of numerous different pathologies, ranging from early- to late-stage, within one document. One option might be to focus in on pathologies that are associated with degeneration of the tissue where tissue engineering might be able to bolster the early- to mid-stage degeneration via repair or replace the tissue completely for late-stage pathologies. Finally, as discussed with the FDA paradigm, clinical endpoints must be measured. A major hurdle remaining is the development of standardized indices or measurement systems for fibrocartilage in general. Evaluating tissue engineered fibrocartilage by an FI was suggested for tissue engineering and preclinical studies but remains a question for measurement of clinical endpoints in phased human trials.

In summary, tissue engineering of fibrocartilage addresses the limitations of current clinical treatments. There has been limited translation of tissue engineered fibrocartilage

products from the bench to the bedside. Throughout the FDA paradigm, there are many considerations to be included in the guidance document as discussed earlier. However, there are still several hurdles and remaining questions before the creation of a fibrocartilage guidance document analogous to that which exists for articular cartilage can come to fruition.

Conclusion

This review has highlighted tissue engineering of fibrocartilage, using the knee meniscus and TMJ disc as primary examples. Anatomy, function, epidemiology, pathologies, and current clinical treatments were reviewed to elucidate the need for tissue engineered solutions that are both biochemically and mechanically reminiscent of native tissue. Prior to tissue engineering fibrocartilage, design criteria must be attained via characterization of native tissue in the species of interest. Design parameters such as cell sourcing, scaffold versus scaffold-free methods, as well as biochemical and mechanical stimuli alone or in combination were discussed to create a fibrocartilage spectrum. Evaluation of the resultant tissue engineered fibrocartilages was also examined for comparison to previously characterized properties of native tissue.

Navigation of the FDA paradigm was discussed to motivate the translation of studies from laboratory bench to bedside in the clinic. We have recommended collaboration and open communication with the FDA to create a fibrocartilage guidance document analogous to that which exists for articular cartilage. Regulation of tissue engineered fibrocartilage and considerations for preclinical animal models and clinical trials were highlighted to encourage standardization amongst the field. Ultimately, this review looks to the future of tissue engineered fibrocartilage products, which are the culmination of decades-long research efforts. While there remains much to be accomplished, the field is now closer than ever to alleviating prominent fibrocartilage conditions.

Chapter 2: Remaining Hurdles for Tissue-Engineering the Temporomandibular Joint Disc[2]

Abstract

The temporomandibular joint (TMJ) disc, a fibrocartilaginous structure between the mandible and temporal bone, is implicated in temporomandibular disorders (TMDs). TMDs symptomatically affect approximately 25% of the population, of which 70% have internal derangement of the disc. Treatments lack efficiency, motivating novel therapies, including tissue-engineering toward TMJ disc regeneration. Recent developments in scaffold-based or scaffold-free approaches, cell sources, and biochemical and mechanical stimulation result in constructs exhibiting native tissue mechanics. Safety and efficacy of tissue-engineered implants show promising results in orthotopic animal studies. However, many hurdles need to be overcome in tissue-engineering approaches, and clinical and regulatory pathways. Future studies present an opportunity for clinicians and researchers to work together toward safe and effective clinical trials.

Highlights

- Current treatments for TMJ disorders lack long-term efficacy and are palliative, motivating tissue-engineering for repair or replacement of the injured or ailing tissues in the TMJ, such as the disc.
- Scaffold-based or scaffold-free approaches, cell sources, biochemical stimuli, and mechanical stimuli are all elements of the tissue-engineering process that need to be considered to tailor TMJ disc construct properties.

[2] **Chapter published as:** Donahue, R.P., Hu, J.C., Athanasiou, K.A. Remaining hurdles for tissue-engineering the temporomandibular joint disc. *Trends in Molecular Medicine*, March 2019, 25(3): 241-256.

- Large animals can serve as models of human TMD; orthotopic implantation in large animal models is a necessary translational step.
- The first successful orthotopic study of the TMJ disc in a large animal model has primed the field for translation of tissue-engineered constructs; however, there are still numerous hurdles prior to human clinical trials.

Motivation for Tissue-Engineering of the Temporomandibular Joint Disc

The temporomandibular joint (TMJ) is a ginglymoarthrodial joint**,** central to speaking and chewing functions [12]. The TMJ contains a disc between a condyle and the glenoid fossa-articular eminence region [39] (Figure 2-1). The TMJ disc is biconcave and fibrocartilaginous in nature [39]. As the TMJ articulates, the TMJ disc may distribute the stresses that develop within the joint [169] (Figure 2-1). Trauma [170] and age-related degeneration [8] can cause abnormal loading in the TMJ, leading to temporomandibular disorders (TMDs). TMDs are characterized by orofacial pain and/or limitation in jaw movement [171-173], and symptoms are present in approximately 25% of the population [5]. Perplexingly, TMDs affect females up to 8.0-fold more than males [5, 174-176]. In addition, TMDs affect mostly younger patients between 20-50 years of age [54, 55, 174]. As the second most common musculoskeletal condition resulting in pain and disability, TMDs cost an estimated $4 billion per annum in the United States (https://www.nidcr.nih.gov/research/data-statistics/facial-pain).

A specific subset of TMDs involve discal pathologies such as internal derangement (ID), disc thinning, and disc perforation. *ID* affects about 70% of TMD patients [7]. Severe cases of ID present disc thinning and eventual disc perforation (Figure 2-2

Figure 2-2: Internal derangement of the TMJ disc.
(A) A healthy closed jaw position is shown. (B) The most common type of internal derangement is shown, where the disc is displaced anteriorly. Progression of the joint in this configuration often causes (C) disc thinning and (D) eventual disc perforation.

) in approximately 5-15% of ID patients [8-10]. However, ID and disc perforation can occur independently; the independent cases of disc perforation can be due to age-related wear

[8]. These discal pathologies are the most prevalent manifestation of TMDs [7]. Osteoarthritis (OA) is also commonly seen in conjunction with ID [9, 57], but the relationship between ID and OA is not understood; it is not known whether one precedes the other or if both share common causative events [57]. However, it is thought that TMJ disc pathologies such as ID or disc perforation are the first steps in a series of degenerative changes (i.e., OA) seen throughout the adjacent articulating, soft tissue surfaces [177].

Management of disc-related TMDs varies with disease severity [178]. Non- and minimally-invasive strategies include physical therapy [179], occlusal splints or adjustments [180], pharmacologic agents [181], sodium hyaluronate and corticosteroid injections [182], arthrocentesis [183], and arthroscopy [9]. However, these treatments are only palliative. Only 5% of TMDs are candidates for surgical intervention [13]; surgeries for TMDs include discectomy with or without disc replacement [69] and partial or full joint reconstruction with autologous [184] or alloplastic materials [185]. Discectomy has shown promise for symptom reduction but has shown degenerative remodeling of the joint as a result [186, 187]. Costochondral rib grafts are used to reconstruct the mandibular condyle [184], but no autologous grafts exist for the complete joint [54]. Alloplastic total joint prostheses have been indicated for severe ankylosis, failure of autologous grafts, failure of Proplast-Teflon implants, or severe OA [188]. Most TMD patients range between 20-50 years of age [54, 55, 174], but the typical lifetime of alloplastic total joint prostheses is 10-15 years [189], making revisions likely within a patient's lifetime [54]. The use of alloplastic total joint prostheses is reserved as an option of last resort for a small subset of patients, creating a gap in terms of treatment options between non-invasive or minimally invasive strategies and end-stage surgical techniques.

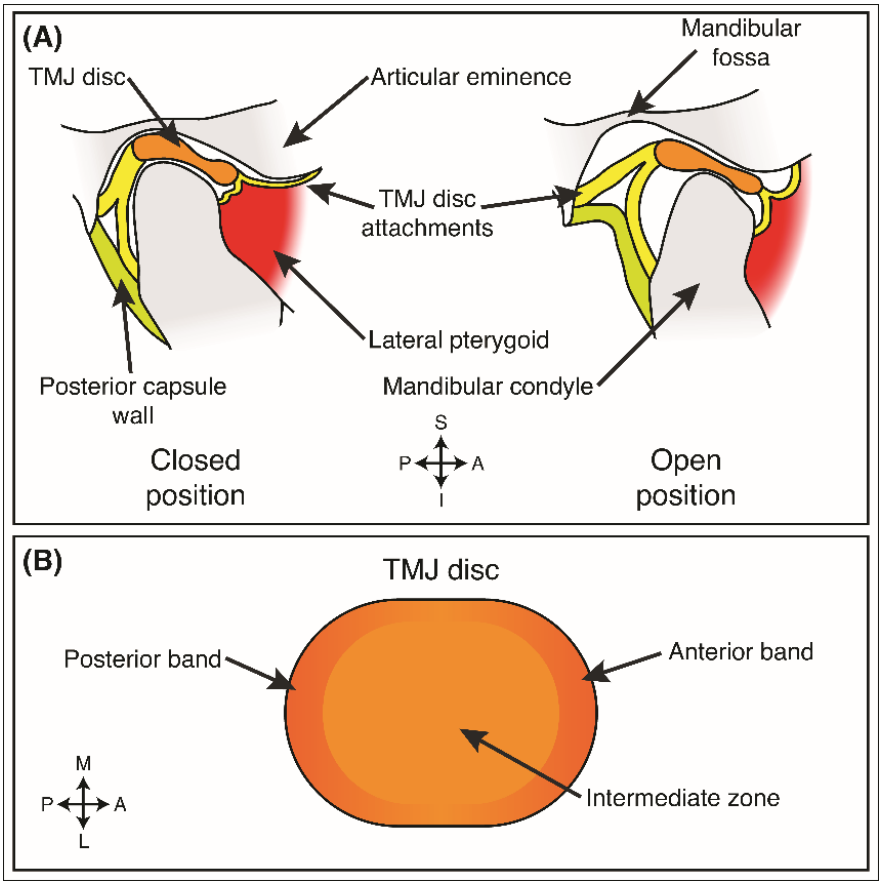

Figure 2-1: TMJ disc anatomy.
(A) Depending on the open or closed position of the joint, the TMJ disc is situated between the mandibular condyle and the articular eminence-mandibular fossa region. In this sagittal view, the disc is held in place by disc attachments, present at all angles (e.g., lateral, medial, posterior, anterior), surrounding the disc. The joint is separated into two joint capsules delineated by the TMJ disc. (B) The disc is regionally composed of two bands in the anterior and posterior portions of the disc. The middle portion of the disc is referred to as the intermediate zone. S – superior, I – inferior, A – anterior, P – posterior, M – medial, L – lateral.

The treatments described above do not provide mid-stage intervention for patients. To fill this gap, novel treatment strategies to improve patient outcomes must be developed. Tissue-engineering aims to regenerate the pathological tissues in TMD with biological neotissues to restore long-term function. Here, we focus on TMJ disc pathologies due to their overarching prevalence in TMDs [7]. In particular, we discuss recent tissue-engineering efforts (Table 2-1) and remaining hurdles for TMJ disc tissue-engineering.

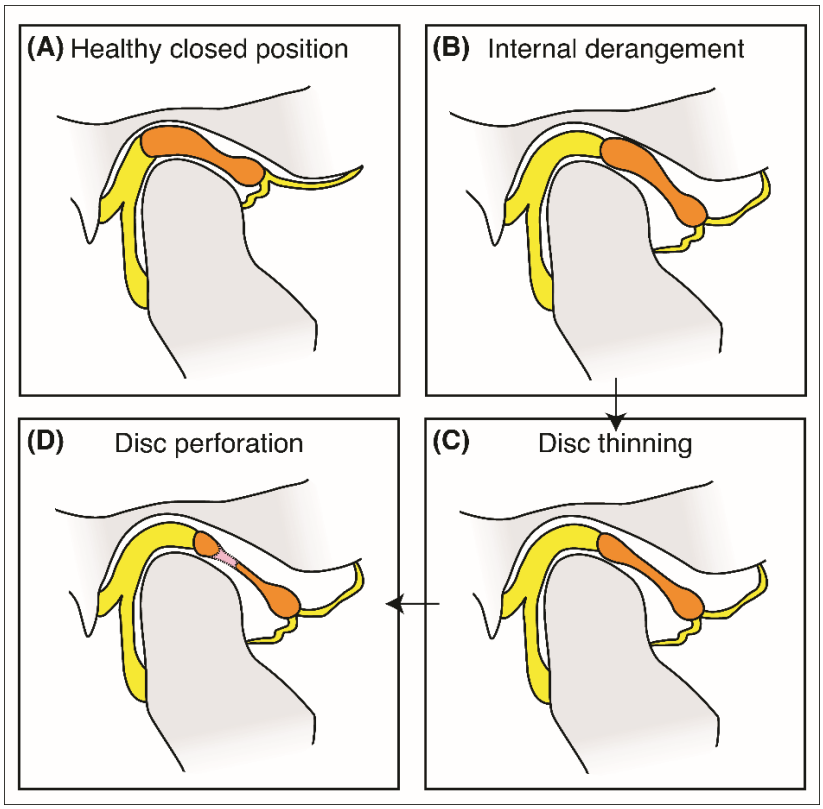

Figure 2-2: Internal derangement of the TMJ disc.
(A) A healthy closed jaw position is shown. (B) The most common type of internal derangement is shown, where the disc is displaced anteriorly. Progression of the joint in this configuration often causes (C) disc thinning and (D) eventual disc perforation.

Recent Tissue-Engineering Efforts

Tissue-engineering employs scaffolds, cells, and various signals such as biochemical and mechanical stimuli (Figure 2-3). As discussed in this section, advances in materials engineering have resulted in a variety of scaffolds [145, 190, 191], while scaffold-free approaches, such as the self-assembling process [17, 23, 133], have also emerged in TMJ disc tissue-engineering. In terms of cell sources, primary chondrocytes, mesenchymal stem cells (MSCs), and cell expansion technologies are also reviewed below (Table 2-1). Signals such as biochemical and mechanical stimuli for mechanical improvement of the TMJ disc (Table 2-1) are also discussed. This section also examines small animal models that have been used for examining the performance of these implants [23, 75, 76, 140, 191, 192].

Table 2-1: Recent tissue-engineering studies of the TMJ disc published since 2013.
Summary of the scaffold-based or scaffold-free approaches, cell sources, species, biochemical stimuli, mechanical stimuli, and implantation sites of the constructs are provided. * — It is unclear what biochemical stimuli are in the chondrogenic medium used in the study by Bousnaki, *et al.* because it is a proprietary formulation.

Author, Year	Ref.	Scaffold-based or Scaffold-free Approach	Cell Sources	Species of Cell Sources	Biochemical Stimuli	Mechanical Stimuli	Animal Model Tested (Implantation Site)
Vapniarsky, *et al*. (2018)	[23]	Self-assembling process	CCs expanded to passage 3	Yucatan Minipig	TGF-β1, C-ABC, LOXL2	Passive axial compression	Yucatan Minipig (Orthotopic)
Matuska, *et al.* (2018)	[193]	Decellularized TMJ discs	Wharton's jelly-derived MSCs	Human	None	None	None
Bousnaki, *et al*. (2018)	[194]	Chitosan and alginate scaffolds	Dental pulp stem cells or human nucleus pulposus cells	Human	Unidentified*	None	None
Wang, *et al*. (2018)	[147]	Coculture cell sheet seeded on PLGA electrospun scaffolds	TMJ disc cells and synovium-derived MSCs	Rabbit	TGF-β3	None	None
Ronald & Mills (2016)	[190]	Titanium dioxide nanofilms	TMJ disc cells	Cow	None	None	None
Tarafder, *et al*. (2016)	[191]	Polycaprolactone scaffolding with PLGA microspheres	Bone marrow-derived and synovium derived MSCs	Human/Rabbit	CTGF, TGF-β3	None	Rabbit (Orthotopic)
Legemate, *et al*. (2016)	[145]	PCL scaffolding with PLGA microspheres	Bone marrow-derived MSCs	Human	CTGF, TGF-β3	None	None
Juran, *et al*. (2015)	[195]	Decellularized TMJ discs with laser micropatterning	Wharton's jelly-derived MSCs	Pig	Epidermal growth factor, platelet-derived growth factor BB	None	None
Wu, *et al*. (2014)	[192]	Fibrin gel and chitosan scaffold	Synovium derived-MSCs	Rat	TGF-β3	None	Nude Mice (Subcutaneous)
MacBarb, *et al*. (2013)	[133]	Self-assembling process	ACs and MCs	Cow	TGF-β1, C-ABC	Passive axial compression	None
Ahtiainen, *et al*. (2013)	[140]	Poly(lactic acid) scaffold	Subcutaneous adipose-derived MSCs	Rabbit	TGF-β1	None	Rabbit (Orthotopic)

Novel scaffold-based and scaffold-free approaches

The primary purpose of scaffolds is to provide a template for cells to form tissues. Scaffolds can be functionalized with biomolecules to direct cell behavior and manufactured with mechanical properties similar to the tissues they are intended to replace. Ideally, scaffold degradation rates would match the rate of tissue formation. Scaffolds recently used in tissue-engineering the TMJ disc include natural materials and synthetic materials (Table 2-1). Two particularly interesting developments include novel scaffold fabrication methods and the emergence of scaffold-free approaches.

New fabrication methods allow for surface modifications of scaffolding materials. Layer-by-layer nanoassembly is one such fabrication method [190, 196] Titanium dioxide nanofilms are used to modify surfaces of scaffolds for tissue-engineering of bone [196] as well as cartilage [190]. These nanofilms are created by layer-by-layer nanoassembly, based on the principle of electrostatic charge, to coat various surfaces allowing for increased cell attachment, control of cell phenotype, and control of differentiation. In a study using titanium dioxide surface modification with seeded TMJ disc cells, cell proliferation and extracellular matrix (ECM) deposition increased with increasing thickness of nanofilms [190]. The matrix was reminiscent of a fibrous ECM, in contrast to a cartilaginous ECM. Type I collagen and decorin, approximately 0.34mg/mL and 0.31mg/mL, were present in higher amounts than type II collagen and aggrecan, approximately 0.14mg/mL and 0.28mg/mL, after 14 days of culture on 20 layers of titanium dioxide nanofilms [190]. Additional work needs to be performed to couple layer-by-layer nanoassembly with typical scaffold materials such as polycaprolactone (PCL) or polylactic acid (PLA).

Three-dimensional (3D) printing is a fabrication technique that achieves microprecise placement of scaffolding materials and functional biomolecules. 3D printing can create regional variation in scaffolds reminiscent of the native TMJ disc. For example, a dual-nozzle setup in a PCL-poly(lactic-co-glycolic acid) (PLGA) microsphere system allowed spatiotemporal delivery of

transforming growth factor beta 3 (TGF-β3) and connective tissue growth factor (CTGF) [145, 191]. The 100mg dosages of growth factor-embedded microspheres resulted in increased intermediate zone type II collagen and aggrecan deposition by approximately 2-fold compared to the 50mg dosage when analyzing immunofluorescence images of constructs seeded with bone marrow-derived MSCs [145]. However, growth factor-embedded microsphere application decreased compressive modulus in both dosages by at least 2-fold when compared to empty microspheres in both areas analyzed [145]. Similar trends were apparent in instantaneous and relaxation moduli indicating that mechanical properties did not necessarily trend with growth factor application and ECM content [145]. Compared to traditional scaffold-based approaches, 3D printing offers the ability to create regional variation which can resemble native ECM content.

Scaffold-free approaches, such as the self-assembling process [17, 23, 133], have been developed to bypass issues related [156] to scaffold degradation products, e.g., acidity due to PLA degradation [197], fabrication byproducts, e.g., crosslinkers and plasticizers [197], and stress-shielding of cells [198]. The self-assembling process recapitulates developmental aspects of cartilage formation to generate functional neotissues with characteristics resembling those of native tissues [156, 199]. Specifically, it is the most prominent of these techniques for TMJ disc tissue-engineering because it has generated mechanically robust tissue [17]. Stimulation of self-assembled TMJ disc constructs by bioactive agents and mechanical compression resulted in values of approximately 3.5%, 2.75 MPa, and 2.25 MPa for collagen per wet weight, tensile Young's modulus, and ultimate tensile strength (UTS), respectively. Additional analysis of constructs created from cocultures of hyaline articular chondrocytes (ACs) and knee meniscus cells (MCs) found collagen fibril alignment reminiscent of native TMJ discs, exhibiting direction-dependent strains in finite element analysis. This was promising because it showed anisotropic tissue on par with the alignment of native tissue [133], which further substantiates scaffold-free tissue-engineering as an alternative to scaffold-based approaches.

While scaffold-free approaches do not necessarily have the flexibility of scaffold-based approaches, e.g., scaffold functionalization with biomolecules, these limitations can be overcome with exogenous stimulation, which can have various effects on scaffold-free constructs such as increased mechanical properties [163, 200]. In addition, variation of the cell source can also have a large influence on the eventual properties of the resulting constructs.

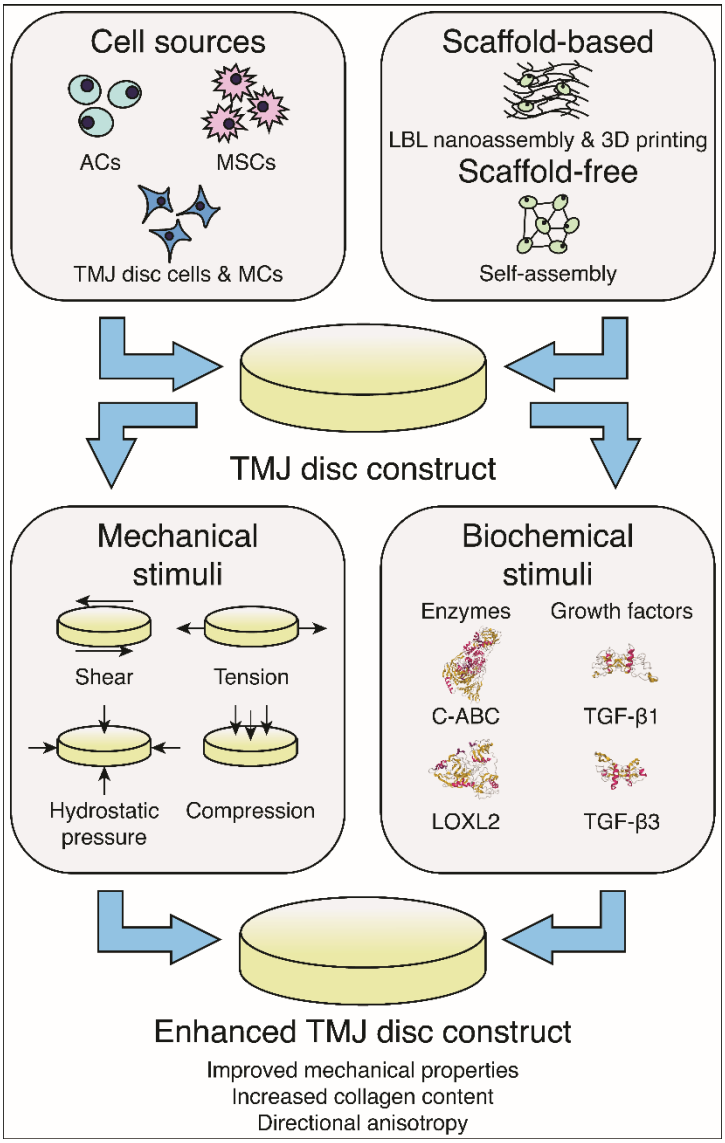

Figure 2-3: Tissue-engineering paradigm of TMJ disc constructs.
Combination of an appropriate cell source and scaffold-based or scaffold-free approaches can be used for fabrication of a TMJ disc construct (upper panels). Via the application of various biochemical and mechanical stimuli, an enhanced, biomimetic construct can be tissue-engineered (lower panels). ACs – hyaline articular chondrocytes, MSCs – mesenchymal stem cells, MCs – knee meniscus cells, LBL – layer-by-layer, 3D – three-dimensional, C-ABC – chondroitinase ABC, LOXL2 – lysyl oxidase-like 2, TGF-β – transforming growth factor beta.

Cell sources

Selection of a cell source is one of the most important considerations for TMJ disc tissue-engineering (Table 2-1). Options for primary cells range from native TMJ disc cells [118, 190] to other cells from hyaline articular cartilage and the knee meniscus [133]. In addition, recent advances in cell expansion technologies [144, 149, 150] have allowed exploration of costal cartilage-derived cells [23]. MSCs are also heavily used [118, 140, 145, 191-195].

Potential primary cell sources for TMJ disc tissue-engineering include TMJ disc cells, ACs, MCs, and costal chondrocytes (CCs). TMJ disc cells have been used in multiple studies [118, 190], but the dearth of available, healthy tissue raises concerns for this source [20]. Thus, ACs and MCs have been considered [133]. Using AC-MC coculture with the self-assembling process resulted in a functional, anisotropic TMJ disc as discussed above [133]. With recent advances in cell expansion technologies that preserve chondrogenic phenotype [144, 149, 150], CCs might allow for either an autologous or allogeneic approach to replacing cartilages, as demonstrated previously in articular cartilage [19, 201] and the TMJ disc [23]. Allogeneic CCs can be harvested from cadaveric tissue, while autologous tissue harvest procedures are conducted routinely for rhinoplasty and autologous TMJ reconstruction. Thus, existing surgical procedures may be sufficient for tissue regeneration purposes. The use of CCs can also remove or reduce donor site morbidity and virtually eliminate the potential of harvesting cells from OA tissue. When used in a hyaline articular cartilage model, CC constructs have attained a functionality index (FI, described below) of 55% compared to the medial condyle cartilage properties [19]. These techniques and results offer promise of an alternative source of chondrocytes that can create mechanically stable constructs for other parts of the body such as the TMJ disc.

The functionality index compares constructs properties to native tissue values. Values for biochemical content, such as overall collagen (Col) and glycosaminoglycan (GAG) content, accompany values for various mechanical properties such as ultimate tensile strength (UTS), Young's modulus (E^T), compressive relaxation modulus (E^r), and compressive instantaneous modulus (E^i). Ranging from 0% to 100%, a value of 100% represents perfect recapitulation of native values. Subscripts serve to designate native (N) or tissue-engineered (TE) values.

$$\mathrm{FI(TE|N)} = \frac{1}{6}\left[\begin{array}{l}\left(1-\left|\frac{\mathrm{GAG_N}-\mathrm{GAG_{TE}}}{\mathrm{GAG_N}}\right|\right)+\left(1-\left|\frac{\mathrm{Col_N}-\mathrm{Col_{TE}}}{\mathrm{Col_N}}\right|\right)+\left(1-\left|\frac{\mathrm{E_N^i}-\mathrm{E_{TE}^i}}{\mathrm{E_N^i}}\right|\right) \\ +\left(1-\left|\frac{\mathrm{E_N^r}-\mathrm{E_{TE}^r}}{\mathrm{E_N^r}}\right|\right)+\left(1-\left|\frac{\mathrm{E_N^T}-\mathrm{E_{TE}^T}}{\mathrm{E_N^T}}\right|\right)+\left(1-\left|\frac{\mathrm{UTS_N}-\mathrm{UTS_{TE}}}{\mathrm{UTS_N}}\right|\right)\end{array}\right]*100\%$$

An array of MSCs from both adult and fetal tissues have been used, as previously reviewed [202]. MSCs from various tissues (Table 2-1) offer an autologous or allogeneic approach and can be isolated in large quantities, making these sources clinically relevant for construct formation. Perhaps the most interesting MSCs are those derived from the synovium because they were shown to synthesize cartilage oligomeric matrix protein, link protein, and glycosaminoglycans (GAGs), similar to ACs [203]. For example, synovium-derived MSCs on fibrin-chitosan scaffolds increased type I collagen expression approximately 2-fold *in vitro* and ECM deposition *in vivo* as evidenced by histological analysis when compared to pure chitosan scaffolds [192]. Progress using MSCs has resulted in morphological and biochemical biomimicry evaluated via histology, gene expression, and other biochemical assays [118, 140, 191, 192], but future research should next focus on assaying functional properties of MSC-derived constructs via mechanical testing.

The choice of cell source remains a challenge within the field of TMJ disc tissue-engineering. Lack of standardization of mechanical testing modalities makes it difficult to compare sources head-to-head and to determine if one cell source is more suitable than another. Perhaps the most important characteristic to consider when choosing a cell source is mechanical stability of the resulting tissue-engineered construct due to the dynamic joint environment.

Improvement of mechanical properties of TMJ disc fibrocartilage

The TMJ disc functions in a dynamic environment of compression, tension, and shear [204, 205]. Finite element analysis shows stresses in the TMJ disc during mouth opening to be greater than 7 MPa in compression, 4 MPa in tension, and 1 MPa in shear [32]. For comparison, the hip experiences approximately 7-10 MPa in compression and up to 18 MPa during stressful activities such as standing up [33, 206]. Characterization of the native tissue should aim to define the gold-standard, design criteria for tissue-engineered TMJ disc constructs; the expectation is that replicating the native tissue's mechanical properties would allow for restoration of mechanical function. Thus, to engineer constructs with physiological levels of mechanical stresses in mind, various biochemical and mechanical stimuli, and also changes in scaffold processing (Figure 2-3) have been developed. For scaffold-free approaches, self-assembled constructs have approached native values in mechanical properties due to synergistic effects of biochemical and mechanical stimulation [23, 133]

A majority of recent scaffold-based studies use only biochemical stimuli to improve construct mechanical properties (Table 2-1). Constructs stimulated with biochemical stimuli have been previously found to exhibit native tissue structure-function relationships. For example, insulin-like growth factor I and TGF-β applied to constructs created from TMJ disc cells increased collagen synthesis by greater than 400% at 3 weeks of culture, leading to higher aggregate moduli of 5 kPa [121]. However, constructs sometimes do not follow native tissue structure-function relationships [145] (e.g., increased matrix deposition leading to increased mechanical properties). To overcome such deficiencies, mechanical stimulation may be considered. However, mechanical stimulation has not been employed in scaffold-based TMJ disc approaches, though it has been used in other fibrocartilages such as the knee meniscus. For example, hydrostatic pressure combined with TGF-β1 led to 4-fold higher collagen deposition and 3-fold higher GAG deposition, as compared to the unpressurized growth factor controls in MC-seeded PLA scaffolds [137]. Studies showing recapitulation of native tissue

structure-function relationships should serve as models for future studies toward identifying additional stimuli. Biochemical stimuli must continue to be investigated, but, additionally, mechanical stimuli can be used to increase mechanical properties of engineered discs to withstand the dynamic *in vivo* environment.

Scaffold-free approaches have combined biochemical stimuli and mechanical stimuli to generate stiffer, stronger, anisotropic constructs, followed by examination of the resulting constructs in large animal models. Using a scaffold-free approach with AC-MC coculture, TGF-β1, chondroitinase ABC (C-ABC), and lysyl oxidase-like 2 (LOXL2) have been identified in the past as efficacious for fibrocartilage tissue-engineering, enhancing tensile Young's modulus and UTS by 245% and 186%, respectively [83]. In a self-assembled TMJ disc model using AC-MC coculture stimulated with only TGF-β1 and C-ABC, tensile Young's modulus, UTS, and collagen per wet weight increased by 2-fold or greater in the intermediate zone of the disc, as compared to controls [133]. Passive axial compression and these biochemical stimuli were combined and noted to exhibit synergism, showing 5.8-fold, 14.7-fold, and 13.8-fold increases in collagen per wet weight, tensile Young's modulus, and UTS, respectively, compared to unstimulated controls [133]. Moving to *in vivo* studies, TMJ discs engineered using all three stimuli (TGF-β1, C-ABC, and LOXL2) coupled with passive axial compression, yielded an FI of 42% of native properties with a passaged, allogeneic CC source [23]. By combining these three biochemical stimuli with mechanical stimulation, increased functional properties were achieved as compared to either alone. Thus, further synergistic effects of other biochemical and mechanical stimuli should be explored.

As reviewed elsewhere [163], strategies for other tissues, such as hyaline articular cartilage, can help inform further mechanical improvement of constructs. Similar designs and models can be used to engineer the fibrocartilage of the TMJ disc. For example, in a recent study on tension and its effects for articular cartilage engineering, continuous stimulation combined with a bioactive regimen increased the tensile properties by 5.8-fold over

unstimulated controls in AC-derived, self-assembled constructs [207]. By improving mechanical stability using biochemical and mechanical stimuli, constructs continue to approach native tissue values. Attaining mechanical biomimicry is a crucial characteristic for constructs to perform satisfactorily when implanted into the orthotopic environment.

Current animal models

Prior to human clinical trials, tissue-engineered implants are examined in relevant animal models to demonstrate initial safety and efficacy. Similar to TMJ disc tissue-engineering, development of animal models is based on design criteria. For the TMJ, similar anatomies, chewing patterns, and diets compared to humans, and ease of surgical access are included in the design criteria. In addition, relative size of TMJ structures and animal cost may also determine which model to use. Animal models exist for various purposes such as observing the adverse reactions to an implant subcutaneously to examining surgically induced pathologies in orthotopic studies. Small animals such as mice and rats are economical, serve as pain models [208, 209], and simulate OA and associated degenerative changes in the joint [210, 211]. However, their small TMJ disc size limits studies to simple subcutaneous implantation as opposed to orthotopic studies in larger animals such as rabbits [75]. Moving toward orthotopic studies, rabbits allow for additional biochemical and histological analysis, and reliable mechanical testing [76], but present substantial differences from human size and loading conditions [75]. This motivates the use of large animal models that more closely resemble human anatomies and conditions [76].

Many preliminary studies involve subcutaneous implantation to examine possible adverse reactions and establish proof-of-concept. These studies, as reviewed [75], are commonly performed in mice or rats due to their low cost, without much consideration of anatomical or dietary similarities. For example, a fibrin-chitosan scaffold with synovium-derived rat MSCs was embedded into explanted TMJ discs with perforation defects and implanted into

nude mice subcutaneously in a xenogeneic approach [192]. Histological analysis showed increased type I and II collagen deposition in the fibrin-chitosan scaffold, compared to the pure chitosan scaffold [192]. Although this study represents a disc perforation model, additional biochemical and mechanical analyses must be performed in larger animals to show reparative ability in the fully loaded orthotopic environment.

Recent studies employed the rabbit for orthotopic evaluation of tissue-engineered TMJ discs [140, 191]. For example, 3D printed PCL-PLGA microsphere scaffolds seeded with allogeneic, synovium-derived MSCs were implanted into the disc and noted histologically to degrade by 6 weeks [191]. Cells retained their chondrocyte-like phenotype *in vivo* [191]. Scoring of the condylar surfaces with an OA score resulted in values of approximately 3.9 and 2.4 for the scaffolds without and with growth factors, respectively, where a lower score represents a better outcome [191]. While these studies [140, 191] demonstrate feasibility for implantation of tissue-engineered TMJ discs via histological analysis, mechanical testing is of paramount importance to show the integrity of tissue-engineered constructs.

Strides in animal studies are promising to the research community as they point to a feasible translation pathway for tissue-engineered constructs. The use of ectopic small animal and larger orthotopic models (e.g., the mouse and rabbit models) is a crucial first step in proof-of-concept work for the field. However, it will ultimately be regenerative studies in orthotopic animal models in species such as the minipig that will be most impactful for translation of tissue-engineered TMJ discs toward human clinical studies.

The Path to Translation

Translational hurdles that remain (see Outstanding Questions) include tuning of construct mechanical properties toward biomimicry (Figure 2-3) as well as scale-up of area and thickness of implants (Figure 2-4). A recent minipig study, showing safe and efficacious implantation of TMJ constructs [23], establishes this orthotopic large animal model as a cogent element in the

translational pathway (Figure 2-4). Clinical and regulatory hurdles are also significant for translation of TMJ disc constructs (Figure 2-4).

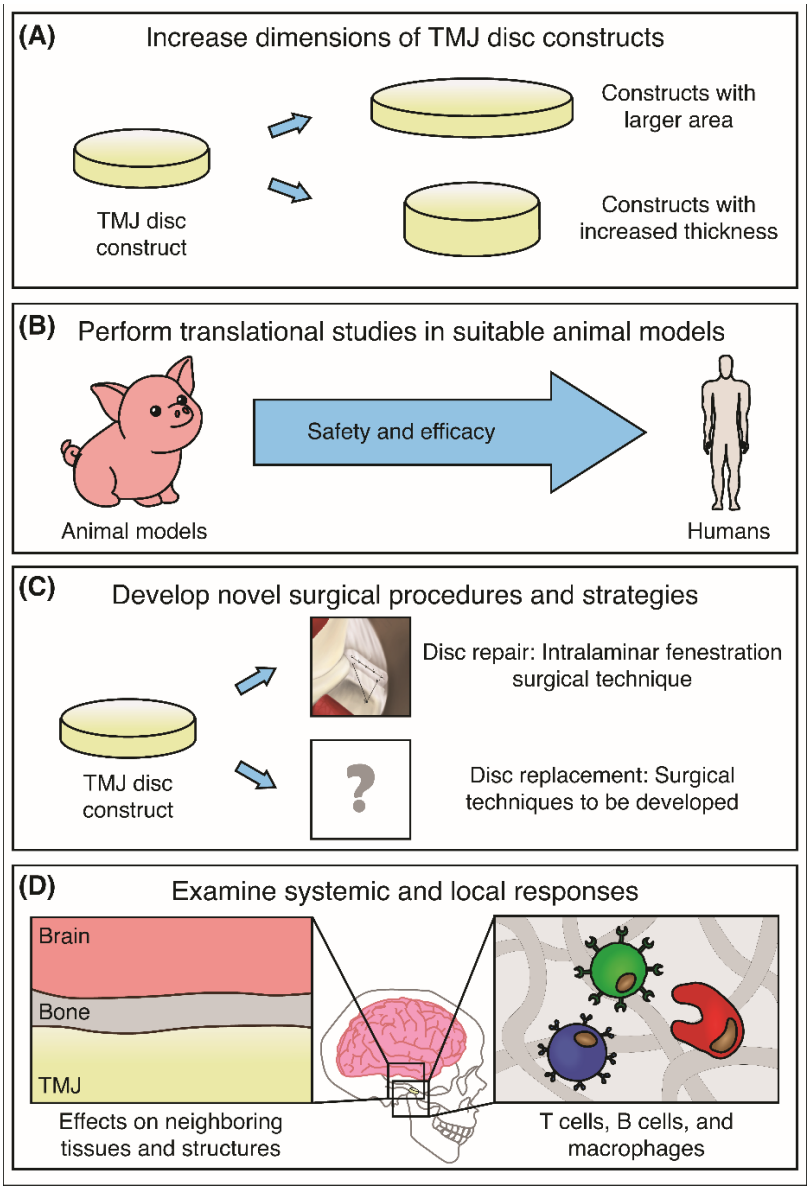

Figure 2-4: Toward the path to translation.
(A) Constructs should be tailored for human discal pathologies and size, potentially increasing in both area and thickness. (B) Prior to translation through regulatory bodies such as the FDA, animal studies must be performed in proper large animals, such as the minipig. (C) Novel surgical procedures for disc repair and disc replacement need to be developed as well. (D) Additional studies also need to be performed to examine local and systemic responses to tissue-engineered TMJ discs in the orthotopic environment. Upon overcoming these hurdles, the TMJ disc tissue-engineering field will be closer to human clinical trials.

Application of proper tissue-engineering parameters for tuning of TMJ disc constructs to the TMJ mechanical environment

Constructs must be tuned to the mechanical environment of the TMJ disc because they will be subject to compressive, tensile, and shear forces [204, 205]. Theoretically, the required mechanical properties will depend on surgical technique, model, and animal. For example, it was shown that an FI of 42% was shown to be sufficient when implanted via the intralaminar fenestration surgical technique (Figure 2-5) in a focal thinning model in the Yucatan minipig [23]. When moving toward perforation or larger defects, this implant might be insufficient. On the opposite end, some constructs might be too stiff or strong compared to native values, as observed in some scaffold-based approaches [145], causing stress concentrations and possible degeneration on the articulating surfaces. Also, a mismatch in the rates of scaffold degradation versus tissue formation can lead to failure. Therefore, it is important to consider tuning mechanical properties by application of proper stimulation regimens, whether using a scaffold-based or scaffold-free tissue-engineering approach (Figure 2-3).

Tailoring of tissue-engineered TMJ discs to human discal pathologies and size

As the translational direction points to additional large animal orthotopic studies before human clinical trials commence, defect models must increase in size. As such, constructs must also scale-up (Figure 2-4). In the recent minipig study [23], a one-sided 3mm defect, mimicking disc thinning, was used. Future studies need to scale-up to a larger defect area to mimic increased disc thinning, in addition to two-sided defects to mimic disc perforation. To scale-up constructs to larger thicknesses, one might consider using larger scaffolds. But as scaffolds and constructs trend upward in thickness, it should be kept in mind that diffusion limitations increase. Decreased diffusion can result in shell-like neotissues with necrotic centers, that display inadequate mechanics. However, scaffold-free approaches might prove advantageous for creation of larger constructs to mimic disc thinning. Self-assembled articular cartilage constructs

made of passaged ACs up to 25 mm dia. have been made by combining cytochalasin D, TGF-β1, C-ABC, and LOXL2, under a compressive load and in mechanical confinement [212]. This approach may allow for examining TMJ disc healing in larger defects that mimic clinically observed disc thinning. As such, a significant portion of future TMJ disc studies should investigate the scale-up of defects and constructs for relevance to human TMJ anatomy.

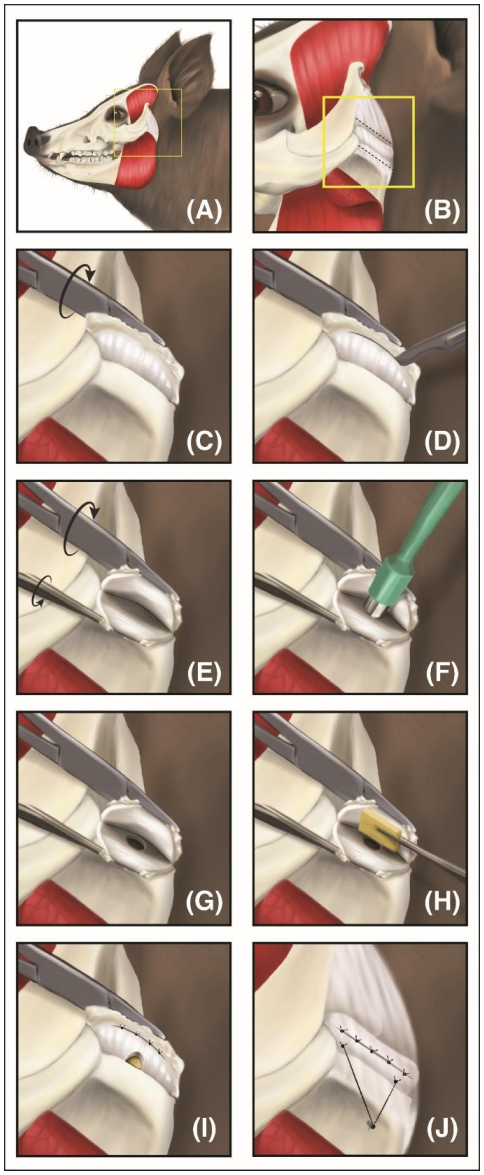

Figure 2-5: The intralaminar fenestration surgical technique.
(A-B) Through a preauricular incision, the TMJ was exposed. (C-E) Surgeons fileted the disc open with a scalpel, and (F-G) created a one-sided thinning defect via a biopsy punch. (H) A tissue-engineered disc was placed between the two laminae and (I) sutured back together. Sutures attached to the side of the disc instead of on the articulating surfaces allowed for continued loading of the TMJ disc while healing; this placement avoided possible stress concentrations and resulting degeneration. (J) The lateral attachment is recreated by use of an anchoring system. From Vapniarsky, *et al*., 2018 [23]. Reprinted with permission from AAAS.

Novel and cogent translational studies

Orthotopic large animal models need to be performed to examine the safety and efficacy of tissue-engineered constructs prior to translation. Toward selection, possible species for performing regenerative studies include sheep [213], goats [214], dogs [215], farm pigs [216], and minipigs [24]. The farm pig and minipig are two suitable models that have been recently used for regenerative studies due to their similarities to humans in chewing patterns, diet, and anatomy [24, 80, 169, 217-219].

In a recent study demonstrating safety and efficacy of a self-assembled, allogeneic, tissue-engineered implant for disc repair, a novel TMJ disc thinning model was created in the Yucatan minipig [23]. Because the implants were created from a CC source, implantation into the TMJ disc represented non-homologous use. Implants approaching native tissue values were stimulated by a regimen of biochemical and mechanical stimulation. To affix implants securely, the intralaminar fenestration surgical technique was developed (Figure 2-5) [23]. Although this was an allogeneic, non-homologous use which has potential to elicit an immune response, implant safety was shown by minimal to no immune response to the constructs, as assayed by histological staining for CD3, CD20, and CD68 for T cells, B cells, and macrophages. However, it was specified that additional work needs to further elucidate the immunological response [23], such as macrophage activation due to tissue-engineered implants [220-222] (Figure 2-4). In terms of efficacy, results showed that the tensile Young's modulus, integration at the repair-to-native tissue interface, and percent of defect closure were 3.4-fold, 3.2-fold, and 4.4-fold higher, respectively, compared to empty defect controls [23]. OA scores of the condylar surface treated with implants were 3.0-fold less than the empty defect controls [23], yielding a better clinical outcome overall. Together, these results demonstrate the feasibility of allogeneic TMJ disc tissue-engineered constructs in the orthotopic environment and pave the way for additional orthotopic large animal studies and future human clinical trials (Figure 2-4).

Overcoming additional clinical and regulatory hurdles

In stark contrast to diarthrodial joints such as the knee, there is limited knowledge surrounding the TMJ, especially when it comes to developing new processes and products for repair or replacement of the TMJ disc. Compared to the TMJ, a greater variety of products, treatments, and studies exist for the knee. To illustrate these differences, one can consider indications and contraindications in the TMJ versus the knee. For example, in the knee, there are clear guidelines as to what constitutes small, large, partial thickness, and full thickness defects with concomitant treatment algorithms [223]. In contrast, it is not clear when a tissue-engineered treatment would be indicated in the TMJ. Currently, in the knee, tissue-engineered products are contraindicated for the OA milieu [224]. This has not been confirmed for the TMJ, though the expectation is that the constructs under OA conditions might succumb to the same fate as the native tissue [225]. Development of treatment guidelines and additional studies specific to the TMJ should continue, toward bringing TMJ-related knowledge to levels of other diarthrodial joints.

One must also consider fixation and associated surgical approaches. The intralaminar fenestration surgical technique (Figure 2-5) was successful in treating early-stage disc thinning, but in the minipig [23]. However, in 5% of TMD cases requiring surgery [13], it is not yet obvious how one may be able to attach a partial or whole, tissue-engineered disc (Figure 2-4). Surgeons and researchers must continue to collaborate to develop surgical approaches for implantation of tissue-engineered implants, as they are of utmost importance to the success of the tissue-engineered treatment.

With regard to clearing the regulatory hurdle, the TMJ's proximity to the brain (Figure 2-4) may necessitate more stringent safety requirements than products for other joints such as the knee. These requirements may include analysis of the synovial fluid in the TMJ, but also the neighboring cerebrospinal fluid. Notoriously, mechanical failure and resulting degradation of the Proplast-Teflon disc implants resulted in exposure of the brain cavity [226-228]. Additionally,

current large animal work has yet to investigate fully immunological implications related to TMJ disc implants (Figure 2-4) or how immunomodulation may be used in a proinflammatory environment [167]. In terms of regulation, the FDA has not previously guided a tissue-engineered TMJ disc product [15], thus raising the question of establishing TMJ-specific safety and efficacy guidance documents. Future research in the field needs to establish the safety of tissue-engineered TMJ discs by elucidating the immune response. Additionally, researchers need to communicate with regulatory bodies, such as the FDA, to obtain guidance on how tissue-engineered TMJ disc products need to be demonstrated as safe and efficacious.

Concluding Remarks

While recent advances propel TMJ disc tissue-engineering forward, many hurdles still exist. To summarize, the pressing challenges include improvement of mechanical properties of constructs, scale-up of implant dimensions, determination of indications for tissue-engineered discs, development of surgical techniques, analysis of the immunological response, and regulation by the FDA (see Outstanding Questions). Tissue-engineering and basic science investigations for TMDs will continue to drive the field. The field should focus toward addressing questions in the clinical and regulatory spaces. Specifically, studies should pay attention to developing novel surgical techniques and associated fixation methods toward human clinical trials. For each new tissue-engineering approach, regulatory requirements need to be satisfied by demonstration of TMJ-specific safety and efficacy in large animal models. As regulatory bodies turn their attention toward clinical trials, these data will be the primary preclinical assessment of implants. Considering the momentum toward significant preclinical studies, it is an exciting time to be in the field of TMJ disc tissue-engineering. After the early success shown in the orthotopic study performed in the Yucatan minipig [23] and the identification of clinical and regulatory hurdles discussed here, there is new impetus to develop tissue-engineering solutions

to begin addressing the various intractable TMJ trauma and degenerative ailments. The possibility of translating tissue-engineered TMJ discs is increasingly being realized.

Outstanding Questions

- How do researchers achieve tuning of tissue-engineered constructs to the mechanical environment of the TMJ disc?
- Can researchers scale-up constructs, in area and thickness, to be relevant to human discal pathologies and size?
- For what cases will tissue-engineered products be indicated (or contraindicated)?
- Can novel surgical procedures be developed for accessing the TMJ, and fixing and implanting tissue-engineered TMJ disc constructs orthotopically?
- What is the local and systemic responses to tissue-engineered TMJ discs *in vivo*?
- How would tissue-engineered constructs for the TMJ disc be regulated by the FDA?

Chapter 3: Knee Orthopaedics as a Template for the Temporomandibular Joint[3]

Abstract

Although the knee joint and temporomandibular joint (TMJ) experience similar incidence of cartilage ailments, the knee orthopaedics field has greater funding and more effective end-stage treatment options. Translational research has resulted in the development of tissue-engineered products for knee cartilage repair, but the same is not true for TMJ cartilages. Here, we examine the anatomy and pathology of the joints, compare current treatments and products for cartilage afflictions, and explore ways to accelerate the TMJ field. We examine disparities such as a 6-fold higher article count and 2,000-fold higher total joint replacement frequency in the knee compared to the TMJ, despite similarities in osteoarthritis incidence. Using knee orthopaedics as a template, basic and translational research will drive the development and implementation of clinical products for the TMJ. With more funding opportunities, training programs, and federal guidance, millions of people afflicted with TMJ disorders could benefit from novel, life-changing therapeutics.

Highlights

- The knee and the TMJ have similar incidence of cartilage ailments
- The knee field has more treatment options and funding than the TMJ field
- Tissue-engineered products have been developed for the knee but not the TMJ
- Using knee orthopaedics as a template, novel TMJ therapeutics will be developed

[3] **Chapter published as:** Bielajew, B.J.,* Donahue, R.P.,* Espinosa, M.G.,*, Arzi, B., Wang, D., Hatcher, D.C., Paschos, N.K., Wong, M.E.K., Hu, J.C., Athanasiou, K.A. Knee orthopaedics as a template for the temporomandibular joint. *Cell Reports Medicine*, April 2021, 2(5): 100241. (* These authors contributed equally.)

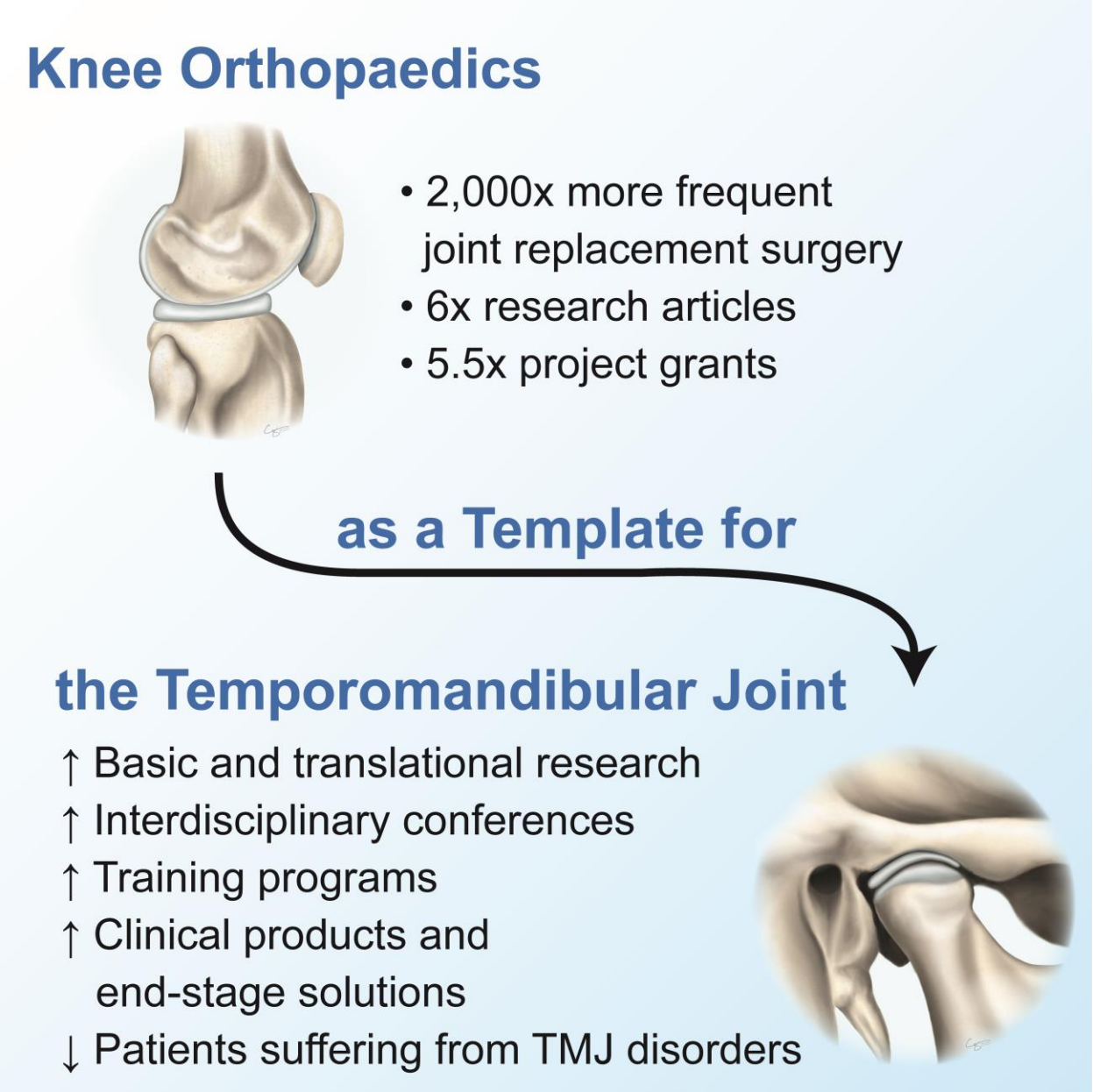

Introduction

The knee joint and temporomandibular joint (TMJ) are two of the most used joints in the body. They are both diarthrodial hinge joints consisting of a fibrocartilaginous meniscus/disc between two articulating surfaces (Figure 3-1) [34, 229]. The knee is better described as two joints, the tibiofemoral joint and the patellofemoral joint; these work together for flexion, extension, and rotation of the lower legs. The knee is the largest joint in the body and is essential for walking,

running, and jumping [230]. The TMJ is one of the most complex joints in the body and functions in rotation and translation to perform crucial activities such as chewing, speaking, and breathing [231]. Both joints are critical for performing many day-to-day movements, where they withstand large, repeated forces.

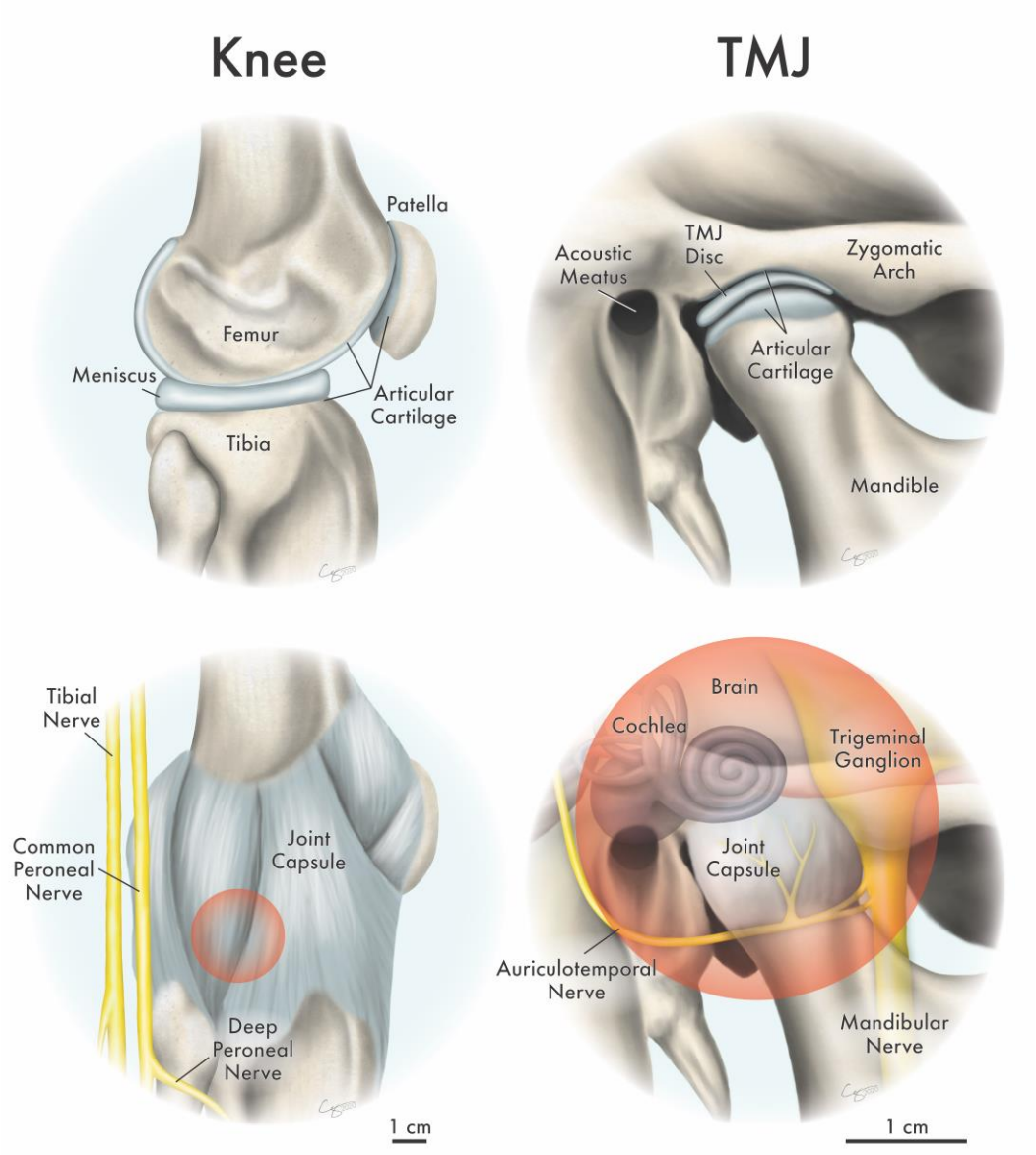

Figure 3-1: Knee and TMJ anatomy and proximity to crucial sensory structures.
(Top) Both the knee and TMJ are diarthrodial joints with two articular surfaces and an interpositional fibrocartilage. Specifically, the meniscus is situated between the tibia and the femur in the knee, while the TMJ disc is situated between the zygomatic arch and the mandible. (Bottom) Within a 3 cm sphere (red circle representation in 2D space) centered around the meniscus and the TMJ disc, the knee has no crucial sensory structures, while the TMJ has numerous structures present including components of the inner ear, the brain, the trigeminal ganglion, and the mandibular and auriculotemporal nerves.

While there are analogous structures in the knee and TMJ (Figure 3-1), there are some biomechanical and biochemical differences between the two joints. When performing simple motions, the knee withstands comparatively large forces; light jogging can put over four times the body's weight (e.g., 3080-3600 N) on the knee [232, 233], compared to the TMJ, which experiences forces equivalent to the body's weight (e.g., 770-900 N) when biting [232, 234]. While compression and shear are major loading types in both joints [235], tensile loading plays a greater role in the TMJ than the knee [236]. The knee meniscus contains zonal differences in collagen type I and II ratios, while the TMJ disc is almost completely composed of collagen type I [237]. While both articular surfaces contain growth plates, the mandibular condyle contains a unique fibrous zone [238], unlike the articular cartilages of the knee which are completely hyaline. Despite these differences, the two joints manifest pathologies and disorders leading to pain and dysfunction.

Approximately 25% of adults have some sort of cartilage affliction [239]. Arthritides, diseases involving joint inflammation and cartilage degeneration, frequently occur from overuse, aging, trauma, or pathology. Osteoarthritis (OA) is the most common form, with the knee being one of the most frequently affected joints; about 14% of the adult U.S. population is afflicted by knee OA [240]. Other disorders of the knee joint include meniscus tears, common in young athletes [241], resulting in the development of OA in the knee; one study showed that 85% of patients with medial meniscus tears also developed OA [242]. Although epidemiological studies of OA incidence in the TMJ are not extensive, one article indicates evidence of TMJ-OA in 8-16% of the population [243]. Temporomandibular disorders (TMDs), an umbrella term to describe a wide variety of TMJ pathologies, includes TMJ-OA (also referred to as degenerative joint disease) as well as other ailments such as disc pathologies and myofascial dysfunction. Joint disorders also involve changes to muscles, ligaments, tendons, and bones; this Review will be focused primarily on the cartilages of the knee joint and the TMJ.

Although the joints have similar anatomy and OA incidence, the knee and TMJ fields display stark differences in primary research, funding, cell-based products in development, and total joint replacement procedures (Table 3-1). Compared to the TMJ, the knee has a greater quantity of basic and translational research, resulting in more product development and marketed treatments. For example, the knee has a 5.5-fold higher amount of R01 research project grants from the National Institutes of Health (NIH) compared to the TMJ in 2019. The NIH is part of the U.S. Department of Health and Human Services and is the largest biomedical research agency in the world. It is broken down into 27 institutes and centers which fund scientific grants. There is also a major difference in the amount of end-stage surgical procedures performed on knee and TMJ patients; the knee has approximately a 2,000-fold higher frequency of total joint replacements compared to the TMJ. The dearth of TMJ research presents a pressing challenge toward developing novel cartilage therapies, but, by bolstering primary and translational research of the TMJ, new products for its cartilages may be developed [16]. The lack of translational advancement for the TMJ represents a chokepoint in the development of safe and effective therapeutics for people afflicted by TMDs, which, according to the TMJ Association, totals over 35 million adults in the U.S [244]. In this Review, we compare the pathologies, anatomical challenges, clinical practices, and products for the cartilages of the two joints within the U.S. medical system and call for improved treatment options for specific TMJ indications. By using the knee orthopaedics field as a template to follow in translational pathways, TMJ experts can drive the implementation of new cartilage therapies for millions of TMD patients.

Table 3-1: Comparison of the knee and TMJ fields.
Despite similar incidence of osteoarthritis, the TMJ lags behind in research output, grant funding, cell-based products, and practicing physicians.
***** PubMed was searched using the following keyword schemes: [(((tibiofemoral) OR (knee)) AND ((cartilage) OR (meniscus)))] [(((temporomandibular) OR (jaw)) AND ((cartilage) OR (meniscus) OR (disc) OR (disk)))]
** NIH RePORTER was searched using the following keyword schemes limited to project abstracts: [(((tibiofemoral) OR (knee)) AND ((cartilage) OR (meniscus)))] [(((temporomandibular) OR (jaw)) AND ((cartilage) OR (meniscus) OR (disc) OR (disk)))]
*** Related to treating cartilage, meniscus, and disc pathologies.
**** Based on searches based in clinicaltrials.gov across all countries.

	Knee	TMJ
Osteoarthritis incidence	~14% [240]	8-16% [243]
Professional membership	AAOS membership: 39,195 [245]	AAOMS membership: 11,436 [246]
PubMed articles*	1,852 (in 2019)	288 (in 2019)
R01s (research project grant)**	33 (in 2019)	6 (in 2019)
R21s (exploratory/developmental research project grant)**	9 (in 2019)	1 (in 2019)
Cell-based therapeutics in development or clinical trials (worldwide)***	18 [247]	1****
Projected number of joint replacement procedures in 2020 (U.S. only)	882,000-1,783,000 [248] (range of 2020 projections from a variety of historical data)	709 [249] (2020 projection from historic data from 2005-2014)

Pathology

The TMJ requires improved diagnostic modalities despite similarities in osteoarthritis progression

Knee and TMJ OA pathologies have several similarities. This disease involves mechanical and biochemical degradation of cartilage, subchondral bone, and synovium [250]. Pain is the most common OA symptom, which can range from barely noticeable to severe and debilitating [251]. Other symptoms include joint stiffness and reduced function or range of motion, and, with severe TMJ-OA, changes in occlusion. Knee OA is traditionally diagnosed with radiography, and early damage can be detected using magnetic resonance imaging (MRI) [252]. For TMJ-OA, panoramic radiography has a low sensitivity for diagnosis [253]. Cone beam computed tomography (CBCT), a widely used imaging modality, is used as a more reliable diagnostic

technique [254], and MRI can be used to assess different signs of dysfunction [255]. Dynamic MRI scoring algorithms, similar to those used to evaluate cardiac wall motion [256], can be used for the TMJ, for example, to assess the causes of reduced joint mobility. Reduced mobility is often caused by a displaced disc [257], but capsule and ligament pathology may also play a role; these are not routinely examined with imaging. An unusual caveat with TMJ imaging is that radiographic signs alone may not be associated with pain; one study performed CBCT imaging on TMJs of healthy adults with no TMJ complaints, and nearly 40% of the TMJs showed degenerative changes [258]. Conversely, TMJ pain may not be associated with radiographic signs of disease [259]. For determining the source of pain in the TMJ, positron emission tomography paired with a computed tomography scan (PET/CT) is being used to image inflammation and bone changes in the TMJ and may be useful for diagnosing TMJ-OA [260]. While knee OA is similar in nature to TMJ-OA, additional assessment tools are needed to improve the accuracy of OA diagnosis correlating with symptoms in the TMJ [261], thus, improving indications for TMJ repair.

TMJ disorders are more prevalent in women

Women experience higher levels of knee pain than men [262], with about a 1.6-fold higher incidence of knee OA [263]. This difference is likely caused by biomechanical, hormonal, and neural differences [264], but a better understanding is needed. Epidemiological studies on gender differences in TMJ-OA are not extensive, but the higher prevalence of TMDs in women has been widely documented; TMDs are up to four times more prevalent in women than men, with women presenting more severe symptoms [265]. There is evidence of increased amounts of hormone receptors in the TMJ discs of women with TMDs [266], but there is conflicting literature showing relationships between TMD prevalence and estrogen levels [267]. This coincides with a high proportion of young TMD patients compared to knee OA patients [268, 269]. An earlier onset of TMJ-OA challenges the “overuse phenomenon” — that OA occurs

when functional demands exceed the adaptive capacity of the cartilage [270]. One stark example of age and gender bias in TMDs is the incidence of idiopathic condylar resorption of the TMJ. This disease occurs nine times more frequently in women than men and rarely develops after the age of 20 [271]. In these young patients, TMDs may profoundly affect facial growth, occlusion, and airway dimensions [272]. Given the severe, unexplained gender discrepancy in the TMJ, which has been called the “TMJ gender paradox” [273], deeper understanding of what drives the higher TMD occurrence in young women remains a major milestone for the field.

The anatomical challenge of sensory structures near the TMJ versus the knee

A major difference between the joints is the location relative to vital structures, which affects joint symptoms, treatment effectiveness, surgical approaches, and adverse events. In the knee, the tibial, peroneal, and saphenous nerves are near the joint (Figure 3-1), but nerve damage is rare during knee surgery. The TMJ is near multiple important sensory nerves, parts of the inner ear, and the brain (Figure 3-1). The TMJ’s sensory nerves innervate surrounding masticatory muscles, and spasms in these muscles might be associated with TMJ pain [274]. One study on 501 TMD patients showed that 60 also had trigeminal neuritis, a condition causing severe, chronic pain [275]. TMJ disc displacement may compress the mandibular nerve, causing neuropathic pain [276]. People with TMDs are more likely to have severe tinnitus and vertigo, potentially due to the TMJ’s proximity to the inner ear [277]. The complex anatomy and associated symptoms can complicate diagnosis and make treatment difficult [278], and the outcome of patients with neural and joint symptoms is inconsistent, often resulting in unsuccessful treatments [279]. As shown in Figure 3-1, a 3cm sphere centered on the TMJ disc contains major nerve structures, the inner ear, and the brain, while the same sphere centered on the knee meniscus contains no major sensory structures. In addition to the aforementioned lack of diagnostic modalities, a major hurdle in performing surgery is the TMJ’s close proximity

to the brain [280], illustrating the anatomical challenge of diagnosing and treating cartilage disorders of the TMJ compared to the knee.

Current Clinical Practices

Divergence of end-stage treatment strategies for osteoarthritis of the knee and TMJ

The treatment strategies for knee and TMJ cartilage pathologies are similar at first glance (Figure 3-2A). Both the American Academy of Orthopaedic Surgeons (AAOS) and the American Association of Oral and Maxillofacial Surgeons (AAOMS) list physical therapy, analgesics, and mechanical stabilizers as conservative treatment options for OA [281, 282]. These relatively noninvasive, early-stage therapies are often undertaken by a variety of providers, such as physicians and physical therapists or, for the TMJ, dentists and dental specialists. If such therapies prove ineffective, frequently, orthopaedic and oral and maxillofacial (OMF) surgeons employ injection-based therapies [57, 283]. There are greater differences between surgical treatment options. Few late-stage TMD patients are referred to an OMF surgeon, indicated by the small number of TMJ surgeries performed. Only 5% of TMD patients are considered candidates for surgery [14], despite a lack of positive outcomes with non-surgical approaches. This is reflected in the decline of TMJ surgeries; the number of TMJ arthroscopic surgeries has steadily decreased since the 1990s [284]. This is in contrast to total knee arthroplasties, which are projected to increase by up to 800% by 2050 [285]. The declining trend in the TMJ field may be attributed to a number of causes, such as disagreement over the suitability or efficacy of surgical approaches [284]. Conversely, knee cartilages have well-defined treatment algorithms. For example, focal defects are treatable with widely accepted surgical techniques [247]. In the U.S., Current Procedural Terminology (CPT) codes are used to report medical or dental services provided by a physician to insurance companies for reimbursement or payment. A higher specificity of knee treatments is shown in a higher quantity of CPT codes compared to the TMJ. For example, TMJ arthroplasty has only three CPT codes while knee arthroplasty has

ten [286, 287]. Knee treatment is covered by medical insurance, while TMDs can be covered under either medical or dental insurance. It is clear that TMD patients need greater access to effective, end-stage treatments with indications that are well-vetted among OMF surgeons with specialized training in the TMJ.

Training disparities between knee and TMJ surgeons

Quality surgical treatment is directly related to physician training. OMF and orthopaedic surgery training consists of four years of dental or medical school followed by residency (Figure 3-2B). OMF surgery residency lengths and degree requirements vary significantly across countries; this is reviewed elsewhere [288]. In the U.S., OMF surgery residency may either be a four-year program (single degree) or an MD-granting six-year program (dual degree). Dual degree programs make up to 46% of the residency programs [289]. One measure of surgical training is resident case log volume throughout the duration of the program (Figure 3-2B). Regardless of residency duration, the Commission on Dental Accreditation (CODA) requires that OMF residents log 175 major procedures in their final year [290]. A survey of senior OMF residents in the U.S. showed that only ~3.5% of these cases involve TMJ arthroscopic or open joint procedures [291]. Most TMJ-specific treatments performed by residents were injection-based [291]. At programs lacking OMF residencies, TMDs may be covered by plastic surgery or otorhinolaryngology residencies, but TMDs are not a focus. In general, orthopaedic surgery residents log 200-600 cases in the final year [292, 293], and, in 2019, knee-specific arthroscopy and open joint surgery accounted for ~16% [294]. Following their five-year residency, most orthopaedic surgeons complete a fellowship year [295], and those interested in knee cartilage typically choose a sports medicine or arthroplasty fellowship. While the CODA-accredited endoscopic maxillofacial fellowship provides more substantial TMJ-related training [296], fellowships are not as popular among OMF surgeons [297]. If better end-stage treatment

options are to become available, there will be a greater need for TMJ specialization to meet the surgical needs of TMD patients.

From incidence to clinic: Gender imbalances in physician populations and clinical trials

Gender imbalances are present in the demographics of knee and TMJ patients and the surgeons that treat them, and these disparities have a clinical impact on the treatment of knee- and TMJ-related ailments. Because there are significantly more women who experience OA and TMDs, it is important to account for gender-based differences in treatment development. For example, women report more pain before and after total knee arthroplasty when compared to men [298]. Similarly, the percentage of women reporting orofacial pain at routine dental visits was triple that of men [299]. While some have focused on psychosocial factors to explain this difference [300-302], it is important to consider the ample evidence showing that women's analgesic response is physiologically different from men's [303]. Interestingly, a recent review noted that physicians are more likely to recommend greater pain intervention for patients of the same gender [304]. This is important, given that most knee and TMJ OA patients are female, while orthopaedic and OMF surgeons are predominantly male (Figure 3-2C). In the last decade, approximately half of medical and dental school graduates were women, but the percentage of female residents in both orthopaedic and OMF surgery programs has only been about 15% [305, 306]. This imbalance is greater within professional societies; women make up only 6.5% and 8.0% of the AAOS and AAOMS membership, respectively [307, 308]. Reducing this disparity among orthopaedic and OMF practitioners will help ensure that gender-based differences are not overlooked in patient treatment.

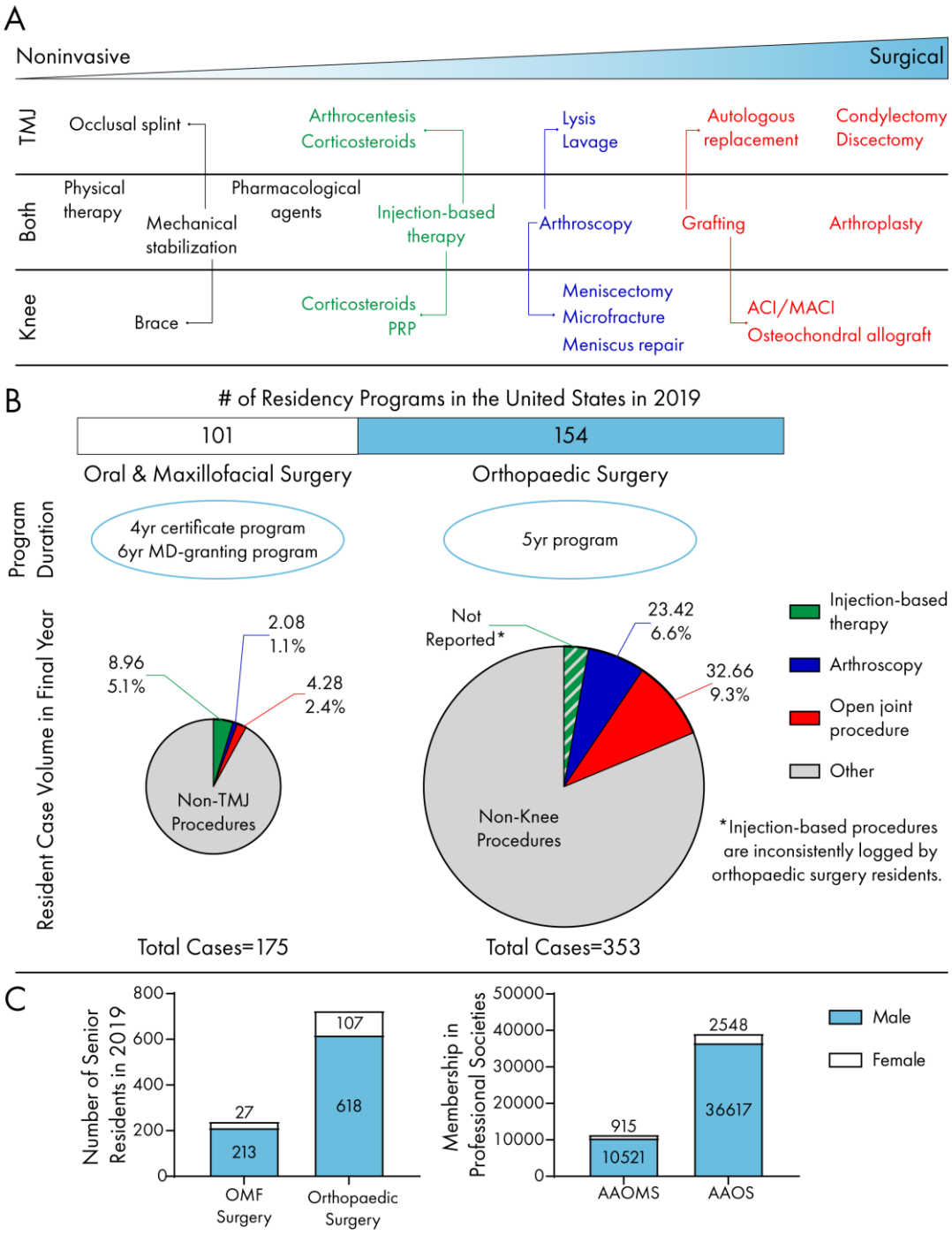

Figure 3-2: Clinical practices for the knee and TMJ.
(A) The cartilages of knee and TMJ share similar treatment pathways. Progressing from non-invasive to surgical approaches, conservative treatment is often indicated prior to end-stage surgeries such as autologous grafting (e.g., fat, rib) for the TMJ and osteochondral allografts for the knee. (B) Orthopaedic surgery leads oral and maxillofacial surgery in residency program quantity. Oral and maxillofacial surgery residents are exposed to a lower quantity and percentage of total cases in open joint and arthroscopic procedures compared to orthopaedic residents. (C) Males are overrepresented in both senior resident numbers and professional society membership in AAOMS and AAOS.

Potential therapeutics must go through preclinical and clinical trials to gain regulatory approval. Potential product sponsors must consider careful design of such trials, specifically, the gender of the participants. With a vast majority of people experiencing TMDs being women, the NIH's policy on "sex as a biological variable" is particularly relevant [309, 310]. This strongly encourages researchers to consider gender-based differences throughout the translational process. Unfortunately, meta-analytic studies have shown that gender differences in clinical trials are underreported [311]. Translational scientists must consider how gender disparities in knee and TMJ OA patients may not only affect the demographics of clinical trials but, subsequently, the landscape of commercial products.

Commercial Products

Joint prostheses: Successes in the knee and catastrophic setbacks in the TMJ

Partial or total joint replacement is the current solution for patients with cartilage pathologies that fail to improve with less invasive treatments. The first hemiarthroplastic knee device, a tibial plateau prosthesis, was designed by McKeever in 1957 [312, 313]. In 1963, Christensen published on a fossa-eminence prosthesis for TMJ hemiarthroplasty [314]. These devices paved the way for the development of total joint implants in the U.S. The early total knee devices include the Freeman-Swanson knee and the Geomedic knee [313]. In the 1970s and '80s, the Oxford knee and the New Jersey Low-Contact-Stress knee significantly improved mobility and are still used [315]. Today, there are over a dozen knee replacement manufacturers collectively offering a wide range of customization options [315, 316].

Unlike the knee, TMJ prosthesis development has been slow and controversial. In 1983, the U.S. Food and Drug Administration (FDA), the regulatory body responsible for determining safety and efficacy of therapeutics, cleared Vitek's Proplast-Teflon implant for TMJ disc replacement, despite evidence of fragmentation with similar Teflon-based hip replacements [317]. Given the joint's proximity to the brain, the implant's failure led to catastrophic outcomes,

such as particulate migration and cranial breaching [227, 318]. By 1990, the FDA rescinded clearance of the implant and issued a recall a year later [319]. In 1993, the FDA reclassified all TMJ prostheses as Class III, a designation reserved for devices posing the greatest risk [189], requiring more rigorous premarket approval and stifling production of all TMJ implants. Currently, there are only four FDA-approved TMJ implants [184, 320, 321]. Nexus makes both a partial and total metallic joint, and Zimmer-Biomet and TMJ Concepts make metal/polymer total joint replacements [317]. This is in stark contrast to the hundreds of total joint replacement systems available for the knee [313].

The TMJ field trails the progress of tissue engineering in the knee

An important measure of an implant's success is its long-term performance and lifetime. Approximately 82% of total knee replacements survive 25 years [322]. Although most surveillance studies for TMJ implants are ongoing, Zimmer-Biomet reports that implant survival is 86% after 10 years [323]. The average age of a TMJ implant recipient is only 34.9 years compared to 67.5 years for knee implant recipients [269, 324]. Assuming an implant lifetime of 20 years and an average life expectancy of 78.6 years in the U.S. [325], a TMJ patient is likely to need two revision surgeries; a knee patient is unlikely to need any. This disparity underscores the TMD patient's dire need for high quality, long-lasting replacement options for treatment of late-stage, degenerative TMDs. Tissue engineering offers a promising long-term alternative to alloplastic implants, thus, potentially eliminating the need for revision surgeries.

In 2016, the FDA approved matrix-induced autologous chondrocyte implantation (MACI), a two-surgery process utilizing expanded cells seeded on a porcine collagen membrane, for the repair of knee cartilage defects [326]. Several more tissue-engineered products, such as NOVOCART 3D for articular cartilage and Chondrogen for the meniscus, are currently proceeding through the regulatory pipeline [247]. Some tissue-engineered products employ an allogeneic approach; one example, Revaflex, reports encouraging results in clinical trials [247,

327]. Given this established precedent, continued development of tissue-engineered products for the knee cartilages will proceed. Development of cell-based therapeutics for the TMJ cartilages is still in its nascent stage, with only one clinical trial based in Brazil [328]. Although autologous grafts (e.g., fat, rib) for the TMJ offer a tissue-based option [184, 321], there are still no approved, tissue-engineered products for the TMJ cartilages in the U.S.

Future Directions

The vicious cycle of translating TMJ research

Tissue engineering can potentially offer long-term solutions for knee and TMJ cartilage ailments. With multiple products, either approved or in trials, tissue engineering toward regeneration of knee cartilages is poised to be a major early success of regenerative medicine, acting as a template for other joints such as the TMJ. Although the knee and TMJ fields had similar start points in the 1950s and ‘60s with joint replacement devices, the catastrophic failure of the Proplast-Teflon protheses affects the TMJ field to this day. The knee field enjoys much success in terms of quantity of research output, funding, marketed products, and regulatory guidance, while the TMJ field is relatively stagnant in nearly all areas. Low research output, especially in translational science, leads to fewer innovative therapeutics that make it to clinical trials. The resulting dearth of products for TMJ cartilages limits commercial success, disincentivizing financial and regulatory support, feeding back into the vicious cycle as a lack of precedent (Figure 3-3). By increasing research output, bolstering training opportunities, narrowing and specifying indications for TMJ cartilages, establishing a commercial TMJ landscape, and publishing guidance documents, the field can accelerate translational research to break the vicious cycle.

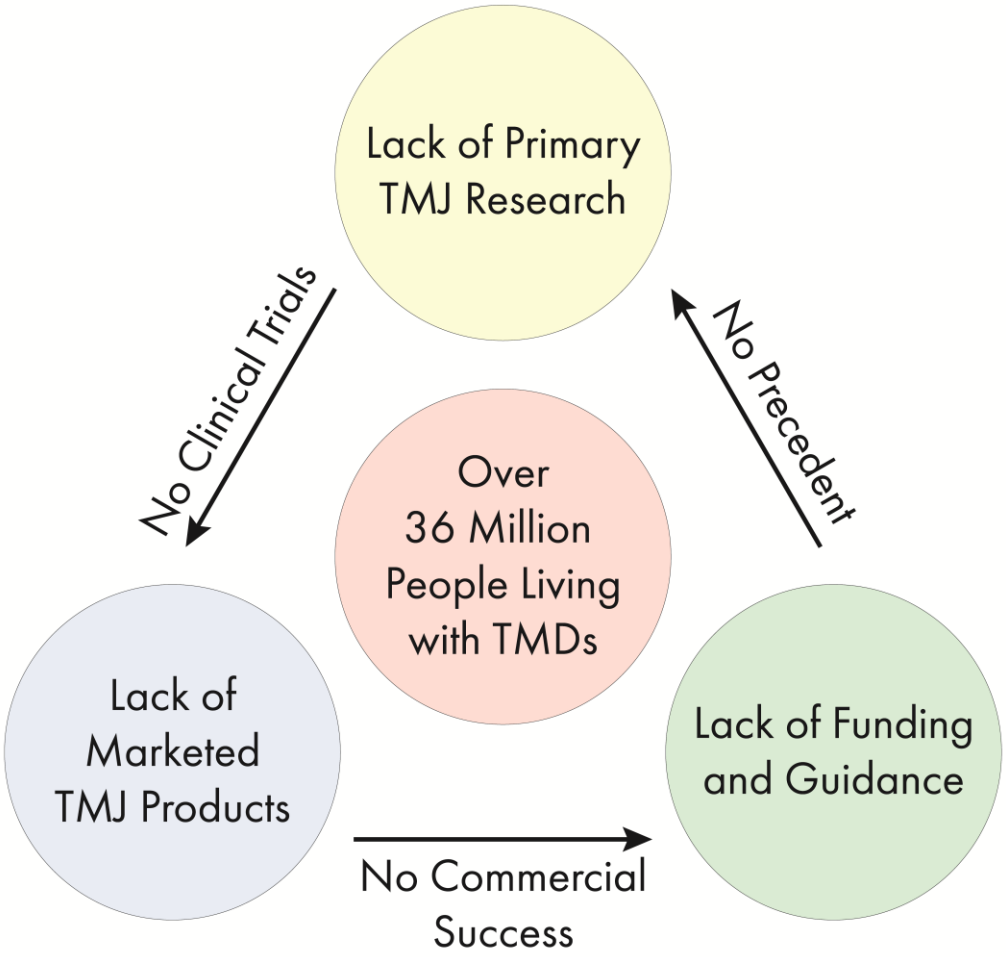

Figure 3-3: The vicious cycle of TMJ translational research.
Primary research is lacking in the TMJ field, leading to little translation and resulting human clinical trials. Without clinical trials, approved, marketed products do not exist, resulting in little to no commercial market for TMJ products. This disincentivizes regulatory and funding agencies from publishing guidance and providing funding for the TMJ field, feeding back into the loop and resulting in a lack of precedent for researchers.

Increasing the quantity of rigorous TMJ research

There is a critical need for increased basic and translational research output to energize the TMJ field. Within the U.S., the number of TMJ-related, NIH-funded grants drastically trails those of the knee (Table 3-1), illustrating the need to further mature the TMJ field. In a recent report, the National Academies of Science, Engineering, and Medicine recommended bolstering different aspects of TMJ research [329]. For example, the report calls for the creation of a national collaborative research consortium and expansion of TMJ research. For orthopaedics,

the Orthopedic Research Society (ORS) helps facilitate these activities through their annual meeting. This meeting brings together orthopaedic surgeons, biologists, engineers, and other experts across various fields. This fosters a collaborative environment for those within orthopaedics, both researchers and practitioners, to discuss interdisciplinary research and form collaborations. While the TMJ Bioengineering Conference occurs every two years and achieves the same goal as the ORS annual meeting on a smaller scale, the TMJ field is more fragmented. There are multiple different symposiums, such as the meetings of the American Society of TMJ Surgeons, the AAOMS, the American College of Oral and Maxillofacial Surgeons, and the American Academy of CranioMaxillofacial Surgeons that discuss the TMJ, but the field does not have one meeting that brings together experts from different fields at the same scale of ORS. One can consider a TMJ meeting, modeled after ORS, where researchers and clinicians meet to discuss current treatment issues and how interdisciplinary approaches can be developed toward relieving TMJ ailments. Additionally, ORS may consider cosponsoring a TMJ-specific meeting to bring together researchers, orthopaedic surgeons, and OMF surgeons to discuss how treatments and approaches in the knee cartilages could be transferred to the TMJ. By using orthopaedic meetings as a template, the TMJ field can accelerate the basic and translational research toward clinical trials to develop effective TMJ therapeutics.

Without a large quantity of interdisciplinary research, the TMJ field will not be able to establish a base to propel itself forward. One of the major issues is that TMDs disproportionately affect up to 17% of all American women [244, 265]. Understanding fundamental science will shape the approach of translational research, such as in the design of preclinical animal studies. Although basic science and translational research have already resulted in a steady rise of TMJ-related publications since 2006 [330], federal bodies such as the National Institute of Dental and Craniofacial Research (NIDCR), NIH, and FDA still push for increased research [329]. This will not only lead to increased output but also maintain a high standard of scientific rigor, as those bodies require that grant applications and manuscripts undergo peer-review. On average, an

R01 grant from the NIH leads to 7.36 published research articles with almost 300 citations [331]. Similar to ORS sponsoring a combined meeting, the NIDCR and institutes such as the National Institute of Arthritis and Musculoskeletal and Skin Diseases (NIAMS), two U.S. NIH institutes which the TMJ and knee commonly fall under, may consider publishing dual requests for applications that study the knee and TMJ cartilages under one grant. These could focus on transferring the knee knowledge, equipment, and protocols to the cartilages of the TMJ, providing incentive for established musculoskeletal researchers to extend a branch into the TMJ field. By increasing grant funding through various channels such as the NIH, TMJ research output will be closer to the level of the knee field.

Bolstering training opportunities for researchers and physicians

As research output rises, more trained researchers and surgeons will be needed. The NIH F-series of grants is targeted toward students and postdoctoral fellows to support both individuals (e.g., salary, stipend, tuition) as well as their proposed research. The funding success rates of the NIDCR grants for pre- (F31) and post-doctoral (F32) candidates are 70% and 35% in 2019, respectively [332]. Considering both of these success rates trend in the top third of all NIH institutes [332], the NIDCR is commended for their commitment to funding junior researchers. However, total funds disbursed by the NIDCR ranked in the bottom half of all NIH institutes [332]. Compared to the NIDCR, the NIAMS F31 and F32 success rates were lower in 2019, about 18% for both mechanisms [332]. Although the number of candidates funded were similar for each mechanism, the total number of applicants for NIAMS fellowships was drastically larger than those of the NIDCR [332]; thus, the NIDCR could improve their outreach and advertising of such mechanisms. A mechanism to bridge postdoctoral scientists to their early career (e.g., junior faculty) is the K99/R00 grant which includes both a mentored and independent research phase. In 2019, the K99 application numbers were comparable between the NIDCR and NIAMS, but the NIDCR maintained a higher success rate of 36.8% compared to 20.0% [332]. Clearly,

the NIDCR is committed to developing researchers' careers in the craniofacial, dental, and TMJ fields. By maintaining high success rates, increasing funding disbursed, and bolstering outreach efforts for these awards, the NIDCR will increase the number of trainees pursuing a TMJ-related career.

As discussed above, orthopaedic surgery residents gain exceptional experience in open joint surgeries and arthroscopy of the knee (~16% of cases) [294], compared to the equivalent for the TMJ (~3.5%) for OMF residents [291]. Development of reliable diagnostic modalities and clear treatment algorithms to address specific pathology will increase TMJ surgery case volume for OMF residents, thus, better equipping future surgeons for implementing new therapeutics. An additional option would be to develop a TMJ-specific surgical fellowship for OMF residents, modeled after fellowships for orthopaedic surgeons. Lastly, as the field matures, the need for dual degree clinician-researchers will grow, which is expected to spur the development of novel therapeutics. The dual degree F30 fellowship success rate for the NIDCR in 2019 was in excess of 80% [332], indicating that the institute is committed to developing clinician-researchers and their ideas toward therapeutics. Early career medical professionals might bridge their careers into research with a K08 clinical investigator award, which provides these individuals with an intensive, research career development experience. In contrast to the F30 mechanism, the K08 success rate for the NIDCR (25.0%) trails that of NIAMS (56.3%) although they maintain relatively similar applicant numbers [332]. Encouragement of clinician-researchers to apply for funding at the success rate of the F30 award and continuing to increase success rates at the K08 level will grow and sustain the number of TMJ physicians and translation of novel therapeutics.

Narrowing and specifying indications for TMDs toward establishing the commercial landscape for TMJ cartilage products

As researchers and clinical practitioners continue to grow the field in number and research output, there will be a push to narrow and specify indications for the TMJ-specific conditions amenable to surgical management. Currently, the term TMD encompasses many different conditions, including muscle and joint problems [333]. This has led to confusion in the field today that causes conflicting paradigms for treating certain indications. Toward solving this, the National Academies' report recently recommended establishing a national TMD registry to track incidences, indications, and treatment pathways toward establishing best practices [329]. A template for the TMJ field may be the AAOS American Joint Replacement Registry that has recorded procedural data, post-operative data, and patient-reported outcome measures on over 2,000,000 joint replacement procedures for the knee and hip since 2009 [334]. Continued clinical research output, specifically retrospective and meta-analytic studies on certain indications, will additionally improve the clinical body of knowledge.

Establishing specific indications for TMDs is crucial to a healthy market for the TMJ field; without a clear indication, there is no commercial product. Due to a lack of indications, it is not clear how TMJ tissue-engineered products might be implemented [225]. By establishing indications, more TMJ scientists and clinicians will attempt to translate technologies, therapeutics, and devices from the benchtop to the bedside. In the knee, MACI is indicated for patients with symptomatic, full-thickness knee cartilage defects who have failed conservative treatments [335]. The TMJ market would benefit from using MACI and other knee cartilage therapeutics as a template for TMJ tissue-engineered products. As translation occurs for various TMJ therapeutics, additional CPT codes and surgical procedures will likely be needed. Historically, only 5% of TMDs are candidates for surgical intervention [13]. These few surgical cases only include three CPT codes for TMJ arthroplasty, compared to ten for knee arthroplasty. As therapeutics are developed, specifically those for late-stage pathology, it is likely that the

number of CPT codes and surgical TMD cases will increase [286, 287]. CPT codes for these indications will need to be sufficiently supported by science for third party reimbursers to support payment for the procedures. Furthermore, additional CPT codes specifying indications for late-stage pathology may further bolster medical insurance support (i.e., as compared to dental insurance). Additionally, following the specificity seen in CPT codes for the knee as a template, progress is also needed in delineating CPT codes for early-stage TMDs to support non-surgical treatment. Finally, specific terminology delineating between the various muscle and joint problems would be a step toward dismantling the umbrella term “TMD.” This would clarify communication among researchers, physicians, and patients, improving granularity in treatment algorithms, and garnering support for TMDs for treatment under medical insurance as opposed to dental insurance. A recent example of this is the recommendation provided by the International Research Diagnostic Criteria for Temporomandibular Disorders Consortium Network and Orofacial Pain Special Interest Group which attempts to delineate among the various myogenous and arthrogenous conditions [6], but this report has been deemed to fall short [333]. Additional work is needed in order to delineate the term further and identify appropriate indications. As more entrepreneurial ventures are established, a larger market for therapeutics indicated for specific, end-stage TMDs will arise, laying the groundwork for the TMJ commercial landscape.

Implementing industry guidance for treatment of TMJ cartilages

As scientific entrepreneurs establish TMJ startup companies, they will look to regulatory agencies for guidance. The FDA has previously given specific guidance for products intended to repair or replace knee cartilage, with specific recommendations to establish safety and efficacy [37]. Analogous FDA guidance for the TMJ is necessary if new cartilage products are to emerge; to this end, the knee cartilage guidance document may serve as a template for the TMJ. Specific considerations, such as proximity to crucial sensory structures, the mechanical loading

environment of the joint, and appropriate animal models, should be included. Defining regulatory jurisdiction would also be helpful by delineating various types of therapeutics (e.g., drug, biologic, device, or combination product), not only for the TMJ but also the knee. Autologous materials have been used in the past for the TMJ [16], but recent animal studies suggest that allogeneic approaches are also safe [23]. Assays required to show safety for allogeneic approaches compared to autologous approaches may be considered. Due to the dearth of precedent for both the knee and TMJ, the FDA might consider providing early communication and advice through existing designations and programs, such as Breakthrough and Fast Track designations and Priority Review and Accelerated Approval programs, as applicable to product sponsors. Additionally, establishing regulatory guidance in the benchtop and preclinical phases of the translational paradigm would be useful. For example, for NIH-funded grants with animal studies, perhaps the FDA and the appropriate NIH institute could collaborate to provide early regulatory advice to the principal investigator. This guidance and support would undoubtedly improve the success of translational TMJ research.

Conclusion

The nature of translational research is inherently arduous, with many choke points frequently leading to a vicious cycle (Figure 3-3). However, there are just as many possibilities to break this cycle. As the NIDCR moves forward with funding various projects, they should consider funding TMJ cartilage-specific grants to encourage focused research in the field. While current support at the R-series level is insufficient (Table 3-1), early career researchers are well funded through F-series mechanisms, which bodes well for the future of the TMJ field. Increasing funding and outreach for such mechanisms while maintaining success rates would be beneficial to the field. For surgical trainees, bolstering the number of TMJ cases encountered throughout residency, developing TMJ surgical fellowships, and encouraging clinicians to apply for F30/K08 awards will increase the supply of TMJ-specific OMF surgeons to perform technically

challenging cartilage procedures and explore the clinical efficacy of new therapeutics. Clarification of indications and treatments for TMDs through a national registry will be of great value to entrepreneurs attempting to translate technologies. By doing so, markets for such technologies will arise so that additional CPT codes specific to cartilage indications will be established, enabling additional insurance coverage for TMDs. Finally, guidance published by the FDA will enable translational studies to support safety and efficacy of TMJ cartilage products, especially tissue-engineered implants. These documents should include specific considerations for TMJ cartilages such as proximity to crucial structures and timely guidance for nascent products. Similar approaches and suggestions have resulted in the development and translation of tissue-engineered products for knee cartilages and can thrust the TMJ field forward. With knee orthopaedics as a template, the TMJ field can make great strides toward ameliorating the symptoms that millions of TMD patients experience on a day-to-day basis, drastically improving their quality of life.

Chapter 4: Long-term Safety and Efficacy of Temporomandibular Joint Disc Regeneration in the Yucatan Minipig[4]

Abstract

Up to 25% of the US population exhibits symptoms of temporomandibular joint (TMJ) disorders (TMDs). A subset of those include disc perforations, which can develop as a result of disc displacement. Toward addressing the disc perforation indication, the objective of this study was to examine the long-term safety and efficacy of tissue-engineered implants derived from allogeneic costal chondrocytes in the Yucatan minipig toward healing TMJ disc perforations of 3 mm in diameter. It was hypothesized that implants would not elicit a significant systemic or local immune response, and implant-treated discs would exhibit superior healing, with significantly higher functional properties compared to empty defect controls. After 24 weeks, implants were well-tolerated. Systemically, there was no response as evidenced by complete blood count and comprehensive metabolic panel parameters, and implant-treated discs exhibited a local immune response of T cells, B cells, and macrophages that dampened after 8 weeks. Implant-treated discs appeared to heal better than controls. When testing the repair tissue of implant-treated discs and the fill tissue of empty defects under uniaxial tension, repair tissue was 6.2-times tougher, 8.9-times more resilient, 3.4-times stronger, and had a 2.5-times higher strain at failure compared to fill tissue. Additionally, collagen type I and collagen type III were significantly higher and lower in repair tissue compared to fill tissue of controls. These values in implant-treated discs, 99.4% and 103.1% of native tissue values, respectively, indicated more native-like regeneration, unlike scar tissue in control discs. Overall, tissue-engineered implants proved to be safe and efficacious for healing TMJ disc perforations, establishing the translational potential of neocartilage implants for addressing discal TMD indications.

[4] **Chapter in preparation for submission as:** Donahue, R.P., Bielajew, B.J., Vapniarsky, N., Heney, C.M., Arzi, B., Hu, J.C., Athanasiou, K.A. Long-term safety and efficacy of temporomandibular joint disc regeneration in the Yucatan minipig. For submission in *Nature Biomedical Engineering*.

Introduction

The temporomandibular joint (TMJ) is a ginglymoarthrodial joint involved in speaking, chewing, and breathing [16]. Temporomandibular disorders (TMDs), a group of ailments affecting the joint and surrounding structures, symptomatically affect between 5-25% of the US population [1-5], are the second most common musculoskeletal condition in the US [16], and cost the US healthcare system up to $4 billion per year [6]. Pathologies of the TMJ disc, a fibrocartilaginous structure between the temporal bone of the skull and mandible, are central to TMDs. These pathologies include disc displacement, which can lead to disc thinning developing into disc perforation. It has been reported that approximately 70% of all TMD cases involve disc displacement [7], where the disc is mispositioned relative to its normal anatomic location. Concurrently with or independent of displacement, disc thinning and perforation can also occur. Up to 15% of displaced discs develop perforations, affecting up to 9 million people in the US alone [8-10]; thus, disc perforations are a significant clinical indication. While not all discal TMDs require medical intervention, a large portion of them cause intractable day-to-day pain and dysfunction.

Unlike joints such as the knee where there are established algorithms for treatment of cartilage afflictions, current treatments for discal TMDs are not well-defined [11]. Generally, treatment options depend on severity of the disc condition [12]. For example, analgesics, mechanical stabilizers, and some arthroscopic procedures may be suitable for early-stage cases [11], but open surgical procedures are reserved for the most severe cases, with only 5-10% of TMD patients being candidates for surgery [13, 14]. Discectomy and total joint replacements are plagued with the need for revision surgeries due to joint degradation after disc removal and young patient age coupled with average joint replacement lifetime [16]. Currently, there is no suitable intermediate solution between noninvasive and late-stage surgical interventions for the TMJ disc that can significantly halt progression of TMJ disc pathologies or regenerate damaged

tissues. Thus, the field would benefit from new interventions that would provide a long-term alternative to joint replacements.

Tissue engineering has gained traction as a long-term solution to discal TMDs. Tissue-engineered implants for TMJ disc regeneration must withstand joint loading, especially under high tensile strains [32]. Recently, several orthotopic preclinical studies examining safety and efficacy of tissue-engineered implants in large animal models have been performed. For example, a recent study investigated poly(glycerol sebacate) and gelatin scaffolds toward regeneration of osteochondral defects in the goat mandibular condyle [336]. Work in the TMJ discs of Yucatan minipigs also showed success in healing disc thinning defects using scaffold-free, self-assembled neocartilage [23]. For large animal models, the minipig has recently emerged as the gold-standard for preclinical studies in the TMJ [76] due to its similarities in anatomy, biochemical and mechanical properties, diet, and joint loading [24].

A major challenge in cartilage tissue-engineering is cell sourcing. Numerous cell sources have been investigated as alternates to directly harvesting TMJ chondrocytes due to issues such as donor site morbidity and potential harvest of diseased cells from TMD-affected tissues unsuitable for tissue engineering [337]. For example, due to their vast availability and expansion capabilities, mesenchymal stem cells derived from bone marrow have been used with 3D-printed TMJ disc scaffolds as a potential replacement [145]. Previously, costal cartilage has been used for autologous replacement of the TMJ disc [184], motivating the use and investigation of costal chondrocytes as a cell source. Costal chondrocytes are more abundant and more easily harvested than other chondrocyte sources, including both TMJ chondrocytes and knee articular chondrocytes, and have been shown to create robust neocartilage implants [16, 338]. Additionally, previous work examined the feasibility of using an allogeneic approach with costal chondrocytes in the Yucatan minipig, resulting in healing of TMJ disc thinning defects [23]. Therefore, costal chondrocytes have been proven to be a suitable cell source for TMJ disc tissue engineering.

Our recent study showed short-term (i.e., 8-week) safety and efficacy of a nonhomologous, allogeneic approach using costal chondrocyte-derived implants in the Yucatan minipig TMJ disc [23]. Using self-assembled neocartilage implants, TMJ disc thinning (i.e., partial thickness) defects successfully healed without a significant local or systemic immune response, indicating immunogenic tolerance to an allogeneic donor source. Additionally, there was 4.4-times greater defect closure in implant-treated groups compared to empty defect controls, and the osteoarthritis (OA) score was 3.0-times higher (indicative of a worse clinical outcome) in controls compared to implant-treated groups. Importantly, implants facilitated mechanically robust healing, resulting in 3.4-times stiffer repair tissue (tissue filling in the implant-treated defect) compared to empty defect fill tissue (tissue filling in the control defect). Additionally, intralaminar fusion (measuring the integration of the two laminae of the pocket) was 3.2-times stiffer when treated with an implant. Given these promising results, additional research into the capabilities of self-assembled implants to heal TMJ disc perforations (i.e., full thickness defects), further down the degenerative pathway compared to thinning defects, is essential given the widespread prevalence of TMJ disc perforations in human populations.

Driven by success in disc thinning models and the pervasiveness of disc perforations, the objective of this study was to validate the long-term (i.e., 24-week) safety and efficacy of self-assembled neocartilage implants derived from allogeneic costal chondrocytes in perforation defects of the Yucatan minipig TMJ disc. It was hypothesized that 1) compared to untreated empty defect controls, implant-treated discs would heal with repair tissues that have a collagen profile more consistent to native TMJ discs, and 2) repair tissues of implant-treated discs would exhibit superior mechanical properties compared to control fill tissue. Additionally, it was hypothesized that the extracellular matrix of the neocartilage implants would remodel toward that of native TMJ discs. Finally, it was expected that implants would not elicit a significant systemic or local immune response. Upon completion of this study, substantial preclinical data

will be generated toward translation of self-assembled neocartilage implants for eventual human use.

Results

Tissue-engineered implants approached native tissue values, and the intralaminar perforation surgical technique secured tissue-engineered implants in the Yucatan minipig TMJ disc

Implants were fabricated from donor costal cartilage for a nonhomologous, allogeneic approach in the Yucatan minipig TMJ disc (Figure 4-1A). Specifically, costal chondrocytes harvested from the minipig rib underwent three passages [149] to an expansion factor of 64 and were placed into aggregate rejuvenation for 11 days prior to self-assembly [25]. During the self-assembling process (Figure 4-1B), chondrocytes were treated with bioactive factors and passive axial compression [201], previously shown to improve functional properties [23, 201]. Implants (originally 8x13 mm) were trimmed to approximately 8x8 mm (Figure 4-1C) for use in the intralaminar perforation surgical technique (Figure 4-2). Prior to implantation, implants exhibited matrix staining for glycosaminoglycans (GAGs) via safranin O staining with fast green counterstain (SO/FG) and collagen via picrosirius red staining (PSR) with cells being homogeneously distributed after 28 days of self-assembly as seen through hematoxylin and eosin staining (H&E) (Figure 4-1D), consistent with prior studies [339]. Prior to surgery, the implants' mechanical properties were as follows: tensile Young's modulus of 7.05±1.39 MPa, ultimate tensile strength (UTS) of 2.28±0.45 MPa, compressive 20% relaxation modulus of 177±55 kPa, and compressive 20% instantaneous modulus of 777±115 kPa, similar to the mechanical properties of the native minipig TMJ disc [24]. Thus, these implants were considered suitable for implantation into perforation defects in the Yucatan minipig in both short-term pilot studies and long-term safety and efficacy studies (Figure 4-1A).

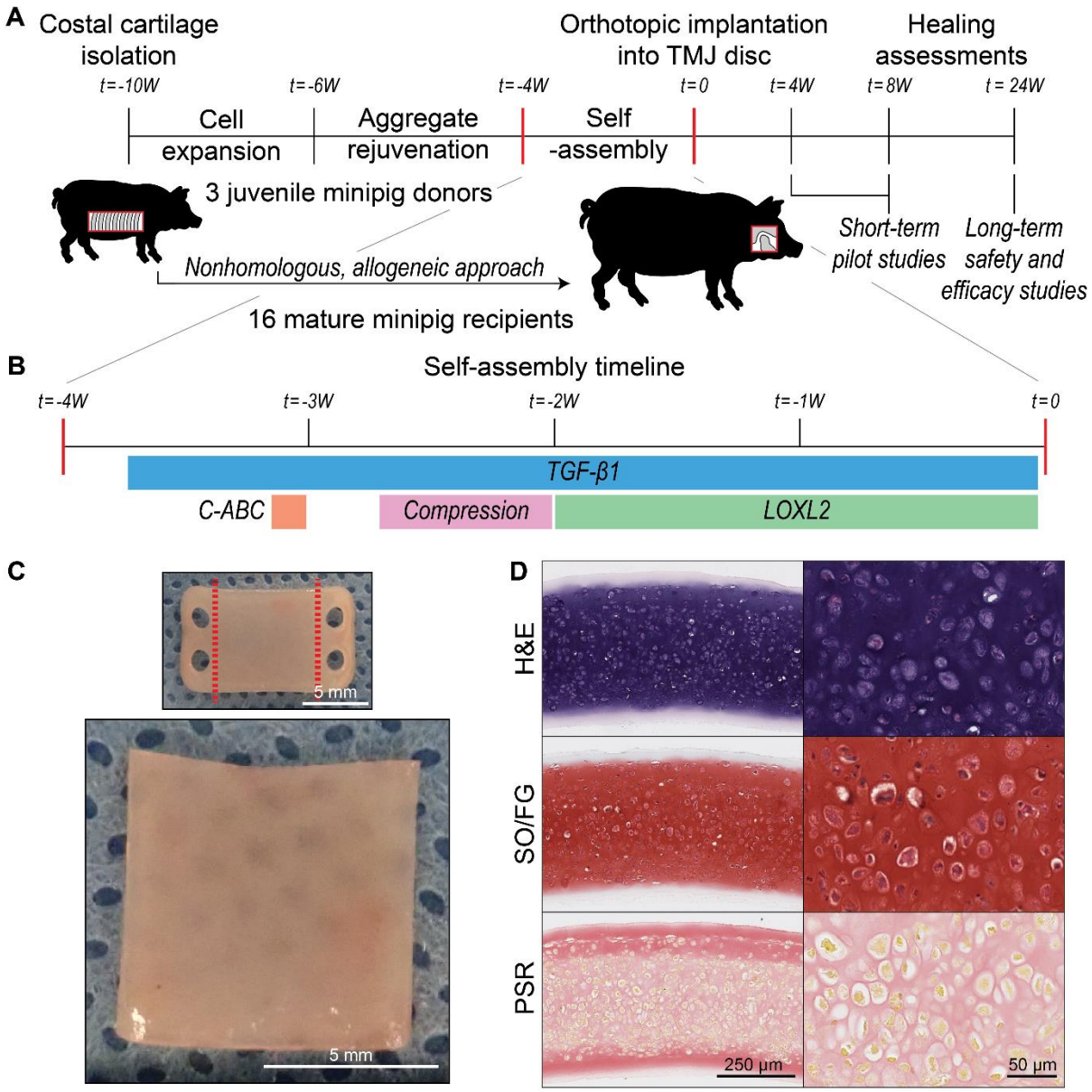

Figure 4-1: Neocartilages were fabricated using the self-assembling process and exhibited robust matrix content for implantation into the TMJ disc.
(A) After costal cartilage isolation from three juvenile minipigs, chondrocytes underwent expansion, aggregate rejuvenation, and self-assembly prior to nonhomologous, allogeneic implantation into the TMJ disc. After implantation, minipigs were euthanized and assessed for healing in the short-term or long-term studies. (B) The self-assembling process included addition of bioactive factors, such as transforming growth factor beta 1 (TGF-β1), chondroitinase ABC (C-ABC), and lysyl oxidase-like 2 (LOXL2), and passive axial compressive to improve the functional properties of implants. (C) The original implant (8x13 mm) was trimmed to 8x8 mm for implantation. (D) The implant exhibited homogenous chondrocyte distribution in the matrix, seen in hematoxylin and eosin staining (H&E), and staining with safranin O staining with fast green counterstaining (SO/FG) and picrosirius red staining (PSR) showed glycosaminoglycan and total collagen distribution, respectively.

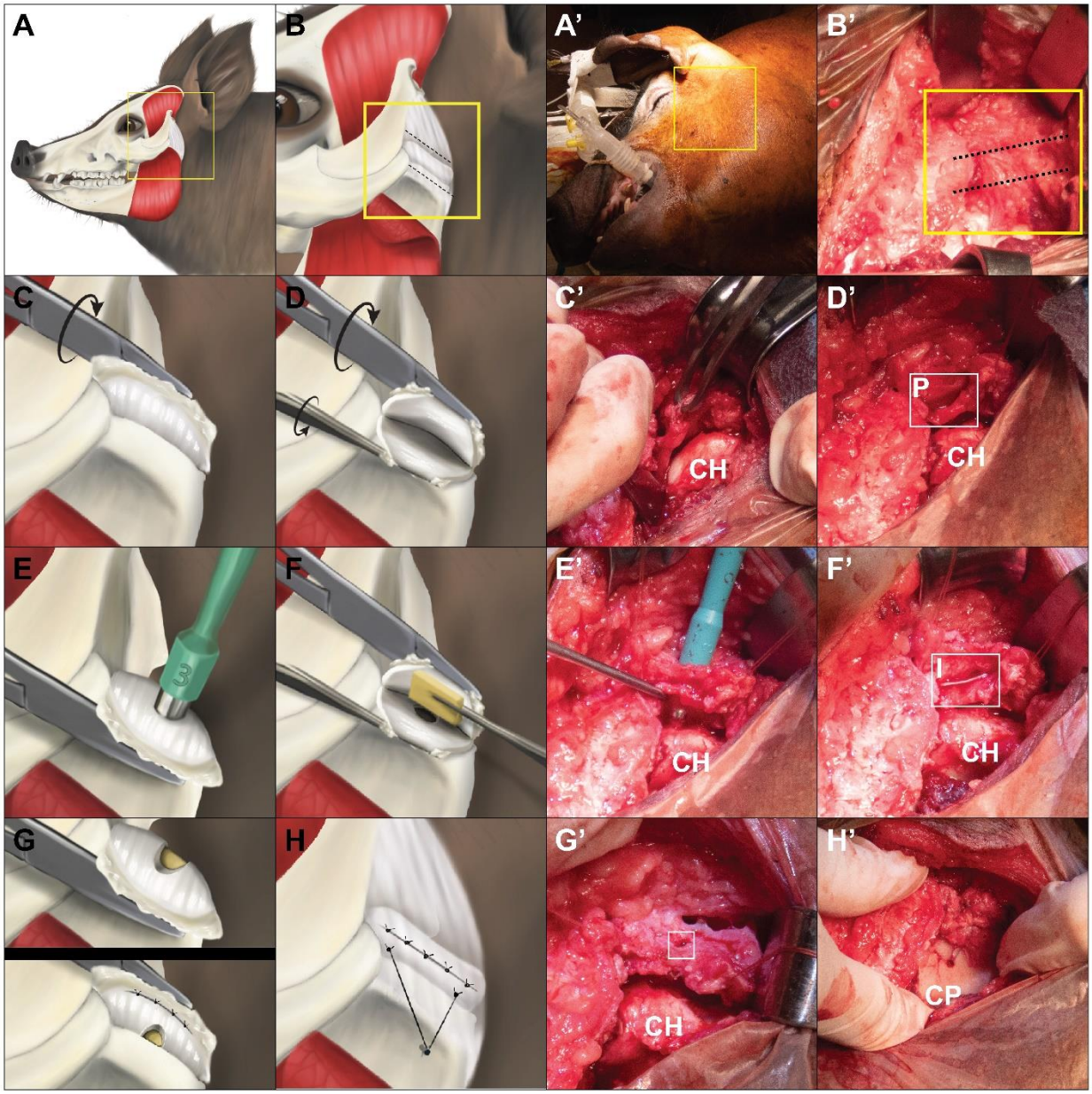

Figure 4-2: The intralaminar perforation surgical technique secured tissue-engineered implants in perforation defects.
(A) The animal was prepared for surgical intervention, and (B) the TMJ was identified (dashed lines). (C) Upon freeing the TMJ disc, the condylar head (labeled as "CH") was identified, and the superior and inferior joint spaces were clearly visible. (D) The incision was created, and the pouch ("P") was deepened, where the implant was placed. (E) The 3 mm diameter perforation defect was created with a disposable biopsy punch. (F) The implant ("I") was placed in the pocket, and (G) the pocket was sutured shut along the lateral edge. Upon rotation, the defect (white box) was present on the superior surface of the disc. (H) The lateral portion of the disc was attached back to the condylar process ("CP") with a double-armed Mitek bone anchor.

The intralaminar perforation surgical technique has been previously described and used to secure implants in the TMJ disc (Figure 4-2) [23]. Here, the surgical approach was altered

from a disc thinning (i.e., one-sided or partial thickness) defect model to a perforation (i.e., two-sided or full thickness) defect model. Using a preauricular approach, the TMJ disc was identified, and a horizontal incision in the disc was created (Figure 4-2A-D). A perforation defect was then made in the centrolateral region of the disc with a 3 mm diameter disposable biopsy punch, and the implant was placed in the horizontal pocket (Figure 4-2E-F, Supplementary Figure 4-1). The incision was sutured shut on the lateral edge of the disc, avoiding placement of sutures on the disc articulating surface, and the lateral aspect of the disc was attached to the condylar process using a Mitek bone anchor (Figure 4-2G-H). This surgical technique effectively secured the implant in place without the need for sutures on the articulating surfaces of the TMJ disc, avoiding stress concentrations which have been shown to cause degradation of the articular surfaces [340].

Perforation defects in the TMJ disc healed with tissue-engineered implants

Initial pilot studies at 4 and 8 weeks demonstrated efficacy of healing perforation defects with tissue-engineered implants. All four minipigs (n=2 animals/timepoint) exhibited complete defect closure (Supplementary Figure 4-2). Moving forward, a statistically driven safety and efficacy study examining the long-term healing of perforation defects in the TMJ disc consisting of 12 animals (n=6/group, with implant-treated and empty defect control groups) was performed. After 24 weeks, all six implant-treated discs exhibited complete repair tissue fill (Figure 4-3A, Supplementary Figure 4-3). In comparison, control discs also had some degree of tissue fill, as seen in images depicting their gross morphologies; one of the six discs still had defects present on the superior and inferior surfaces of the disc (Figure 4-3A, Supplementary Figure 4-3). Control discs appeared worse in gross morphology images than implant-treated discs, exhibiting surface abrasions on the superior surfaces of the discs (Figure 4-3A). This same morphology was found only in the worst-cases of the implant-treated group (Figure 4-3A, Supplementary Figure 4-3). Opposing condylar surfaces also presented a heterogeneous response to surgical

intervention (Supplementary Figure 4-4). When quantifying the osteoarthritic changes on the articulating surface of the condyle via a modified ICRS score, there was no significant difference between the two groups (Supplementary Table 4-1). Although there were some condylar changes, this was most likely due to the suture rubbing on the condyle over the study length.

When assessing anteroposterior cross sections of the discs, controls did not completely heal along the entire incision (Figure 4-3B). In contrast, a majority of implant-treated discs exhibited complete healing in the central biconcave portion of the disc (Figure 4-3B). When testing the intralaminar fusion between the two laminae under tension in the superoinferior direction, it was noted that there were no significant differences between the groups (Supplementary Table 4-2). When examining implant location via histology, all discs that received tissue-engineered implants had posterior migration of the implant (Figure 4-3B) compared to the original centrolateral implantation site and defect location (Supplementary Figure 4-1). This is most likely due to the biomechanical loading of the joint during articulation, which applies compressive loads to the disc transmitted through the condyle. When these compressive forces are applied in the center of the TMJ disc, it develops high tensile strains in the periphery of the disc, causing the implant to migrate into the thicker portion of the posterior band. The H&E staining of the areas surrounding implants revealed a cellular response after 24 weeks; the implant was surrounded by cells from the host response, compared to the control which remained open and lacked any cellular response (Figure 4-3B). Despite the varied healing responses in the two groups, implant-treated discs exhibited more robust gross morphologic healing.

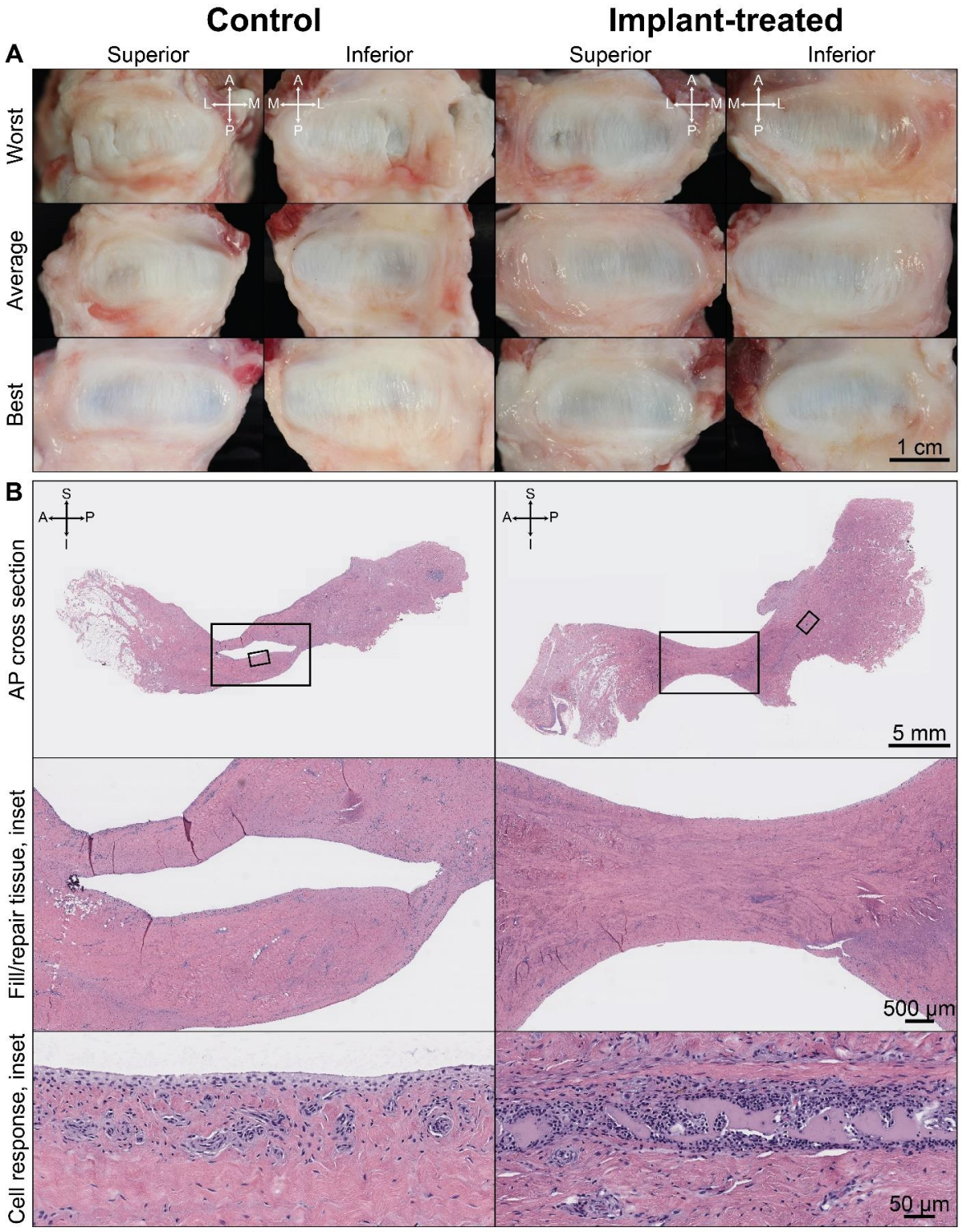

Figure 4-3: Gross morphology and histological cross sections of TMJ discs showed lack of complete healing in controls and repair tissue in implant-treated groups.
(A) All six implant-treated discs appeared better than controls. (B) When examining anteroposterior (AP) cross sections of the TMJ discs, the incision did not completely heal in controls. In implant-treated discs, which did completely heal with repair tissue, there was a cellular host response to the implant, while control discs remained open and lacked a cellular response. A, anterior, I, inferior, L, lateral, M, medial, P, posterior, S, superior.

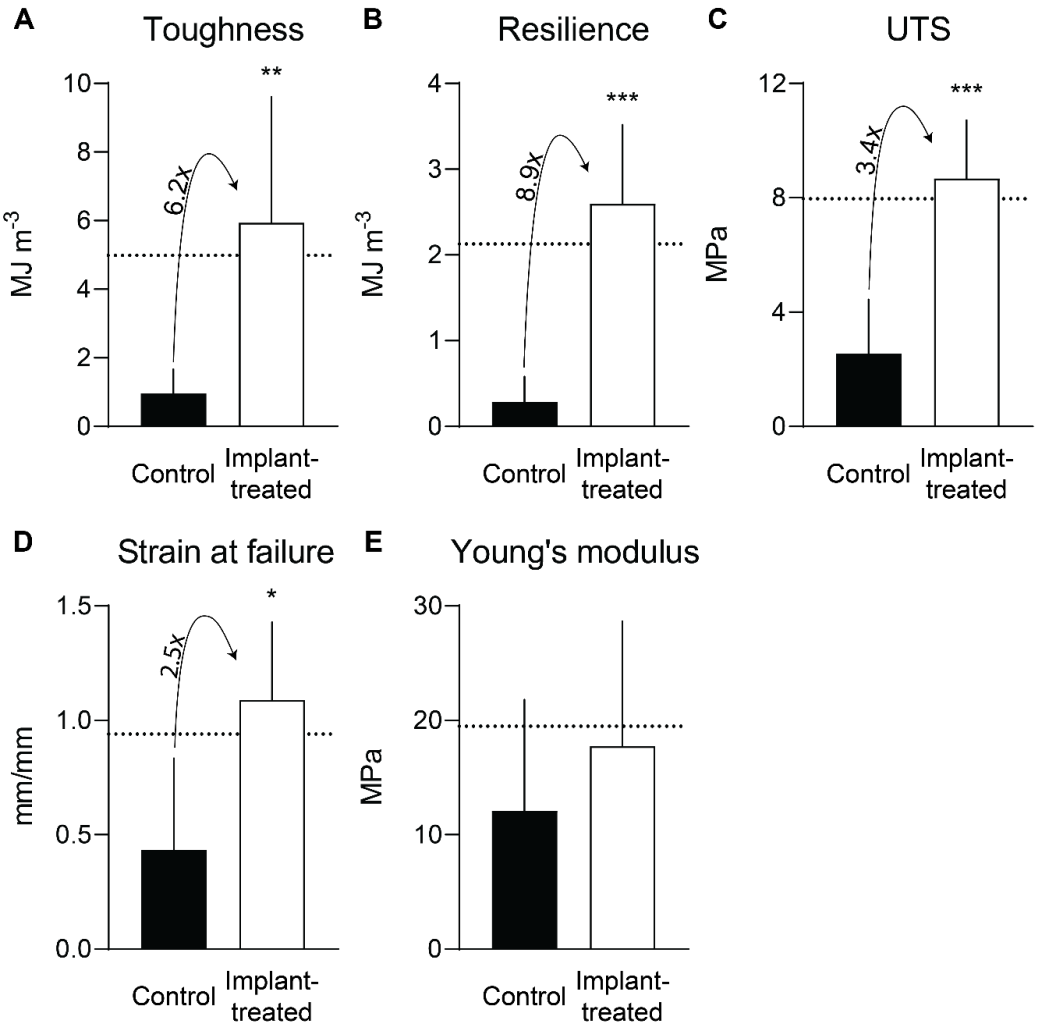

Figure 4-4: Tensile properties of repair tissue of implant-treated discs were higher compared to fill tissue of controls.
When compared to fill tissue of control discs, repair tissue had a (A) 6.2-times higher toughness, (B) 8.9-times higher resilience, (C) 3.4-times higher ultimate tensile strength (UTS), and (D) 2.5-times higher strain at failure. (E) Young's modulus of repair tissue trended up with implant treatment but was not significantly different to control fill tissue. Dashed lines represent native TMJ disc values.

Tissue-engineered implants facilitated regeneration of mechanically robust repair tissue that reached native TMJ disc tensile properties

Despite a heterogeneous gross morphological healing response, tissue-engineered implants facilitated robust healing when compared to controls, as indicated by multiple statistically significant outcome measures on disc function. The tissues that filled in the defects in the centrolateral portion of the disc were tested under uniaxial tension to determine toughness,

resilience, UTS, strain at failure, and tensile Young's modulus (Figure 4-4). Implant-treated discs exhibited repair tissue values above 90% of contralateral control disc values (dashed lines), while fill tissue values in controls were under 50% of native tissue values for every measure except tensile Young's modulus (Figure 4-4). Importantly, repair tissue of implant-treated discs was 6.2-times tougher, 8.9-times more resilient, 3.4-times stronger, and had a 2.5-times higher strain at failure than control fill tissue, all of which were statistically significant (Figure 4-4A-D). While Young's modulus trended upwards with implant treatment, this difference was not significant (Figure 4-4E). Ultimately, tissue-engineered implants resulted in more robust repair tissue compared to the fill tissue found in control discs.

Repair tissue of implant-treated discs mimicked the native TMJ disc biochemical content

Mechanical properties develop from structure-function relationships with the extracellular matrix of TMJ discs. Collagen is the major component of the TMJ disc, encompassing more than 90% of the dry weight (DW) of the disc (dashed line, Figure 4-5A). When comparing to fill tissue of controls, the total collagen content of repair tissues of implant-treated discs trended upwards toward native TMJ disc values (Figure 4-5A), but this trend was not significant. However, significant differences emerge among the tissues when analyzing individual collagen subtypes. Collagen type I, the main collagen type found in the TMJ disc, was significantly lower per total protein (PROT) content in fill tissue of controls compared to repair tissue (Figure 4-5B). The repair tissue contained 99.4% of native tissue collagen type I, indicating the regenerative capacity of the tissue-engineered implants. Additionally, mature pyridinoline (PYR) and immature dihydroxylysinonorleucine (DHLNL) crosslinks in the repair tissue of the implant-treated group also were on par with native tissue crosslink content (Supplementary Table 4-3). In contrast, collagen type III was 53.9% lower in repair tissue of implant-treated discs than in fill tissue of controls, which contained 2.2-times more collagen type III than native TMJ disc (Figure 4-5C). Because collagen type III is associated with scarring [341], it is possible that the lower

mechanical properties of the control fill tissue resulted from scar tissue formation; scar tissues have previously been shown to have inferior mechanics compared to healthy tissues [342]. The full bottom-up proteomics results for fill and repair tissues are reported in Supplementary Table 4-4. Overall, repair tissue from implant-treated discs displayed a matrix composition biomimetic to native TMJ discs, unlike the inferior scar-like tissue of control discs.

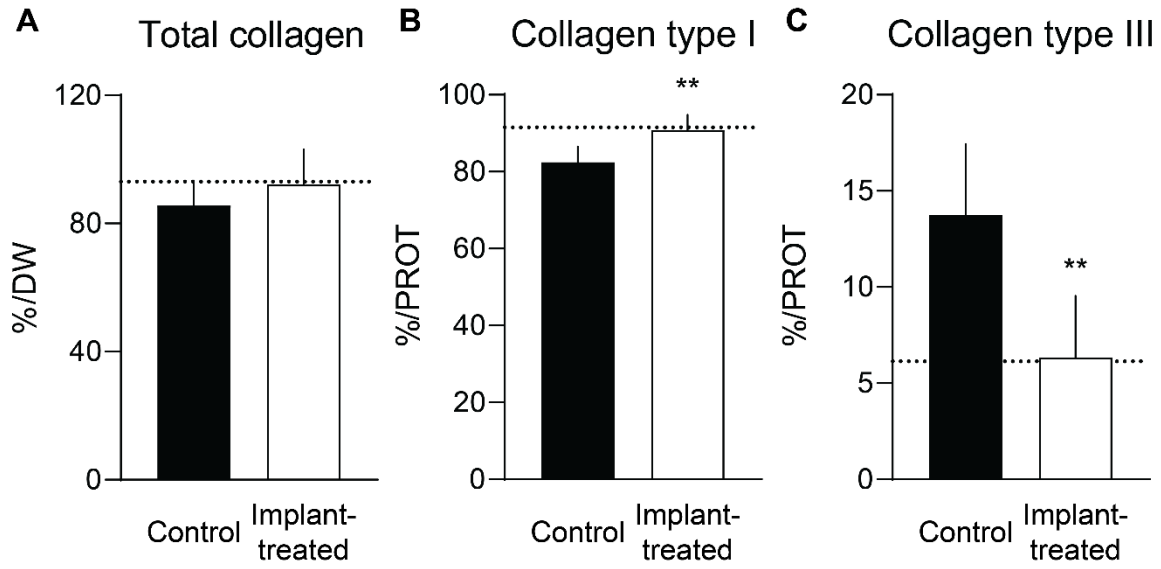

Figure 4-5: Collagens in the matrix of repair tissue was reminiscent of native TMJ disc content.
(A) Total collagen per dry weight (DW) was not significantly different between the two groups but trended upwards in implant-treated discs. In the control group, (B) there was less collagen type I per total protein (PROT) and (C) more collagen type III per PROT, indicative of a scar-like tissue. In contrast, implant-treated discs exhibited native-like regeneration of collagen type I in their repair tissue. Dashed lines represent native TMJ disc values.

Implantation of tissue-engineered neocartilages resulted in no abnormal systemic effects

Following surgery, animals were returned to their pens and examined daily for behavior and food intake. Within 2 hours of surgery, animals were alert and ambulating. In the days following surgery, animals were provided a soft diet and water bowls as opposed to spigots to minimize joint loading. Throughout the study, jaw function continued, and minipigs maintained or gained weight. Animals were then euthanized at the predetermined timepoint (i.e., 4, 8, or 24 weeks). Full body necropsy was then performed to examine signs of toxicity due to the implant. All organ systems including the integumentary, cardiovascular, respiratory, musculoskeletal (other than

the TMJ), digestive, urogenital, endocrine, and nervous systems displayed normal morphology and exhibited no signs of cellular damage, inflammation, or neoplastic growth.

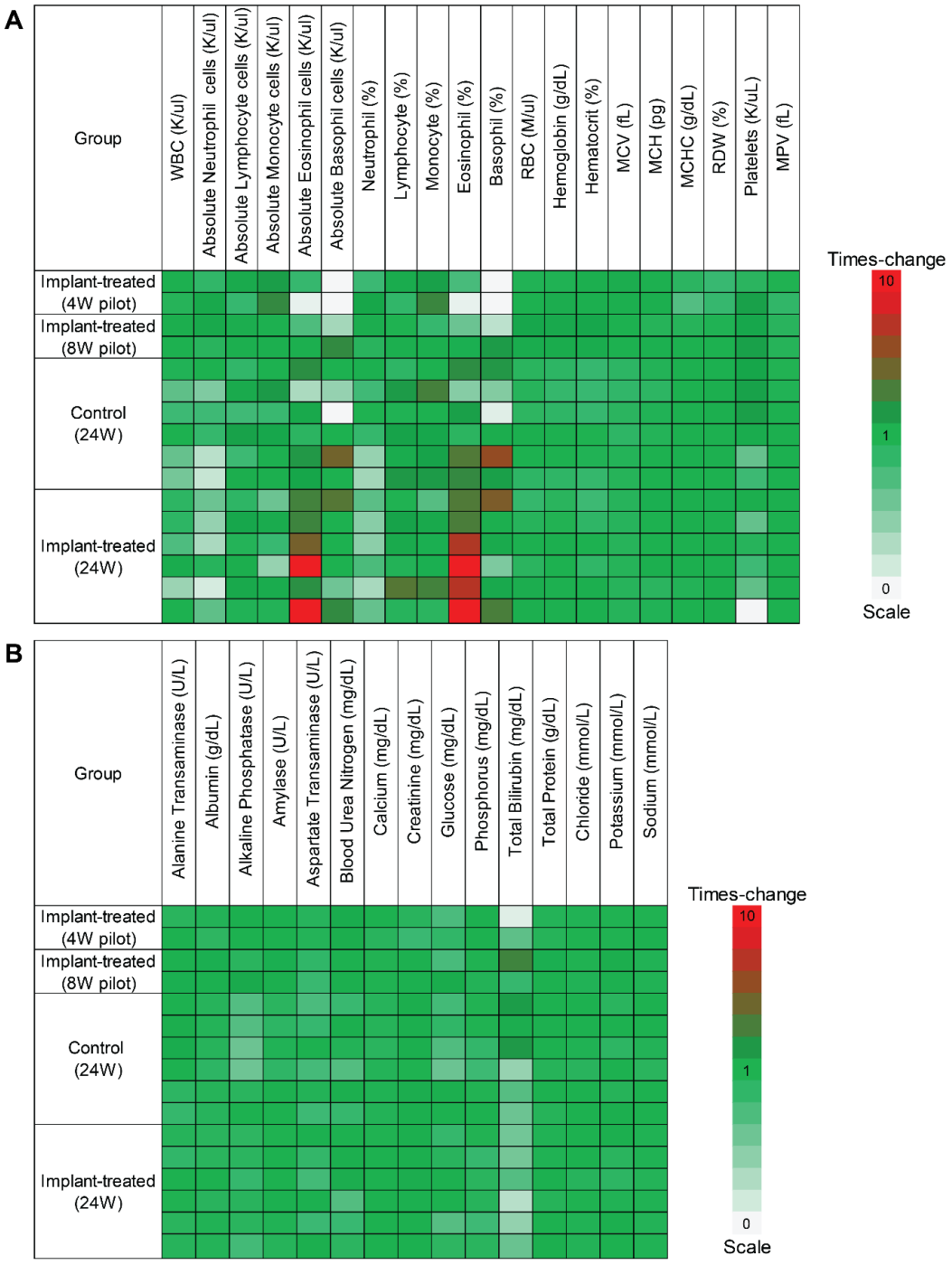

Figure 4-6: Heatmap of normalized complete blood count and comprehensive metabolic panel parameters show no abnormal systemic effects.
(A) The complete blood count and (B) comprehensive metabolic panel parameters were normalized to the pre-operative values. Each row represents a different animal. Eosinophils and basophils showed some large changes from pre-operative values but could not be attributed to implant treatment.

To examine the systemic response to tissue-engineered implants, a complete blood count and comprehensive metabolic panel were performed (Figure 4-6, Supplementary Table 4-5). Implants were well-tolerated with little to no differences in white blood cell counts from baseline values (WBC column, Figure 4-6A). A few animals exhibited large increases in eosinophils in the implant-treated group (Figure 4-6A), indicating eosinophilia, but the direct cause could not be directly attributed to implant treatment. Specifically, it was noted that little to no eosinophils were found in histological sections of implant-treated animals (Figure 4-3, Figure 4-7), suggesting a cause other than implant treatment. Otherwise, all blood count parameters were within normal ranges (Supplementary Table 4-5). In the comprehensive metabolic panel, all values were within normal limits, and little to no differences were observed for all analytes (Figure 4-6B). Overall, tissue-engineered implantation did not result in any adverse systemic effects.

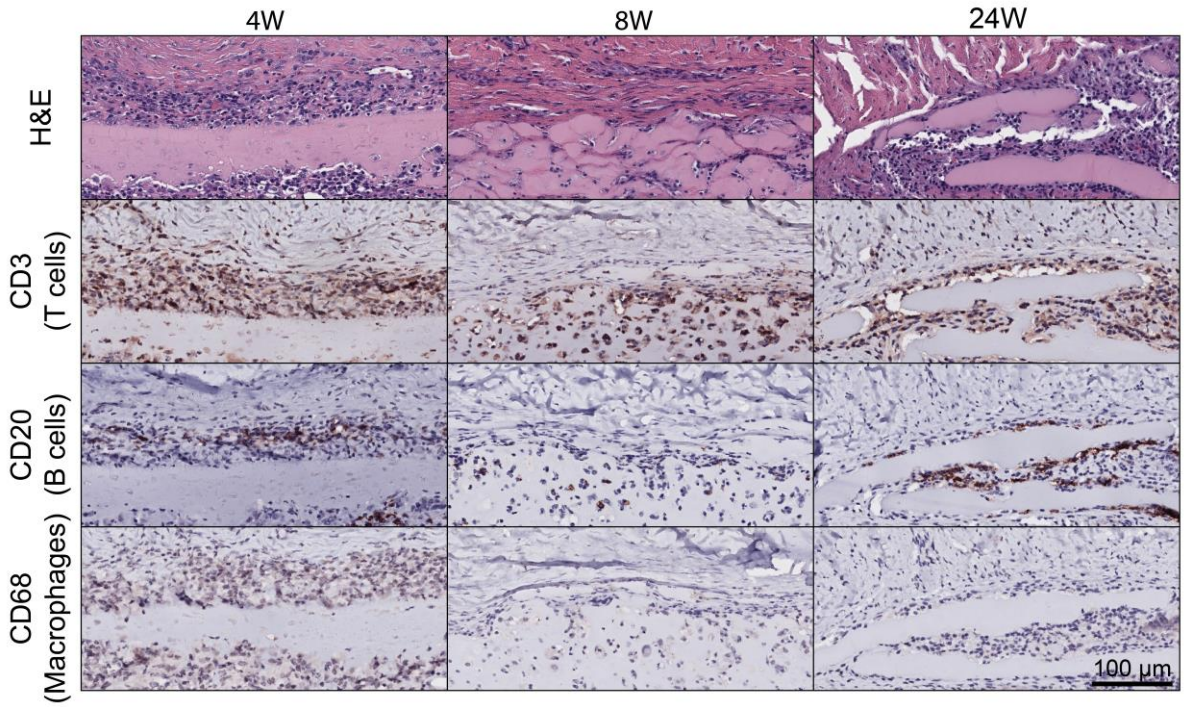

Figure 4-7: Immunohistochemical staining for T cells, B cells, and macrophages showed immunogenic tolerance to tissue-engineered implants.
Over time, cellularity decreased as seen in H&E, while T cell (CD3) and B cell (CD20) staining remained relatively consistent. CD68 staining for macrophages decreased.

Tissue-engineered implants were well-tolerated immunologically

After surgery, acute joint swelling occurred for every animal, consistent with surgical intervention of the TMJ. After 2 weeks, joint swelling subsided in both groups, and all incisions were completely healed upon suture removal. The incision site had minimal scarring present at animal euthanasia. After euthanasia, TMJs were excised *en bloc* for examination and analysis, and there was no sign of inflammation or neoplastic growth. In all animals, the joint capsule was intact and appeared morphologically normal. The synovium appeared normal, and synovial fluid volume was minimal and clear in color, similar to a healthy joint. Histologically, the synovium showed no abnormal cellular response and was nonreactive in both control and implant-treated joints (Supplementary Figure 4-5).

When examining the local immune response to tissue-engineered implants in the TMJ disc, cellularity around the implant generally decreased over time between 4 and 8 weeks, while animals at 24 weeks exhibited similar overall cellularity compared to animals after 8 weeks (Figure 4-7), indicating that the animals were reaching a steady state in terms of the immune response to the implant. Specifically, when considering immunohistochemical staining for CD3 (T cells), CD20 (B cells), and CD68 (macrophages) (Figure 4-7) with the appropriate positive and negative controls (), it became apparent that immune cells were mounting a response to the implant. Specifically, T cells and B cells were sustained throughout all timepoints, being located around the periphery of the implant (Figure 4-7). However, macrophage numbers generally decreased over time (Figure 4-7). Additionally, through H&E staining, no multinucleated giant cells, polymorphonuclear cells, or capsule formation were noted (Figure 4-7). Thus, implants were well-tolerated immunogenically over time.

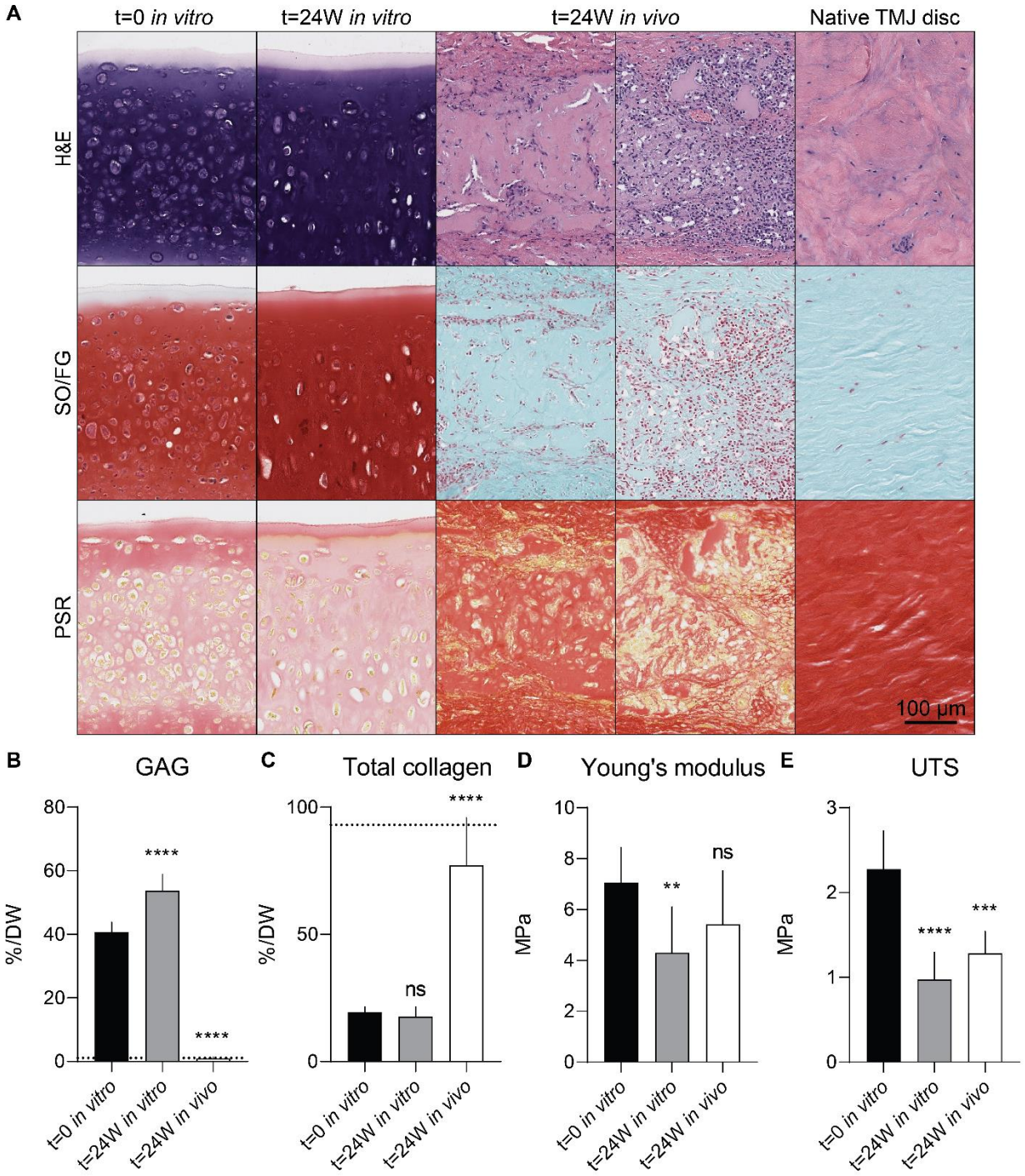

Figure 4-8: Histological and biochemical properties of neocartilages after implantation showed remodeling toward native TMJ discs.
(A) In terms of matrix content, safranin O staining with fast green counterstaining (SO/FG) and picrosirius red staining (PSR) followed quantitative trends of (B) glycosaminoglycan (GAG) content and (C) total collagen content. (D) Young's modulus and (E) ultimate tensile strength (UTS) also decreased across extended culture. Dashed lines represent native TMJ disc values. ns, not significant.

Tissue-engineered implants remodeled to a native-like tissue

Tissue-engineered implants remodeled after 24 weeks to a native-like tissue. Compared to *in vitro* controls cultured alongside the study, the *in vivo* implants after 24 weeks exhibited matrix components reminiscent of a native TMJ disc; GAG content (stained by SO/FG) drastically decreased while collagen content (stained by PSR) increased (Figure 4-8A). GAG and collagen content of *in vivo* implants after 24 weeks were 87.1% and 82.8% of native tissue values (indicated by dashed lines), significantly lower and higher, respectively, when compared to t=0 *in vitro* controls (Figure 4-8B-C). *In vitro* implants cultured for another 24 weeks after implantation were not significantly different in collagen content compared to values at implantation (Figure 4-8C). Remodeling toward a native-like tissue is further corroborated when examining analytes from bottom-up proteomics (Figure 4-9, Supplementary Table 4-4). For example, the implant was initially high in collagen type II (64.54±3.36%/PROT), which was remodeled toward the native TMJ disc content, having 88.29±5.55%/PROT collagen type I and 0.21±0.13%/PROT collagen type II after 24 weeks of implantation (Figure 4-9A-B). Collagen type III, which is present in low levels in the native TMJ discs due to colocalization with collagen type I, also rose to 8.73±3.36% in implants after 24 weeks *in vivo* (Figure 4-9C). Aggrecan, biglycan, and link protein all were drastically lower in *in vivo* implants compared to *in vitro* controls, similar to native TMJ discs (Figure 4-9E-G). Histone H4, involved with chromatin structure, decreased by 86.7% after implantation *in vivo* (Figure 4-9H), which was consistent with the decrease in cellularity of the implant observed in H&E staining (Figure 4-8A).

For mechanical properties, Young's modulus and UTS significantly dropped 39.0% and 57.2% after 24 weeks of *in vitro* culture, but *in vivo* implants only dropped significantly by 43.6% in UTS dropped after 24 weeks (Figure 4-8D-E). Concurrently, as was seen through H&E staining (Figure 4-8A), the implant was broken down by the immune cells surrounding the implant *in vivo*, which was likely weakening its structure as repair tissue was regenerated. This reduction in tensile properties was also reflected in PYR content, commonly associated with

tensile properties [343], which was only 46.5% of native tissue levels by DW after 24 weeks of implantation (Supplementary Table 4-6). Despite this, the ratio of mature to immature crosslinks (PYR:DHLNL) in implants significantly rose after 24 weeks toward levels of native tissue (Supplementary Table 4-6). Additionally, despite similar collagen quantities between t=0 and t=24W *in vitro* controls (Figure 4-8C), tensile properties of the implants cultured *in vitro* also dropped between these two points. When examining the ratio of Col1α1 and Col1α2 as quantified by bottom-up proteomics, the native tissue had a ratio of approximately two (Figure 4-9D), as would be expected in native tissues composed of collagen type I [344]. Previous studies which examined the mechanical properties of homotrimeric forms of collagen type I, where collagen type I molecules form from three Col1α1 chains rather than the typical two Col1α1 chains and one Col1α2 chain, noted weakening of the tissue in disease-states where this occurred [344]. The same weakening may be occurring in the extended *in vitro* culture as the ratio between the two alpha chains increased over 2-times that of the ratio at implantation (i.e., t=0 *in vitro*) and of native TMJ disc (Figure 4-9D). Compressive properties, which increased with GAG content *in vitro* but were not measured in *in vivo* implants due to tissue availability, are reported in Supplementary Table 4-7. Despite these temporal drops in tensile properties of excised implants, their biochemical components remodeled toward native tissue values of TMJ discs.

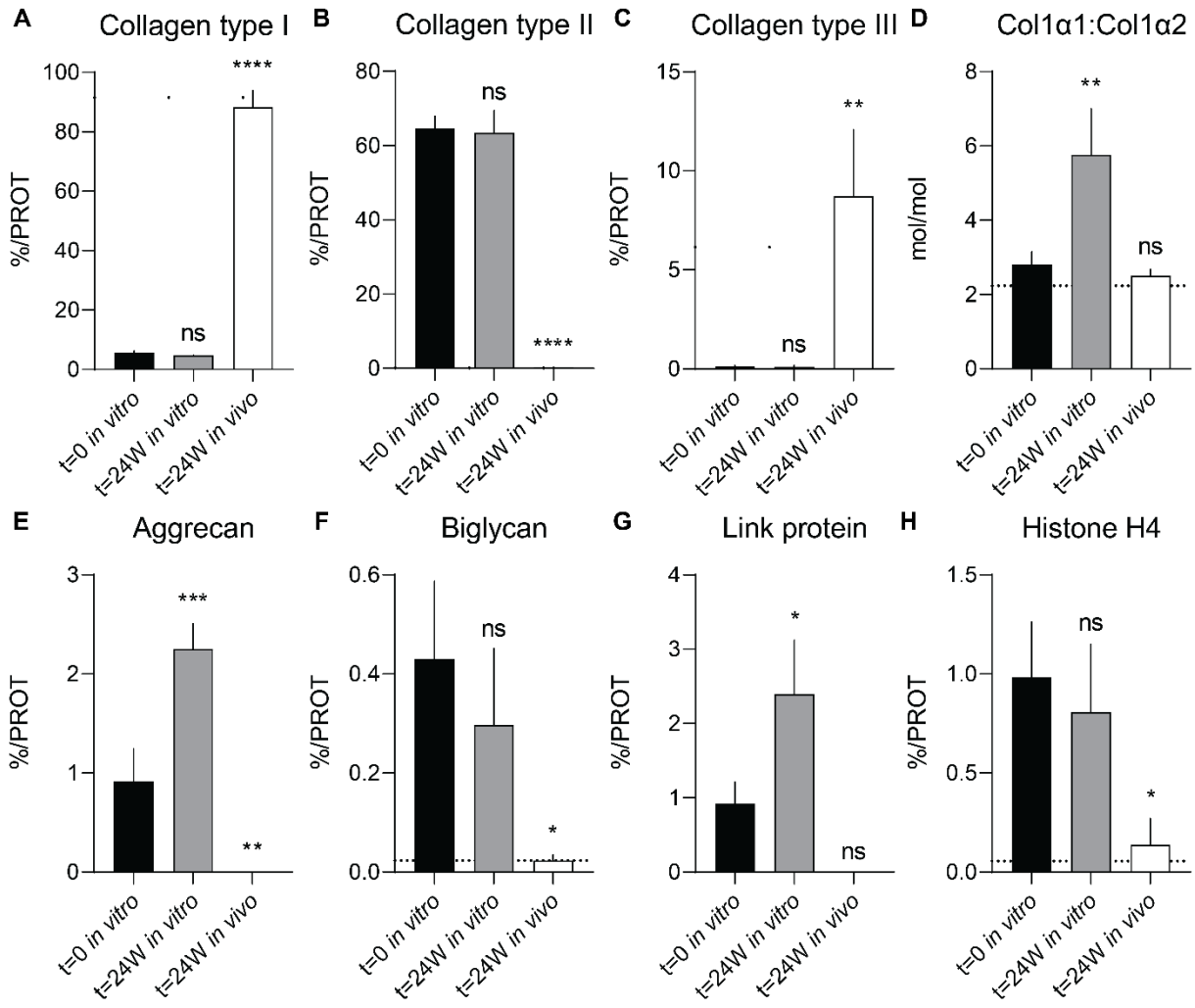

Figure 4-9: Bottom-up proteomic analysis of neocartilages after implantation also showed remodeling toward native TMJ disc content.
Bottom-up proteomics data are presented per total protein (PROT) as a percentage. (A) Collagen type I increased toward native TMJ disc values, while (B) collagen type II decreased. (C) Collagen type III and (D) the ratio between the two collagen type I alpha chains are presented. (E) Aggrecan, (F) biglycan, and (G) link protein all decreased after implantation, and (H) histone H4 followed the trends in cellularity as seen in histology. Dashed lines represent native TMJ disc values. ns, not significant.

Discussion

The objective of this study was to investigate the safety and efficacy of long-term implantation of costal chondrocyte-derived, self-assembled neocartilage implants in TMJ disc perforations. The hypothesis that repair tissue would have a collagen profile similar to native tissue with superior mechanical properties compared to control fill tissue was supported by the *in vivo* data. Implant-treated discs exhibited mechanically robust healing of perforation defects with repair tissue that

mimicked the native TMJ disc biochemically. In contrast, control fill tissue consisted of a biochemical make-up consistent with scar tissue formation, which led to inferior functional properties. Compared to the control fill tissue, the repair tissue of implant-treated discs was 615.4% tougher, 894.5% more resilient, and 340.8% stronger. Additionally, implants underwent significant remodeling; both total collagen and GAG content converged toward native TMJ disc biochemical values. Systemic safety of tissue-engineered implants, as analyzed through necropsy, complete blood counts, and comprehensive metabolic panels, was confirmed. As examined by staining for general cellularity via H&E and immunohistochemical staining for immune cells, the implants were immunogenically well-tolerated over time. This study supports the safety and efficacy of self-assembled TMJ disc implants for long-term healing of disc perforation defects. The data presented here are significant in demonstrating the feasibility of using TMJ disc implants in future clinical studies examining TMJ disc healing in humans.

This study showed that self-assembled implants that underwent expansion, rejuvenation, and self-assembly were suitable for allogeneic, nonhomologous implantation. Previously, our group showed that self-assembled, allogeneic implants derived from expanded and rejuvenated costal chondrocytes were suitable for nonhomologous use in the TMJ disc [23]. Despite being only within the lower range of reported tensile properties in native tissue [24], the TMJ disc implants used here, with an average tensile Young's modulus of 7.05 MPa and UTS of 2.28 MPa, survived the joint loading environment after implantation. As a result, implants surgically placed into discs remodeled over 24 weeks. After 24 weeks, implants still retained more than 50% of their original tensile values. Because the implants survived, their regenerative capacity was activated which allowed for native-like recapitulation of functional properties in the repair tissue and remodeling of the implant over time. Over the 24 weeks examined here, the neocartilage implants proved to be crucial in regenerating the minipig TMJ disc, because controls treated without an implant had inferior mechanical, biochemical, and proteomic properties of their fill tissue.

All implant-treated TMJ discs exhibited healing as indicated by gross morphology, but control discs also exhibited a degree of tissue fill. The gross healing response of both groups exhibited a wide range of morphologies, but implant-treated discs appeared better than those of controls. Furthermore, the repair tissue of implant-treated discs had significantly improved mechanical outcomes compared to fill tissue of controls. Thus, gross morphology may not be the best indicator of a robust healing outcome. Since control fill tissue did not exhibit mechanical robustness, one can expect that the untreated discs may further degenerate with time. This may be due to stress concentrations that develop at the interface between the softer control fill tissue and the stiffer healthy native tissue. This is well documented in knee articular cartilage. For example, when a focal defect develops in articular cartilage, stress concentrations develop in adjacent native cartilage which can induce cell death and, eventually, degeneration [345]. In the TMJ disc, an analogous process would occur at the interface between fill tissue and native fibrocartilage, causing accelerated degeneration which may necessitate future disc removal or total joint replacement in the analogous human TMDs [16]. Thus, use of a tissue-engineered implant to achieve native-like properties of the TMJ disc has potential to halt the degenerative processes in the joint since the TMJ disc is central to TMDs [11, 16].

Similar to the TMJ disc, the condyles showed heterogeneity in osteoarthritic changes as a result of implantation of a tissue-engineered therapeutic into the TMJ disc. There was no significant difference in OA scoring of joints which received an implant compared to those that did not, indicating that the changes in condylar degenerative status are most likely a direct result of surgical intervention in the TMJ disc. For example, in the approach described here, the Mitek anchor sutures pass over the condylar process and small portions of the condyle's articulating surface depending on the individual animal anatomy. This may have caused some degeneration in the areas where the suture contacts the articular cartilage; this phenomenon has been previously reported in the knee [340]. However, a vast majority of the articulating surface in the condylar head was spared of abrasions, with most degenerative changes only appearing on the

condylar process where the suture was placed and a small portion of the articulating surface. Given the double-armed nature of these bone anchor sutures, future studies using the surgical techniques described here may consider only using one arm of the suture to secure the disc or alternative methods to preserving the lateral attachment. Despite the minor degenerative changes seen on the adjacent articulating surface, the use of the intralaminar perforation surgical technique was crucial toward achieving TMJ disc regeneration using a tissue-engineered implant.

It was shown that the tissue-engineering approach in this perforation defect model resulted in robust repair tissue that was similar to the native TMJ disc. Specifically, the repair tissue of implant-treated discs was similar to native tissue in terms of toughness, resilience, UTS, and strain at failure. Additionally, repair tissues were significantly tougher, more resilient, and stronger than the fill tissue of empty defects. Given the structure-function relationships of the matrix content and tissue mechanical properties, the composition of the repair tissue compared to the fill tissue was investigated. Repair tissue in the implant-treated group had significantly more collagen type I, the main collagen type found in the TMJ disc. Collagen type III, which is also present in the TMJ disc at low levels [346], was found to be significantly greater by more than 2-times in fill tissue of empty defects compared to native or repair tissue. This is consistent with scar tissue, where collagen type III is elevated over normal levels and mechanical properties decrease [347]. Given the TMJ disc's mechanical loading under large tensile strains, this is a significant finding which explains the inferior mechanical properties of empty defect fill tissue. The tissue-engineered implant placed in the TMJ disc facilitated more collagen type I deposition which improved repair tissue mechanics toward that of native tissue, in direct opposition to what was seen in controls.

TMJ disc implants demonstrated exceptional systemic safety in the Yucatan minipig model in this study. As examined during necropsy, organ systems displayed no neoplastic growth or abnormalities, demonstrating that the implants do not exhibit systemic tumorigenicity.

This finding was further corroborated by the complete blood count and comprehensive metabolic panel outcomes; there was minimal reaction to the tissue-engineered implant as indicated by the bloodwork. Within the joint space, after 4, 8, or 24 weeks, there was no synovium reaction and no neoplastic growth, indicating that chondrocytes within the implant do not have any effects outside of the TMJ disc. Ultimately, the long-term *in vivo* data show that self-assembled neocartilages were systemically safe for implantation into the TMJ disc, which is a promising step toward seeking future regulatory approval for use in humans.

After implantation *in vivo*, there was a cellular response surrounding and infiltrating the neocartilage as shown through H&E staining. Through immunohistochemical staining for CD3, CD20, and CD68 for T cells, B cells, and macrophages, respectively, it was apparent that the cells surrounding the implant were immune cells. T cells and B cells were present throughout the three timepoints examined, indicating that there was a steady state immune response after implantation; however, CD68 staining decreased over time. While CD68 is typically associated as a pan-macrophage marker, recent studies have shown that it may be a marker of an inflammatory macrophage phenotype [348, 349]. Given the decrease in CD68 staining between 4 and 24 weeks, the acute inflammatory immune response was shown to resolve. In agreement with previous studies examining macrophage response in natural healing cascades [350], over time, it was expected that macrophages polarized toward a pro-healing response. Additional work is necessary to confirm macrophage polarization, such as staining discal sections for pro-healing macrophage markers like CD163 [351]. Additionally, this phenomenon might be examined by looking at *in vitro* cocultures of implants with macrophages polarized toward different states [352]. Ultimately, implants facilitated a long-term healing response toward TMJ disc regeneration as evidenced by not only immunohistochemistry but the long-term mechanical healing of implant-treated discs.

Implants undergo progressive remodeling throughout the long-term healing response. As evidenced by histological and biochemical data, the implant is being remodeled to resemble

native tissue. For example, the implant increased in collagen and decreased in GAG content toward levels of native TMJ discs, reaching 82.8% and 87.1% of native tissue values, respectively. This was further corroborated by the bottom-up proteomics analysis, which showed that GAG-associated proteins, such as aggrecan and link protein, likewise converged toward native TMJ disc levels. Moreover, the collagen type II-rich neocartilage (64.54%/PROT) remodeled to a collagen type I-rich tissue (88.29%/PROT) after implantation, and collagen type III increased to native tissue levels. Importantly, collagen type III in implants (8.73%/PROT) after 24 weeks was lower than that found in fill tissue of control discs (13.74%/PROT), indicating that the remodeling was toward native tissue-like regeneration and not scar tissue. Given these biochemical changes, it would be expected that mechanical properties would increase as well, but the opposite was shown; UTS significantly decreased by 43.5% over 24 weeks of implantation. For the *in vitro* controls cultured under a static environment, Col1α1:Col1α2 ratio increased over 24 weeks of culture, reminiscent of diseased tissues [344]. In contrast, excised *in vivo* implant maintained a similar Col1α1:Col1α2 ratio to native tissue indicating that the orthotopic location is a more appropriate environment for TMJ disc implant remodeling. Most importantly, the remodeled implant activated the regenerative capacity of the TMJ discs and produced repair tissue that was more mechanically robust and biomimetic than fill tissue of controls.

This study generated significant preclinical data toward demonstration of safety and efficacy of TMJ disc implants in healing perforation defects. For safety, both the systemic and local responses showed that implants were well-tolerated. Although there was a local immune response at 4 weeks, it resolved toward a steady state response, indicating that implants were immunogenically well-tolerated. Additionally, implants remodeled toward the native TMJ disc biochemical makeup. Ultimately, neocartilage implants resulted in the regeneration of fibrocartilaginous repair tissue in implant-treated discs. In terms of efficacy, repair tissue exhibited more collagen type I, indicative of TMJ disc regeneration, and less collagen type III,

indicative of scar tissue formation, compared to fill tissue in the control group. The repair tissues of implant-treated discs had robust mechanical properties, which all reached native TMJ disc values, and were many times higher in toughness, resilience, strength, and strain at failure than control fill tissues. Given the regenerative capacity of tissue-engineered implants in the TMJ disc, future interventions may be able to halt the degenerative processes, thus avoiding the need for discectomy or total joint replacement. However, there are many hurdles that need to be overcome prior to translation of TMJ disc implants to widespread human use, including both scientific and regulatory hurdles [16]. This study paves the path toward eventual widespread use of tissue-engineered TMJ disc implants in the millions of people experiencing intractable pain and dysfunction as a result of TMDs.

Materials and Methods

Tissue engineering of implants

Three juvenile Yucatan minipig donors (males, 5-8 months), culled for reasons unrelated to this study, were used for costal chondrocyte sourcing, as previously described [338]. Briefly, costal cartilage was exposed using sterile tools in a biosafety cabinet, perichondrium was removed, and costal cartilage was minced to approximately 1 mm^3 sized pieces. Costal cartilage pieces were digested in 0.4% (w/v) pronase for 1 hour at 37°C and then in 0.2% (w/v) collagenase for 18 hours at 37°C. Enzymes were resuspended in Dulbecco's modified Eagle's medium (DMEM, high glucose, GlutaMAX supplement) with 3% fetal bovine serum (FBS) and 1% penicillin-streptomycin-fungizone (PSF). After collagenase treatment, single-cell suspensions were filtered using 70 µm cell strainers and treated with ammonium-chloride-potassium lysis buffer, as previously described [353].

After lysis buffer treatment, chondrocytes were plated in T225 flasks at 2.5M cells per flask (~11,111 cells/cm^2) in chondrogenic (CHG) medium (DMEM, 1% PSF, 1% nonessential amino acids, 1% insulin-transferrin-selenous acid+, 100 nM dexamethasone, 50 µg/mL

ascorbate-2-phosphate, 40 µg/mL L-proline, 100 µg/mL sodium pyruvate). Expansion medium consisted of CHG medium supplemented with 2% FBS, 1 ng/mL TGF-β1, 5 ng/mL basic fibroblast growth factor (bFGF), and 10 ng/mL platelet-derived growth factor (PDGF) [149]. During expansion, medium was changed every 3-4 days. Chondrocytes were frozen in FBS containing 10% dimethyl sulfoxide (DMSO) after one passage, then thawed for continued downstream expansion. Passaging consisted of lifting cells with 0.05% trypsin-EDTA treatment for 9 minutes, followed by digestion of the lifted cells with 0.2% (w/v) collagenase in DMEM with 3% FBS and 1% PSF for 30 minutes (37°C, agitation every 10 minutes). After three passages, cells underwent aggregate rejuvenation, as previously described [25]. Aggregate rejuvenation medium consisted of CHG medium supplemented with 10 ng/mL TGF-β1, 100 ng/mL growth differentiation factor 5 (GDF-5), and 100 ng/mL bone morphogenetic protein 2 (BMP-2). During aggregate rejuvenation, medium was changed every 3-4 days. After 11 days, aggregates were digested in 0.05% trypsin-EDTA for 45 minutes and 0.2% (w/v) collagenase in DMEM with 3% FBS and 1% PSF for 90 minutes (37°C, agitation every 10 minutes). After collagenase treatment, the solution was filtered with 70 µm cell strainers to yield a single-cell suspension.

After aggregate rejuvenation, self-assembly of neocartilage was performed, as previously described [17]. Briefly, nonadherent wells of 8x13 mm were made using molten 2% agarose and negative molds. Wells were hydrated with CHG medium, which was changed three times prior to cell seeding. Cells (7M/implant) were seeded into each well with 300 µL of CHG medium. After 4 hours, 2 mL of CHG medium was added, and medium was exchanged every day up until day 2, at which point implant were unconfined by releasing them from the wells. From unconfining to end of culture at day 28, neocartilage implants were fed with 7 mL of CHG medium every other day. After day 2 of self-assembly, CHG medium was supplemented with TGF-β1 (10 ng/mL). At day 7 of self-assembly, C-ABC was applied for 4 hours at 1.5 U/mL in CHG medium [201]. C-ABC was activated using 50 mM sodium acetate and quenched using 1 mM zinc sulfate. Passive axial compression was applied from days 10-14 as a mechanical

stimulus and to keep implants flat [201]. From day 14 of self-assembly onward, LOXL2 was added to the CHG medium at 0.15 µg/mL, along with 0.146 mg/mL hydroxylysine and 1.6 µg/mL copper sulfate.

The day prior to surgery, implants for *in vivo* use were placed on ice (4°C) in a 50 mL conical tube with HEPES-buffered CHG medium supplemented with TGF-β1 and LOXL2 for transportation to the veterinary operating room (7 hours). Upon arrival, implants were placed in an incubator at 37°C for equilibrium prior to surgery the following day. The remaining implants (n=9) were split in half under sterile conditions. Half of the implant was used to establish baseline properties prior to implantation as a control (t=0 *in vitro*). The other half remained in culture until animal sacrifice to serve as a measure of *in vitro* remodeling (t=24W *in vitro*).

In vivo experiments

All animal work was approved by the UC Irvine (#AUP-21-033) and UC Davis (#21430) Institutional Animal Care and Use Committees (IACUCs). This study consisted of 16 Yucatan minipigs (n=4 males, n=12 females). For initial pilot studies, two male animals at both 4 and 8 weeks (n=4 total) were used for initial feasibility studies prior to initiating long-term studies (i.e., 24 weeks). For 24-week timepoints, female minipigs (n=12 total) were used; six minipigs were designated as empty defect controls, while the remaining six minipigs received a tissue-engineered implant.

Presurgical medication and anesthesia

Yucatan minipigs were fasted for 24 hours prior to surgery. Animals were pretreated with Telazol (tiletamine/zolazepam) at 3-6mg/kg via intramuscular (IM) administration. An intravenous (IV) catheter was used in the auricular vein for administration of lactated Ringer's solution at 5-10 mL/kg/hr and other medications. Anesthesia was induced using ketamine at 5 mg/kg and diazepam at 0.2-0.5 mg/kg, as well as isoflurane delivered via facemask. Minipig

larynxes were treated with 2% lidocaine (1-2 mL) prior to intubation with a cuffed endotracheal tube (sized based on individual animal). Preemptive analgesia was provided with morphine at 0.5 mg/kg via IM delivery. Throughout surgery, anesthesia was maintained with 1-3% isoflurane in 100% oxygen. End-tidal carbon dioxide was maintained between 35-45 mmHg via positive ventilation. Monitoring via capnography, electrocardiography, thermometer, and blood pressure measurements was performed throughout surgery. Animal body temperature was maintained at physiological temperature (37-38°C) via a heating pad.

Surgical implantation and defect creation

As previously described [23], prior to surgical intervention, the lateral side of the head was shaved and aseptically prepared for surgery using iodine-based solutions followed by alcohol (Figure 4-2A). Subsequently, an approximately 10cm curvilinear incision along the curvature of the ventral aspect of the zygomatic arch and extended superiorly over the temporal process of the zygoma toward the ear was made with a #15 blade (Figure 4-2B) followed by blunt dissection through the subcutaneous adipose tissue and the periosteum. Using a periosteal elevator, the masseter muscle was reflected ventrally and posteriorly, and the tissues of the TMJ were identified, including the condylar process and the mandibular head, the masseter muscle that attaches to the condylar process, and the lateral TMJ disc attachments. Using sharp dissection, the tissue was thinned to further identify the lateral aspects of the joint. The condylar process was subsequently exposed using a combination of sharp and blunt dissections. Using a sharp elevation of the superior TMJ disc attachments of the joint capsule, the superior joint space was exposed. An incision through the inferior TMJ disc attachments of the joint capsule (below the disc) exposed the inferior joint space. The disc and articular cartilages were protected during all blunt and sharp dissections through the joint capsule.

At this juncture, the lateral, superior and inferior aspects of the disc were exposed (Figure 4-2C). Using 3.5x loupe magnification, the intralaminar incision was created in the

lateral edge of the disc using a #15 scalpel blade, yielding an incision approximately 12 mm wide. This incision was deepened into the disc to create a pouch with an inferior and superior lamina measuring approximately 12 mm deep by 12 mm wide (Figure 4-2D). The lateral edges of the laminae were then grasped and held together while a 3 mm diameter disposable biopsy punch was pushed through both laminae, creating a full thickness perforation defect in the centrolateral region of the disc (Figure 4-2E, Supplementary Figure 4-1). Careful manipulation of the biopsy punch ensured that adjacent articulating surfaces were not damaged. A tissue-engineered implant measuring 8x8 mm (Figure 4-1C) was placed between the two laminae (Figure 4-2F), and the pouch was closed on the lateral margin using a 5-0 Monocryl suture in a simple interrupted fashion (Figure 4-2G). The suture was not passed through the implant. The TMJ disc was reattached to the lateral component of the condylar process using a Mitek bone anchor (QuickAnchor Plus, #0 suture) [354]. A Jacob's chuck was used with the supplied 2.0x9.7 mm drill bit to pre-drill a hole prior to placement of the bone anchor with self-expanding flanges. The suture was then used to secure the lateral edge of the TMJ disc to the condylar process (Figure 4-2H). The remaining layers of tissue, including the joint capsule and masseter muscle, were closed using 3-0 Monocryl suture.

Postoperative medication and animal care

For postoperative analgesia, minipigs were administered a mixture of meloxicam at 0.1-0.4 mg/kg via IV, IM, or oral delivery once daily for 3 days, fentanyl at 1-5 μg/kg/hr via patch for 3 days, and buprenorphine at 0.005-0.05mg/kg via a single IM dose. Minipigs also received a single dose of perioperative antibiotics. Until ambulation and mentation, minipigs were closely recovered and observed in narrow padded pens and monitored for postoperative complications. The animals were then returned to their normal housing pens. For diet, a soft diet (i.e., liquid yogurt, softened pellet food) was provided for 3 days after surgery. Additionally, water bowls

were provided for animals instead of standard spigots to minimize postoperative joint loading. Sutures were removed 14 days after surgery.

Animal euthanasia

After 4 weeks, 8 weeks, or 24 weeks, minipigs were humanely euthanized with an IM injection of Telazol (3-6 mg/kg) followed by an IV injection of Euthazol (phenytoin/pentobarbital, 1 mL/4.5kg). Upon animal euthanasia, a veterinary pathologist carried out a full necropsy examining organ systems for any signs of toxicity or neoplastic growth. The TMJ discs and the mandibular heads on the condylar process were removed *en bloc* as one unit.

TMJ sample preparation

Prior to any dissections, TMJ tissue samples were documented photographically. Discs were subsequently removed from the condyle, and the condyle and disc were photographed from multiple angles and views. A small amount of synovium from the inner lateral wall of the inferior joint space was excised for histological analysis. Condyles were also kept for histological analysis. Upon documentation, discs were sectioned anteroposteriorly to identify the implant location and/or the repair or fill tissue (Supplementary Figure 4-7). Careful dissection of the disc was guided by gross morphology images of the disc and observation of irregularities that indicated the location of fill/repair tissue. From these sections, the following samples were identified: implant histological section, implant tensile testing sample, fill/repair tissue tensile testing sample, intralaminar tensile testing sample, implant biochemistry sample, fill/repair tissue biochemistry sample, implant mass spectrometry sample, and fill/repair tissue mass spectrometry sample. Contralateral samples from the centrolateral region of the disc were also excised for use as native tissue controls.

In vitro sample preparation

At time of implantation (t=0) and at animal euthanasia (t=24W), halves of in vitro (non-implanted) implants were sectioned into samples for histological analyses, compressive stress-relaxation testing, uniaxial tensile testing, biochemical testing, and mass spectrometry analyses.

Histology and immunohistochemistry

Synovium, condyle, and disc samples were fixed in 10% neutral buffered formalin for at least 72 hours. After fixation, condyles underwent decalcification with 10% formic acid and were grossly cut to capture any osteoarthritic changes on the articulating surface of the condyle. Samples were subsequently processed, embedded in paraffin wax blocks, sectioned to 4 μm thickness for immunohistochemistry or 5 μm thickness for all other stains using a microtome, and mounted on microscopy slides. Samples were stained with H&E, SO/FG, and PSR, as previously described [355]. Only H&E was performed for condyle and synovium sections. Immunohistochemistry was performed for CD3 (T cells), CD20 (B cells), and CD68 (macrophages) markers using the primary and secondary antibodies listed with the antigen retrieval method, blocking serums, and developments in Supplementary Table 4-8, as previously described [23]. Whole slide scans were then captured using a Roche VENTANA DP 200 slide scanner, and QuPath software was used to visualize the slides digitally [356].

Mechanical testing

Samples from *in vitro* controls were subjected to mechanical testing with compressive stress-relaxation tests and uniaxial tensile tests. Compressive stress-relaxation testing was performed on 3 mm diameter sample punches, taken with a disposable biopsy punch. Sample height was detected using a tare load of 0.1 N, and samples were subjected to 15 preloading cycles of 5% strain, as previously described [24]. Strain of 20% was applied to the punch for 900 seconds until equilibrium. The relaxation modulus, instantaneous modulus, and coefficient of viscosity

were determined by fitting the resulting force-displacement curves to a standard linear solid model with a custom MATLAB script. For tensile tests of *in vitro* controls, dog bone-shaped samples were glued to paper tabs of a predefined gauge length. Samples were tested at 1% strain per second until failure. Resulting force-displacement curves were analyzed with a custom MATLAB script to determine the tensile Young's modulus and UTS of samples.

Tissues excised from the TMJ disc underwent uniaxial tensile testing in the anteroposterior direction for the excised implants, fill/repair tissues, and contralateral native tissue samples. Uniaxial tensile tests for intralaminar fusion were performed in the superoinferior direction. Briefly, the samples were clamped using hemostats attached to a uniaxial testing machine (Instron model 5655). Prior to initiating the uniaxial tensile test, a 0.2 N tare load was applied to remove slack from samples. Images were then taken from the front and side of the sample to calculate the cross-sectional area, and the gauge length was measured using a caliper. The gauge length was defined as the pretest grip-to-grip clamping distance. Samples were then tested at 1% strain per second until failure. Resulting force-displacement curves were analyzed with a custom MATLAB script to determine the Young's modulus, UTS, strain at failure, toughness (entire area under the curve), and resilience (area under the curve of linear region only) of tissue samples.

Biochemical testing

Biochemical assays for total collagen and GAG content were performed on *in vitro* control implants, excised *in vivo* implants, excised fill/repair tissues, and excised contralateral TMJ discs. Prior to assays, hydrated samples were weighed to obtain a wet weight (WW) and then lyophilized for at least 72 hours. After lyophilization, samples were reweighed to obtain a DW. Briefly, a modified hydroxyproline assay was used to quantify total collagen [93] and a dimethylmethylene blue assay kit was used to quantify sulfated GAGs. The total collagen and GAG contents were normalized to DW.

Mass spectrometry analyses for crosslinks quantification and bottom-up proteomics

Pieces of tissue for crosslinks quantification and bottom-up proteomics were split from a singular piece of tissue for mass spectrometry analyses. Collagen crosslink quantification was performed, as previously described [346]. Briefly, tissue pieces (~1 mg WW) were lyophilized for at least 72 hours, and DWs were measured. Samples were reduced for 1 hr in $NaBH_4$, washed overnight in ultrapure water, and hydrolyzed in HCl for 18 hours. Hydrolysates were evaporated, resuspended, filtered, and analyzed on a Waters ACQUITY QDa LC-MS system. PYR, DHLNL, hydroxyproline (OHP), and internal standard pyridoxine were quantified by taking the area under the curve of the extracted ion chromatograms of each analyte's mass.

Bottom-up proteomics analysis was performed, as previously described [346]. Briefly, tissue pieces (~1 mg WW) were lyophilized for at least 72 hours, digested overnight in trypsin in a heat block at 65°C, desalted with Waters Sep-pak C18 cartridges, and analyzed with a Thermo Fisher Scientific Orbitrap Fusion Lumos mass spectrometer. Label-free quantification was performed with MaxQuant [357] to normalize all identified protein analytes to PROT content.

ICRS scoring

Evaluation of the degenerative, osteoarthritic changes on the condyles was carried out using the International Cartilage Repair Society (ICRS) scoring system [358]. Briefly, H&E slides were analyzed by a veterinary pathologist to perform histological grading on decalcified sections of condyles. If a sample required two mediolateral sections to be graded, the grades were averaged and reported. A gross stage was also determined by measuring the percentage of the articulating surface affected by osteoarthritic changes (i.e., osteophytes, chondral or osteochondral defects, fibrillation, etc.). The total OA score was calculated by multiplying the gross stage by the histologic grade.

Statistical analyses

Data were analyzed with a Student's t-test or one-way analysis of variance (ANOVA) followed by a *post hoc* Dunnett's test performed using t=0 *in* vitro samples as the control group. All tests were performed and graphs were generated using GraphPad Prism 9. The number of asterisks were representative of the degree of significance; (ns) represents $p>0.05$, (*) represents $p\leq0.05$, (**) represents $p\leq0.01$, (***) represents $p\leq0.001$, and (****) represents $p\leq0.0001$.

Supplementary Materials

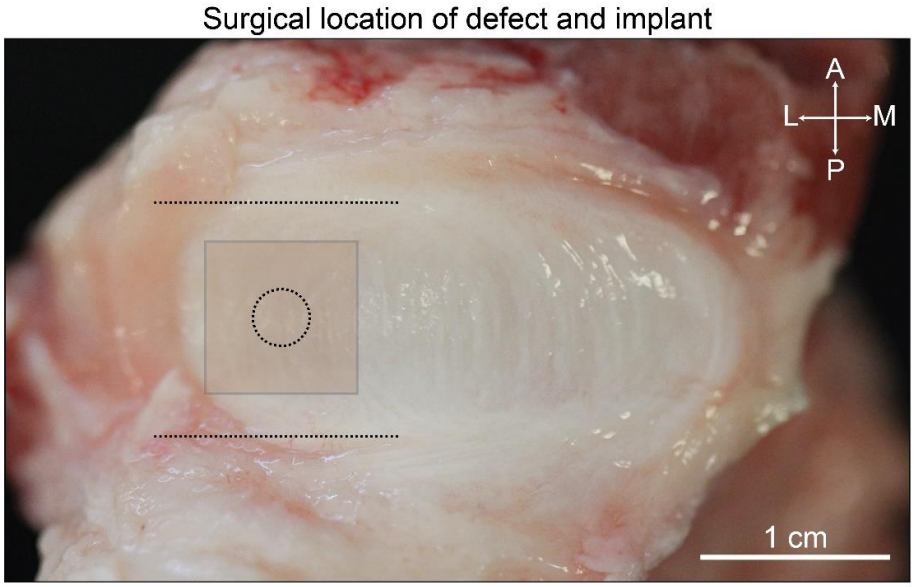

Supplementary Figure 4-1: Depiction of the surgical placement of the incision, defect, and implant.
The defect (dashed circle) was placed in the centrolateral aspect of the disc in the center of the incision margins (dashed lines). The implant (solid square) was positioned within the incision margins. A, anterior, L, lateral, M, medial, P, posterior.

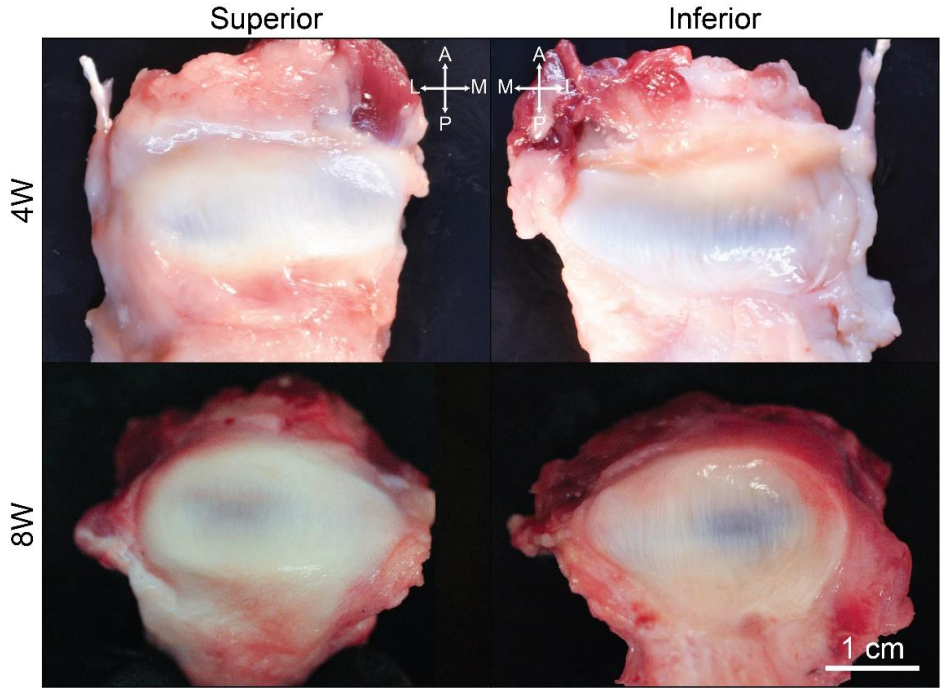

Supplementary Figure 4-2: Short-term gross morphology of implant-treated TMJ discs.
After 4 or 8 weeks of healing, TMJ discs exhibited repair tissue in the defect placed in the centrolateral portion of the disc. A, anterior, L, lateral, M, medial, P, posterior.

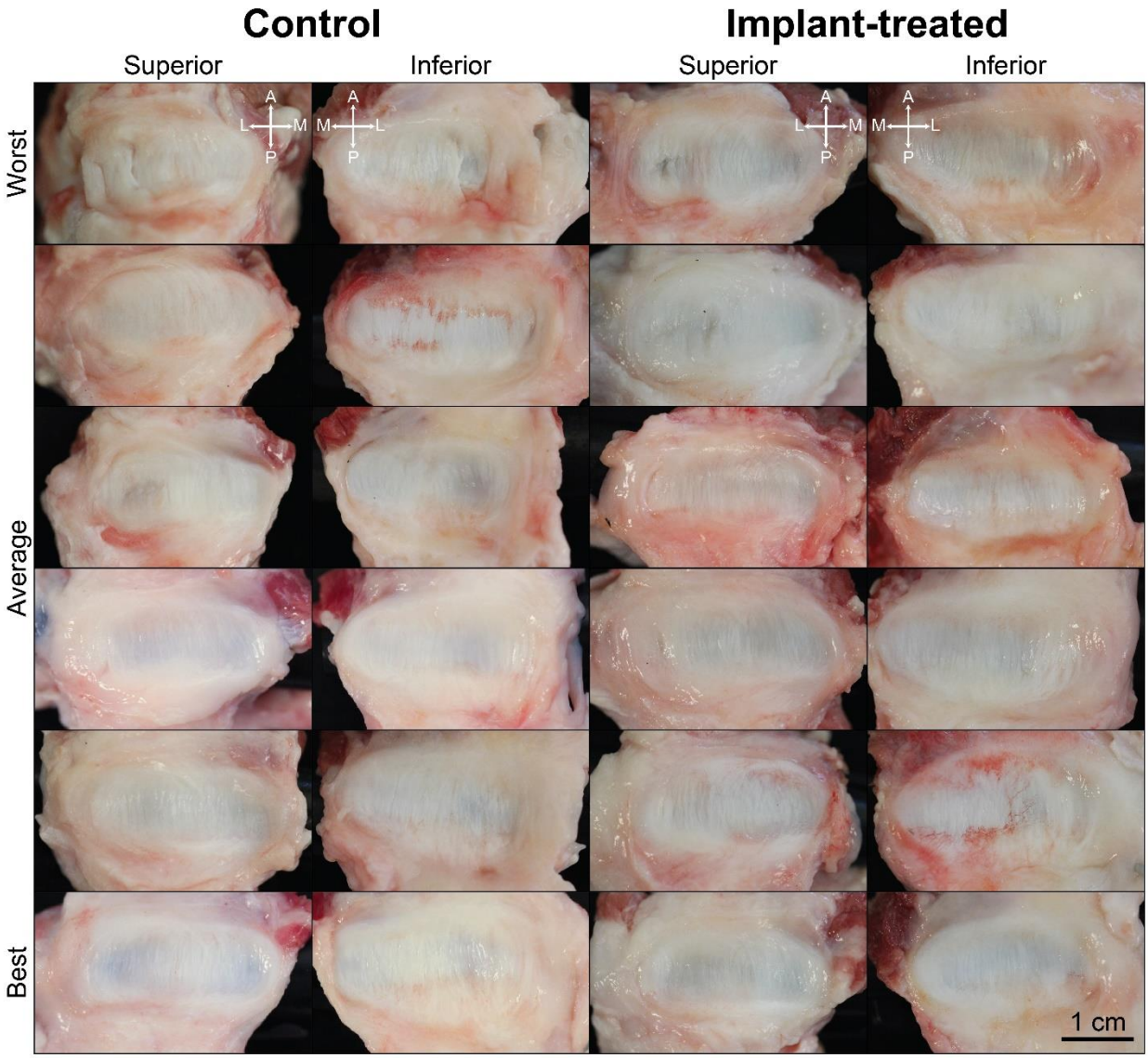

Supplementary Figure 4-3: Gross morphology of all discs in the long-term study.
After 24 weeks, TMJ discs exhibited a heterogeneous healing response. A, anterior, L, lateral, M, medial, P, posterior.

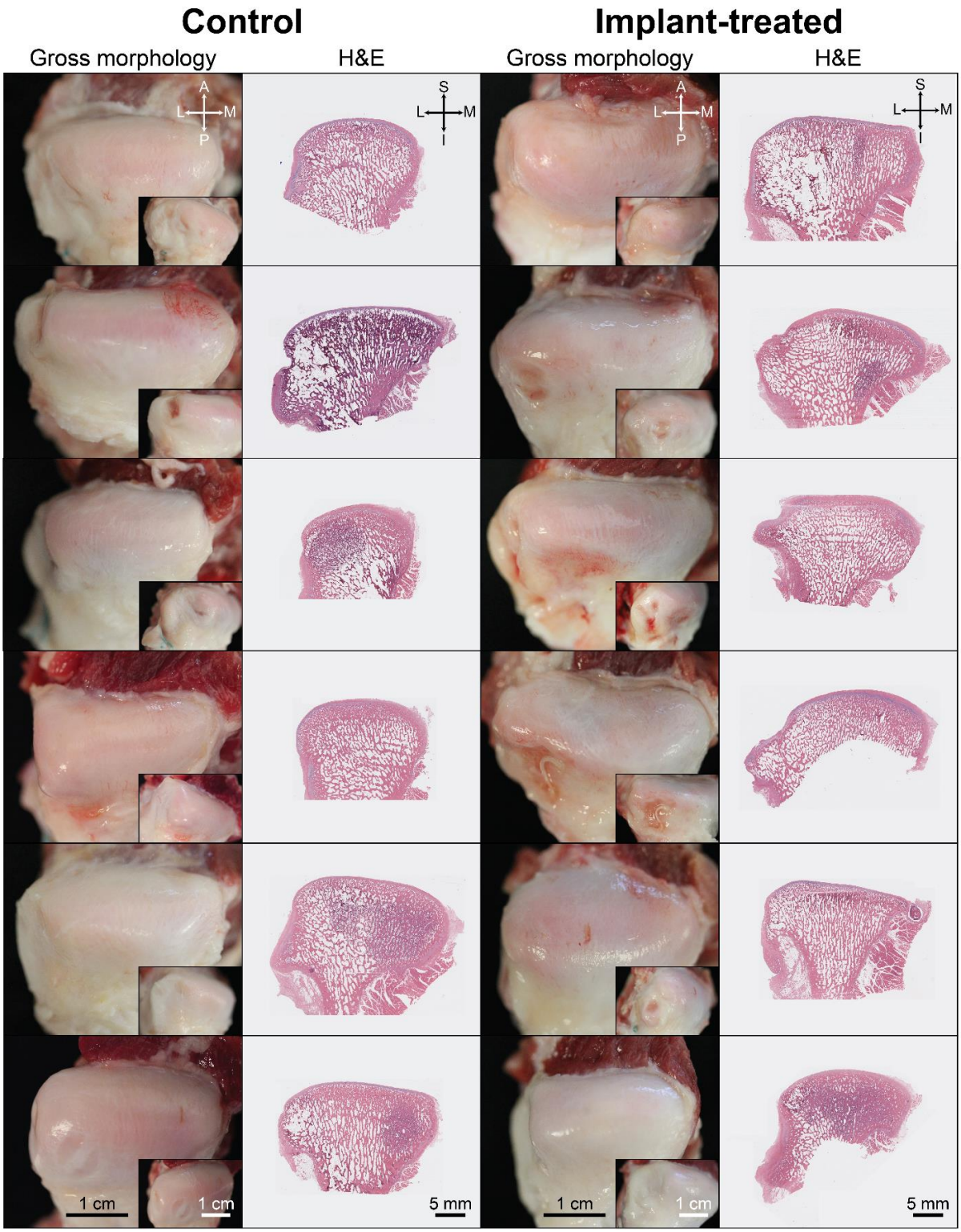

Supplementary Figure 4-4: Gross morphology and mediolateral histological cross sections of condyles. After 24 weeks of implantation, the condyles had a heterogeneous response to the presence of a TMJ disc implant and suture anchor as shown by both gross morphology and hematoxylin and eosin (H&E) sections. Insets are rotated views of the lateral area (left) of the condyle. A, anterior, I, inferior, L, lateral, M, medial, P, posterior, S, superior.

Supplementary Table 4-1: Osteoarthritis scores of condyles.
A histological score and gross stage were assigned to each animal and were multiplied to get the osteoarthritis (OA) score, according to the International Cartilage Repair Society scoring scheme [358]. There was no difference between the groups.

Group	Animal	Histological Grade	Gross Stage	OA Score
Control	1	0.00	1	0.00
	2	6.00	2	12.00
	3	2.25	2	4.50
	4	3.50	2	7.00
	5	2.00	0	0.00
	6	4.50	2	9.00
	Final Score			5.42±4.86
Implant-treated	1	5.50	1	5.50
	2	0.00	0	0.00
	3	1.25	2	2.50
	4	5.00	2	10.00
	5	4.75	1	4.75
	6	4.00	1	4.00
	Final Score			4.46±3.34

Supplementary Table 4-2: Tensile properties of intralaminar fusion.
When tested under uniaxial tension in the superoinferior direction, there was no difference in the intralaminar stiffness or strength between control and implant-treated groups.

Group	Young's modulus (MPa)	UTS (MPa)
Control	1.34±1.18	0.66±0.43
Implant-treated	1.40±0.94	0.68±0.46

Supplementary Table 4-3: Crosslinks in the fill and repair tissues.
For implant-treated discs, mature pyridinoline (PYR) and immature dihydroxylysinonorleucine (DHLNL) crosslinks normalized to dry weight (DW) and hydroxyproline (OHP) were near native TMJ disc levels but were not statistically different compared to controls.

Group	PYR/DW (ng/mg)	PYR/OHP (mmol/mol)	DHLNL/DW (ng/mg)	DHLNL/OHP (mmol/mol)	PYR/DHLNL (mol/mol)
Control	5633±672	42.55±9.33	1603±280	16.56±2.23	2.553±0.293
Implant-treated	4968±755	34.20±8.42	1467±446	14.04±4.47	2.578±0.646
Native TMJ disc	5518±1686	35.94±8.73	1367±500	12.32±3.48	2.968±0.138

Supplementary Table 4-4: Bottom-up proteomics data for all tissues.
Bottom-up proteomics data are presented per total protein as a percentage.

Gene	Protein	t=0 *in vitro*		t=24W *in vitro*		t=24W *in vivo*		Control		Implant-treated		Native TMJ disc	
		Avg	SD	Avg	SD	Avg	SD	Avg	SD	Avg	SD	Avg	SD
ACTB	Actin, cytoplasmic 1	1.09%	0.25%	0.75%	0.16%	0.06%	0.06%	0.09%	0.07%	0.03%	0.03%	0.05%	0.11%
PGCA	Aggrecan core protein (Fragments)	0.92%	0.33%	2.25%	0.26%	0.00%	0.00%	0.00%	0.00%	0.00%	0.00%	0.00%	0.00%
ANXA2	Annexin A2	0.43%	0.17%	0.27%	0.15%	0.00%	0.01%	0.03%	0.02%	0.01%	0.01%	0.03%	0.06%
ATPA	ATP synthase subunit alpha, mitochondrial	0.13%	0.03%	0.06%	0.02%	0.00%	0.01%	0.00%	0.00%	0.00%	0.01%	0.00%	0.01%
ENOB	Beta-enolase	0.13%	0.03%	0.13%	0.01%	0.00%	0.00%	0.00%	0.00%	0.00%	0.00%	0.00%	0.00%
PGS1	Biglycan (Fragments)	0.43%	0.15%	0.29%	0.15%	0.02%	0.01%	0.03%	0.03%	0.04%	0.04%	0.02%	0.02%
Col1a1	Collagen type I alpha 1	4.19%	0.50%	4.03%	0.26%	63.08%	3.17%	56.65%	5.54%	61.49%	4.46%	63.09%	3.52%
Col1a2	Collagen type I alpha 2	1.49%	0.12%	0.72%	0.12%	25.21%	2.60%	25.78%	2.32%	29.43%	3.36%	28.42%	3.03%
Col2a1	Collagen type II alpha 1	64.54%	3.36%	63.48%	5.93%	0.21%	0.13%	0.24%	0.32%	0.21%	0.12%	0.09%	0.05%
Col3a1	Collagen type III alpha 1	0.15%	0.02%	0.11%	0.06%	8.73%	3.36%	13.74%	3.70%	6.34%	3.20%	6.15%	4.07%
Col4a2	Collagen type IV alpha 2	0.00%	0.00%	0.00%	0.00%	0.07%	0.02%	0.02%	0.03%	0.03%	0.05%	0.04%	0.02%
Col5a1	Collagen type V alpha 1	0.36%	0.03%	0.26%	0.06%	0.11%	0.03%	0.20%	0.10%	0.13%	0.07%	0.09%	0.03%
Col5a2	Collagen type V alpha 2	1.07%	0.02%	0.83%	0.07%	0.16%	0.02%	0.21%	0.07%	0.14%	0.05%	0.14%	0.05%
Col5a3	Collagen type V alpha 3	0.00%	0.00%	0.00%	0.00%	0.14%	0.25%	0.23%	0.22%	0.13%	0.15%	0.11%	0.26%
Col6a1	Collagen type VI alpha 1	0.17%	0.07%	0.13%	0.05%	0.06%	0.05%	0.08%	0.05%	0.06%	0.03%	0.05%	0.02%
Col6a2	Collagen type VI alpha 2	0.77%	0.25%	0.63%	0.19%	0.32%	0.25%	0.35%	0.18%	0.34%	0.22%	0.25%	0.18%
Col6a3	Collagen type VI alpha 3	2.71%	0.43%	2.22%	0.62%	1.01%	0.78%	0.83%	0.37%	0.68%	0.29%	0.68%	0.46%
Col9a1	Collagen type IX alpha 1	1.65%	0.12%	1.88%	0.27%	0.00%	0.00%	0.00%	0.00%	0.00%	0.00%	0.00%	0.00%

Col9a2	Collagen type IX alpha 2	0.73%	0.09%	0.94%	0.26%	0.00%	0.00%	0.06%	0.08%	0.01%	0.03%	0.00%	0.00%
Col11a1	Collagen type XI alpha 1	3.12%	0.58%	3.69%	0.32%	0.01%	0.01%	0.01%	0.02%	0.02%	0.01%	0.02%	0.01%
Col11a2	Collagen type XI alpha 2	3.86%	0.03%	4.41%	0.30%	0.06%	0.03%	0.05%	0.05%	0.04%	0.03%	0.03%	0.01%
Col12a1	Collagen type XII alpha 1	3.66%	0.69%	3.75%	1.39%	0.01%	0.01%	0.11%	0.12%	0.14%	0.12%	0.02%	0.01%
Col14a1	Collagen type XIV alpha 1	0.00%	0.00%	0.00%	0.00%	0.19%	0.24%	0.17%	0.15%	0.02%	0.03%	0.05%	0.11%
Col27a1	Collagen type XXVII alpha 1	0.00%	0.00%	0.00%	0.00%	0.00%	0.00%	0.03%	0.06%	0.00%	0.00%	0.02%	0.04%
Col28a1	Collagen type XXVIII alpha 1	0.00%	0.00%	0.07%	0.12%	0.00%	0.00%	0.00%	0.00%	0.00%	0.00%	0.00%	0.00%
CSN4	COP9 signalosome complex subunit 4	0.12%	0.06%	0.05%	0.06%	0.00%	0.00%	0.00%	0.00%	0.00%	0.00%	0.01%	0.01%
CSN6	COP9 signalosome complex subunit 6	0.05%	0.02%	0.04%	0.03%	0.00%	0.00%	0.00%	0.00%	0.00%	0.00%	0.03%	0.06%
PGS2	Decorin	0.02%	0.01%	0.00%	0.00%	0.03%	0.00%	0.08%	0.06%	0.06%	0.03%	0.04%	0.01%
FRIL	Ferritin light chain (Fragment)	0.03%	0.02%	0.06%	0.04%	0.00%	0.00%	0.00%	0.00%	0.00%	0.00%	0.00%	0.00%
FMOD	Fibromodulin (Fragment)	0.07%	0.06%	0.04%	0.03%	0.00%	0.00%	0.01%	0.01%	0.00%	0.01%	0.01%	0.01%
G3P	Glyceraldehyde-3-phosphate dehydrogenase	0.51%	0.17%	0.25%	0.05%	0.00%	0.00%	0.01%	0.01%	0.01%	0.01%	0.00%	0.01%
HSPB1	Heat shock protein beta-1	0.30%	0.07%	0.17%	0.05%	0.00%	0.00%	0.00%	0.00%	0.00%	0.00%	0.00%	0.01%
H33	Histone H3.3	0.27%	0.08%	0.33%	0.09%	0.03%	0.04%	0.09%	0.09%	0.02%	0.03%	0.02%	0.04%
H4	Histone H4	0.98%	0.28%	0.81%	0.34%	0.14%	0.13%	0.21%	0.16%	0.09%	0.07%	0.05%	0.07%
HPLN1	Hyaluronan and proteoglycan link protein 1	0.92%	0.29%	2.39%	0.73%	0.00%	0.00%	0.00%	0.00%	0.00%	0.00%	0.00%	0.00%
MFGM	Lactadherin	0.25%	0.06%	0.58%	0.20%	0.00%	0.00%	0.00%	0.01%	0.00%	0.00%	0.00%	0.01%
LDHA	L-lactate dehydrogenase A chain	0.09%	0.02%	0.06%	0.02%	0.00%	0.00%	0.00%	0.00%	0.00%	0.00%	0.00%	0.00%
PGK1	Phosphoglycerate kinase 1	0.32%	0.06%	0.24%	0.08%	0.00%	0.00%	0.00%	0.00%	0.00%	0.00%	0.00%	0.01%
LMNA	Prelamin-A/C	0.43%	0.06%	0.22%	0.06%	0.06%	0.06%	0.08%	0.06%	0.04%	0.04%	0.05%	0.09%

SMPX	Small muscular protein	0.00%	0.00%	0.01%	0.02%	0.00%	0.00%	0.01%	0.01%	0.01%	0.02%	0.04%	0.07%
TENA	Tenascin	0.04%	0.00%	0.03%	0.02%	0.00%	0.00%	0.03%	0.04%	0.15%	0.14%	0.05%	0.03%
TBA1B	Tubulin alpha-1B chain	0.11%	0.05%	0.09%	0.01%	0.01%	0.01%	0.02%	0.01%	0.01%	0.01%	0.02%	0.02%
TBB5	Tubulin beta chain	0.12%	0.04%	0.08%	0.00%	0.02%	0.02%	0.03%	0.02%	0.01%	0.01%	0.01%	0.02%
UGPA	UTP--glucose-1-phosphate uridylyltransferase	0.05%	0.03%	0.08%	0.04%	0.00%	0.00%	0.00%	0.00%	0.00%	0.00%	0.00%	0.00%
VIME	Vimentin	2.11%	0.65%	2.38%	0.81%	0.20%	0.22%	0.29%	0.19%	0.17%	0.15%	0.20%	0.41%

Supplementary Table 4-5: Raw values for the complete blood count and comprehensive metabolic panel parameters.
The parameters were assayed at implantation (t=0) and animal euthanasia (t=4W, t=8W, or t=24W).

Group	ID # and Assay Point	WBC (K/ul)	Absolute Neutrophil cells (K/ul)	Absolute Lymphocyte cells (K/ul)	Absolute Monocyte cells (K/ul)	Absolute Eosinophil cells (K/ul)	Absolute Basophil cells (K/ul)	Neutrophil (%)	Lymphocyte (%)	Monocyte (%)	Eosinophil (%)	Basophil (%)	RBC (M/ul)	Hemoglobin (g/dL)	Hematocrit (%)	MCV (fL)	MCH (pg)	MCHC (g/dL)	RDW (%)	Platelets (K/uL)	MPV (fL)
Implant-treated (4W pilot)	1680 t=0	8.18	4.58	3.05	0.31	0.22	0.02	55.93	37.26	3.83	2.73	0.25	7.25	12.5	34.9	48.2	17.2	35.8	20.4	450	9.3
	1680 t=4W	8.90	3.91	4.18	0.62	0.18	n/a	43.97	46.97	6.99	2.00	n/a	7.09	12.3	41.5	58.5	18.8	32.0	16.2	407	9.2
	7852 t=0	10.02	3.47	4.24	0.25	2.03	0.02	34.63	42.35	2.51	20.28	0.23	6.92	11.7	35.2	50.8	16.9	33.2	19.6	210	13.0
	7852 t=4W	9.52	5.24	3.43	0.76	0.10	n/a	55.00	36.00	8.00	1.00	n/a	7.13	14.1	41.7	58.5	19.8	22.8	15.9	383	11.1
Implant-treated (8W pilot)	3550 t=0	6.54	2.29	3.00	0.20	1.00	0.03	35.01	45.90	3.36	15.26	0.48	5.59	8.8	28.3	50.6	15.7	31.1	18.4	212	11.3
	3550 t=8W	8.02	3.42	3.66	0.22	0.71	0.01	42.62	45.64	2.73	8.91	0.11	8.48	12.6	43.2	51.0	14.9	29.2	18.1	324	10.4
	3556 t=0	10.82	6.64	3.29	0.34	0.53	0.01	61.37	30.44	3.13	4.93	0.12	5.67	8.5	29.7	52.3	15.0	28.6	16.9	170	13.0
	3556 t=8W	10.82	6.11	3.71	0.38	0.59	0.03	56.48	34.28	3.53	5.44	0.26	7.30	11.5	38.4	52.6	15.8	29.9	17.5	311	12.4
Control (24W)	6586 t=0	11.28	7.24	3.80	0.19	0.05	0.01	64.18	33.68	1.66	0.43	0.05	6.64	11.9	41.3	62.2	17.9	28.8	16.3	243	11.4
	6586 t=24W	10.98	7.41	3.23	0.19	0.14	0.01	67.53	29.42	1.69	1.24	0.12	6.06	10.5	33.2	54.8	17.3	31.6	17.4	399	11.2
	6593 t=0	17.04	12.97	2.96	0.10	0.95	0.05	76.10	17.39	0.59	5.60	0.31	5.93	10.6	35.1	59.2	17.9	30.2	16.2	319	10.4
	6593 t=24W	11.02	6.39	4.10	0.22	0.29	0.02	58.03	37.18	2.04	2.60	0.15	5.53	8.8	27.9	50.4	15.9	31.5	18.8	571	10.2

	6613 t=0	8.56	3.18	4.98	0.20	0.15	0.06	37.15	58.12	2.31	1.74	0.67	6.41	12.0	39.3	61.3	18.7	30.5	16.3	160	10.8
	6613 t=24W	6.64	2.45	3.80	0.16	0.22	0.00	36.95	57.30	2.40	3.30	0.05	5.71	10.4	31.6	55.4	18.2	32.9	18.6	313	11.9
	6615 t=0	12.28	9.33	2.12	0.15	0.66	0.02	75.94	17.30	1.25	5.36	0.16	5.09	9.8	32.6	64.1	19.3	30.1	16.5	378	9.4
	6615 t=24W	12.32	7.71	3.76	0.23	0.59	0.02	62.55	30.56	1.89	4.80	0.20	5.79	10.7	32.4	56.0	18.5	33.0	17.8	486	11.2
	6657 t=0	11.02	5.41	4.73	0.26	0.61	0.01	49.07	42.93	2.32	5.56	0.12	6.25	11.2	36.0	57.6	17.9	31.1	16.8	441	10.0
	6657 t=24W	6.78	1.31	3.70	0.28	1.44	0.05	19.32	54.61	4.07	21.26	0.74	6.37	11.6	35.2	55.2	18.2	33.0	18.1	271	10.6
	6668 t=0	9.46	6.40	2.53	0.16	0.35	0.02	67.69	26.75	1.67	3.73	0.16	5.37	9.8	31.0	57.7	18.2	31.6	17.5	523	9.3
	6668 t=24W	5.10	1.20	3.12	0.19	0.58	0.02	23.49	61.12	3.63	11.45	0.30	4.68	8.5	25.7	54.9	18.2	33.1	17.7	409	9.9
Implant-treated (24W)	6633 t=0	11.34	5.61	4.69	0.31	0.72	0.01	49.48	41.35	2.69	6.39	0.08	6.49	10.6	37.8	58.2	16.3	28.0	16.1	188	10.5
	6633 t=24W	10.02	3.26	4.10	0.18	2.43	0.04	32.53	40.93	1.83	24.28	0.43	5.40	9.7	29.4	54.4	18.0	33.0	17.9	234	11.7
	6639 t=0	6.98	4.37	2.19	0.12	0.28	0.01	62.64	31.36	1.77	4.07	0.16	6.43	10.8	38.3	59.5	16.8	28.2	16.7	351	12.0
	6639 t=24W	6.14	1.74	3.32	0.16	0.91	0.01	28.34	54.08	2.62	14.78	0.19	6.01	10.6	33.3	55.4	17.6	31.8	18.4	218	13.0
	6641 t=0	9.90	5.12	4.22	0.29	0.21	0.05	51.73	42.63	2.95	2.14	0.54	5.94	10.1	34.8	58.6	17.0	29.0	16.0	341	9.0
	6641 t=24W	6.98	1.58	4.04	0.23	1.08	0.05	22.63	57.93	3.26	15.45	0.74	6.43	11.3	35.4	55.0	17.6	31.9	18.0	319	9.3
	6643 t=0	7.26	3.44	3.43	0.28	0.11	0.00	47.39	47.27	3.83	1.45	0.06	6.00	10.3	38.1	63.5	17.2	27.0	16.3	417	8.5
	6643 t=24W	9.26	3.19	4.22	0.11	1.73	0.00	34.45	45.58	4.23	18.70	0.03	5.42	10.5	32.8	60.6	19.4	32.0	17.4	322	9.7
	6652 t=0	24.92	21.20	2.23	0.19	1.13	0.16	85.09	8.95	0.76	4.55	0.65	5.63	11.4	35.3	62.7	20.2	32.3	16.0	449	10.0
	6652 t=24W	9.26	2.50	3.32	0.24	3.12	0.09	26.95	35.82	2.56	33.72	0.94	6.79	12.4	39.8	58.6	18.3	31.2	18.3	289	11.3
	6655 t=0	9.36	4.90	3.91	0.31	0.22	0.02	52.33	41.79	3.35	2.37	0.17	5.18	9.2	30.7	59.3	17.8	30.0	16.3	263	12.0
	6655 t=24W	9.80	3.16	3.81	0.30	2.48	0.06	32.23	38.84	3.04	25.29	0.61	5.78	10.0	32.3	55.8	17.3	31.0	18.7	1.61	12.5

Group	ID # and Assay Point	Alanine Transaminase (U/L)	Albumin (g/dL)	Alkaline Phosphatase (U/L)	Amylase (U/L)	Aspartate Transaminase (U/L)	Blood Urea Nitrogen (mg/dL)	Calcium (mg/dL)	Creatinine (mg/dL)	Glucose (mg/dL)	Phosphorus (mg/dL)	Total Bilirubin (mg/dL)	Total Protein (g/dL)	Chloride (mmol/L)	Potassium (mmol/L)	Sodium (mmol/L)
Implant-treated (4W pilot)	1680 t=0	39.8	4.13	51.7	2102.7	30.5	12.5	9.51	0.982	71.0	5.65	0.258	6.30	101.3	3.86	138
	1680 t=4W	36.6	3.99	61.4	2224.4	28.3	16.0	9.80	0.907	51.2	6.09	0.021	6.02	99.2	3.83	137
	7852 t=0	45.7	4.43	31.5	1601.2	32.0	16.4	10.36	1.146	70.6	4.68	0.138	6.52	101.7	4.37	139
	7852 t=4W	47.9	3.94	31.9	1632.9	30.7	20.4	9.57	0.903	60.3	4.73	0.090	6.17	101.6	4.32	142
Implant-treated (8W pilot)	3550 t=0	26.2	3.96	69.3	2459.7	41.6	13.7	10.26	0.932	110.2	5.64	0.034	6.20	103.8	3.89	140
	3550 t=8W	26.8	4.40	63.3	2711.9	35.6	13.8	10.09	1.015	80.4	5.59	0.112	6.84	102.8	4.77	137
	3556 t=0	30.5	4.54	38.1	1876.2	23.6	14.2	10.55	0.950	88.4	6.12	0.089	6.38	102.7	3.70	141
	3556 t=8W	33.8	4.78	52.1	2171.1	18.8	16.2	10.47	1.014	119.9	5.92	0.072	6.51	99.7	4.05	138
Control (24W)	6586 t=0	39.4	4.84	55.6	1778.1	46.5	14.9	10.42	0.832	77.9	5.15	0.148	7.13	99.8	4.48	136
	6586 t=24W	40.7	4.53	38.3	1616.4	33.5	11.9	9.77	1.027	58.8	5.06	0.304	7.36	102.5	4.08	139
	6593 t=0	33.4	4.18	63.4	2143.6	35.7	11.8	10.30	0.737	85.9	5.54	0.077	6.93	100.6	4.00	138
	6596 t=24W	41.2	4.01	43.4	1888.0	28.7	13.4	9.81	0.836	73.9	5.49	0.094	7.62	102.4	4.20	138
	6613 t=0	33.8	4.58	66.1	2295.3	29.1	12.3	10.91	0.946	93.3	5.83	0.088	7.12	103.0	4.30	142
	6613 t=24W	42.7	4.29	38.5	2237.0	29.5	11.9	9.94	1.126	65.2	4.93	0.199	7.15	101.4	3.82	137
	6615 t=0	42.6	4.81	60.5	1991.2	36.1	22.5	10.51	1.066	122.3	6.17	0.133	7.88	106.9	4.03	145

	6615 t=24W	43.4	4.24	34.5	1723.5	26.9	15.6	10.08	1.065	71.4	4.80	0.052	7.46	98.7	4.07	133
	6657 t=0	38.5	4.80	138.5	2171.6	38.1	13.2	10.42	0.836	76.5	5.44	0.025	7.30	98.5	4.45	135
	6657 t=24W	34.0	4.57	126.2	2392.6	36.8	15.0	10.25	1.008	86.4	5.34	0.017	7.49	99.7	4.22	136
	6668 t=0	42.0	4.28	68.9	1201.8	39.9	13.6	10.07	0.872	73.2	4.87	0.185	7.21	98.6	3.72	135
	6668 t=24W	34.9	3.97	70.4	1234.3	31.0	11.1	9.75	0.981	74.4	5.03	0.107	6.84	101.2	4.31	136
Implant-treated (24W)	6633 t=0	35.7	4.56	50.7	1123.0	25.6	12.9	10.10	0.818	101.9	5.16	0.064	7.43	99.6	3.34	136
	6633 t=24W	33.7	4.19	45.1	1121.6	27.4	13.3	10.03	0.947	84.4	5.07	0.035	7.26	100.6	3.77	134
	6639 t=0	44.6	4.36	52.9	2128.6	33.2	11.9	10.08	0.923	91.7	5.35	0.123	7.06	99.3	4.03	136
	6639 t=24W	37.8	4.00	47.8	2178.0	28.1	13.5	10.12	1.083	84.5	4.34	0.067	6.95	99.4	3.67	134
	6641 t=0	34.1	4.28	57.4	2052.6	27.8	10.7	9.98	0.728	102.3	5.53	0.114	7.08	105.7	4.41	140
	6641 t=24W	35.2	4.29	47.1	2130.8	21.0	12.9	10.26	0.880	110.7	5.05	0.078	7.51	97.9	3.91	134
	6643 t=0	31.8	4.64	86.3	2014.2	30.4	16.0	10.21	0.862	80.2	5.08	0.315	7.66	103.2	3.68	139
	6643 t=24W	31.5	4.28	79.6	2119.3	32.3	11.1	10.21	0.910	82.7	4.76	0.079	7.24	102.7	3.60	137
	6652 t=0	39.0	4.52	52.7	2787.5	48.0	16.6	10.03	1.054	108.9	5.34	0.180	7.21	104.2	4.04	139
	6652 t=24W	35.8	4.41	48.1	2721.9	37.7	13.2	10.38	1.139	74.1	4.11	0.073	7.51	102.1	4.73	134
	6655 t=0	45.9	4.23	88.5	2961.7	33.5	13.5	9.92	0.756	87.4	5.55	0.074	6.99	101.8	4.73	135
	6655 t=24W	43.0	4.06	66.9	2792.6	37.5	12.1	10.32	0.802	77.7	5.07	0.044	7.96	98.1	4.80	132

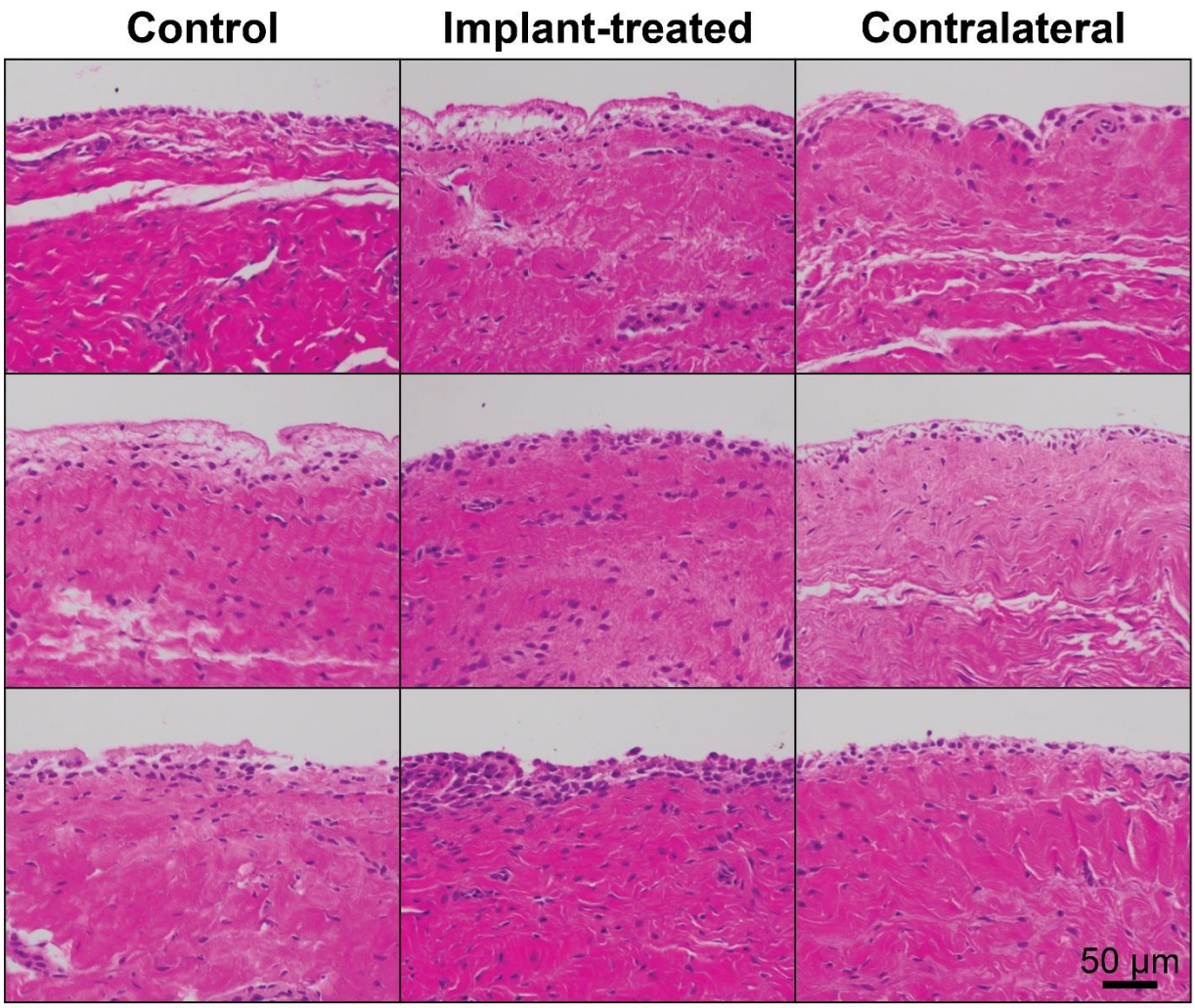

Supplementary Figure 4-5: The synovium of empty defect and implant-treated TMJs.
Consistent with contralateral synovium, control and implant-treated synovium did not exhibit any abnormal cellular response in three different animals (rows) per group (columns).

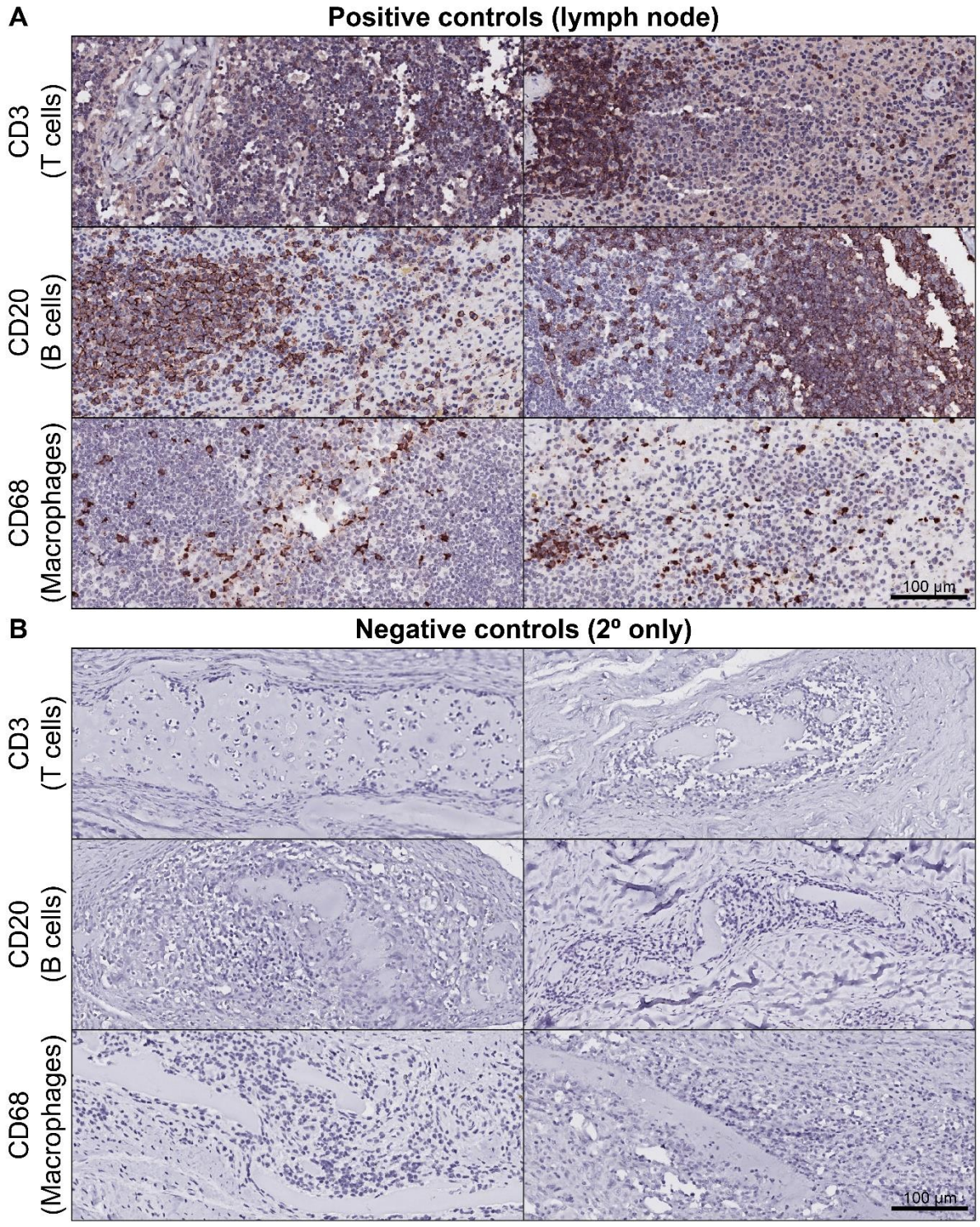

Supplementary Figure 4-6: Controls for immunohistochemical staining.
(A) Lymph node positive controls exhibited staining for T cell, B cells, and macrophages, while (B) negative secondary antibody-only controls lacked staining, as expected.

Supplementary Table 4-6: Crosslinks in the implants after extended culture or implantation.
After 24 weeks of implantation, mature pyridinoline (PYR) and immature dihydroxylysinonorleucine (DHLNL) crosslinks normalized to dry weight (DW) significantly increase compared to pre-implantation values (i.e., t=0 *in vitro*). Those values normalized to hydroxyproline (OHP) approached native TMJ disc values but were not significantly different between groups.

Group	PYR/DW (ng/mg)	PYR/OHP (mmol/mol)	DHLNL/DW (ng/mg)	DHLNL/OHP (mmol/mol)	PYR/DHLNL (mol/mol)
t=0 *in vitro*	490±51	14.68±1.43	250±42	10.60±2.58	1.437±0.262
t=24W *in vitro*	424±37	18.14±2.59	187±58	11.45±4.46	1.732±0.470
t=24W *in vivo*	2570±583****	15.23±3.41	855±186****	7.08±1.73	2.194±0.437**
Native TMJ disc	5518±1686	35.94±8.73	1367±500	12.32±3.48	2.968±0.138

Supplementary Table 4-7: Compressive properties of neocartilage.
Relaxation and instantaneous moduli values increased after 24 weeks of extended culture. Implants after 24 weeks *in vivo* were not tested (nt).

Group	20% Relaxation modulus (kPa)	20% Instantaneous modulus (kPa)	20% Coefficient of viscosity (MPa s)
t=0 *in vitro*	177±55	777±115	55.9±18.8
t=24W *in vitro*	435±151***	1214±465*	59.9±34.0
t=24W *in vivo*	nt	nt	nt

Supplementary Table 4-8: Immunohistochemistry parameters.
For CD3, CD20, and CD68 staining, the brands of primary antibody, dilution ratios, antigen retrieval methods, blocking serums, secondary antibodies, and development methods are listed.

Primary antibody	Brand	Dilution ratio	Antigen retrieval	Blocking serum	Secondary antibody	Development
Rat anti-CD3	Dr. Moore's Leukocyte Antigen Biology Lab clone 3-12	1:10	Dako antigen retrieval solution, 30 min at 95°C	10% horse serum in PBS, 20 min at room temperature	Biocare Medical's 4+ detection systems anti-rat	Streptavidin horseradish peroxidase (HRP) GR608
Rabbit anti-CD20	NeoMarker RB-9013-P1	1:4	Dako antigen retrieval solution, 30 min at 95°C	10% horse serum in PBS, 20 min at room temperature	Biocare Medical's 4+ detection systems anti-rabbit	Streptavidin HPR HP604
Mouse anti-CD68	ThermoFisher Mac387	1:9	EDTA buffer, 30 min at 95°C	10% horse serum in PBS, 20 min at room temperature	Biocare Medical's 4+ detection systems anti-mouse	Streptavidin HPR HP604

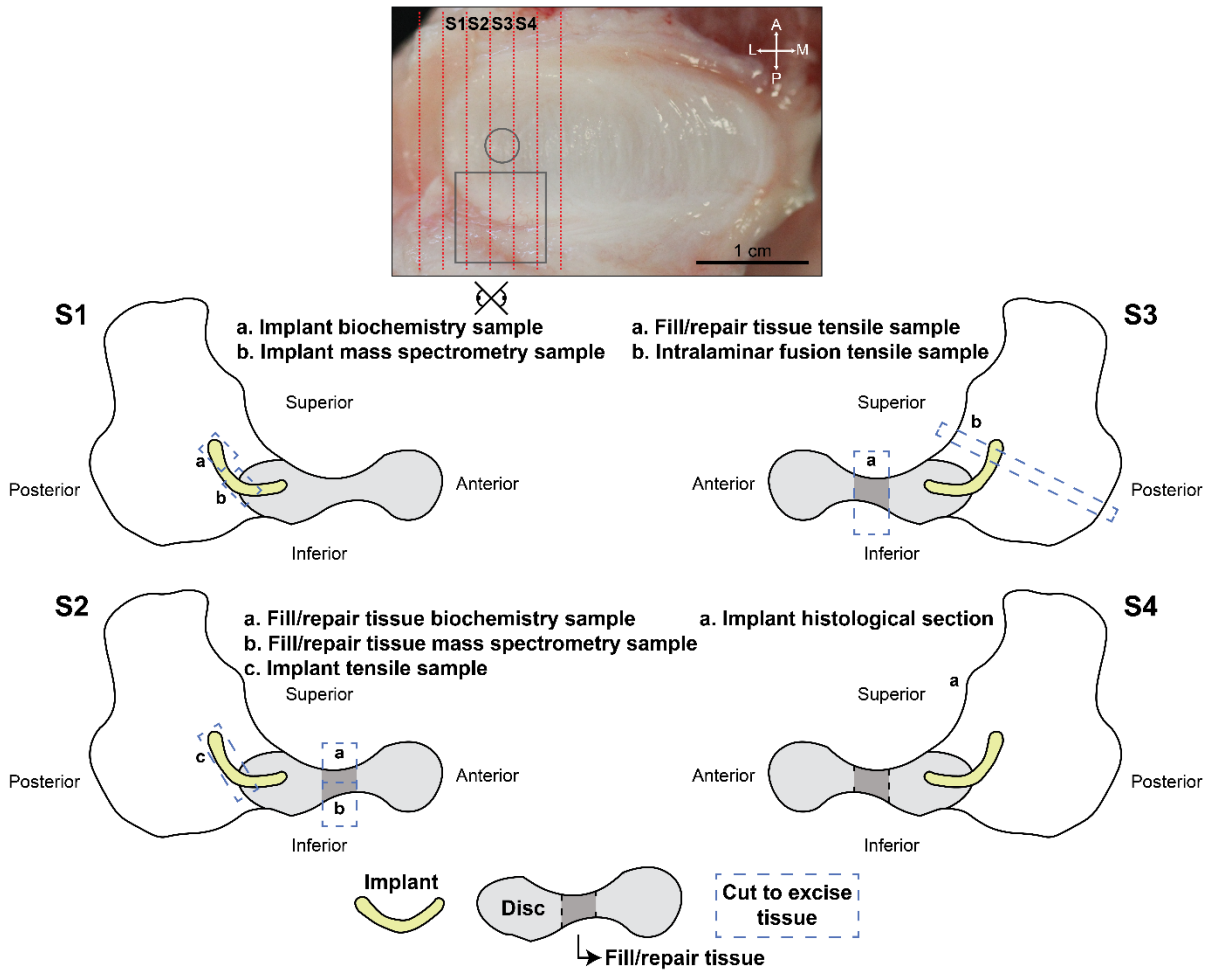

Supplementary Figure 4-7: TMJ disc sample preparation and excision.
From serial sectioning (red lines) of the TMJ disc, the implant (square) and fill/repair tissue (circle) were identified. Upon examining sections, the following samples were identified from approximately four serial sections (as depicted): S1) implant biochemistry sample, implant mass spectrometry sample, S2) fill/repair tissue biochemistry sample, fill/repair tissue mass spectrometry sample, implant tensile testing sample, S3) fill/repair tissue tensile testing sample, intralaminar tensile testing sample, and S4) implant histological section. A, anterior, L, lateral, M, medial, P, posterior.

Chapter 5: The Effect of Neonatal, Juvenile, and Adult Donors on Rejuvenated Neocartilage Functional Properties[5]

Abstract

Cartilage does not naturally heal, and cartilage lesions from trauma and wear-and-tear can lead to eventual osteoarthritis. To address long-term repair, tissue engineering of functional biologic implants to treat cartilage lesions is desirable, but the development of such implants is hindered by several limitations including 1) donor tissue scarcity due to the presence of diseased tissues in joints, 2) dedifferentiation of chondrocytes during expansion, and 3) differences in functional output of cells dependent on donor age. Toward overcoming these challenges, 1) costal cartilage has been explored as a donor tissue, and 2) methods have been developed to rejuvenate the chondrogenic phenotype of passaged chondrocytes for generating self-assembled neocartilage. However, it remains unclear how the rejuvenation processes are influenced by donor age, and, thus, how to develop strategies that specifically target age-related differences. Using histological, biochemical, proteomic, and mechanical assays, this study sought to determine the differences among neocartilage generated from neonatal, juvenile, and adult donors using the Yucatan minipig, a clinically relevant large animal model. Based on the literature, a relatively young adult population of animals was chosen due to a reduction in functional output of human articular chondrocytes after 40 years of age. After isolation, costal chondrocytes were expanded, rejuvenated, and self-assembled, and the neocartilages were assessed. The aggregate modulus values of neonatal constructs were at least 1.65-fold of those from the juvenile or adult constructs. Poisson's ratio also significantly differed among all groups, with neonatal constructs exhibiting values 49% higher than adult constructs. Surprisingly, other functional properties such as tensile modulus and glycosaminoglycan content did not

[5] **Chapter published as:** Donahue, R.P.,* Nordberg, R.C.,* Bielajew, B.J., Hu, J.C., Athanasiou, K.A. The effect of neonatal, juvenile, and adult donors on rejuvenated neocartilage functional properties. *Tissue Engineering Part A*. January 2022, online ahead of print. (* These authors contributed equally.)

significantly differ among groups. Total collagen content was slightly elevated in the adult constructs when compared to neonatal and juvenile constructs. A more nuanced view via bottom-up mass spectrometry showed that *Col2a1* protein was not significantly different among groups, but protein content of several other collagen subtypes (i.e., *Col1a1, Col9a1, Col11a2,* and *Col12a1*) was modulated by donor age. For example, *Col12a1* protein content in adult constructs was found to be 102.9% higher than neonatal-derived constructs. Despite these differences, this study shows that different aged donors can be used to generate neocartilages of similar functional properties.

Impact Statement

Tissue-engineered neocartilage can be generated with functional properties that mimic native cartilage tissue. However, cell sourcing challenges hinder clinical translation of tissue-engineered cartilage. Chondrocytes can be expanded and rejuvenated for the generation of functional self-assembled cartilage, making an allogeneic approach feasible. However, it is currently unclear if donor age impacts functional properties. Here, using the Yucatan minipig as a clinically relevant large animal model, we demonstrate that functional properties of self-assembled neocartilage are relatively consistent regardless of donor age, suggesting that a wider range of donor ages may be used for cartilage tissue engineering than previously expected.

Introduction

Hyaline articular cartilage does not naturally heal, and cartilage lesions from trauma or wear-and-tear can develop into osteoarthritis (OA). OA is associated with pain and loss of joint function [359, 360]. According to the Centers for Disease Control, OA affects over 32 million people in the U.S. [361] and is projected to rise up to 60% in prevalence over the next two decades [362]. Tissue engineering is poised to provide a long-term, regenerative solution

needed for cartilage defects, and the only currently approved cell-based therapy is matrix-assisted autologous chondrocyte implantation (MACI), which consists of expanding a patient's cells in the laboratory and re-implanting the cells on a collagen membrane [363]. For MACI and future cell-based therapies, such as tissue-engineered neocartilage, it is widely recognized that one of the biggest challenges to the field is cell sourcing, and the development of novel cell-based cartilage therapies is hindered by several limitations including 1) donor tissue scarcity due to the presence of diseased tissues in the joints, 2) dedifferentiation of cells during expansion, and 3) the differences in engineering potential of chondrocytes dependent on donor age [31, 364, 365].

Donor tissue scarcity is a major challenge because cartilage tissue engineering techniques require high numbers of chondrocytes, especially when considering the development of large cartilage implants. For example, self-assembled cartilage constructs have been generated up to 9.3 cm^2 but require 50 million chondrocytes [212], which would require harvesting approximately half of the entirety of chondrocytes from one adult donor knee [366, 367]. This is an untenable proposition given that patients who require cartilage therapies have diseased tissues in their joints, further limiting the availability of healthy donor cartilage. Thus, one of the challenges for the translation of cartilage tissue engineering is selecting a cell source that is both functional and scalable. While fully differentiated, primary chondrocytes are a desirable cell source in that they are already primed to function as mature chondrocytes, practically, they are difficult to obtain in large numbers due to donor site morbidity in autologous cases, limited donor tissue supply in allogeneic cases, and prevalence of disease within the donor tissue.

Cell expansion can help address the issue of cell scarcity but is limited due to concerns of chondrocyte dedifferentiation. Passaging chondrocytes can allow for a cumulative expansion factor of $12.6X10^6$-fold [25], but passaging chondrocytes can lead to rapid dedifferentiation and loss of the chondrogenic phenotype [368]. To combat this, aggregate culture methods have

been developed to rejuvenate cells to a chondrogenic phenotype and to restore the ability of passaged chondrocytes to generate functional self-assembled cartilage [25]. Moreover, cartilage is considered relatively immuno-privileged [26], and, therefore, passaged, allogeneic chondrocytes can be utilized to provide cells for a large number of patients. Specifically, at passage 11, it has been estimated that chondrocytes from a single 1 cm^3 biopsy can generate cartilage implants for up to 10 million patients [25]. At such a staggering expansion factor, selecting the appropriate donor source will be critical to the success of a tissue-engineered cartilage implant system.

Toward addressing the current bottleneck of cell sourcing, costal chondrocytes, in particular, are attractive due to their excellent expansion and redifferentiation capabilities [149, 369]. Additionally, previous use of costal cartilage in rhinoplasties [370] and as an interpositional material for the temporomandibular joint (TMJ) [18] make costal chondrocytes a logical cell source for tissue engineering of cartilages. It has been demonstrated that costal chondrocytes have a greater initial yield and capacity for expansion than articular chondrocytes and can redifferentiate without ossification [371]. Harnessing these advantages, recent cartilage tissue engineering research has utilized costal chondrocytes for both scaffold-based [372, 373] and scaffold-free techniques [19]. Moreover, passaged costal chondrocytes can be used to repair fibrocartilage and have been demonstrated to repair defects in the TMJ disc [23]. Therefore, costal chondrocytes can be further developed into a cell source to repair both articular cartilage and fibrocartilage.

When selecting a donor source, a factor that may play a role in the functional properties of a tissue-engineered cartilage construct is the age of the donor. Prior work has demonstrated that donor age can affect the functional output of chondrocytes. For example, it has been reported that the growth factor responsiveness of chondrocytes is modulated by donor age [30]. Also, chondrocytes isolated from the knee of donors under the age of 13 produced significantly more proteoglycans and had greater proliferative capacity than older donors (i.e., up to 72 years

old) [31]. In another study, increased levels of *Col II* and *Sox9* gene expression were reported in juvenile chondrocytes (i.e., 6-month-old donor) during monolayer expansion compared to adult chondrocytes (i.e., 34-year-old donor), and higher *Col II* and *Acan* gene expression were reported in juvenile chondrocyte-derived hydrogel neocartilages [364]. To combat the effect of aging chondrocytes, transforming growth factor beta 1 (TGF-β1), basic fibroblast growth factor (bFGF), and platelet-derived growth factor (PDGF-BB) have been used to support post-expansion chondrogenic capacity for cells derived from older donors [365]. It was found that when these growth factors were applied, chondrocyte proliferation rate was significantly elevated from donors of all age groups (age 20-91 years), but chondrogenic capacity in neocartilage formation was elevated in donors only up to 40 years of age [365]. Additionally, this growth factor combination has been previously shown to increase neocartilage glycosaminoglycan (GAG) content, decrease the ratio of collagen types I to II, and enhance compressive properties [149]. Thus, even in experiments that aim to improve the utility of cells from older donors, it was shown that younger chondrocytes consistently have a higher functional output. Thus, autologous therapeutic strategies are hindered by the lack of methodologies that can enhance an older donor's cells to the levels of productivity associated with cells from younger donors, and allogeneic approaches are limited to using scarcely available young donor sources. Based on the above literature examining articular chondrocytes, the work here focused on characterizing the age-related differences in costal cartilage-derived neotissues from a relatively young range of donors (i.e., neonatal, juvenile, young adult) due to the attractiveness of using these cells for potential therapies and the lack of such characterization in the literature.

Toward the translation of cartilage tissue-engineered products and toward addressing donor tissue scarcity, chondrocyte dedifferentiation, and different functional output of chondrocytes of various ages, the current study examined the effect of donor age on the functional properties of self-assembled neocartilage formed using expanded costal

chondrocytes. Neocartilage constructs were generated from costal chondrocytes isolated from neonatal, juvenile (5-8 months), and skeletally mature adult (18-24 months) Yucatan minipigs. In terms of human age equivalencies, the neonatal minipigs correspond to several days old in the human, juvenile minipigs correspond to the start of sexual maturity at around 8-10 years old in the human [374, 375], and adult minipigs correspond to the end of skeletal maturity at a maximum of 25 years old in the human [24, 376]. It is important to note that, in relation to human age, the adult group of minipigs here is relatively young (i.e., up to 25 years in humans) and were selected for this study as literature has shown a severe reduction in the capacity to create mechanically robust neotissue after 40 years of age in humans [365]. Thus, the objective of this study was to ultimately characterize the functional differences of neocartilage derived from these three minipig donor ages. As with cells derived from articular cartilage, it was hypothesized that donor age will have an effect on the biochemical and mechanical properties of neocartilage constructs derived from costal chondrocytes.

Materials and Methods

Costal cartilage harvest and isolation

Tissues were obtained from Yucatan minipigs culled for reasons unrelated to this study. The ages of the minipigs donors were stillborn (neonatal); 5-8 months (juvenile), corresponding to start of sexual maturity in humans (e.g., 10-12 years old) [374]; and 1.5-2 years (skeletally mature adult), corresponding to completion of epiphyseal closure in humans (e.g., up to 25 years old) [376]. Costal cartilage (green oval, Figure 5-1) was obtained from four minipigs (2 males, 2 females) for each age (12 total for the entire study) and separated from the bone. Soft tissues and perichondrium were removed from the costal cartilage before mincing into ~1 mm^3 pieces. Costal cartilage was digested via agitation at 50 RPM using 0.4% w/v pronase for 1h at 37°C and then 0.2% w/v collagenase for 18h at 37°C. Both enzymes were supplemented with 3% fetal bovine serum (FBS) in Dulbecco's modified Eagle's Medium (DMEM) with 1% penicillin-

streptomycin-fungizone (PSF). Following digestion, a single cell suspension was obtained by passing the cell suspension through a 70 µm strainer, and chondrocytes were rinsed using blank DMEM with 1% PSF in preparation for expansion and aggregate rejuvenation.

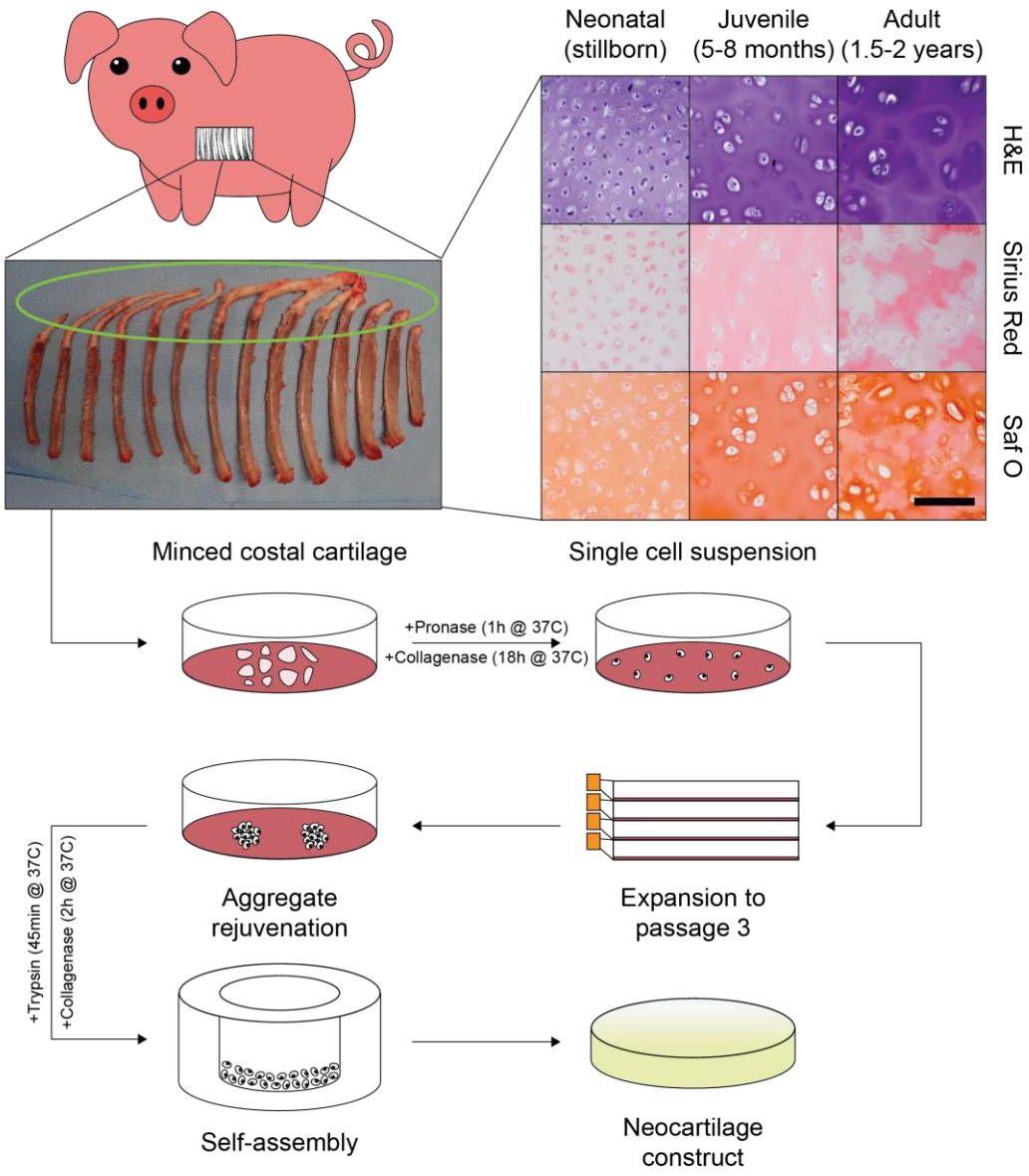

Figure 5-1: Costal cartilage harvest and isolation and the tissue engineering process.
Costal cartilage (green oval) from the ribs of Yucatan minipigs of three different ages of animals was isolated from the surrounding soft tissue and separated from the bone, minced into small pieces, and enzymatically digested to obtain a single cell suspension. Histological staining showed differences in native costal cartilage among the three ages (neonatal, juvenile, and adult). Chondrocytes were then seeded into flasks for expansion to passage 3, then aggregate rejuvenated in nonadherent petri dishes. Subsequent seeding for self-assembly then occurred to obtain a neocartilage construct. Abbreviations: H&E, Hematoxylin and Eosin; Saf O, Safranin O; Sirius Red, Picrosirius Red. Scale bar = 200 µm.

Chondrocyte expansion and aggregate rejuvenation

Immediately following isolation (Figure 5-1), chondrocytes were plated for expansion at 2.5 million per T225 flask (~11,111 cells/cm^2) in chemically defined, chondrogenic (CHG) medium composed of DMEM supplemented with 1% PSF, 1% insulin-transferrin-selenous acid+ (ITS+), 1% nonessential amino acids (NEAA), 100 nM dexamethasone, 50 µg/mL ascorbate-2-phosphate, 40 µg/mL L-proline, and 100 µg/mL sodium pyruvate. CHG medium was further supplemented with 2% FBS, 1 ng/mL TGF-β1, 5 ng/mL bFGF, and 10 ng/mL PDGF-BB during expansion to passage 3 [149]. Cells were frozen after one passage in FBS containing 10% dimethyl sulfoxide (DMSO) for downstream use in multiple experiments and thawed as needed for use at passage 3. Donors were cultured separately up until passage 2 and then subsequently combined based on donor age (i.e., two male and two female donors were combined for each age). Medium changes occurred every 3-4 days. Upon 90% confluence for each passage, cells were lifted using 0.05% Trypsin-EDTA for 9 minutes followed by 0.2% w/v collagenase supplemented with 3% FBS in DMEM with 1% PSF for 40 minutes. After three passages, cells underwent aggregate rejuvenation.

For aggregate rejuvenation, cells were plated at 750,000 cells/mL in CHG medium containing 10 ng/mL TGF-β1, 100 ng/mL growth differentiation factor 5 (GDF-5), and 100 ng/mL bone morphogenetic protein 2 (BMP-2) for 14 days [150]. Petri dishes (25 x 100 mm) were covered with 1% agarose to make the surfaces nonadherent. Dishes were placed on an orbital shaker at 50 RPM for 24 hours after seeding, then switched to static culture for the remaining culture time. Medium changes occurred every 3-4 days. After 14 days, aggregates were digested using 0.05% Trypsin-EDTA for 45 minutes followed by 0.2% w/v collagenase supplemented with 3% FBS in DMEM with 1% PSF for 2 hours. Cells were passed through a 70 µm cell strainer prior to the self-assembling process.

Neocartilage self-assembly

Two days before self-assembly, nonadherent cylindrical 5 mm diameter wells were made using 2% agarose and negative molds. CHG medium was exchanged at least three times prior to cell seeding. Based on prior work [377], 2 million cells per well was identified as the ideal seeding density, and cells were seeded at this density in 100 µL of CHG. After 4 hours, medium was topped off in the well with another 400 µL. CHG medium was then exchanged (450 µL) every day until neocartilage was unconfined from the wells at day 5. From days 5-28, CHG medium was exchanged every other day (2 mL). After 28 days, cell culture was terminated, and samples were analyzed.

Sample processing and photometric biochemical analysis

After 28 days of self-assembly, each construct (n=7-8 per group) was photographed, measured for diameter and thickness (on the outside edge of the construct), and then split into samples for photometric biochemical analysis, pyridinoline (PYR) mass spectrometry analysis, bottom-up mass spectrometry proteomic analysis, mechanical testing, and histology. Pieces for biochemical and PYR analysis were weighed to obtain a wet weight (WW) and frozen at -20 °C for further downstream processing. After lyophilization, a dry weight (DW) was taken for each sample, and biochemical samples were subsequently digested using papain for 18 hours at 60 °C. Total collagen content was quantified using a modified hydroxyproline assay, as previously described [93]. GAGs were also quantified through a dimethylmethylene blue assay (DMMB) per the manufacturer's protocol. Total collagen content and GAG content were normalized to DW. Hydration was calculated by subtracting the ratio of DW to WW from 1 and converted to a percentage by multiplying by 100.

Pyridinoline mass spectrometry analysis

As previously described [378], liquid chromatography-mass spectrometry was performed to quantify PYR content. Briefly, neocartilage samples (~200-500 µg DW) were hydrolyzed in 6 N HCl at 105 °C for 24 hours, then acid was evaporated inside a chemical fume hood. Dried hydrolysates were resuspended in 400 µL of 25% v/v acetonitrile and 0.1% v/v formic acid in water and centrifuged at 15,000 g for 10 minutes through a 100 kDa molecular weight cut-off centrifugal filter, yielding a colorless, transparent, filtered hydrolysate. These filtered hydrolysates (5 µL) were analyzed on a Waters Quattro Premier XE triple quadrupole mass spectrometer with a Cogent Diamond Hydride 2.o HPLC column on a Waters ACQUITY UPLC I-Class core system. Solvent A was 0.1% formic acid in water, and solvent B was 0.1% formic acid in acetonitrile. The gradient was as follows: initial 90% B, 1 minute 90% B, 2 minutes 20% B, 5 minutes 90% B, 10 minutes 90% B, flow rate 400 µL/min, and a total run time of 10 minutes. A standard curve of six serial dilutions of PYR standard was used to quantify the PYR in injected samples using area-under-curve measurements in the QuanLynx module of MassLynx v4.1. PYR samples were then normalized to collagen content.

Bottom-up mass spectrometry proteomic analysis

For bottom-up proteomics, three samples per group were washed twice in 10 mM ammonium citrate and twice in 50 mM ammonium bicarbonate, and mass spectrometry-grade trypsin was added in a 1:20 w/w ratio of trypsin to sample DW. Samples were digested overnight at 65 °C in 200 µL of 50 mM ammonium bicarbonate. Samples were filtered through 100 kDa molecular weight cut-off centrifugal filters and diluted 4:1 in 0.1% formic acid, yielding a colorless, transparent digest. The digests were analyzed using a Thermo Fisher Scientific UltiMate 3000 RSLC system with an Acclaim® PepMap RSLC column coupled to a Thermo Fisher Scientific Orbitrap Fusion Lumos mass spectrometer. Solvent A was 0.1% formic acid in water, and solvent B was 0.1% formic acid in acetonitrile. The gradient was as follows: 4% to 25% solvent

B over 57 minutes, a flow rate of 300 nL/min, and a total run time of 60 minutes. Label-free quantitation was carried out using MaxQuant as previously described [357]. Briefly, raw files were searched using MaxQuant (v. 1.6.0.16) against a FASTA containing the *Sus scrofa* proteome (SwissProt, version from May 2021) and *Sus scrofa* collagen proteins (TrEMBL). For quantification, intensities were determined as the full peak volume over the retention time profile. The resulting quantification values, normalized to total protein content, are displayed in Supplementary Table 5-1.

Mechanical testing and analysis

For mechanical testing, creep indentation and uniaxial tensile tests were performed. For creep indentation testing, a 3 mm diameter punch of neocartilage was indented using a flat 1 mm diameter porous tip under a constant load, and force-displacement curves were fit to a linear biphasic model using finite element optimization and semi-analytical solutions to obtain aggregate modulus, Poisson's ratio, and permeability, as previously described [83]. For uniaxial tensile tests, a dog bone-shaped piece of the neocartilage was glued to paper tabs, loaded into an Instron uniaxial tension machine, and pulled to failure at a rate of 1% strain per second. Force-displacement curves were used to calculate tensile Young's modulus and ultimate tensile strength (UTS) using a custom MathWorks' MATLAB code, as previously described [355].

Histological processing and staining

Immediately after culture, constructs were fixed in 10% neutral-buffered formalin for at least 72 hours. Constructs were then processed, embedded in paraffin, and sectioned at 6 μm thickness using a microtome. Sections were mounted on slides and stained with Safranin O (Saf O), Picrosirius Red (Sirius Red), and Hematoxylin and Eosin (H&E).

Statistical analyses

All statistical analysis was done with GraphPad's Prism 9. Quantitative gross morphological, biochemical, mechanical, and proteomic data was assessed using a one-way analysis of variance (ANOVA) with *post hoc* Tukey's honestly significant difference (HSD) test. Significance levels were set at $\alpha = 0.05$. A connecting letters report is used to show significant differences from the *post hoc* test, where groups that do not share the same letter are significantly different.

Results

Gross morphology and histology

Hydration for juvenile and adult constructs was 83.1±1.5% and 83.3±1.5% respectively (Table 5-1). Neonatal constructs exhibited a significantly lower hydration (80.7±1.1%) when compared to juvenile ($p=0.001$) and adult ($p=0.005$) constructs, which were not significantly different from one another (Table 5-1). Neonatal constructs were significantly larger in diameter than juvenile and adult constructs (both $p<0.0001$), while juvenile constructs were significantly thicker than neonatal and adult constructs (both $p<0.0001$) (Figure 5-2A-C, Table 5-1). Adult constructs also appeared slightly more curved than neonatal and juvenile constructs (Figure 5-2A-C). Staining for general tissue and cellular morphology using H&E and total collagen content using Sirius Red appeared relatively consistent among constructs (Figure 5-2D-I). However, Saf O staining for GAG content appeared slightly more intense in neonatal constructs (Figure 5-2J) when compared to juvenile and adult constructs (Figure 5-2K-L).

Table 5-1: Morphological properties of neocartilage constructs.
Juvenile and adult constructs exhibit significantly higher hydration, while neonatal constructs are significantly larger in diameter, and juvenile constructs are significantly thicker when compared to other groups. Statistics: One-way ANOVA with *post hoc* Tukey's HSD test, $\alpha = 0.05$, n=7-8 per group, superscript letters depict the connecting letters report.

Group	Hydration (%)	Diameter (mm)	Thickness (mm)
Neonatal	80.7 ± 1.1^{B}	6.59 ± 0.12^{A}	0.64 ± 0.04^{B}
Juvenile	83.1 ± 1.5^{A}	5.99 ± 0.19^{B}	0.92 ± 0.07^{A}
Adult	83.3 ± 1.5^{A}	6.02 ± 0.10^{B}	0.71 ± 0.08^{B}

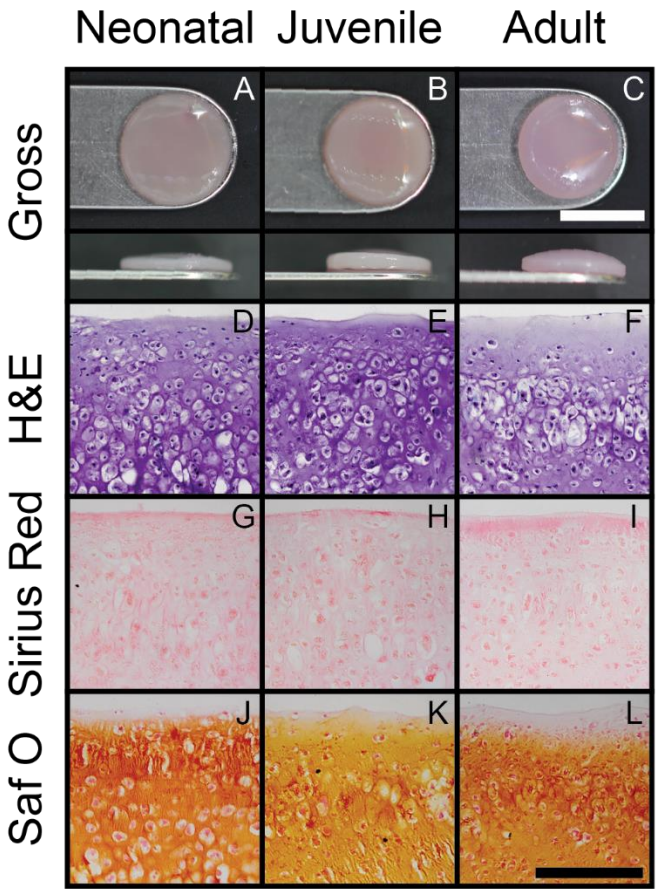

Figure 5-2: Gross morphology and histology of neocartilage constructs.
Of the three groups examined, (A) neonatal, (B) juvenile, and (C) adult constructs, neonatal constructs appear to be the largest in diameter, and juvenile constructs appear thickest. Consistent staining by H&E (D-F) and by Sirius Red (G-I) for total collagen is observed. Slightly increased Saf O staining intensity was observed in (J) neonatal constructs when compared to (K) juvenile and (L) adult constructs. Abbreviations: H&E, Hematoxylin and Eosin; Saf O, Safranin O; Sirius Red, Picrosirius Red. White scale bar = 5 mm, black scale bar = 200 µm.

Biochemical and proteomic properties

Collagen/DW for neonatal and juvenile constructs was 0.092±0.006 µg/µg and 0.098±0.005 µg/µg, respectively, which was significantly less than the adult constructs (0.109±0.010 µg/µg, p=0.001, p=0.017) (Figure 5-3A). GAG/DW for neonatal, juvenile, and adult constructs was 0.498±0.042 µg/µg, 0.481±0.037 µg/µg, and 0.539±0.119 µg/µg, respectively; there was no

statistical difference among the three groups (Figure 5-3B). There was also no statistical difference in PYR/Collagen (Figure 5-3C).

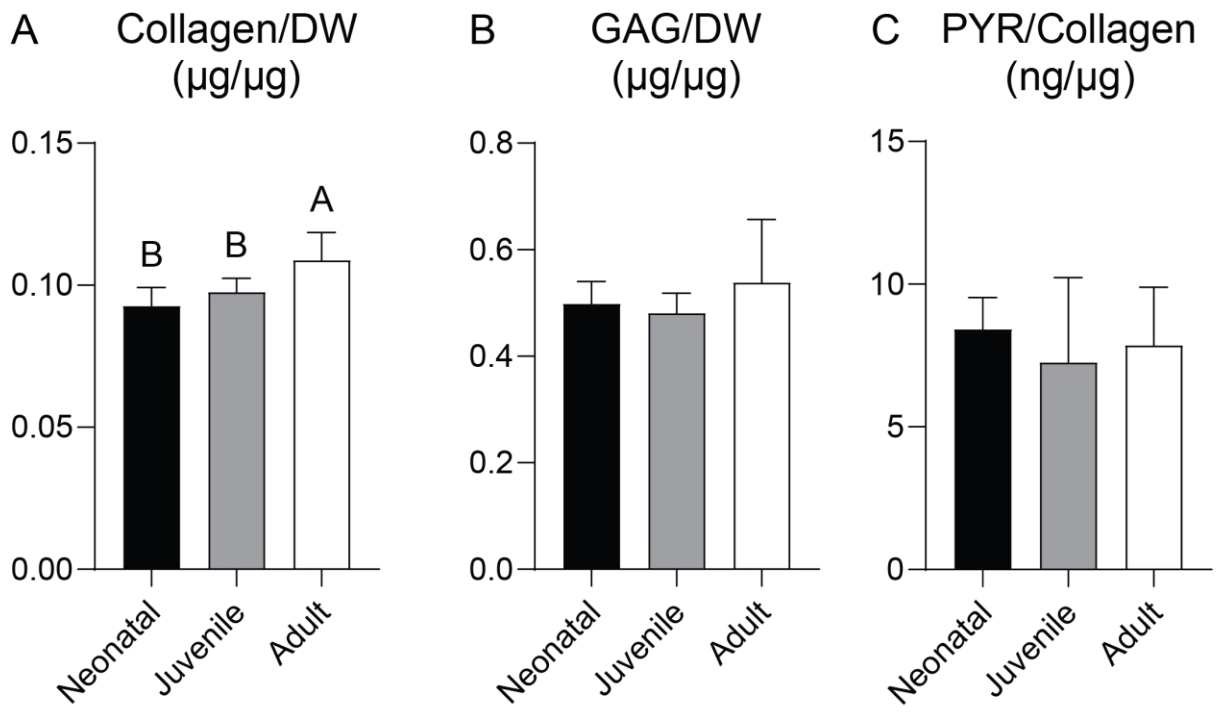

Figure 5-3: Biochemical properties of neocartilage constructs.
(A) Collagen/DW increases with age of construct donors, while (B) GAG/DW and (C) PYR/Collagen did not exhibit any significant differences. Statistics: One-way ANOVA with *post hoc* Tukey's HSD test, $\alpha = 0.05$, n=7-8 per group, letters depict the connecting letters report. Abbreviations: DW, dry weight; GAG, glycosaminoglycan; PYR, pyridinoline.

A full list of proteins quantified with bottom-up mass spectrometry is available in Supplementary Table 5-1. Eight proteins of interest were selected based on known roles in cartilage extracellular matrix. *Col2a1* protein content did not significantly differ among groups, but *Col1a1* (p=0.039), *Col9a1* (p=0.003), and *Col11a2* (p=0.007) protein content were all statistically higher in the neonatal group compared to adult-derived constructs (Figure 5-4A-D). The opposite was true for *Col12a1* protein content, statistically increasing in both juvenile (p=0.001) and adult (p<0.0001) construct groups compared to neonatal-derived constructs (Figure 5-4E). There were no statistical differences in link protein, aggrecan, and biglycan among the groups (Figure 5-4F-H).

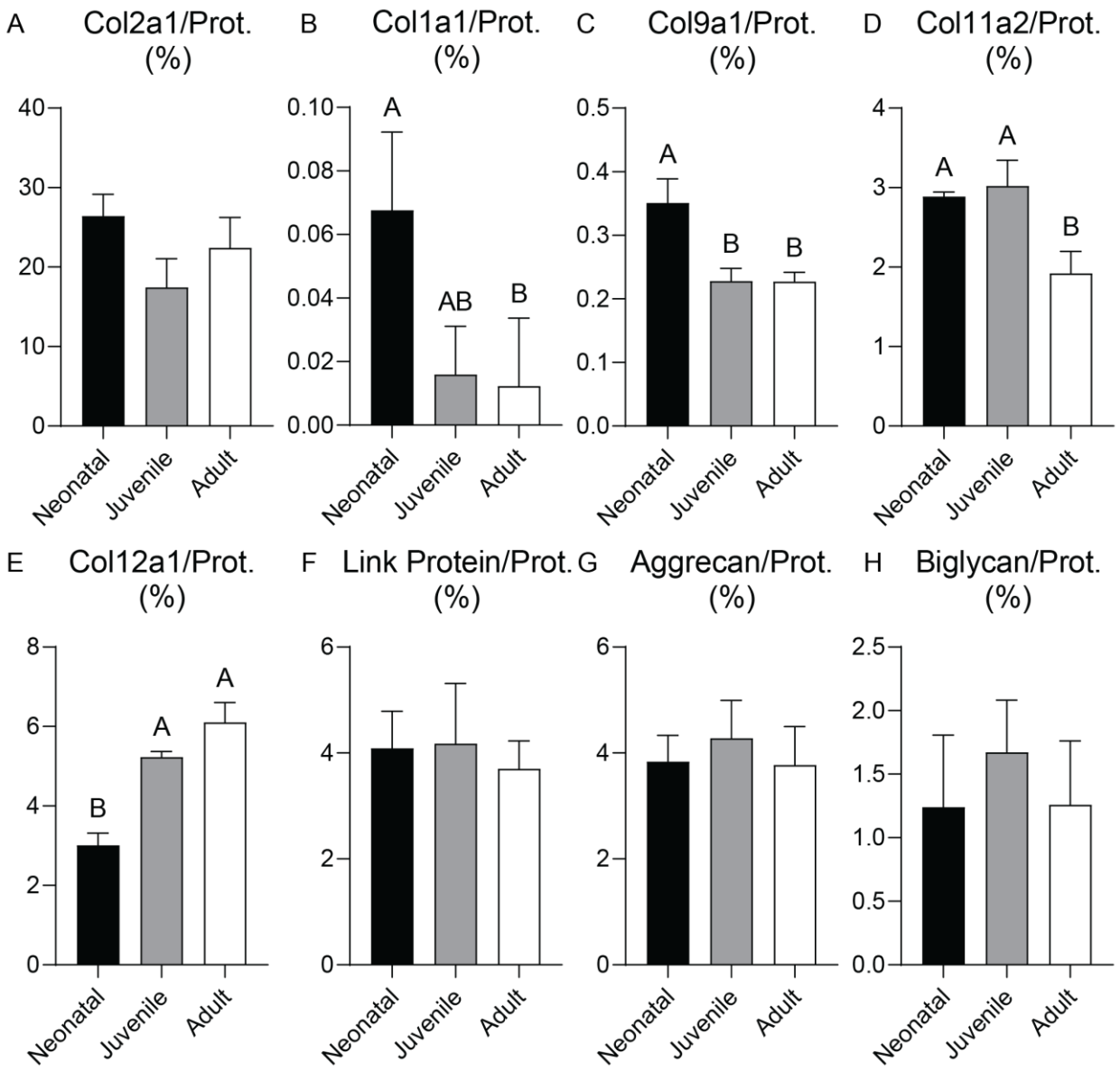

Figure 5-4: Proteomic analysis of neocartilage constructs.
Interestingly, (A) *Col2a1* protein did not significantly differ among groups, while (B) *Col1a1*, (C) *Col9a1*, and (D) *Col11a2* proteins were significantly higher in neonatal constructs compared to adult constructs. Contrastingly, (E) *Col12a1* protein content trends higher in adult-derived constructs, while there were not differences in (F) link protein, (G) aggrecan, and (H) biglycan, three crucial components of the matrix. Statistics: One-way ANOVA with *post hoc* Tukey's HSD test, $\alpha = 0.05$, n=3 per group, letters depict the connecting letters report. Abbreviation: Prot., protein.

Mechanical properties

Tensile properties remained unaffected as donor age was varied for constructs. When compared to neonatal constructs (1.91±0.49 MPa), Young's modulus values of juvenile and adult constructs decreased by 23.9% and 24.5%, respectively; however, this trend was not

significant (Figure 5-5A). UTS values varied from 0.37±0.19 MPa for juvenile constructs to 0.52±0.16 MPa for neonatal constructs (Figure 5-5B). Strain at failure increased with donor age, from 0.35±0.06 mm/mm to 0.49±0.15 mm/mm, although no groups were statistically different from one another (Figure 5-5C).

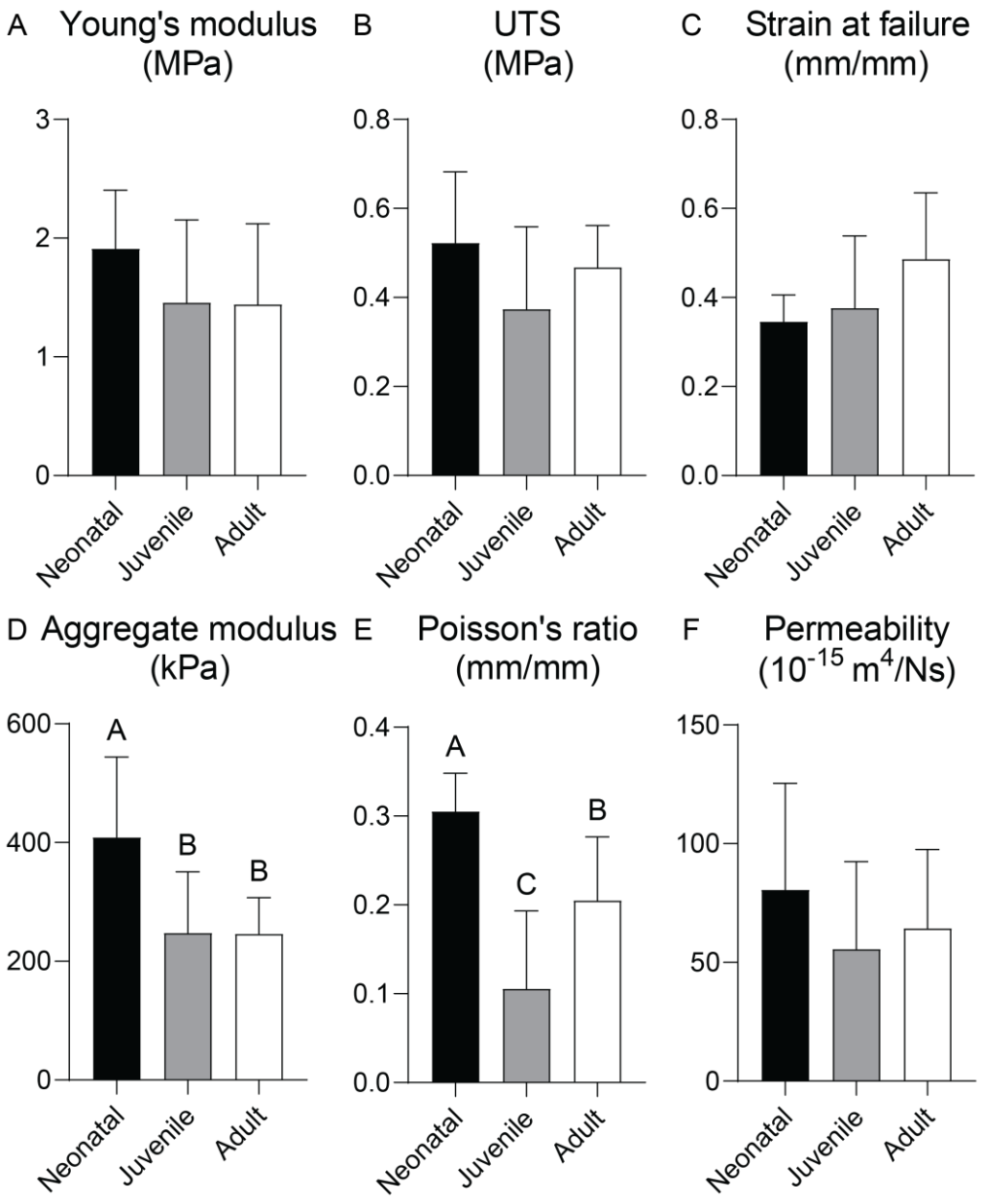

Figure 5-5: Mechanical properties of neocartilage constructs.
Tensile properties, including (A) Young's modulus, (B) UTS, and (C) strain at failure, did not exhibit any significant differences. (D) Aggregate modulus significantly decreased with age of cell source from neonatal to juvenile and adult constructs, while (E) Poisson's ratio was significantly different among all groups. (F) Permeability remained unaffected by donor age. Statistics: One-way ANOVA with *post hoc* Tukey's HSD test, α = 0.05, n=7-8 per group, letters depict the connecting letters report. Abbreviation: UTS, ultimate tensile strength.

Compressive measurements include aggregate modulus, Poisson's ratio, and permeability from creep indentation testing. Aggregate modulus values significantly decreased between neonatal (409±135 kPa) and juvenile (248±104 kPa) constructs (p=0.0199) (Figure 5-5D). Additionally, the aggregate modulus of adult constructs significantly decreased by 39.8% from neonatal constructs (p=0.023) (Figure 5-55D). The juvenile and adult groups did not differ in aggregate modulus values (Figure 5-5D). Poisson's ratio significantly changed among all groups; neonatal-derived constructs were significantly higher than both juvenile- (p<0.0001) and adult-derived (p=0.041) constructs (Figure 5-5E). For permeability, the values ranged between 56±37 10^{-15} m^4/Ns and 81±45 10^{-15} m^4/Ns (Figure 5-5F).

Discussion

Tissue engineering of functional biologic implants is emerging as a potential solution for articular cartilage lesions, but neotissue development may be hindered by 1) donor tissue scarcity due to diseased tissue, 2) dedifferentiation of mature chondrocytes during expansion, and 3) varying functional output of chondrocytes due to differences in donor age. Toward overcoming two of three of these hurdles, costal cartilage, used here, has been explored as a donor tissue due to the cells' exceptional capability to expand and redifferentiate toward a chondrogenic phenotype. Toward addressing the last hurdle, this study's objective was to investigate the age-dependent, functional differences among neocartilage formed from neonatal, juvenile, and adult donors. It should be noted that the skeletally mature adult minipig donors used here would be equivalent to a young adult human, up to 25 years old [376]. Generally, it was hypothesized that donor age will affect the biochemical and mechanical properties of neocartilage constructs. Surprisingly, despite age having been shown as a significant factor in the utility of articular chondrocytes [31, 364, 365], for costal chondrocytes processed using the methods described here, such effects were generally not observed, most likely due to the rejuvenation process. Our results showed that age-related differences among constructs are minimal using costal chondrocytes from

relatively young donors in conjunction with the tissue engineering processes described here and that differences in the production of minor collagens and compressive properties may be what differentiates younger and older donor neocartilages.

Gross morphological, biochemical, and mechanical analyses showed only minute differences in the measured outcomes. For gross measurements, neonatal-derived constructs were 9.5% larger in diameter, while juvenile-derived constructs were 29.5% thicker, than adult-derived constructs. The most drastic increase was in the aggregate modulus values of neonatal-derived constructs, with a significant 65% increase over adult constructs. Poisson's ratio also differed among constructs of different donor ages. However, the other measures including GAG content, PYR content, permeability, Young's modulus, UTS, and strain at failure were not significantly different among groups. The tissue engineering process used here appears to modulate expanded then redifferentiated costal chondrocytes to a similar baseline of functional properties, showing few mechanical and biochemical differences among groups. Interestingly, the total collagen content was significantly higher in adult constructs, rising 11.5% over juvenile-derived constructs. In short, these results suggest that the use of costal cartilage in conjunction with aggregate rejuvenation may yield constructs with minimal functional differences due to age-related variability within younger donor populations.

To further investigate the differences in neocartilage matrix content, bottom-up proteomic analysis was used to highlight the differences in matrix proteins among constructs derived from neonates, juveniles, and young adults. The most abundant collagen subtype, collagen type II, did not exhibit significant differences among groups. Collagen type I was reduced with age, with the highest content in neonatal-derived constructs. Collagen types IX and XI also displayed this trend, which is expected, because their expression in native articular cartilage decreases with age [379, 380]. These collagen subtypes (IX and XI) are colocalized with collagen type II in articular cartilage [237, 381]. Interestingly, collagen type XII, a fibril-associated collagen that colocalizes with collagen type I fibrils in ligament, perichondrium,

periosteum, dermis, and skeletal muscle [382-385], increased with donor age. A study on collagen type XII spatial and temporal expression has shown that staining was present in the chondrocytes of the growth plate but was not associated at any developmental stage with the secondary ossification center [386]. Postnatally, collagen type XII expression also increased in chondrocytes in the articular surface with age [386]. This corroborates our finding that collagen type XII is present in higher amounts in the adult-derived constructs. Additionally, as is the case with a majority of biochemical and mechanical properties, other matrix content, including link protein, aggrecan, and biglycan, did not significantly differ among the three age groups. Although there are differences in the collagen subtype profile, it is not yet apparent how individual collagen subtypes might affect the mechanical properties of neocartilage; thus, future studies should investigate the structure-function properties of these minor collagens and neocartilage mechanical properties.

The biochemical and mechanical values reported here are on par with those of previous studies that use various ages and species under control conditions (i.e., no supplementation of the self-assembling process with bioactive factors or mechanical stimulation) to engineer neocartilage constructs. For example, the Young's modulus and UTS reported here ranged from 1.44-1.91 MPa and 0.15-0.36 MPa, respectively. Previous studies utilizing porcine costal chondrocytes derived from 6-month-old animals (i.e., juvenile), then expanded three times and redifferentiated for 14 days, averaged approximately 1.35 MPa in Young's modulus [144]. Similarly, constructs derived from the costal cartilage of 1-year-old sheep, expanded three passages then redifferentiated for 11 days, yielded Young's modulus of approximately 1.4 MPa and UTS of approximately 0.33 MPa [201], on par with the values reported here. Additionally, the GAG and total collagen contents (approximately 1.5-2% per WW and 7-8% per WW, respectively) are on par with the values here [201]. Values of total collagen per WW in a separate study examining skeletally mature minipig costal chondrocytes expanded then redifferentiated are also on par with those presented here [23]. Even across separate studies

using expanded then redifferentiated costal chondrocytes in the self-assembling process, similar values of functional properties are found among a variety of species and ages, indicating that costal cartilage is a consistent cell source, further bolstering its use as a donor tissue source.

Despite the small differences in functional properties shown here, constructs isolated from different aged donors displayed unexpectedly similar properties after the same amount of expansion, aggregate rejuvenation, and self-assembly. A potential explanation of this result is that previous studies demonstrated that passage number, rather than donor age, may more greatly affect the functional properties of constructs derived from mesenchymal stem cells [387]. Thus, at a standard passage number, donor age may be less of a factor than expected with the tissue engineering process being more influential on functional output. For example, the tissue engineering process used here includes applying a cocktail of growth factors during expansion to passage 3, which has been shown to rescue cells from dedifferentiation, increasing post-expansion chondrogenic potential in subsequent 3D culture [149, 388-390]. Expansion of human articular chondrocytes, in the presence of TGF-β1, PDGF-BB, and bFGF, was reported to be up to 3.7-fold more in all age groups and decreased only slightly with age when compared to cells cultured in control medium [365]. Additionally, TGF-β1, GDF-5, and BMP-2 added during aggregate rejuvenation, have all been developmentally inspired, are implicated in chondrogenesis that occurs during mesenchymal condensation, and are shown to be effective in redifferentiation of articular chondrocytes [150]. The data presented combined with the historical studies discussed here suggest that these growth factor cocktails, in conjunction with aggregate rejuvenation culture, at least partially ameliorate the age-dependent changes in costal chondrocyte function.

This study shows that the tissue engineering processes described here (i.e., expansion to passage 3, aggregate rejuvenation, and the self-assembling process) result in similarly robust constructs derived from neonates, juveniles, and skeletally mature adults. It is unclear whether this could be applied to older donors (i.e., 24+ month minipigs, corresponding to humans older

than 25 years in age) or diseased chondrocytes. The adult minipigs of this study were 18-24 months old. Because Yucatan minipigs reach skeletal maturity at approximately 16-18 months [24] and can have a life span up to 15 years [391], these are still relatively young adults, corresponding to a maximum of 25 years old in humans [376]. Therefore, a limitation of this work is the exclusion of older donors from the study. However, based on literature from human articular chondrocytes [365], it would be expected that functional properties would decrease in constructs derived from older donors (i.e., 40+ years of age in humans) compared to those examined here. Moreover, the chondrocytes were isolated from healthy cartilage tissue, and, thus, future studies should investigate whether these trends would apply to diseased chondrocytes. Lastly, future studies should focus on additional improvements in functional properties by use of additional stimuli such as bioactive factors [83] and mechanical bioreactors [201, 207] toward improving neocartilage properties to native tissue values. Once design criteria are met, the *in vivo* performance of constructs in both healthy adults and diseased elderly patients should be examined in a clinically relevant defect model, establishing the potential reparative or regenerative effects of constructs derived from different donor ages. Despite the need for continued work in this area, the current study is significant in that it demonstrates that a range of relatively young donor ages may be used to generate mechanically robust, self-assembled neocartilage of similar functional properties.

Conclusion

This is the first study to investigate the effects of donor age on the self-assembling process. Using costal chondrocytes which were expanded and rejuvenated, it was demonstrated that, while neonatal chondrocytes yielded constructs with significantly higher aggregate modulus values and skeletally mature constructs had higher total collagen content, the majority of functional properties of the constructs were not significantly different among groups. This phenomenon is most likely due to the rejuvenation step used in the construct engineering

process, which may have overcome any apparent age-related functional differences. Although functional properties were largely similar among donors of different ages, several minor collagens were modulated by donor age. These findings suggest that the tissue engineering processes used to fabricate self-assembled and mechanically robust neocartilage from passaged and rejuvenated chondrocytes are effective on chondrocytes isolated from young donors (i.e., 0-25 years in human age) of different developmental stages. Translationally, this is significant in that donors from a wide range of ages, from neonates to young adults, may be able to donate cells for expansion and the generation of allogeneic cartilage implants, which can help facilitate an efficient and comprehensive donor selection process.

Supplementary Materials

Supplementary Table 5-1: Full list of proteins returned from bottom-up mass spectrometry analysis.
Three individual data points from each group (n=3), neonatal (N), juvenile (J), and adult (A), were run and normalized to total protein content and expressed as a percentage with calculated means and standard deviations.

Accession	Gene	Protein	Label-free Quantification Value (Normalized to Total Protein, %)														
			Neonatal					Juvenile					Adult				
			N1	N2	N3	Mean	SD	J1	J2	J3	Mean	SD	A1	A2	A3	Mean	SD
A0A286ZWS8	Col2a1	Collagen type II alpha 1 chain	26.85%	28.89%	23.46%	26.40%	2.74%	14.03%	21.23%	17.10%	17.45%	3.61%	26.85%	20.03%	20.42%	22.43%	3.83%
P02543	VIME	Vimentin	19.50%	17.15%	16.07%	17.57%	1.76%	28.43%	21.67%	22.40%	24.16%	3.71%	19.59%	22.93%	21.58%	21.37%	1.68%
F1RQI0	Col12a1	Collagen type XII alpha 1 chain	2.96%	2.73%	3.34%	3.01%	0.31%	5.08%	5.25%	5.36%	5.23%	0.14%	5.64%	6.63%	6.03%	6.10%	0.50%
Q6QAQ1	ACTB	Actin, cytoplasmic 1	4.33%	4.72%	4.65%	4.57%	0.21%	3.04%	3.44%	3.56%	3.35%	0.27%	4.12%	4.29%	4.72%	4.38%	0.31%
P10859	HPLN1	Hyaluronan and proteoglycan link protein 1	4.35%	3.29%	4.62%	4.09%	0.70%	3.23%	3.87%	5.43%	4.18%	1.14%	3.30%	4.30%	3.52%	3.70%	0.53%
Q29011	PGCA	Aggrecan core protein (Fragments)	4.41%	3.50%	3.61%	3.84%	0.49%	3.50%	4.91%	4.42%	4.28%	0.71%	3.14%	4.56%	3.62%	3.77%	0.72%
P62802	H4	Histone H4	3.22%	2.83%	4.38%	3.47%	0.81%	5.18%	3.92%	4.18%	4.43%	0.67%	4.49%	3.30%	3.28%	3.69%	0.69%
I3LUR7	Col6a3	Collagen type VI alpha 3 chain	3.22%	3.17%	3.73%	3.37%	0.31%	2.75%	2.81%	2.89%	2.82%	0.07%	2.82%	3.27%	3.34%	3.14%	0.28%
P00355	G3P	Glyceraldehyde-3-phosphate dehydrogenase	2.79%	2.74%	3.23%	2.92%	0.27%	2.67%	4.29%	4.17%	3.71%	0.90%	2.29%	2.90%	2.31%	2.50%	0.35%
A0A5G2Q7A4	Col11a2	Collagen type XI alpha 2 chain	2.85%	2.87%	2.95%	2.89%	0.06%	3.30%	3.10%	2.67%	3.02%	0.32%	1.63%	1.96%	2.18%	1.92%	0.28%
A0A5G2RKA4	Col11a1	Collagen type XI alpha 1 chain	1.97%	2.10%	2.12%	2.06%	0.08%	2.99%	2.05%	2.20%	2.41%	0.50%	2.03%	1.82%	1.80%	1.88%	0.13%
Q71LE2	H33	Histone H3.3	1.63%	1.98%	1.44%	1.68%	0.28%	1.98%	0.97%	0.95%	1.30%	0.59%	1.46%	1.73%	2.04%	1.74%	0.29%
P19620	ANXA2	Annexin A2	1.22%	0.95%	1.47%	1.21%	0.26%	1.22%	1.30%	1.62%	1.38%	0.21%	1.79%	1.71%	1.52%	1.67%	0.14%
Q9GKQ6	PGS1	Biglycan (Fragments)	1.88%	0.81%	1.03%	1.24%	0.57%	2.15%	1.46%	1.41%	1.67%	0.41%	1.73%	1.31%	0.73%	1.26%	0.50%
P03970	INHBA	Inhibin beta A chain	0.00%	4.22%	2.26%	2.16%	2.11%	1.09%	1.54%	0.00%	0.87%	0.79%	1.12%	0.76%	0.98%	0.96%	0.18%
Q3ZD69	LMNA	Prelamin-A/C	1.29%	1.16%	1.40%	1.29%	0.12%	1.10%	1.27%	1.24%	1.21%	0.09%	1.23%	1.33%	1.43%	1.33%	0.10%
Q1KYT0	ENOB	Beta-enolase	1.13%	1.20%	1.23%	1.19%	0.05%	0.65%	1.11%	1.49%	1.08%	0.42%	0.91%	0.65%	0.89%	0.82%	0.14%

I3LQ84	Col6a2	Collagen type VI alpha 2 chain	0.87%	0.92%	1.41%	1.07%	0.30%	0.93%	0.86%	0.91%	0.90%	0.03%	1.00%	0.77%	0.95%	0.91%	0.12%
F1SF83	Col28a1	Collagen type XXVIII alpha 1 chain	0.00%	0.47%	1.26%	0.58%	0.64%	0.01%	0.00%	0.23%	0.08%	0.13%	0.70%	0.55%	4.51%	1.92%	2.24%
I3L8B2	Col9a2	Collagen type IX alpha 2 chain	0.81%	0.90%	1.58%	1.10%	0.42%	0.65%	0.51%	0.47%	0.54%	0.09%	0.68%	0.58%	0.74%	0.67%	0.08%
P79385	MFGM	Lactadherin	0.61%	0.50%	0.71%	0.61%	0.11%	0.73%	0.52%	0.60%	0.62%	0.11%	0.93%	1.06%	0.75%	0.91%	0.16%
Q767L7	TBB5	Tubulin beta chain	0.73%	0.59%	1.09%	0.80%	0.26%	0.55%	0.70%	0.79%	0.68%	0.12%	0.47%	0.50%	0.50%	0.49%	0.02%
Q7SIB7	PGK1	Phosphoglycerate kinase 1	0.74%	0.70%	0.77%	0.74%	0.04%	0.49%	0.57%	0.76%	0.61%	0.14%	0.54%	0.53%	0.48%	0.52%	0.03%
Q2XVP4	TBA1B	Tubulin alpha-1B chain	0.49%	0.52%	0.37%	0.46%	0.08%	0.43%	0.58%	0.83%	0.61%	0.21%	0.47%	0.51%	0.52%	0.50%	0.03%
Q29371	TPIS	Triosephosphate isomerase	0.45%	0.71%	0.49%	0.55%	0.14%	0.35%	0.55%	0.51%	0.47%	0.11%	0.32%	0.40%	0.38%	0.37%	0.04%
P00339	LDHA	L-lactate dehydrogenase A chain	0.59%	0.55%	0.66%	0.60%	0.05%	0.28%	0.45%	0.65%	0.46%	0.19%	0.27%	0.35%	0.35%	0.32%	0.04%
P80021	ATPA	ATP synthase subunit alpha, mitochondrial	0.35%	0.25%	0.52%	0.37%	0.14%	0.63%	0.39%	0.52%	0.51%	0.12%	0.42%	0.55%	0.48%	0.49%	0.06%
P79303	UGPA	UTP--glucose-1-phosphate uridylyltransferase	0.37%	0.36%	0.45%	0.40%	0.05%	0.79%	0.43%	0.53%	0.58%	0.19%	0.32%	0.41%	0.30%	0.34%	0.06%
Q5S1U1	HSPB1	Heat shock protein beta-1	0.26%	0.24%	0.25%	0.25%	0.01%	0.44%	0.51%	0.69%	0.55%	0.13%	0.48%	0.50%	0.55%	0.51%	0.04%
P06348	H1T	Histone H1t	0.08%	0.36%	0.32%	0.26%	0.16%	0.56%	0.32%	0.38%	0.42%	0.12%	0.36%	0.52%	0.42%	0.43%	0.08%
A5A779	PGTA	Geranylgeranyl transferase type-2 subunit alpha	0.25%	0.24%	0.47%	0.32%	0.13%	0.00%	0.36%	0.37%	0.24%	0.21%	0.62%	0.36%	0.34%	0.44%	0.16%
P10668	COF1	Cofilin-1	0.34%	0.32%	0.32%	0.33%	0.01%	0.62%	0.33%	0.30%	0.42%	0.18%	0.22%	0.19%	0.29%	0.23%	0.06%
Q6S4N2	HS71B	Heat shock 70 kDa protein 1B	0.24%	0.31%	0.38%	0.31%	0.07%	0.36%	0.33%	0.33%	0.34%	0.02%	0.21%	0.25%	0.25%	0.24%	0.02%
A0A481AEJ4	Col9a1	Collagen type IX alpha 1 chain	0.40%	0.33%	0.33%	0.35%	0.04%	0.22%	0.25%	0.22%	0.23%	0.02%	0.21%	0.23%	0.24%	0.23%	0.01%
P20305	GELS	Gelsolin (Fragment)	0.33%	0.34%	0.32%	0.33%	0.01%	0.18%	0.29%	0.25%	0.24%	0.06%	0.22%	0.26%	0.22%	0.23%	0.02%
Q1T7A9	Col6a1	Collagen type VI alpha 1 chain	0.26%	0.22%	0.32%	0.27%	0.05%	0.12%	0.33%	0.31%	0.25%	0.12%	0.27%	0.23%	0.27%	0.26%	0.02%
Q29214	RLA0	60S acidic ribosomal protein P0	0.28%	0.20%	0.26%	0.25%	0.05%	0.15%	0.19%	0.38%	0.24%	0.12%	0.31%	0.29%	0.20%	0.27%	0.06%

Q2EN75	S10A6	Protein S100-A6	0.31%	0.24%	0.18%	0.24%	0.07%	0.38%	0.20%	0.21%	0.26%	0.10%	0.20%	0.14%	0.29%	0.21%	0.08%
O02705	HS90A	Heat shock protein HSP 90-alpha	0.24%	0.20%	0.26%	0.24%	0.03%	0.15%	0.26%	0.29%	0.23%	0.07%	0.24%	0.22%	0.21%	0.22%	0.02%
Q29549	CLUS	Clusterin	0.55%	0.00%	0.00%	0.19%	0.32%	0.00%	0.03%	0.19%	0.07%	0.10%	0.21%	0.48%	0.28%	0.32%	0.14%
Q29092	ENPL	Endoplasmin	0.16%	0.15%	0.22%	0.18%	0.04%	0.17%	0.18%	0.22%	0.19%	0.03%	0.19%	0.18%	0.15%	0.17%	0.02%
P02550	TBA1A	Tubulin alpha-1A chain	0.20%	0.17%	0.13%	0.17%	0.04%	0.22%	0.19%	0.24%	0.21%	0.03%	0.16%	0.15%	0.13%	0.14%	0.02%
P34935	BIP	Endoplasmic reticulum chaperone BiP (Fragment)	0.15%	0.25%	0.05%	0.15%	0.10%	0.00%	0.22%	0.36%	0.19%	0.18%	0.15%	0.21%	0.18%	0.18%	0.03%
Q29116	TENA	Tenascin	0.20%	0.20%	0.09%	0.16%	0.06%	0.11%	0.16%	0.18%	0.15%	0.03%	0.19%	0.19%	0.16%	0.18%	0.02%
P26042	MOES	Moesin	0.21%	0.12%	0.04%	0.12%	0.09%	0.22%	0.19%	0.22%	0.21%	0.02%	0.18%	0.14%	0.14%	0.15%	0.03%
Q2EN76	NDKB	Nucleoside diphosphate kinase B	0.18%	0.17%	0.28%	0.21%	0.06%	0.10%	0.13%	0.19%	0.14%	0.05%	0.15%	0.13%	0.11%	0.13%	0.02%
Q4GWZ2	RSSA	40S ribosomal protein SA	0.16%	0.15%	0.07%	0.13%	0.05%	0.13%	0.20%	0.21%	0.18%	0.05%	0.10%	0.22%	0.17%	0.17%	0.06%
Q0Z8U2	RS3	40S ribosomal protein S3	0.14%	0.12%	0.08%	0.11%	0.03%	0.11%	0.20%	0.22%	0.18%	0.06%	0.16%	0.16%	0.18%	0.17%	0.01%
Q59IP2	Col5a2	Collagen type V alpha 2 chain	0.13%	0.25%	0.00%	0.13%	0.12%	0.13%	0.17%	0.22%	0.17%	0.04%	0.17%	0.14%	0.13%	0.15%	0.02%
P62936	PPIA	Peptidyl-prolyl cis-trans isomerase A	0.13%	0.14%	0.11%	0.13%	0.02%	0.17%	0.16%	0.20%	0.17%	0.02%	0.14%	0.14%	0.15%	0.14%	0.01%
Q9GMB0	RPN1	Dolichyl-diphosphooligosaccharide--protein glycosyltransferase subunit 1	0.13%	0.09%	0.13%	0.11%	0.02%	0.27%	0.16%	0.20%	0.21%	0.06%	0.09%	0.12%	0.13%	0.11%	0.02%
P28491	CALR	Calreticulin	0.18%	0.17%	0.12%	0.16%	0.03%	0.11%	0.18%	0.18%	0.15%	0.04%	0.11%	0.14%	0.11%	0.12%	0.02%
P00346	MDHM	Malate dehydrogenase, mitochondrial	0.09%	0.10%	0.09%	0.10%	0.01%	0.14%	0.20%	0.15%	0.16%	0.03%	0.11%	0.14%	0.12%	0.12%	0.02%
Q29387	EF1G	Elongation factor 1-gamma (Fragment)	0.11%	0.11%	0.10%	0.11%	0.01%	0.23%	0.13%	0.15%	0.17%	0.05%	0.10%	0.08%	0.10%	0.09%	0.01%
P63053	RL40	Ubiquitin-60S ribosomal protein L40	0.07%	0.15%	0.14%	0.12%	0.04%	0.12%	0.09%	0.14%	0.12%	0.02%	0.11%	0.17%	0.11%	0.13%	0.04%

Q9MZ16	VDAC1	Voltage-dependent anion-selective channel protein 1	0.11%	0.06%	0.11%	0.10%	0.03%	0.22%	0.12%	0.12%	0.15%	0.06%	0.12%	0.12%	0.11%	0.12%	0.01%
Q29121	GALT1	Polypeptide N-acetylgalactosaminyltransferase 1	0.16%	0.00%	0.29%	0.15%	0.15%	0.40%	0.06%	0.06%	0.18%	0.20%	0.00%	0.06%	0.05%	0.04%	0.03%
Q8HXW0	GGLO	L-gulonolactone oxidase	0.18%	0.08%	0.19%	0.15%	0.06%	0.40%	0.06%	0.12%	0.19%	0.19%	0.01%	0.00%	0.00%	0.01%	0.01%
P68137	ACTS	Actin, alpha skeletal muscle	0.08%	0.08%	0.13%	0.09%	0.03%	0.14%	0.11%	0.18%	0.14%	0.04%	0.13%	0.14%	0.03%	0.10%	0.06%
P83686	NB5R3	NADH-cytochrome b5 reductase 3 (Fragment)	0.12%	0.08%	0.07%	0.09%	0.03%	0.17%	0.10%	0.06%	0.11%	0.06%	0.12%	0.14%	0.15%	0.14%	0.02%
P02554	TBB	Tubulin beta chain	0.11%	0.13%	0.16%	0.13%	0.03%	0.06%	0.11%	0.16%	0.11%	0.05%	0.06%	0.08%	0.08%	0.07%	0.01%
Q95342	RL18	60S ribosomal protein L18	0.10%	0.08%	0.15%	0.11%	0.04%	0.16%	0.06%	0.08%	0.10%	0.05%	0.11%	0.11%	0.09%	0.10%	0.01%
Q9GL01	RPN2	Dolichyl-diphosphooligosaccharide--protein glycosyltransferase subunit 2	0.08%	0.09%	0.09%	0.08%	0.01%	0.04%	0.10%	0.15%	0.10%	0.05%	0.15%	0.10%	0.10%	0.12%	0.03%
A0A5G2RJ53	Col4a2	Collagen type IV alpha 2 chain	0.00%	0.00%	0.02%	0.01%	0.01%	0.23%	0.00%	0.21%	0.15%	0.13%	0.18%	0.11%	0.12%	0.14%	0.04%
A1XQU9	RS20	40S ribosomal protein S20	0.11%	0.15%	0.09%	0.12%	0.03%	0.03%	0.11%	0.12%	0.09%	0.05%	0.09%	0.10%	0.08%	0.09%	0.01%
Q6QRN9	ADT3	ADP/ATP translocase 3	0.09%	0.06%	0.05%	0.07%	0.02%	0.06%	0.11%	0.12%	0.10%	0.04%	0.11%	0.11%	0.11%	0.11%	0.00%
D2SW95	COPB	Coatomer subunit beta	0.07%	0.05%	0.12%	0.08%	0.04%	0.12%	0.08%	0.10%	0.10%	0.02%	0.06%	0.05%	0.08%	0.06%	0.02%
P79403	GANAB	Neutral alpha-glucosidase AB	0.08%	0.03%	0.04%	0.05%	0.03%	0.06%	0.10%	0.14%	0.10%	0.04%	0.08%	0.10%	0.10%	0.10%	0.01%
Q52NJ2	RAB1A	Ras-related protein Rab-1A	0.09%	0.05%	0.09%	0.08%	0.02%	0.10%	0.07%	0.12%	0.10%	0.02%	0.11%	0.03%	0.06%	0.07%	0.04%
Q29205	RL11	60S ribosomal protein L11	0.07%	0.10%	0.17%	0.11%	0.05%	0.00%	0.04%	0.08%	0.04%	0.04%	0.13%	0.07%	0.05%	0.08%	0.04%
P05024	AT1A1	Sodium/potassium-transporting ATPase subunit alpha-1	0.08%	0.08%	0.07%	0.08%	0.01%	0.06%	0.10%	0.08%	0.08%	0.02%	0.09%	0.08%	0.06%	0.08%	0.01%
A1XQU3	RL14	60S ribosomal protein L14	0.11%	0.04%	0.00%	0.05%	0.06%	0.02%	0.07%	0.16%	0.09%	0.07%	0.10%	0.10%	0.08%	0.09%	0.01%

A7Y521	CSN4	COP9 signalosome complex subunit 4	0.00%	0.03%	0.00%	0.01%	0.02%	0.58%	0.01%	0.01%	0.20%	0.33%	0.00%	0.00%	0.00%	0.00%	0.00%
Q9MZ15	VDAC2	Voltage-dependent anion-selective channel protein 2	0.06%	0.05%	0.10%	0.07%	0.03%	0.00%	0.08%	0.08%	0.05%	0.05%	0.07%	0.08%	0.11%	0.09%	0.02%
Q29228	AL9A1	4-trimethylaminobutyraldehyde dehydrogenase	0.08%	0.03%	0.06%	0.06%	0.03%	0.21%	0.05%	0.03%	0.10%	0.10%	0.04%	0.05%	0.08%	0.06%	0.02%
P29797	GNAS	Guanine nucleotide-binding protein G(s) subunit alpha	0.07%	0.03%	0.13%	0.08%	0.05%	0.06%	0.07%	0.05%	0.06%	0.01%	0.06%	0.06%	0.07%	0.07%	0.01%
P03974	TERA	Transitional endoplasmic reticulum ATPase	0.07%	0.05%	0.06%	0.06%	0.01%	0.06%	0.07%	0.08%	0.07%	0.01%	0.07%	0.07%	0.08%	0.07%	0.00%
Q9TSX9	PRDX6	Peroxiredoxin-6	0.08%	0.05%	0.08%	0.07%	0.02%	0.07%	0.07%	0.07%	0.07%	0.00%	0.08%	0.07%	0.04%	0.06%	0.02%
P63246	RACK1	Receptor of activated protein C kinase 1	0.07%	0.03%	0.06%	0.06%	0.02%	0.16%	0.05%	0.05%	0.09%	0.06%	0.05%	0.05%	0.05%	0.05%	0.00%
Q29201	RS16	40S ribosomal protein S16	0.07%	0.04%	0.07%	0.06%	0.02%	0.04%	0.07%	0.09%	0.07%	0.03%	0.07%	0.07%	0.06%	0.07%	0.01%
Q9XSZ6	FCERG	High affinity immunoglobulin epsilon receptor subunit gamma	0.10%	0.03%	0.02%	0.05%	0.05%	0.10%	0.09%	0.06%	0.08%	0.02%	0.10%	0.04%	0.03%	0.05%	0.04%
P62272	RS18	40S ribosomal protein S18	0.07%	0.10%	0.00%	0.06%	0.05%	0.00%	0.05%	0.03%	0.03%	0.03%	0.07%	0.14%	0.10%	0.10%	0.04%
A7TX81	CSN6	COP9 signalosome complex subunit 6	0.00%	0.00%	0.00%	0.00%	0.00%	0.54%	0.01%	0.00%	0.18%	0.31%	0.00%	0.00%	0.00%	0.00%	0.00%
P20112	SPRC	SPARC	0.08%	0.06%	0.07%	0.07%	0.01%	0.00%	0.07%	0.08%	0.05%	0.04%	0.06%	0.06%	0.05%	0.06%	0.00%
P52552	PRDX2	Peroxiredoxin-2 (Fragment)	0.05%	0.04%	0.06%	0.05%	0.01%	0.10%	0.08%	0.05%	0.08%	0.02%	0.05%	0.04%	0.05%	0.04%	0.00%
P00336	LDHB	L-lactate dehydrogenase B chain	0.07%	0.04%	0.09%	0.07%	0.02%	0.06%	0.03%	0.09%	0.06%	0.03%	0.05%	0.03%	0.04%	0.04%	0.01%
P62197	PRS8	26S proteasome regulatory subunit 8	0.00%	0.05%	0.00%	0.02%	0.03%	0.38%	0.06%	0.02%	0.15%	0.20%	0.00%	0.00%	0.00%	0.00%	0.00%
A1XQU5	RL27	60S ribosomal protein L27	0.08%	0.05%	0.11%	0.08%	0.03%	0.00%	0.07%	0.09%	0.05%	0.05%	0.04%	0.03%	0.05%	0.04%	0.01%

P49171	RS26	40S ribosomal protein S26	0.04%	0.03%	0.05%	0.04%	0.01%	0.10%	0.05%	0.07%	0.07%	0.03%	0.05%	0.05%	0.06%	0.05%	0.00%
Q29315	RLA2	60S acidic ribosomal protein P2	0.05%	0.05%	0.06%	0.05%	0.00%	0.04%	0.04%	0.07%	0.05%	0.02%	0.07%	0.05%	0.04%	0.05%	0.02%
Q29381	OST48	Dolichyl-diphosphooligosaccharide--protein glycosyltransferase 48 kDa subunit	0.06%	0.03%	0.04%	0.05%	0.02%	0.05%	0.04%	0.05%	0.05%	0.01%	0.05%	0.05%	0.06%	0.05%	0.01%
P08059	G6PI	Glucose-6-phosphate isomerase	0.06%	0.08%	0.04%	0.06%	0.02%	0.09%	0.05%	0.04%	0.06%	0.03%	0.05%	0.05%	0.00%	0.03%	0.03%
P11708	MDHC	Malate dehydrogenase, cytoplasmic	0.05%	0.08%	0.06%	0.06%	0.01%	0.04%	0.03%	0.05%	0.04%	0.01%	0.05%	0.05%	0.03%	0.04%	0.01%
P08132	ANXA4	Annexin A4	0.06%	0.04%	0.03%	0.05%	0.02%	0.07%	0.06%	0.06%	0.06%	0.01%	0.04%	0.03%	0.02%	0.03%	0.01%
P02540	DESM	Desmin	0.00%	0.00%	0.36%	0.12%	0.21%	0.00%	0.00%	0.00%	0.00%	0.00%	0.00%	0.00%	0.00%	0.00%	0.00%
P08835	ALBU	Albumin	0.05%	0.00%	0.00%	0.02%	0.03%	0.05%	0.03%	0.12%	0.07%	0.05%	0.00%	0.06%	0.05%	0.03%	0.03%
P04163	S10AA	Protein S100-A10	0.00%	0.04%	0.00%	0.01%	0.02%	0.04%	0.05%	0.07%	0.05%	0.01%	0.04%	0.05%	0.06%	0.05%	0.01%
P19619	ANXA1	Annexin A1	0.03%	0.00%	0.06%	0.03%	0.03%	0.00%	0.04%	0.03%	0.02%	0.02%	0.07%	0.05%	0.07%	0.06%	0.01%
Q2YGT9	RL6	60S ribosomal protein L6	0.00%	0.06%	0.00%	0.02%	0.04%	0.06%	0.00%	0.07%	0.04%	0.04%	0.06%	0.05%	0.05%	0.05%	0.01%
P79401	CP3AT	Cytochrome P450 3A29	0.00%	0.00%	0.00%	0.00%	0.00%	0.00%	0.00%	0.00%	0.00%	0.00%	0.00%	0.13%	0.20%	0.11%	0.10%
Q9XT00	DHB8	Estradiol 17-beta-dehydrogenase 8	0.00%	0.00%	0.09%	0.03%	0.05%	0.15%	0.00%	0.00%	0.05%	0.09%	0.09%	0.00%	0.00%	0.03%	0.05%
A5GFY8	SERA	D-3-phosphoglycerate dehydrogenase	0.05%	0.05%	0.12%	0.08%	0.04%	0.01%	0.03%	0.04%	0.02%	0.02%	0.00%	0.00%	0.03%	0.01%	0.02%
Q29308	RS19	40S ribosomal protein S19 (Fragment)	0.04%	0.02%	0.08%	0.05%	0.03%	0.05%	0.02%	0.02%	0.03%	0.01%	0.03%	0.03%	0.03%	0.03%	0.00%
P12682	HMGB1	High mobility group protein B1	0.00%	0.04%	0.04%	0.03%	0.02%	0.05%	0.05%	0.04%	0.05%	0.01%	0.02%	0.03%	0.05%	0.03%	0.01%
C0HL13	LRP2	Low-density lipoprotein receptor-related protein 2	0.00%	0.32%	0.00%	0.11%	0.18%	0.00%	0.00%	0.00%	0.00%	0.00%	0.00%	0.00%	0.00%	0.00%	0.00%
P60982	DEST	Destrin	0.00%	0.06%	0.03%	0.03%	0.03%	0.07%	0.00%	0.07%	0.05%	0.04%	0.04%	0.03%	0.02%	0.03%	0.01%

P62279	RS13	40S ribosomal protein S13 (Fragment)	0.05%	0.04%	0.00%	0.03%	0.03%	0.00%	0.05%	0.06%	0.03%	0.03%	0.04%	0.04%	0.03%	0.04%	0.01%
P50578	AK1A1	Aldo-keto reductase family 1 member A1	0.04%	0.02%	0.03%	0.03%	0.01%	0.05%	0.03%	0.03%	0.04%	0.01%	0.03%	0.03%	0.04%	0.03%	0.01%
A0A1S7J210	Col1a1	Collagen type I alpha 1 chain	0.09%	0.07%	0.04%	0.07%	0.03%	0.03%	0.02%	0.00%	0.02%	0.02%	0.00%	0.00%	0.04%	0.01%	0.02%
Q29293	RL3	60S ribosomal protein L3 (Fragment)	0.00%	0.05%	0.04%	0.03%	0.03%	0.05%	0.03%	0.00%	0.03%	0.03%	0.04%	0.06%	0.00%	0.03%	0.03%
P16276	ACON	Aconitate hydratase, mitochondrial	0.03%	0.03%	0.03%	0.03%	0.00%	0.00%	0.05%	0.04%	0.03%	0.02%	0.04%	0.03%	0.04%	0.04%	0.01%
F1SFA7	Col1a2	Collagen type I alpha 2 chain	0.04%	0.00%	0.06%	0.03%	0.03%	0.00%	0.02%	0.01%	0.01%	0.01%	0.04%	0.05%	0.05%	0.05%	0.01%
Q29561	KCY	UMP-CMP kinase	0.02%	0.02%	0.02%	0.02%	0.00%	0.10%	0.03%	0.02%	0.05%	0.04%	0.01%	0.02%	0.03%	0.02%	0.01%
P67985	RL22	60S ribosomal protein L22	0.02%	0.02%	0.04%	0.03%	0.01%	0.04%	0.03%	0.03%	0.03%	0.01%	0.04%	0.02%	0.03%	0.03%	0.01%
Q52NJ1	RB11A	Ras-related protein Rab-11A	0.03%	0.02%	0.03%	0.03%	0.00%	0.03%	0.04%	0.04%	0.04%	0.00%	0.02%	0.03%	0.02%	0.02%	0.01%
P19133	FRIL	Ferritin light chain (Fragment)	0.02%	0.01%	0.04%	0.02%	0.01%	0.02%	0.02%	0.08%	0.04%	0.03%	0.03%	0.02%	0.02%	0.02%	0.01%
P67937	TPM4	Tropomyosin alpha-4 chain	0.05%	0.05%	0.00%	0.03%	0.03%	0.00%	0.00%	0.06%	0.02%	0.03%	0.00%	0.05%	0.04%	0.03%	0.03%
Q06A98	SRSF2	Serine/arginine-rich splicing factor 2	0.05%	0.00%	0.00%	0.02%	0.03%	0.11%	0.04%	0.00%	0.05%	0.06%	0.03%	0.03%	0.00%	0.02%	0.02%
Q9XSD9	PGS2	Decorin	0.03%	0.03%	0.08%	0.05%	0.03%	0.00%	0.04%	0.03%	0.02%	0.02%	0.00%	0.00%	0.01%	0.01%	0.01%
Q29197	RS9	40S ribosomal protein S9 (Fragment)	0.03%	0.02%	0.00%	0.02%	0.02%	0.00%	0.02%	0.05%	0.02%	0.02%	0.03%	0.03%	0.03%	0.03%	0.00%
P53027	RL10A	60S ribosomal protein L10a (Fragment)	0.03%	0.00%	0.00%	0.01%	0.02%	0.04%	0.04%	0.04%	0.04%	0.00%	0.02%	0.02%	0.02%	0.02%	0.00%
P61288	TCTP	Translationally-controlled tumor protein	0.03%	0.07%	0.04%	0.05%	0.02%	0.00%	0.03%	0.02%	0.02%	0.02%	0.00%	0.01%	0.00%	0.01%	0.01%
Q56P28	PRAF3	PRA1 family protein 3	0.04%	0.02%	0.00%	0.02%	0.02%	0.01%	0.03%	0.02%	0.02%	0.01%	0.03%	0.03%	0.03%	0.03%	0.00%
Q29223	RL34	60S ribosomal protein L34	0.00%	0.00%	0.00%	0.00%	0.00%	0.00%	0.00%	0.03%	0.01%	0.02%	0.05%	0.06%	0.04%	0.05%	0.01%

Q6Q7J2	GDIB	Rab GDP dissociation inhibitor beta	0.03%	0.02%	0.01%	0.02%	0.01%	0.00%	0.03%	0.02%	0.02%	0.02%	0.02%	0.03%	0.01%	0.02%	0.01%
Q1RPR6	ITB6	Integrin beta-6	0.00%	0.02%	0.00%	0.01%	0.01%	0.07%	0.02%	0.02%	0.04%	0.03%	0.02%	0.00%	0.03%	0.02%	0.01%
P16582	LSHR	Lutropin-choriogonadotropic hormone receptor	0.00%	0.00%	0.00%	0.00%	0.00%	0.00%	0.17%	0.00%	0.06%	0.10%	0.00%	0.00%	0.00%	0.00%	0.00%
P27594	MX1	Interferon-induced GTP-binding protein Mx1	0.17%	0.00%	0.00%	0.06%	0.10%	0.00%	0.00%	0.00%	0.00%	0.00%	0.00%	0.00%	0.00%	0.00%	0.00%
A5A8V7	HS71L	Heat shock 70 kDa protein 1-like	0.02%	0.02%	0.02%	0.02%	0.00%	0.07%	0.03%	0.02%	0.04%	0.03%	0.00%	0.00%	0.00%	0.00%	0.00%
Q6QAT1	RS28	40S ribosomal protein S28	0.03%	0.02%	0.02%	0.02%	0.01%	0.00%	0.01%	0.02%	0.01%	0.01%	0.03%	0.03%	0.00%	0.02%	0.02%
P62831	RL23	60S ribosomal protein L23	0.03%	0.03%	0.00%	0.02%	0.02%	0.00%	0.00%	0.03%	0.01%	0.02%	0.06%	0.00%	0.00%	0.02%	0.03%
Q95JC8	ARGI1	Arginase-1	0.00%	0.03%	0.03%	0.02%	0.01%	0.00%	0.04%	0.04%	0.03%	0.02%	0.00%	0.03%	0.00%	0.01%	0.02%
Q95266	KCC2D	Calcium/calmodulin-dependent protein kinase type II subunit delta	0.02%	0.01%	0.00%	0.01%	0.01%	0.04%	0.02%	0.03%	0.03%	0.01%	0.00%	0.02%	0.03%	0.02%	0.01%
Q7M2W6	CRYAB	Alpha-crystallin B chain	0.00%	0.00%	0.02%	0.01%	0.01%	0.02%	0.02%	0.02%	0.02%	0.00%	0.02%	0.02%	0.03%	0.02%	0.00%
P18434	ATP4B	Potassium-transporting ATPase subunit beta	0.14%	0.00%	0.00%	0.05%	0.08%	0.00%	0.00%	0.00%	0.00%	0.00%	0.00%	0.00%	0.00%	0.00%	0.00%
Q29238	CLIC1	Chloride intracellular channel protein 1 (Fragment)	0.00%	0.03%	0.02%	0.02%	0.02%	0.00%	0.00%	0.00%	0.00%	0.00%	0.03%	0.03%	0.03%	0.03%	0.00%
P49923	LIPL	Lipoprotein lipase	0.02%	0.02%	0.01%	0.01%	0.01%	0.04%	0.03%	0.03%	0.03%	0.00%	0.00%	0.00%	0.00%	0.00%	0.00%
Q95274	TYB4	Thymosin beta-4	0.00%	0.02%	0.00%	0.01%	0.01%	0.00%	0.03%	0.04%	0.02%	0.02%	0.00%	0.03%	0.01%	0.02%	0.02%
P28839	AMPL	Cytosol aminopeptidase	0.02%	0.02%	0.00%	0.01%	0.01%	0.00%	0.02%	0.02%	0.02%	0.01%	0.02%	0.02%	0.02%	0.02%	0.00%
P00506	AATM	Aspartate aminotransferase, mitochondrial	0.00%	0.01%	0.01%	0.01%	0.01%	0.00%	0.02%	0.02%	0.01%	0.01%	0.02%	0.02%	0.03%	0.02%	0.00%
Q6JTA8	PRLR	Prolactin receptor	0.04%	0.00%	0.00%	0.01%	0.02%	0.00%	0.00%	0.00%	0.00%	0.00%	0.03%	0.04%	0.00%	0.02%	0.02%
A6M931	IF4A3	Eukaryotic initiation factor 4A-III	0.00%	0.04%	0.00%	0.01%	0.02%	0.00%	0.04%	0.04%	0.03%	0.02%	0.00%	0.00%	0.00%	0.00%	0.00%

Q29554	ECHA	Trifunctional enzyme subunit alpha, mitochondrial	0.00%	0.00%	0.00%	0.00%	0.00%	0.00%	0.02%	0.02%	0.01%	0.01%	0.03%	0.02%	0.02%	0.02%	0.00%
Q00655	KSYK	Tyrosine-protein kinase SYK	0.00%	0.02%	0.00%	0.01%	0.01%	0.00%	0.02%	0.01%	0.01%	0.01%	0.00%	0.06%	0.00%	0.02%	0.03%
Q95281	RL29	60S ribosomal protein L29	0.00%	0.03%	0.00%	0.01%	0.02%	0.00%	0.01%	0.02%	0.01%	0.01%	0.00%	0.02%	0.02%	0.01%	0.01%
P00571	KAD1	Adenylate kinase isoenzyme 1	0.02%	0.03%	0.00%	0.02%	0.02%	0.00%	0.02%	0.02%	0.01%	0.01%	0.00%	0.00%	0.01%	0.00%	0.01%
P02067	HBB	Hemoglobin subunit beta	0.00%	0.00%	0.00%	0.00%	0.00%	0.10%	0.00%	0.00%	0.03%	0.06%	0.00%	0.00%	0.00%	0.00%	0.00%
A5GFS8	VAPB	Vesicle-associated membrane protein-associated protein B	0.00%	0.00%	0.06%	0.02%	0.03%	0.00%	0.03%	0.00%	0.01%	0.02%	0.00%	0.01%	0.00%	0.00%	0.01%
Q06AU7	RAB1B	Ras-related protein Rab-1B	0.01%	0.01%	0.00%	0.01%	0.01%	0.02%	0.01%	0.01%	0.01%	0.01%	0.01%	0.01%	0.01%	0.01%	0.00%
P01315	INS	Insulin	0.00%	0.00%	0.00%	0.00%	0.00%	0.00%	0.05%	0.00%	0.02%	0.03%	0.00%	0.02%	0.03%	0.02%	0.01%
Q9N1F5	GSTO1	Glutathione S-transferase omega-1	0.00%	0.03%	0.00%	0.01%	0.02%	0.00%	0.00%	0.02%	0.01%	0.01%	0.02%	0.02%	0.00%	0.02%	0.01%
Q29195	RL10	60S ribosomal protein L10	0.00%	0.00%	0.00%	0.00%	0.00%	0.00%	0.02%	0.05%	0.02%	0.03%	0.00%	0.02%	0.00%	0.01%	0.01%
Q3YLA6	SRSF1	Serine/arginine-rich splicing factor 1	0.03%	0.02%	0.00%	0.02%	0.01%	0.00%	0.00%	0.03%	0.01%	0.02%	0.00%	0.00%	0.01%	0.00%	0.01%
Q29036	DAD1	Dolichyl-diphosphooligosaccharide--protein glycosyltransferase subunit DAD1	0.00%	0.01%	0.00%	0.00%	0.00%	0.02%	0.01%	0.00%	0.01%	0.01%	0.03%	0.01%	0.01%	0.02%	0.01%
Q29099	PTBP1	Polypyrimidine tract-binding protein 1	0.02%	0.01%	0.01%	0.01%	0.00%	0.00%	0.02%	0.01%	0.01%	0.01%	0.00%	0.00%	0.00%	0.00%	0.00%
P59083	PHP14	14 kDa phosphohistidine phosphatase	0.02%	0.03%	0.00%	0.02%	0.02%	0.00%	0.00%	0.01%	0.01%	0.01%	0.00%	0.01%	0.00%	0.00%	0.01%
Q6SA96	RS23	40S ribosomal protein S23	0.00%	0.02%	0.00%	0.01%	0.01%	0.00%	0.01%	0.03%	0.01%	0.02%	0.00%	0.00%	0.01%	0.00%	0.01%
F1S021	Col5a1	Collagen type V alpha 1 chain	0.00%	0.01%	0.00%	0.00%	0.01%	0.00%	0.03%	0.03%	0.02%	0.02%	0.00%	0.00%	0.00%	0.00%	0.00%
Q29221	CAZA2	F-actin-capping protein subunit alpha-2	0.01%	0.02%	0.00%	0.01%	0.01%	0.01%	0.00%	0.00%	0.00%	0.00%	0.00%	0.03%	0.00%	0.01%	0.02%

P16960	RYR1	Ryanodine receptor 1	0.00%	0.00%	0.00%	0.00%	0.00%	0.00%	0.00%	0.00%	0.00%	0.00%	0.03%	0.02%	0.02%	0.02%	0.00%
P80031	GSTP1	Glutathione S-transferase P	0.01%	0.01%	0.00%	0.01%	0.01%	0.01%	0.02%	0.02%	0.02%	0.01%	0.00%	0.00%	0.00%	0.00%	0.00%
Q06AU6	RAB5A	Ras-related protein Rab-5A	0.00%	0.00%	0.00%	0.00%	0.00%	0.00%	0.00%	0.03%	0.01%	0.02%	0.02%	0.02%	0.00%	0.01%	0.01%
Q29290	CYTB	Cystatin-B	0.00%	0.02%	0.00%	0.01%	0.01%	0.01%	0.01%	0.02%	0.01%	0.01%	0.00%	0.00%	0.00%	0.00%	0.00%
Q2EN81	ATPO	ATP synthase subunit O, mitochondrial	0.01%	0.01%	0.01%	0.01%	0.00%	0.00%	0.01%	0.01%	0.01%	0.01%	0.00%	0.00%	0.00%	0.00%	0.00%
P60662	MYL6	Myosin light polypeptide 6	0.00%	0.00%	0.02%	0.01%	0.01%	0.00%	0.00%	0.01%	0.00%	0.01%	0.01%	0.01%	0.00%	0.01%	0.01%
P19130	FRIH	Ferritin heavy chain	0.00%	0.01%	0.01%	0.01%	0.01%	0.00%	0.03%	0.00%	0.01%	0.02%	0.00%	0.00%	0.00%	0.00%	0.00%
Q6QN13	IOD1	Type I iodothyronine deiodinase	0.00%	0.00%	0.00%	0.00%	0.00%	0.00%	0.00%	0.00%	0.00%	0.00%	0.00%	0.00%	0.05%	0.02%	0.03%
A0A286ZQ85	Col3a1	Collagen type III alpha 1 chain	0.00%	0.02%	0.00%	0.01%	0.01%	0.00%	0.03%	0.00%	0.01%	0.02%	0.00%	0.00%	0.00%	0.00%	0.00%
Q710C4	SAHH	Adenosylhomocysteinase	0.01%	0.02%	0.00%	0.01%	0.01%	0.00%	0.00%	0.00%	0.00%	0.00%	0.00%	0.00%	0.02%	0.01%	0.01%
P49666	RL21	60S ribosomal protein L21	0.04%	0.00%	0.00%	0.01%	0.02%	0.00%	0.00%	0.00%	0.00%	0.00%	0.00%	0.00%	0.00%	0.00%	0.00%
P01269	PTHY	Parathyroid hormone	0.00%	0.00%	0.00%	0.00%	0.00%	0.00%	0.00%	0.00%	0.00%	0.00%	0.00%	0.04%	0.00%	0.01%	0.02%
P28768	SODM	Superoxide dismutase [Mn], mitochondrial (Fragment)	0.00%	0.00%	0.00%	0.00%	0.00%	0.00%	0.01%	0.00%	0.00%	0.01%	0.00%	0.02%	0.01%	0.01%	0.01%
Q9TTB4	FMOD	Fibromodulin (Fragment)	0.00%	0.00%	0.00%	0.00%	0.00%	0.00%	0.00%	0.00%	0.00%	0.00%	0.01%	0.02%	0.00%	0.01%	0.01%
P01965	HBA	Hemoglobin subunit alpha	0.00%	0.00%	0.00%	0.00%	0.00%	0.00%	0.00%	0.00%	0.00%	0.00%	0.00%	0.02%	0.00%	0.01%	0.01%
P79281	PTN	Pleiotrophin	0.00%	0.00%	0.00%	0.00%	0.00%	0.00%	0.00%	0.00%	0.00%	0.00%	0.00%	0.00%	0.01%	0.00%	0.01%
Q6QAP7	RS17	40S ribosomal protein S17	0.00%	0.00%	0.00%	0.00%	0.00%	0.00%	0.00%	0.00%	0.00%	0.00%	0.00%	0.00%	0.01%	0.00%	0.01%

Chapter 6: Proteomic, Mechanical, and Biochemical Development of Tissue-Engineered Neocartilage[6]

Abstract

The self-assembling process of cartilage tissue engineering is a promising technique to heal cartilage defects, preventing osteoarthritic changes. Given that chondrocytes dedifferentiate when expanded, it is not known if cellular expansion affects the development of self-assembled neocartilage. The objective of this study is to use proteomic, mechanical, and biochemical analyses to quantitatively investigate the development of self-assembled neocartilage derived from passaged, rejuvenated costal chondrocytes. It was found that temporal trends in neocartilage formation are similar to those seen in native hyaline articular cartilage development. For example, between days 7 and 84 of culture, tensile Young's modulus increases 4.4-times, total collagen increases 2.7-times, DNA content decreases 69.3%, collagen type II increases 1.5-times, and aggrecan drops 55.3% mirroring trends shown in native knee cartilage. Importantly, collagen type X, which is associated with cartilage calcification, remains at low levels (≤0.05%) at all neocartilage developmental time points, similar to knee cartilage (<0.01%) and unlike donor rib cartilage (0.98%). In this work, bottom-up proteomics, a powerful tool to interrogate tissue composition, is used to quantify the proteome of maturing neocartilage vis-à-vis native hyaline cartilages. Furthermore, it is shown that self-assembled, costal chondrocyte-derived neocartilage is suitable for a non-homologous approach in the knee.

Introduction

Focal cartilage defects occur in 12% of the population [392] and 36% of athletes [393], and cartilage defects are well-known not to heal. Existing surgical procedures to address focal

[6] **Chapter submitted as:** Bielajew, B.J.,* Donahue, R.P.,* Lamkin, E.K., Hu, J.C., Hascall, V.C., Athanasiou, K.A. Proteomic, mechanical, and biochemical development of tissue-engineered neocartilage. Submitted to *Biomaterials*. (* These authors contributed equally.)

cartilage defects, such as microfracture or matrix-assisted autologous chondrocyte implantation, only provide short-term relief [247, 394]. Focal cartilage defects can eventually degenerate to osteoarthritis (OA) [395], which affects over 32.5 million adults in the US [361]. Tissue engineering holds promise for regenerating cartilage defects by alleviating pain, restoring function, and preventing the onset of OA [247, 396, 397]. For successful translation of tissue-engineered cartilages from the laboratory to human usage, neocartilages must be well-characterized for quality control with appropriate release criteria for preclinical and clinical trials. The quality and safety profile of any implant will benefit greatly from the ability to quantitatively define the implant's composition.

Toward the precise determination of tissue composition for quality control and release criteria of tissue-engineered implants, it is desirable to quantify many analytes in a single sample with low sample volume. The advent of powerful quantitative bottom-up proteomics techniques [398] enables the simultaneous quantification of hundreds of proteins in biological samples, for example, in cartilage extracellular matrix (ECM). This engenders tissue engineers to establish new quality control protocols, where bottom-up proteomics can be used as a basis for a multitude of release criteria. Applications of bottom-up proteomics to investigate tissue composition is applicable to any neotissue that has ECM-dependent functionality (e.g., cartilage, skin, tendon/ligament, heart valve). Moreover, quantitative bottom-up proteomics can be used as a tool to interrogate developmental changes in neotissues, such as in tissue-engineering approaches for hyaline articular cartilage.

Self-assembled neocartilage derived from primary articular chondrocytes matures similarly to the way that native cartilage develops (i.e., it mimics aspects of mesenchymal condensation) [399]. Additionally, self-assembled neocartilages have been produced with native-like mechanical properties, such as a tensile modulus of 8.4 MPa [207] and an aggregate modulus of 400 kPa [400]; these robust mechanical properties are crucial for implant survival and functionality [401]. However, harvesting primary articular chondrocytes, which were used in

these neocartilages, can lead to donor site morbidity or yield cells with an osteoarthritic phenotype [15]. Thus, recent tissue-engineering efforts have focused on alternative cell sources such as costal chondrocytes from the rib [402]. For example, self-assembled neocartilages have recently been made from expanded, rejuvenated costal chondrocytes [338], which allows for thousands of robust neocartilage implants to be made from one biopsy [25]. However, it is unknown whether neocartilage produced from expanded chondrocytes develops similarly to native cartilage, given that chondrocyte expansion results in dedifferentiation [368, 403-406]. Furthermore, it is not known whether neocartilage made with costal chondrocytes is suitable for non-homologous implantation into the knee.

The objective of this study is to determine, through mechanical, biochemical, and proteomic analyses, whether neotissues formed from passaged, rejuvenated, and self-assembled costal chondrocytes display features of the native hyaline cartilage developmental process. The study design compares multiple protein analytes throughout maturation of self-assembled neocartilage, thereby informing how ECM components form mechanically robust tissue. The hypothesis of this work is that self-assembled neocartilage derived from passaged, rejuvenated costal chondrocytes will follow temporal trends in mechanical, biochemical, and proteomic properties that have previously been characterized in native hyaline cartilage development [407]. Specifically, as the self-assembled neocartilage develops from nascent tissue to mature neocartilage, it is expected that, 1) in mechanics, tensile and compressive properties will increase, 2) in biochemical composition, collagen content will increase, and glycosaminoglycan (GAG) and DNA content will decrease, and 3) in proteomics, collagen type II will increase, aggrecan and link protein will decrease, and, unlike in native costal cartilage, collagen type X will only be deposited at low levels (<0.1%). This work will further the understanding of how the self-assembling process mimics native cartilage development and will determine the suitability of costal chondrocyte-derived neocartilage for non-homologous implantation into the knee.

Methods

Costal cartilage harvest and isolation

Costal chondrocytes were harvested from the rib cartilage of three juvenile (aged 5-8 months) Yucatan minipig donors that were culled for reasons unrelated to this study (Figure 6-1A). Briefly, using sterile tools in a biosafety cabinet, costal cartilage was exposed, and the perichondrium was removed. Then, costal cartilage was minced to approximately 1 mm^3 pieces and digested at 37°C in 0.4% w/v pronase for 1 hour followed by 0.2% w/v collagenase for 18 hours. Both enzymes were dissolved in Dulbecco's modified Eagle's medium (DMEM, high glucose, GlutaMAX supplement) supplemented with 3% fetal bovine serum (FBS) and 1% penicillin-streptomycin-fungizone (PSF). The resulting cell suspension was filtered through a 70 µm cell strainer and treated with ammonium-chloride-potassium lysis buffer, as previously described [353].

Costal chondrocyte expansion and aggregate rejuvenation

After isolation, costal chondrocytes were plated at 2.5M cells per T225 flask (~11,111 cells/cm^2) in chemically defined chondrogenic (CHG) medium (Figure 6-1A), which consisted of DMEM, 1% PSF, 1% nonessential amino acids, 1% insulin-transferrin-selenous acid+, 100 nM dexamethasone, 50 µg/mL ascorbate-2-phosphate, 40 µg/mL L-proline, and 100 µg/mL sodium pyruvate. CHG medium was further supplemented with 2% FBS, 1 ng/mL transforming growth factor beta 1 (TGF-β1), 5 ng/mL basic fibroblast growth factor (bFGF), and 10 ng/mL platelet-derived growth factor (PDGF) during monolayer expansion to retain post-expansion chondrogenic potential [149]. Medium was changed every 3-4 days during expansion. After one passage, chondrocytes were frozen in FBS containing 10% dimethyl sulfoxide (DMSO) for downstream use. Cells were thawed and plated in CHG medium containing FBS and growth factors, as described above. Between passages, cells were lifted using 0.05% trypsin-EDTA solution for 9 minutes, and the cell sheet was digested using 0.2% w/v collagenase in DMEM

containing 3% FBS and 1% PSF for approximately 30 minutes with agitation every 10 minutes. After six passages, the expanded cells underwent aggregate rejuvenation for 14 days to return them to a chondrogenic phenotype (Figure 6-1A), as previously described [150]. Medium was changed every 3-4 days during aggregate rejuvenation. Cells were cultured in CHG medium supplemented with 10 ng/mL TGF-β1, 100 ng/mL growth differentiation factor 5 (GDF-5), and 100 ng/mL bone morphogenetic protein 2 (BMP-2). Aggregates were then digested after culture in 0.05% trypsin-EDTA solution for 45 minutes followed by 0.2% w/v collagenase solution in DMEM supplemented with 3% FBS and 1% PSF for 90 minutes with agitation every 10 minutes. The resulting cell suspension was filtered through a 70 µm cell strainer prior to the self-assembling process.

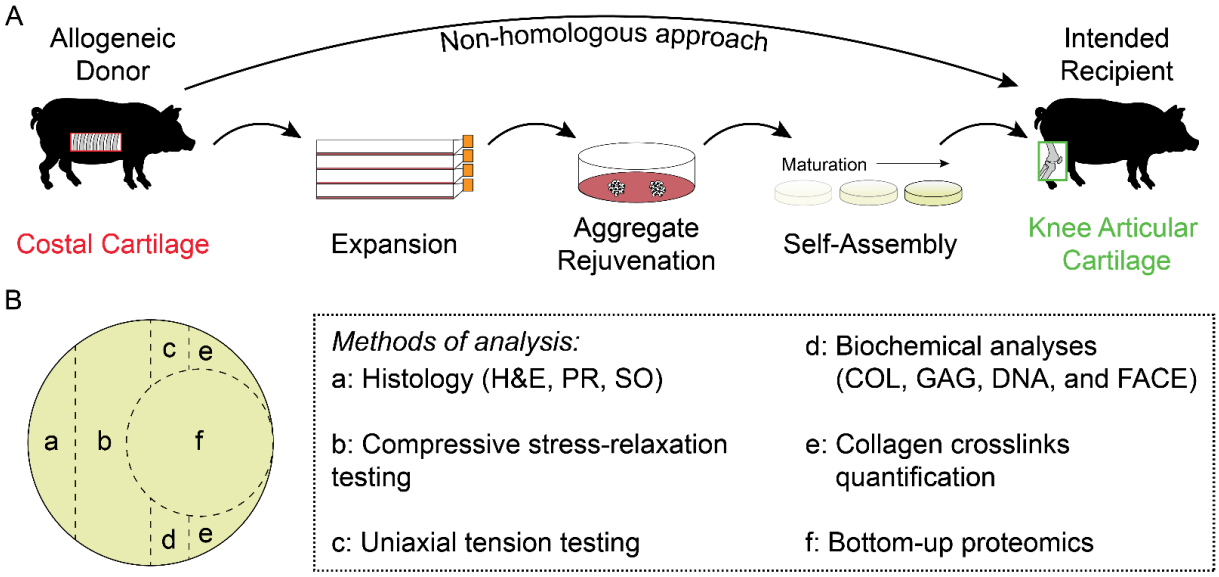

Figure 6-1: The tissue-engineering process using costal chondrocytes and neocartilage sample preparation. (A) Self-assembled constructs are envisioned to be used in the knee through an allogeneic, non-homologous approach. Donor costal chondrocytes were expanded, rejuvenated, and self-assembled for eventual implantation into the knee. (B) At specific maturation time points (i.e., days of culture), the neocartilage constructs were divided and assayed by various methods. Histological analysis included staining with hematoxylin and eosin (H&E), picrosirius red (PR), and safranin O with fast green counterstains (SO). Mechanical analysis included uniaxial tensile testing and compressive stress-relaxation testing. Biochemical analyses for total collagen (COL), glycosaminoglycan (GAG), and DNA content and fluorophore assisted carbohydrate electrophoresis (FACE) were performed from a papain digest.

Neocartilage self-assembly and bioactive factor treatment

As previously described [25], scaffold-free neocartilage self-assembly was carried out for a total of 84 days (Figure 6-1A). Briefly, nonadherent wells of 5 mm diameter in size were made using molten 2% agarose and negative molds. The wells were hydrated with CHG medium, and the medium was changed at least three times prior to cell seeding. As previously optimized [377], 2M cells per well were seeded in 100 µL CHG medium. After 4 hours, medium was topped off with an additional 400 µL CHG medium, and, subsequently, medium was exchanged every day until day 3 when constructs were unconfined from agarose wells. From day 3 onward, neocartilage constructs were fed 2 mL CHG medium every 2 days. Constructs were treated with bioactive factors, as previously described [25]. Briefly, TGF-β1 (10 ng/mL) was supplemented continuously in CHG medium. Chondroitinase ABC (c-ABC) was applied to constructs at 2 U/mL in 0.4 mL of CHG for 4 hours on day 7 of self-assembly. C-ABC was activated with 50 mM of sodium acetate and quenched with 1 mM zinc sulfate. Lysyl oxidase-like 2 at was added to the medium 0.15 µg/mL with 0.146 mg/mL hydroxylysine and 1.6 µg/mL copper sulfate from day 7 until the end of self-assembly.

Sample preparation

Self-assembled neocartilage constructs (n=7-9 per time point) were removed from culture after 1, 4, 7, 14, 28, 56, or 84 days of culture and photographed. Constructs at days 1 and 4 of culture disintegrated upon handling, and, thus, were not able to be photographed. Constructs were cut with a biopsy punch and scalpel for histological, mechanical, biochemical, and proteomic analyses as depicted in Figure 6-1B. Samples for photometric biochemical assays and crosslinks mass spectrometry were weighed to obtain the wet weights (WWs). WWs were not able to be taken on day 1 constructs because they disintegrated upon contact with the weigh boat. After at least 72 hours of lyophilization, samples were reweighed to obtain dry weights (DWs). Hydration was calculated based on the ratio of sample DW to WW.

Histology

As previously described [355], samples were fixed in 10% neutral buffered formalin for at least 72 hours, processed, embedded in paraffin, sectioned to 5 μm thickness, and mounted on microscopy slides. Samples were then stained with hematoxylin and eosin (H&E), safranin O with fast green counterstain, or picrosirius red. Representative images were taken at 20x magnification using a brightfield microscope.

Mechanical testing

Mechanical properties of constructs were quantified with compressive stress-relaxation and uniaxial tension tests. Punches of 3 mm diameter from neocartilage constructs were subjected to compressive stress-relaxation testing. Because day 1 and day 4 constructs disintegrated upon handling, they were not included in the mechanical testing analysis. As previously described [24], the sample height was determined using a tare load of 0.1 N. Samples were subjected to 15 preloading cycles of 5% strain based on the determined sample height. Strains of 10% and 20% were applied to the punch and held for 600 and 900 seconds, respectively. The force-displacement curves were fit to a standard linear solid model using a custom MATLAB code to determine relaxation modulus, instantaneous modulus, and coefficient of viscosity for each strain level. For tensile testing, samples were trimmed into dog bone shapes (approximately 0.75 mm by 0.45 mm) and glued to paper tabs of a predefined gauge length (1.55 mm), as previously described [355]. Samples were pulled until failure at 1% strain per second. Force-displacement curves were analyzed using a custom MATLAB code to extract Young's modulus and ultimate tensile strength (UTS).

Collagen, GAG, and DNA assays

Construct pieces were subjected to overnight digestion with papain, followed by biochemical assays for quantification of total collagen (COL), GAG, and DNA contents, as previously

described [378]. Briefly, COL was quantified using a modified hydroxyproline assay [93], GAG was quantified using a dimethylmethylene blue assay kit, and DNA was quantified using a PicoGreen assay kit. The COL, GAG, and DNA measurements were normalized to WW and DW.

Fluorophore assisted carbohydrate electrophoresis (FACE)

Papain digest aliquots (50 µL) from each sample were lyophilized, and GAGs were precipitated with alcohol and digested with c-ABC. Chondroitin-6-sulfate (CS6) and chondroitin-4-sulfate (CS4) were derivatized using 2-aminoacridone, and CS6 was separated from CS4 using FACE, as previously described [408]. CS6 and CS4 were quantified by integrating the optical density of CS6 and CS4 bands in ImageJ, then comparing the resulting integrated optical density in samples and standards. CS6 was divided by CS4 to obtain the chondroitin sulfate ratio.

Collagen crosslink quantification

Quantification of collagen crosslinks was performed, as previously described [346]. Briefly, construct pieces approximately 1 mg in WW were lyophilized, weighed, reduced in $NaBH_4$, washed on a rocker plate overnight in ultrapure water, and hydrolyzed overnight in HCl. HCl was evaporated, hydrolysates were resuspended and filtered, and then hydrolysates were subjected to liquid chromatography-mass spectrometry with a Waters ACQUITY QDa quadrupole mass spectrometer to quantify mature pyridinoline (PYR), immature dihydroxylysinonorleucine (DHLNL), hydroxyproline (OHP), and internal standard pyridoxine. Because day 1 constructs disintegrated during the washing process, they were not included in the crosslinks analysis.

Bottom-up proteomics

Bottom-up proteomics was performed, as previously described [346]. Three samples per group, chosen at random, were used for bottom-up proteomics. Briefly, construct pieces approximately 1 mg in WW were lyophilized, weighed, washed by vortexing twice in 10 mM ammonium citrate and twice in 50 mM ammonium bicarbonate, digested overnight in trypsin, and subjected to liquid chromatography-tandem mass spectrometry on a Thermo Fisher Scientific Orbitrap Fusion Lumos mass spectrometer. MaxQuant was used for label-free quantification [357], yielding a list of proteins normalized to total protein content (PROT). PROT/DW was quantified by dividing COL/DW from the hydroxyproline assay by COL/PROT from bottom-up proteomics (sum of all collagen proteins per PROT). Because day 1 and day 4 constructs disintegrated during the washing process, they were not included in the bottom-up proteomics analysis.

Statistical analysis

Data from this study were analyzed using a one-way analysis of variance (ANOVA), with the only factor being culture time, followed by a *post hoc* Tukey's honestly significant difference test performed in JMP Pro 14. All bar graphs were created in GraphPad Prism 9. A connecting letters report is used to show statistical significance in all bar graphs; bars that do not share the same letter are significantly different from each other.

Results

Neocartilage histology

Representative images for histology of H&E staining for cellular morphology, picrosirius red staining for collagen, and safranin O staining for GAGs, as well as gross morphology, are reported in Figure 6-2. At earlier time points such as 1 and 4 days of culture, staining intensity is localized to the cells for both H&E and picrosirius red stainings. As the tissue matures to 7-28 days of culture, the staining becomes more intense for hematoxylin in the ECM of the

neocartilage, but rapidly decreases after 56-84 days of culture, exhibiting almost no staining. However, the picrosirius red staining becomes more intense over time. Safranin O staining follows a similar pattern to the H&E staining for 7-84 days of culture but yields minimal staining for the earlier 1- and 4-day time points. From 7 to 84 days of culture, constructs appear flat and robust.

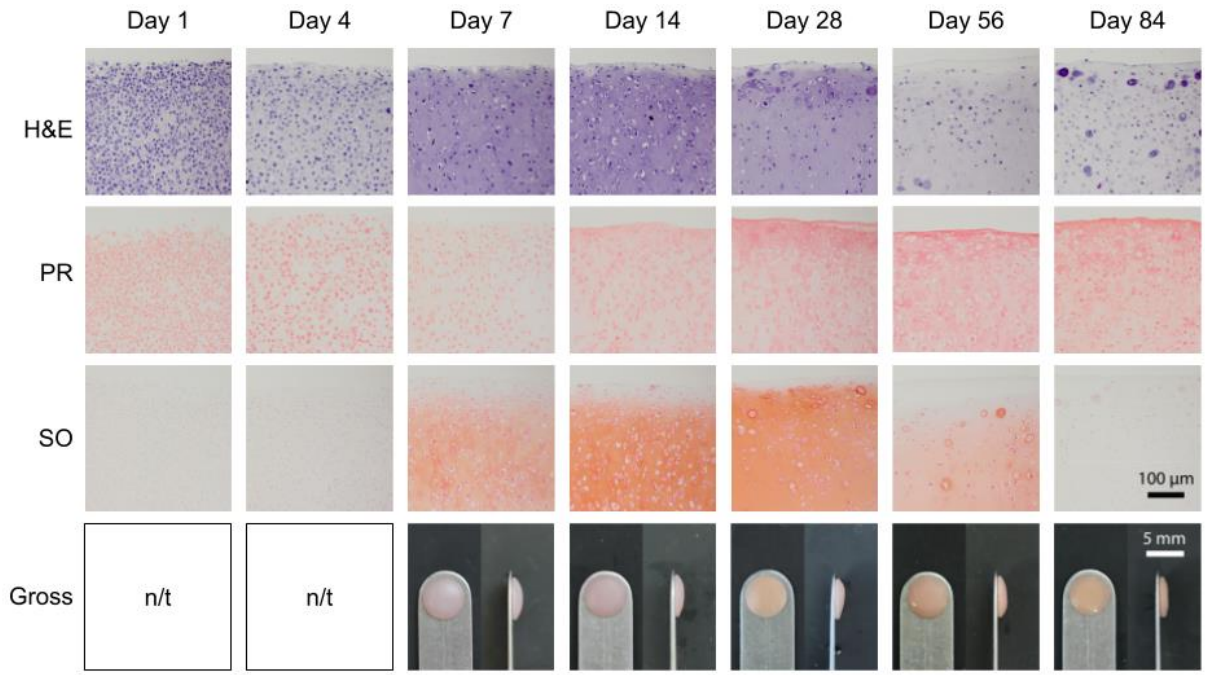

Figure 6-2: Histology and gross morphology of neocartilage constructs.
Staining with hematoxylin and eosin (H&E), picrosirius red (PR), and safranin O with fast green counterstain (SO) is shown in self-assembled neocartilage constructs at different time points in culture. Gross morphology is shown in front and side views. Gross morphology pictures for day 1 and day 4 of culture were not taken (n/t).

Mechanical properties

Mechanical properties from compressive stress-relaxation testing and uniaxial tension testing are reported in Figure 6-3. Across culture times, instantaneous modulus for both 10% and 20% strain levels peaked at 14 days of culture. The maximum values for 10% and 20% instantaneous modulus obtained at 14 days were 266±43 kPa and 565±87 kPa, respectively, significantly higher than the values at both 7 days (216±27 kPa for 10%, 304±46 kPa for 20%, $p<0.05$) and 56 days of culture (202±20 kPa for 10% and 404±39 kPa for 20%, $p<0.01$);

however, they were not different from 28 days of culture (Figure 6-3A, C). For both 10% and 20% relaxation modulus, maximal points were observed at 28 days of culture, with significant decreases at 56 and 84 days ($p<0.0001$) (Figure 6-3B, D). Young's modulus (4.7±1.9 MPa) and UTS (1.2±0.3 MPa) peaked at 56 days, 5.9-times and 4.0-times higher than their respective values of 0.8±0.3 MPa and 0.3±0.1 MPa at 7 days (Figure 6-3E-F). Young's modulus slightly decreased to 3.7±0.8 MPa at 84 days of culture, which was 4.6-times higher than day 7, but the difference between 56 and 84 days of culture was not significant (Figure 6-3E). UTS exhibited a significant increase from 7 to 14 days of culture ($p<0.0001$), at which point it plateaued without any significant changes at any later time points (Figure 6-3F). Additional outcomes including 10% and 20% coefficients of viscosity, strain at failure, and toughness are reported in Supplementary Table 6-1.

Biochemical properties

For biochemical analysis of ECM content, COL, GAG, and DNA content are reported in Figure 6-4. For COL/DW and COL/WW values, steady increases were observed over culture time, with the highest value seen at day 84 for both measurements (24.8±1.9% and 4.4±0.8%, respectively) (Figure 6-4A-B). The COL/DW increased 27.6-times from day 1 to day 84 and 2.7-times from day 7 to day 84 (Figure 6-4B). Interestingly, GAG/DW peaked at 7 days of culture (45.7±4.4%), which was significantly higher than any other group ($p<0.0001$) (Figure 6-4D), while GAG/WW peaked at 28 days of culture (6.0±0.9%) but was not significantly different from 7 days of culture (5.1±1.2%) (Figure 6-4C). By 84 days of culture, GAG content decreased toward those levels seen at 1-4 days of culture in both measures (Figure 6-4C-D). DNA/DW also trended down with time, exhibiting an 84.6% decrease from days 1 to 84 and a 69.3% decrease from days 7 to 84 (Figure 6-4F). Similarly, DNA/WW also significantly decreased between 14 days of culture to 84 days ($p<0.0001$) (Figure 6-4E). Generally, hydration also decreased with time, exhibiting a 9.6% decrease from 7 days of culture to 56 days ($p<0.0001$)

(Figure 6-4G). The CS6:CS4 ratio rose until 14 days of culture (1.2 w/w) before exhibiting a stark and significant decrease between 56 and 84 days (0.8±0.4 w/w to 0.1±0.1 w/w, $p<0.01$) (Figure 6-4H).

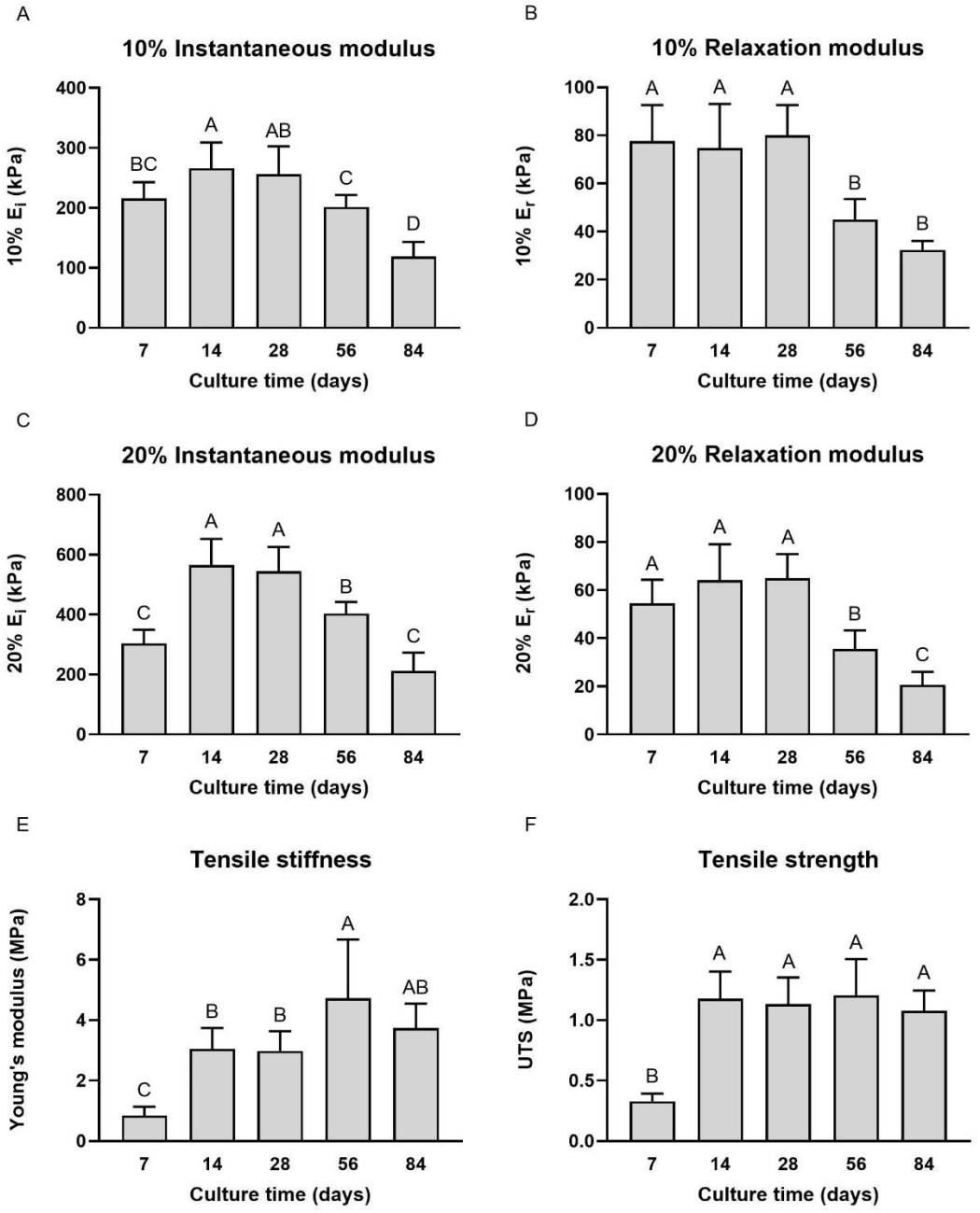

Figure 6-3: Mechanical properties of neocartilage constructs.
At different time points throughout self-assembled neocartilage culture, compressive properties are shown in the 10% and 20% instantaneous modulus (E_i) (A, C) and relaxation modulus (E_r) (B, D) graphs. Tensile properties are shown in the Young's modulus (E) and ultimate tensile strength (UTS) graphs (F). Bars that do not share the same letter are significantly different from each other.

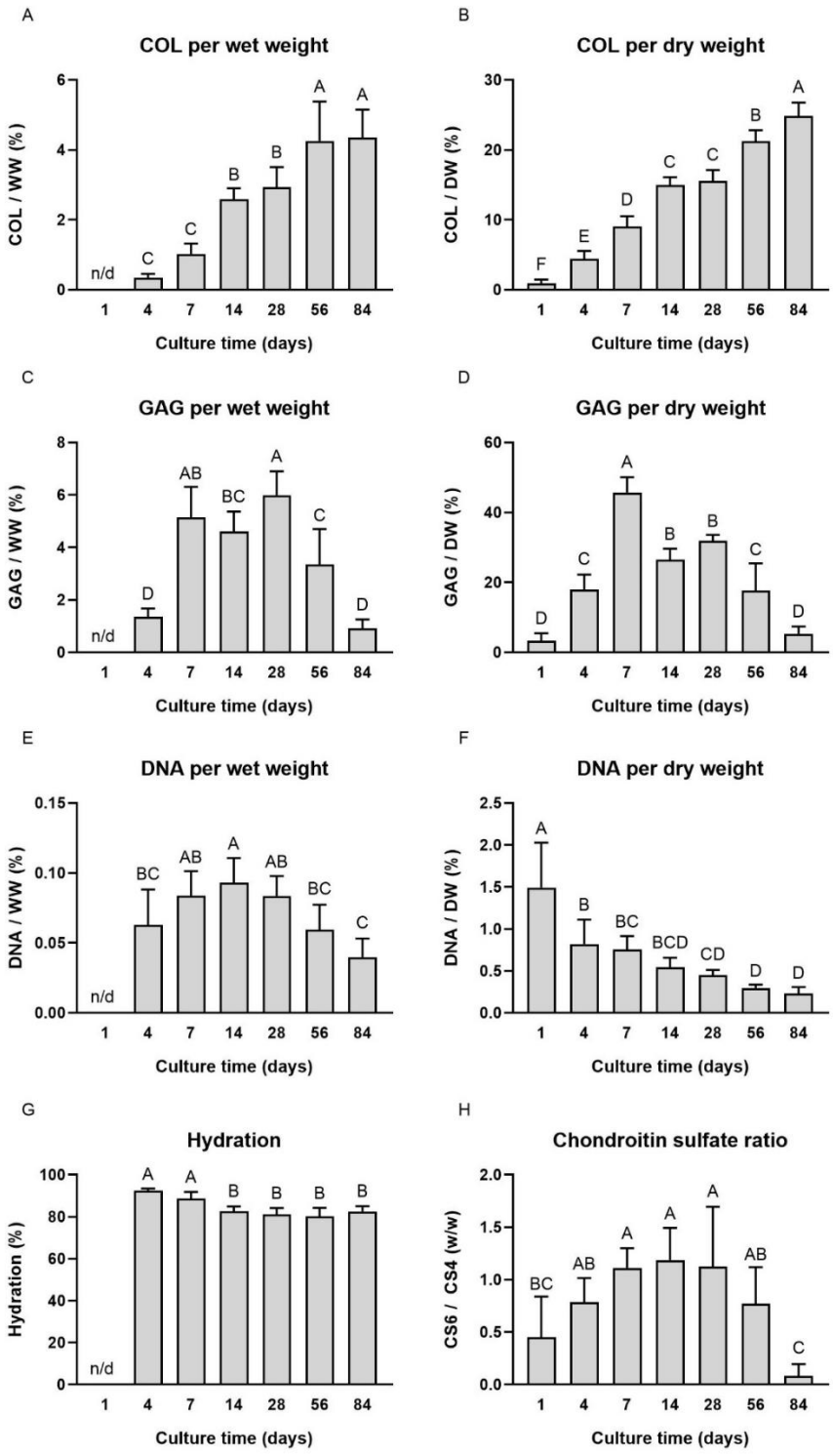

Figure 6-4: Biochemical composition of neocartilage constructs.
At different time points throughout self-assembled neocartilage culture, the biochemical composition is shown. Total collagen (COL) content (A-B), glycosaminoglycan (GAG) content (C-D), and DNA content (E-F) are normalized to both wet weight (WW) and dry weight (DW). Hydration (G) is reported, along with the chondroitin-6-sulfate (CS6) to chondroitin-4-sulfate (CS4) ratio (H). Bars that do not share the same letter are significantly different from each other.

Crosslink quantification

Collagen crosslink analysis is reported in Figure 6-5. PYR/DW was at a maximum after 84 days of culture, measuring 1273±51 ng/mg (Figure 6-5A). PYR/OHP significantly increased between 4 days (7.9±1.7 mmol/mol) and 7 days (20.3±6.9 mmol/mol) of culture ($p<0.01$) but had no significant differences between days 7 and 84 (Figure 6-5B). For DHLNL/DW, the values significantly increased over time from 100±79 ng/mg after 4 days of culture to a maximum of 708±430 ng/mg at 56 days of culture ($p<0.01$) (Figure 6-5C). The opposite trend was observed for DHLNL/OHP; between 4 days (14.4±4.1 mmol/mol) and 28 days (7.3±1.3 mmol/mol) of culture, there was a significant decrease in immature crosslinks ($p<0.05$) (Figure 6-5D). Overall, the maturity of the crosslinking within the constructs' ECM increased, as depicted by the PYR/DHLNL ratio (Figure 6-5E), significantly increasing 4.0-times from 4 days (0.6±0.2 mol/mol) to 84 days of culture (2.4±1.1 mol/mol, $p<0.05$).

Bottom-up proteomic analysis

Bottom-up proteomics analysis identified and quantified a total of 364 protein analytes. Those with an intensity greater than 0.1%/PROT in at least one sample and all collagen chains (86 analytes total) are reported as averages in Supplementary Table 6-2. For *post hoc* analysis, 15 proteins of interest were chosen, and these data are reported in Figure 6-6. Overall, PROT/DW significantly increased with culture time, rising 4.4-times from 7 days (5.30±0.66%) to 84 days (23.50±1.35%) of culture ($p<0.0001$) (Figure 6-6A). Similar trends were seen in collagen types I, II, V, VI, IX, XI, and XII, and decorin (Figure 6-6C-D, F-K). For example, per PROT, collagen type II increased 1.5-times from 7 days (38.40±0.74%) to 84 days (57.58±0.81%) of culture (Figure 6-6D). Aggrecan per PROT decreased over time, exhibiting a significant drop of 55.3% between 7 days (0.47±0.03%) and 84 days (0.21±0.04%) of culture ($p<0.01$) (Figure 6-6B). Link protein followed a similar trend (Figure 6-6M). Most cell-associated proteins such as histone H4, tubulin, and vimentin all also decreased over time (Figure 6-6L, O-P). Tenascin exhibited a

parabolic-shaped trend, peaking after 28 days of culture (Figure 6-6N). Collagen type X remained at levels below or equal to 0.05%/PROT for all culture time points (Supplementary Table 6-2).

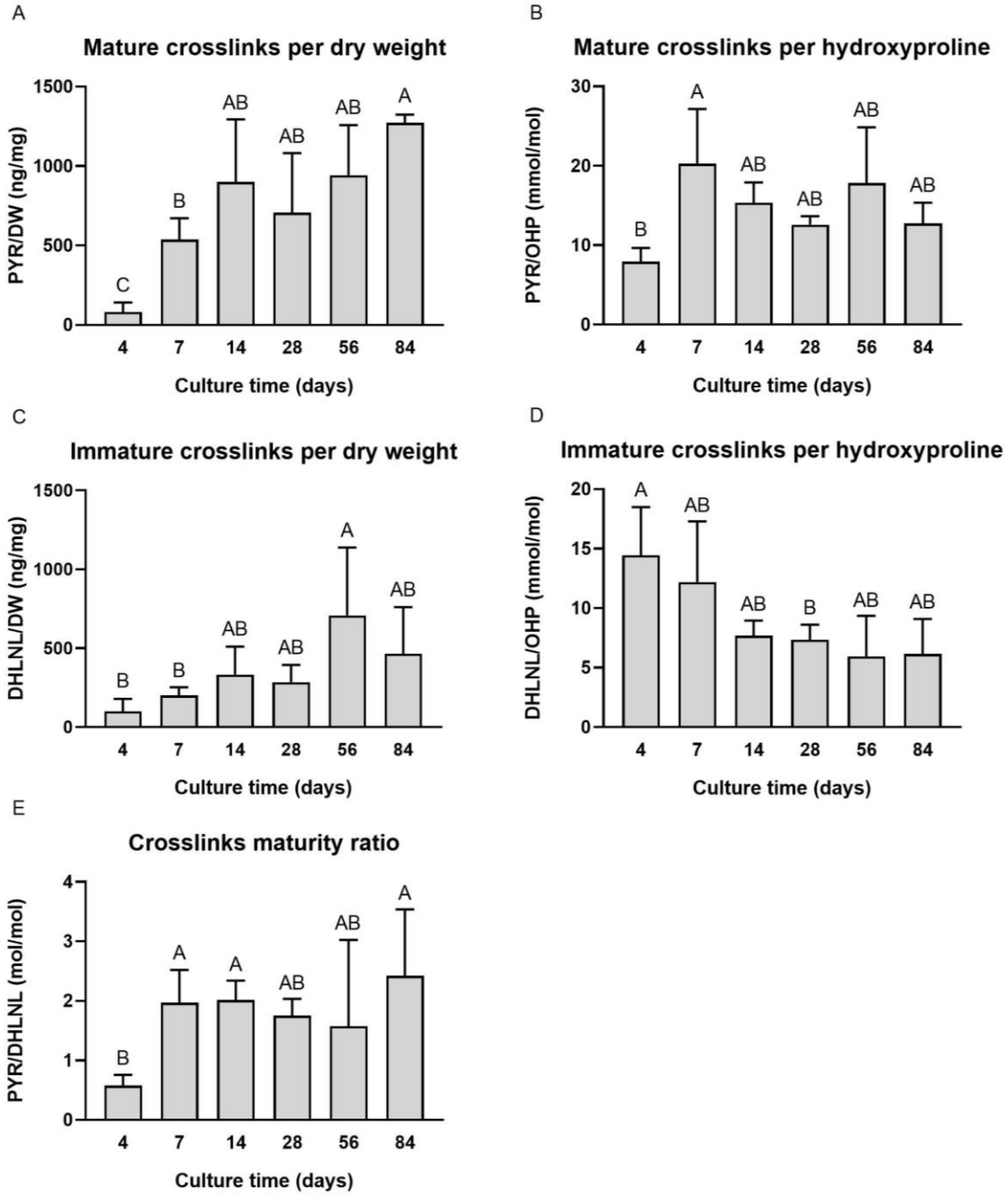

Figure 6-5: Collagen crosslink composition of neocartilage constructs.
Throughout self-assembled neocartilage culture, mature pyridinoline crosslinks (PYR) and immature dihydroxylysinonorleucine crosslinks (DHLNL) are reported. PYR is normalized to dry weight (DW) (A) and hydroxyproline (OHP) (B). DHLNL is normalized to DW (C) and OHP (D). The PYR to DHLNL ratio is reported (E). Bars that do not share the same letter are significantly different from each other.

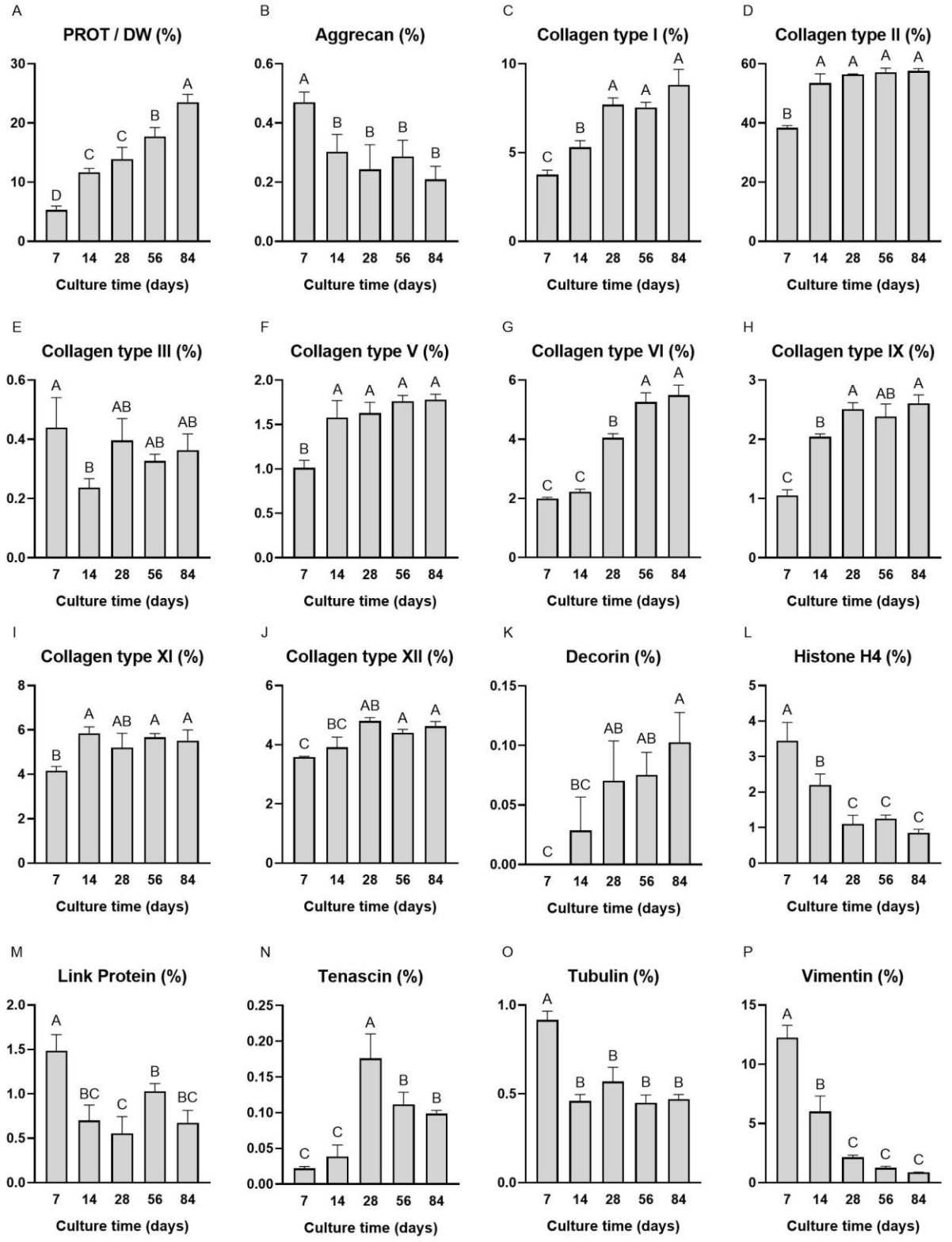

Figure 6-6: Bottom-up proteomics analysis of neocartilage constructs.
Total protein (PROT) content (A) and 15 selected protein analytes of interest are reported. Graphs (B-P) are reported as percent protein per PROT. Bars that do not share the same letter are significantly different from each other.

Discussion

The self-assembling process has recently emerged as a tissue engineering method that creates neocartilage constructs on par with native hyaline cartilage functional properties [23, 207]. The objective of this study was to characterize the self-assembling process via mechanical, biochemical, and proteomic assays and determine whether the process using expanded and rejuvenated costal chondrocytes mirrors aspects of the development of native hyaline cartilage tissue. The hypotheses of this study were confirmed; self-assembled neocartilage derived from passaged, rejuvenated costal chondrocytes exhibited certain temporal trends in mechanics, biochemistry, and proteomics that were reminiscent of native hyaline cartilage development [407]. For example, our group has previously characterized increases in tensile properties, COL, and collagen type II, and decreases in DNA, aggrecan, and link protein when comparing juvenile to fetal porcine knee cartilage [407]. Throughout maturation of self-assembled neocartilage, these same trends were mirrored with tensile properties, COL, and collagen type II increasing and DNA, aggrecan, and link protein decreasing during culture. Ultimately, this study 1) elucidated similarities in the ECM maturation of self-assembled neocartilage and native hyaline cartilage, 2) identified specific ECM components with quantities parallel to those in native hyaline articular cartilage and costal cartilage, 3) explored the proteomics of self-assembled cartilage ECM, including structure-function relationships and protein targets for future tissue-engineering techniques, and 4) established optimal time points for future implantation of self-assembled cartilage. Combined, these findings allow tissue engineers to identify targets and measures for potential quality control and release criteria for mechanically robust cartilage therapeutics, required for future preclinical and clinical studies.

The maturation of self-assembled neocartilage derived from expanded and rejuvenated costal chondrocytes followed mechanical trends of native hyaline cartilage development. In native porcine knee articular cartilage, there was a 10.5-times increase in tensile Young's modulus properties from the fetal to juvenile stage, then a slight decrease to mature tissue [407].

The neocartilage in this experiment exhibited a similar trend in tensile Young's modulus, increasing 5.9-times from 7 days to 56 days of culture, before a slight decrease at 84 days of culture. In compressive properties, similar trends applied to both native knee cartilage and self-assembled neocartilage. Native cartilage increased in compressive properties from the fetal to juvenile stages [407], and self-assembled neocartilage instantaneous moduli increased from 7 days to 28 days of culture. A subsequent drop in compressive properties was seen in both native articular cartilage and neocartilage; the 20% relaxation modulus of native knee articular cartilage dropped 1.8-times from juvenile to mature [407], and, in neocartilage, this same property dropped 3.2-times from 28 days to 84 days of culture. While mechanical properties are the primary design criteria for tissue-engineered cartilages, the biochemical and proteomic properties are also of crucial importance.

Biochemical and proteomic analysis of the neocartilage in this study also revealed many similarities to native articular cartilage development. COL content in both native articular cartilage [407] and self-assembled neocartilage increased throughout development. In terms of specific collagen subtypes, collagen type II increased over time in both native articular cartilage [407] and neocartilage. The collagen subtype profiles in native tissue and neocartilage had some developmental differences; in native articular cartilage, collagen types I, VI, and XII did not significantly change with tissue age, while collagen types IX and XI decreased [407], but in neocartilage, collagen types I, VI, IX, XI, and XII all increased throughout culture. The collagen crosslink maturity ratio, which did not change throughout tissue development in native knee cartilage [407], increased in neocartilage; this was likely due to medium supplementation of lysyl oxidase-like 2, an enzyme that catalyzes the production of mature collagen crosslinks [25, 409]. The GAG content of native tissue decreased from neonatal to juvenile articular cartilage [407], and this trend was seen in later time points of self-assembly (i.e., days 28 and beyond); however, in earlier timepoints of self-assembly (i.e., days 1-14), GAG rapidly accumulated in the ECM. Similar to native knee cartilage [407], aggrecan and link protein, parts of hyaline

cartilage's proteoglycan structure, decreased in neocartilage throughout development. In agreement with a previous study on matrix maturation in self-assembled cartilage, the CS6:CS4 ratio decreases in later time points of self-assembly [399]. However, the decrease in the CS6:CS4 ratio is opposite to the trend previously shown in aging knee cartilage [407]. DNA and cellularity (from H&E staining) also decreased over time in neocartilage constructs, similar to the trends found in native tissue [407]. As expected due to their respective roles in chromatin and cytoskeletal structure, histone H4, tubulin, and vimentin decreased in parallel with cellularity, similar to native cartilage trends. Tenascin, previously associated with fetal articular cartilage development, decreases during later tissue maturation [410]. Thus, the increases seen here in tenascin in early stages of self-assembly may be correlated with the deposition of more ECM by the chondrocytes, but the subsequent decrease may be due to maturation of the neocartilage. Altogether, there were many mechanical, biochemical, and proteomic trends that are mirrored between native articular cartilage development and culture of self-assembled neocartilage made from expanded, rejuvenated costal chondrocytes.

In the allogeneic, non-homologous cartilage tissue engineering approach used in this study (Figure 6-1A), costal chondrocytes from the rib were intended for tissue-engineering of knee articular cartilage. In this study, there were specific analytes where the neocartilage is more reminiscent of donor costal cartilage than recipient knee cartilage. For example, collagen type I in neocartilage comprised 7.55-7.70%/PROT between days 28 and 56 of culture, which was similar to the collagen type I quantity in native porcine floating costal cartilage (6.69%/PROT) and is higher than in the femoral condyle (1.22%/PROT) [346]. Collagen type V was found to be in the range of 1.63-1.76%/PROT in neocartilage between 28 and 56 days of culture, which was between the quantities reported for floating costal cartilage (3.13%/PROT) and femoral condyle articular cartilage (0.29%/PROT) [346]. While these collagen subtype quantities showed aspects of donor tissue phenotype, importantly, collagen type X, associated with hypertrophic and calcified cartilage [411, 412], remained at or below 0.05%/PROT in all

neocartilage time points. The quantity of collagen type X in native floating costal cartilage was 0.98%/PROT, and, in native femoral condyle cartilage, it was less than 0.01%/PROT [346]. If there were an abundant presence of collagen type X, self-assembled neocartilage implants could potentially calcify, rendering them unsuitable for use in the knee. However, the self-assembling process was shown to change the costal chondrocyte phenotype toward that of articular chondrocytes and away from calcification as found in native costal cartilage. This is significant because costal cartilage offers important advantages as a cell source, such as isolation from non-diseased tissues and use in either autologous or allogeneic approaches [338]. While future tissue engineering studies will need to address these differences of donor and recipient tissues, the self-assembling process using costal chondrocytes produced a neocartilage that is suitable for non-homologous use in the knee.

Bottom-up proteomics was used to quantify all proteins in developing neocartilages, giving insight to structure-function relationships and protein targets for future tissue-engineering studies. Well-documented structure-function relationships in articular cartilage predict a direct relationship between tensile properties and COL content [33], but the UTS in neocartilages plateaued after 14 days of culture while COL continues to increase throughout the entire culture time. Bottom-up proteomics may hint as to why this contradiction arises; the overall collagen subtype profile became less abundant in collagen type II relative to the other collagens after day 14, where collagen type II plateaued and collagen types I, VI, IX, and XII continued to increase. Given the role of collagen types IX and XII in fibrillogenesis [237], it is possible that these other collagen types inhibited maturation of the collagen type II fibrils, and, thus, why tensile properties did not continue to increase after day 14. Collagen type IX was abundant in fetal knee cartilage (7.43%/PROT) but dropped in mature cartilage (0.80%/PROT) [407]. In neocartilage, collagen type IX started at 1.05%/PROT at day 7 of culture and increased to 2.61%/PROT at day 84; the drop seen in native tissue was not observed. Unlike in native knee cartilage development, collagen type IX in neocartilage was not replaced by more collagen type

II. Interestingly, there was no detectable collagen type XIV in neocartilages, but there was a small amount present in native articular cartilages (0.95%/PROT in fetal cartilage, <0.01%/PROT in mature cartilage) [407]. Contrastingly, collagen type XII was abundant in neocartilage constructs (3.59-4.80%/PROT) compared to native cartilages (0.15-0.35%/PROT), approximately a 10-times difference. Because both collagen type XII and XIV play similar roles in fibrillogenesis [237], the neocartilage may have been producing excessive collagen type XII as compensation for the lack of collagen type XIV. It would be of great interest to cartilage tissue engineers to determine novel mechanical or biochemical stimuli leading to the deposition of collagen type XIV. The field of tissue engineering will continue to benefit from bottom-up proteomic studies through deeper understanding of structure-function relationships and development of novel tissue-engineering strategies to target specific protein analytes, improving the functionality of engineered neotissues.

It is crucial to create neocartilages that can withstand the joint loading environment; thus, it is important to select an appropriate time of culture which maximizes neocartilage mechanical properties. For knee articular cartilage, the main form of loading is compression [33], and, thus, it is desired to implant neocartilage when it has maximal compressive properties. Here, we showed that both instantaneous and relaxation moduli reached their maximum around 28 days of culture and decreased at later time points, making 28 days the optimal time point for knee articular cartilage implantation. While articular cartilage functions under tensile stresses as well, the tensile magnitudes are not as large as those seen in fibrocartilages [15]. Tensile stiffness and strength increased beyond 28 days of culture, with 56 and 84 days of culture exhibiting the greatest tensile stiffness and strength. Thus, these later time points may also be considered for fibrocartilage therapeutics. In addition to tensile properties, collagen type I also increased significantly at 28-84 days of culture compared to earlier time points, further mimicking the biochemical makeup of fibrocartilages like the knee meniscus and temporomandibular joint disc. This study identified optimal culture times for neocartilage (i.e., 28 days for knee articular

cartilage and 56-84 days for fibrocartilages) which will be important as this technology is translated toward preclinical and clinical studies.

Tissue-engineered cartilage products are proceeding through the regulatory pipeline, with matrix-assisted autologous chondrocyte implantation already approved for use in the U.S. and many more in development [247]. Recent tissue engineering approaches, such as the developmentally inspired self-assembling process, have resulted in robust neocartilages that have functional properties similar to native cartilage. Through this study, we observed that neocartilage made from passaged, rejuvenated costal chondrocytes had many similarities in ECM development to native knee cartilage, as shown through mechanical, biochemical, and proteomic analyses. Optimal time points were identified to maximize compressive and tensile properties for eventual implantation into suitable large animal models for hyaline cartilage and fibrocartilage ailments. Through bottom-up proteomics it was shown that there were some similarities to donor costal cartilage, such as the presence of collagen type I, and some differences in ECM composition of native knee cartilage and tissue-engineered cartilage, such as the temporal trends of collagen types IX, XI, and XII. Importantly, collagen type X in the neocartilage was approximately 20-times lower than in native floating rib cartilage, supporting the non-homologous approach of using costal chondrocytes to produce neocartilages for the knee. Toward translation of engineered cartilages and other tissues, bottom-up proteomics should be considered for the study of structure-function relationships, development of quality control protocols, and creation of a multitude of release criteria. Because the ultimate goal of tissue engineering is to reach native tissue mimicry, bottom-up proteomics is a demonstrably powerful tool for investigating differences in, for example, native and engineered tissues. A deeper understanding of ECM composition will enable new tissue engineering strategies to recapitulate the unique biochemical and mechanical properties of native tissue, improving clinical outcomes for patients as tissue-engineered products undergo preclinical studies, clinical trials, and eventual widespread usage in humans.

Supplementary Materials

Supplementary Table 6-1: Additional mechanical outcomes of neocartilage constructs.
Additional outcomes for compressive stress-relaxation and uniaxial tension tests are reported as mean ± standard deviation. Cells that do not share the same letter are significantly different from each other.

Outcome	Culture time (days)				
	7	14	28	56	84
Compressive stress-relaxation					
10% Coefficient of viscosity (MPa s)	11.6 ± 2.5^{A}	2.1 ± 0.7^{B}	1.4 ± 0.6^{B}	1.1 ± 0.2^{B}	1.4 ± 1.2^{B}
20% Coefficient of viscosity (MPa s)	30.7 ± 7.8^{A}	15.0 ± 4.9^{B}	6.2 ± 2.0^{C}	4.0 ± 1.0^{C}	2.9 ± 1.6^{C}
Uniaxial tension					
Strain at failure (mm/mm)	0.52±0.13	0.59±0.15	0.57±0.11	0.43±0.09	0.46±0.11
Toughness (MPa m^{-3})	0.13 ± 0.05^{B}	0.38 ± 0.16^{A}	0.34 ± 0.15^{A}	0.30 ± 0.10^{A}	0.27 ± 0.08^{AB}

Supplementary Table 6-2: Bottom-up proteomics analytes of neocartilage constructs.
All analytes are reported as a percentage per total protein (PROT) content. Of 364 identified analytes, those with an intensity greater than 0.1%/PROT in at least one sample and all collagen chains (86 proteins total) are reported.

Gene	Protein	Protein / Total Protein (%)				
		Culture time (days)				
		7	14	28	56	84
HMDH	3-hydroxy-3-methylglutaryl-coenzyme A reductase	0.03%	0.05%	0.03%	0.13%	0.04%
RS16	40S ribosomal protein S16	0.10%	0.07%	0.05%	0.04%	0.05%
RS20	40S ribosomal protein S20	0.08%	0.07%	0.03%	0.04%	0.02%
RS3	40S ribosomal protein S3	0.13%	0.10%	0.08%	0.07%	0.09%
RS9	40S ribosomal protein S9 (Fragment)	0.09%	0.04%	0.03%	0.04%	0.04%
RSSA	40S ribosomal protein SA	0.12%	0.10%	0.08%	0.06%	0.06%
RLA0	60S acidic ribosomal protein P0	0.06%	0.02%	0.03%	0.02%	0.03%
RL11	60S ribosomal protein L11	0.05%	0.10%	0.06%	0.05%	0.05%
RL14	60S ribosomal protein L14	0.07%	0.03%	0.05%	0.03%	0.04%
RL18	60S ribosomal protein L18	0.09%	0.07%	0.06%	0.04%	0.04%
RL6	60S ribosomal protein L6	0.15%	0.10%	0.05%	0.04%	0.02%
ACTS	Actin, alpha skeletal muscle	0.20%	0.10%	0.03%	0.05%	0.03%
ACTB	Actin, cytoplasmic 1	3.17%	1.96%	1.96%	1.53%	1.50%
PGCA	Aggrecan core protein	0.47%	0.30%	0.24%	0.28%	0.21%
ALBU	Albumin	0.35%	0.36%	0.09%	0.23%	0.27%
CRYAB	Alpha-crystallin B chain	0.03%	0.04%	0.09%	0.12%	0.07%
ANXA2	Annexin A2	1.14%	0.44%	0.37%	0.41%	0.38%
ARGI1	Arginase-1	0.09%	0.09%	0.07%	0.06%	0.07%
ATPA	ATP synthase subunit alpha, mitochondrial	0.27%	0.18%	0.23%	0.19%	0.22%

ENOB	Beta-enolase	0.95%	0.78%	0.43%	0.14%	0.13%
PGS1	Biglycan	0.75%	0.69%	0.34%	0.95%	0.37%
CALR	Calreticulin	0.18%	0.09%	0.05%	0.06%	0.02%
COF1	Cofilin-1	0.17%	0.13%	0.07%	0.06%	0.04%
COL1A1	Collagen type I alpha 1	2.45%	3.24%	4.63%	4.77%	5.58%
COL1A2	Collagen type I alpha 2	1.31%	2.06%	3.07%	2.78%	3.23%
COL2A1	Collagen type II alpha 1	38.40%	53.49%	56.36%	57.20%	57.58%
COL3A1	Collagen type III alpha 1	0.44%	0.24%	0.40%	0.32%	0.36%
COL4A2	Collagen type IV alpha 2	<0.01%	0.04%	0.02%	0.05%	0.06%
COL4A4	Collagen type IV alpha 4	0.01%	0.03%	0.00%	0.00%	0.04%
COL4A5	Collagen type IV alpha 5	0.00%	0.03%	0.01%	0.01%	0.00%
COL5A1	Collagen type V alpha 1	0.33%	0.45%	0.38%	0.49%	0.42%
COL5A2	Collagen type V alpha 2	0.67%	1.12%	1.24%	1.26%	1.36%
COL5A3	Collagen type V alpha 3	0.01%	0.01%	0.01%	0.01%	0.00%
COL6A1	Collagen type VI alpha 1	0.12%	0.13%	0.15%	0.34%	0.25%
COL6A2	Collagen type VI alpha 2	0.51%	0.38%	0.72%	1.06%	1.03%
COL6A3	Collagen type VI alpha 3	1.46%	1.82%	3.26%	4.16%	4.44%
COL9A1	Collagen type IX alpha 1	0.63%	1.36%	1.75%	1.57%	1.82%
COL9A2	Collagen type IX alpha 2	0.42%	0.69%	0.77%	0.82%	0.79%
COL10A1	Collagen type X alpha 1	<0.01%	0.05%	0.02%	0.02%	0.03%
COL11A1	Collagen type XI alpha 1	2.11%	2.77%	2.33%	2.75%	2.46%
COL11A2	Collagen type XI alpha 2	2.05%	3.08%	2.88%	2.92%	3.06%
COL12A1	Collagen type XII alpha 1	3.59%	3.92%	4.80%	4.40%	4.62%
COL28A1	Collagen type XXVIII alpha 1	0.00%	0.03%	0.52%	0.05%	0.55%
PGS2	Decorin	0.00%	0.03%	0.07%	0.08%	0.10%
RPN1	Dolichyl-diphosphooligosaccharide-protein glycosyltransferase subunit 1	0.13%	0.09%	0.07%	0.08%	0.07%
EF1G	Elongation factor 1-gamma (Fragment)	0.17%	0.11%	0.05%	0.04%	0.05%
BIP	Endoplasmic reticulum chaperone BiP (Fragment)	0.18%	0.08%	0.06%	0.09%	0.07%
ENPL	Endoplasmin	0.33%	0.14%	0.09%	0.09%	0.09%
FMOD	Fibromodulin (Fragment)	0.09%	0.04%	0.03%	0.03%	0.01%
GELS	Gelsolin (Fragment)	0.19%	0.09%	0.07%	0.07%	0.08%
G6PI	Glucose-6-phosphate isomerase	0.14%	0.05%	0.01%	<0.01%	<0.01%
G3P	Glyceraldehyde-3-phosphate dehydrogenase	3.94%	1.58%	0.92%	0.49%	0.57%
HS71B	Heat shock 70 kDa protein 1B	0.66%	0.40%	0.42%	0.31%	0.24%
HSP76	Heat shock 70 kDa protein 6	0.12%	0.00%	0.02%	0.00%	<0.01%
HSPB1	Heat shock protein beta-1	0.49%	0.18%	0.18%	0.19%	0.13%
HS90A	Heat shock protein HSP 90-alpha	0.41%	0.19%	0.16%	0.13%	0.15%
H1T	Histone H1t	0.26%	0.20%	0.19%	0.10%	0.10%
H33	Histone H3.3	0.89%	0.48%	0.45%	0.39%	0.32%
H4	Histone H4	3.45%	2.21%	1.10%	1.25%	0.85%
HPLN1	Hyaluronan and proteoglycan link protein 1	1.49%	0.70%	0.55%	1.03%	0.67%
MX2	Interferon-induced GTP-binding protein Mx2	0.00%	0.02%	0.17%	0.02%	0.08%

MFGM	Lactadherin	0.18%	0.17%	0.30%	0.54%	0.46%
GGLO	L-gulonolactone oxidase	0.09%	0.08%	0.05%	0.00%	<0.01%
LDHA	L-lactate dehydrogenase A chain	0.41%	0.19%	0.08%	0.05%	0.04%
GANAB	Neutral alpha-glucosidase AB	0.11%	0.07%	0.04%	0.03%	0.03%
NDKB	Nucleoside diphosphate kinase B	0.15%	0.07%	0.02%	0.02%	0.01%
PPIA	Peptidyl-prolyl cis-trans isomerase A	0.22%	0.11%	0.07%	0.04%	0.03%
PRDX6	Peroxiredoxin-6	0.11%	0.05%	0.06%	0.03%	0.03%
PGK1	Phosphoglycerate kinase 1	0.91%	0.51%	0.32%	0.20%	0.13%
UBC	Polyubiquitin-C	0.18%	0.10%	0.16%	0.08%	0.12%
LMNA	Prelamin-A/C	1.66%	1.09%	0.63%	0.45%	0.37%
PPCE	Prolyl endopeptidase	0.36%	0.00%	0.00%	0.00%	0.00%
S10A6	Protein S100-A6	0.13%	0.18%	0.15%	0.11%	0.06%
RAB1B	Ras-related protein Rab-1B	0.13%	0.05%	0.05%	0.05%	0.06%
RYR1	Ryanodine receptor 1	0.00%	0.26%	0.00%	0.17%	0.16%
STAT1	Signal transducer and activator of transcription 1	0.23%	0.10%	0.44%	0.22%	0.09%
SPRC	SPARC	0.09%	0.02%	<0.01%	<0.01%	0.00%
TENA	Tenascin	0.02%	0.04%	0.18%	0.11%	0.10%
THIO	Thioredoxin	0.14%	0.01%	0.03%	<0.01%	0.00%
TPIS	Triosephosphate isomerase	0.86%	0.42%	0.14%	0.02%	0.02%
TPM4	Tropomyosin alpha-4 chain	0.11%	0.07%	0.01%	<0.01%	0.00%
TBA1B	Tubulin alpha-1B chain	0.55%	0.19%	0.33%	0.24%	0.27%
TBB5	Tubulin beta chain	0.37%	0.27%	0.24%	0.21%	0.20%
UGPA	UTP--glucose-1-phosphate uridylyltransferase	0.21%	0.04%	0.03%	0.03%	0.04%
VIME	Vimentin	12.25%	6.01%	2.14%	1.26%	0.87%
VDAC1	Voltage-dependent anion-selective channel protein 1	0.13%	0.06%	0.07%	0.06%	0.07%

Chapter 7: Proteomic, Mechanical, and Biochemical Characterization of Cartilage Development[7]

Abstract

The objective of this work is to examine the development of porcine cartilage by analyzing its mechanical properties, biochemical content, and proteomics at different developmental stages. Cartilage from the knees of fetal, neonatal, juvenile, and mature pigs was analyzed using histology, mechanical testing, biochemical assays, fluorophore-assisted carbohydrate electrophoresis, and bottom-up proteomics. Mature cartilage has 2.2-times the collagen per dry weight of fetal cartilage, and fetal cartilage has 2.1-times and 17.9-times the glycosaminoglycan and DNA per dry weight of mature cartilage, respectively. Tensile and compressive properties peak in the juvenile stage, with a tensile modulus 4.7-times that of neonatal. Proteomics analysis reveals increases in collagen types II and III, while collagen types IX, XI, and XIV, and aggrecan decrease with age. For example, collagen types IX and XI decrease 9.4-times and 5.1-times respectively from fetal to mature. Mechanical and biochemical measurements have their greatest developmental changes between the neonatal and juvenile stages, where mechanotransduction plays a major role. Bottom-up proteomics serves as a powerful tool for tissue characterization, showing results beyond those of routine biochemical analysis. For example, proteomic analysis shows significant drops in collagen types IX, XI, and XIV throughout development, which shows insight into the permanence of cartilage's matrix. Changes in overall glycosaminoglycan content compared to aggrecan and link protein indicate non-enzymatic degradation of aggrecan structures or hyaluronan in mature cartilage. In addition to tissue characterization, bottom-up proteomics techniques are critical in tissue engineering efforts toward repair or regeneration of cartilage in animal models.

[7] **Chapter published as:** Bielajew, B.J.,* Donahue, R.P.,* Lamkin, E.K., Hu, J.C., Hascall, V.C., Athanasiou, K.A. Proteomic, mechanical, and biochemical characterization of cartilage development. *Acta Biomaterialia*. February 2022, online ahead of print. (* These authors contributed equally.)

Introduction

Cartilage does not heal, and current clinical treatments for cartilage degeneration are palliative, not reparative. This motivates cartilage tissue engineering, which aims to design neotissues for cartilage repair or replacement. Many researchers have attempted to engineer neocartilages by recapitulating aspects of cartilage development, including the self-assembling process which is reminiscent of mesenchymal condensation [17, 399]. Toward ensuring that developmentally accurate neocartilage is produced, developing native cartilage must be characterized — especially its mechanical properties as a function of its biochemical and proteomic content. Through these characterizations, design criteria for tissue-engineered cartilages may be established such that the neocartilage implants are capable of bearing loads experienced by adults in daily activities. Additionally, tissue engineering strategies that mimic developmental processes will be informed by a characterization of these structure-function relationships over developmental time points from fetal to mature tissue.

The extracellular matrix (ECM) content and mechanics of cartilage change during development and aging [33]. Knee articular cartilage forms as a result of endochondral ossification during embryonic development. During this process, mesenchymal condensation occurs which results in an interzone region at the future joint. Chondrogenesis of mesenchymal progenitor cells in the perichondrium region of the interzone leads to formation of early cartilage tissues which will later develop into mature cartilage [413]. This process continues into postnatal development where cartilage continues to mature. Collagens and glycosaminoglycans (GAGs), two main ECM components of cartilage, change in quantity and type throughout this process [414, 415]. For example, collagen type II, the principal collagen subtype of hyaline cartilage, is known to increase with tissue maturity [399, 414], but it is not known how other minor collagen subtypes develop. Along with these biochemical changes, mechanical properties of cartilage are altered throughout development [416-418]. For example, human cartilage reaches peak stiffness between 30 and 50 years of age [419]. After cartilage is fully developed, further age-

related ECM changes occur, including proteolytic degradation and other post-translational modifications [420]. Biochemical changes alter mechanical properties of the cartilage; for example, cartilage shear modulus has a strong negative correlation with age and osteoarthritis grade [421]. These age-related changes can result in cartilage degeneration and pathology, affecting approximately nearly 1 in 4 US adults [422]. A promising solution to these age-related degenerative changes is tissue engineering, which is poised to provide a long-term regenerative solution to cartilage ailments toward improving pain and function and enhancing quality of life for patients.

Toward informing design criteria for neocartilage, characterization studies have investigated the biochemical and mechanical properties of cartilage. For example, healthy human articular cartilage has an aggregate modulus of 0.08-2 MPa and tensile modulus of 5-25 MPa, depending on tissue location and depth [33]. These properties arise from the biochemical makeup of cartilage, mainly being composed of collagen type II and GAGs. Cartilage contains 50-75% collagen by dry weight (DW) and 15-30% GAG by DW, including chondroitin sulfate (CS) [33]. However, the subtypes of collagens and GAGs are rarely quantified, especially in developmental studies. This study investigates the proteomic development of cartilage ECM using bottom-up proteomics for the first time, as well as isomers of CS (chondroitin-6-sulfate, CS6, and chondroitin-4-sulfate, CS4), via fluorophore-assisted carbohydrate electrophoresis (FACE), in addition to biochemical and mechanical characterization.

Prior to the development of human tissue-engineered therapeutics, preclinical studies must be done in animal models. There are many accepted animal models for cartilage. For example, the sheep and horse are suggested by the U.S. Food and Drug Administration for preclinical studies that aim to repair or replace knee cartilage due to the biochemical and mechanical similarities to human cartilage [423]. In developmental biology, the porcine model has long been used due to its similarity to human development [424]; this is best illustrated by its use in anatomy courses from the high school to graduate levels. The porcine model has

recently emerged as a model for knee cartilage studies due to its cartilage biomechanics [425]. Additionally, minipigs have been used for their lower terminal weight, which offers practical and financial advantages for long-term studies, including easier handling and less food intake [24]. Here, the porcine model is investigated due to its well-studied developmental pathway and suitability as a cartilage preclinical animal model.

The objective of this work is to interrogate the development of knee articular cartilage by analyzing the mechanics, biochemical content, and proteomics of knee articular cartilage from different aged pigs. The hypothesis of this work is that age-dependent changes in the mechanical, biochemical, and proteomic properties will be observed. Specifically, as a function of developmental age, increases in the tensile and compressive mechanical properties, increases in collagen, and decreases in GAG and DNA will be observed. Increases and decreases in proteomic biomarkers will also be observed; however, the specific targets are not known *a priori*. Toward this objective, a wide breadth of characterization analyses were performed on the cartilage of pigs ranging from fetal to 2+ years, including compressive and tensile mechanical testing; photometric collagen, GAG, and DNA assays; mass spectrometry for collagen crosslinks; FACE for CS isomers; and bottom-up proteomic approaches for cartilage proteins.

Methods

Sample collection

Fresh-frozen whole fetal and neonatal pigs (*Sus scrofa domesticus*, Yorkshire cross, female and male) were purchased from Nebraska Scientific. According to the provided growth chart, the pigs were determined to be of 80d, 90d, or 100d gestational age, or stillborn (neonatal). Knees from juvenile (5-6 month old) and mature (2-3 year old) pigs (*Sus scrofa domesticus*, Yorkshire cross, female and castrated male), culled for purposes unrelated to this research, were purchased from Corona Cattle, Inc. For fetal and neonatal pigs, unilateral (only the right) knee

joints were used, and for juvenile and mature pigs, bilateral knee joints were used. Prior to sample collection, juvenile and mature knees were fresh-frozen *en bloc* and subsequently thawed to ensure consistency with fetal and neonatal groups. Knee joint capsules were then opened, and macroscopic joint health of patellofemoral joints was checked to ensure that they were absent of osteoarthritic changes such as osteophytes and cartilage fibrillation or defects. A total of 44 knees were used, as follows: 7 knees from fetal 80d, 7 knees from fetal 90d, 7 knees from fetal 100d, 7 knees from neonatal, 8 knees from juvenile, and 8 knees from mature pigs. Osteochondral samples were taken from three locations on the condyles with disposable 3 mm diameter biopsy punches as depicted in Figure 7-1, and subchondral bone was then trimmed off at the tidemark with a scalpel blade. The center of the condyle was defined as the intersection of midpoints of the height and width of each condyle. Punch 1 from the center of the lateral condyle was cut into a dog-bone shape (approximately 0.5 mm width by 1.0 mm thickness) for tensile testing, and the removed portions were used for crosslinks and bottom-up proteomics analyses. Punch 2 from the center of the medial condyle was used for compression testing and histology, with a 2 mm diameter sample (full-thickness, approximately 1 mm in height) from the center used for stress-relaxation test, and the remaining portion used for histology. Punch 3 was taken adjacent to punch 1 as shown in Figure 7-1, and this full-thickness sample was used for the biochemical analysis, including the collagen, GAG, DNA, and FACE assays. Mechanical testing samples were stored in phosphate-buffered saline after collection and tested within 24 hours.

Histology

Hematoxylin and eosin (H&E), picrosirius red (PR), and safranin O (SO) histological stains were performed. A full-thickness slice of cartilage was fixed in 10% neutral buffered formalin, processed, embedded in paraffin, sectioned to 5 μm thickness, mounted on microscopy slides, and stained with H&E, PR, or SO, as previously described [339]. For all stains, all samples were

stained simultaneously to ensure consistency. Representative images were taken at 20x magnification on a brightfield microscope. All histology slides were reviewed by a histopathologist to ensure quality of staining.

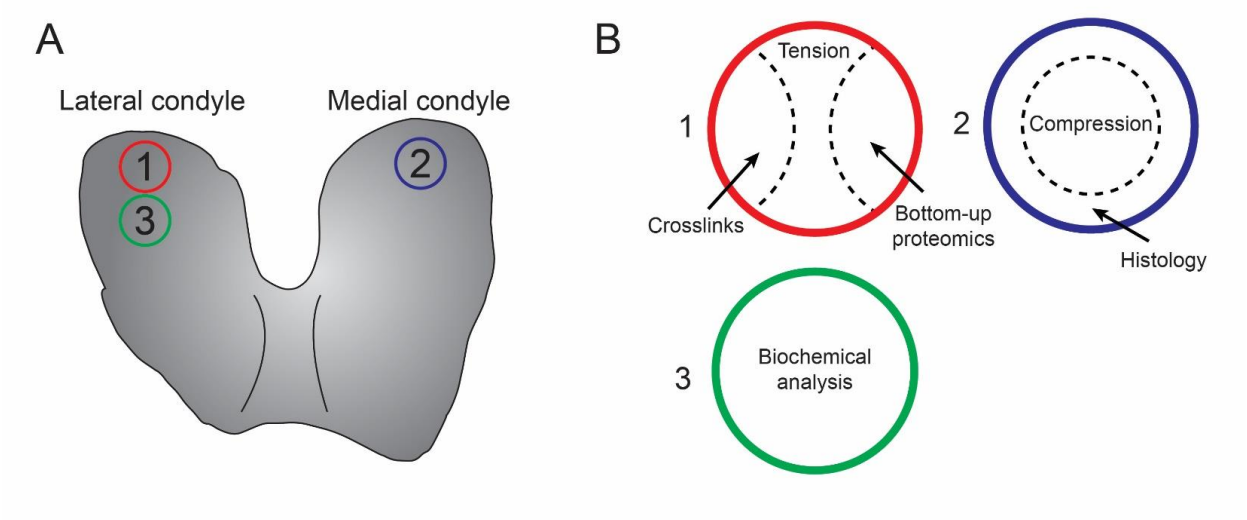

Figure 7-1: Sample collection diagram.
This illustration shows the (A) lateral and medial condyles with punch locations (not to scale) and (B) sample locations within each punch.

Mechanical testing

Tensile and compressive mechanical testing was performed, as previously described [24]. Briefly, dog-bone shaped specimens were glued to paper tabs for uniaxial tensile tests. Tabs were gripped in a uniaxial testing machine with a gauge length of 1.55 mm, and samples were subjected to a pull-to-failure test at 1% strain per second. A custom MATLAB code was used to determine the tensile Young's modulus and ultimate tensile strength (UTS) from the engineering stress-strain curves which were generated from force-displacement curves. For compressive stress-relaxation tests, 2 mm diameter tissue punches were subjected to 15 preloading cycles of 5% strain followed by application of 10% and 20% strain held for 600 and 900 seconds, respectively, until relaxation equilibrium. The loading rate was 10% strain per second. The force-displacement curves were fit to a standard linear solid model using a custom MATLAB code to obtain instantaneous modulus and relaxation modulus at both strain levels.

Photometric biochemical assays for total collagen, GAG, and DNA content

Hydration was measured by comparing the wet weight (WW) to the post-lyophilization DW. Cartilage was digested overnight with papain, and photometric biochemical assays were performed, as previously described [378]. Briefly, overall collagen content (COL) was measured with a modified hydroxyproline assay [93]. GAG content was measured with a dimethylmethylene blue assay kit, and DNA was measured with a PicoGreen assay kit. The resulting COL, GAG, and DNA values were normalized to both WW and DW.

Fluorophore assisted carbohydrate electrophoresis (FACE)

Aliquots of the papain digests (50 µL) were lyophilized and subjected to a series of ethanol precipitations and digestion with chondroitinase ABC. The digested disaccharides were fluorescently derivatized with 2-aminoacridone and separated using FACE, as previously described [408]. CS6 and CS4 contents were quantified using ImageJ software measurements of band integrated optical density with CS6 and CS4 standards, and CS6 content was divided by CS4 content to obtain the CS6/CS4 ratio.

Crosslink quantification and bottom-up proteomics

Collagen crosslink quantification and bottom-up proteomics were performed, as previously described [346]. Briefly, cartilage pieces ~1 mg in WW from the lateral condyle punch were used for both assays. For crosslinks, cartilage pieces were hydrolyzed in HCl, and hydrolysates were subjected to aqueous normal phase chromatography and mass spectrometry with a Waters ACQUITY QDa quadrupole mass spectrometer to quantify pyridinoline (PYR), dihydroxylysinonorleucine (DHLNL), hydroxyproline (OHP), and internal standard pyridoxine. For bottom-up proteomics, cartilage pieces were digested in trypsin then subjected to reverse-phase chromatography and tandem mass spectrometry on a Thermo Fisher Scientific Orbitrap Fusion Lumos mass spectrometer, then label-free quantification was performed with MaxQuant

[357] to quantify all identified proteins, normalized to total protein content. Total protein content was determined by dividing the COL/DW from the hydroxyproline assay by the sum of all collagen proteins per total protein, yielding total protein per DW.

Statistical analysis

Experimental data were analyzed with a one-way analysis of variance (ANOVA) with the factor being tissue age followed by a *post hoc* Tukey's honestly significant difference test. A sample size of 7-8 per group (i.e., one from each knee) was used for mechanical testing, biochemical analysis, and crosslink quantification. For bottom-up proteomics, three randomly selected samples per group were used. Normality was verified by a Shapiro-Wilk test. Statistical analyses were performed in JMP Pro 14, and graphs were generated in GraphPad Prism 9. In all bar graphs, bars represent the mean ± standard deviation, and statistical significance is represented with a connecting letters report; bars that do not share a letter are significantly different from each other. Reported p-values presented in the text refer to multiple pairwise comparisons, all of which are described by the stated p-value inequality. For example, $p<0.0001$ means that all pairwise comparisons yielded p-values below 0.0001.

Results

Histology

Representative histological images from each cartilage age are shown in Figure 7-2. H&E staining shows the relative hypercellularity of fetal and neonatal cartilage compared to juvenile and mature, which is consistent with DNA content. Throughout cartilage development, the number of cells decreased and spacing among cells increased. PR staining showed a more intense red staining on the juvenile and mature cartilage than the other groups, which is consistent with the quantitative hydroxyproline assay. All cartilages stained intensely for GAGs with SO.

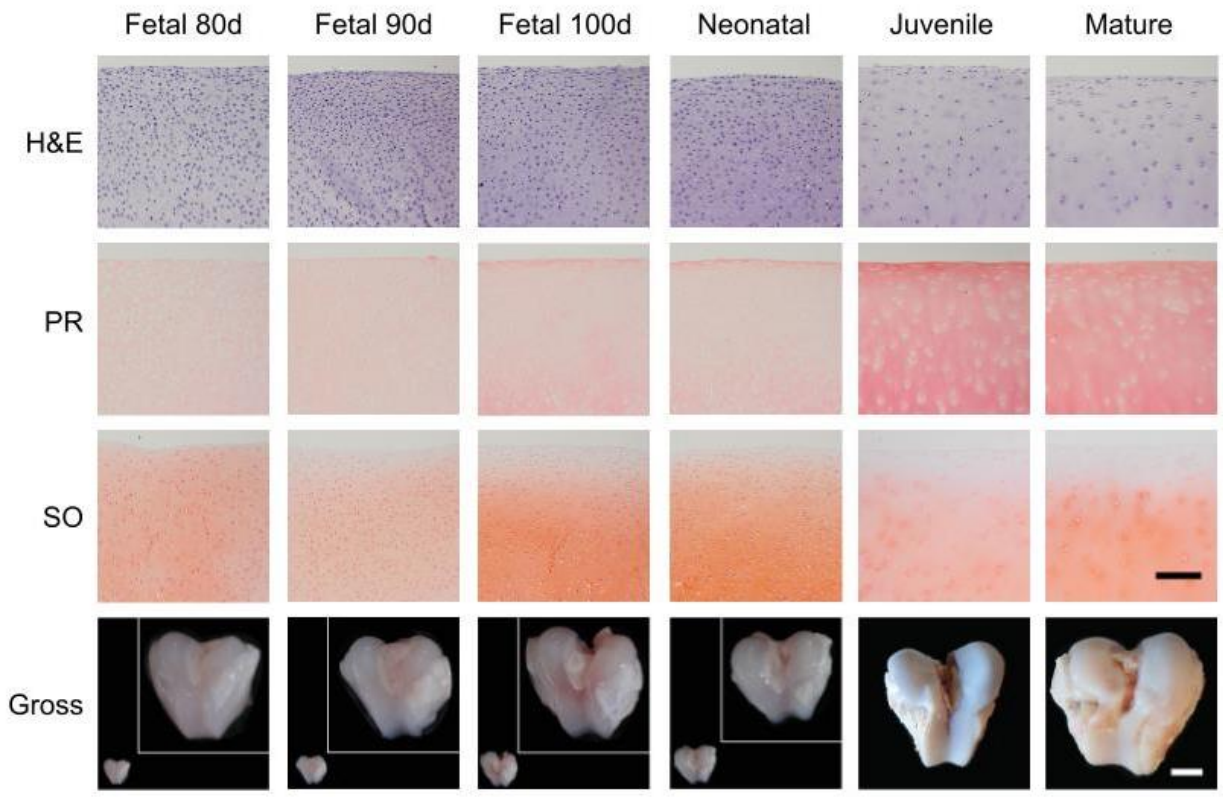

Figure 7-2: Representative histology and gross morphology images for porcine articular cartilage of different developmental ages.
Fetal and neonatal gross morphology images are shown in actual size (bottom left) and zoomed in (inset). Juvenile and mature are shown in actual size. Scale bars: histology, 100 μm, gross morphology, 2 cm. H&E, hematoxylin and eosin. PR, picrosirius red. SO, safranin O.

Mechanical testing

The mechanical testing results are depicted in Figure 7-3. For compressive properties, the juvenile cartilage had the highest instantaneous and relaxation moduli ($p<0.01$). For the 10% instantaneous modulus, the juvenile cartilage was 1.5-times that of neonatal cartilage and 3.0-times that of mature cartilage. The other compressive measurements had similar results, with the juvenile cartilage having between 1.4- and 6.9-times the moduli of all other groups. In tensile testing, the juvenile cartilage had the highest tensile Young's modulus of 37.2±20.1 MPa, significantly higher than any of the other groups ($p<0.0001$). This stiffness was 10.5-times that of the fetal 80d cartilage, 4.7-times that of neonatal cartilage, and 3.1-times that of mature cartilage. The juvenile cartilage also had the highest UTS at 15.6±7.1 MPa ($p<0.0001$), over

double that of any other cartilage. The fetal tissues had the lowest UTS, which had means ranging from 0.6-1.0 MPa.

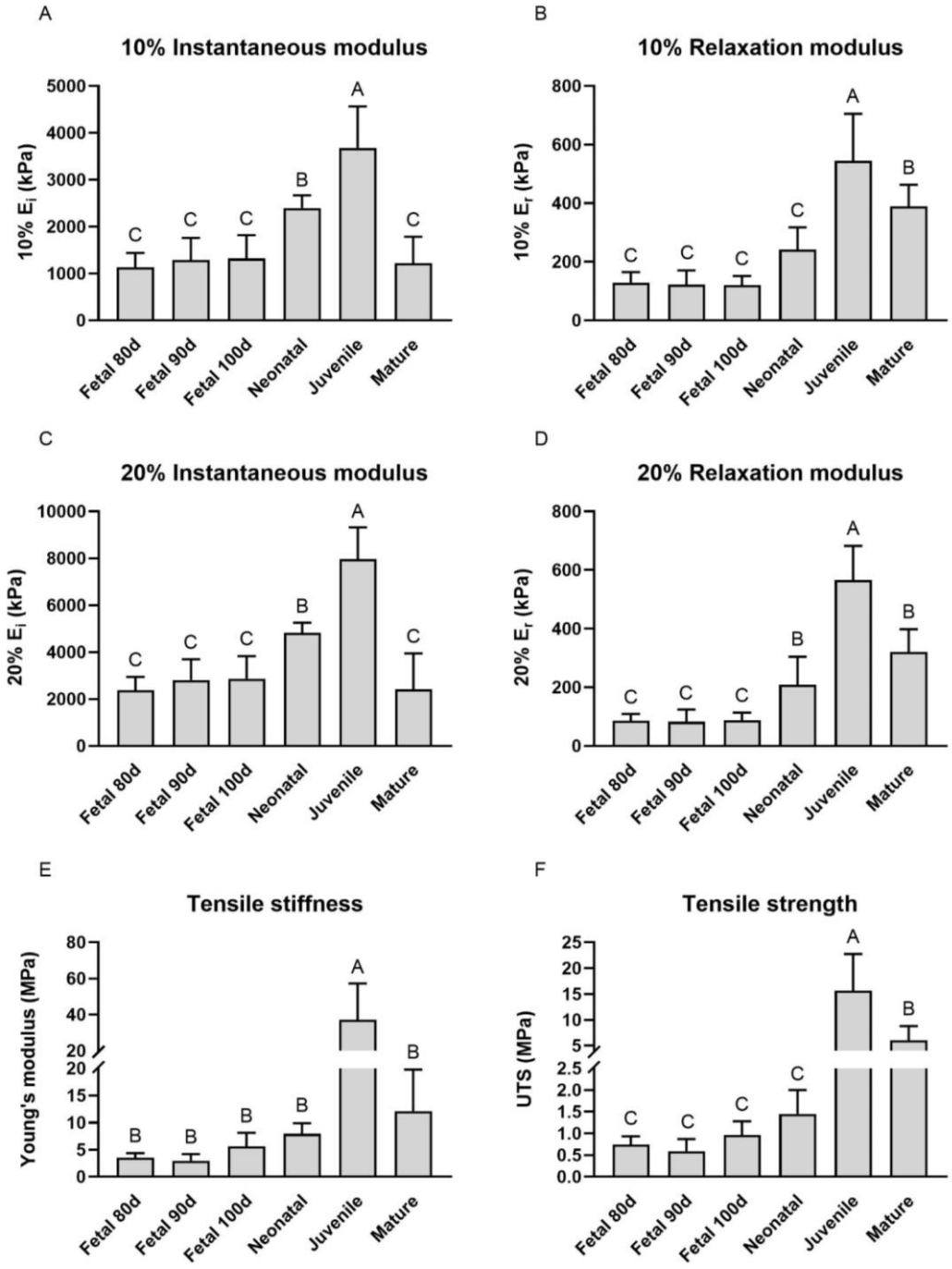

Figure 7-3: Mechanical results for porcine articular cartilage of different developmental ages.
These graphs show the (A) 10% instantaneous modulus, (B) 10% relaxation modulus, (C) 20% instantaneous modulus, (D) 20% relaxation modulus, (E) tensile stiffness, and (F) tensile strength. Ei, instantaneous modulus. Er, relaxation modulus. UTS, ultimate tensile strength. Bars that do not share a letter are significantly different from each other.

Biochemical content

The biochemical analysis results are shown in Figure 7-4. COL/DW and COL/WW were significantly greater in the juvenile and mature tissues than in fetal or neonatal tissues ($p<0.0001$). Juvenile and mature cartilages contained about 2.2-times the COL/DW of fetal and neonatal cartilages. While there were no significant differences in GAG/WW among the different age groups, GAG/DW was significantly lower in the juvenile and mature tissues than in the fetal or neonatal tissues ($p<0.01$), dropping about 1.6-times from neonatal to juvenile. DNA/WW and DNA/DW were significantly lower in juvenile and mature tissues than in fetal or neonatal tissues ($p<0.01$). The fetal 80d cartilage had 12.0-times the DNA/DW of juvenile cartilage, and 17.9-times the DNA/DW of the mature cartilage. The hydration of the juvenile and mature tissues was significantly less than that of the younger tissues ($p<0.01$), dropping from a maximum of 87.0±0.7% in the fetal 90d cartilage to a minimum of 75.2±3.8% in the mature cartilage. The CS6/CS4 ratio was significantly higher in the mature cartilage than the other ages ($p<0.001$), at 1.85±1.29, while the other tissues ranged from 0.10±0.03 (fetal 90d) to 0.37±0.10 (juvenile).

Crosslinks analysis

The crosslink quantification results are shown in Figure 7-5. There were no significant differences among any tissue ages for PYR/DW or DHLNL/DW. The fetal 80d group had significantly more PYR/OHP than other groups ($p<0.01$) at 12.0±2.1 mmol/mol, but there were no other significant differences among groups, and there were no differences in DHLNL/OHP. The fetal 80d cartilage contained 1.9-times the PYR/OHP of juvenile cartilage, and 1.6-times that of mature cartilage. The maturity ratio, which compares the molar amounts of PYR and DHLNL, did not have any significant differences among tissue ages. The highest mean PYR/DHLNL was in the fetal 80d cartilage (1.4±0.4 mol/mol), while the lowest mean PYR/DHLNL was in the mature cartilage (1.0±0.2 mol/mol), but this difference was not significant.

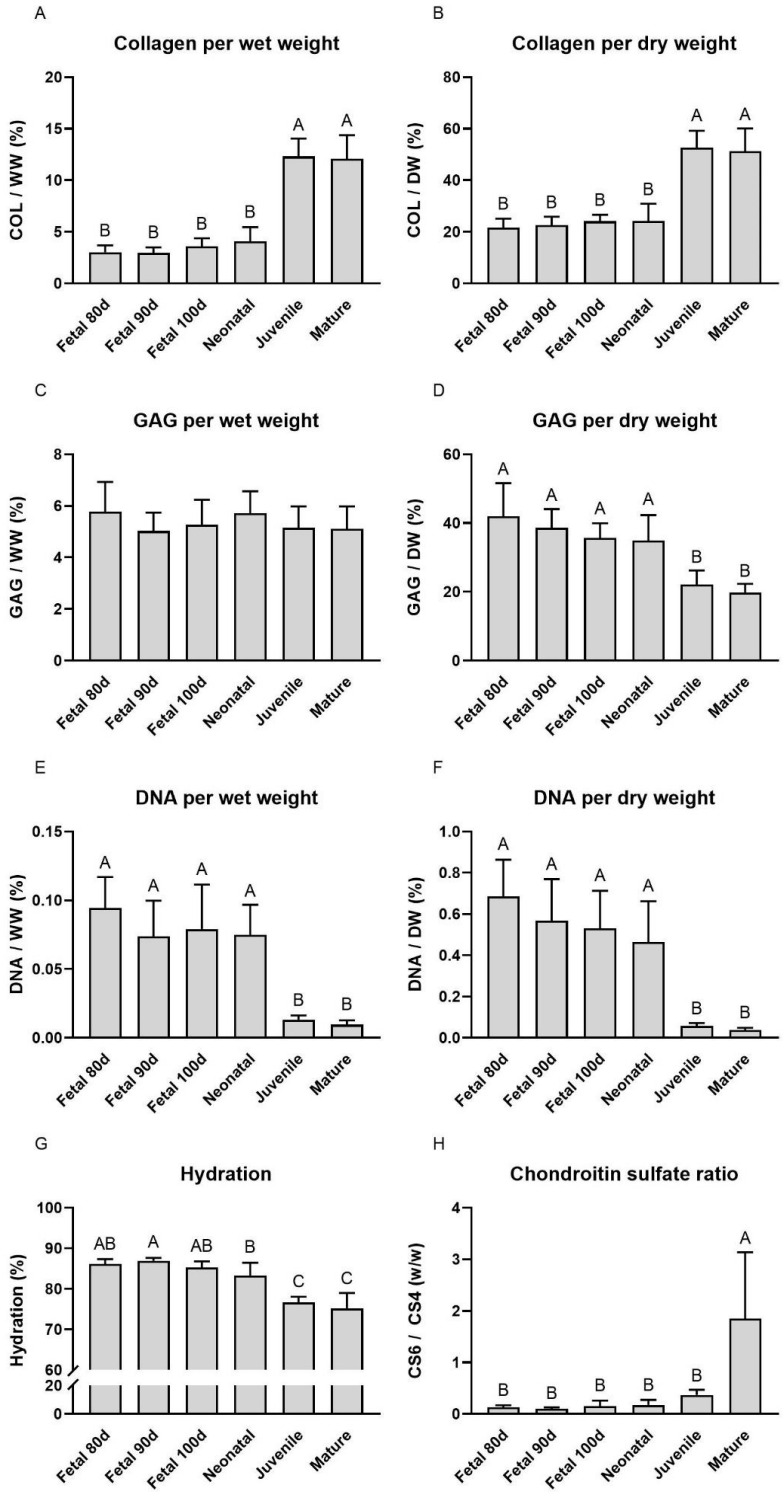

Figure 7-4: Biochemical results for porcine articular cartilage of different developmental ages.
(A, B) Collagen per wet weight and dry weight, respectively. (C, D) Glycosaminoglycan per wet weight and dry weight, respectively. (E, F) Double-stranded DNA per wet weight and dry weight, respectively. (G) Hydration of tissue. (H) Ratio of chondroitin 6-sulfate to chondroitin 4-sulfate. COL, collagen. WW, wet weight. DW, dry weight. GAG, glycosaminoglycan. CS6, chondroitin-6-sulfate. CS4, chondroitin-4-sulfate. Bars that do not share a letter are significantly different from each other.

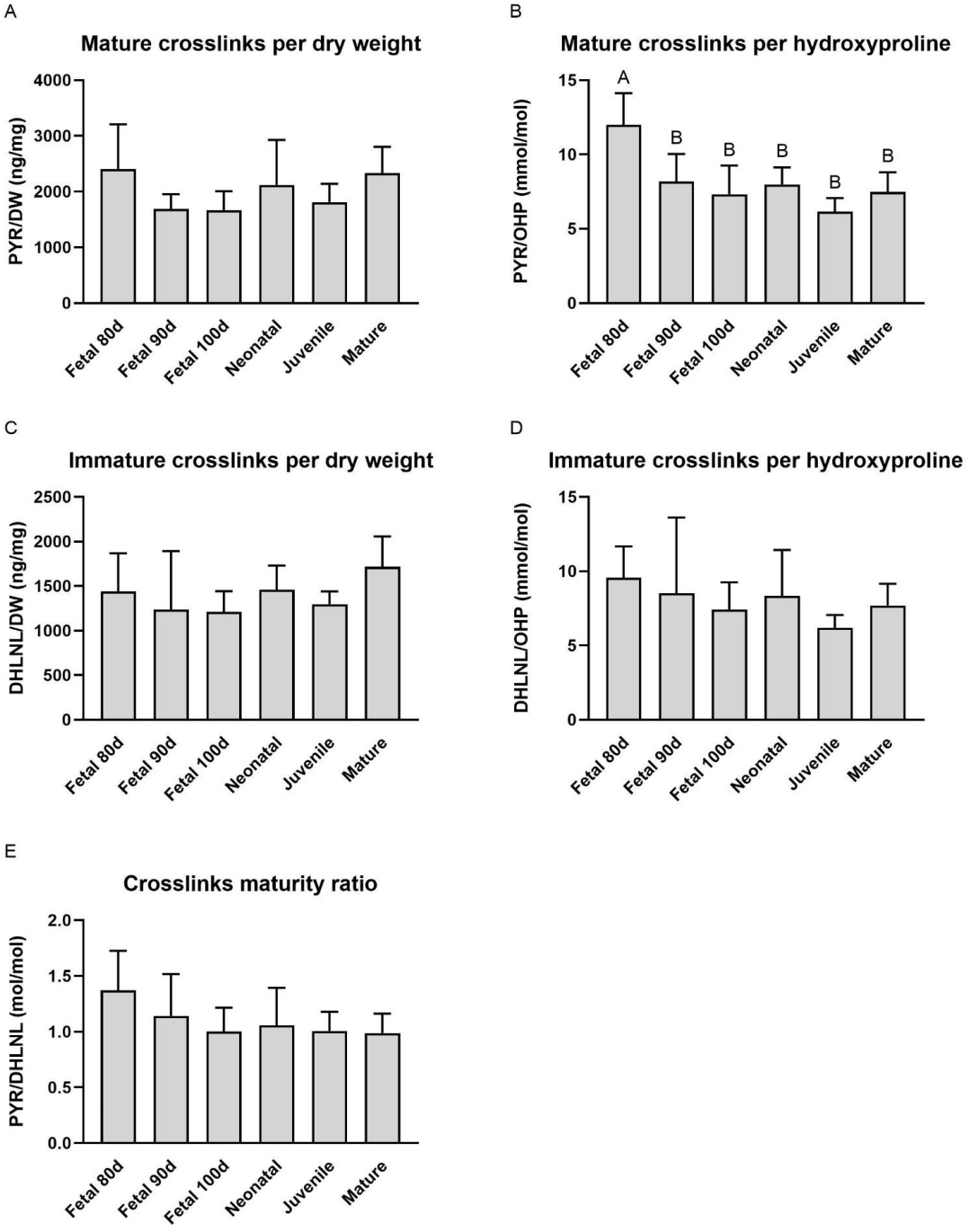

Figure 7-5: Crosslink quantification results for porcine articular cartilage of different developmental ages.

(A, B) Mature pyridinoline crosslinks normalized to dry weight and hydroxyproline, respectively. (C, D) Immature dihydroxylysinonorleucine crosslinks normalized to dry weight and hydroxyproline, respectively. (E) Crosslinks maturity ratio, calculated as the molar ratio of pyridinoline to dihydroxylysinonorleucine. PYR, pyridinoline. DW, dry weight. OHP, hydroxyproline. DHLNL, dihydroxylysinonorleucine. Bars that do not share a letter are significantly different from each other.

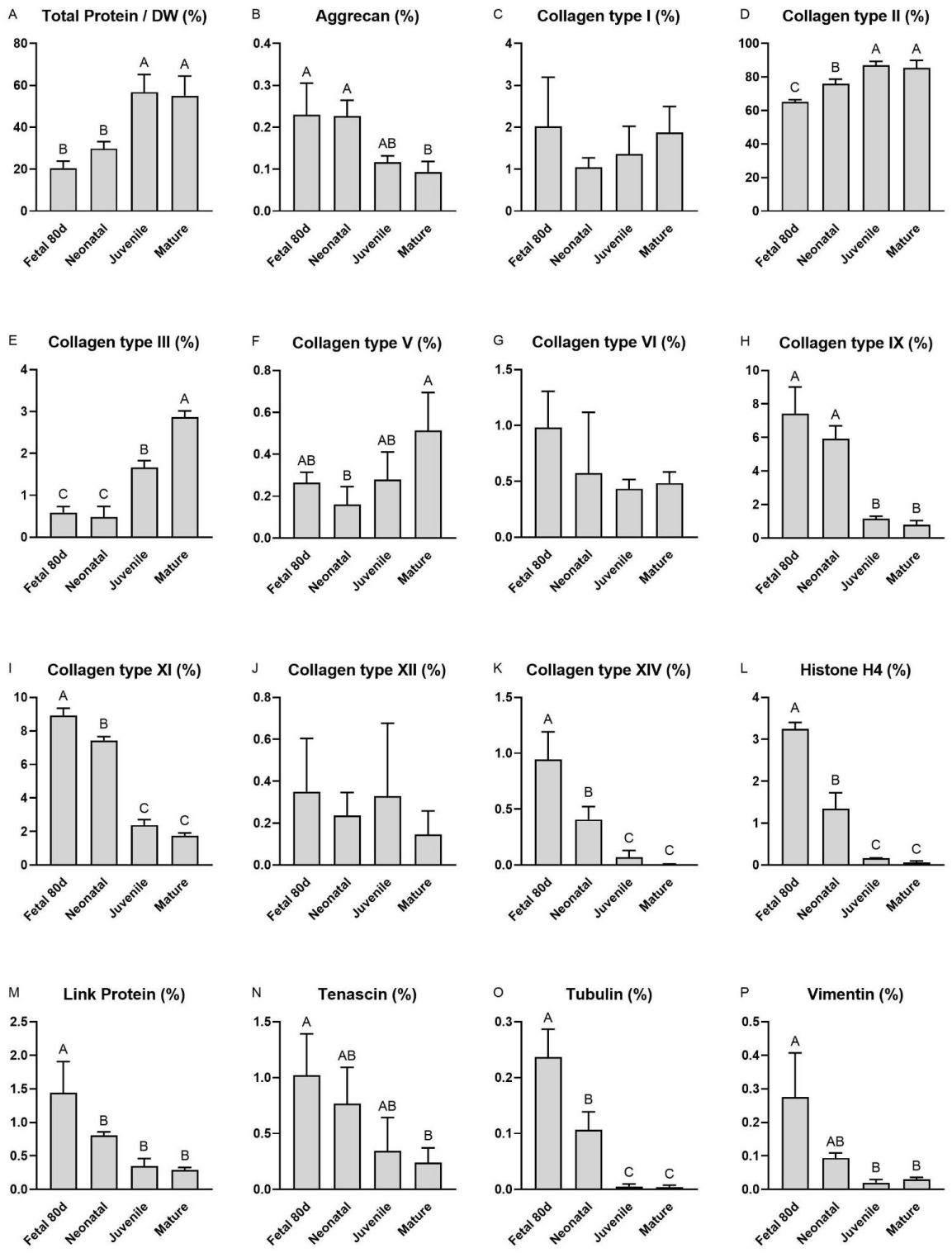

Figure 7-6: Bottom-up proteomic results for porcine articular cartilage of different developmental ages.

Orbitrap results showing (A) total protein content and (B-P) 15 different proteins of interest in different ages of porcine cartilage. All proteins are normalized to total protein content and calculated as a percentage. A table containing averaged data from the four ages can be found in Supplementary Table 7-1. DW, dry weight. Bars that do not share a letter are significantly different from each other.

Bottom-up proteomics

Over 400 individual proteins were quantified through the bottom-up proteomics approach, which were narrowed down to 42 proteins, including 13 collagen types, that had an intensity of >0.1% per protein in at least one sample. Of the 42 proteins, 15 selected analytes of interest are shown in Figure 7-6 (the larger list of 42 proteins is presented in Supplementary Table 7-1). Significant differences were found in several proteomic targets. Collagen types II and III increased with age; aggrecan, collagen types IX, XI, XIV, histone H4, link protein, tenascin, tubulin, and vimentin decreased with age; and collagen types I, VI, and XII did not significantly change with age.

Discussion

In this study, the objective was to elucidate the mechanical, biochemical, and proteomic changes in cartilage throughout development by analyzing knee cartilage from fetal, neonatal, juvenile, and mature pigs. The hypotheses that there will be age-dependent increases in collagen and mechanical properties, as well as age-dependent decreases in GAG and DNA were confirmed. The proteomics analysis revealed that as cartilage ages, its collagen profile shows increases in types II and III and decreases in types IX, XI, and XIV. Aggrecan core protein and link protein, both associated with the GAG bottlebrush structure [426], decrease with age. Some intracellular proteins, such as histones, decrease with age, which is expected given the measured decrease in DNA with age. Some collagen types, such as types I, VI, and XII did not change throughout development. As described below, the proteomics analysis yielded insights into cartilage development because of the quantification of individual collagen subtypes, GAG structural components, and cellular proteins, beyond what can be accomplished in traditional assays for collagen, GAG, and DNA.

Throughout cartilage development, mechanical properties increased from fetal to juvenile, then decreased between juvenile and mature time points. The greatest changes occurred between neonatal and juvenile cartilage in most mechanical and biochemical

measurements. Specifically, when comparing neonatal to juvenile tissues, the tensile Young's modulus increased 4.7-times, the 20% relaxation modulus increased 2.7-times, the COL/DW increased 2.2-times, and the DNA/DW decreased 8.2-times. With this developmental stage occurring in the few months following birth, it is likely that mechanotransduction and hormones are major drivers of cartilage developmental changes. Once neonates begin to walk, cartilage loading and strain increase, which can lead to ECM synthesis through osmo-mechanosensitive ion channels [427]. Growth hormone, which stimulates growth of articular chondrocytes and contributes to cartilage growth and maturity [428], circulates at high levels in neonatal pigs [429]. Maximum mechanical properties occurred at the juvenile stage; from juvenile to mature cartilage, tensile Young's modulus decreased by 3.1-times, and 20% relaxation modulus decreased 1.8-times. However, these changes were not reflected in biochemical properties; collagen, GAG, and DNA had no significant differences between juvenile and mature cartilages. One potential explanation for the decreases in mechanical properties is that farm pigs have been characterized as a model of spontaneously occurring osteoarthritis, where 80-week old pigs exhibit more lameness and higher chondropathy scores than juvenile pigs, and these degenerative changes worsen as the pigs age to 3-4 years [430]. The mature pigs used in the present study were 2-3 years old, and even though the joints were undamaged to the naked eye, the mechanical properties may be signs of a pre-osteoarthritic state. Rapid weight gain, which is caused by selective breeding and intensive feeding [431], may have led to excessive force and wear on the articular cartilage of the mature pigs, leading to degenerative states that were not detectable via gross observation. Future studies should closely consider not only the biomechanics of weight bearing regions of porcine stifle joint cartilage due to differences compared to humans [73, 432] but also the phenotype of chondrocytes within the matrix through RNA sequencing to gain further insight into this pre-osteoarthritic state.

The existence of different CS isomeric forms and the prevalence and ratios of these isomers in different tissue ECMs suggests tissue specific functionality [433]. Of particular

interest is the CS6/CS4 ratio in maturing cartilage. Changes in this ratio may be due to ECM remodeling through cartilage development, or may be an indicator of disease and aging. In previous studies, mature porcine cartilage was shown to contain a very small ratio of CS6/CS4, and a decrease in this ratio is correlated with tissue maturation [399, 434]. However, FACE analysis for this study showed lower CS6/CS4 ratios in less developed tissues and a significant increase in mature samples. This inconsistency with previous experiments may be a result of the previously discussed pre-osteoarthritic state of the mature cartilage, because, as osteoarthritic cartilage degrades, GAGs are cleaved from cartilage ECM and released into synovial fluid [435], which may lead to different sulfation ratios with GAG turnover. With the pre-osteoarthritic state of the mature cartilage in this work, it is likely that many of these GAGs are cleaved from the surface of the cartilage, because the surface zone stains less with SO with increasing age Figure 7-2. Further investigation into CS6/CS4 ratios, especially at different cartilage depths, in developmental and disease states is needed to fully understand the spike in the CS6/CS4 ratio for the mature cartilage in this study.

Bottom-up proteomic techniques have recently received attention as critical tools in tissue characterization, capable of simultaneous quantification of hundreds of proteins [237], and been used to show signaling pathways of osteoarthritic diseases [436], to compare different cartilages [346, 437], and to compare the proteome of neocartilage engineered from different aged chondrocytes [338]. While developmental proteomic studies have been performed in mice [438], this study was novel in that it used bottom-up proteomics to show developmental changes in a clinically relevant large animal model for the first time. The hydroxyproline assay showed an increase in overall collagen throughout development, and the proteomics analysis showed that the collagen types that increase are mostly collagen types II and III, which increased by factors of 1.3 and 4.8, respectively, from fetal to mature. Other types of collagen such as types IX and XI, and XIV decreased throughout tissue maturity; types IX and XI dropped by factors of 9.4 and 5.1, respectively, and type XIV dropped from 0.95% in fetal cartilage to <0.01% in mature

cartilage (Supplementary Table 7-1). Collagen types IX and XI are known to decrease with age as finer fibrils mature to thicker and more variably sized fibrils in mature cartilage [439], but the same was not known of collagen type XIV. Collagen type XIV is involved in fibrillogenesis by regulating collagen fibril diameter [440]. Using values reported in Supplementary Table 7-1 and Figure 7-6, the sums of the means reported for collagen types IX, XI, and XIV were 17.3% for fetal, 13.8% for neonatal, 3.6% for juvenile, and 2.6% for mature cartilage; the higher proportion of these collagen subtypes in younger tissue indicates that they are critical for collagen development in cartilage, where fibrils assemble into mature fibers of mainly collagen type II. Radiocarbon dating shows that the collagen matrix of articular cartilage has little to no turnover, and once the collagen type II matrix matures, it is essentially a permanent structure [441]. The drop in collagen types IX, XI, and XIV shown here may either be a cause or an effect of this permanence; either the cartilage loses the tools to rebuild its collagen structure during tissue maturation, or these tools are degraded and replaced as they become no longer needed. The application of bottom-up proteomics techniques to elucidate developmental changes in the collagen profile of cartilage is a novel, exciting aspect of this study that can also be applied to the full cartilage proteome.

The bottom-up proteomics data offer additional insights in non-collagen proteins as well. For example, the amount of aggrecan core protein per total protein dropped 2.6-times from fetal to mature cartilage. This was similar to the 2.1-times drop in GAG/DW across the same ages. This may indicate that entire proteoglycan structures consisting of aggrecan and GAGs are removed from the ECM with aging. Age-related enzymatic degradation of GAG structures typically involve depletion of CS and cleavage of aggrecan without removal of link protein [442]. It is likely that the changes seen here are a result of mostly non-enzymatic breakdown of aggrecan structures or hyaluronan, as these pathways remove link protein [442], and link protein dropped by 5.0-times from fetal to mature, more than the drop in aggrecan. Interestingly, vimentin, an intermediate filament protein, dropped 9.3-times from fetal to mature cartilage, less

than the decreases in cellularity seen in the 17.9-times drop in DNA/DW and 54.2-times drop in Histone H4. Thus, the cells that remain in maturing cartilage tissue deposit increasing amounts of vimentin with age. Vimentin intermediate filaments have previously been shown to increase in chondrocytes that experience more mechanical stress [443]; thus, the increase in vimentin per cell shown here (Vimentin/DNA increased 5.2-times from fetal to mature) is likely a result of increases in loading as the animals gain weight and their knees experience greater forces. As cartilage matures, protein markers such as collagen types II and III increased, mirroring the increases in mechanical properties throughout development; however, despite the significant drop-off in mechanics from juvenile to mature cartilage described above, no significant differences were found between these two ages in any proteomic targets except for an increase in collagen type III. It is clear that this pre-osteoarthritic state cannot be sufficiently described by individual biochemical or proteomic biomarkers, and additional studies on cartilage proteomics will be crucial in studying age-related changes that both strengthen cartilage throughout development and weaken it with aging. Proteomic characterization of structural and cellular components of cartilage and other tissues can provide a deeper understanding of tissue development beyond what is offered by routine benchtop assays for collagen, GAG, and DNA, which is of particular use to researchers in the fields of tissue characterization and tissue engineering.

Porcine animal models have recently shown promise as large animal models for cartilage tissue engineering due to similarities in cartilage thickness, and, in the case of the Yucatan minipig, low mature animal weight and mild temperament [24, 444, 445]. While the pigs in this study are not Yucatan minipigs, as used more commonly in orthotopic cartilage large animal studies, the developmental states between the Yorkshire cross breed and the Yucatan minipig breed would likely be conserved between fetal and juvenile states. Because minipigs gain weight less rapidly and typically are on a more controlled diet within closed research herds, the age-related spontaneous pre-osteoarthritic state may not translate. However, tissue

engineers may use the results of this work as benchmarks for preclinical porcine studies. Because of cartilage's role as a mechanical tissue, ideal neocartilages will match the mechanical properties of native cartilage, and the results of this study offer comparison points for tensile and compressive properties. Furthermore, through the elucidation of temporal changes in mechanics, biochemistry, and proteomics, tissue engineers can attempt to more closely mimic the developmental processes of cartilage using tissue engineering techniques toward further improving the mechanical properties of neocartilage. For example, in addition to collagen type II, tissue engineers may also seek to build robust cartilage ECM through collagen types IX, XI, and XIV, which are needed for forming mature collagen type II-based fibers. Modulation, expression, or deposition of these collagen types can conceivably be manipulated to build new cartilage ECM in people who have cartilage degeneration due to injury or disease. Before this is possible, proteomic characterization of human cartilage at different developmental and aging time points is crucial. This work indicates that bottom-up proteomics will continue to be a powerful tool in the fields of tissue characterization, tissue degeneration, and tissue engineering in cartilage and a multitude of other tissues in the body.

Supplementary Materials

Supplementary Table 7-1: Bottom-up proteomics results on porcine knee cartilage. All analytes are reported as protein percentage per total protein. Over 400 individual proteins were quantified through the bottom-up proteomics approach, and 42 proteins that had an intensity of >0.1% per protein in at least one sample are shown here.

Protein	Protein / Total Protein (%)			
	Fetal	Neonatal	Juvenile	Mature
Actin, cytoplasmic 1	0.41%	0.31%	0.06%	0.04%
Aggrecan core protein	0.23%	0.22%	0.12%	0.09%
Biglycan	0.34%	0.29%	0.19%	0.14%
Collagen type I alpha 1	1.50%	0.88%	1.06%	1.44%
Collagen type I alpha 2	0.52%	0.16%	0.30%	0.44%
Collagen type II alpha 1	65.13%	76.02%	86.92%	85.51%
Collagen type III alpha 1	0.59%	0.48%	1.67%	2.86%
Collagen type IV alpha 2	0.08%	0.04%	0.28%	0.15%
Collagen type IV alpha 5	0.03%	0.00%	0.06%	0.11%
Collagen type V alpha 1	0.12%	0.06%	0.08%	0.14%
Collagen type V alpha 2	0.13%	0.08%	0.12%	0.37%
Collagen type V alpha 3	0.02%	0.02%	0.08%	<0.01%
Collagen type VI alpha 1	0.04%	0.02%	0.02%	0.02%
Collagen type VI alpha 2	0.16%	0.12%	0.10%	0.13%
Collagen type VI alpha 3	0.78%	0.43%	0.32%	0.34%
Collagen type IX alpha 1	5.33%	3.83%	0.75%	0.48%
Collagen type IX alpha 2	2.10%	2.10%	0.40%	0.32%
Collagen type X alpha 1	0.01%	0.07%	<0.01%	0.01%
Collagen type XI alpha 1	3.81%	2.92%	1.11%	0.71%
Collagen type XI alpha 2	5.11%	4.52%	1.27%	1.04%
Collagen type XII alpha 1	0.35%	0.24%	0.33%	0.15%
Collagen type XIV alpha 1	0.95%	0.41%	0.07%	<0.01%
Collagen type XVI alpha 1	0.07%	0.09%	0.04%	0.05%
Collagen type XXVIII alpha 1	0.36%	0.47%	1.19%	1.28%
Cytochrome P450 2E1	0.15%	0.06%	0.00%	0.00%
Decorin	0.03%	0.09%	0.04%	0.08%
Glyceraldehyde-3-phosphate dehydrogenase	0.13%	0.20%	0.03%	0.02%
Hemoglobin subunit alpha	0.16%	0.28%	0.01%	0.02%
Hemoglobin subunit beta	0.20%	0.30%	0.01%	0.01%
Histone H1t	0.56%	0.18%	0.01%	0.01%
Histone H3.3	1.62%	0.48%	0.03%	0.02%
Histone H4	3.25%	1.35%	0.16%	0.06%
Hyaluronan and proteoglycan link protein 1	1.44%	0.81%	0.35%	0.29%
Lactadherin	<0.01%	0.01%	0.04%	0.12%

Phosphoglycerate kinase 1	0.11%	0.05%	0.02%	<0.01%
Prelamin-A/C	0.17%	0.10%	<0.01%	<0.01%
Ryanodine receptor 1	0.12%	0.08%	0.26%	0.07%
Tenascin	1.02%	0.76%	0.34%	0.24%
Transforming growth factor-beta-induced protein ig-h3	0.12%	0.11%	0.10%	0.10%
Tubulin beta chain	0.11%	0.05%	<0.01%	<0.01%
Tubulin alpha-1B chain	0.13%	0.05%	<0.01%	<0.01%
Vimentin	0.28%	0.09%	0.02%	0.03%

Chapter 8: The Functionality and Translatability of Neocartilage Constructs are Improved with the Combination of Fluid-induced Shear Stress and Bioactive Factors[8]

Abstract

Neocartilage tissue engineering aims to address the shortcomings of current clinical treatments for articular cartilage indications. However, advancement is required toward neocartilage functionality (mechanical and biochemical properties) and translatability (construct size, gross morphology, passage number, cell source, and cell type). Using fluid-induced shear (FIS) stress, a potent mechanical stimulus, over four phases, this work investigates FIS stress' efficacy toward creating large neocartilage derived from highly passaged minipig costal chondrocytes, a species relevant to the preclinical regulatory process. In Phase I, FIS stress application timing was investigated in bovine articular chondrocytes and found to improve aggregate modulus of neocartilage by 151% over unstimulated controls when stimulated during the maturation stage. In Phase II, FIS stress stimulation was translated from bovine articular chondrocytes to expanded minipig costal chondrocytes, yielding a 46% improvement in aggregate modulus over nonstimulated controls. In Phase III, bioactive factors were combined with FIS stress to improve the shear modulus by 115% over bioactive factor-only controls. The translatability of neocartilage was improved in Phase IV by utilizing highly passaged cells to form constructs more than 9-times larger in area (11x17mm), yielding an improved aggregate modulus by 134% and a flat morphology compared to free-floating, bioactive factor-only controls. Overall, this study represents a significant step toward generating mechanically robust, large constructs necessary for animal studies, and, eventually, human clinical studies.

[8] **Chapter published as:** Salinas, E.Y.,* Donahue, R.P.,* Herrera, J.M.,* Hu, J.C., Athanasiou, K.A. The functionality and translatability of neocartilage constructs are improved with the combination of fluid-induced shear stress and bioactive factors. *The FASEB Journal*, April 2022, 36(4): e22225. (* These authors contributed equally.)

Introduction

Articular cartilage is a stiff and resilient tissue that protects bones and distributes forces during movement. Native articular cartilages vary widely in compressive aggregate modulus values, ranging from about 250 kPa to about 1400 kPa depending on the location and species [446-448]. Cartilage trauma and wear can cause defects that do not naturally heal [239]. Currently, the most common treatments for articular cartilage lesions are chondroplasty and microfracture, neither of which are considered effective for more than 5 years post-treatment [377, 449]. If cartilage lesions are not properly treated, they can progress to osteoarthritis (OA). OA currently affects 32 million people in the U.S. and is projected to rise up to 60% in prevalence over the next 20 years [361, 362]. Compared to the current short-term solutions applied to cartilage lesions, an emerging solution for articular cartilage defects is tissue engineering, which aims to provide a long-term regenerative solution [239]. Additionally, tissue-engineered cartilage derived from expanded cells has the potential to provide an inexhaustible amount of implant material, addressing the major clinical problem of donor tissue scarcity [25]. Although several advances in cartilage tissue engineering have been developed over the last several years, including the self-assembling process [23, 25, 207, 450], certain improvements must still be made before the successful implantation of neocartilage in humans, such as 1) finding the ideal timing of neocartilage stimulation regimens toward functional improvement, 2) establishing the reproducibility of the effects of mechanical stimuli across multiple species and cell types, 3) exploring the additive effects of multiple types of stimuli (i.e., biochemical and mechanical), and 4) scaling-up of constructs.

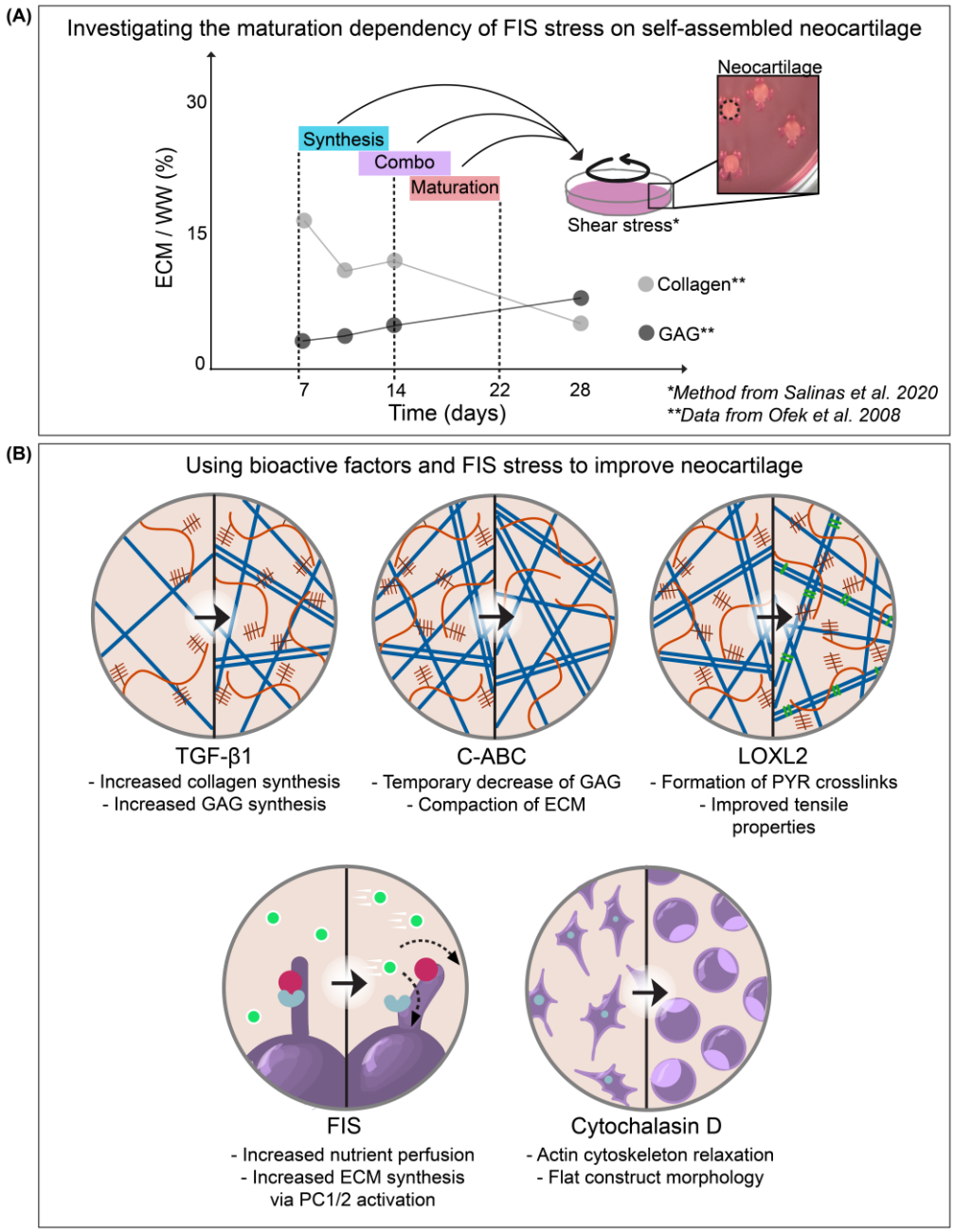

Figure 8-1: Maturation dependency and modes of action.
(A) The design of the experimental groups of Phase I follows the stages of the self-assembling process of neocartilage. The synthesis stage occurs from day 7 to day 14 of culture when glycosaminoglycan content increases slowly, and collagen content decreases slowly. During the maturation stage, from day 15 to day 22, glycosaminoglycan content continues to increase, and collagen content continues to decrease, but the total matrix production increases. The neocartilage constructs were either nonstimulated controls or stimulated with FIS stress during the synthesis stage, the maturation stage, or a combination stage (days 11-18). *Shear stress refers to fluid-induced shear stress, described previously in Salinas *et al.* (2020) [450]. **Data obtained from Ofek *et al.* (2008) [399]. (B) Schematic representation of the modes of action for bioactive and mechanical (FIS stress) signaling factors are shown. All the bioactive and mechanical signaling factors shown were used to create the neocartilage constructs in Phase IV. Abbreviations: chondroitinase ABC (C-ABC), combination (Combo), extracellular matrix (ECM), fluid-induced shear (FIS), glycosaminoglycan (GAG), lysyl oxidase-like 2 (LOXL2), polycystin 1/2 (PC1/2), pyridinoline (PYR), transforming growth factor beta 1 (TGF-β1), wet weight (WW).

Certain magnitudes of mechanical stimulation regimens improve neocartilage tissue properties toward those of native tissue, but the timeline of application is not typically scrutinized. For example, fluid-induced shear (FIS) stress has been previously shown by our group and others to mechano-regulate ion channels on the primary cilia of chondrocytes, leading to enhancements in neocartilage extracellular matrix (ECM) content and mechanical properties [450-454]. A previous study investigating the use of FIS stress found that applying 0.05-0.21 Pa of shear stress on neocartilage improved both bovine and human constructs [450]; however, the timeline of application is has not been previously investigated. Determining an ideal application window for neocartilage mechanical stimulation is critical because timed mechanical cues help maintain tissue health in native cartilages. For example, during embryonic development, chondrocytes are stimulated by mechanical loading to synthesize ECM [455, 456], and during postnatal development, mechanical loading regulates cartilage thickness and maturation [33, 457]. Certain tissue engineering methods, such as the neocartilage self-assembling process, have also been shown to follow similar developmental steps and may exhibit the same maturation-dependent mechanical signaling needs [156, 399, 458]. For example, self-assembled neocartilage undergoes the synthesis stage (days 7-14), when the chondrocytes produce ECM, and the maturation stage (days 15-22), when production of glycosaminoglycans is increased and collagen content is decreased (Figure 8-1A) [201, 399]. The maturation-dependency of mechanical stimulation regimens, such as FIS stress, should be investigated toward maximizing mechanical properties of neocartilage [163].

To translate mechanical stimulation technologies to the clinic, the reproducibility of tissue engineering techniques across species and sources must be examined. This is a necessary design criterion because the Food and Drug Administration (FDA) requires analogous products to be tested in animal studies prior to use in human clinical trials. For neocartilages, exploratory experiments may be conducted using bovine articular chondrocytes since they are inexpensive and easily obtainable. Eventually, the species and source will need to be translated to a

commonly used preclinical animal model for *in vivo* testing. The Yucatan minipig is considered a suitable animal model for most preclinical work because of its similarity to humans in weight, anatomy, immunology, physiology, and bone biology [24, 459-462]. Specifically, it is widely used for cartilage therapeutic testing in articular cartilage, knee meniscus, and temporomandibular joint disc investigations [23, 24, 461, 463]. Another consideration is the cell source. For example, costal chondrocytes may be advantageous over articular chondrocytes due to their ability to be harvested autologously and allogeneically without further damaging diseased joints that require treatment. Costal chondrocytes are also advantageous because they regain their chondrogenic phenotype via redifferentiation methods after expansion [19, 365, 402]. To eventually translate a mechanical stimulus for human use, analogous sources should be tested with an appropriate species that will be used in preclinical studies to satisfy regulatory guidance toward eventual human use.

To improve neocartilage functional properties, exogenous growth factors, enzymes, and other small molecules (i.e., bioactive factors) have been extensively studied to optimize their dosage and timeline of application [83, 339, 464-467]. Nevertheless, how bioactive factors work in conjunction with mechanical stimulation is of interest because of the potential for additive improvements in neocartilage functional properties. For example, transforming growth factor beta 1 (TGF-β1) alone has lead to enhanced collagen and glycosaminoglycan synthesis during the self-assembling process (Figure 8-1B) [83] and in scaffold-based neocartilages [468]. TGF-β signaling has been shown to be regulated through the primary cilia [469], the main mode of action of FIS stress [450]. This is significant because exogenous TGF-β1 addition and FIS stress might act in a similar manner to improve ECM content. Other bioactive factors, such as chondroitinase ABC (C-ABC), lysyl oxidase-like 2 (LOXL2), and insulin-like growth factor 1, have been studied in conjunction with TGF-β1 toward further improving functional properties of neocartilage [470], including self-assembled neocartilage (Figure 8-1B) [83]. Additionally, the use of bioactive factors independently or together with tensile and compressive stimulation has

been explored [207, 339, 399], motivating further exploration and combination with other mechanical stimulation regimens, such as FIS stress.

To repair larger cartilage defects, large neocartilage constructs (e.g., 11x17mm) that are mechanically robust and have a flat morphology must be generated, and more cells will be necessary to create these large constructs. While the process of further expanding chondrocytes is simple, recent studies have shown that maintaining a chondrogenic phenotype in highly passaged cells is exceedingly complex due to dedifferentiation [403, 404] and leads to the creation of neocartilage constructs that are not flat [25]. For example, protocols for creation of flat, robust neocartilages have been developed using aggregate rejuvenation combined with the use of bioactive factors, such as TGF-β1, C-ABC, and LOXL2. This work has yielded small constructs that maintain flat morphology and mechanical robustness despite using cells that have been passaged up to 11 times [25]. However, further attempts at increasing the size of self-assembled constructs in the past have yielded constructs that fold or become wavy due to the actin cytoskeleton exerting internal tensile forces within the construct [212]. In large constructs, the addition of cytochalasin D, a potent inhibitor of actin polymerization, has been shown to yield flat neocartilage construct morphology (Figure 8-1B) [212]. Moreover, cytochalasin D addition has also been known to restore the primary cilia on extensively passaged chondrocytes, which could further enhance the effects of FIS stress in this phase [469]. For addressing articular cartilage indications of larger sizes, it will be critical to develop protocols for larger constructs with both biochemical and mechanical stimulation which generate mechanically robust and flat neocartilages.

Toward successful implantation of neocartilage in humans, the global objective of this work was to improve the functional and translational aspects of neocartilage constructs using FIS stress and bioactive factors. In particular, the functional properties investigated were mechanical properties and ECM content, while the translational aspects investigated were construct size (5mm diameter circular vs. 11x17mm rectangular), gross morphology (flat

neocartilage), passage number (passages 0, 3, and 6), cell source (bovine vs. minipig), and cell type (articular chondrocytes vs. costal chondrocytes). We hypothesized that the combination of FIS stress and bioactive factors would yield flat, large, neocartilage constructs that are mechanically robust. This series of studies was divided into four phases. In Phase I, the objective was to determine if application of FIS stress during the synthesis stage (days 7-14) or during the maturation stage (days 15-22) of the self-assembling process was most beneficial for biochemical and mechanical properties (Figure 8-1A). In Phase II, a clinically relevant and widely accepted animal model and cell source (i.e., costal chondrocytes from the Yucatan minipig) were used with the appropriate timing derived from Phase I [24, 461]. In Phase III, bioactive factors previously shown to improve functional aspects of neocartilage constructs were used in conjunction with FIS stress with the goal of increased functionality (Figure 8-1B). Finally, in Phase IV, the combination of FIS stress timing and bioactive factors discovered in Phases I to III was applied to constructs derived from highly passaged minipig costal chondrocytes to create large, flat neocartilage constructs for larger articular cartilage indications.

Methods

Overview of experimental phases

In Phase I, the ideal FIS stress application window was determined by creating neocartilage constructs from bovine articular chondrocytes and stimulating them with FIS stress during the synthesis stage (days 7-14), maturation stage (days 15-22), or a combination of both stages (days 11-18) (Figure 8-1A). In Phase I, nonstimulated neocartilage created from bovine articular chondrocytes served as a control group. Next, in Phase II, Yucatan minipig costal chondrocytes were expanded to passage 3 and used to create neocartilage constructs that were either stimulated with FIS stress during the optimal period or not stimulated with FIS stress. In Phase III, the combination of FIS stress and bioactive factors (TGF-β1, C-ABC, and LOXL2) was investigated to further improve functionality of neocartilage constructs created from Yucatan

minipig costal chondrocytes. Bioactive factors were included in the creation of all the neocartilage constructs for Phase III, including controls. Finally, in Phase IV, the results from all previous phases were used to create large (11x17mm), neocartilage constructs from highly passaged Yucatan minipig costal chondrocytes.

Isolation of bovine articular chondrocytes

For Phase I of this study, bovine articular chondrocytes were isolated by mincing cartilage from the femoral condyles and trochlear grooves of the knees of six, 2-month old Jersey calves. Minced pieces from each leg were stored in 30ml of wash medium, which consisted of Dulbecco's Modified Eagle's Medium (DMEM) and 1% penicillin-streptomycin-fungizone (PSF). The minced tissue from each leg was washed 2-3 times with wash medium and digested in a petri dish using collagenase II solution (0.2% w/v, Worthington Biochemical's Collagenase type II in wash medium, 3% fetal bovine serum (FBS)) for 18hr on an orbital shaker at 37°C at 60RPM. Following this, the solution with cells was filtered through 70µm cell strainers and centrifuged for 5 minutes at 400g to remove the collagenase. The resulting cell pellet was washed with phosphate-buffered saline (PBS). The chondrocytes were then washed with ammonium-chloride-potassium (ACK) lysis buffer, followed by several washes with PBS [353]. Finally, chondrocytes were counted and frozen in 90% FBS and 10% dimethyl sulfoxide (DMSO) for downstream self-assembly.

Isolation of minipig costal chondrocytes

For Phases II, III, and IV of this study, minipig costal cartilage was obtained from three, 6-month old Yucatan minipigs. Costal cartilage was minced into ~1mm^3 pieces. The cartilage pieces were then digested with pronase solution (0.4% w/v, in wash medium, 3% FBS) for 1hr followed by 18hr in collagenase II solution on an orbital shaker at 60RPM. Finally, the cells were strained,

treated with ACK lysis buffer, washed several times, counted, and frozen in 90% FBS and 10% DMSO either immediately as primary cells or after one passage, as previously described [23].

Passaging and aggregate rejuvenation of minipig costal chondrocytes

Cell vials were thawed by placing in a 37°C water bath and adding cells drop-wise to wash medium to ensure high viability. The tubes were spun down at 400g for 5 minutes, and cells were resuspended in pre-warmed chondrogenic medium (CHG), which consisted of DMEM, 1% PSF, 1% nonessential amino acids, 1% insulin-transferrin-selenous acid, 50 µg/ml ascrobate-2-phosphate, 40µg/ml L-proline, 100µg/ml sodium pyruvate, and 100nM of dexamethasone. The cells were seeded in 27ml per flask of CHG, plus 2% FBS and growth factors (1ng/ml TGF-β1 + 5ng/ml basic fibroblast growth factor + 10ng/ml platelet derived growth factor), at 2.5 million cells per flask. Finally, the flasks were checked for confluence every 1-2 days, and the cells were fed every 3-4 days with CHG, plus 2% FBS and growth factors.

The cells were passaged every two weeks or until the cells were confluent, whichever came first. Cells for Phase II and III were expanded to passage 3, while Phase IV utilized passage 6 cells. Wash medium was added to each flask to rinse, and, subsequently, 0.05% Trypsin-EDTA was added to each flask. The flasks were placed in an incubator for 8-9 minutes, and wash medium, plus 10% FBS, was added to the growth surface of the flask to neutralize the Trypsin-EDTA. The suspension of cells were spun down, and the supernatant was discarded. The cell pellet was resuspended in collagenase II solution and placed in a 37°C water bath. The cell suspension was pipetted up and down every 10-15 minutes for 20-30 minutes. The cell suspension was spun down to remove the supernatant, and the cells were counted in wash medium. The cells were plated for the next passage until the terminal passage when they were placed into aggregate rejuvenation. The three individual costal chondrocyte donors were passaged individually until the last passage when they were combined for the remainder of culture.

Finally, the cells were then placed into aggregate rejuvenation, which allowed the cells to recover their chondrogenic phenotype [149]. Petri dishes were coated with molten 1% agarose to create a nonadherent surface. The cells were seeded at a final density of 750 thousand cells per ml of medium in 30ml (22.5 million cells per dish) of CHG plus growth factors (10 ng/ml TGF-β1 + 100ng/ml growth differentiation factor 5 + 100ng/ml bone morphogenetic protein 2). The petri dishes were placed on an orbital shaker for 24hrs at 50RPM, then subsequently cultured under static conditions. The aggregates were fed every 3-4 days for 14 or 11 days for Phases II/III or IV, respectively. It has been previously shown that expanded chondrocytes that are placed in aggregate rejuvenation maintain a chondrogenic phenotype throughout the self-assembling process, exhibiting high expression of aggrecan, collagen type II, and SRY-box transcription factor 9 and minimal expression of osteocalcin and collagen type I [150].

Self-assembly of neocartilage constructs

Custom made well-makers were used to make negative molds in 2% agarose wells. CHG was added and exchanged twice before seeding chondrocytes. Wells were 5mm diameter cylinders for Phases I, II, and III. For Phase IV, wells were are scaled-up from prior studies to 11x17mm rectangular wells [201, 207]. As described previously, chondrocytes were seeded into the 2% agarose wells at densities of 4 million bovine chondrocytes per well for Phase I, 2 million minipig chondrocytes per well for Phases II and III, and 15 million minipig chondrocytes per well for Phase IV to begin the self-assembling process. After seeding, 0.5ml of CHG was added to each well in Phases I, II, and III, while 5ml of CHG was added to each well for Phase IV, at the 4hr timepoint. Seven or two days after seeding for small circular or large rectangular constructs, respectively, the self-assembled neocartilage constructs were unconfined from the agarose wells and cultured in 24- or 6-well plates. The small circular and large rectangular constructs received changes of medium (0.5ml or 5.0ml) every day up until unconfining, and 1ml or 10ml of medium on alternating days for the remainder of the 28 day culture period.

Table 8-1: Timeline of FIS stress and bioactive factor application.
The specific timeline of application for FIS stress, TGF-β1, C-ABC, LOXL2, and cytochalasin D is shown. Abbreviations: chondroitinase ABC (C-ABC), lysyl oxidase-like 2 (LOXL2), transforming growth factor beta 1 (TGF-β1).

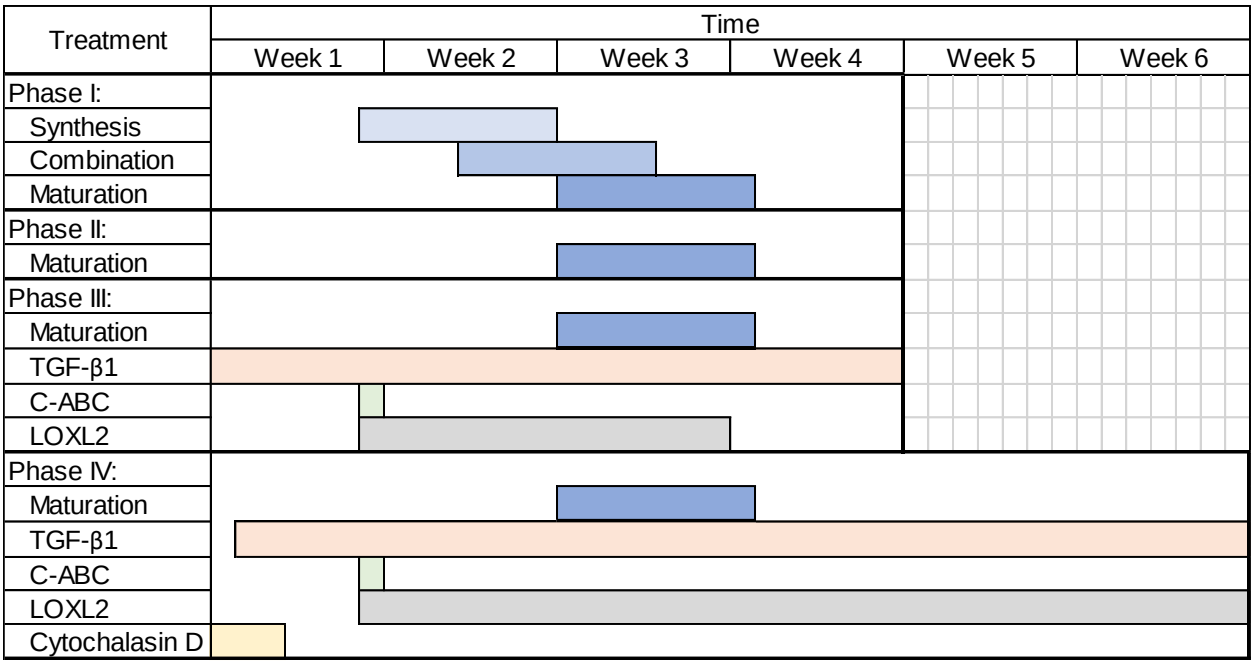

FIS stress stimulation and devices

FIS stress was applied to the treatment groups by placing the neocartilage constructs in a FIS stress device at the previously specified stages of maturation (Table 8-1). The device for 5mm neocartilage constructs was created by adding 25ml of 3% agarose to a 100x25mm petri dish, placing the device mold to create small protruding agarose poles, and removing the mold once the agarose solidified, as described previously [450]. Each of the neocartilage constructs were positioned between four surrounding poles to keep the constructs in place, and 20ml of CHG was added to the device (Figure 8-2A). A new device was created for the stimulation of 11x17mm neocartilage constructs using an acrylic base and stainless-steel metal rods (Figure 8-2B). As with the original device, the new device was designed to be placed inside a petri dish (100x25mm), and the neocartilage constructs were loaded into the device. Acrylic weights were also used to hold the neocartilage constructs in place (Figure 8-2B). Three constructs were loaded per FIS stress device, and 30ml of CHG was added to the device. The FIS stress device

was then placed on an orbital shaker at 50RPM, and, as the orbital shaker rotated, it allowed the medium in the FIS stress device to flow over the neocartilage constructs, thereby applying 0.05-0.21Pa of FIS stress, as previously characterized [450]. Since both devices were designed to have the same radius and are placed on the orbital shaker at the same rotational speed, the fluid-flow and resulting FIS stress applied to the neocartilage constructs are not altered, as is shown by previous computational fluid dynamic modeling studies [471-474].

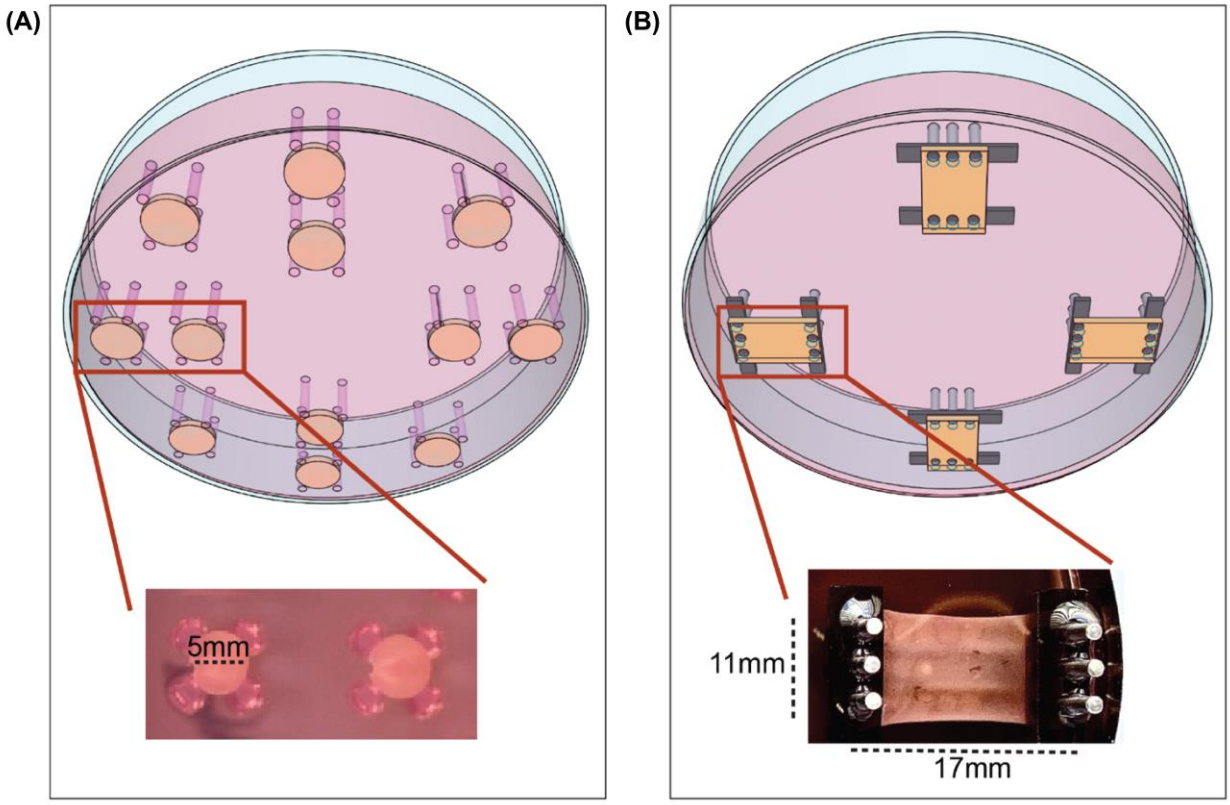

Figure 8-2: The two FIS stress devices used for stimulation of circular and rectangular neocartilage constructs.
(A) The FIS stress device for 5mm diameter neocartilage constructs was created using a 3% agarose base inside a 100mm diameter petri dish. Neocartilage constructs of 5mm diameter were placed within four agarose posts to be held in place during FIS stress stimulation. (B) A novel design of the FIS stress device was necessary to stimulate 11x17mm neocartilage constructs. The new FIS stress device was created using an acrylic base and stainless-steel metal rods. The acrylic base was placed inside a 100mm diameter petri dish, and the 11x17mm neocartilage constructs were held in place by the six metal rods and acrylic weights. Previous studies have shown that the changes created in the new design for rectangular constructs does not significantly alter the fluid flow or FIS stress applied to the neocartilage [471-474]. For both designs, previous computational fluid dynamic modeling studies have shown that a speed of 50RPM on an orbital shaker achieves 0.05-0.21Pa of FIS stress on neocartilage constructs [450].

Bioactive factor treatment

The timeline of application for bioactive factor treatment is summarized in Table 8-1. The use of these bioactive factors was used in accordance with previous studies showing that 1) bioactive factors improved the functional properties of self-assembled constructs [23, 25, 83, 201, 207, 212, 339, 355, 378] and 2) bioactive factors improved flatness of large constructs derived from highly passaged cells [212, 339]. For Phase III, TGF-β1 (10ng/ml) was applied for the entire duration of the 28 days of self-assembly, while C-ABC (2.0U/ml) was applied on day 7 for 4hr to temporarily deplete glycosaminoglycan content, as previously described [355]. LOXL2 was applied at 0.15μg/ml in conjunction with copper sulfate (1.6μg/ml) and hydroxylysine (0.146mg/ml) from days 7-21. For Phase IV, the culture time was extended to 42 days to maximize construct thickness and mechanical properties; LOXL2 treatment was extended until the end of culture and C-ABC was treated as described above. TGF-β1 was modified for large constructs in Phase IV to be applied after unconfining (day 2) for the remaining duration of the culture, and cytochalasin D (2μM) was applied from days 1-3, as previously described [212].

Analysis of mechanical properties

After completion of culture, mechanical testing of the neocartilage constructs was performed. To determine the compressive properties, a circular 2mm diameter punch was taken from the center of the construct, and a creep indentation test was performed to determine aggregate modulus and shear modulus, as previously described [475]. For Phase IV, 3mm diameter circular punch specimens were also examined in a compressive stress-relaxation test at 10% strain on a uniaxial Instron machine (Model 5665) to determine the instantaneous modulus and relaxation modulus, as determined from a standard linear solid model using MATLAB software [24].

Tensile testing was conducted using an uniaxial Instron machine, as previously described [476]. Neocartilage constructs were cut into dog bone-shaped samples and were

glued to paper tabs with a predefined gauge length of 1.55mm. The thickness and width of the dog bone-shaped samples were measured using ImageJ, and a subsequent cross-sectional area was calculated. A uniaxial strain-until-failure test was conducted with a strain rate of 1% per second. Load–displacement curves were normalized to the cross-sectional area and gauge length of each sample. Finally, the Young's modulus and ultimate tensile strength were calculated using MATLAB software.

Analysis of biochemical properties

For ECM content, wet weight (WW) and dry weight (DW) of the samples were measured, and specific assays were used to quantify collagen content and glycosaminoglycan content. First, the samples were frozen to allow for sublimation during a 72hr lyophilization cycle. After lyophilization, DWs were measured, and the tissue was digested in a buffered papain solution for 18hr at 65°C. The glycosaminoglycan and collagen contents were normalized per WW and is reported in percentage. Glycosaminoglycan content was measured using a BioColor Blyscan glycosaminoglycan assay kit according to the manufacturer's directions. The total collagen content was measured using a modified chloramine T hydroxyproline assay and a Sircol collagen standard, as previously described [93].

Histology

Construct samples from Phase IV were fixed in 10% neutral buffered formalin for at least 48hr immediately after culture completion. Samples were then processed, embedded in paraffin, and sectioned at 5µm for subsequent staining with hematoxylin and eosin (H&E), safranin O (Saf O), with fast green counterstain, and picrosirius red (Picro Red).

Statistics

For Phase I, one-way analysis of variance (ANOVA) and Tukey's *post hoc* tests were performed using $p < 0.05$ to determine statistically significant differences among groups. Groups deemed significantly different by the Tukey's *post hoc* tests are denoted using alphabetical letters via a connecting letters report, where groups not sharing the same letter are statistically significant. For Phases II, III, and IV, Student's *t*-test was used at $p < 0.05$ to determine statistically significant differences between groups.

Results

Phase I: FIS stress stimulation during the maturation stage yields the largest functional increases over nonstimulated controls

To determine which stimulation time would lead to the most mechanically robust neocartilage constructs, FIS stress was applied at the different stages of neocartilage development (Figure 8-1A). For the compressive stiffness, the neocartilage constructs stimulated during the maturation stage improved 2.51-times over the nonstimulated control in aggregate modulus values ($p<0.0001$) (Figure 8-3A). They also trended higher than the neocartilage constructs stimulated during the combination stage (Figure 8-3A). When considering tensile properties, neocartilage stimulated during the maturation and combination stages saw improvements in ultimate tensile strength over nonstimulated controls, showing an 100% increase ($p=0.0185$ and $p=0.0144$, respectively) (Figure 8-3B). In parallel, collagen content of constructs stimulated during the maturation stage was improved over the collagen content of nonstimulated neocartilage ($p<0.0001$), exhibiting an 82% increase (Figure 8-3C). Toward achieving the maximal improvement in neocartilage biochemical and mechanical properties, FIS stress stimulation during the maturation stage was selected to move forward to Phases II through IV.

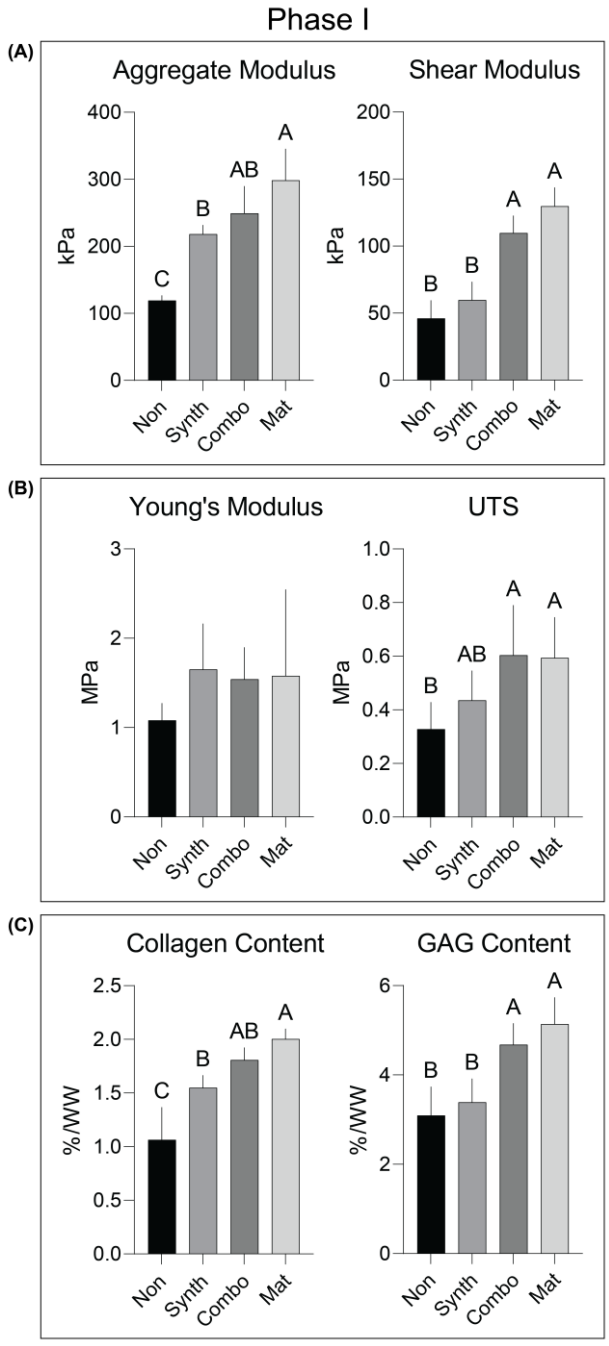

Figure 8-3: Identifying the best time of application for FIS stress.
Phase I constructs were derived from bovine articular chondrocytes in small 5mm diameter circular shapes and included four groups to determine an optimal FIS stress stimulation stage: nonstimulated, stimulated with FIS stress during the synthesis stage, stimulated with FIS stress during the maturation stage, and stimulated with FIS stress during combination of synthesis and maturation stages. (A) The aggregate modulus and shear modulus under compressive conditions, (B) the Young's modulus and the ultimate tensile strength under tensile conditions, (C) and the collagen content and the glycosaminoglycan content of neocartilage constructs are shown. Bars not sharing the same letter are statistically different when evaluated at $p < 0.05$ using a one-way ANOVA and Tukey's *post hoc* test. Abbreviations: combination (Combo), glycosaminoglycan (GAG), kilopascals (kPa), maturation stage (Mat), megapascals (MPa), nonstimulated (Non), synthesis stage (Synth), percent by wet weight (%/WW).

Phase II: FIS stress yields similar neocartilage functional increases using expanded and rejuvenated minipig costal chondrocytes

To evaluate the translatability of FIS stress stimulation across chondrocytes from different sources and species, Phase II explored the use of Yucatan minipig costal chondrocytes to produce neocartilage constructs. As in Phase I, neocartilage derived from Yucatan minipig costal chondrocytes was stimulated during the maturation stage. Compressive properties were examined, and it was found that the aggregate modulus values of neocartilage stimulated with FIS stress during the maturation stage were 46% higher than nonstimulated neocartilage ($p=0.0020$) (Figure 8-4A). Furthermore, tensile properties were also improved; the ultimate tensile strength of neocartilage stimulated with FIS stress during the maturation stage was 78% higher than that of nonstimulated neocartilage ($p=0.0002$) (Figure 8-4B). Similarly, the Young's modulus of neocartilage stimulated with FIS stress during the maturation stage was 78% higher than nonstimulated neocartilage ($p=0.0041$) (Figure 8-4B). An improvement in Young's modulus had not been previously seen in self-assembled neocartilage constructs made with bovine articular chondrocytes stimulated with FIS stress. As in neocartilage created with bovine neocartilage constructs in Phase I, an increase in glycosaminoglycan content was observed in minipig neocartilage stimulated during the maturation stage compared to the nonstimulated control (Figure 8-4C); a 136% increase in glycosaminoglycan content was observed ($p=0.0008$). Interestingly, although collagen content trended higher, a significant increase in collagen content was not observed in the FIS stress-stimulated neocartilage created with minipig costal chondrocytes (Figure 8-4C). As the Yucatan minipig is a widely used preclinical model for treatment of cartilage lesions [23, 24, 461, 463], this phase showed that FIS stress can be applied across various sources and species for similar functional improvements.

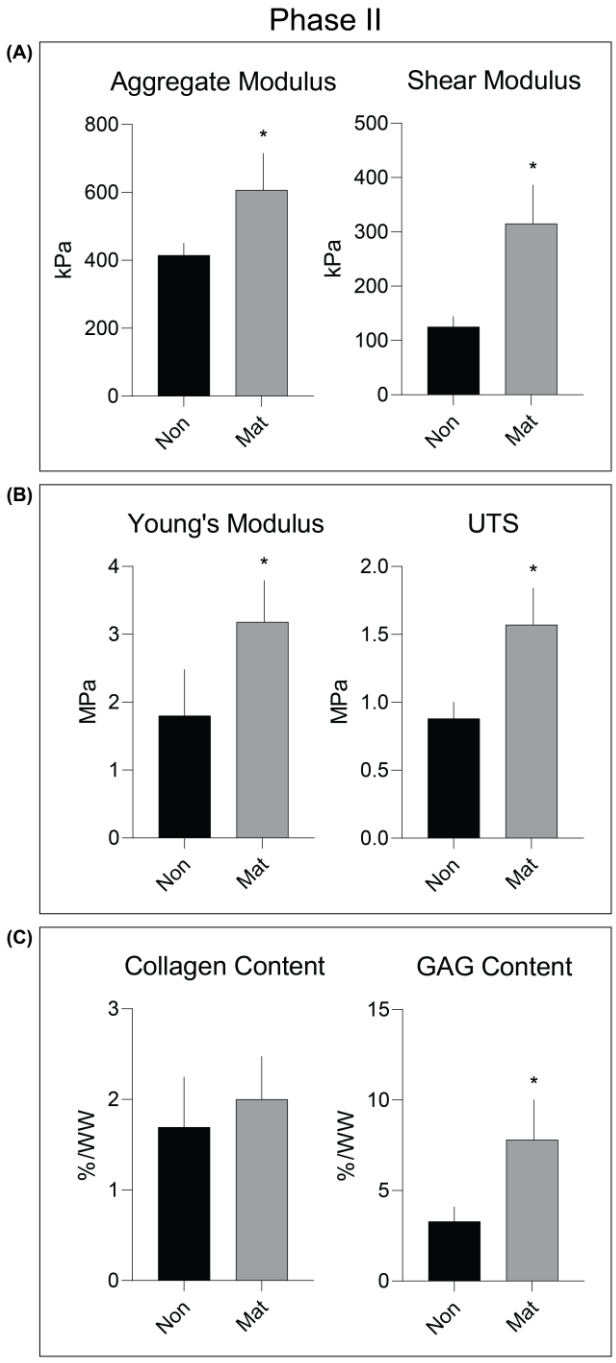

Figure 8-4: Translating FIS stress stimulation to costal chondrocytes from the Yucatan minipig.
Phase II constructs were derived from passage 3 minipig costal chondrocytes in small 5mm diameter circular shapes and included two groups to assess the translatability of the FIS stress stimulation regimen across cell sources and species: nonstimulated and stimulated with FIS stress during the maturation stage. (A) The aggregate modulus and the shear modulus under compressive conditions, (B) the Young's modulus and the ultimate tensile strength under tensile conditions, (C) and the collagen content and the glycosaminoglycan content of neocartilage constructs are shown. The asterisk (*) above the bars indicates statistically different groups when evaluated at $p < 0.05$ using Student's *t*-test. Abbreviations: glycosaminoglycan (GAG), kilopascals (kPa), maturation stage (Mat), megapascals (MPa), nonstimulated (Non), percent per wet weight (%/WW).

Phase III: Bioactive factors in conjunction with FIS stress yield further functional improvements over bioactive factors alone

Bioactive factors have been previously found to further enhance neocartilage constructs [83], and they were applied here in conjunction with FIS stress toward further functional improvement. FIS stress in combination with bioactive factor treatment significantly increased aggregate modulus ($p=0.0006$) and shear modulus ($p<0.0001$) values by 48% and 115%, respectively, over bioactive factor-only controls (Figure 8-5A). Both measures of tensile properties, Young's modulus and ultimate tensile strength, were also significantly higher with application of FIS stress and bioactive factors compared to bioactive factor-only controls ($p=0.0047$ and $p=0.0014$, respectively) (Figure 8-5B). In terms of ECM content, glycosaminoglycan and collagen content were measured (Figure 8-5C); glycosaminoglycan content was significantly higher ($p<0.0001$) with the application of FIS stress and bioactive factors compared to bioactive factor-only controls. The combination of bioactive factors and FIS stress led to improved neocartilage properties when compared to bioactive factors alone. However, when comparing the magnitudes of aggregate modulus and Young's modulus values of the FIS stress plus bioactive factor group of Phase III to those from the FIS stress-stimulated group of Phase II, the neocartilage properties did not further improve when stimulated with bioactive factors. However, application of bioactive factors is important for examining large constructs as it has been previously demonstrated that rejuvenated constructs stimulated with bioactive factors yield mechanically robust and flat constructs [25], an important clinical feature for tissue-engineered cartilage therapeutics. Despite this, stimulation with bioactive factors and FIS stress yielded improved functionality when compared to neocartilage stimulated with only bioactive factors.

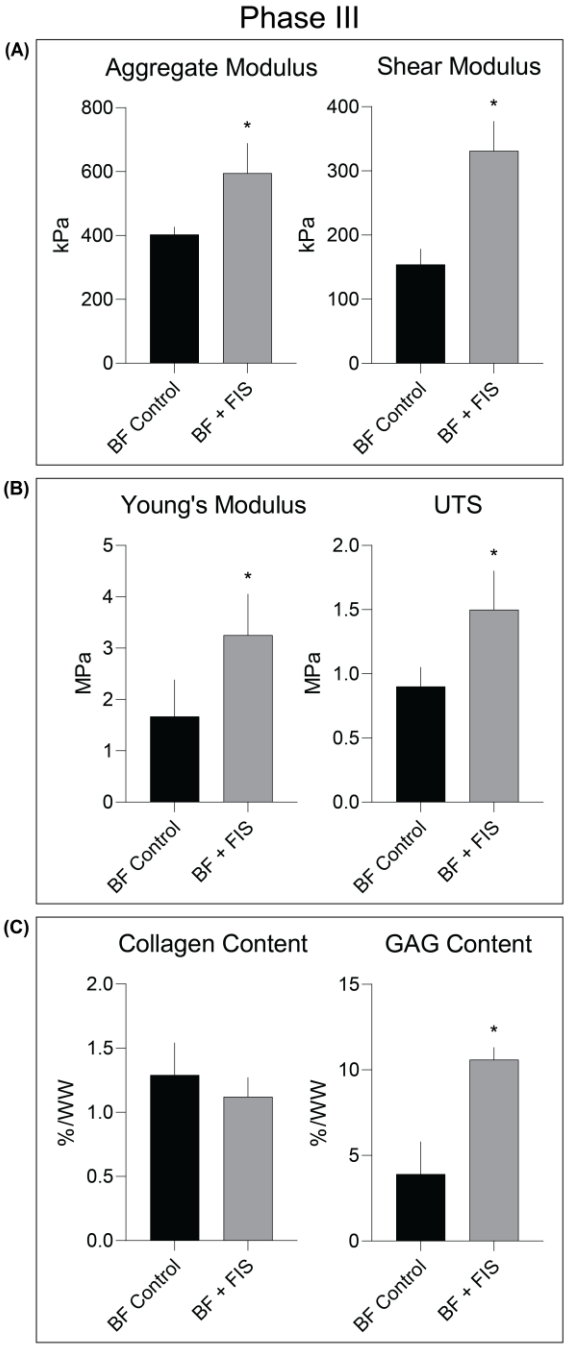

Figure 8-5: Combining bioactive factors and FIS stress to further improve the functional properties of neocartilage constructs.

Phase III constructs were derived from passage 3 minipig costal chondrocytes in small 5mm diameter circular shapes and included two groups: treated with bioactive factors alone, and treated with bioactive factors and FIS stress stimulation during the maturation stage. (A) The aggregate modulus and the shear modulus under compressive conditions, (B) the Young's modulus and the ultimate tensile strength under tensile conditions, (C) and the collagen content and the glycosaminoglycan content of neocartilage constructs are shown. The asterisk (*) above the bars indicate statistically different groups when evaluated at $p < 0.05$ using Student's *t*-test. Abbreviations: bioactive factors (BF), fluid-induced shear (FIS), glycosaminoglycan (GAG), kilopascals (kPa), megapascals (MPa), percent per wet weight (%/WW).

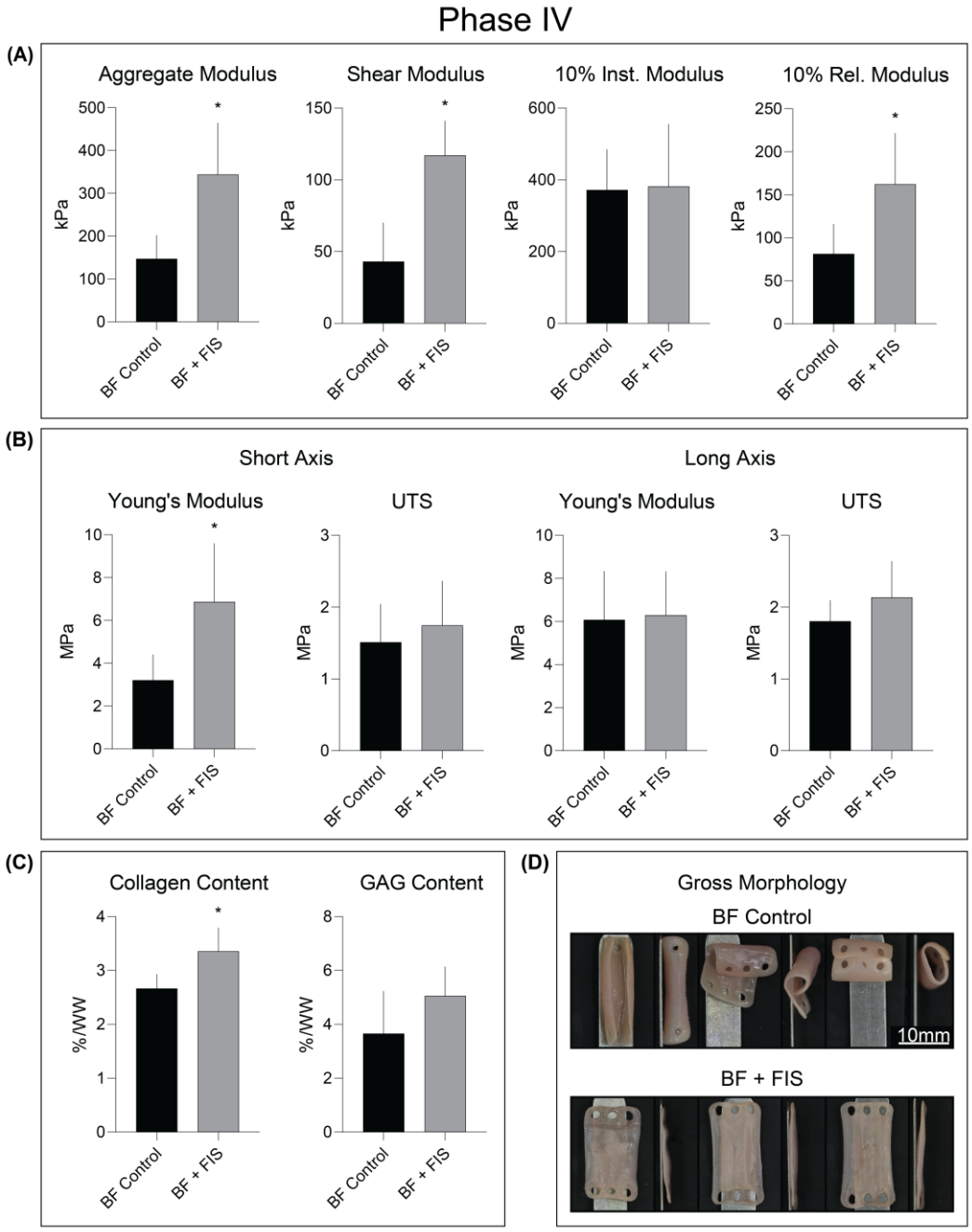

Figure 8-6: Scaling-up the size of neocartilage constructs created from highly passaged chondrocytes using FIS stress and bioactive factors.
Phase IV constructs were derived from passage 6 minipig costal chondrocytes in 11x17mm rectangular shapes and included two groups: treated with bioactive factors plus cytochalasin D, and treated with bioactive factors, cytochalasin D, plus FIS stress stimulation during the maturation stage. (A) The aggregate modulus, the shear modulus, and the 10% instantaneous and relaxation moduli under compressive conditions, (B) and the Young's modulus and the ultimate tensile strength for both the long and short axis of neocartilage constructs under tensile conditions are shown. (C) The collagen content and the glycosaminoglycan content, and (D) images of the gross morphology of neocartilage constructs are shown. The asterisk (*) above the bars indicates statistically different groups when evaluated at $p < 0.05$ using Student's *t*-test. Abbreviations: bioactive factors (BF), fluid-induced shear (FIS), instantaneous (Inst.), glycosaminoglycan (GAG), kilopascals (kPa), megapascals (MPa), percent per wet weight (%/WW), relaxation (Rel.).

Phase IV: Large constructs derived from highly passaged cells are mechanically robust and flat

Phase IV examined the effect of FIS stress in conjunction with bioactive factors on large rectangular 11x17mm neocartilage constructs derived from passage 6 costal chondrocytes. Although the functional properties of neocartilage stimulated with a combination of FIS stress and bioactive factors in Phase III did not significantly improve over FIS stress-stimulated groups of Phase II, the addition of bioactive factors and cytochalasin D has previously been necessary to create neocartilage constructs larger than 5mm diameter, specifically when using highly passaged chondrocytes [25, 212]. Compressive properties were examined using both creep indentation and stress-relaxation. Aggregate modulus increased 2.34-times over bioactive factor-only controls ($p=0.0251$), while shear modulus increased 2.72-times over controls ($p=0.0064$) (Figure 8-6A). Under 10% strain, the relaxation modulus significantly increased by 100% ($p=0.0251$) and the instantaneous modulus did not significantly differ (Figure 8-6A). The constructs were also measured under uniaxial tension in both axes (i.e., short and long) (Figure 8-2B). The only significant difference was in the short axis Young's modulus, which increased significantly when stimulated with FIS stress over bioactive factor-only controls ($p=0.0216$). For biochemical content, collagen increased when treated with FIS stress compared to bioactive factor-only controls ($p=0.0209$) (Figure 8-6C). While glycosaminoglycan trended upwards with application of FIS stress, it was not significant (Figure 8-6C). Compared to free-floating constructs stimulated only with bioactive factors, those to which FIS stress was applied exhibited a flatter morphology and less curling (Figure 8-6D). Histologically, samples stimulated with FIS stress and bioactive factors had increased staining intensity in Saf O (Figure 8-7A), indicative of neocartilage constructs with more glycosaminoglycan content, but similar staining intensities under H&E (Figure 8-7B). Picro Red staining shows spatial organization of collagens within the matrix. The groups seem to have similar overall intensities, but FIS stress increased the peripheral staining, indicating stronger collagen deposition on the outer edges of the neocartilage constructs (Figure 8-7C). These staining trends from Figure 8-7 follow those

quantitative metrics for glycosaminoglycan and total collagen content presented in Figure 8-6C. Combined, these results indicate that large constructs derived from highly passaged cells respond in a similar manner to the combination of bioactive factors and FIS stress during the maturation stage compared to small constructs from Phases I through III. Additionally, mechanical confinement in the form of the novel FIS stress device also improves construct flatness. This represents a significant step toward treating larger articular cartilage defects using large constructs.

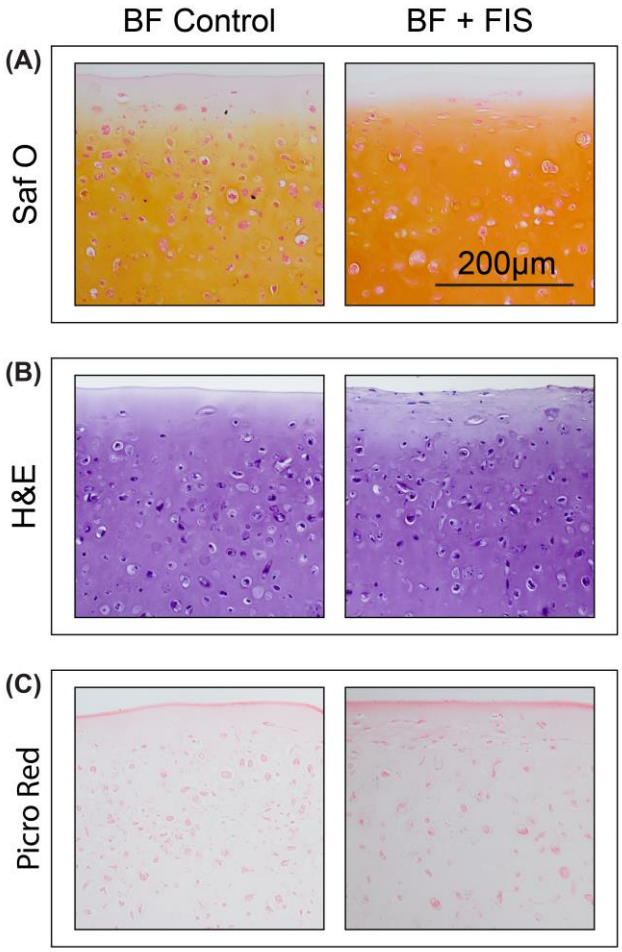

Figure 8-7: Combining bioactive factors and FIS stress increases intensity for glycosaminoglycan staining.
Phase IV constructs were derived from passage 6 minipig costal chondrocytes in 11x17mm rectangular shapes and included two groups: treated with bioactive factors plus cytochalasin D, and treated with bioactive factors, cytochalasin D, plus FIS stress stimulation during the maturation stage. Representative images of (A) safranin O staining for glycosaminoglycan content, (B) hematoxylin and eosin staining for general cellular and tissue morphology, and (C) picrosirius red staining for general collagen are shown. Abbreviations: bioactive factors (BF), fluid-induced shear (FIS), hematoxylin and eosin (H&E), picrosirius red (Picro Red), safranin O (Saf O).

Discussion

In this series of studies, the global objective of this work was to improve the functional and translational aspects of neocartilage constructs. Specifically, this work tackled four critical aspects of neocartilage engineering across the four phases presented, including 1) finding the ideal application window of FIS stress stimulation for biochemical and mechanical improvement, 2) establishing the reproducibility of FIS stress stimulus across bovine and minipig cell sources, 3) exploring the beneficial effects of combining FIS stress and bioactive factors, and 4) scaling-up the size of neocartilage constructs using highly passaged cells while maintaining a flat morphology and other improvements in functional properties seen with application of FIS stress and bioactive factors. Overall, it was hypothesized that the appropriate combination of FIS stress and bioactive factors would yield flat, large neocartilage constructs with improved mechanical properties and ECM content. Indeed, both the functional characteristics (mechanical properties and ECM content) and the translational aspects (construct size, gross morphology, passage number, cell source, and cell type) were improved. Namely, in Phase I, FIS stress applied during the maturation stage improved compressive stiffness by 151%, tensile stiffness by 45%, and collagen content by 82% in self-assembled neocartilage constructs engineered from bovine articular cartilage cells. In Phase II, the FIS stress stimulation regimen from Phase I was implemented using costal chondrocytes from the Yucatan minipig and also led to similar increases in compressive stiffness (46%) and tensile stiffness (78%). Then, in Phase III, the combination of FIS stress with bioactive factors improved the compressive stiffness (48%) and tensile stiffness (94%) of neocartilage constructs over bioactive factor-only controls. Finally, in Phase IV, the methods from Phases I through III were combined to engineer large neocartilage constructs derived from highly passaged cells, while maintaining the earlier increases seen via application of FIS stress and bioactive factors.

Toward achieving native tissue functionality, the ideal window of FIS stress time of application was identified. This objective is significant because, in native articular cartilage,

chondrocytes depend on mechanical loading during embryonic development to synthesize ECM [455, 456], and, during postnatal development, timed mechanical signaling regulates cartilage thickness and maturation for proper function [33, 457]. Similarly, previous studies showed that self-assembled neocartilage also follows chronological steps and may exhibit maturation-dependent mechanical signaling needs [156, 399]. For example, when nonstimulated neocartilage constructs enter the maturation stage, the production of glycosaminoglycan is increased, whereas collagen content shows a stark decrease [399]. In contrast, when FIS stress is applied during the maturation stage (days 15-22) in Phase I of this work, collagen content increased by 82% over nonstimulated constructs and by 33% over constructs stimulated during the synthesis stage (days 7-14). The neocartilage constructs also improved in compressive and tensile properties. These results indicate that, like native cartilage, carefully timed mechanical signaling is crucial to the development of robust neocartilage. Although further study is necessary to determine the precise pathways leading to these results, FIS stress has been previously shown to activate ECM producing protein pathways via the perturbation of the PC1/PC2 complex on the primary cilia of chondrocytes [450, 453, 454, 477]. Inasmuch as previous studies on self-assembled cartilage have seldom investigated time of application of mechanical stimulation, this study showed that stimulation during the maturation stage is optimal in terms of producing a mechanically robust neocartilage suitable for preclinical *in vivo* implantation toward eventual FDA approval for human studies.

As specified by the FDA, tissue-engineered therapeutics must undergo preclinical studies in an appropriate animal model prior to human clinical studies, and, for these, an analogous animal product should be investigated. Therefore, an important translational feature of this study is the demonstration that the FIS stress stimulus is efficacious in an animal model, such as the Yucatan minipig. Furthermore, transferring the FIS stress stimulus to a different cell type, namely, costal chondrocytes, is significant for translation because of their ability to be harvested autologously and allogeneically without further damaging diseased joints that require

treatment. For example, in a recent study using bioactive factor-stimulated constructs derived from costal cartilage, the Yucatan minipig was used as a model for temporomandibular joint disc cartilage repair [23]. Similarly, several researchers are performing *in vivo* meniscus and articular cartilage repair in the minipig [478-480]. Here, constructs were generated from the costal cartilage of the Yucatan minipig and stimulated during the maturation stage. Similar to constructs derived from bovine articular chondrocytes, compressive stiffness and tensile strength and stiffness of minipig-derived neocartilage significantly increased by 46%, 78%, and 78%, respectively, when FIS stress was applied. Although increases in shear modulus are similar between Phases I and II, aggregate modulus increases were larger in Phase I compared to Phase II. These differences are most likely due to changes in the ECM-producing capacity of the different cell types (i.e., articular vs. costal chondrocytes) when stimulated with FIS stress. For example, the increases in collagen are also different between the two phases. Despite these small differences, these are significant results because, 1) FIS stress has not been previously investigated in the costal cartilage cell source, and 2) the Yucatan minipig is a widely used preclinical model. Previous studies have also corroborated the findings shown here that FIS stress stimulation, as well as tensile stimulation, of self-assembled constructs can be translated across cell passage numbers and species (e.g., bovine and human articular chondrocytes) [207, 450]. Although additional studies examining FIS stress during the maturation stage in human costal chondrocytes will eventually need to be performed, the work done here shows promise that use of FIS stress on neocartilage would be feasible and beneficial across different cell passage numbers, cell sources, and cell types.

Previously identified cocktails of bioactive factors have been shown to individually improve functionality and morphology of neocartilage constructs [25, 83], but their interactions with FIS stress have not been previously investigated. This is of scientific interest because healthy cartilage, whether native or engineered, is dependent on a variety of signals which include both mechanical and biochemical cues [33, 83, 156, 339, 399, 457, 464-467]. Phases III

and IV relied on a plethora of past studies which used bioactive factors, employing the regimens described here, to improve the functional properties of self-assembled cartilage compared to nonstimulated controls [83, 139, 212, 339, 464-466]. Here, the addition of bioactive factors (TGF-β1, C-ABC, and LOXL2) was investigated in combination with FIS stress stimulation to further improve the functional properties of neocartilage constructs and, eventually, keep constructs derived from high passage cells flat. Indeed, it was found that, similar to Phase II, increases were observed in Phase III when FIS stress was combined with bioactive factors, increasing compressive stiffness (by 48%) and tensile stiffness (by 94%). It appears that FIS stress dominates the functional increases seen in constructs regardless of bioactive factor stimulation. As previously shown [23, 25, 83, 201, 207, 212, 339, 355, 378], future studies should include a direct comparison between bioactive factor-stimulated and nonstimulated groups to ensure that the beneficial effects of bioactive factors are maintained in the Yucatan minipig costal cartilage source. The increases in mechanical properties seen here may be due to increased perfusion of growth factors in neocartilage by FIS stress, but this is unknown as the perfusion rates in FIS stress-stimulated neocartilage constructs have not been explored [450]. However, previous studies have shown that the primary cilia is implicated in both TGF-β signaling and FIS stress stimulation. Future studies should determine whether perfusion, primary cilia perturbation, or a combination is the exact cause of further improved functional properties of neocartilage constructs [469]. The findings of this study mirror the results of previous studies which used these bioactive factors in conjunction with other mechanical stimuli, such as tension and compression [201, 207]. For example, combination of passive axial compression and bioactive factors yielded significantly higher relaxation modulus values compared to bioactive factor-only controls [201]. Additionally, previous studies have shown that bioactive factors are an important element for maintaining mechanical robustness for highly passaged cells and large constructs [25, 212]. Thus, the combination of FIS stress and bioactive

factors is important when considering generation of self-assembled neocartilages larger than 5mm in diameter.

Toward addressing larger cartilage lesions, this study examined creation of large, flat, mechanically robust constructs generated from highly passaged costal chondrocytes stimulated with bioactive factors and FIS stress. This phase represents a significant step toward functional and translational improvements for implantation by increasing the tissue-engineered implant in size from 5mm diameter to 11x17mm, representing more than a 9-times increase in construct area. This increase in size also increased the number of cells needed by 7.5-times. Therefore, in Phase IV, in order to accommodate for the high number of cells needed (i.e., 15 million per construct), the number of passages costal chondrocytes undergo, compared to Phases II and III, was doubled from three to six. Although this may seem straightforward, as passage number increases, it has been shown that the cells undergo more dedifferentiation toward a fibroblastic phenotype [368]. Using the expansion and aggregate rejuvenation process described (i.e., no bioactive factors), constructs up to passage 5 have exhibited flat morphologies, but then started to display unwanted morphological characteristics at passage 7 (e.g., decreased diameter, biconcave structure) [25]. This same study further examined bioactive factor use, as described here, during self-assembly of small 5mm diameter constructs and noted additional increases in functional properties, especially for higher passage constructs, and maintenance of a flat morphology [25]. While 5mm diameter constructs remained relatively flat, larger constructs of 25mm diameter did not remain flat due to internal stresses through the actin cytoskeleton, applying forces to the ECM [212]. Previous studies noted that application of bioactive factors, cytochalasin D (an actin polymerization inhibitor), and mechanical confinement in the form of an agarose coverslip are necessary to maintain flatness [212]. Cytochalasin D was applied here in a similar regimen toward keeping constructs flat, but it has also been shown to recover primary cilia of chondrocytes after passaging [481], thus, potentially making cytochalasin D-treated cells here more sensitive to FIS stress to yield further increases in functional properties. Similarly,

this study showed that mechanical confinement in the form of the novel FIS stress device was necessary to keep constructs flat. As expected, the FIS stress system and other bioactive factors also maintained the functional properties seen in earlier phases of this study. Thus, the combination of highly passaged cells with FIS stress and bioactive factors was successful in generating mechanically robust neocartilage constructs toward improving the range of cartilage lesion indications that can be potentially addressed by self-assembled neocartilage.

This work represents substantial progress toward generating a tissue-engineered neocartilage solution for addressing articular cartilage lesions. Using FIS stress, functional properties, such as aggregate modulus and collagen content, of constructs derived from primary bovine articular chondrocytes and passaged and rejuvenated minipig costal chondrocytes were improved toward native tissue values. For example, compressive aggregate modulus values reported here for neocartilages range from approximately 120-600 kPa. These values are within the range reported for native articular cartilages (250-1400 kPa) [446-448]. Additionally, bioactive factors have been previously used in conjunction with other forms of mechanical stimuli (i.e., passive axial compression and tension), but have not been examined in combination with FIS stress, as performed here. The addition of bioactive factors with FIS stress stimulation did not adversely affect functional improvements when compared to bioactive factor-only controls. Finally, combining all the previous phases, large constructs derived from highly passaged costal chondrocytes exhibited mechanical robustness and flatness, important translational features. Combined, the four phases of this study represent significant steps toward generating mechanically robust, flat, large neocartilage constructs necessary for a wide range of preclinical animal studies, and, eventually, human clinical studies for various articular cartilage indications.

Chapter 9: Isolation and Characterization of Porcine Macrophages and their Inflammatory and Fusion Responses in Different Stiffness Environments[9]

Abstract

Evaluating the host immune response to biomaterials is an essential step in the development of medical devices and tissue engineering strategies. To aid in this process, *in vitro* studies, whereby immune cells such as macrophages are cultured on biomaterials, can often expedite high throughput testing of many materials prior to implantation. While most studies to date utilize murine or human cells, the use of porcine macrophages has been less well described, despite the prevalent use of porcine models in medical device and tissue engineering development. In this study, we describe the isolation and characterization of porcine bone marrow- and peripheral blood-derived macrophages, and their interactions with biomaterials. We confirmed the expression of the macrophage surface markers CD68 and F4/80 and characterized the porcine macrophage response to the inflammatory stimulus, bacterial lipopolysaccharide. Finally, we investigated the inflammatory and fusion response of porcine macrophages cultured on different stiffness hydrogels, and we found that stiffer hydrogels enhanced inflammatory activation by more than two-fold and promoted fusion to form foreign body giant cells. Together, this study establishes the use of porcine macrophages in biomaterial testing and reveals a stiffness-dependent effect on biomaterial-induced giant cell formation.

[9] **Chapter published as:** Meli, V.S., Donahue, R.P., Link, J.M., Hu, J.C., Athanasiou, K.A., Liu, W.F. Isolation and characterization of porcine macrophages and their inflammatory and fusion responses in different stiffness environments. *Biomaterials Science*, November 2021, 9(23): 7851-7861.

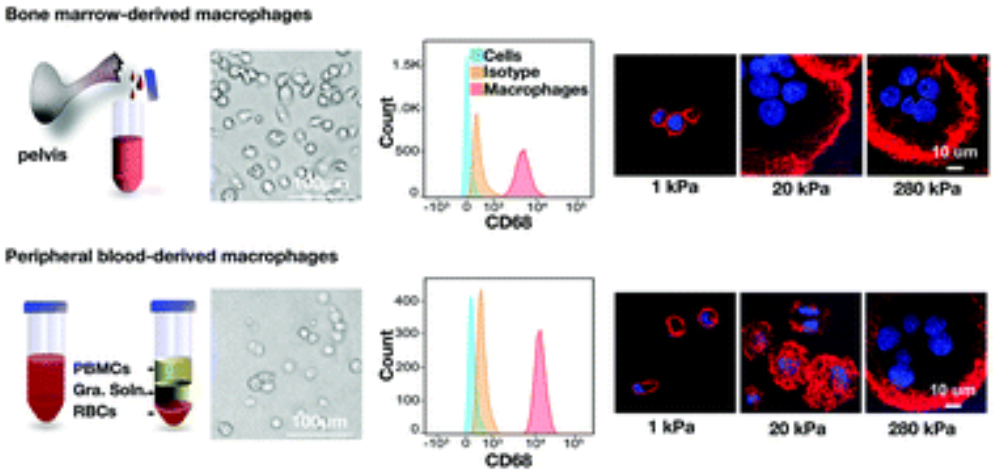

Introduction

Porcine models are essential tools for the translation of tissue engineering and regenerative medicine research to the clinic [425, 482]. Their use has increased over the years, particularly for musculoskeletal tissue engineering applications, where it is critical for the animal model to mimic the biomechanical environment present in humans [425]. Despite some anatomical and morphological differences, porcine and human musculoskeletal tissues have many similarities in their mechanical loading profiles and biochemical properties, and, thus, porcine models have been widely chosen for studies of the cartilages, ligaments, and bones in joints such as the knee and temporomandibular joint [483, 484]. In the context of injury response, porcine and human wound healing are also thought to occur through similar processes, and responses to wound therapies in porcine models are reported to be 78% consistent with responses in humans [485, 486]. While there have been many advances in the field of tissue engineering, one of the major challenges hindering their success has been adverse innate and adaptive immune responses that result from implantation of engineered materials. The host immune response involves an acute inflammatory response followed by tissue fibrosis around the implant or infiltrating the construct, which can lead to altered function and device failure [487-490]. Therefore, the ability to evaluate immune responses to engineered tissues in a porcine model is critical for developing new tissue-engineered and regenerative therapies

Cell culture platforms are a valuable tool for assessing the host response to biomaterials or implants, bridging the design and fabrication of new materials with *in vivo* pre-clinical studies. *In vitro* culture of cells on biomaterials can be completed more rapidly and at a higher throughput compared to *in vivo* studies, where materials are implanted into animals, often individually, and the inflammatory or fibrotic response is assessed at various time points afterwards. Culture models also allow the study of basic mechanisms underlying immune cell-biomaterial interactions, which can lead to new immunomodulatory strategies. Previous work from our laboratory and others has shown a robust correlation between the extent of inflammatory cytokine secretion by macrophages cultured on biomaterials with the inflammatory responses elicited by these materials after implantation in animals [491-493]. These include studies evaluating libraries of new chemistries [491] as well as of materials with different physical and topographical properties [492, 493], suggesting that the methods are broadly applicable to a wide range of materials. However, these findings have largely been established using rodent models, where material implantation and biocompatibility studies are common and immune cells are easily accessible through bone marrow harvest. To date, few studies have used cells derived from large animals, such as porcine sources, despite the established use of these models in tissue engineering.

Biomaterial stiffness has become widely appreciated for its role in regulating many cellular behaviors in healthy and pathological states [494-497], including immune activation and foreign body responses. In the context of medical devices, compliance mismatch between the implant and the surrounding tissue is thought to be a major driver of the foreign body response [498, 499]. At the cellular level, our laboratory has demonstrated that macrophages cultured on soft fibrin or polyacrylamide (PA) hydrogels suppress the inflammatory activation compared to stiffer PA, polystyrene, or glass [492, 500]. Similar observations were made when the macrophages were cultured on soft PEG hydrogels, leading to significantly less expression of tumor necrosis factor (TNF-α), interleukin 1 beta (IL-1β), and interleukin 6 (IL-6) [501].

Furthermore, subcutaneous implantation of softer hydrogels recruited significantly fewer macrophages to the implant surface and led to a less severe foreign body reaction when compared to a stiff hydrogel [492, 501], suggesting that stiffness can regulate tissue repair responses *in vivo*. Taken together, material stiffness can play a critical role in immune cell activation and foreign body response to biomaterials, but the role of stiffness in regulating porcine immune cells has not yet been examined.

Here, we describe the isolation and characterization of porcine bone marrow-derived and peripheral blood-derived macrophages, as well as their responses in different stiffness environments. We identify candidate bones to consistently isolate maximal number of cells and confirm the expression of commonly expressed macrophage cell surface markers after differentiation including CD68 and F4/80. Both bone marrow-derived and peripheral blood-derived macrophages demonstrated an increased secretion of TNF-α with increased lipopolysaccharide (LPS) doses, as well as characteristic changes in inflammation-associated cell shape. Finally, we investigated the role of substrate stiffness on porcine macrophage behavior and found that culture on stiffer substrates increases their inflammatory activation, similar to our previous studies using murine and human cell systems [492, 500]. Interestingly, fusion to foreign body giant cells was also enhanced in higher stiffness environments, specifically for bone-marrow derived macrophages. Together, this study will aid in the evaluation of new biological and synthetic biomaterials for tissue engineering.

Results

Isolation of porcine bone marrow- and peripheral blood-derived macrophages

A schematic for isolation of bone marrow-derived and peripheral blood-derived macrophages is shown in Figure 9-1. To determine the optimal method of harvesting macrophages from porcine bone marrow, different bones including the radius, ulna, humerus, scapula, and pelvis were harvested from the minipig and cleaned of muscle and soft tissues to harvest bone marrow cells.

Quantities of bone marrow cells harvested were analyzed to determine the ideal bones to use for future harvest. We found that the pelvis yielded more than five times greater number of cells compared to any of the other bones tested and proceeded with isolating cells from only the pelvis in subsequent harvests. The cells were cultured in differentiation media containing recombinant porcine granulocyte macrophage colony stimulating factor (rpGM-CSF) to differentiate monocytes to macrophages, which are adhesive and can be isolated by removing nonadherent cells [502]. We also attempted culture with human macrophage colony stimulating factor (hM-CSF)-containing media, as has been previously reported [503], but found that cells did not adhere to the tissue culture plate in this culture medium. We isolated ~28 x 10^7 bone marrow cells, which yielded ~64 x 10^6 macrophages after differentiation, and therefore, approximately 20% of the cells differentiated over seven days. We further confirmed this differentiation efficiency in two subsequent minipig donors, totaling three donors for later experiments. In conclusion, pelvises were determined to be the optimal bone for efficient isolation of macrophages, and rpGM-CSF was appropriate for cell differentiation.

To isolate peripheral blood mononuclear cells (PBMCs), blood was processed within 24 h of collection and stored in either sodium ethylenediaminetetraacetic acid (EDTA) or sodium citrate as anti-coagulants. PBMCs were then isolated using Sepmate^{TM}-50 tubes for density gradient centrifugation. The cells were cultured in rpGM-CSF-containing media for seven days with fresh media added on day 3. We isolated ~10 x 10^7 PBMCs from 75 ml blood, which yielded ~14 x 10^6 macrophages after 7 days of differentiation. Further, we found that the blood stored in sodium citrate as an anti-coagulant resulted in less red blood cell contamination (Supplementary Figure 9-1), and, thus, we continued using sodium citrate for future isolations.

Finally, we found that it was possible to freeze down differentiated macrophages for later experimentation, alleviating the need to perform experiments on the day of cell harvest. Of note, we found that bone marrow cells that were frozen prior to differentiation, in either 90% heat-inactivated fetal bovine serum (FBS) and 10% dimethyl sulfoxide (DMSO) or 45% FBS and 10%

DMSO, did not survive thawing and failed to adhere to the plate. However, both peripheral blood- and bone marrow- derived cells that had been cultured in differentiation media for seven days were successfully frozen using media supplemented with 20% FBS and 10% DMSO and exhibited greater than 90% viability upon thawing. Together, these results describe a method to isolate and store porcine macrophages for downstream biological studies.

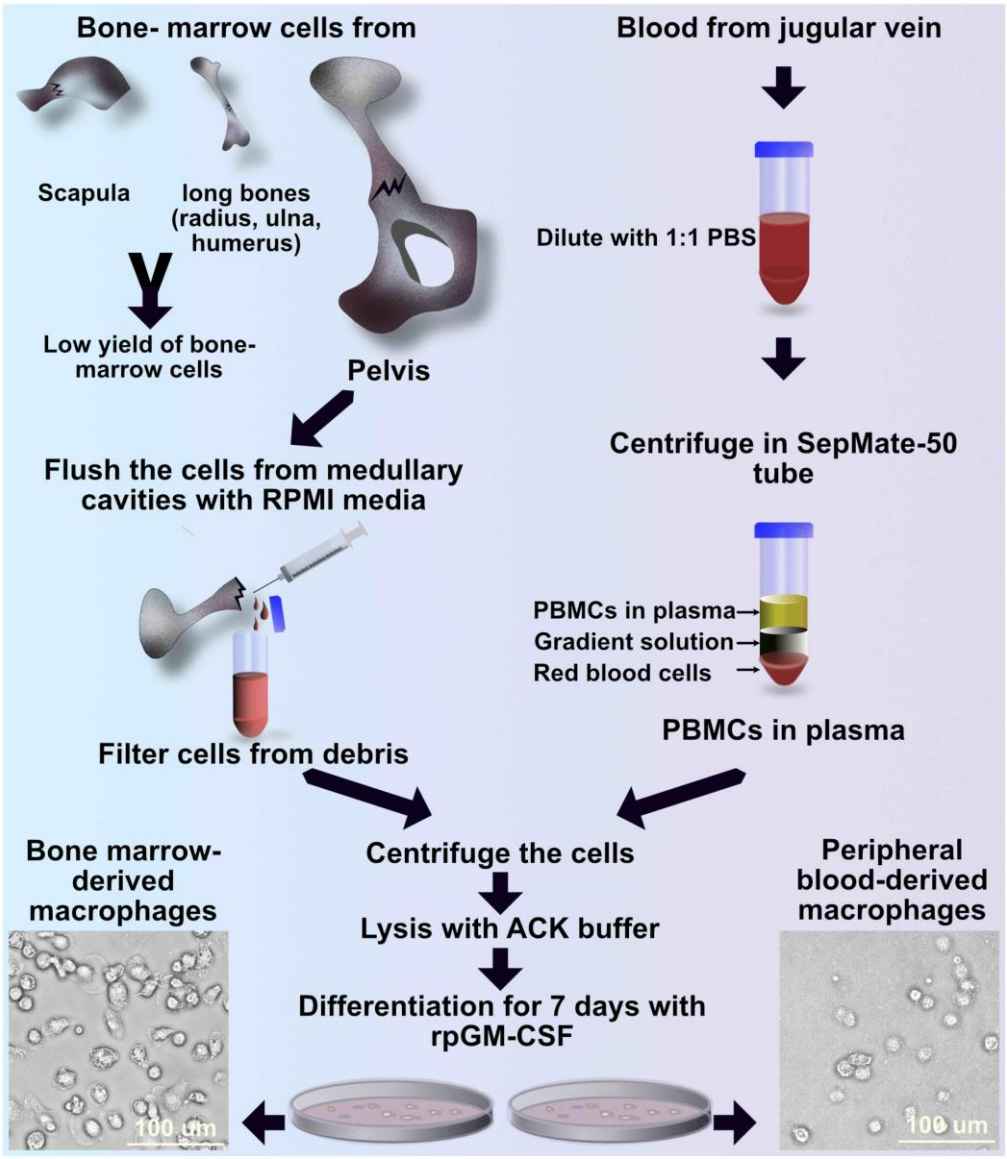

Figure 9-1: Schematic representation of the protocol used to isolate and differentiate bone marrow- and peripheral blood-derived macrophages.
Bone marrow-derived macrophages were isolated from the pelvises and differentiated for seven days using rpGM-CSF. Peripheral blood was used to isolate PBMCs using SepMate^{TM}-50 tube with density gradient solution. Isolated PBMCs were differentiated for seven days using rpGM-CSF.

Porcine macrophages express F4/80 and CD68 on the cell surface

Following differentiation, macrophages were dissociated from the tissue culture plate for further analysis. The transmembrane protein cluster of differentiation 68 (CD68) is a marker highly expressed by macrophages and other mononuclear phagocytes, and it is often used to detect macrophages by flow cytometry and immunostaining [504, 505]. Flow cytometry was performed to evaluate CD68 expression in porcine macrophages using a porcine-specific CD68 antibody, clone BA4D5 [506]. Staining the cells with BA4D5 antibody after 7 days of differentiation showed substantial CD68 staining in both bone marrow-derived and peripheral blood-derived macrophages (Figure 9-2A) compared to isotype control. We confirmed the protein expression of CD68 by immunofluorescence (Figure 9-2C-D) in the bone marrow- and peripheral blood-derived macrophages. Another marker, F4/80 protein, which is encoded by the *ADGRE1* gene, has been widely used as a macrophage marker in mice. However, recent RNA-seq analysis identified *ADGRE1* gene expression in monocyte-derived and alveolar macrophages of eight different mammalian species including pig [507]. Therefore, we confirmed *ADGRE1* gene expression by quantitative real time polymerase chain reaction (qRT-PCR) (Figure 9-2B) and expression of F4/80 protein in both bone marrow and peripheral blood-derived porcine macrophages by immunostaining (Figure 9-2C-D). Secondary antibody only controls showed no positive staining (Supplementary Figure 9-2). Together, our data show that porcine peripheral blood- and bone marrow-derived macrophages express CD68 and F4/80, two well-documented macrophage-specific markers.

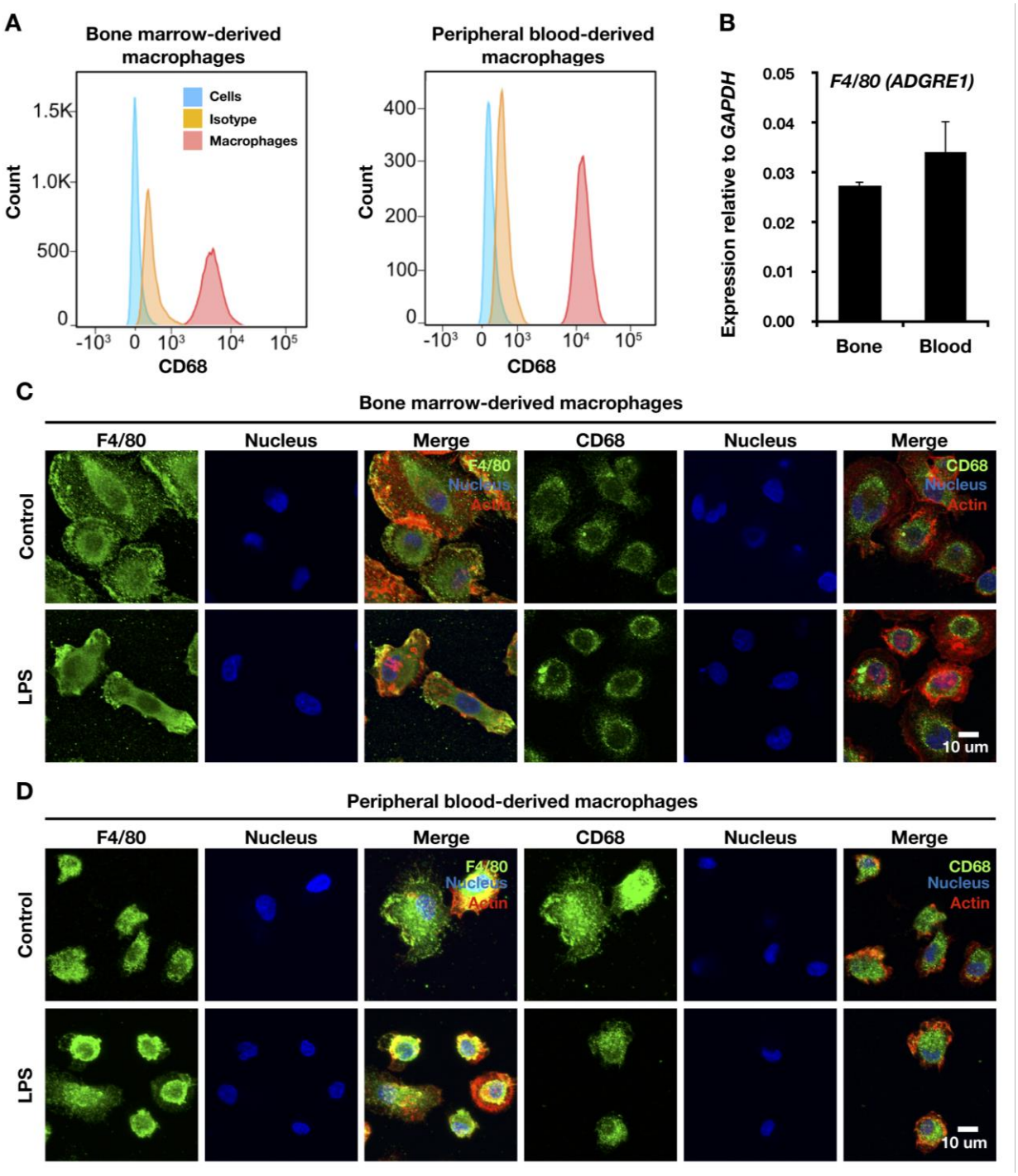

Figure 9-2: Bone marrow- and peripheral blood derived-macrophages express CD68 and F4/80 upon differentiation.

(A) Representative flow cytometry histograms with unstained macrophages in light blue curves, isotype controls indicated using orange, and CD68 with red curves for bone marrow- (left) and peripheral blood-derived (right) macrophages after 7 days of differentiation using rpGM-CSF on tissue culture-treated polystyrene. (B) Expression of *ADGRE1* (F4/80) relative to *GAPDH* assessed by quantitative PCR in bone marrow- and peripheral blood-derived macrophages after 7 days of differentiation. The values are the mean ± SEM from three porcine donors. Immunofluorescence confocal images of F4/80 (left) and CD68 (right) of bone marrow- (C) and peripheral blood-derived macrophages (D) after 24 h adhesion and 6 h stimulation with LPS.

Porcine macrophages respond to LPS and increase the expression of inflammatory genes.

To demonstrate the effect of inflammatory stimuli on the differentiated macrophages, cells were seeded onto glass or polystyrene for 24 h, and then stimulated with varied concentrations of bacterial LPS, a potent agonist of Toll-like receptor 4 (TLR-4), for 6 h. We found that both bone marrow- and peripheral blood-derived macrophages showed dose-dependent secretion of the inflammatory cytokine TNF-α in response to LPS (Figure 9-3A). Expression of inflammatory genes *iNOS, TNFα* and *IL6* in bone marrow- and peripheral blood-derived macrophages also increased compared to unstimulated cells (Figure 9-3B-C). In bone marrow-derived macrophages, *iNOS* expression was 1.25 fold higher than the unstimulated cells with a p- value of 0.001. Expression of other inflammatory genes *TNFα* and *IL6* were at least 1.65 fold higher, and significantly different, compared to the unstimulated cells, with a p-value of 0.026 and 0.027, respectively. In blood-derived macrophages *iNOS, TNFα,* and *IL-6* expression were at least 1.8 fold higher, and significantly different, than the unstimulated cells with p-values of 0.003, 0.04 and 0.05, respectively. In addition, we performed immunostaining using an antibody targeting the inflammatory marker inducible nitric oxide synthase (iNOS) (Figure 9-3C). We chose iNOS as an inflammatory marker in our study. iNOS is an enzyme that synthesizes nitric oxide from L-arginine. Its expression is enhanced with M1 (LPS and IFNγ) stimulation in mouse and rat macrophages and plays a critical role in systemic inflammation and sepsis [508], although the levels have been reported to be varied in porcine models [509-511]. Nonetheless, detection of iNOS is feasible and valuable because it is intracellular across different cell types [512-514]. On the contrary, TNF-α and IL-6 are secreted cytokines, and their levels as detected through immunofluorescence staining may not represent the true expression. We observed the expression of iNOS, both in unstimulated and LPS stimulated macrophages, suggesting that this marker does not show changes in inflammation at this time point (6 h post stimulation). Together, our data show that inflammatory cytokine gene expression and protein secretion can be used to evaluate responses to agonists such as LPS.

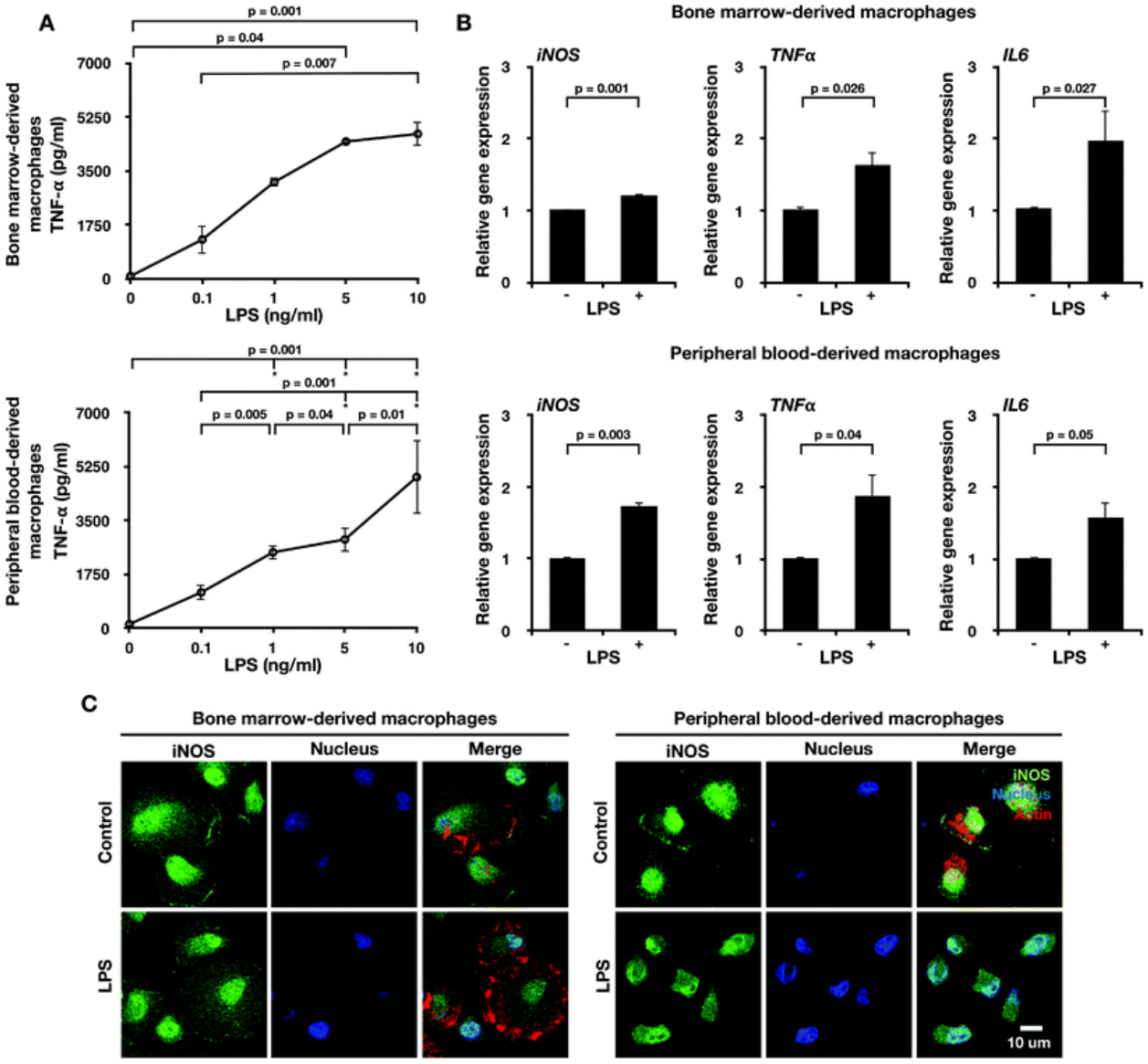

Figure 9-3: Differentiated bone marrow- and peripheral blood-derived macrophages are activated upon LPS stimulation.

(A) Secretion of TNF-α by bone marrow- (top) and blood- (bottom) derived macrophages after 24 h of adhesion and 6 h of stimulation with increasing concentrations of LPS. (B) Relative expression of *iNOS, TNFα* and *IL6* genes in bone marrow- and peripheral blood-derived macrophages when stimulated with 10 ng/ml LPS, analyzed by qRT-PCR, and normalized to M0 (no LPS) condition. (C) Immunofluorescence confocal images of iNOS in bone marrow- and peripheral blood-derived macrophages cultured on glass for 24 h and stimulated with LPS for 6 h. The values are the mean ± SEM from three donors. Statistics: p values are depicted in the graph for each comparison, assessed by one-way ANOVA with Tukey's multiple comparisons for LPS titration experiment and two-tailed Student's t-test for qRT-PCR analysis.

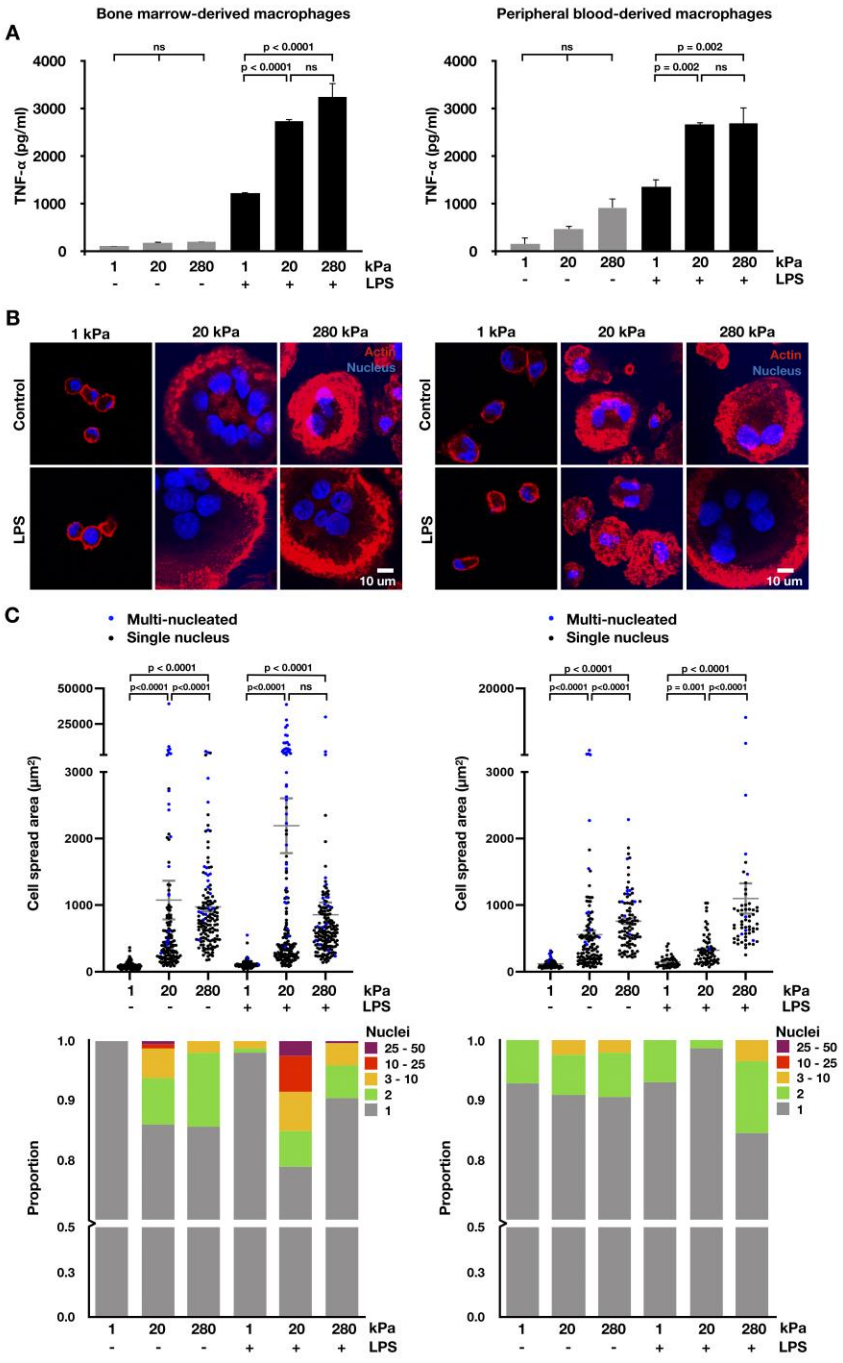

Figure 9-4: Substrate stiffness enhances inflammatory activation and fusion of macrophages.
(A) Secretion of TNF-α by bone marrow- (left) and peripheral blood- (right) derived macrophages after 24 h of adhesion to PA gels of varying stiffness and 6 h of stimulation with 10 ng/ml LPS. (B) Immunofluorescence confocal images of F-actin (phalloidin, red) and nuclei (blue) in bone marrow- and peripheral blood-derived macrophages cultured on PA gels of varying stiffness for 24 h and stimulated with 10 ng/ml LPS for 6 h. The values are the mean ± SEM from three donors. Statistics: One-way ANOVA with Tukey's multiple comparisons test was used, and the determined p value is reported in the graph. (C) Cell spread (top) and proportion of multinucleated cells (bottom) in bone marrow-derived macrophages (left) or peripheral blood-derived macrophages (right) cultured on PA gels of different stiffness. Each condition had 50-100 cells analyzed. Statistics: For the cell spread, the determined p value is reported in the graph, assessed by Kruskal-Wallis test with Dunn's multiple comparisons. ns: not significant.

Substrate stiffness influences porcine macrophage inflammatory activation and fusion

Our previous work has shown that culture of murine and human macrophages on stiffer substrates enhances their inflammatory activation, whereas culture on soft substrates reduces their response to LPS [492, 500]. To examine whether stiffness also plays a role in the inflammatory activation in porcine macrophages, we cultured bone marrow- and peripheral blood-derived macrophages on PA gels with stiffnesses of 1, 20, or 280 kPa, coated with 20 □g/ml of fibronectin. After 24 h of culture, cells were stimulated with 10 ng/ml LPS for 6 h, and the supernatants were collected and analyzed for TNF-α secretion. Irrespective of the PA gel stiffness, LPS stimulation enhanced the section of TNF-α secretion. Macrophages cultured on 20 and 280 kPa PA gels and stimulated with LPS, secreted at least two-fold higher inflammatory cytokine TNF-α compared to the cells cultured on soft (1 kPa) PA gels ($p \leq 0.002$) (Figure 9-4A). However, TNF-α secretion from cells cultured on 20 kPa was not significantly different from the secretion by cells on 280 kPa PA gels. These results are consistent with what we have previously observed in human and murine macrophages [492].

To evaluate the effects of stiffness on cell morphology, we stained cells with phalloidin to visualize their actin cytoskeleton. We found that macrophages cultured on 1 kPa PA gels were rounded with intense cortical actin staining, whereas cells cultured on 20 and 280 kPa exhibited significantly higher spread area compared to cells cultured on 1 kPa both with and without LPS stimulation, with cytoplasmic actin staining, along with membrane ruffles. (Figure 9-4B-C). Analysis of spread area of cells cultured on different stiffness PA gels showed heterogeneity with respect to cell size, particularly for the cells cultured on 20 and 280 kPa gels (Figure 9-4C). In addition, LPS stimulation did not significantly increase the cell area of bone marrow-derived and peripheral blood-derived macrophages on any of the stiffness tested (Figure 9-4C). Interestingly, we also observed a striking increase in cell fusion, with the presence of many giant cells containing up to 50 nuclei on 20 and 280 kPa, whereas greater than 95% of cells on 1 kPa surfaces remained as single cells, although sometimes clustered together (Figure 9-4B-C).

Multinucleated giant cells were observed in both bone marrow-derived and peripheral blood-derived macrophages, although giant cells with two or more nuclei were more abundant in bone marrow-derived macrophages compared to peripheral blood-derived macrophages (Figure 9-4B-C). In addition, LPS stimulation enhanced cell fusion, increasing the number of nuclei per giant cell on 20 kPa, but not on 280 kPa, in bone marrow-derived macrophages, and on 280 kPa, but not 20 kPa, in peripheral blood-derived macrophages. The fusion responses may at least in part explain the increases in cell area, since the well spread cells tended to have multiple nuclei (indicated by the blue dots in the cell area plot). Together, these data not only show that increased substrate stiffness enhances the inflammatory response of porcine macrophages to LPS, similar to human and murine macrophages, but also reveal that stiffness causes an increase in cell fusion and giant cell formation.

Discussion

Large animal models have been increasingly used for medical device development, tissue engineering, and regenerative medicine [425, 515]. Porcine models in particular offer better homology with humans in terms of their anatomy and biomechanics of musculoskeletal tissues and are also thought to exhibit more similar immune responses to wound healing therapies [486, 516], However, large animals are costly, particularly for long term studies, and *in vitro* testing can offer a lower cost and expedient alternative for screening materials and developing tissue engineering strategies prior to studies in animals. This motivated our current study to isolate porcine macrophages and to characterize their responses to different biomaterial environments. We determined the pelvis yields the highest number of bone marrow cells and differentiated macrophages, and optimal differentiation occurs with rpGM-CSF. While L929–conditioned media, human M-CSF, and porcine GM-CSF have all been used as differentiating factors for porcine macrophages [502, 503, 517], we found that recombinant human M-CSF did not result in monocyte differentiation to macrophages, and cells remained in suspension, whereas rpGM-

CSF yielded many adherent macrophages. After differentiation for seven days, we analyzed the macrophages for the expression of CD68 and F4/80 and found that both markers were highly expressed. While F4/80 (*ADGRE1*) is often thought to be a mouse-specific macrophage marker, a recent study also reported its expression in other species including porcine sources [507]. Taken together, we successfully isolated and differentiated bone marrow cells and PBMCs to bone marrow- and peripheral blood-derived macrophages, respectively.

Inflammation is a key aspect of the tissue repair process. It is caused by injury to the tissue and presence of a foreign biomaterial and is also needed to initiate wound healing responses. However, chronic inflammation is associated with poor healing and fibrosis [496]. We tested the inflammatory response to LPS, a bacterial component and agonist of TLR4, and found that bone marrow- and peripheral blood-derived porcine macrophages responded to LPS by secreting the inflammatory cytokine TNF-α, consistent with an earlier study [502]. In addition, we found a dose-dependent increase and saturation of the response at approximately 5 ng/ml of LPS. We also observed that LPS induced expression of inflammatory genes including *iNOS, IL6, and TNFα,* although iNOS protein analyzed by immunofluorescence staining appeared to be expressed regardless of LPS stimulation. Dynamic changes in nitric oxide (NO) synthesis has been observed in porcine macrophages in response to LPS [510]. Another study also showed that regardless of *iNOS* gene expression after LPS treatment, cells did not produce any detectable NO or iNOS protein, contrary to what we show here [518, 519]. Using TNF-α secretion to measure inflammation, we also examined porcine macrophage response to substrate stiffness. We found that porcine macrophages stimulated with LPS cultured on stiffer substrates secreted significantly higher TNF-α levels than the softer substrate, with cells cultured on 1 kPa exhibiting significantly less inflammation compared to cells on 20 or 280 kPa, consistent with what we have observed in human and murine macrophages [492].

Macrophages often exhibit characteristic cell shape changes in response to their biochemical and biophysical environment, and we found that porcine macrophages indeed

exhibit a flattened, “fried-egg” morphology, when stimulated with LPS. In addition, we observed a profound increase in cell fusion and the presence of multi-nucleated giant cells, particularly in bone marrow-derived macrophages cultured on stiffer PA hydrogels, which was not observed in cells cultured on soft PA hydrogels. Fusion responses are common during the foreign body response to biomaterial implant, during which macrophages can exhibit “frustrated phagocytosis” as they are unable to engulf large materials [520]. *In vitro* studies have demonstrated that macrophage fusion requires stimulation with IL-4 and CCL2/MCP-1 [521-523]. A recent study has also shown that this response occurs in different biomaterial contexts [524]. Here, we observed fusion of up to 50 cells after only 24 h of culture on stiffer PA hydrogels in the presence of rpGM-CSF and a further increase with LPS stimulation. Interestingly, fusion occurred the most in cells cultured on 20 kPa hydrogels, to a lesser extent on 280 kPa, and was nearly absent in cells on 1 kPa in bone marrow-derived macrophages. Moreover, while fusion was less prominent in peripheral blood-derived macrophages, the most occurred in cells cultured on 280 kPa gels. The differential response between bone marrow- and peripheral blood-derived macrophages may be caused by differences in cell origin, and thus diverse experiences in their respective mechanical environments [28, 525]. Nonetheless, fusion of cells is thought to require fusogens, cell surface proteins such as integrins and ion channels, as well as cytoskeletal rearrangements [526-531], and further studies will be needed to elucidate the molecular underpinnings of stiffness-dependent porcine macrophage fusion.

In summary, we describe here an efficient method to isolate porcine macrophages from peripheral blood and bone marrow and characterize their response to LPS and the stiffness of the environment. Since macrophages are recruited abundantly to biomaterial implants and tissue-engineered constructs, it is crucial to understand the macrophage response to the integrative effects of chemical and physical stimuli. The findings from this study will assist in studying the immunomodulatory properties of new tissue-engineered constructs and biomaterials used in medical devices.

Methods

Isolation of bone marrow- and peripheral blood derived-macrophages and differentiation

Pelvis, scapula, radius, ulna, and humerus from 5 to 8 month old Yucatan minipigs were obtained within 6 h of postmortem. The bones were cleaned of muscle and other soft tissues. Using a sterile chisel and hammer, the bone marrow was exposed and flushed with phosphate buffered saline (PBS) or un-supplemented 1X RPMI-1640 media. The cells were then passed through a 70 µm filter, centrifuged, rinsed with PBS, treated with ACK lysing buffer to remove any red blood cells, and subsequently washed with PBS. Cells were then seeded at approximately 10 million cells per 100 x 25 mm petri dishes or 0.176 million per cm^2 in differentiation culture media composed of RMPI-1640 (Fisher Scientific), L-glutamine (Fisher Scientific), and 1% penicillin-streptomycin (Fisher Scientific), supplemented with 10% FBS and 20 ng/mL rpGM-CSF (R&D Systems) or hM-CSF (PeproTech) to differentiate cells to macrophages. Cells were fed with the same media on day 3 and dissociated from the culture plate on day 7 for experiments or frozen down in 1X RPMI media with 20% FBS and 10% DMSO for future use.

Blood from the jugular vein was collected in sodium citrate or sodium EDTA as an anti-coagulant and stored at 4° C until use. The PBMCs from the blood were isolated by density gradient centrifugation using SepMate™ -50 tubes (Stem Cell Technologies) following the manufacturer's protocol. The isolated PBMCs were incubated with ACK lysing buffer to remove red blood cells and subsequently washed with PBS. Finally, the cells were resuspended and differentiated using the differentiation media and protocol described above.

Flow cytometry

After 7 days of differentiation with rpGM-CSF, the cells were dissociated from the plate using dissociation buffer (ThermoFisher) and blocked using anti-CD16 (clone 2.4G2, Tonbo Biosciences) on ice. The cells were stained with mouse anti-pig macrophage antibody, clone

BA4D5, specific for porcine CD68 (Bio-Rad) and IgG2b isotype control. The unbound and excess antibody was washed thoroughly using 1X PBS. Flow cytometry was performed on a BD LSRII flow cytometer using BD FACSDiva software (BD Biosciences). Data acquisition was performed until at least 10,000 events were collected, and post processing of the data was performed in FlowJo (Tree Star).

Assessment of cytokine secretion by ELISA and immunofluorescence staining of the cells

After 7 days of cell culture with rpGM-CSF, the cells were dissociated from the plate using cell dissociation buffer and seeded on tissue culture polystyrene or cover glass. Cells were seeded at a density of 0.1 million cells/well in 24 well plates. After 24 h of culture, the cells were stimulated with 10 ng/ml ultrapure LPS (InvivoGen). Supernatants were collected 6 h after stimulation for assessment of cytokine secretion by enzyme-linked immunosorbent assay (ELISA) following the manufacturer's protocol (R&D Systems). Further, the cells were immediately fixed in 4% PFA (Electron Microscopy Sciences) for 10 min at room temperature (RT). The cells were washed 3 times with PBS and permeabilized using 0.3% Triton X-100 in PBS. Samples were then blocked with 2% bovine serum. The samples were incubated in the following primary antibodies overnight at 4 °C: F4/80 (Thermo Fisher Scientific, BM8) or CD68 monoclonal antibody (KP1; MA5-13324, Thermo Fisher Scientific). Cells were then washed with 2% bovine serum albumin (BSA) in PBS and incubated with secondary antibody anti-rat IgG-488 (for F4/80) and anti-mouse Alexa fluor 488 (for CD68) at RT for 1 h. Nuclei and actin were stained using Hoechst and Alexa fluor 594-phalloidin (Invitrogen), diluted in 2% BSA in PBS for 30 min at RT. Finally, the cells were washed with PBS and mounted on glass slides using Fluoromount G (Southern Biotech). Images were acquired at 40X using an Olympus FV3000 laser scanning confocal microscope.

Polyacrylamide hydrogel synthesis

PA hydrogels with tunable mechanical properties were synthesized on glass coverslips according to the previously described protocol [532]. The PA coated glass coverslips were conjugated with 20 µg/ml fibronectin using sulfo-SANPAH (Thermo Scientific) overnight at 4°C. Cells were cultured for 24 h on the gel and stimulated with 10 ng/ml LPS for 6 h and the supernatant was collected for ELISA, and cells were fixed immediately for immunostaining.

RNA isolation, cDNA preparation, and qRT-PCR analysis

After the collection of supernatants, cells were lysed using TRI Reagent (Sigma), and RNA was isolated following the manufacturer's protocol. The pellet was briefly air-dried and the RNA was dissolved in DEPC treated water. cDNA was synthesized using the High Capacity cDNA Reverse Transcription Kit from Applied Biosystems (Cat. no. 4368814) with 1 µg of total RNA following the manufacturer's protocol. PerfeCTa® SYBR® Green SuperMix Reaction Mixes from QuantaBio was used for quantitative real-time PCR, and a total of 40 cycles were performed on Bio-Rad's CFX-96 real-time PCR system. Relative gene expression was analyzed by $2^{-\Delta\Delta CT}$ method, expressed relative to the housekeeping gene *GAPDH,* and normalized to the unstimulated condition. The primers used for qPCR in this study are in Supplementary Table 9-1.

Statistical analysis

One-way ANOVA with Tukey's *post hoc* test was used for bone marrow- and peripheral blood-derived macrophages to assess LPS dose response and the response to substrate stiffness. Student's *t*-tests were performed to compare the gene expression of inflammatory genes in bone marrow- and peripheral blood-derived macrophages. For cell spread, Kruskal-Wallis test with Dunn's multiple comparisons was performed for both bone marrow- and peripheral blood-derived macrophages. For all the statistical tests, p values less then or equal to 0.05 were

considered significant. The determined p value is reported in the graph for each comparison made. Values presented here are mean ± standard error of the mean (SEM).

Supplementary Materials

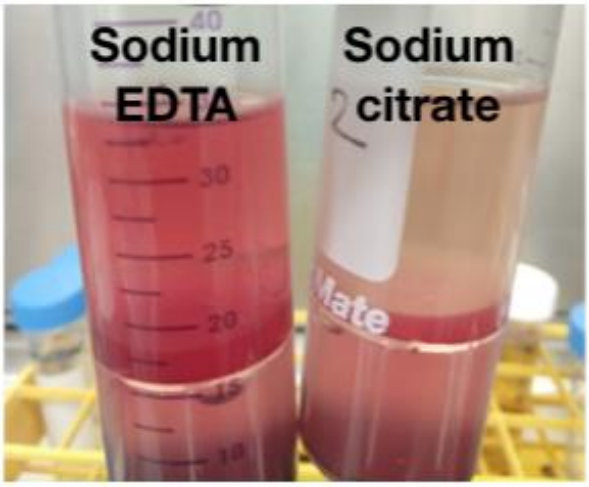

Supplementary Figure 9-1: Comparison of anti-coagulants.
Isolation of peripheral blood-derived macrophages from blood stored in sodium EDTA and sodium citrate.

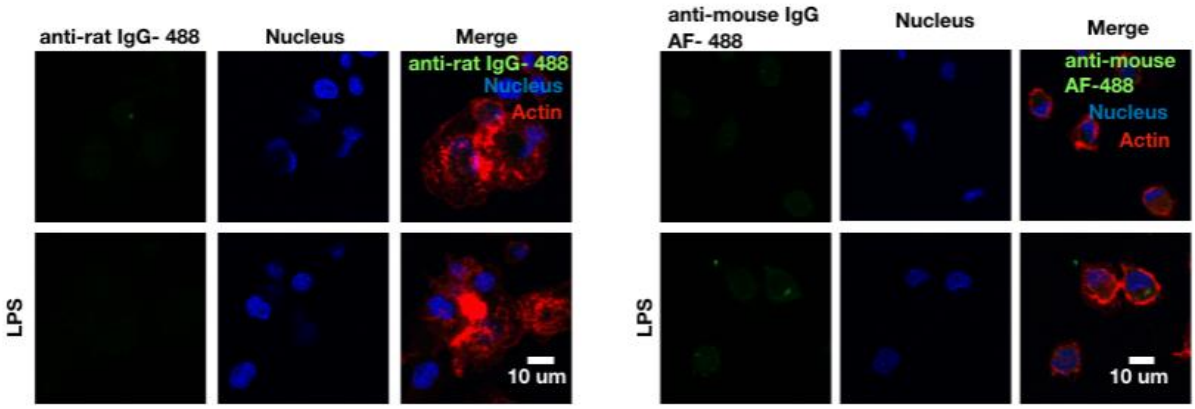

Supplementary Figure 9-2: Immunofluorescence confocal images of secondary antibodies stained for 1h in bone marrow-derived macrophages.
Cells were cultured on glass for 24 h and stimulated with LPS for 6 h.

Supplementary Table 9-1: List of primers used in this study for qRT-PCR analysis.

Gene Name	Forward primer (5'-3')	Reverse primer (5'-3')
TNF-α	TCCACCAACGTTTTCCTCAC	ATCATCCTTCTCCAGCTGGAAG
IL6	TGGCAGAAAAAGACGGATGC	TACTAATCTGCACAGCCTCGAC
iNOS	TGCCTTTGCTCATGACATCG	AGAGCTTGGGGATCTGAATGTG
ADGRE1	ATGTGTCCGGCATATGCAAC	TGGCAGGTTCTTGCAGATTG
GAPDH	TGGCAAAGTGGACATTGTCG	TCACCCCATTTGATGTTGGC

Chapter 10: Stiffness- and Bioactive Factor-Mediated Protection of Self-assembled Cartilage against Macrophage Challenge in a Novel Co-culture System[10]

Abstract

Tissue-engineered cartilage implants must withstand the potential inflammatory and joint loading environment for successful long-term repair of defects. The work's objectives were to develop a novel, direct cartilage-macrophage co-culture system and to characterize interactions between self-assembled neocartilage and differentially stimulated macrophages. In Study 1, it was hypothesized that the proinflammatory response of macrophages would intensify with increasing construct stiffness; it was expected that the neocartilage would display a decrease in mechanical properties after co-culture. In Study 2, it was hypothesized that bioactive factors would protect neocartilage properties during macrophage co-culture. Also, it was hypothesized that interleukin 10 (IL-10)-stimulated macrophages would improve neocartilage mechanical properties compared to lipopolysaccharide (LPS)-stimulated macrophages. As hypothesized, stiffer neocartilage elicited a heightened proinflammatory macrophage response, increasing tumor necrosis factor alpha (TNF-α) secretion by 5.47-times when LPS-stimulated compared to construct-only controls. Interestingly, this response did not adversely affect construct properties for the stiffest neocartilage but did correspond to a significant decrease in aggregate modulus for soft and medium stiffness constructs. Additionally, bioactive factor-treated constructs were protected from macrophage challenge compared to chondrogenic medium-treated constructs, but IL-10 did not improve neocartilage properties, although stiff constructs appeared to bolster the anti-inflammatory nature of IL-10-stimulated macrophages. However, co-culture of bioactive factor-treated constructs with LPS-treated macrophages reduced TNF-α secretion by over 4-

[10] **Chapter published as:** Donahue, R.P.,* Link, J.M.,* Meli, V.S., Hu, J.C., Liu, W.F., Athanasiou, K.A. Stiffness- and bioactive factor-mediated protection of self-assembled cartilage against macrophage challenge in a novel co-culture system. *Cartilage*, January 2022, 13(1): 19476035221081466. (* These authors contributed equally.)

times compared to macrophage-only controls. In conclusion, neocartilage stiffness can mediate macrophage behavior, but stiffness and bioactive factors prevent macrophage-induced degradation. Ultimately, this co-culture system could be utilized for additional studies to develop the burgeoning field of cartilage mechano-immunology.

Introduction

Key initial mediators of the immune response to tissue-engineered therapeutics are macrophages, which orchestrate the inflammatory and healing processes after injury, infection, and therapeutic implantation [27]. Macrophages can interact with tissue-engineered cartilages indirectly through cytokines released from those embedded in the synovium [533, 534]. Macrophages have also been observed to directly interact with chondrocytes in tissue engineering studies through the formation of granular pannus tissue in a cartilage defect [26, 535, 536]. Depending on the healing or disease state, the spectrum of macrophage behavior and phenotype can polarize toward proinflammatory or anti-inflammatory states [537]. Biochemical signals identified as having polarizing effects include, for example, tumor necrosis factor alpha (TNF-α) and lipopolysaccharide (LPS), an outer membrane component of Gram-negative bacteria [538-540]; these can activate macrophages toward a proinflammatory phenotype [27, 540]. Conversely, interleukin 10 (IL-10) or a combination of IL-4 and IL-13 can drive macrophages toward an anti-inflammatory phenotype [538, 541]. These phenotypic states are particularly important in cartilages such as hyaline articular cartilage, the knee meniscus, and the temporomandibular joint (TMJ) disc, which lack innate healing capacity [15, 16, 247]. Small defects that may emanate from wear-and-tear or traumatic injury can lead to inflammation and often result in osteoarthritis (OA), leading to pain and loss of joint function [359, 360]. According to the Centers for Disease Control, OA affects over 32 million people in the U.S. [361], and this number is projected to rise up to 60% in the next two decades [362]. To prevent

degenerative changes and to induce repair, these defects are often targets for surgical treatment, which alone can cause an immune response [247].

Current approaches for repair of cartilage defects do not provide robust long-term solutions, in part because they encourage the development of mechanically inferior repair tissue, which can lead to further degeneration, OA, and inflammation, further activating macrophages and the immune response. Inflammation and immune cell activation can induce chondrocyte apoptosis and/or hypertrophy, all of which can impede healing [359]. In native cartilages, proinflammatory macrophages have been shown to enhance cartilage inflammation and resulting degeneration [542]. However, anti-inflammatory macrophage states have been shown to prevent extracellular matrix (ECM) degradation and to promote healing [543, 544]. Characterization of these macrophage phenotypes in the context of tissue-engineered cartilages is limited. Thus, in addition to overcoming the challenge of mechanically inferior repair in future therapies, it is also necessary to consider the inflammatory immune response.

The effect of biophysical cues on macrophage polarization, such as material topography, applied mechanical forces, and ECM stiffness, has also been recently explored [28, 545, 546]. The ability of macrophages to sense biophysical cues, particularly ECM stiffness, has been shown to be a complex interplay between integrins, ion channels, transcriptional regulators, and the actin cytoskeleton [28, 492, 547]. Within the context of cartilage tissue engineering, ECM stiffness is of particular interest because repeated loading of the joint would require stiff neocartilage implants [199]. For example, transforming growth factor beta 1 (TGF-β1), chondroitinase ABC (C-ABC), and lysyl oxidase-like 2 (LOXL2) (termed TCL) treatment has been previously shown to increase matrix content and subsequent mechanical properties (e.g., stiffness) when applied to self-assembled neocartilage constructs [83]. Paradoxically, substrate stiffness has been previously shown to correlate positively with macrophage-induced proinflammatory responses [29]. For example, stiffer hydrogels elicit increased TNF-α and IL-1β levels [548], which can lead to breakdown of the ECM [542]. This finding is in direct

contradiction to the goal of cartilage tissue engineering, which is to produce neocartilage tissues with stiff ECM to withstand the loading environment of the joint. Characterizations investigating these conflicting conditions have not been previously performed on cartilage neotissue, representing a novel direction for advancing therapeutics for repair or replacement of articular cartilage. Thus, characterization of the interactions between macrophages and neocartilages meant to repair or replace native articular cartilage should be performed *in vitro* to inform strategies for more effective *in vivo* cartilage repair.

Toward translation of *in vitro* strategies for *in vivo* applications, tissue-engineered cartilages are fabricated with regulatory guidance in mind. For example, the Food and Drug Administration guidance on therapeutics intended to repair or replace articular cartilage of the knee indicates that therapeutics must be tested in a suitable large animal model [37]. Here, the Yucatan minipig was selected due to its similarities to humans in weight, anatomy, immunology, physiology, and bone biology [24, 459-462]. Additionally, costal chondrocytes from the rib cartilage have been previously identified as a cell source for tissue engineering applied to synovial joints since they can be harvested without further damaging diseased joints requiring treatment and can result in neocartilages mimicking articular cartilages of synovial joints [19, 144, 149, 150, 201, 369]. Specifically, our group can extensively passage chondrocytes and redifferentiate cells back toward a chondrogenic phenotype using an aggregate culture [25]. Subsequent self-assembly of the rejuvenated costal chondrocytes results in a robust neocartilage construct [17, 339]. These neocartilage constructs can then be used to investigate their interactions with macrophages.

Another reason to consider the immune response in developing new cartilage therapies is that allogeneic cell sources will be necessary to overcome the donor site morbidity and cell sourcing issues associated with autologous approaches [23, 26]. An allogeneic approach increases the risk of an immune response [549], despite various cartilages having been cited as immunoprivileged [15, 16, 26]. For example, recent work toward regeneration of the TMJ disc

cartilage has shown that an allogeneic approach elicits a minor local immune response through some positive immunohistochemical staining for T cells, B cells, and macrophages, without exhibiting any systemic effects [23]. The study also demonstrated excellent disc healing as evidenced by more complete defect closure, less OA on adjacent articulating condylar surfaces, and increased repair tissue robustness, when compared to empty defect controls [23]. However, given the likelihood that tissue-engineered cartilages will be produced from an allogeneic source, it is possible for an immune response to be mounted against the allogeneic implant, potentially affecting its mechanical integrity. Thus, this allogeneic approach warrants additional investigation. Within the field of cartilage tissue engineering, the potential interactions between neocartilage and immune system components have not been extensively studied.

In this study, a novel, direct co-culture system to explore the interaction between self-assembled neocartilage and macrophages is described. A direct co-culture system was selected to study the physical interaction between neotissue stiffness and cells that would likely occur *in vivo*, for example, through the formation of a granular pannus. Although synovial fibroblasts can also be found in the pannus tissue [550] and partially contribute to some of the inflammation seen during OA [551], in this study, macrophages were investigated as the immune cell of choice due to the well-established effects of biophysical cues, specifically ECM stiffness, on macrophage phenotype [28, 500, 552]. The global objective was to characterize the interaction between macrophages in differentially activated states and neocartilage constructs formed under a variety of conditions. The objective of Study 1 was to investigate the stiffness-mediated proinflammatory response of macrophages. It was hypothesized that stiffer constructs would polarize macrophages toward a proinflammatory phenotype, and, thus, would cause a decrease in the mechanical properties of the constructs. Study 2 aimed to determine the protective effects of various bioactive factors against the potential degradation of neocartilage constructs under macrophage co-culture. It was hypothesized that neocartilage-specific bioactive factors (i.e., TCL treatment) would protect neocartilage during macrophage co-culture.

It was also hypothesized that co-culture with IL-10-stimulated macrophages would result in improved neocartilage mechanical properties compared to those exposed to LPS-stimulated macrophages. The characterization of macrophage-neocartilage interactions performed here sets the stage for future studies spanning from mechanisms of neocartilage-macrophage interactions to immunomodulatory approaches for preclinical and clinical *in vivo* cartilage repair.

Materials and Methods

Isolation, expansion, and aggregate rejuvenation of chondrocytes

Costal cartilage from three Yucatan minipigs between 5 and 8 months of age (Premier BioSource) was obtained within 48 hours postmortem. All tissues used in this study were obtained from animals that were culled for reasons unrelated to this study. The cartilage was obtained from the entirety of the rib cage, minced into 1 mm^3 pieces, and digested using 0.4% w/v pronase (Sigma Aldrich) supplemented with 3% fetal bovine serum (FBS) (R&D Systems) for 1 hour at 37°C followed by 0.2% w/v collagenase (Collagenase, type 2, Worthington Biochemical) supplemented with 3% FBS for 18 hours at 37°C. Chondrocytes were filtered, counted, treated with ammonium-chloride-potassium (ACK) lysis buffer [353], and washed with phosphate buffered saline (PBS).

Costal chondrocytes were subsequently cultured in chemically defined chondrogenic medium (CHG) composed of Dulbecco's modified Eagle's medium (DMEM) (high glucose, GlutaMAX supplement) (Gibco), 1% penicillin-streptomycin-fungizone (Lonza), 1% insulin, transferrin, and selenous acid+ (ITS+) premix (Corning), 1% nonessential amino acids (Gibco), 100 nM dexamethasone (Sigma Aldrich), 50 µg/mL ascorbate-2-phosphate (Sigma Aldrich), 40 µg/mL L-proline (Sigma Aldrich), and 100 µg/mL sodium pyruvate (Sigma Aldrich) supplemented with 2% FBS at a density of 2.5 million cells per T-225 flask. During monolayer expansion, culture was further supplemented with 1 ng/mL TGF-β1 (PeproTech), 5 ng/mL basic fibroblastic growth factor (bFGF) (PeproTech), and 10 ng/mL platelet derived growth factor

(PDGF) (PeproTech), termed TFP, which has been previously shown to increase proliferation and postexpansion chondrogenic potential [144]. Medium was exchanged every 3-4 days. Upon 90% confluence, cells were lifted and digested using 0.05% Trypsin with 0.02% EDTA (Gibco) for 9 minutes followed by 0.2% w/v collagenase supplemented with 3% FBS for 40 minutes and frozen at passage 1 for downstream use. Cells were thawed for each experiment and expanded to passage 6 in CHG supplemented with TFP, as described above. Each passage had an approximate expansion factor of 4, which is calculated by dividing the final cell count by the initial seeding density. Doublings per passage, in this case two doublings, can be calculated by the following formula [25]: log(expansion factor)/log(2). This represents a cumulative expansion factor of 4096 as calculated by the following formula: expansion factor$^{\text{number of passages}}$. Toward addressing the issue of cell scarcity in donor cells for neocartilage tissue engineering, we employed passage 6 cells. The use of passage 6 cells is based on prior experiments optimizing efficient passaging and aggregate rejuvenation of chondrocytes toward creating a flat, robust construct [25, 247].

At passage 6, cells were placed into aggregate culture, termed aggregate rejuvenation [25], with CHG containing 10 ng/mL TGF-β1, 100 ng/mL growth differentiation factor 5 (GDF-5) (PeproTech), and 100 ng/mL bone morphogenetic protein 2 (BMP-2) (PeproTech), collectively termed TGB. Aggregate rejuvenation has been previously shown to promote redifferentiation of cells toward a chondrogenic phenotype, specifically exhibiting high expression of collagen type II, aggrecan, and SRY-box transcription factor 9 and low expression of collagen type X and osteocalcin [150]. Cells were plated on 1% agarose-coated plates at a density of 750,000/mL with medium changes every 3-4 days. Plates were kept on an orbital shaker at 50 RPM for 24 hours and subsequently cultured under static conditions. After 14 days of aggregate rejuvenation, cells were digested with 0.05% Trypsin with 0.02% EDTA for 45 minutes followed by 0.2% w/v collagenase supplemented with 3% FBS for 2 hours. Cells were passed through a 70 μm filter for subsequent self-assembly.

Isolation of bone marrow-derived monocytes and differentiation into macrophages

Pelvises from three Yucatan minipigs between 5 and 8 months of age (Premier BioSource) were obtained within 6 hours postmortem. Costal cartilage and pelvises were not obtained from the same animals. Bones were cleaned of muscle and other soft tissues. Using a sterilized chisel and hammer, the bone marrow was exposed and rinsed from the pelvic bone cavity using RPMI-1640 (L-glutamine) (Gibco). Resulting cells were passed through a 70 µm filter, spun down, and rinsed with PBS. Cells were treated with ACK lysis buffer and subsequently washed with PBS. Cells were plated at approximately 10 million cells per 100 mm diameter petri dish in a chemically defined macrophage culture medium (MΦM) composed of RPMI-1640, and 1% penicillin-streptomycin (Gibco), supplemented with 10% FBS and 20 ng/mL granulocyte-macrophage colony-stimulating factor (GM-CSF) (R&D Systems) to differentiate cells to bone marrow-derived macrophages. Recombinant porcine GM-CSF was selected for macrophage differentiation, as previously described [502, 553]. Cells were fed every 3-4 days and lifted after 7 days and frozen for downstream use. As previously reported in another study by our group [553], macrophage differentiation was confirmed through flow cytometry for cluster of differentiation 68 (CD68), immunofluorescence staining for CD68 and F4/80, and TNF-α secretion via an LPS dose response.

Formation of self-assembled cartilage constructs

After expansion and aggregate rejuvenation, chondrocytes underwent the self-assembling process [17]. Prior to seeding, non-adherent agarose wells were formed using 2% agarose (Fisher Scientific) in PBS and a negative mold to form the shape of 5 mm diameter cylindrical constructs, and CHG was exchanged on the wells 3 times prior to seeding. Chondrocytes were subsequently seeded at 2 million per well in 100 µL of CHG. Four hours after seeding, wells were topped off with another 400 µL of CHG. Medium was exchanged (500 µL) every day until day 3 when constructs were unconfined from agarose wells, transferred to untreated dishes,

and fed with 2 mL medium every other day up to 27 days. Study 1 consisted of CHG only. Study 2 consisted of CHG coupled with TCL treatment which is TGF-β1 continuously until day 27 (10 ng/mL), C-ABC (Sigma Aldrich) on day 7 for four hours, and LOXL2 (SignalChem) from days 14-27 to enhance engineered cartilage properties, as previously described [355]. Because C-ABC is used in this study both 1) as a culture supplement during the early period of tissue engineering culture and also 2) immediately before macrophage co-culture, the two different treatments are denoted as denoted as C-ABC$_{eng.}$ and C-ABC$_{comp.}$ to differentiate the culture additive and stiffness modulation, respectively. Briefly, C-ABC$_{eng.}$ (2 U/mL) consisted of activation with 50 mM sodium acetate (Sigma Aldrich) and quenching with 1 mM zinc sulfate (Sigma Aldrich). LOXL2 treatment consisted of 0.15 µg/mL of the enzyme coupled with 0.146 mg/mL hydroxylysine (Sigma Aldrich) and 1.6 µg/mL copper sulfate (Sigma Aldrich) [83].

Co-culture of macrophages and self-assembled cartilage constructs

After the self-assembling process, co-culture was initiated according to the steps illustrated in Figure 10-1. First, immediately prior to macrophage seeding, constructs were treated with C-ABC to modulate compressive stiffness via depletion of glycosaminoglycan (GAG) content (denoted as C-ABC$_{comp.}$ further). On day 27, constructs were treated with 0.0, 0.5, or 1.0 U/mL (1 mL/construct) of C-ABC$_{comp.}$ for 2 hours with activation and quenching, as described above. Macrophages were also thawed and cultured in MΦM overnight. On day 28, constructs were placed at the bottom of 2% agarose wells in 50 µL CHG. Based on previous work with biomaterials [500, 554], macrophages were then seeded at a density of 25,000 in 50 µL MΦM on top of constructs inside the agarose well to confine macrophages to the construct surface. Three macrophage donors were used separately in duplicate co-cultures for a total of six samples per co-culture condition. After 4 hours, a 1:1 mixture of CHG and MΦM was added to the co-culture system to sustain cell and tissue viability. Stimulation occurred the following day with 0.1 ng/mL of LPS in Study 1 and either 1.0 ng/mL LPS or 10 ng/mL IL-10 in Study 2. LPS

stimulation concentrations were chosen based on a previous study [553]. Medium was exchanged with half the total volume every 3 days, and co-culture continued for 2 weeks. Both studies also included constructs cultured in 1:1 CHG:MΦM within agarose wells in the absence of macrophages (i.e., construct-only control), as well as 25,000 macrophages cultured in 1:1 CHG:MΦM within agarose wells without constructs (i.e., macrophage-only control).

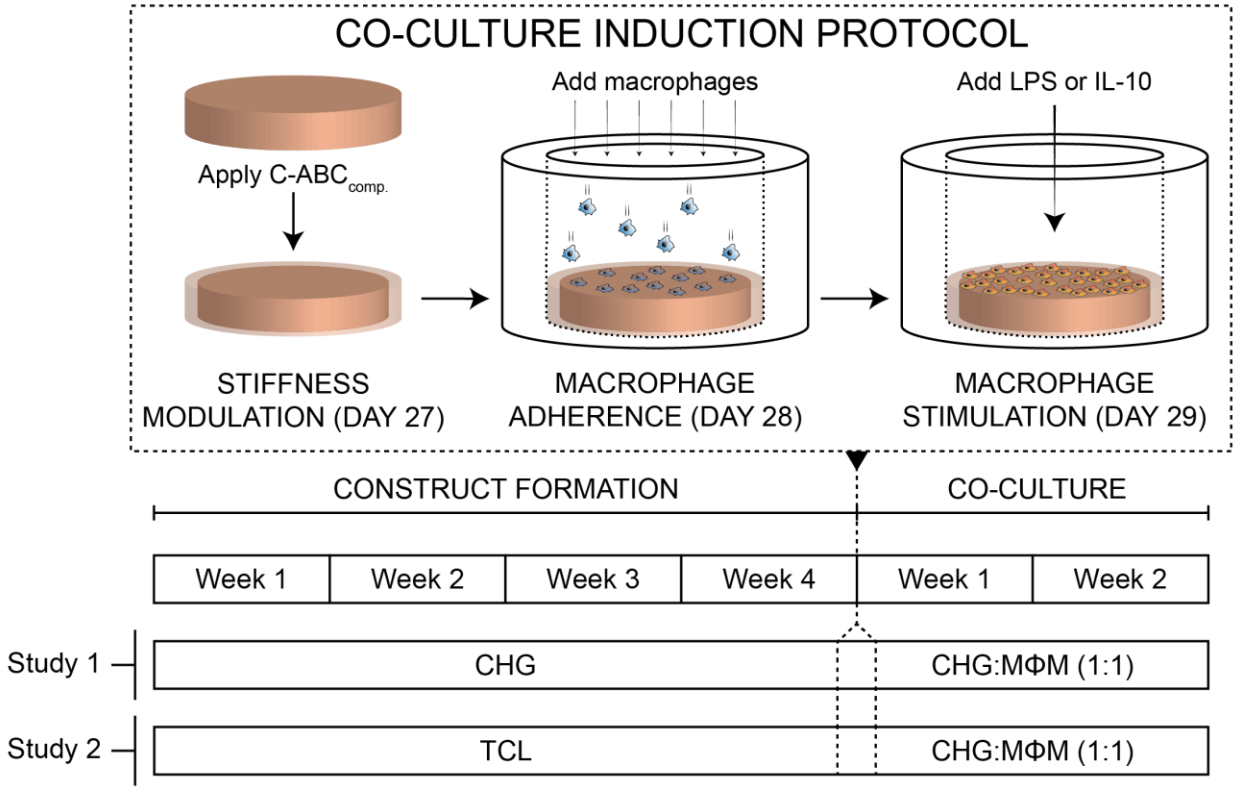

Figure 10-1: Stiffness is modulated via C-ABC$_{comp.}$, and macrophages are adhered and stimulated in a direct co-culture system.
Constructs were cultured in either CHG only or with TCL treatment. After 27 days, compressive stiffness was modulated via C-ABC$_{comp.}$ application. Constructs were assayed for baseline properties (t=0). The next day, macrophages adhered and were cultured in a 1:1 mix of CHG and MΦM medium, then stimulated with LPS in Study 1 and LPS or IL-10 in Study 2. Unstimulated macrophage controls, construct-only controls, and macrophage-only controls were also included. After 2 weeks of co-culture, constructs were assayed again (t=2W). Abbreviations: C-ABC$_{comp.}$, chondroitinase ABC to modulate compressive stiffness; CHG, chondrogenic medium; IL-10, interleukin 10; LPS, lipopolysaccharide; MΦM, macrophage medium; TCL, transforming growth factor beta 1/chondroitinase ABC$_{eng.}$/lysyl oxidase like 2.

Sample processing and biochemical analyses

Following culture, construct samples were weighed before and after lyophilization to obtain wet weight (WW) and dry weight (DW), and subsequently digested in papain for biochemical

analysis. Total collagen (Col) content was measured via a modified hydroxyproline assay, as previously described [93]. GAG content was measured by a dimethylmethylene blue dye-binding assay kit (Biocolor).

Mechanical testing

Constructs were analyzed under creep indentation and uniaxial tension to obtain compressive and tensile properties, respectively. As previously described [83], constructs were trimmed into dog bone-shaped specimens and glued to paper tabs which were gripped to a uniaxial testing machine (Instron 5565). A pull-to-failure test was performed at 1% strain per second. Tensile Young's modulus and ultimate tensile strength (UTS) were determined using the force-displacement curves from a custom MATLAB (MathWorks) code. Creep indentation was performed on cylindrical pieces of construct, as previously described [555]. Briefly, 3 mm diameter punches from self-assembled cartilage constructs were indented with a flat, porous tip under a constant load. A linear biphasic model and finite element analysis were used to obtain aggregate modulus, permeability, and shear modulus from experimental curves [446].

Histology

Construct samples were fixed in 10% neutral-buffered formalin for histological evaluation. Samples were subsequently processed, embedded in paraffin, and sectioned at 5 μm thickness. Samples were stained with hematoxylin and eosin (H&E) to show tissue and cellular morphology and Safranin O/Fast Green (Saf-O) to visualize GAG content.

Enzyme linked immunosorbent assays for cytokine analysis

Medium for enzyme-linked immunosorbent assays (ELISAs) was collected from sample wells either 24 or 48 hours after stimulation. Kits for TNF-α were purchased and used per the manufacturer's instructions (R&D Systems).

Statistical analysis

All statistical analyses were performed using Prism 9 (GraphPad Software). Quantitative data including more than two groups were assessed using either a one-way or two-way analysis of variance (ANOVA) with a *post hoc* Tukey's honestly significant difference (HSD) test at a significance level of $\alpha = 0.05$. Two-way ANOVA factors and interactions were analyzed to determine the individual factor effects as well as any interactions between those factors. P-values for ANOVA factors are capitalized. Significance among particular groups is illustrated by a "connecting letters report" with Latin characters (i.e., bars that do not share the same Latin character(s) are statistically significant), and p-values for *post hoc* tests are lower case. For two-way ANOVAs, *post hoc* Tukey's HSD tests were only used to compare groups within the dotted lines in each figure. For each set of quantitative data that only included two groups, a Student's t-test was performed at a significance level of $\alpha = 0.05$.

Results

Study 1

C-ABC$_{comp.}$ modulates compressive stiffness in CHG-treated constructs

To modulate compressive stiffness of constructs, C-ABC$_{comp.}$ was applied at a concentration of 0.0 U/mL (stiff), 0.5 U/mL (medium), or 1.0 U/mL (soft). Directly following this treatment, constructs were evaluated to establish baseline properties (t=0). Application of 1.0 U/mL (soft) and 0.5 U/mL (medium) of C-ABC$_{comp.}$ significantly decreased soft ($p = 0.0008$) and medium ($p = 0.02$) group WWs compared to the stiff group (Table 10-1). Similarly, GAG/WW significantly decreased by 28.0% in the soft group compared to the stiff group ($p = 0.02$) but was not significantly different from the medium group ($p = 0.15$) (Figure 10-2A). As expected, this led to subsequent decreases in aggregate modulus values; compared to constructs from the stiff group (341.7 ± 65.6 kPa), constructs from the soft and medium groups exhibited significantly lower aggregate modulus values, 133.7 ± 67.2 kPa ($p = 0.009$) and 182.7 ± 22.4 kPa ($p = 0.03$),

respectively (Figure 10-2B). Tensile Young's modulus and UTS did not differ significantly among the groups at t=0 (Table 10-1).

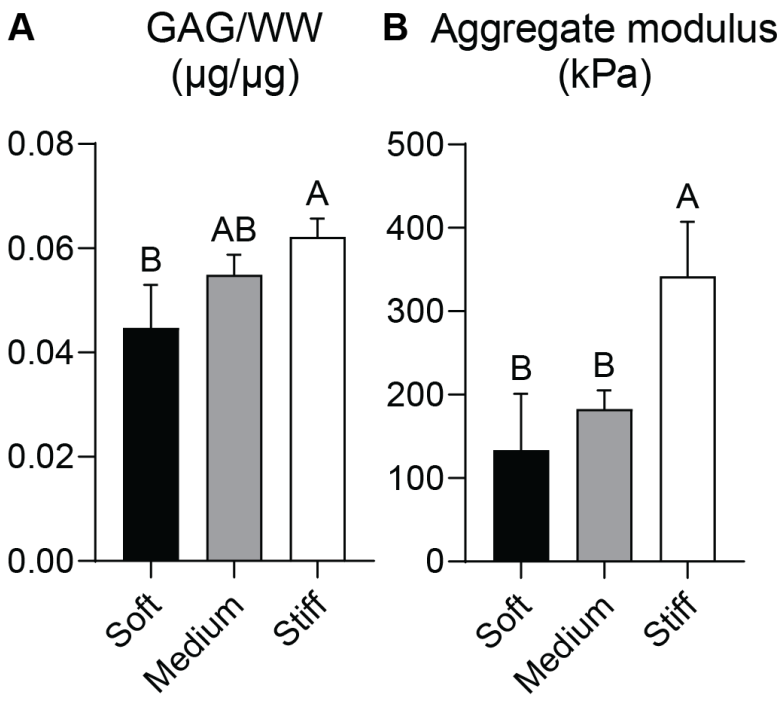

Figure 10-2: C-ABC$_{comp.}$ modulates the compressive stiffness of CHG-treated constructs.
A) GAG/WW increased across soft to stiff groups and decreased as higher C-ABC$_{comp.}$ concentrations were used to modulate compressive stiffness. B) Similarly, aggregate modulus also trended higher from soft to stiff, as expected. Abbreviations: GAG, glycosaminoglycan; WW, wet weight. Statistics: One-way ANOVA with *post hoc* Tukey's HSD, $\alpha = 0.05$, n=3 per group.

Table 10-1: Additional properties of CHG-treated constructs.
Significance is seen in construct WW among construct stiffnesses at t=0, significantly increasing from soft to stiff groups. Additionally, construct WW also decreases with the addition of macrophages to constructs, as seen in all groups. Abbreviations: Col, collagen; LPS, lipopolysaccharide; UTS, ultimate tensile strength; WW, wet weight. Statistics: Uppercase letters represent a connecting letters report from a one-way ANOVA with *post hoc* Tukey's HSD test comparing t=0 properties among stiffnesses (α = 0.05), n=3 per group. Lowercase letters represent a two-way ANOVA with *post hoc* Tukey's HSD test comparing properties after 2 weeks of co-culture only within individual stiffnesses (α = 0.05), n=3-6 per group. Gray-shaded table cells indicate statistical comparisons.

Time	Stiffness	Macrophage Condition	Construct WW (mg)	Col/WW (ug/ug)	Young's modulus (MPa)	UTS (MPa)	Shear modulus (kPa)	Permeability (10^{-15} m^4/Ns)
t=0	Soft	None	15.443±0.660^{C}	0.023±0.002^{A}	1.825±0.516	0.701±0.094	66.8±33.6^{B}	6.1±2.2
	Medium		17.106±0.693^{B}	0.017±0.001^{B}	3.190±2.695	0.515±0.094	91.3±11.3^{AB}	13.7±19.5
	Stiff		18.781±0.166^{A}	0.022±0.002^{A}	2.048±1.017	0.538±0.115	157.7±35.4^{A}	2.6±1.6
t=2W	Soft	None	18.635±0.537^{a}	0.030±0.002	2.357±0.611	0.747±0.279	68.9±6.0^{a}	25.5±11.7
		Unstimulated	15.012±0.632^{b}	0.027±0.002	2.508±0.738	0.868±0.257	31.8±13.4^{b}	36.9±54.2
		LPS	16.443±1.049^{ab}	0.031±0.002	2.488±0.443	0.903±0.143	42.7±31.8^{ab}	60.0±82.0
	Medium	None	20.288±0.761^{a}	0.031±0.004	2.092±0.372^{ab}	0.779±0.060^{ab}	102.2±27.4^{a}	32.2±13.4
		Unstimulated	16.182±1.736^{b}	0.028±0.003	2.113±0.514^{b}	0.754±0.215^{b}	44.9±14.6^{b}	15.8±14.4
		LPS	14.095±1.991^{b}	0.028±0.004	3.439±1.136^{a}	1.147±0.398^{a}	25.8±6.4^{b}	14.1±5.1
	Stiff	None	25.435±2.600^{a}	0.024±0.003	1.076±0.392	0.389±0.135	66.8±14.9	76.4±14.6^{a}
		Unstimulated	17.987±1.321^{b}	0.025±0.005	2.283±0.858	0.697±0.303	60.4±18.4	20.3±11.9^{ab}
		LPS	17.038±1.353^{b}	0.025±0.002	2.106±0.964	0.697±0.096	53.8±14.5	11.4±4.7^{b}

Stiff, CHG-treated constructs are protected from macrophage inflammatory challenge even in the presence of an elevated proinflammatory response

CHG-treated neocartilage cultured for 2 weeks in the presence of macrophages demonstrated differences in tissue morphological characteristics dependent on construct stiffness per H&E staining for general cellular and tissue morphology (Figure 10-3). The unstimulated co-culture group for the stiff group did not appear to lose as much staining intensity relative to the corresponding construct-only control compared to the soft and medium group. Additionally, stiff construct-only controls did not exhibit cells near the construct edge, unlike the other construct-only control (none) groups. As an experimental factor, macrophage co-culture significantly decreased construct WW across all stiffnesses ($P < 0.0001$) (Table 10-1). Similarly, the macrophage co-culture factor was also significant ($P = 0.006$) for GAG/WW (Figure 10-4A), decreasing with macrophage application. For medium stiffness constructs, a significant decrease in GAG/WW was observed between the construct-only control (none) (0.066 ± 0.007 μg/μg) and LPS-stimulated macrophage co-culture (0.035 ± 0.018 μg/μg) ($p = 0.01$) (Figure 10-4A). Stiffness was a significant factor for Col/WW ($P = 0.001$) (Table 10-1). Macrophage co-culture factor was not significant for Col/WW ($P = 0.34$) (Table 10-1).

Aggregate modulus values trended, as expected, with GAG/WW (Figure 10-4). Interestingly, aggregate modulus for soft and medium groups significantly decreased from 160.3 ± 15.3 kPa and 180.5 ± 36.1 kPa for construct-only controls to 91.2 ± 60.1 kPa and 57.8 ± 17.7 kPa ($p = 0.04$ and $p = 0.001$), respectively, when co-cultured with LPS-stimulated macrophages Figure 10-4B). Significant changes in aggregate modulus for soft and medium groups also occurred when comparing construct-only controls to unstimulated macrophage co-culture groups, decreasing by 59.9% and 46.4% ($p = 0.002$ and $p = 0.02$), respectively (Figure 10-4B). Construct-only controls (159.7 ± 47.2 kPa) in the stiff group did not differ from unstimulated (134.5 ± 44.8 kPa) ($p = 0.60$) or LPS-stimulated (123.8 ± 32.9 kPa) ($p = 0.36$) co-culture groups (Figure 10-4B).

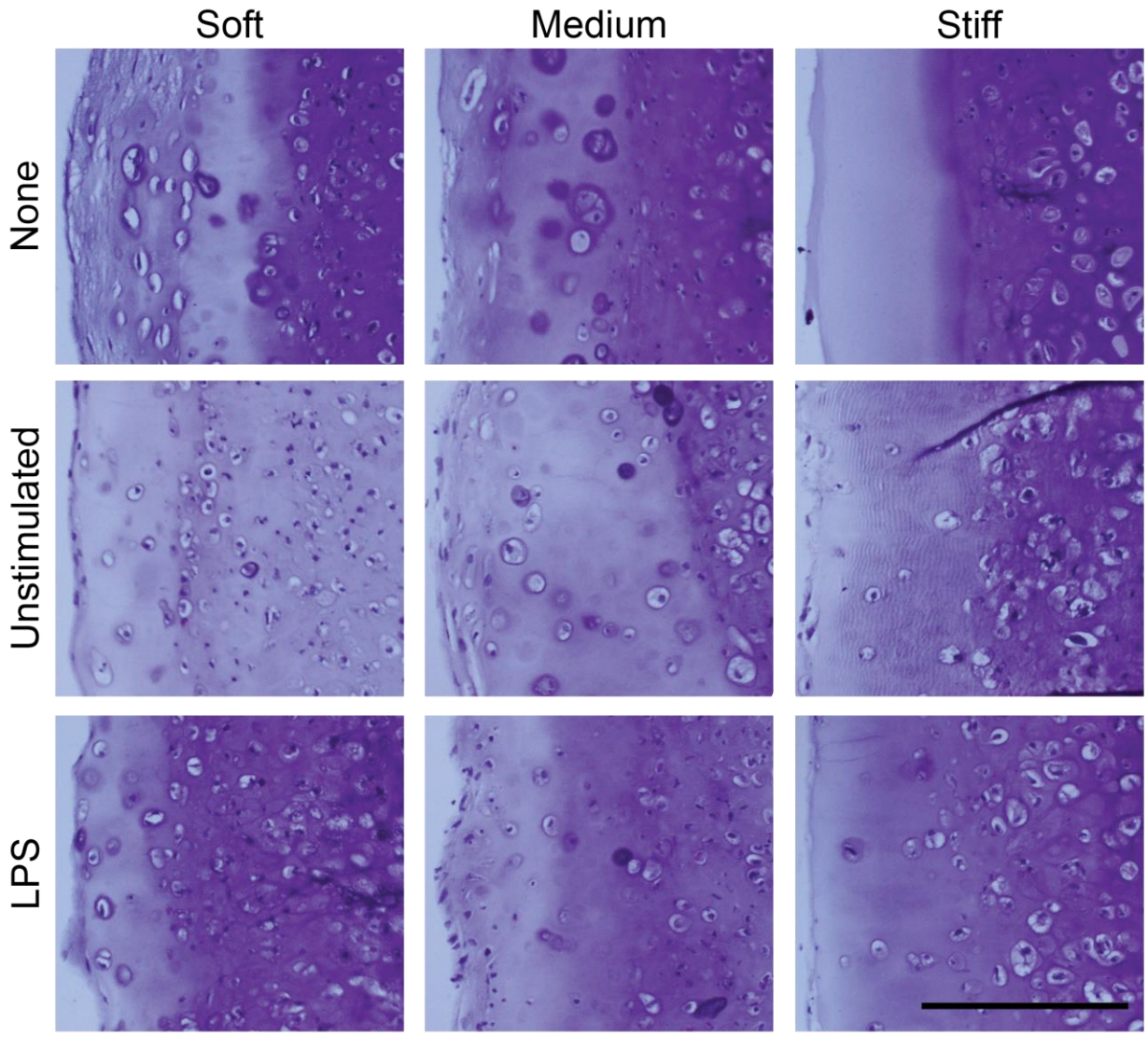

Figure 10-3: CHG-treated constructs of soft and medium stiffness differ in staining intensity.
Following 2 weeks of co-culture, stiff constructs maintain cell morphology and tissue staining intensity in co-culture groups more than the soft and medium groups. Abbreviation: LPS, lipopolysaccharide. Scale bar = 200 µm.

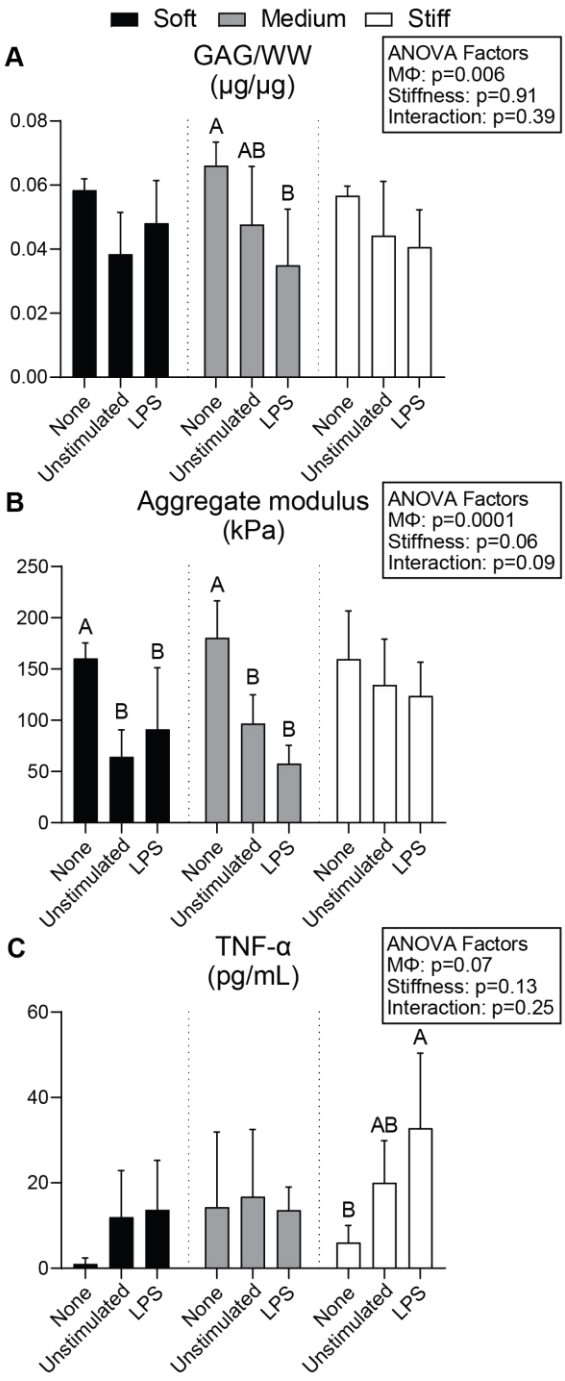

Figure 10-4: Soft and medium stiffness CHG-treated constructs suffer losses in aggregate modulus values despite no increases in TNF-α production.
A) GAG/WW was significantly affected by the MΦ factor, with significant decreases within the medium stiffness constructs between the construct-only control and LPS-stimulated co-culture group. B) Trending with GAG/WW, aggregate modulus significantly decreased with the addition of macrophages (unstimulated or LPS-stimulated) in soft and medium stiffness constructs. C) Conversely, after 48h of co-culture, only the stiff construct group had significant increases in TNF-α secretion between the construct-only control and the LPS-stimulated group. Abbreviations: GAG, glycosaminoglycan; LPS, lipopolysaccharide; MΦ, macrophage; TNF-α, tumor necrosis factor alpha; WW, wet weight. Statistics: Two-way ANOVA with *post hoc* Tukey's HSD among groups within a stiffness (dotted lines), α = 0.05, n=3-6 per group.

After 48 hours of stimulation, TNF-α levels significantly increased by 5.47-times in the stiff group when stimulated with LPS compared to construct-only controls (p=0.01), but there were no significant differences when comparing either of those groups to unstimulated co-culture groups, although TNF-α levels in the LPS group trended 1.64-times higher than the unstimulated group (p = 0.19) (Figure 10-4C). Interestingly, for soft and medium constructs, TNF-α levels did not differ significantly when the two macrophage co-culture conditions were compared against each other (p = 0.97 and p = 0.90) (Figure 10-4C). However, for the soft and medium groups, significant decreases in aggregate modulus values were observed when the constructs were exposed to either unstimulated (p = 0.002 and p = 0.02) or LPS-stimulated macrophages (p = 0.04 and p = 0.001) (Figure 10-4B). Conversely, the stiff co-culture groups did not experience significant decreases in aggregate modulus (p = 0.60 and p = 0.36) compared to construct-only control (Figure 10-4B).

Study 2

C-ABC$_{comp.}$ modulates compressive stiffness in TCL-treated constructs

Directly following C-ABC$_{comp.}$ treatment, TCL-treated constructs were evaluated to establish baseline properties (t=0). As shown in Figure 10-5C, the soft group, which was treated with 1.0 U/mL C-ABC$_{comp.}$, had reduced ECM and GAG content at the periphery of the construct. Conversely, the stiff group (i.e., 0.0 U/mL C-ABC$_{comp.}$) exhibited intense matrix and GAG content all the way to the edge of the construct. As expected, the construct WW was also significantly higher in the stiff group compared to the soft group at t=0 (p = 0.03) (Table 10-2), although GAG/WW was not significantly different between the two stiffnesses (p = 0.78) (Figure 10-5A). Aggregate modulus for the stiff group (165.6 ± 20.7 kPa) was significantly higher (p < 0.0001) than the soft group (76.8 ± 18.6 kPa) (Figure 10-5B). Thus, although C-ABC$_{comp.}$ did not change GAG/WW between the soft and stiff groups, it still had a significant effect on aggregate modulus,

decreasing with higher concentrations of the enzyme. Additional properties are reported in Table 10-2.

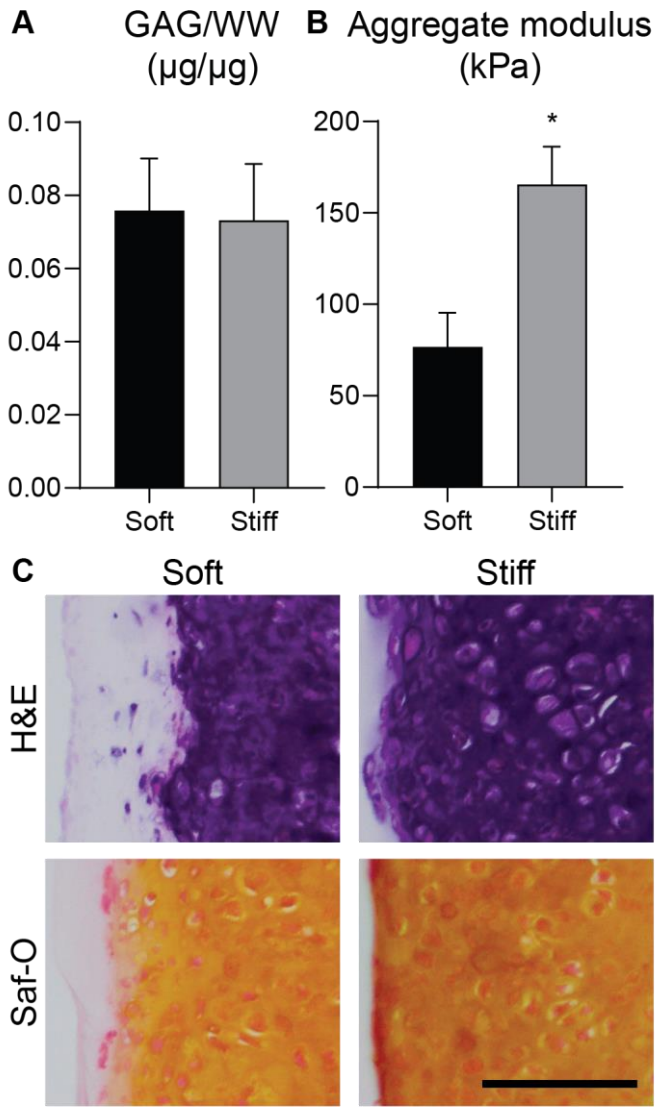

Figure 10-5: C-ABC$_{comp.}$ modulates the compressive stiffness of TCL-treated constructs.
A) GAG/WW does not differ significantly for TCL-treated constructs at t=0. B) Aggregate modulus significantly decreases with application of C-ABC$_{comp.}$. C) Soft constructs show less intense Saf-O and H&E staining due to C-ABC$_{comp.}$ application and only peripheral loss of GAG. Also, some cells are visible near the soft construct edge. Conversely, stiff constructs show intense Saf-O staining at the periphery indicating high GAG content, and cells are not present at the periphery of the construct. Abbreviations: GAG, glycosaminoglycan; H&E, hematoxylin and eosin; Saf-O, Safranin O; WW, wet weight. Scale bar = 100 µm. Statistics: Student's t-test, $\alpha = 0.05$.

Table 10-2: Additional properties of TCL-treated constructs.
Significance is seen in construct WW among construct stiffnesses at t=0, similar to CHG-treated constructs. Additionally, construct WW also generally decreases in both stiffnesses after 2 weeks of co-culture. Abbreviations: Col, collagen; IL-10, interleukin 10; LPS, lipopolysaccharide; UTS, ultimate tensile strength; WW, wet weight. Statistics: Asterisks (*) represent a Student's t-test comparing t=0 properties among stiffnesses (α = 0.05), n=5 per group. Lowercase letters represent a two-way ANOVA with *post hoc* Tukey's HSD test comparing properties after 2 weeks of co-culture only within individual stiffnesses (α = 0.05), n=5-6 per group. Gray-shaded table cells indicate statistical comparisons.

Time	Stiffness	Macrophage Condition	Construct WW (mg)	Col/WW (ug/ug)	Young's modulus (MPa)	UTS (MPa)	Shear modulus (kPa)	Permeability (10^{-15} m^4/Ns)
t=0	Soft	None	9.805±0.470	0.031±0.003	7.352±3.323	2.097±0.662	32.9±7.9	4.9±4.4
	Stiff		10.826±0.612*	0.025±0.003*	6.471±1.038	1.703±0.219	73.0±11.9*	7.3±6.9
t=2W	Soft	None	13.100±0.645[a]	0.034±0.003	11.726±4.720	2.994±1.001	71.9±26.8[a]	15.7±16.5
		Unstimulated	11.678±0.302[b]	0.039±0.003	8.874±1.932	2.395±0.491	56.1±15.9[ab]	11.4±8.1
		LPS	11.783±0.707[ab]	0.038±0.004	7.803±1.046	2.274±0.503	38.0±14.1[b]	10.5±8.3
		IL-10	12.522±0.656[ab]	0.038±0.002	7.510±1.1792	2.223±0.711	41.2±11.3[ab]	9.7±6.2
	Stiff	None	15.455±1.049[a]	0.032±0.002	7.273±2.142	2.081±0.340	75.5±26.5	29.0±20.6[a]
		Unstimulated	13.435±1.323[b]	0.031±0.004	7.285±0.987	2.066±0.571	74.6±20.9	19.9±14.7[ab]
		LPS	13.462±1.264[b]	0.033±0.004	9.322±3.323	2.313±1.033	59.9±24.0	8.8±7.6[b]
		IL-10	14.229±0.904[ab]	0.030±0.004	9.560±6.197	1.947±0.402	70.1±21.8	12.0±12.6[ab]

TCL-treated constructs better withstand macrophage challenge

Saf-O staining of constructs illustrated variability in GAG content across macrophage donors as well as within the construct-only controls (none) (Figure 10-6). Compared to other conditions within stiffnesses, it appeared as though staining intensity was slightly diminished in the LPS-stimulated group. In the soft group, GAG/WW significantly decreased by 26.2% ($p = 0.02$), 33.8% ($p = 0.002$), and 31.8% ($p = 0.004$) for the unstimulated, LPS-stimulated, and IL-10-stimulated groups, respectively, when compared to the construct-only control (none) group (Figure 10-7A). For the stiff group, no condition caused GAG/WW to change (Figure 10-7A). However, in terms of aggregate modulus (Figure 10-7B), in the soft group, only the LPS-stimulated group and construct-only control were significantly different from each other ($p = 0.04$); the LPS group had an aggregate modulus that was 43.8% of the construct-only control. This is in contrast to CHG-treated co-cultures from the soft and medium groups in Study 1 which significantly decreased in aggregate modulus no matter the stimulation condition (Figure 10-4B). For the soft group from Study 2, the unstimulated group and IL-10 group had aggregate moduli that were 76.5% and 48.5% of the construct-only control, but these trends were not statistically significant ($p = 0.66$ and $p = 0.07$) (Figure 10-7B). For the stiff group, there were no significant differences in aggregate modulus, which were 186.0 ± 91.4 kPa, 173.0 ± 56.3 kPa, 144.0 ± 82.0 kPa, and 160.5 ± 65.3 kPa for the construct-only, unstimulated, LPS-stimulated, and IL-10-stimulated conditions, respectively (Figure 10-7B). Additional data after 2 weeks of co-culture are presented in Table 10-2.

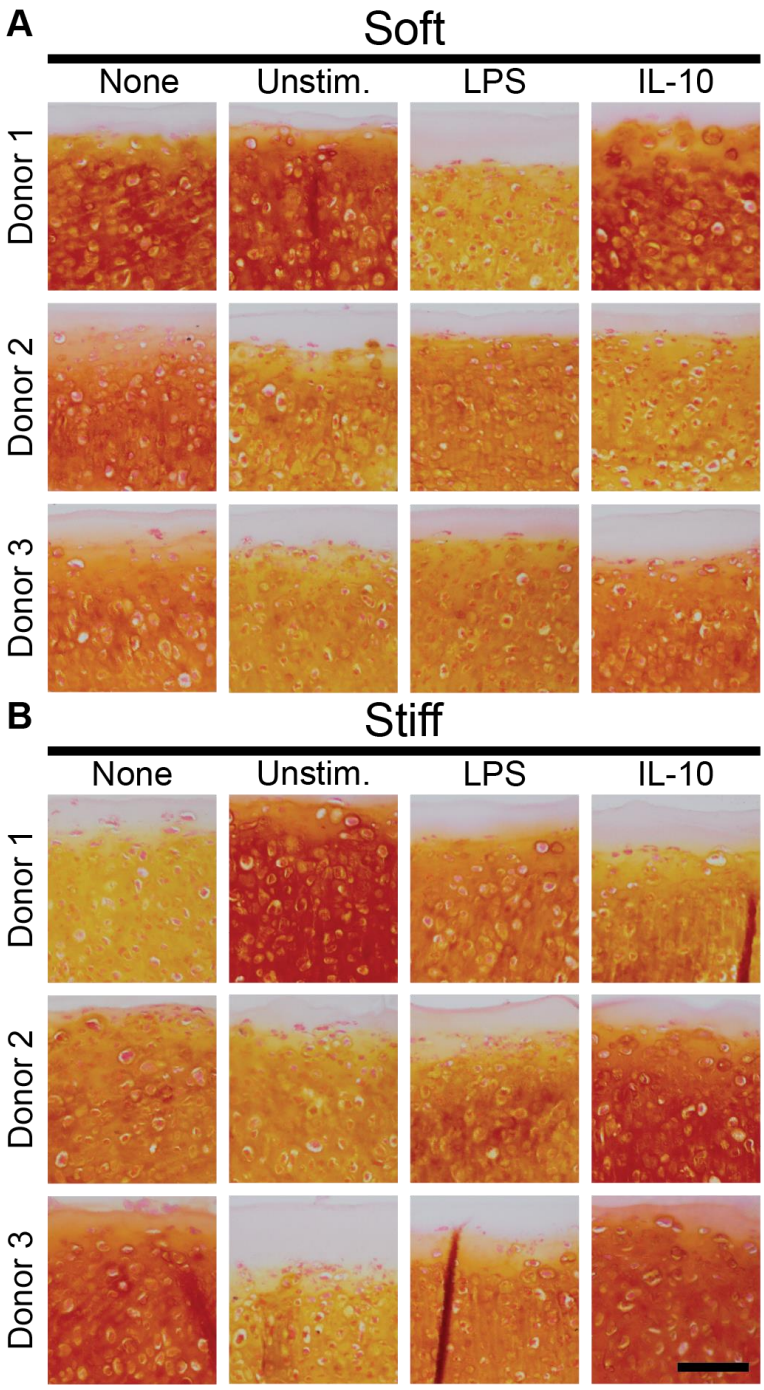

Figure 10-6: Saf-O staining after 2 weeks of macrophage co-culture shows donor-related variation, with diminished staining among LPS-stimulated co-cultures.
Both construct-only controls and co-culture groups show variability between donors. However, on average, staining is slightly diminished in some LPS-stimulated groups compared to construct-only controls. Abbreviations: IL-10, interleukin 10; LPS, lipopolysaccharide, Unstim., unstimulated. Scale bar = 100 µm.

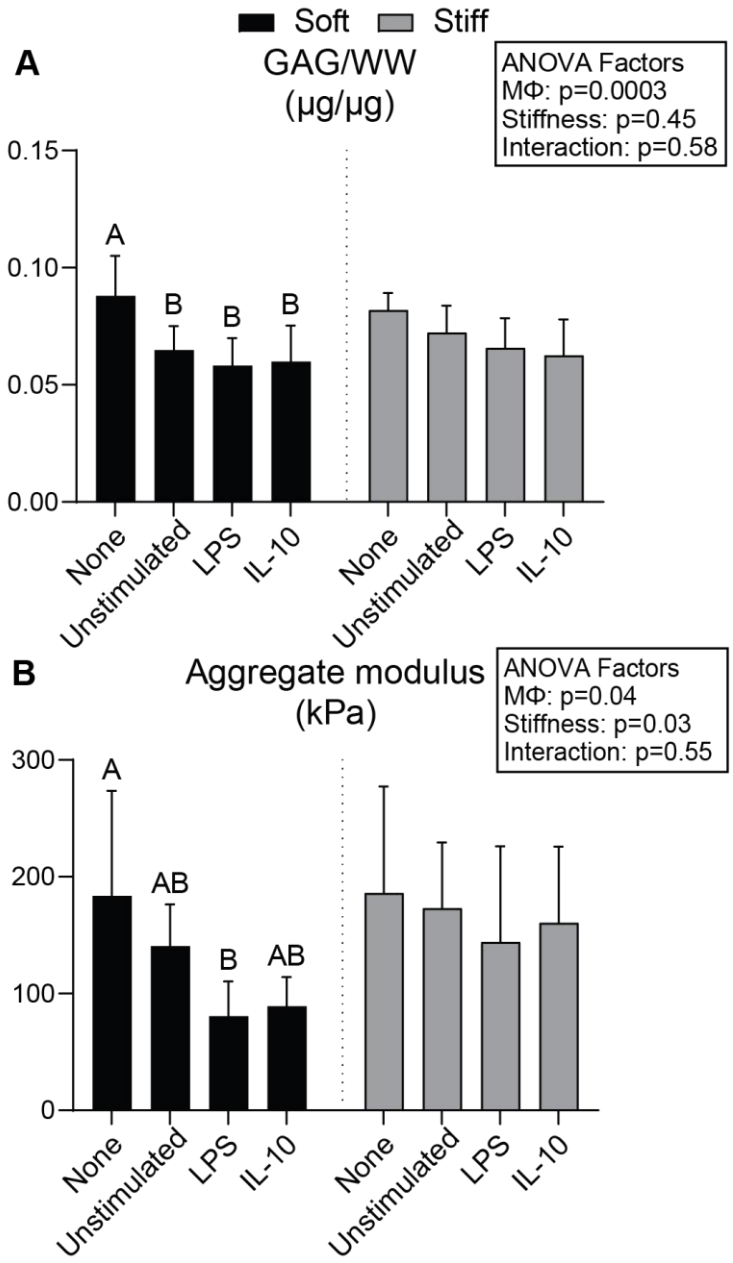

Figure 10-7: Aggregate modulus values of TCL-treated constructs only decrease in soft construct, LPS-stimulated co-cultures.

A) The construct-only control and macrophage co-cultures in the soft constructs are significantly different in GAG/WW, while the stiff group does not exhibit significant differences between groups. B) Aggregate modulus also trends downward for the soft group when co-cultured with macrophages, but only the LPS-stimulated co-culture group is significantly different from the construct-only control. Stiff group aggregate moduli were largely unaffected by macrophage treatment. Abbreviations: GAG, glycosaminoglycan; IL-10, interleukin 10; LPS, lipopolysaccharide; MΦ, macrophage; WW, wet weight. Statistics: Two-way ANOVA with post hoc Tukey's HSD among groups within a stiffness (dotted lines), $\alpha = 0.05$, n=5-6 per group.

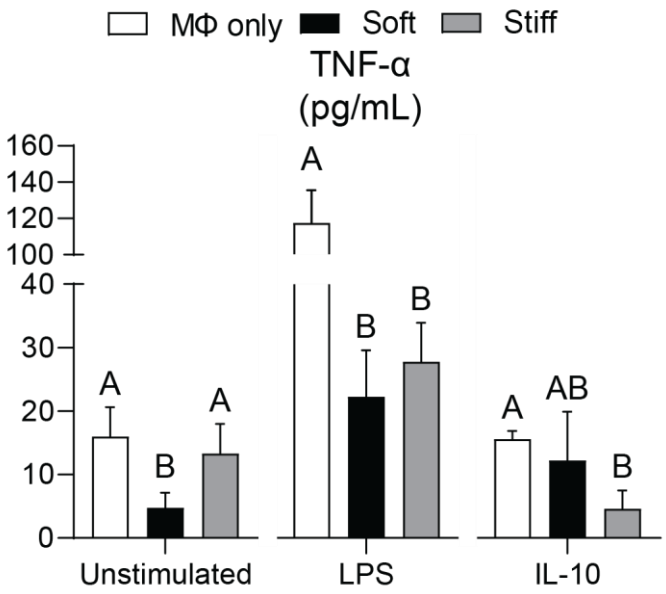

Figure 10-8: TNF-α secretion of TCL-treated construct co-cultures increases with stiffness, decreases with construct co-culture, and diminishes when macrophages are stimulated toward an anti-inflammatory phenotype.
In unstimulated co-culture conditions, TNF-α production increases with stiffness. Similarly, TNF-α secretion also trends higher for stiff construct co-culture compared to the soft construct condition in the LPS-stimulated groups. Interestingly, construct addition significantly decreases the TNF-α production compared to macrophage-only controls in LPS-stimulated groups. For IL-10 stimulation, a decrease in TNF-α levels is seen with increasing construct stiffness. Abbreviations: IL-10, interleukin 10; LPS, lipopolysaccharide; MΦ, macrophage; TNF-α, tumor necrosis factor alpha. Statistics: One-way ANOVA with *post hoc* Tukey's HSD (for each stimulation condition), α = 0.05, n=5-6 per group.

Co-culture with TCL-treated constructs suppress LPS-induced TNF-α production, and increased stiffness enhances the anti-inflammatory effect of IL-10-stimulated macrophages

Similar to Study 1, there was a stiffness-mediated effect with increasing construct stiffness. There was a significant increase in TNF-α secreted by unstimulated, stiff co-cultures compared to the soft co-culture group ($p = 0.006$) (Figure 10-8). LPS stimulation increased the secretion of TNF-α overall. LPS-stimulated macrophages produced 117.6 ± 18.0 pg/mL TNF-α. Both soft and stiff constructs caused a significant 81.0% ($p < 0.0001$) and 76.4% ($p < 0.0001$) reduction in TNF-α levels compared to the LPS-stimulated macrophage-only control (Figure 10-8).

When stimulating macrophages toward an anti-inflammatory phenotype, IL-10-stimulated macrophages secreted 15.6 ± 1.3 pg/mL TNF-α. When IL-10-stimulated macrophages were co-cultured with soft constructs, no significant difference in TNF-α levels

was observed compared to macrophage-only control (p = 0.48) (Figure 10-8). However, stiff constructs significantly reduced the TNF-α secretion to 4.6 ± 2.9 pg/mL compared to macrophage-only controls (p = 0.005) (Figure 10-8).

Table 10-3: CHG-treated constructs decrease aggregate modulus values compared to TCL-treated constructs which maintain or increase aggregate modulus values after 2 weeks of macrophage co-culture.
CHG-treated constructs drop from t=0 baseline values of aggregate modulus across all stiffnesses when co-cultured with macrophages, ranging from 31.6-68.2% of original values. Conversely, TCL-treated constructs either maintain or increase from baseline values, ranging from 87.0-183.2%, when co-cultured with macrophages. Abbreviations: CHG, chondrogenic medium; IL-10, interleukin 10; LPS, lipopolysaccharide; TCL, transforming growth factor beta 1/chondroitinase $ABC_{eng.}$/lysyl oxidase like 2.

Study	Time	Stiffness	Macrophage Condition	Change from t=0 (%)
Study 1: CHG-treated	t=2W	Soft	None	119.9±11.4
			Unstimulated	48.1±19.7
			LPS	68.2±45.0
		Medium	None	98.8±19.7
			Unstimulated	53.0±15.4
			LPS	31.6±9.7
		Stiff	None	46.7±13.8
			Unstimulated	39.4±13.1
			LPS	36.2±9.6
Study 2: TCL-treated		Soft	None	239.1±117.2
			Unstimulated	183.2±46.4
			LPS	104.8±38.8
			IL-10	116.1±32.4
		Stiff	None	112.3±55.2
			Unstimulated	104.5±34.0
			LPS	87.0±49.5
			IL-10	96.9±39.4

Study 1 and Study 2 Comparison

TCL-treated constructs maintain or increase aggregate modulus compared to CHG-treated constructs after 2 weeks of co-culture

To compare the culture regimens of constructs and how construct mechanical properties change after macrophage co-culture, Table 10-3 presents the percent changes of aggregate modulus after 2 weeks of co-culture compared to baseline properties (t=0). For CHG-treated co-

culture groups, unstimulated and LPS-stimulated, all groups had a marked decrease from baseline properties at t=0, ranging between 31.6 ± 9.7% and 68.2 ± 45.0%. In comparison, co-culture groups for TCL-treated constructs either maintained or increased the aggregate modulus compared to t=0 controls, ranging from 87.0 ± 49.5% to 183.2 ± 46.4% of baseline values.

Discussion

Substantial progress has been made toward tissue-engineered cartilages with properties approaching or on par with native tissue [207, 339, 378]. While achieving biomimetic properties should be a part of the translational tissue engineering process, other factors must be considered to evaluate the potential success of a neocartilage implant. For example, as part of the innate immune response to surgical trauma, macrophages migrate to the treated area and would likely interact with the implant [556]. Due to the potentially deleterious effect macrophages can have on engineered tissue *in vivo*, the objective of this study was to develop a novel, *in vitro* direct co-culture model to study the interactions between differentially stimulated macrophages and self-assembled neocartilage. Two separate studies were conducted. Study 1 investigated the inflammatory response of macrophages to neocartilage of varying stiffnesses. The hypothesis for Study 1 was confirmed; macrophages secreted more TNF-α, indicative of a proinflammatory phenotype, during co-culture with neocartilages of increasing stiffnesses. Interestingly, this response did not cause a reduction in construct mechanical properties compared to construct-only controls. However, over the 2 week co-culture period, aggregate modulus values decreased in all CHG-treated co-culture groups compared to t=0 timepoints. Toward rescuing constructs that had a significant decrease in mechanical properties (i.e., the CHG-treated soft and medium groups) and investigating additional protection measures, Study 2 was performed with bioactive factors that have been shown to increase the mechanical properties of neocartilage and polarize macrophages toward an anti-inflammatory phenotype. Macrophage polarization toward an anti-inflammatory phenotype did not improve neocartilage

mechanical properties compared to LPS-stimulation (i.e., proinflammatory phenotype). However, the neocartilage bioactive factors (i.e., TCL treatment) examined here prevented neocartilage mechanical degradation over time (i.e., with respect to t=0) when compared to CHG-treated constructs, regardless of macrophage stimulation condition or construct stiffness.

This study showed that increasing neocartilage stiffness drives polarization of macrophages to an enhanced proinflammatory phenotype, but sufficiently stiff neocartilage may also be protected from macrophage-related deleterious effects. Interestingly, there was a significant increase in TNF-α production between construct-only controls and LPS-stimulated co-cultures in the stiff group (Figure 10-4C). This stiffness-mediated effect on macrophage phenotype was not limited to proinflammatory macrophages. In Study 2, IL-10-stimulated (i.e., anti-inflammatory phenotype) macrophages co-cultured with stiff constructs had TNF-α levels decrease by 62.5% compared to soft constructs exposed to the same co-culture condition (Figure 10-8). This apparent stiffness-dependent macrophage behavior has been seldom examined on tissue substrates and has not been previously examined on cartilage neotissue, but this has been well documented on less complex substrates such as hydrogels [557]. For example, it has been observed that when LPS-stimulated macrophages were seeded on polyethylene glycol (PEG) hydrogels of increasing stiffness, TNF-α and IL-1β expression increased alongside stiffness [492, 552, 558]. To our knowledge, this is the first time that modulation of macrophage phenotype using substrate stiffness has been shown for cartilage neotissue.

Proinflammatory cytokines such as TNF-α are known to have catabolic effects on native articular cartilage mechanical properties [542]. This is well-established in the literature to be mediated through enzymatic degradation of the cartilage via matrix metalloproteinases (MMPs), which are upregulated when exposed to inflammatory cytokines such as TNF-α in multiple species, including the pig [559-561]. For example, as a result of age-related OA, advanced glycation end-products (AGEs) can cause cartilage to become stiffer and more brittle [562]. As a

result of AGEs and associated stiffening, it is likely that increased pro-inflammatory cytokines and MMPs could be secreted from macrophages within the joint, causing breakdown of the cartilage ECM [563]. However, contrary to this potential mechanism and the literature, stiff self-assembled neocartilage did not experience a drop in properties relative to its corresponding construct-only control after exposure to elevated TNF-α levels due to macrophage co-culture in Study 1 (Figure 10-4). The opposite was true for soft and medium stiffness co-cultured constructs in Study 1; they experienced a significant decrease in aggregate modulus, without a corresponding increase in TNF-α secretion (Figure 10-4). Similarly, we hypothesized that constructs co-cultured with macrophages stimulated with IL-10 might improve mechanical properties when compared to co-culture with LPS. However, there were no significant differences in aggregate modulus values between these co-culture conditions in either stiffness in Study 2 (Figure 10-7B). While the mechanism for this stiffness-mediated behavior is unclear, it was clear that additional factors, both neocartilage (i.e., TCL treatment) and macrophage (IL-10 stimulation) specific, for protection of soft neocartilage constructs against macrophage challenge was necessary.

Previous studies have investigated the use of TCL treatment for increasing robustness of neocartilage constructs. Here, TCL treatment prevents construct reductions in mechanical properties experienced by CHG-only treated neocartilage subjected to macrophage challenge. Compared to soft and medium CHG-treated constructs from Study 1, which had a significant decrease in aggregate modulus no matter the co-culture condition (Figure 10-4B), only the soft, TCL-treated constructs exposed to LPS-stimulated macrophages from Study 2 significantly differed in aggregate modulus from the corresponding construct-only control (Figure 10-7B). Additionally, TCL-treated constructs co-cultured with macrophages in Study 2 either maintained or increased their aggregate modulus compared to baseline values at t=0 (Table 10-3). In comparison, CHG-treated constructs co-cultured with macrophages all experienced a reduction in aggregate modulus ranging from 31.6-68.2% of the corresponding values at t=0 (Table 10-3).

Macrophage co-culture reduced construct properties in CHG-treated constructs, but TCL treatment prevented such deleterious effects. When looking at constructs of similar baseline aggregate modulus values, the medium CHG-treated group corresponded to the stiff TCL-treated group. Since the medium CHG-treated group experienced a marked drop in properties from baseline (31.6-53.0%), whereas the stiff TCL-treated group did not (87.0-104.5%), this suggests that an effect inherent to TCL treatment confers protection to constructs. While further exploration would be necessary to determine the mechanism responsible for this behavior, this is a significant finding toward developing future immunomodulatory approaches using tissue engineering techniques such as TCL treatment.

The mechanism of protection via TCL treatment is not fully known, but it may, in part, be due to TCL-treated constructs being less susceptible to macrophage infiltration compared to CHG-treated constructs. It is also known that TGF-β1 binds to cartilage ECM [564], thus, potentially suppressing the proinflammatory phenotype [565] of the co-cultured macrophages. Alternatively, it is possible that alterations in construct surface topology and ECM contents driven by TCL treatment alters the behavior and phenotype of macrophages [557]. LPS-stimulated macrophage TNF-α production was reduced by more than 4-times when co-cultured with TCL-treated constructs (Figure 10-8), suggesting that TCL-treated constructs have an anti-inflammatory effect on macrophage phenotype. This behavior could possibly be due to the increased collagen deposition as compared to CHG-treated constructs, since collagen gels and collagen type II have both been shown to promote an anti-inflammatory macrophage phenotype [359, 566]. Ultimately, due to their stability, robustness, and potential anti-inflammatory effects, TCL-treated constructs should be used for future cartilage mechano-immunology studies.

In tissues such as neocartilage constructs, mechanical properties and biochemical content are inherently linked due to structure-function relationships. Here, we modulate compressive stiffness by removing GAG, which leads to changes in aggregate modulus values. Variations in GAG content as a result of C-ABC$_{comp.}$ treatment in the construct could contribute

to changes in macrophage behavior. For example, it has been shown that individual GAGs can modulate macrophage phenotype by eliciting production of nitric oxide [567]. Because self-assembled neocartilage is a complex biological tissue, it would be challenging, but potentially worthwhile to develop a way to decouple changes in stiffness from changes in ECM content and construct surface topology. Future studies may consider altering collagen content via collagenase or crosslinking via addition exogenous lysyl oxidase in varying concentrations to modulate other mechanical properties (e.g., tensile).

The novel, direct co-culture model developed in this study investigated the interactions between macrophages and neocartilage constructs for the first time, and sets the stage for future investigations that foster the development of the nascent field of cartilage mechano-immunology. Future studies could include investigation of disease or injury modeling, biomolecular pathways that drive macrophage polarization and chondrocyte behavior, or anti-inflammatory macrophage-assisted cartilage tissue engineering. For example, the exact mechanism of TCL-mediated protection could be elucidated by using this co-culture system in future studies by extracting macrophages and chondrocytes and exploring gene expression via single cell RNA sequencing for each cell type. Furthermore, these *in vitro* studies could inform the development and engineering of neocartilage implants that minimize inflammation by tuning the mechanical properties of the neocartilages, and, thus, modulate the macrophage-mediated immune response after implantation. Another example is combining this co-culture system with an *in vitro* integration system, where integration between excised native tissues and engineered cartilages is assessed over various co-culture times as an *in vitro* surrogate for healing potential *in vivo*. Eventually, large animal, orthotopic approaches in native cartilages will ultimately inform whether or not future immunomodulatory approaches will be feasible in humans. In conclusion, through the development of a novel, *in vitro* co-culture system, this study demonstrated that variable neocartilage stiffness can alter macrophage behavior, but that stiffness, as well as

bioactive factor treatments (e.g., TCL treatment), can protect construct integrity in the presence of proinflammatory factors.

Chapter 11: Tissue-Engineered Implants Regenerate Large Perforations in the Yucatan Minipig Temporomandibular Joint Disc[11]

Abstract

The temporomandibular joint (TMJ) disc in the jaw is frequently perforated in people with temporomandibular disorders (TMDs). Current surgical procedures for TMDs ameliorate pain temporarily but are ineffectual in the long-term. Arthroscopy studies have shown that most perforations consist of more than one third of the TMJ disc area, signifying the need to develop novel treatments for large defects. In this study, the objective was to validate the safety and efficacy of tissue-engineered neocartilage implants to regenerate large (6 mm diameter) perforations in the TMJ disc of the Yucatan minipig. It was hypothesized that large TMJ disc perforations treated with self-assembled neocartilage would result in mechanically robust, regenerated tissue. Furthermore, it was predicted that empty defect controls would remain perforated. All implant-treated perforations fully closed while all control discs remained perforated, with a defect perimeter of 14.6 ± 5.8 mm. Regenerated tissue was mechanically robust, with Young's modulus and ultimate tensile strength values that were 81.2% and 79.2% of native TMJ disc values, respectively. The biochemical and proteomic composition of regenerated tissue was shown to be similar to that of the native TMJ disc. For example, collagen types I and III were within native TMJ disc ranges. In the control TMJs, mandibular condyle cartilage showed degenerative changes, and tissue adjacent to the disc perforations showed significant decreases in collagen type I and significant increases in collagen type III, which may be indicative of degeneration. After 8 weeks, self-assembled neocartilage implants were shown to be safe via necropsy, complete blood count, and comprehensive metabolic panel,

[11] **Chapter in preparation for submission as:** Donahue, R.P.,* Bielajew, B.J.,* Vapniarsky, N., Heney, C.M., Arzi, B., Hu, J.C., Athanasiou, K.A. Tissue-engineered implants regenerate large perforations in the Yucatan minipig temporomandibular joint disc. For submission in *Nature Medicine* (* These authors contributed equally.)

and, as predicted, there was a mild cellular response to the implant. With safety and efficacy shown in large perforation defects, self-assembled neocartilage implants are primed for translation to clinical trials and human usage, where they are envisioned to improve clinical outcomes for millions of TMD patients.

Introduction

The temporomandibular joint (TMJ) is crucial for everyday functions including eating, talking, and breathing. Temporomandibular disorders (TMDs), which can result in debilitating pain and loss of function of the TMJ, symptomatically affect up to 83 million people in the U.S. [1-5]. Most TMD cases involve anterior displacement of the TMJ disc [7], and up to 15% of these cases also involve perforation of the disc [8-10]; however, perforation can also occur independently of disc displacement [8]. While many of these TMD patients seek medical treatment to decrease pain and improve function, long-term outcomes of most treatments are ineffectual [16]. Despite the high prevalence, the critical need for TMD treatments, including those for TMJ disc perforation, remains a largely unresolved clinical problem.

Current clinical treatments for TMDs are lacking. Even though osteoarthritis incidence in the TMJ is similar to that in the knee, the TMJ has only a fraction of current procedural terminology (CPT) codes for joint arthroplasty and approximately a 2000-fold fewer projected total joint procedure frequency when compared to the knee [11]. While there exist non-invasive, early-stage therapies such as physical therapy, analgesics, and splints for TMDs [282], most non-surgical approaches are only palliative [16], and surgery is not considered until pain becomes intolerable [14]. Moreover, due to the average implant lifetime coupled with the young age of patients, end-stage surgical treatments such as discectomy and total joint replacements often require revision [11]. Thus, the TMJ surgical field would benefit immensely from an effective and lasting mid-stage intervention to avoid revision surgeries and to treat patients

earlier in the disease timeline. A potential solution to address this unmet clinical need would be a safe and effective tissue engineering approach to treat mid-stage discal TMDs.

Tissue engineering has recently shown promise as a treatment for TMDs, with research focusing on regeneration of cartilage defects to replacing entire TMJ discs. For example, recent approaches include the use of 3D-printed gelatin-genipin scaffolds for TMJ cartilage regeneration [568] and biodegradable polymeric TMJ disc implants [569]. However, despite the need for mid-stage treatments, there is only one cell-based therapeutic approach for TMDs in clinical trials worldwide [328]. To bring new tissue-engineered therapeutics to market, preclinical safety and efficacy must be validated in large animal models. The Yucatan minipig has recently been indicated as an exemplary large animal model for TMDs [24], and it has recently been used in tissue-engineering experiments using self-assembled neocartilage implants in small disc thinning [23] and small perforation [570] indications. In the small (i.e., 3 mm diameter) perforation study, self-assembled neocartilage implants were shown to facilitate the deposition of a regenerated tissue with mechanical properties and extracellular matrix (ECM) components similar to native fibrocartilage, unlike the inferior fill tissue of empty defect controls [570]. With these advancements, tissue engineering is a promising solution to the unmet clinical needs, including disc perforation, of TMD patients.

It remains unknown whether self-assembled cartilage can regenerate larger perforations in the TMJ disc. According to one arthroscopic study, nearly 70% of TMJ disc perforations have an area larger than one third of the TMJ disc surface [9], indicating a need to show efficacy in larger defect sizes. Thus, the present study scales up the defect size and uses self-assembled neocartilage implants to treat large (6 mm dia.) perforations in the TMJ disc. The objective of this study is to validate the safety and efficacy of self-assembled neocartilage implants for the regeneration of large TMJ disc perforations in the Yucatan minipig. Safety measures include blood analysis, complete necropsy, and histology for immune response. Efficacy validation includes mechanical testing, biochemical analysis, and bottom-up proteomics of implant-treated

discal tissues compared to empty defect controls and native TMJ discs. The hypothesis is that large TMJ disc perforations treated with self-assembled neocartilage implants will produce regenerated tissue that is mechanically robust and comprises an ECM similar to native TMJ disc in glycosaminoglycan (GAG), total collagen, and collagen subtype content. It is also predicted that control discs will not heal, resulting in no tissue fill. Additionally, it is predicted that implants will be well-tolerated, both systemically and locally, indicating a safe intervention for TMJ disc perforations. Because the clinical application of self-assembled neocartilage implants is dependent on validation of safety and efficacy in large animal models, this work represents a crucial step toward translating tissue-engineered TMJ disc implants to human clinical use.

Results

Tissue-engineered implants were suitable for implantation

Self-assembled neocartilage implants made from high-passage (passage 7) costal chondrocytes had a robust cartilaginous ECM. This study used a nonhomologous, allogeneic approach to engineer neocartilage implants for TMJ disc perforations in the Yucatan minipig (Figure 11-1A). After isolation of costal chondrocytes from three juvenile minipigs [338], implants were fabricated using the self-assembling process (Figure 11-1B), yielding an implant of approximately 11x17 mm in size that was trimmed to 11x11 mm for implantation into the TMJ disc (Figure 11-1C). After 6 weeks of self-assembly with bioactive factor application with transforming growth factor beta 1 (TGF-β1), chondroitinase ABC (C-ABC), and lysyl oxidase-like 2 (LOXL2) (Figure 11-1B) [83], the neocartilage implants stained intensely for GAGs and collagen (Figure 11-1D), consistent with previous histology of self-assembled neocartilages [355]. The mechanical properties of the implant prior to surgery were as follows: tensile Young's modulus of 6.15 ± 1.52 MPa, ultimate tensile strength (UTS) of 2.49 ± 0.85 MPa, 20% compressive relaxation modulus of 255 ± 85 kPa, and 20% compressive instantaneous modulus of 1061 ± 251 kPa. These implants, derived from highly passaged costal chondrocytes, were

engineered to achieve functional properties approaching native TMJ disc values [24] and were deemed sufficient to proceed with implantation in skeletally mature minipigs.

The intralaminar perforation surgical technique was successful in securing implants in large perforation defects

Modeled after previous surgical approaches for small TMJ disc defects [23, 570], the intralaminar perforation technique was used to create and treat large perforation defects (6 mm diameter) in the Yucatan minipig TMJ disc (Figure 11-2). Previously, this technique was used in a small TMJ disc thinning (3 mm diameter, one-sided, partial thickness) defect model [23], and, more recently, a small perforation (3 mm diameter, two-sided, full thickness) model [570]. After the TMJ disc was approached and identified, an incision was created along the lateral edge of the disc and deepened toward the medial aspect to create a pocket (Figure 11-2A), and, using a 6 mm biopsy punch, a large perforation was created in the centrolateral region of the disc (Figure 11-2B). The neocartilage implant was placed inside the pocket (Figure 11-2C), the two laminae were sutured shut (Figure 11-2D), and the lateral edge of the disc was anchored to the condylar process using a bone anchor. This procedure allowed the implant to be secured without placing sutures in the disc articular surface, which has been previously reported to result in abrasion of the adjacent articular surfaces and dislodgement of the implant from the defect [23]. The application of the surgical technique to large defects was successful in securing and protecting the implant.

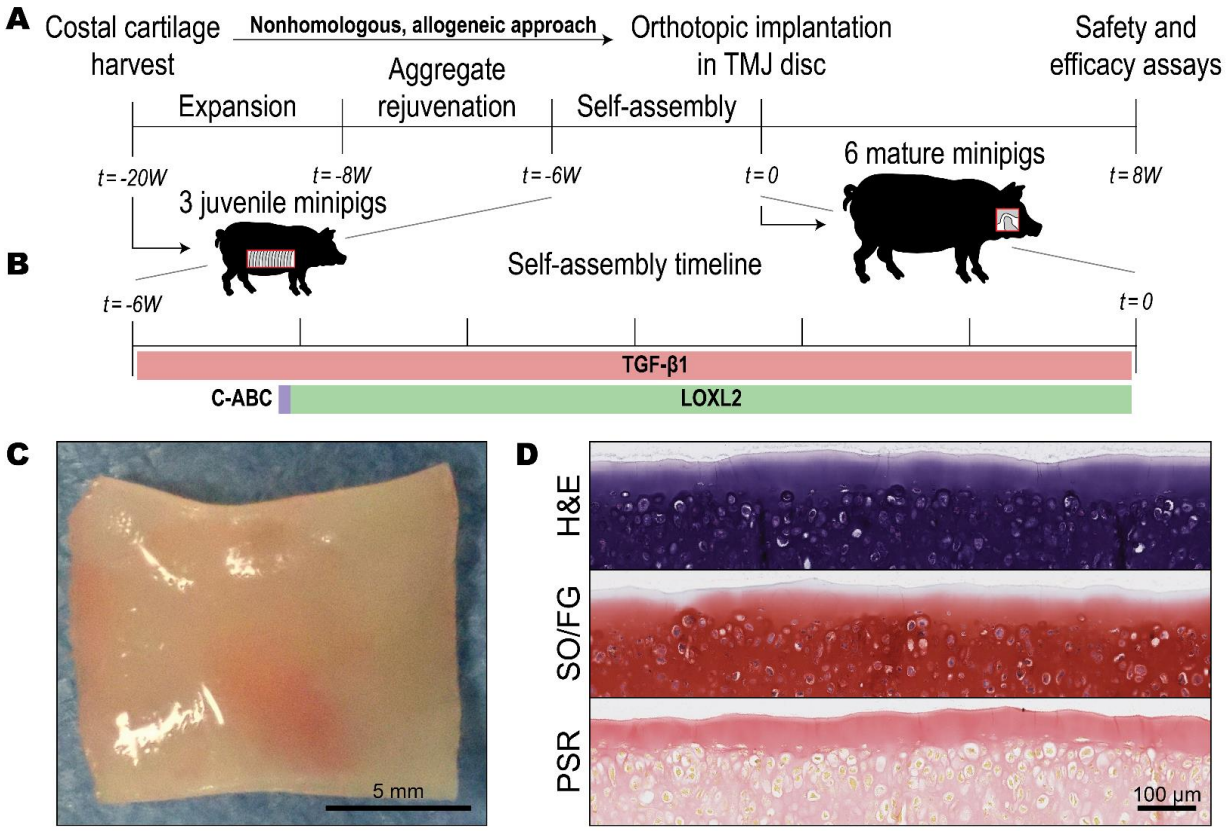

Figure 11-1: Tissue-engineered implants were suitable for nonhomologous usage in the TMJ disc.
(A) Costal chondrocytes from the rib cartilage of juvenile minipigs were expanded, rejuvenated, and self-assembled prior to implantation into the minipig TMJ disc of mature animals. After 8 weeks *in vivo*, safety and efficacy assays were performed. (B) The self-assembly timeline is presented, including application of transforming growth factor beta 1 (TGF-β1), chondroitinase ABC (C-ABC), and lysyl oxidase-like 2 (LOXL2) over the course of 6 weeks. (C) The implant measured approximately 11x11 mm after trimming and (D) showed intense staining with hematoxylin and eosin (H&E), safranin O with fast green counterstain (SO/FG) for glycosaminoglycan content, and picrosirius red (PSR) for total collagen content.

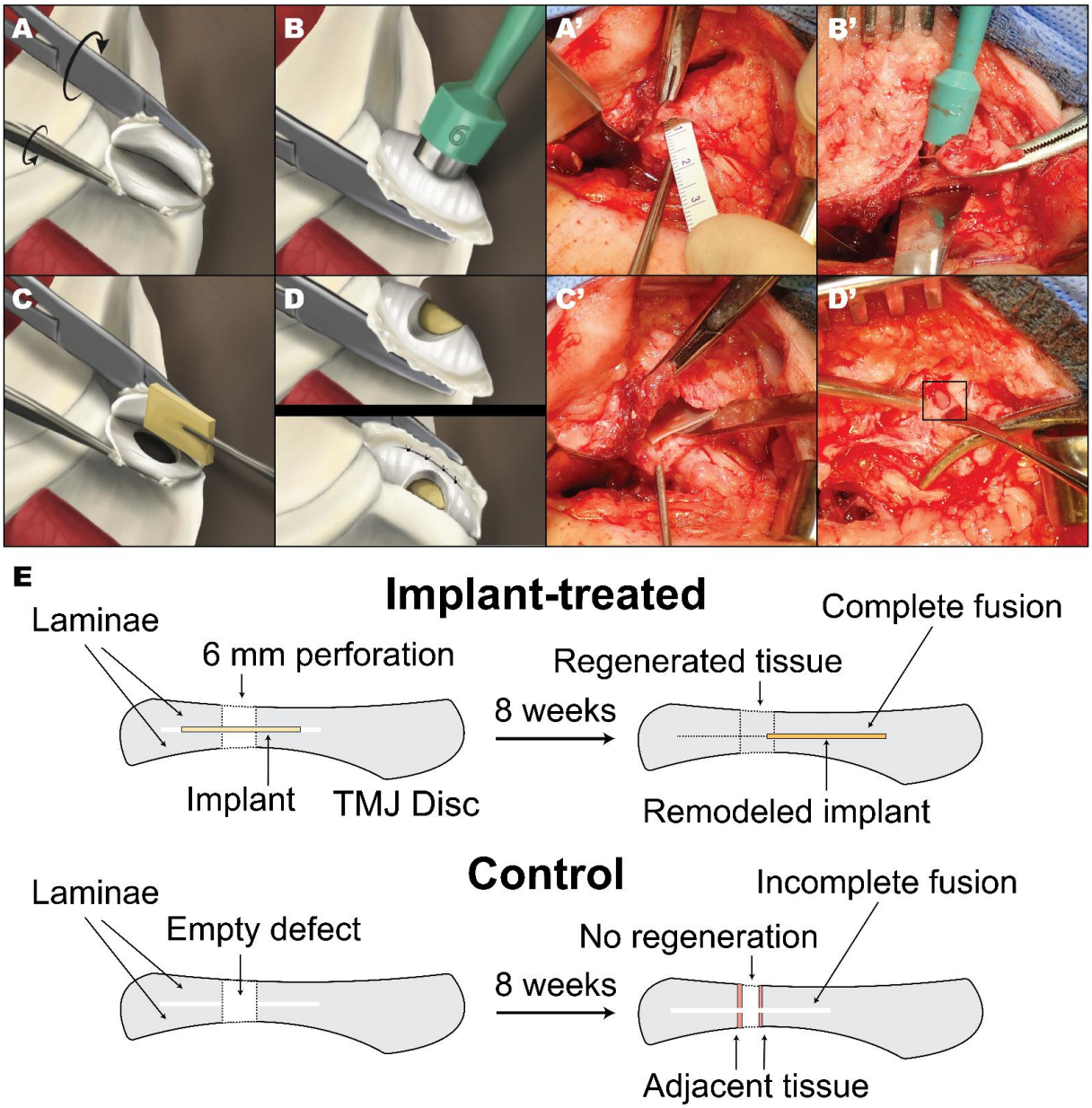

Figure 11-2: The intralaminar perforation technique secured implants in place toward regeneration of large perforation defects.
After TMJ identification, (A) an incision was made into the lateral edge of the disc and deepened to accommodate the implant. (B) A 6 mm diameter disposable biopsy punch was used to create the perforation defect. (C) The 11x11 mm implant was placed into the lateral incision, and (D) it was viewable through the defect after implantation and suturing along the edge of the disc. After surgery, (E) implant-treated discs facilitated cartilage regeneration, resulting in intralaminar fusion and regenerated tissue deposition. Implants remodeled over 8 weeks and migrated in the posterior direction. Control discs did not regenerate, and tissue adjacent to the defect underwent biochemical changes.

Implants achieved tissue regeneration after 8 weeks; controls did not heal

Self-assembled neocartilage implants in the TMJ disc facilitated the deposition of regenerated tissue, while control discs remained empty and perforated after 8 weeks (Figure 11-2E). Here, the term “regenerated tissue” refers to the tissue that fills the perforations after 8 weeks in implant-treated TMJ discs. As seen in the gross morphological images of the excised TMJ discs, all three implant-treated animals exhibited remarkable healing of large perforations after 8 weeks, while the three control discs remained perforated (Figure 11-3A). Upon sectioning anteroposterioly, implants were identified. Non-closure of the laminae and lack of tissue fill was observed in the controls (Figure 11-4A-B). Further examination of implant-treated discs showed incomplete intralaminar fusion in one disc (Figure 11-4C). Regardless, regenerated tissues for the treated discs were present when examined under hematoxylin and eosin (H&E) staining (Figure 11-4C-D). The perimeter of the perforation after 8 weeks in controls was 14.6 ± 5.8 mm, significantly higher than implant-treated discs, which had a perimeter of zero (Figure 11-5A). Similarly, implant-treated discs exhibited no measurable defect area after 8 weeks of healing compared to control discs which had a defect area of 10.2 ± 7.8 mm^2 (Figure 11-5B). When examining the intralaminar fusion by mechanically testing the two laminae, Young’s modulus and UTS values were 6.8-times and 3.0-times higher in implant-treated discs compared to controls, respectively, although these increases were not statistically significant (Supplementary Table 11-1). Both implant-treated and control condyles exhibited degenerative changes on the lateral condylar process due to suture anchor placement (Figure 11-3B), consistent with previous work [570]. However, control animals also had cartilage defects on two of three articulating surfaces, while implant-treated condyles did not exhibit cartilage defects (Figure 11-3B). Ultimately, when examining the gross morphology of the implant-treated discs and condyles, self-assembled neocartilage implants facilitated exceptional healing of discs, unlike the controls that all displayed disc perforations and condylar articular cartilage degeneration.

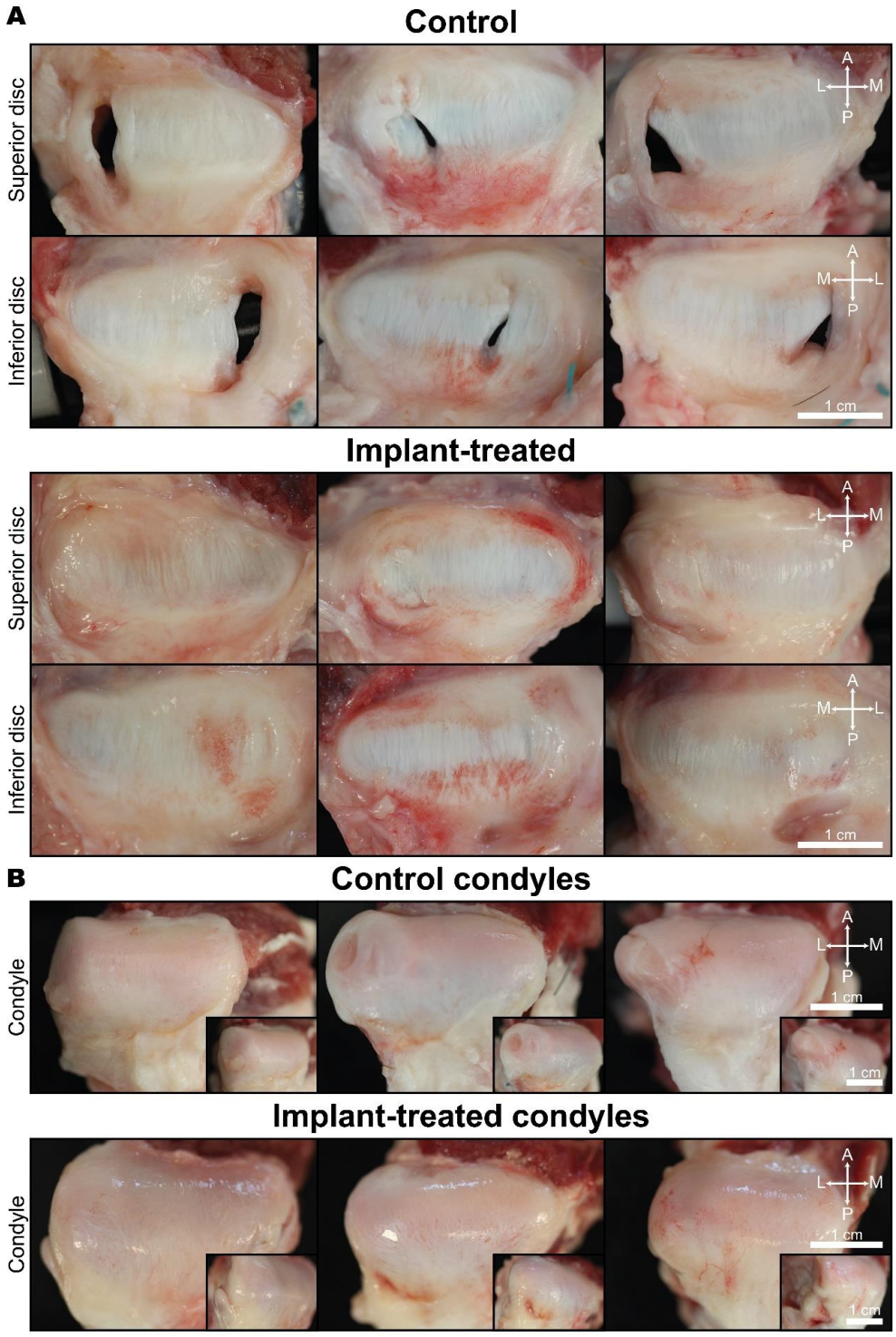

Figure 11-3: Control discs and condyles showed degenerative changes compared to implant-treated discs and condyles after 8 weeks.
(A) In control discs, the created perforations were still present after 8 weeks, while implant-treated discs exhibited complete filling of defects with regenerated tissue. (B) Condyle articular cartilage defects were also present on two of the three articulating surfaces in the control group. In the implant-treated group, minor degenerative changes were shown on the condyles due to suture rubbing associated with surgical intervention. A, anterior, L, lateral, M, medial, P, posterior.

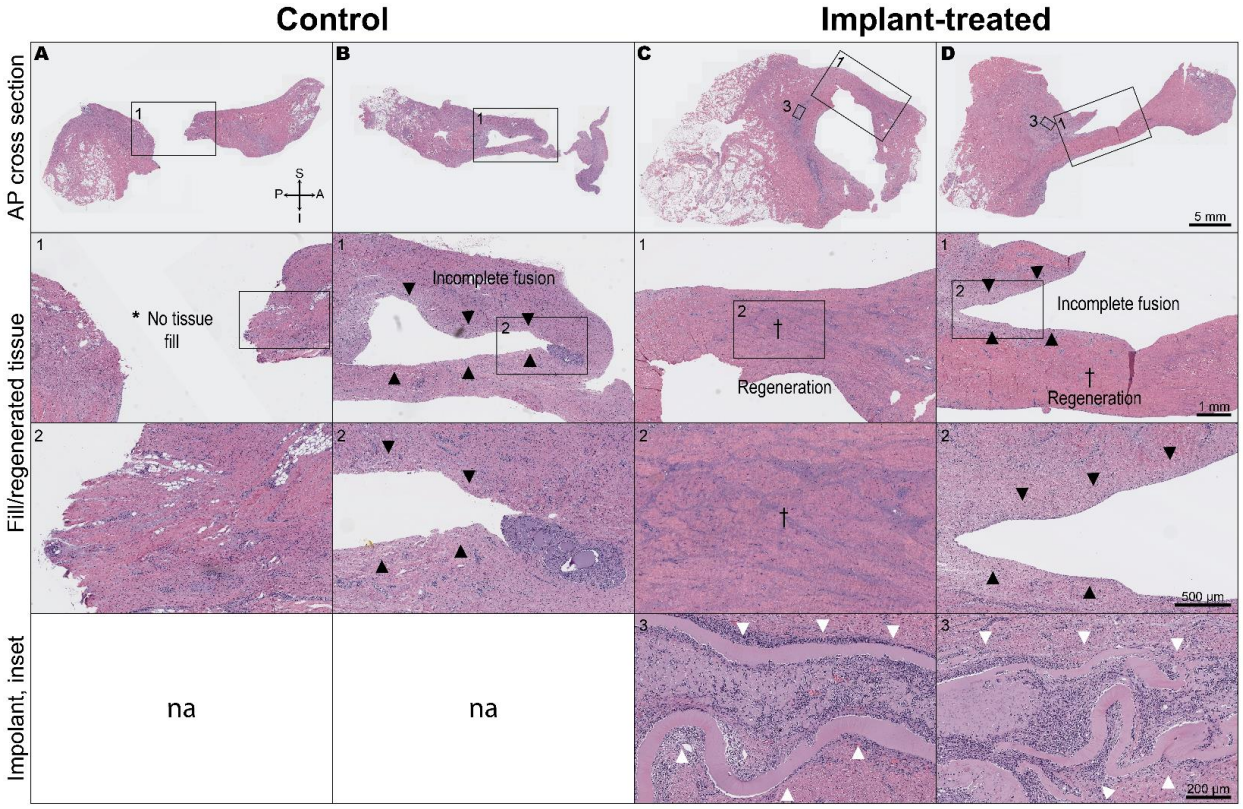

Figure 11-4: Implant-treated discs exhibited regeneration in the centrolateral region of the TMJ disc, and controls displayed lack of healing.
When sectioned in an anteroposterior (AP) direction, four different samples between the two groups displayed various indications of healing and lack thereof. In column (A), a control disc did not exhibit tissue fill in the centrolateral portion (*) of the disc. In column (B), the pocket incision made during surgical implantation (black arrowheads) did not fuse in another control disc. In comparison, both implant-treated discs in columns (C) and (D) exhibited regenerated tissue (†) in the centrolateral portion of the disc, but column (D) did not exhibit complete fusion of the incision (black arrowheads). Both implant-treated discs also had implant remaining (white arrowheads) after 8 weeks of implantation. A, anterior, I, inferior, na, not available, P, posterior, S, superior.

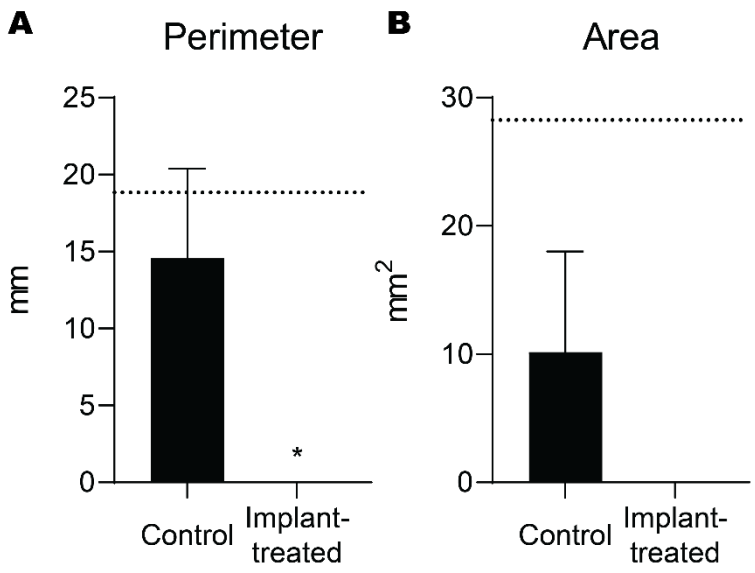

Figure 11-5: Defect perimeter and area after 8 weeks of implantation were higher in controls.
Compared to implant-treated discs, empty defect controls still had measurable defects, which were significantly larger in perimeter. Dashed lines represent the original perforation defect perimeter and area.

Regenerated tissue, only present in implant-treated discs, displayed robust tensile properties

Regenerated tissue was mechanically robust, with mechanical properties approaching those of native TMJ disc fibrocartilage. The controls remained completely perforated; thus, with no tissue present, their mechanical properties were determined to be zero. Mechanical testing of regenerated tissue yielded a tensile Young's modulus of 18.09 ± 5.22 MPa and UTS of 4.77 ± 2.00 MPa, which were 81.2% and 79.2% of the values of the contralateral, native tissue controls, respectively (Figure 11-6A-B). Strain at failure, resilience, and toughness were 86.1%, 64.5%, and 64.4% of native tissue values, respectively (Figure 11-6C-E). All regenerated tissue mechanical outcomes were significantly higher than controls. Thus, after 8 weeks of *in vivo* implantation, exceptional healing was further evidenced by the robust mechanical properties of regenerated tissue in the implant-treated discs.

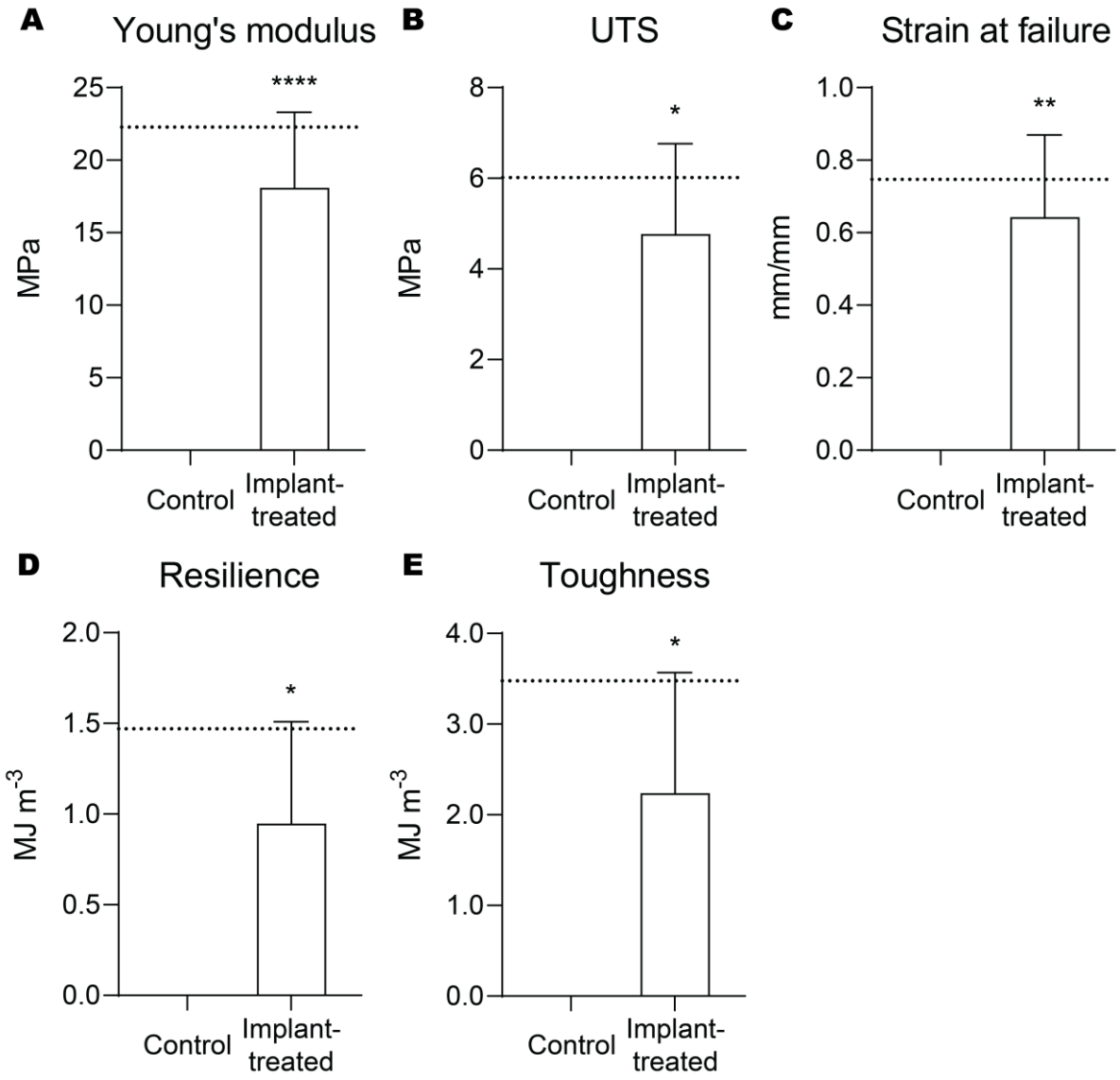

Figure 11-6: Regenerated tissue tensile properties approached native tissue values.
In (A) Young's modulus, (B) ultimate tensile strength (UTS), (C) strain at failure, (D) resilience, and (E) toughness, regenerated tissue of implant-treated discs approached native tissue values (dashed lines), reaching an average of 75.1% of native tissue values across all outcomes.

Regenerated tissue biochemical and proteomic composition was reminiscent of native TMJ discs

The biochemical and proteomic makeup of the regenerated tissue was similar to that of the native TMJ disc controls (tissue removed via biopsy punch during surgery). Due to lack of regenerated tissue in controls, biochemical measures for controls were all zero. In the

regenerated tissue, total collagen content per dry weight (DW) was 72.8 ± 20.9%, which was 85.9% of the value of the native TMJ disc (Figure 11-7A). Collagen types I and III were 92.25 ± 2.99% and 5.99 ± 2.04% per total protein (PROT), respectively, both within native TMJ disc ranges (Figure 11-7B-C). The collagen crosslink profile of regenerated tissue was also similar to native TMJ disc, with mature pyridinoline (PYR) crosslinks, immature dihydroxylysinonorleucine (DHLNL) crosslinks, and crosslink maturity ratios all on par with native tissue values (Figure 11-7D-F). All biochemical and proteomic measurements were significantly higher in regenerated tissues than in controls (Figure 11-7). Other bottom-up proteomic analytes and crosslink measurements are reported in Supplementary Table 11-2 and Supplementary Table 11-3, respectively. Over the course of 8 weeks of healing, implant treatment facilitated the regeneration of TMJ disc fibrocartilage, as shown through the native-like biochemical and proteomic contents in the regenerated tissue.

Tissue adjacent to perforations in controls deviated from native TMJ disc composition

The biochemical and proteomic properties of the tissue adjacent to the control perforations (referred to as “adjacent tissue”) were different than those of control TMJ disc tissue. Because the regenerated tissue was grossly indistinguishable from native TMJ disc, and because there was no discernible border between regenerated tissue and native tissue, the adjacent tissue was compared to native TMJ discs. Total collagen content per DW was not significantly different in adjacent tissue compared to native control TMJ discs (Figure 11-8A); however, collagen type I, the primary collagen subtype in the TMJ disc [237], was significantly lower in the adjacent tissue (89.79 ± 2.05%/PROT) than in native TMJ disc (95.01 ± 3.10%/PROT) (Figure 11-8B). Collagen type III, associated with scar tissue formation [341], was significantly higher in the adjacent tissue (9.17 ± 1.55%/PROT) than in native TMJ disc (4.31 ± 2.69%/PROT) (Figure 11-8C). Mature PYR crosslinks per hydroxyproline (OHP) were also lower in the adjacent tissue (8.2 ± 3.7 mol/mol) than in native TMJ disc (16.4 ± 2.2 mol/mol), indicating that the collagen of

the adjacent tissue was less crosslinked (Figure 11-8D). Immature DHLNL crosslinks and the collagen crosslinks ratio were not significantly different, but the means were lower in adjacent tissue (Figure 11-8E-F). Additional proteomic and biochemical properties of adjacent tissue are reported in Supplementary Table 11-2 and Supplementary Table 11-4, respectively. The lower crosslink and collagen type I content and higher collagen type III content show that tissues adjacent to control perforations are undergoing postoperative biochemical changes, potentially indicating pathological progression of the control TMJ discs.

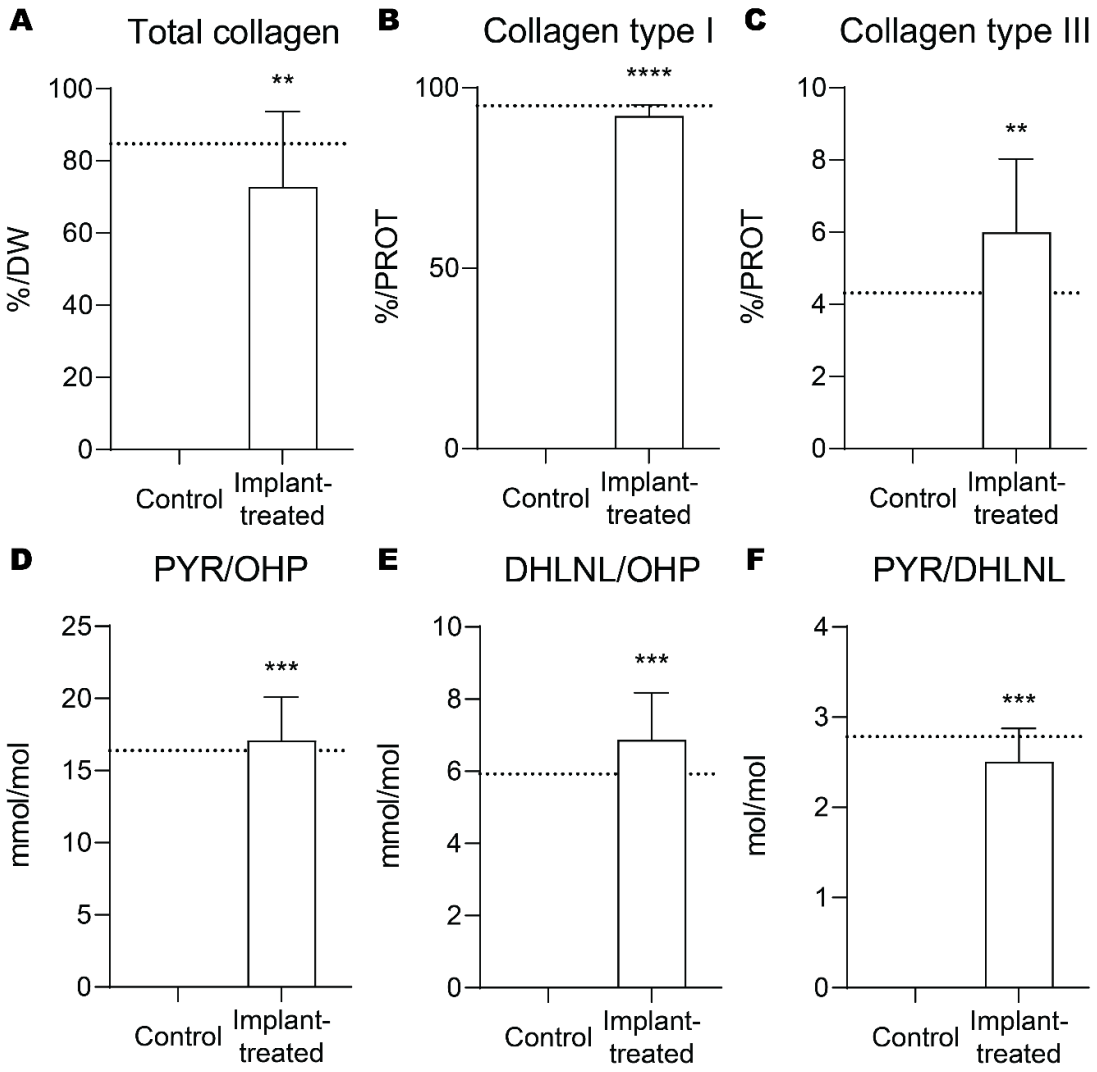

Figure 11-7: Biochemical and crosslink content of regenerated tissue recapitulated native TMJ disc content. After 8 weeks of healing, (A) total collagen, (B) collagen type I, and (C) collagen type III contents were on par with those of native TMJ discs (dashed lines). Collagen types I and III are reported per total protein (PROT). Similarly, (D) pyridinoline (PYR) and (E) dihydroxylysinonorleucine (DHLNL) content per hydroxyproline (OHP) and (F) their ratio were also near native tissue values.

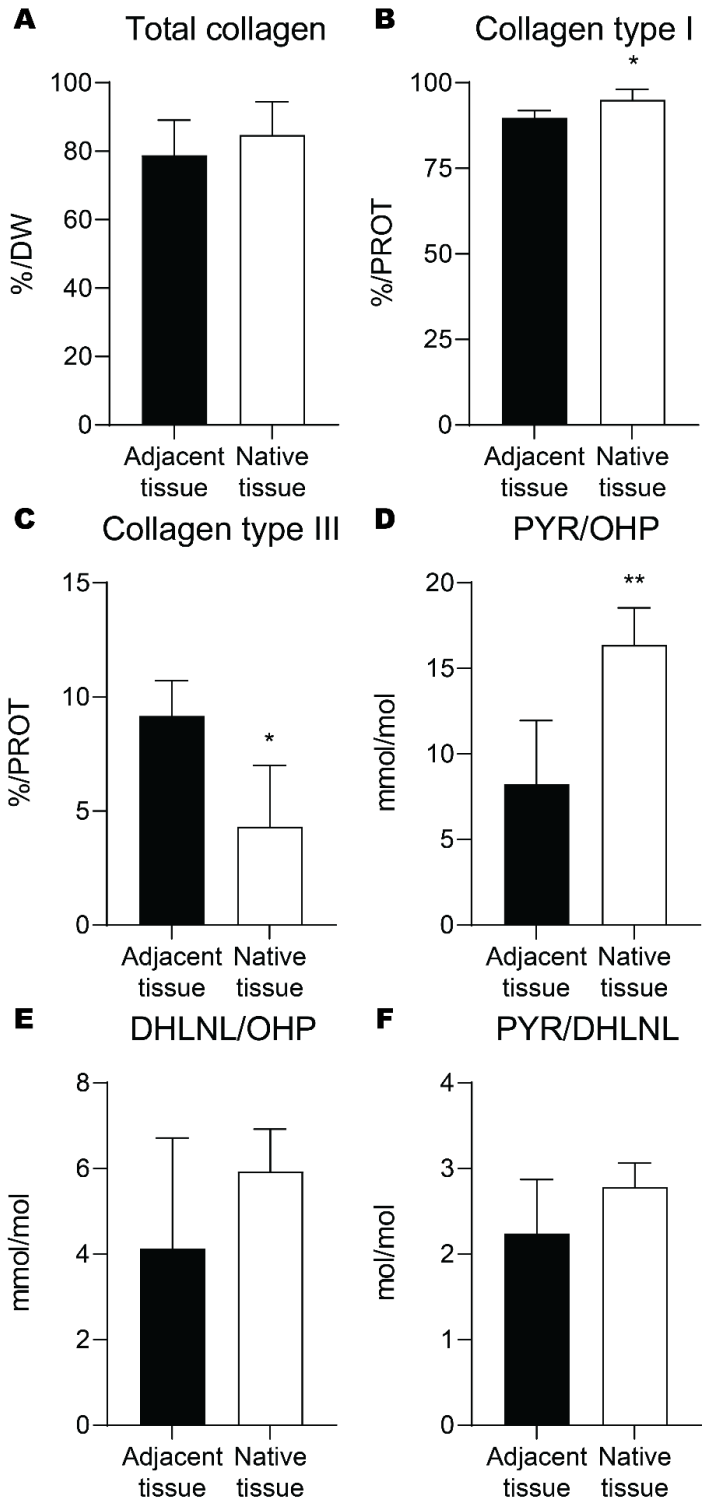

Figure 11-8: Adjacent tissue to control perforations deviated from native tissue in biochemical and crosslink content.
(A) Total collagen, (B) collagen type I, and (C) collagen type III are reported for tissue adjacent to control defects and native TMJ discs. Collagen types I and III are reported per total protein (PROT). Crosslinks data including (D) pyridinoline (PYR) and (E) dihydroxylysinonorleucine (DHLNL) per hydroxyproline (OHP) and (E) their ratio are reported.

Implants remodeled, exhibiting biochemical and proteomic contents similar to native TMJ discs

The implants exhibited significant biochemical changes over the implantation period, where they remodeled toward the makeup of native TMJ disc (Figure 11-9). When compared to t=0 *in vitro* controls, t=8W *in vivo* implants had many significant differences in biochemistry, mechanics, collagen crosslinks, and proteomics. Between the t=0 *in vitro* and t=8W *in vivo* implants, total collagen significantly increased from 19.4 ± 1.2%/DW to 33.0 ± 13.6%/DW, a 1.7-times increase, although this value was still lower than native TMJ disc (84.8%/DW, dashed line) (Figure 11-10A). In contrast, implants cultured *in vitro* for 8 weeks did not have significantly different total collagen compared to the t=0 *in vitro* implants (Figure 11-10A). GAG content decreased from t=0 *in vitro* controls in both the t=8W *in vitro* and t=8W *in vivo* implants; however, only the GAG of the t=8W *in vivo* implants (0.3 ± 0.5%/DW) dropped to levels similar to native TMJ discs (1.2%/DW, dashed line) (Figure 11-10B). Some mechanical measurements of the implant significantly decreased after 8 weeks *in vivo*, with the UTS, resilience, and toughness dropping by 55.5%, 73.2%, and 58.9%, respectively (Figure 11-10C-F). Compressive properties of implants are reported in Supplementary Table 11-5, but t=8W *in vivo* implants were not tested due to lack of tissue availability. Despite these drops in tensile properties, biochemical content of implants remodeled toward native tissue levels of TMJ discs.

The collagen crosslink profile of the implants also underwent *in vivo* remodeling, with PYR/DW and DHLNL/DW both significantly increasing by 3.8-times and 3.1-times, respectively (Figure 11-11A, C). However, given the 1.7-times increase in total collagen in the t=8W *in vivo* implants compared to t=0 *in vitro* baseline values (Figure 11-10A), the increases in crosslinking per DW were likely conflated with increases in total collagen. The degree of collagen crosslinking (i.e., PYR/OHP) was significantly lower in t=8W *in vivo* implants (Figure 11-11B), which potentially led to inferior tensile properties (Figure 11-10C-F). However, most collagen crosslink measures of the t=8W *in vivo* implants were closer to native tissue values than t=0 *in vitro* implants (Figure 11-11). The proteome of the neocartilage implants was also shown to

remodel toward fibrocartilage over the 8-week implantation period. Collagen type I, the main collagen subtype of fibrocartilage [237], significantly increased 6.1-times over 8 weeks of implantation, while collagen type II, the main collagen subtype of hyaline cartilage [237], decreased by over 99.9% (Figure 11-12A-B). Collagen type III significantly increased 39.6-times toward levels of the native TMJ disc (Figure 11-12C). Importantly, collagen type X, associated with cartilage calcification [237], was minimal (<0.01%/PROT) in t=0 *in vitro* controls and was not found in t=8W *in vivo* implants, indicating that the costal chondrocyte-derived implants did not have a propensity to calcify. Other proteomic analytes, including aggrecan, biglycan, and link protein dropped to levels similar to native TMJ discs (Figure 11-12E-H). All bottom-up proteomic analytes are reported in Supplementary Table 11-2. Bottom-up proteomics further revealed that the ECM of the implants remodeled toward native tissue levels after 8 weeks, where they recapitulated the biochemical and proteomic profile of TMJ discs.

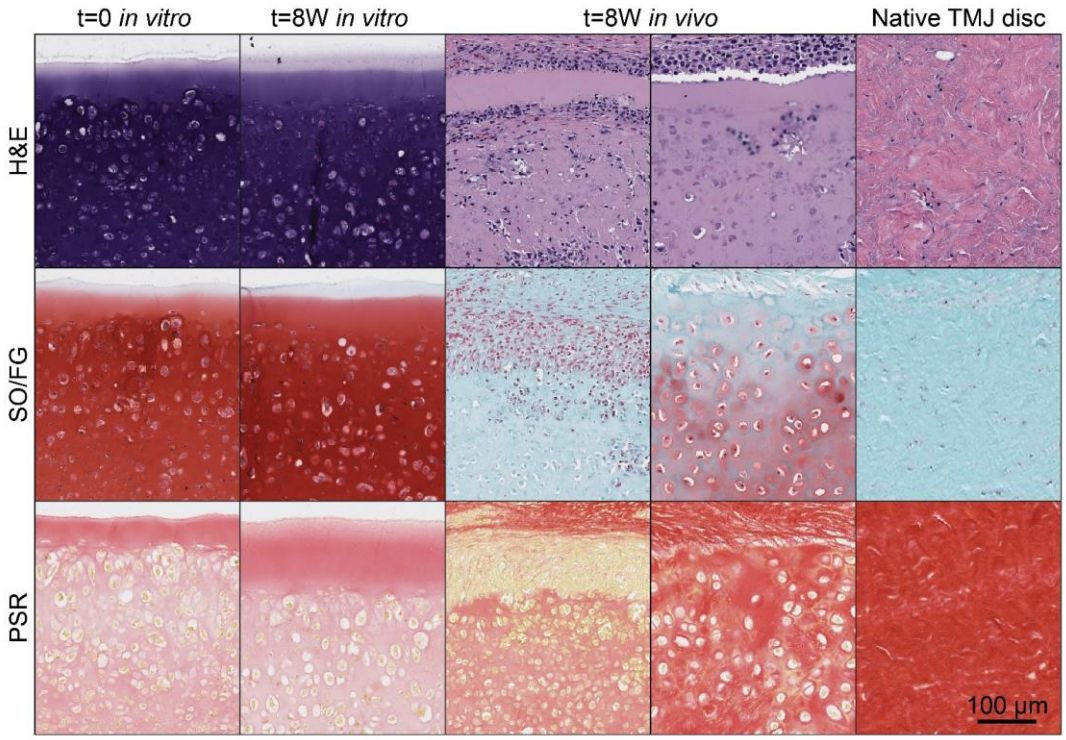

Figure 11-9: Histology of neocartilage implanted for 8 weeks displayed similarities to native TMJ discs.
Hematoxylin and eosin (H&E) for general tissue and cellular morphology, safranin O with fast green counterstain (SO/FG) for glycosaminoglycans, and picrosirius red (PSR) for total collagen are shown. Generally, there were few differences between t=8W *in vitro* implants t=0 *in vitro* implants, while implants placed *in vivo* for 8 weeks remodeled toward the native TMJ disc content in both animals presented (columns).

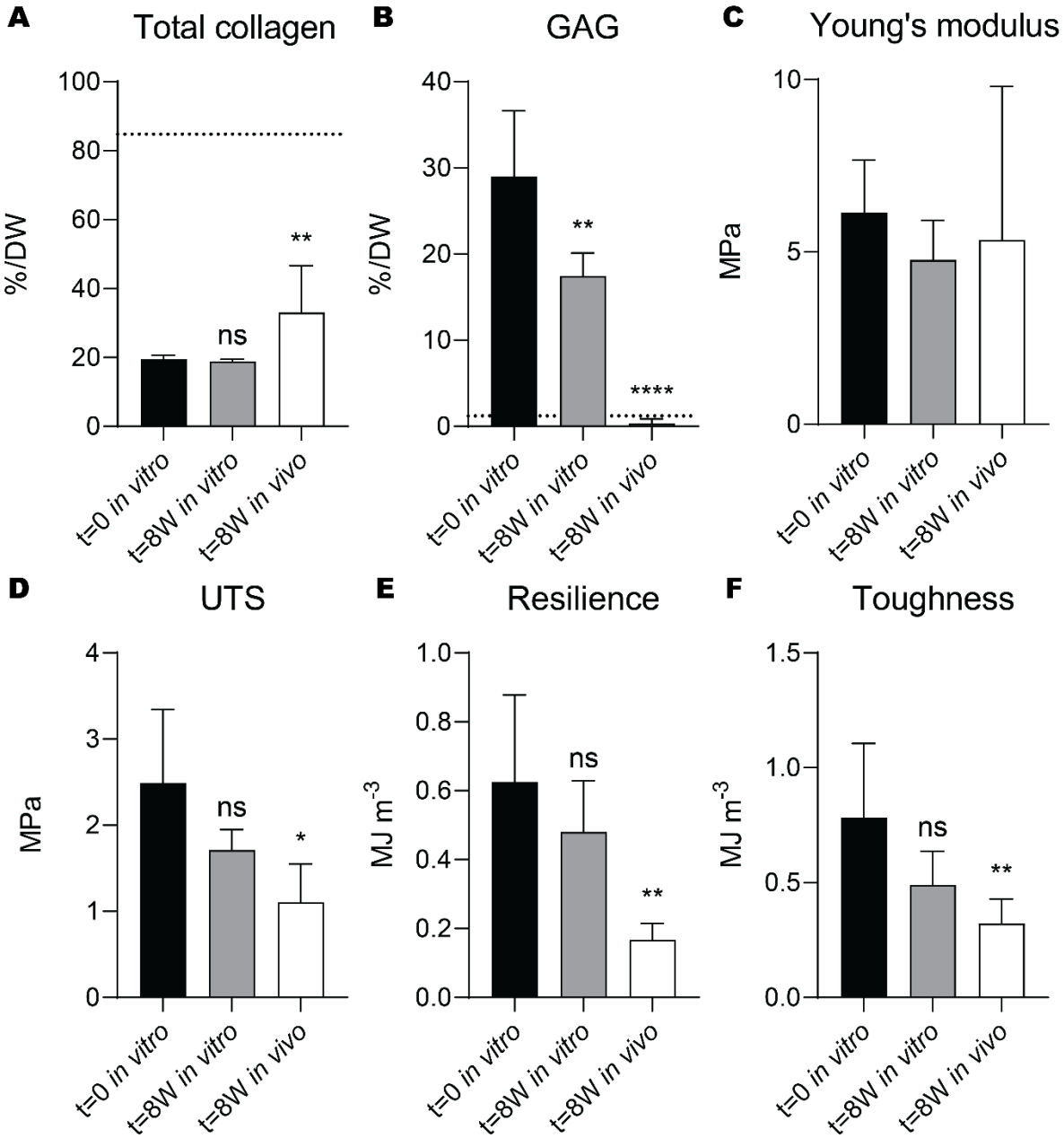

Figure 11-10: Biochemical properties of implants after 8 weeks remodeled toward native tissue values. Over 8 weeks, (A) total collagen and (B) glycosaminoglycan (GAG) contents trended toward native tissue values (dashed lines) in implants placed *in vivo*. (C) Young's modulus, (D) ultimate tensile strength (UTS), (E) resilience, and (F) toughness decreased after implantation.

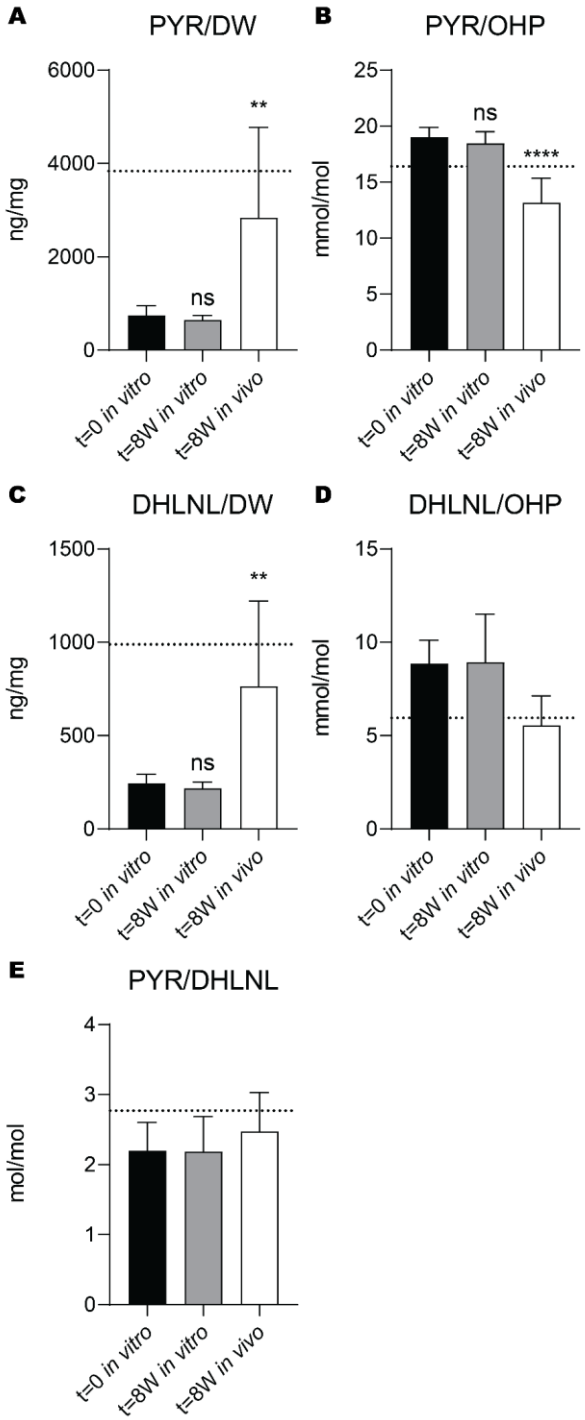

Figure 11-11: Crosslink content after 8 weeks remodeled toward native tissue values.
(A) Pyridinoline (PYR) per dry weight (DW) and (B) per hydroxyproline (OHP), (C) dihydroxylysinonorleucine (DHLNL) per DW and (D) per OHP, and (E) their ratios are reported.

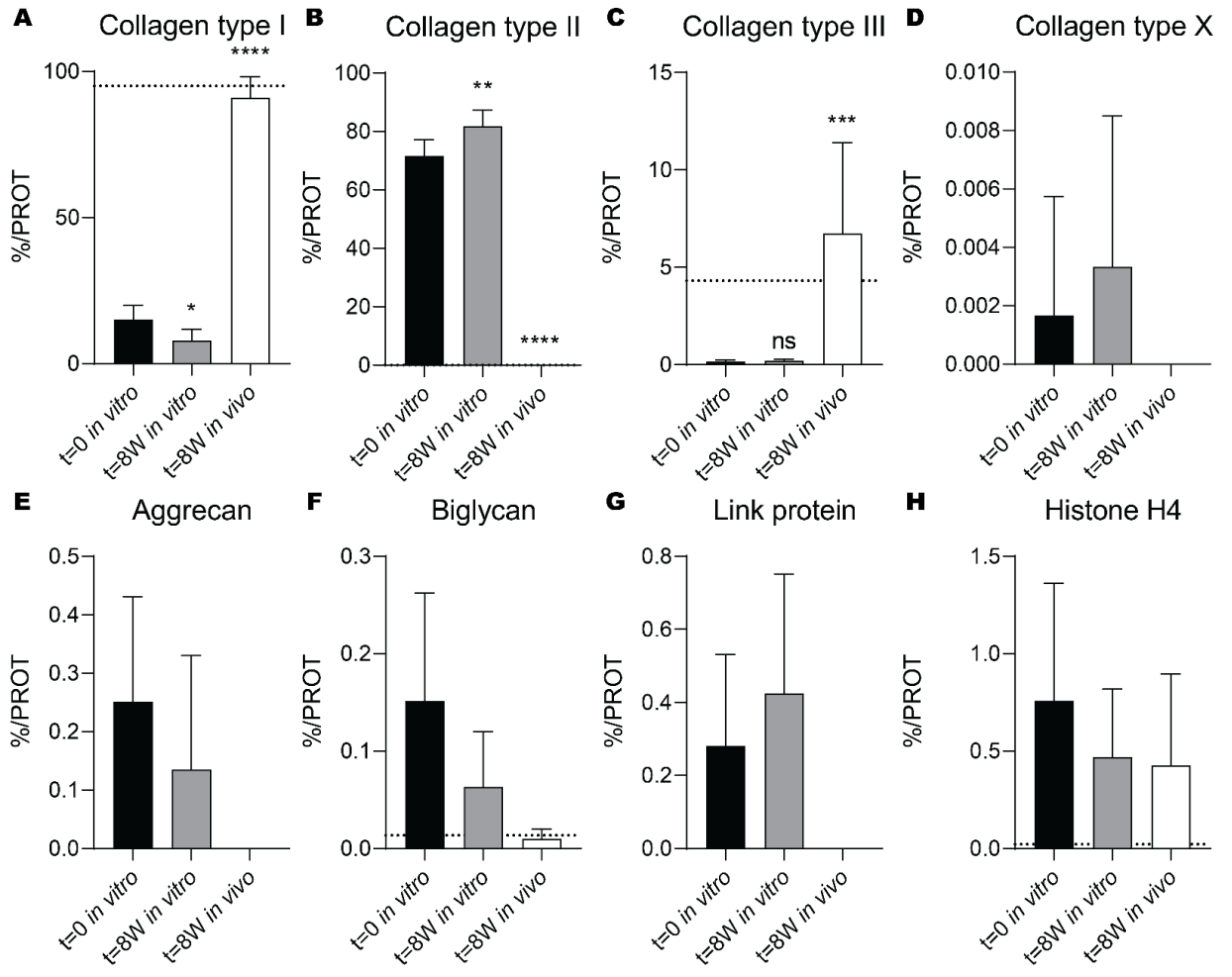

Figure 11-12: Proteomic analytes after 8 weeks of implantation further approached native tissue values.
(A) Collagen type I, (B) collagen type II, (C) collagen type III, (D) collagen type X, (E) aggrecan, (F) biglycan, (G) link protein, and (H) histone H4 are presented per total protein (PROT) content as a percentage. Dashed lines represent native tissue values. Panels without dashed lines had no detectable protein in native tissue samples.

Implants exhibited safety, as shown by no adverse systemic response and minimal local response

Self-assembled neocartilage implants were immunogenically well-tolerated by the recipient minipigs. After surgery, animal jaw function was normal, and minipigs maintained or gained weight, as expected. After euthanasia, a full necropsy of the integumentary, cardiovascular, respiratory, musculoskeletal (non-TMJ), digestive, urogenital, endocrine, and nervous systems revealed normal morphology without cellular damage, inflammation, or neoplastic growth. The

complete blood count and comprehensive metabolic panel (Figure 11-13, Supplementary Table 11-6) revealed few differences at 8 weeks from preoperative blood work. Two animals had moderate increases in eosinophil count (one in the control group at 4.46 K/μL, one in the implant-treated group at 2.62 K/μL, reference range 0.00-2.00 K/μL) (Figure 11-13A). Because the value observed in the implant-treated animal was closer to the reference value than the value observed in the control animal, the elevated eosinophil levels were considered to not be a result of the tissue-engineered implants. The comprehensive metabolic panel showed that all measurements were within normal limits, with only minor differences from baseline values (Figure 11-13B).

Locally, joints exhibited acute swelling and inflammation after surgical intervention which subsided within 2 weeks, as expected. Incisions healed and presented with minimal scarring at 8 weeks. Minipig TMJs exhibited no signs of inflammation or neoplastic growth as examined during *en bloc* excision. Additionally, the synovium appeared non-reactive through gross observation, the joint capsule was intact, and the synovial fluid was minimal and clear in color, indicative of a healthy joint. When further examining cross sections of implants surrounded by native TMJ disc through H&E, there was a moderate cellular immune response (Figure 11-14), consistent with previous 8-week studies [23, 570]. Through H&E, it was determined there were no multinucleated giant cells, polymorphonuclear cells, or capsule formation. Overall, through the examination of the systemic and local responses, safety of self-assembled neocartilage implants was shown.

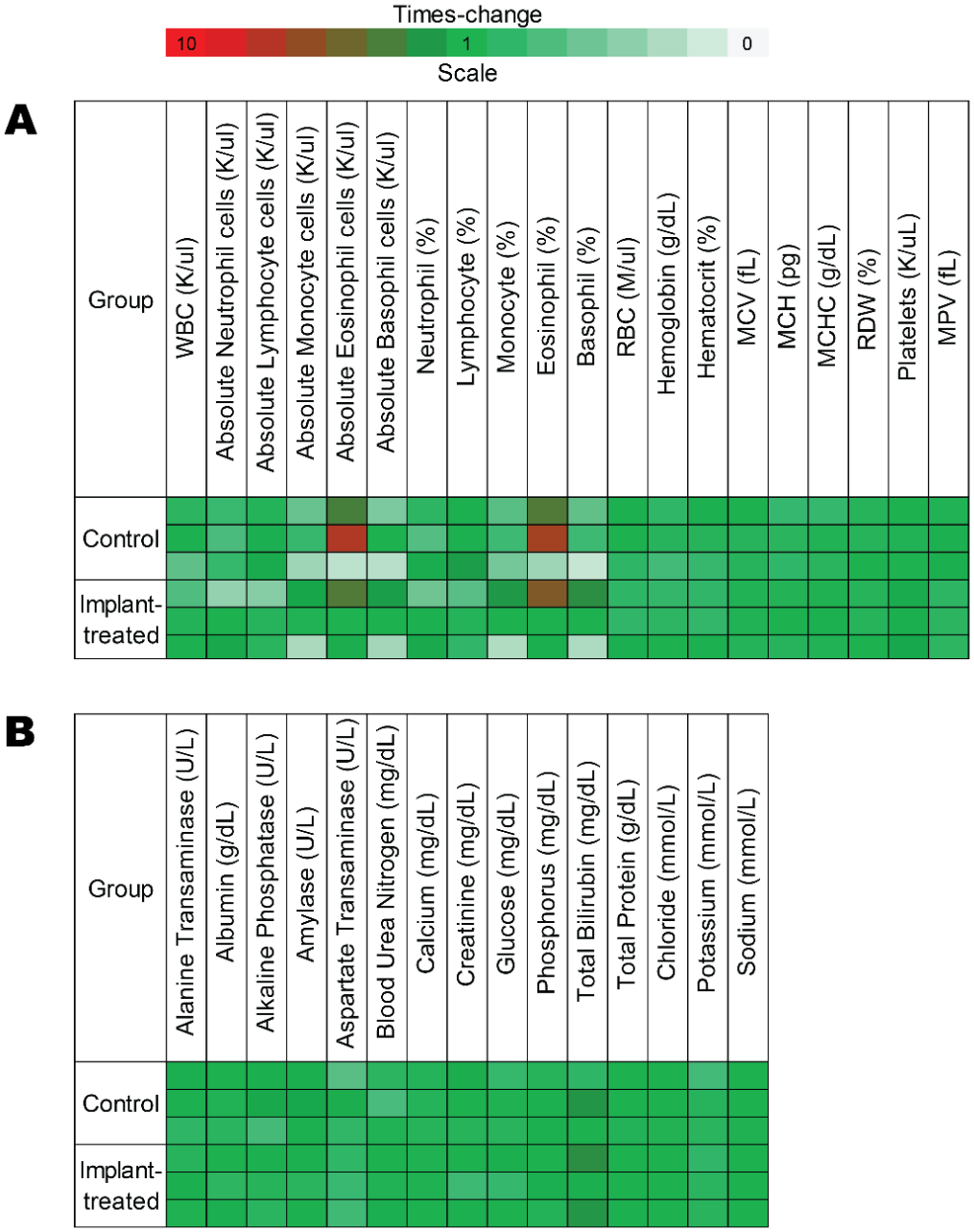

Figure 11-13: Heatmap of normalized complete blood count and comprehensive metabolic panel parameters showed no abnormal systemic effects due to implants.
A majority of parameters after 8 weeks were within normal limits, despite some changes from t=0 baseline values. Each row represents a different animal. Moderate numbers of eosinophils were detected in one control and one implant-treated animal; this was determined to not be due to the implant treatment.

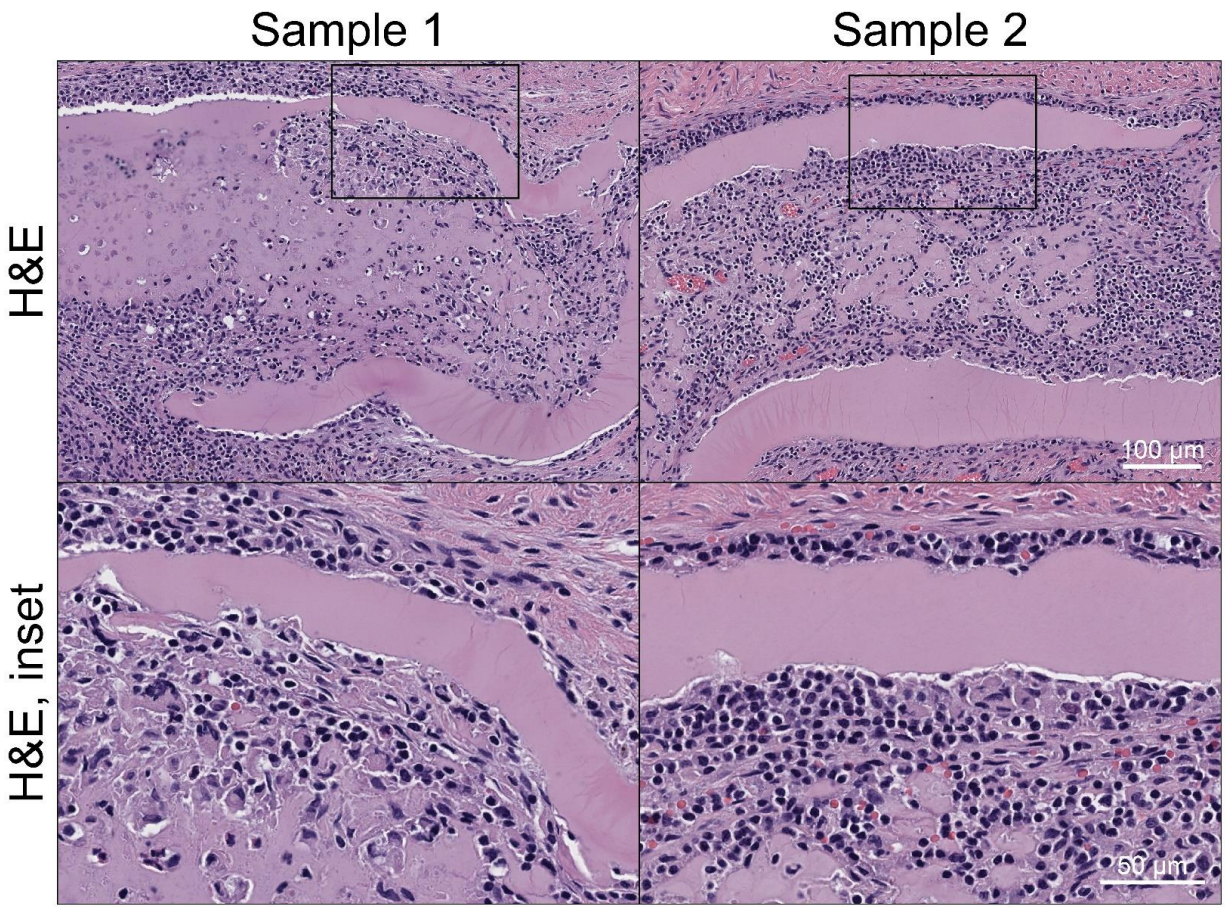

Figure 11-14: H&E revealed moderate cellular response to TMJ disc implants.
After examination through hematoxylin and eosin (H&E), no multinucleated giant cells, polymorphonuclear cells, or capsule formation were observed.

Discussion

Cartilage tissue engineering has the potential to treat TMDs in millions of patients in the U.S. and worldwide, but safety and efficacy of the tissue-engineered implants must be validated through preclinical animal models and clinical trials before they can be widely used in humans. This work represents a significant step in showing safety and efficacy of self-assembled neocartilage implants for regenerating TMJ disc perforations in a clinically relevant, large animal model. Specifically, it was shown that 1) neocartilage implants safely resulted in regenerated TMJ disc fibrocartilage, 2) implanted neocartilages remodeled toward a TMJ disc fibrocartilaginous tissue, 3) TMJ disc fibrocartilage regeneration occurred within 8 weeks, and 4)

perforations of 6 mm diameter were shown to be a critical defect size after 8 weeks. Through this work, the regeneration of fibrocartilage in large perforations of the TMJ disc using self-assembled neocartilage represents substantial progress for translation of tissue-engineered cartilage treatments for TMDs.

The present work represents a significant step forward in showing the safe and effective regenerative capability of self-assembled neocartilage. In this TMJ disc study, no neoplastic growth, cellular damage, or changes from preoperative values as a result of implant treatment were observed systemically. Locally, consistent with previous 8-week studies [23, 570], a moderate cellular response with no signs of multinucleated giant cells, polymorphonuclear cells, or capsule formation was present, indicating neocartilage safety. The differences in the gross morphological appearances of the implant-treated TMJ discs and controls were stark; all control discs remained perforated after 8 weeks, while the implant-treated discs appeared similar in morphology to healthy TMJ discs. The regenerated tissue's tensile properties were, on average, 75.1% of native tissue values, with a biochemical makeup similar to native tissue. Shown through bottom-up proteomics, collagen type I and III quantities were 97.1% and 139.0% of native TMJ disc values, respectively, both within the range of native values. Altogether, the morphological, mechanical, biochemical, and proteomic results showed that neocartilage implants were effective for regenerating TMJ disc fibrocartilage. Cartilage regeneration has remained elusive despite the longstanding effort to develop regenerative approaches [239]. In this work, safe and efficacious fibrocartilage regeneration was achieved, representing a significant step forward in cartilage tissue engineering efforts.

Neocartilage implants were shown to remodel over time toward a fibrocartilaginous biochemical makeup. At t=8W *in vivo*, the implants increased in collagen content by 1.7-times and decreased in GAG by 98.9% compared to t=0 *in vitro* controls. Given the high amount of collagen and low GAG content of fibrocartilages [24], these changes represent fibrocartilaginous remodeling in the neocartilage implant. This is further reinforced by the proteomics data;

collagen type II was initially the primary collagen type upon implantation, accounting for 71.62% of protein, but this value drops to less than 0.05% after 8 weeks *in vivo*, the level of the native TMJ disc. Collagen types I and III, the main collagen subtypes of TMJ discs [237], increased 6.1-times and 39.6-times, respectively, also showing remodeling toward protein proportions of native TMJ disc controls. Other protein analytes, such as aggrecan, biglycan, link protein, and histone H4 also converge to levels similar to native TMJ discs. Given the hypocellularity of the implants at 8 weeks and the immune cells surrounding the implant, it was likely the remodeling seen here was driven by the host response to the implant. This can be verified in future *in vivo* work by implementation of cell tracking technology (e.g., GFP-transfected neocartilage or chromosomal *in situ* hybridization), which would show whether cells in the implant remain and deposit new ECM, or if they are cleared away over time. Though how the remodeling occurs remains to be fully understood, the results presented here are significant in showing that neocartilage implants remodeled toward the phenotype of native TMJ discs after an 8-week maturation time *in vivo*, further reinforcing the safety of the tissue-engineered implant.

In this work, regenerated tissue and implant analyses were performed 8 weeks after implantation. Comparisons to previous long-term studies (i.e., 24 weeks) [570] may help predict how the implants in this study would continue to heal large perforations in the long term. For example, it can be hypothesized that mechanical properties of the regenerated tissue would improve beyond 8 weeks. In the present study, the 8-week regenerated tissue had a UTS of 4.77 ± 2.00 MPa, which was 79.2% of the strength of native tissue. In a 24-week study on smaller perforations [570], the regenerated tissue had a UTS of 8.67 ± 2.04 MPa, 1.8-times higher than this 8-week study. While the ~80% recovery of native UTS in 8 weeks is promising, the increase seen at 24 weeks indicates long-term survivability and functionality of the regenerated tissue. Differences in implant remodeling were also seen between the 24-week study [570] and the present 8-week study. Proteomic analysis showed that the collagen subtypes of the implants remodeled toward fibrocartilage (i.e., more collagen types I and III, less

collagen type II) in both studies; however, visualized with H&E staining, implant degradation appeared to begin between 8 and 24 weeks. The implant appeared hypocellular and intact after 8 weeks *in vivo* (Figure 11-9), but during the 24 week study [570], neocartilage implants were infiltrated by immune cells and underwent additional remodeling. It can be hypothesized that longer term studies (i.e., one year long) would show the neocartilage implant completely remodel, leaving behind only regenerated TMJ disc. To completely assess the safety and efficacy of healing large perforations with self-assembled tissue-engineered implants, studies up to one year in length will be necessary to assess functionality and safety outcomes.

Defects of 6 mm diameter were considered to be a critical defect size after 8 weeks. In comparison to the 24-week study [570], all but one of the 3 mm perforations in control discs closed. Here, all three 6 mm empty defects remained perforated after 8 weeks, and it was shown that tissue adjacent to these perforations had changes such as significantly lower collagen type I and mature crosslinking, and significantly higher collagen type III compared to native tissue. Given the cartilage degeneration on the mandibular condyle in the control group, it is possible that these changes are indicative of degeneration around the periphery of the perforation. However, longer term studies of large perforations will be crucial in determining whether these were degenerative changes (e.g., further decreases in collagen type I and crosslinks, further increases in collagen type III) or reparative changes (e.g., closure of the perforation). While additional studies must be performed to determine whether untreated 6 mm perforations are capable of healing in the long-term, the 8-week time point was demonstrated to be an appropriate short-term endpoint for assessing regeneration of TMJ disc fibrocartilage in the Yucatan minipig model.

The intralaminar perforation technique has been used in three large animal models to date: a small disc-thinning model [23], a small perforation model [570], and, in the present study, a large perforation model. The 6 mm perforation (two-sided, full thickness) defect in this study represents an 8-times scale up in area from the initial 3 mm disc-thinning (one-sided, partial

thickness) defect [23]. Through additional modifications to the technique, other TMD models, such as large disc-thinning (i.e., perforating one of the two laminae with a 6 mm biopsy punch) can be performed in the Yucatan minipig. Defects of the mandibular condyle are also common in TMDs and can occur in conjunction with discal TMDs [174]. With the development of chondral or osteochondral tissue engineering strategies targeted toward the condylar cartilages, a broader array of pathologies could potentially be treated with a combination of the intralaminar perforation technique and an additional technique for the condyle. Arthroscopic implementation of the intralaminar perforation technique will also be beneficial, given improvements in recovery time for arthroscopies versus open surgeries [571, 572]. While the intralaminar perforation surgical approach was used in this study to regenerate disc perforations, extending the technique to address additional TMD indications will be beneficial to a wider patient population.

This work is impactful because it fulfills one of the most important translational objectives prior to clinical trials—showing safety and efficacy in a large animal model. The ultimate goal for TMJ cartilage tissue engineering is to create an effective human therapeutic, and large animal studies generate important preclinical data to begin translation of biomedical technologies to the clinic. With the safety and efficacy of neocartilage implants shown here, long-term, pivotal animal studies would be the next step toward beginning an investigational new drug (IND) and/or investigational device exemption (IDE) application to the US Food and Drug Administration (FDA). The minipig has been established as an appropriate animal model for translation to human TMJ work [24, 76, 570], and robust neocartilage implants have been produced with human chondrocytes [25]. Thus, with FDA approval, the tissue engineering process in this work can be applied in human clinical trials to advance the translation of neocartilage implants toward widespread human usage.

In 1983, the FDA approved the use of Vitek Inc.'s Proplast-Teflon implant for TMJ disc replacement. This implant was used in about 10,000 people, but, after surgery, the implant degraded and released Teflon into surrounding vasculature and tissue, causing catastrophic

side effects including cranial breaching [227, 318]. Given the TMJ's close proximity to the brain and other sensory structures [11], safe, cell-based therapeutics made from materials recognized by the human body represents an exciting and hopeful prospect for people who suffer debilitating pain from TMDs. Despite the need to correct past mistakes of the TMJ field and provide modern solutions to TMDs, there are no FDA-approved, cell-based TMJ implants today [11, 16]. The regeneration of TMJ disc perforations in this study represents a critical step along the translational pathway, where, through the rigorous FDA-guided regulatory process, tissue-engineered TMJ cartilage therapeutics are envisioned to substantially improve TMD outcomes in millions of people.

Materials and Methods

Tissue engineering of implants

Costal chondrocytes were sourced from three male juvenile (5-8 month) Yucatan minipigs, culled for purposes unrelated to this study, as previously described [338]. Briefly, in a biosafety cabinet, ribcages were dissected using sterile tools to reveal costal cartilage, and, after perichondrium removal, cartilage was cut into small pieces, approximately 1 mm^3 in size. Pronase and collagenase solutions were made by resuspending the enzymes at 0.4% (w/v) and 0.2% (w/v), respectively, in Dulbecco's modified Eagle's medium (DMEM, high glucose, GlutaMAX supplement) with 3% fetal bovine serum (FBS) and 1% penicillin-streptomycin-fungizone (PSF). Cartilage was digested in pronase solution for 1 hour followed by collagenase solution for 18 hours, both in a 37°C incubator. Digests were filtered through 70 µm cell strainers and treated with a lysis buffer [353]. After this single-cell suspension was obtained, medium formulations were based on chondrogenic (CHG) medium, which contained DMEM, 1% PSF, 1% nonessential amino acids, 1% insulin-transferrin-selenous acid+, 100 nM dexamethasone, 50 µg/mL ascorbate-2-phosphate, 40 µg/mL L-proline, and 100 µg/mL sodium pyruvate.

For expansion, chondrocytes were seeded into T225 flasks at 2.5M cells per flask (~11,111 cells/cm^2) in CHG medium supplemented with 2% FBS, 1 ng/mL TGF-β1, 5 ng/mL basic fibroblast growth factor (bFGF), and 10 ng/mL platelet-derived growth factor (PDGF), as previously described [149]. Medium was changed every 3-4 days during expansion. To passage the cells, 0.05% trypsin-EDTA was added to flasks for 9 minutes, cell sheets were aspirated with a serological pipette and placed into 50 mL conical tubes, and cell sheets were digested in collagenase solution for 30 minutes at 37°C with agitation every 10 minutes. After one passage, chondrocytes were frozen for future usage in FBS with 10% dimethyl sulfoxide (DMSO). Thawed chondrocytes were plated for continued expansion. After seven passages, cells were transferred to aggregate rejuvenation culture [25]. For aggregate rejuvenation, medium was comprised of CHG medium supplemented with 10 ng/mL TGF-β1, 100 ng/mL growth differentiation factor 5 (GDF-5), and 100 ng/mL bone morphogenetic protein 2 (BMP-2). During aggregate rejuvenation, medium was changed every 3-4 days. After 11 days of aggregate rejuvenation, 0.05% trypsin-EDTA was added to aggregates for 45 minutes at 37°C followed by collagenase solution for 90 minutes at 37°C with agitation every 10 minutes to digest aggregates into a single-cell suspension. Cells were then filtered through 70 µm cell strainers.

After aggregate rejuvenation, chondrocytes underwent self-assembly to form neocartilage [17]. Briefly, 11x17 mm negative mold wells were made from 2% molten agarose. CHG medium was pipetted into the wells after they were solidified, and medium was changed three times. Cells (15M/well) were then seeded with 600 µL of CHG medium into each well. CHG medium (5 mL/well) was added 4 hours later, and medium was exchanged every day until implant unconfinement on day 2, where implants were released from wells. After day 2 of self-assembly, CHG medium was supplemented with TGF-β1 (10 ng/mL), and, every 2 days, neocartilage implants were fed with 10 mL of CHG medium until day 42. On day 7 of self-assembly, implants were treated with 1.5 U/mL C-ABC for 4 hours [201]. After day 7, CHG

medium was supplemented with 10 ng/mL TGF-β1, 0.15 µg/mL LOXL2, 0.146 mg/mL hydroxylysine, and 1.6 µg/mL copper sulfate, as previously described [83].

For transportation to the surgical suite, neocartilage implants for surgery were kept for 7 hours in a cooler with ice in 50 mL conical tubes with HEPES-buffered CHG medium supplemented with 10 ng/mL TGF-β1, 0.15 µg/mL LOXL2, 0.146 mg/mL hydroxylysine, and 1.6 µg/mL copper sulfate. Implants were placed in an incubator at 37°C overnight for surgery the next day. Neocartilage implants that were not used for surgery were cut in half with a scalpel; one half was used as a t=0 control (t=0 *in vitro*), and the other half was cultured for an additional 8 weeks (t=8W *in vitro*).

In vivo experiments

All *in vivo* work was approved by the Institutional Animal Care and Use Committees (IACUCs) at University of California, Irvine (#AUP-21-033) and University of California, Davis (#21430). This study consisted of six Yucatan minipigs (n=6 females). Three minipigs were controls (empty defect), while the remaining three received tissue-engineered implants.

Presurgical medication and anesthesia

Minipigs were fasted for 24 hours before surgery. Prior to surgery, minipigs were pretreated with intramuscular (IM) Telazol (3-6mg/kg). Lactated Ringer's solution (5-10 mL/kg/hr) was administered via an intravenous (IV) catheter placed in the auricular vein. Ketamine (5 mg/kg), diazepam (0.2-0.5 mg/kg), and isoflurane via facemask were used to induce anesthesia. Prior to intubation, 2% lidocaine (1-2 mL) was used to treat larynxes, then minipigs were intubated with cuffed endotracheal tubes that were sized based on the individual animal. Morphine (0.5 mg/kg, IM) was used for preemptive analgesia. During surgery, 1-3% isoflurane in 100% O_2 was used to maintain anesthesia. Positive ventilation was used to maintain end-tidal carbon dioxide between 35-45 mmHg. Throughout surgery, minipigs were monitored via capnography,

electrocardiography, and thermometer and blood pressure measurements. A heating pad was used to maintain animal body temperatures at a physiological state (37-38°C).

Surgical implantation and defect creation

Prior to surgical intervention, skin by the operated joint was shaved and aseptically prepared for surgery with alcohol- and iodine-based solutions. As previously described [23], a ~10cm curvilinear incision was made with a #15 scalpel blade following the curvature of the zygomatic arch. This incision was extended superiorly over the temporal process of the zygoma toward the ear, and then blunt dissection was used to continue the incision through the subcutaneous adipose tissue and the periosteum. Periosteum was reflected ventrally and posteriorly using a periosteal elevator, and the TMJ was identified, with the locations noted for the condylar process and mandibular head, the masseter muscle, and lateral TMJ disc attachments. The tissue was thinned out using sharp dissection to further identify the lateral aspects of the joint, and the condylar process was exposed by dissecting through the masseter muscle. The superior joint space was exposed by using a sharp elevation of the superior TMJ disc attachments. The inferior joint was exposed by incising the inferior TMJ disc attachments. The disc and articular cartilages were protected during all dissections.

After these dissections, the lateral, superior, and inferior aspects of the TMJ were accessible. Using a #15 scalpel blade, an incision (~12 mm wide) was created in the lateral edge of the disc. The incision was deepened into the disc (~12 mm deep) to create a pouch with inferior and superior laminae (Figure 11-2A). Holding the lateral edges of the laminae, a 6 mm diameter disposable biopsy punch was used to create a full thickness perforation through both laminae in the centrolateral region of the disc, avoiding adjacent articulating surfaces (Figure 11-2B). The resulting TMJ disc punch was stored in phosphate-buffered saline. For the three minipigs that received tissue-engineered implants, implants were trimmed to 11x11 mm (Figure 11-1C) and inserted into the lateral incision (Figure 11-2C). Next, the incision was closed on the

lateral edge (Figure 11-2D) using 5-0 Monocryl sutures, avoiding the implant. A Mitek bone anchor (QuickAnchor Plus, #0 suture) was used to reattach the TMJ disc to the condylar process [354]. A hole in the condylar process was created using a Jacob's chuck with the supplied drill bit to place the bone anchor. The lateral aspect of the TMJ disc was attached to the double-armed suture to secure the disc to the condylar process, then the remaining layers of tissue were closed with 3-0 Monocryl suture.

Postoperative medication and animal care

Minipigs were given meloxicam (0.1-0.4 mg/kg via IV, IM, or oral delivery) once daily for 3 days, fentanyl (1-5 µg/kg/hr via patch) for 3 days, and buprenorphine (0.005-0.05mg/kg via IM dose) once for postoperative analgesia. Minipigs also received a single dose of perioperative antibiotics. Minipigs were closely observed in narrow pens lined with pads until ambulation and mentation were recovered, then minipigs were returned to housing pens. Minpigs were fed a soft diet for 3 days after surgery, and water bowls were provided rather than spigots. Sutures were removed 14 days after surgery.

Animal euthanasia

Minipigs were humanely euthanized 8 weeks after surgery with Telazol (3-6 mg/kg, IM) followed by Euthazol (phenytoin/pentobarbital, 1 mL/4.5kg, IV). After euthanasia, a full necropsy was performed by a veterinary pathologist to examine organ systems for signs of toxicity or neoplastic growth. TMJ discs and the mandibular heads on the condylar process were removed *en bloc*.

Sample preparation

TMJ tissue samples were photographed prior to dissections. Discs were removed, and the mandibular heads and discs were photographed. If defects were still present in the excised

discs, the defect perimeter and area were measured using ImageJ on both the superior and inferior surfaces and averaged to obtain a final measurement. Discs were cut into sections in the anteroposterior direction. From these sections, the implant, regenerated tissue, and tissue adjacent to empty defects were identified. Implants, regenerated tissues, and adjacent tissues were divided into sections for histology, mechanics (tissue mechanics and intralaminar mechanics), biochemistry, and proteomics. The 6 mm punch taken during surgery was used as a native tissue control for collagen, GAG, crosslinks, and proteomics assays, and contralateral TMJ disc samples from the same region of the disc as the perforation were used for mechanical testing and histological controls. Halves of non-implanted neocartilages were divided into samples for histological, mechanical, biochemical, and proteomic analysis at time of implantation (t=0) and at animal euthanasia (t=8W).

Histology

Samples were fixed using 10% neutral buffered formalin for at least 72 hours. Next, samples were processed and embedded in paraffin blocks. Sections of 5 μm thickness were created using a microtome, and sections were mounted on microscopy slides. H&E, safranin O and fast green counterstain (SO/FG), and picrosirius red (PSR) stains were performed on the sections, as previously described [339]. Slides were scanned and digitally visualized using a Roche VENTANA DP 200 slide scanner and QuPath software [356].

Mechanical testing

For *in vitro* controls, dog bone-shaped samples were glued to paper tabs of a predefined gauge length for tensile testing. For TMJ disc samples (excised implants, regenerated tissues, contralateral native tissues, intralaminar fusion samples), hemostats were used to clamp samples, a 0.2 N tare load was applied to remove slack, and calipers were used to measure the gauge length (pretest grip-to-grip clamping distance). Front and side views were photographed

to calculate cross-sectional area. All samples underwent 1% strain per second until failure, and a custom MATLAB script was used to analyze the resulting force-displacement curves, determining the Young's modulus and UTS. Strain at failure, toughness (entire area under the curve), and resilience (area under the curve of linear region only) were also calculated. All TMJ disc tissues underwent uniaxial tensile testing in the anteroposterior direction, except for the intralaminar fusion tests, which were performed in the superoinferior direction.

Compressive stress-relaxation tests were performed on *in vitro* controls. Punches of 3 mm diameter for stress-relaxation were taken with a disposable biopsy punch. Using a tare load of 0.1 N, sample height was detected, then samples were preloaded with 15 cycles of 5% strain, as previously described [24]. The relaxation modulus, instantaneous modulus, and coefficient of viscosity were determined by applying 20% strain to the punch for 900 seconds, then fitting the resulting force-displacement curves to a standard linear solid model with a custom MATLAB script.

Biochemical testing

Biochemical assays for total collagen and GAG content were performed. Briefly, samples were weighed to obtain a wet weight (WW), they were lyophilized for at least 72 hours, and DWs were taken. Collagen was measured with a modified hydroxyproline assay [93], while sulfated GAG was measured with a dimethylmethylene blue assay kit.

Mass spectrometry analyses for crosslinks quantification and bottom-up proteomics

Mass spectrometry analyses for collagen crosslinks quantification and bottom-up proteomics were performed, as previously described [346]. Briefly, for collagen crosslinks, tissue pieces approximately 1 mg in WW were lyophilized for at least 72 hours, measured for DW, reduced in $NaBH_4$ for 1 hour, washed in mass spectrometry grade water overnight, and hydrolyzed in 6 N HCl for 18 hours. Resulting hydrolysates were evaporated in a heat block, resuspended in 0.1%

formic acid, filtered with centrifugal filters, and analyzed using a Waters ACQUITY QDa LC-MS system. Quantification of PYR, DHLNL, OHP, and internal standard pyridoxine was performed by taking the area under the curve of the extracted ion chromatograms of each analyte's mass in the TargetLynx module of MassLynx v4.1 software.

For bottom-up proteomics analysis, tissue pieces approximately 1 mg in WW were lyophilized for at least 72 hours, digested in mass spectrometry grade trypsin in a heat block at 65°C overnight, desalted with Waters Sep-pak C18 cartridges, and analyzed with a Thermo Fisher Scientific Orbitrap Fusion Lumos mass spectrometer. MaxQuant was used to perform label-free quantification [357], reporting protein analytes normalized to PROT content.

Statistical analyses

A Student's t-test or a one-way analysis of variance (ANOVAs) with *post hoc* Dunnett's tests was performed on the data. For the Dunnett's tests, t=0 *in vitro* implants served as controls. Bar graphs were created using GraphPad Prism 9. The degree of significance was depicted by the symbols (ns), (*), (**), (***), and (****), to represent $p>0.05$ (not significant), $p\leq0.05$, $p\leq0.01$, $p\leq0.001$, and $p\leq0.0001$, respectively.

Supplementary Materials

Supplementary Table 11-1: Intralaminar fusion metrics.
When tested under uniaxial tension in the superoinferior direction, fusion between the two laminae and implant was higher in Young's modulus and ultimate tensile strength (UTS), but the difference was not significant.

Group	Young's modulus (MPa)	UTS (MPa)
Control	0.26±0.45	0.17±0.30
Implant-treated	1.78±1.16	0.51±0.15

Supplementary Table 11-2: Bottom-up proteomics raw data.
All data for bottom-up proteomics analysis is reported per total protein content as a percentage with the mean and standard deviation (SD) for each group.

Gene	Protein	t=0 *in vitro*		t=8W *in vitro*		t=24W *in vivo*		Regenerated tissue		Adjacent tissue		Native TMJ disc	
		Average	SD	Average	SD	Average	SD	Average	SD	Average	SD	Average	SD
ACTB	Actin, cytoplasmic 1	0.36%	0.17%	0.15%	0.03%	0.39%	0.61%	0.16%	0.17%	0.03%	0.04%	0.00%	0.00%
PGCA	Aggrecan core protein (Fragments)	0.25%	0.18%	0.14%	0.19%	0.00%	0.00%	0.00%	0.00%	0.00%	0.00%	0.00%	0.00%
CRYAB	Alpha-crystallin B chain	0.03%	0.05%	0.00%	0.00%	0.00%	0.00%	0.00%	0.00%	0.00%	0.00%	0.00%	0.00%
ENOB	Beta-enolase	0.06%	0.03%	0.02%	0.01%	0.00%	0.00%	0.00%	0.00%	0.00%	0.00%	0.00%	0.00%
PGS1	Biglycan (Fragments)	0.15%	0.11%	0.06%	0.06%	0.01%	0.01%	0.01%	0.00%	0.00%	0.00%	0.01%	0.02%
COL1A1	Collagen type I alpha 1	11.61%	3.63%	6.01%	2.89%	63.03%	6.48%	63.35%	2.74%	64.02%	5.99%	66.38%	1.96%
COL1A2	Collagen type I alpha 2	3.54%	1.08%	1.83%	0.94%	27.94%	0.98%	28.90%	0.26%	25.77%	3.96%	28.64%	2.28%
COL2A1	Collagen type II alpha 1	71.62%	5.60%	81.79%	5.47%	0.03%	0.01%	0.03%	0.02%	0.07%	0.04%	0.02%	0.02%
COL3A1	Collagen type III alpha 1	0.17%	0.07%	0.20%	0.06%	6.73%	4.66%	5.99%	2.04%	9.17%	1.55%	4.31%	2.69%
COL5A1	Collagen type V alpha 1	0.35%	0.05%	0.20%	0.04%	0.07%	0.07%	0.07%	0.02%	0.07%	0.01%	0.05%	0.02%
COL5A2	Collagen type V alpha 2	1.16%	0.12%	0.87%	0.09%	0.13%	0.10%	0.10%	0.02%	0.15%	0.02%	0.09%	0.03%
COL5A3	Collagen type V alpha 3	0.00%	0.00%	0.00%	0.00%	0.00%	0.00%	0.00%	0.00%	0.25%	0.44%	0.14%	0.35%
COL6A2	Collagen type VI alpha 2	0.17%	0.09%	0.10%	0.04%	0.05%	0.04%	0.11%	0.03%	0.04%	0.02%	0.03%	0.01%
COL6A3	Collagen type VI alpha 3	0.73%	0.37%	0.34%	0.13%	0.20%	0.15%	0.30%	0.03%	0.13%	0.07%	0.09%	0.03%
COL9A1	Collagen type IX alpha 1	0.49%	0.24%	0.41%	0.10%	0.00%	0.00%	0.00%	0.00%	0.00%	0.00%	0.00%	0.00%
COL9A2	Collagen type IX alpha 2	0.29%	0.07%	0.27%	0.07%	0.00%	0.00%	0.00%	0.00%	0.00%	0.00%	0.00%	0.00%
COL10A1	Collagen type X alpha 1	0.00%	0.00%	0.00%	0.00%	0.00%	0.00%	0.00%	0.00%	0.00%	0.00%	0.00%	0.00%
COL11A1	Collagen type XI alpha 1	2.55%	0.93%	2.59%	1.20%	0.01%	0.00%	0.01%	0.01%	0.00%	0.00%	0.01%	0.01%
Col11A2	Collagen type XI alpha 2	2.10%	0.88%	2.29%	0.61%	0.00%	0.00%	0.00%	0.00%	0.00%	0.00%	0.00%	0.01%
COL12A1	Collagen type XII alpha 1	0.85%	0.18%	0.45%	0.16%	0.01%	0.01%	0.02%	0.00%	0.00%	0.00%	0.01%	0.01%
COL14A1	Collagen type XIV alpha 1	0.00%	0.00%	0.00%	0.00%	0.06%	0.04%	0.02%	0.03%	0.00%	0.00%	0.01%	0.01%
COL14A1	Collagen type XVI alpha 1	0.03%	0.02%	0.02%	0.01%	0.00%	0.01%	0.00%	0.00%	0.00%	0.00%	0.00%	0.00%
PGS2	Decorin	0.00%	0.00%	0.00%	0.00%	0.11%	0.10%	0.05%	0.04%	0.09%	0.06%	0.07%	0.07%
BIP	Endoplasmic reticulum chaperone BiP (Fragment)	0.11%	0.04%	0.05%	0.02%	0.01%	0.01%	0.01%	0.01%	0.00%	0.00%	0.00%	0.00%
FMOD	Fibromodulin (Fragment)	0.11%	0.07%	0.05%	0.05%	0.00%	0.00%	0.01%	0.01%	0.00%	0.00%	0.00%	0.00%

G3P	Glyceraldehyde-3-phosphate dehydrogenase	0.11%	0.04%	0.03%	0.02%	0.01%	0.01%	0.01%	0.01%	0.00%	0.00%	0.00%	0.00%
HS71B	Heat shock 70 kDa protein 1B	0.07%	0.03%	0.04%	0.01%	0.00%	0.00%	0.00%	0.00%	0.00%	0.00%	0.00%	0.00%
HBA	Hemoglobin subunit alpha	0.02%	0.04%	0.00%	0.00%	0.02%	0.03%	0.01%	0.02%	0.00%	0.00%	0.06%	0.07%
H4	Histone H4	0.76%	0.60%	0.47%	0.35%	0.43%	0.47%	0.37%	0.40%	0.04%	0.05%	0.02%	0.03%
HPLN1	Hyaluronan and proteoglycan link protein 1	0.28%	0.25%	0.43%	0.33%	0.00%	0.00%	0.00%	0.00%	0.00%	0.00%	0.00%	0.00%
MFGM	Lactadherin	0.35%	0.13%	0.36%	0.10%	0.00%	0.00%	0.00%	0.00%	0.00%	0.00%	0.00%	0.00%
NU2M	NADH-ubiquinone oxidoreductase chain 2	0.02%	0.04%	0.00%	0.00%	0.00%	0.00%	0.00%	0.00%	0.00%	0.00%	0.00%	0.00%
PGK1	Phosphoglycerate kinase 1	0.10%	0.02%	0.05%	0.03%	0.00%	0.00%	0.00%	0.00%	0.00%	0.00%	0.00%	0.00%
LMNA	Prelamin-A/C	0.08%	0.02%	0.03%	0.02%	0.11%	0.15%	0.05%	0.05%	0.01%	0.01%	0.00%	0.00%
TBB	Tubulin beta chain	0.04%	0.04%	0.01%	0.00%	0.02%	0.04%	0.02%	0.04%	0.00%	0.00%	0.00%	0.00%
VIME	Vimentin	0.75%	0.18%	0.58%	0.11%	0.49%	0.60%	0.31%	0.30%	0.10%	0.09%	0.01%	0.01%

Supplementary Table 11-3: Dry weight crosslink normalizations and biochemical data for regenerated tissue.
Pyridinoline (PYR), dihydroxylysinonorleucine (DHLNL), and glycosaminoglycan (GAG) content per dry weight (DW) are reported.

Group	PYR/DW (ng/mg)	DHLNL/DW (ng/mg)	GAG (%/DW)
Control	0±0	0±0	0±0
Implant-treated	3860±217****	1119±150***	0.352±0.347
Native TMJ disc	3802±920	995±289	1.200±0.492

Supplementary Table 11-4: Dry weight crosslink normalizations and biochemical data for adjacent tissue.
Pyridinoline (PYR), dihydroxylysinonorleucine (DHLNL), and glycosaminoglycan (GAG) content per dry weight (DW) are reported.

Group	PYR/DW (ng/mg)	DHLNL/DW (ng/mg)	GAG (%/DW)
Adjacent tissue	2954±1007	1046±549	0.886±0.177
Native TMJ disc	3802±920	995±289	1.200±0.492

Supplementary Table 11-5: Compressive properties of implants cultured *in vitro*.
Since there was not enough tissue, t=24W *in vivo* samples were not tested (nt).

Group	20% Relaxation modulus (kPa)	20% Instantaneous modulus (kPa)	20% Coefficient of viscosity (MPa s)
t=0 *in vitro*	255±85	1061±251	52.2±35.0
t=8W *in vitro*	258±83	1004±258	37.9±37.3
t=8W *in vivo*	nt	nt	nt

Supplementary Table 11-6: Raw complete blood count and complete metabolic panel data.
Parameters were assayed at implantation (t=0) and animal euthanasia (t=8W).

Group	ID # and Assay Point	WBC (K/ul)	Absolute Neutrophil cells (K/ul)	Absolute Lymphocyte cells (K/ul)	Absolute Monocyte cells (K/ul)	Absolute Eosinophil cells (K/ul)	Absolute Basophil cells (K/ul)	Neutrophil (%)	Lymphocyte (%)	Monocyte (%)	Eosinophil (%)	Basophil (%)	RBC (M/ul)	Hemoglobin (g/dL)	Hematocrit (%)	MCV (fL)	MCH (pg)	MCHC (g/dL)	RDW (%)	Platelets (K/uL)	MPV (fL)
Control	6819 t=0	12.56	5.86	6.20	0.35	0.13	0.02	46.63	49.39	2.79	1.06	0.14	4.94	10.8	28.0	56.7	21.9	38.6	17.9	396	10.6
	6819 t=8W	11.30	4.67	5.95	0.21	0.46	0.01	41.30	52.63	1.89	4.09	0.09	5.24	9.3	29.7	56.7	17.7	31.3	17.0	399	10.4
	1177 t=0	8.62	4.34	3.66	0.38	0.22	0.02	50.35	42.43	4.43	2.57	0.23	6.38	11.1	33.8	53.0	17.4	32.8	20.7	379	9.3
	1177 t=8W	9.10	3.13	4.06	0.31	1.58	0.02	34.39	44.65	3.45	17.32	0.18	6.43	10.3	31.9	49.6	16.0	32.3	19.5	368	10.1
	1329 t=0	11.10	3.29	2.35	0.96	4.46	0.04	29.61	21.21	8.68	40.14	0.37	8.04	15.1	44.0	54.7	18.8	34.3	19.2	334	9.4
	1329 t=8W	7.18	2.72	3.10	0.34	1.02	0.01	37.89	43.17	4.71	14.15	0.07	7.01	11.3	35.9	51.2	16.1	31.5	19.6	332	11.0
Implant-treated	2661 t=0	10.62	3.76	5.80	0.37	0.68	0.01	35.42	54.58	3.52	6.38	0.10	7.72	12.5	42.2	54.7	16.2	29.6	19.7	194	12.0
	2661 t=8W	7.46	1.52	2.71	0.59	2.62	0.02	20.34	36.33	7.95	35.10	0.28	6.68	10.5	35.8	53.6	15.7	29.3	18.7	258	10.6
	3774 t=0	9.80	2.39	4.77	0.64	1.98	0.02	24.34	48.72	6.48	20.24	0.22	6.78	10.6	36.3	53.6	15.6	29.0	20.3	329	10.8
	3774 t=8W	9.46	2.42	4.42	0.63	1.97	0.02	25.62	46.75	6.62	20.80	0.22	5.77	9.4	30.5	52.9	16.3	30.8	19.2	367	9.7
	4525 t=0	8.06	1.80	3.34	0.68	2.21	0.03	22.36	41.43	8.41	27.38	0.41	6.18	10.8	33.4	54.0	17.5	32.3	19.8	251	11.0
	4525 t=8W	8.68	2.69	3.06	0.21	2.72	0.01	30.95	35.21	2.39	31.34	0.12	6.83	11.1	35.2	51.6	16.3	31.5	19.8	389	9.8

Group	ID # and Assay Point	Alanine Transaminase (U/L)	Albumin (g/dL)	Alkaline Phosphatase (U/L)	Amylase (U/L)	Aspartate Transaminase (U/L)	Blood Urea Nitrogen (mg/dL)	Calcium (mg/dL)	Creatinine (mg/dL)	Glucose (mg/dL)	Phosphorus (mg/dL)	Total Bilirubin (mg/dL)	Total Protein (g/dL)	Chloride (mmol/L)	Potassium (mmol/L)	Sodium (mmol/L)
Control	6819 t=0	30.0	4.16	38.2	2252.9	36.7	16.4	10.71	0.903	117.8	5.66	0.038	6.76	99.6	4.37	138
	6819 t=8W	33.1	4.22	42.9	2561.3	24.5	14.7	10.26	1.089	97.1	5.35	0.033	6.86	101.2	3.28	138
	1177 t=0	27.0	4.33	29.8	2954.4	18.2	12.5	10.21	1.168	70.5	5.59	0.056	6.65	100.6	3.96	137
	1177 t=8W	28.6	4.27	44.7	4484.4	22.4	9.1	9.81	1.187	70.0	6.07	0.138	6.83	101.5	3.69	140
	1329 t=0	28.5	4.66	56.9	3600.6	29.1	13.3	10.31	1.136	89.7	5.59	0.216	6.67	102.8	3.82	138
	1329 t=8W	24.9	4.22	42.5	3917.0	24.8	12.9	9.79	1.073	82.9	5.90	0.222	6.46	100.9	3.51	137
Implant-treated	2661 t=0	33.9	4.53	67.6	2343.2	30.0	15.5	10.65	0.843	63.7	5.52	0.053	6.73	98.3	4.35	136
	2661 t=8W	31.4	4.7	72.1	2518.2	25.8	16.2	10.55	0.886	71.8	5.65	0.151	6.93	101.2	3.70	140
	3774 t=0	28.8	4.29	35.9	2101.3	25.0	12.1	10.29	0.982	89.8	5.10	0.025	6.10	102.7	4.43	136
	3774 t=8W	32.2	3.82	34.0	1914.4	19.9	11.9	10.21	0.768	73.1	5.63	0.030	6.19	103.1	4.02	137
	4525 t=0	21.3	4.72	66.0	2522.4	23.1	12.8	10.58	0.884	85.5	5.68	0.056	6.79	102.7	3.63	139
	4525 t=8W	21.1	5.22	59.7	2708.8	17.7	14.2	10.60	0.933	87.1	5.47	0.135	7.32	104.0	3.35	143

Conclusions and Future Directions

Temporomandibular joint (TMJ) disorders (TMDs) affect millions of patients on a day-to-day basis. Specifically, arthrogenous indications include disc perforation, affecting up to 9 million in the US alone. To address disc perforations, there are no good intermediate solutions between current non-surgical treatments and end-stage surgical interventions. As evidenced by this dissertation, tissue-engineered implants have the potential to address unmet clinical needs for the millions that are afflicted by disc perforations. This work started by describing the unmet clinical needs and considerations for translation of tissue-engineered fibrocartilages, including the TMJ disc. There are several remaining hurdles for tissue engineering the TMJ disc, and the oral and maxillofacial field should consider treating certain TMJ disc indications similar to how knee cartilage indications are treated in orthopaedics. These reviews developed a roadmap for tissue-engineered TMJ disc implants. Based on prior success in healing partial thickness defects, the long-term safety and efficacy of regenerating focal (3 mm diameter) disc perforations using self-assembled implants were established, showing that implants resulted in significantly improved mechanical outcomes when compared to empty defect controls. Prior to scale-up of defects, a number of tissue engineering investigations were performed, including 1) identifying a donor age of costal chondrocytes, 2) finding an appropriate time of self-assembly to maximize tensile properties of constructs, and 3) scaling-up of constructs and improving their translatability and functionality. Together, these three studies described the generation of large (11x17 mm) constructs that were robust and flat for future implantation into larger perforation defects. Immunological reaction to tissue-engineered implants was also of concern given that stiff substrates can elicit a macrophage-mediated inflammatory response; thus, the macrophage-mediated response to increasing stiffnesses of neocartilage implants and subsequent effects were investigated. It was shown that the robust matrix content and addition of neocartilage bioactive factors protected constructs from macrophage-mediated inflammation and subsequent catabolic breakdown. Using this information, the preclinical safety and efficacy

of large implants were examined in perforation defects 4-times the area (i.e., 6 mm diameter) of initial studies. In stark contrast across the 8-week study, implant-treated discs completely healed with regenerated tissue while empty defect controls did not heal at all, exhibiting through-and-through perforations. Ultimately, this work represents substantial progress in demonstrating the preclinical safety and efficacy of TMJ disc implants for healing perforation defects, toward potentially reducing pain and increasing function for millions of patients afflicted with discal TMDs.

Disc perforations in the human can be a significant clinical indication, inducing pain and dysfunction of the TMJ. Prior to this work, only partial thickness defects assessed in preclinical animal models were examined in the literature [23]. Thus, a more clinically relevant indication of disc perforation was selected to be examined here. In Aim 1, the objective was to assess the long-term safety and efficacy of small neocartilage implants in focal perforation (i.e., full thickness) defects in the TMJ disc. Using previously optimized tissue engineering methodologies for self-assembly of implants derived from minipig costal chondrocytes, initial safety and efficacy were proven. Systemically, full body necropsy revealed no signs of inflammation or neoplastic growth in any organ systems. Locally, T cells, B cells, and macrophages surrounded the implant after implantation, but the local response dampened over time, indicating that implants were well-tolerated immunogenically and safe for treatment of perforations. For repair metrics, implant treatment resulted in repair tissue that was 6.2-times tougher, 8.9-times more resilient, 3.4-times stronger, and had a 2.5-times higher strain at failure, compared to fill tissue of controls. Additionally, collagen type I and collagen type III were significantly higher and lower in repair tissue, reaching 99.4% and 103.1% of native tissue values, respectively, compared to fill tissue of controls. Overall, implant treatment resulted in more native-like tissue regeneration compared to the scar-like fill tissue of empty defects, proving that self-assembled implants are efficacious in healing focal disc perforations. This work established the translational potential of neocartilage implants for addressing discal TMDs.

Although there have been many advances in the self-assembling process over the last two decades, certain optimizations had not yet been performed toward maximizing functionality of neocartilage constructs, especially those derived from costal chondrocytes. Toward this, Aim 2's objective was to examine, optimize, and scale-up the tissue engineering process toward generation of large neocartilage constructs. First, the age of costal chondrocyte donors used in the self-assembling process was examined. Previous studies reported that donor age plays a large role in the functional outcome of tissue-engineered cartilages [30, 31], but the effect of donor age in the self-assembling process here was minimal. Only slight differences in certain functional outcomes in the neonatal group, such as aggregate modulus, Poisson's ratio, and total collagen content, were observed compared to the adult group. Thus, the juvenile donors were selected to be carried forward in future studies toward balancing these minor differences found between the neonatal and adult donor sources. Second, the self-assembling process was examined longitudinally, and it was found that there are many biochemical, mechanical, and proteomic differences among the various culture timepoints examined. The self-assembling process was also shown to be similar to native porcine knee development as well. For self-assembled neocartilage, tensile properties after 56 days of culture were found to be maximal. Since previous optimizations of the self-assembling process were found to produce superior functional properties at 28 days of culture [399], the difference between the two timepoints (i.e., 42 days of culture) was carried forward. Finally, fluid-induced shear stress was examined toward improving the functionality and translatability of constructs derived from highly passaged costal chondrocytes. Since large implants will require additional cells for tissue engineering, passage 6 costal chondrocytes were examined in this study with fluid-induced shear stress as a mechanical stimulus and bioactive factors as biochemical stimuli for improving the functional properties of constructs. It was found that constructs were mechanically robust and flat after 42 days of culture. Ultimately, these three chapters optimized the tissue engineering methodologies

used in the self-assembling process with highly passaged costal chondrocytes to generate large constructs for implantation into large disc perforation defects.

The *in vivo* immune response as a result of surgical implantation is a crucial factor to the success of a tissue-engineered implant, including those intended for the TMJ disc. The goal of tissue engineering is to implant a stiff and robust construct that survives the joint loading environment. However, recent evidence suggests that stiffer substrates increase the macrophage-mediated inflammatory immune response [29], which could potentially break down robust implants before resolving toward a healing response. Given that macrophages are a crucial initial mediator of the inflammatory and healing responses *in vivo* [27], the objective of Aim 3 was to evaluate the stiffness mediated-macrophage response to neocartilage implants. First, isolation and characterization of minipig macrophages derived from the blood and bone marrow were described. Since the minipig is a widely used preclinical animal model for both tissue engineering and immunology studies, the investigation of these sources represented a novel direction toward further establishing the minipig model. The effects of macrophage co-culture with neocartilage constructs were then examined. In the first study, it was found that, despite a 5.47-times increase in macrophage secretion of tumor necrosis factor alpha (TNF-α) in the stiffest construct co-culture groups, a significant decrease in aggregate modulus values was not observed. In contrast, softer constructs exhibited lower mechanical properties after 2 weeks of coculture with macrophages despite no concomitant increases in TNF-α. Toward rescuing the functionality of softer constructs, neocartilage bioactive factors were applied during construct culture in the second study, and it was found that the same decreases in aggregate modulus values seen in the first study did not occur except for the softest construct cocultured with LPS-stimulated (proinflammatory) macrophages. Additionally, bioactive factor-treated constructs also further increased in aggregate modulus values over the 2-week co-culture period, compared to control constructs which all lost mechanical integrity. Overall, through the studies in this aim, stiffness- and bioactive factor-mediated protection of neocartilage implants

against macrophage inflammatory challenge was observed in an *in vitro* co-culture system, thereby supporting the protection of such constructs *in vivo* from an initial inflammatory cascade, common after implantation.

Using the information derived from Aims 1, 2, and 3, investigation of healing large perforations in the Yucatan minipig was used to further bolster the *in vivo* safety and efficacy of self-assembled implants in Aim 4. Since TMJ arthroscopic studies have shown that perforations encompass more than one-third of the disc in about 70% of cases [9], the objective of this aim was to assess the safety and efficacy of large neocartilage implants in a large perforation defect in the TMJ disc. In this study, a stark contrast in the implant-treated discs and empty defect controls was observed; implant-treated discs had complete closure and regeneration in the defect while controls remained perforated after 8 weeks. The perimeter of the control discs was 14.6 ± 5.8 mm, while the implant-treated discs did not exhibit a measurable defect perimeter. Furthermore, the regenerated tissue was mechanically robust, reaching 64.4% to 81.2% of native tissue values depending on the mechanical outcome measure in just 8 weeks of healing. Biochemical and proteomic contents of regenerated tissue were also similar to native TMJ disc contents. Notably, when compared to native tissue, adjacent tissue to empty defects showed lower collagen type I and pyridinoline content, and higher collagen type III content, potentially indicating pathological progression of the defects toward degeneration. Importantly, adjacent articulating surfaces of the condyles exhibited cartilage defects in two of three control animals, indicating that the empty defects in the disc are indeed progressing toward osteoarthritic changes in the TMJ as a whole. For safety, no multinucleated giant cells, polymorphonuclear cells, or capsule formation were observed in the vicinity of the implant, and full body necropsy, complete blood counts, and comprehensive metabolic panels showed no systemic effects specific to implant treatment. This work further bolstered self-assembled implant safety and efficacy for healing perforation defects of the TMJ disc.

Tissue-engineered implants are poised for translation to clinical use after the studies presented in this dissertation. In the US, regulation of the cell-based, neocartilage implants would fall under the Food and Drug Administration (FDA), which regulates biologics, devices, and drugs. Since these TMJ disc implants are derived from isolated, living chondrocytes with a cartilaginous matrix component produced by the cells, it is expected that they would be regulated as a combination product (i.e., a device and biologic), with primary jurisdiction to the Center for Biologics Evaluation and Research (CBER) and secondary jurisdiction to the Center for Devices and Radiological Health (CDRH) [37]. Additionally, since the chondrocytes isolated from the costal cartilage are put through the expansion, aggregate rejuvenation, and self-assembling processes described throughout this dissertation, it is likely that a future product based on self-assembled neocartilage would be regulated under Section 351 of the Public Health Service Act, as opposed to Section 361, which describes regulations for products which are minimally manipulated, for homologous use, and uncombined with another article. According to guidance documents for cartilage products intended to repair or replace knee cartilage [37], preclinical safety and efficacy are required to be examined in a suitable large animal model prior to human clinical studies. For the TMJ disc, preclinical safety and efficacy of self-assembled implants were proven in the preliminary studies performed here for both focal and large perforation defects in the Yucatan minipig, a suitable large animal model for TMJ disc pathologies [24]. Based on the knee cartilage guidance document and pharmacology/toxicology reviews for similar cell-based products [37, 573], the FDA will likely require a long-term (i.e., 1 year) pivotal study in the Yucatan minipig for an investigational new drug (IND) or investigational device exemption (IDE) application; however, the data generated here can be used as supporting data to such a pivotal study and bolster the IND/IDE application. Additionally, according to the FDA guidance document for knee cartilage products [37], the chemistry, manufacturing, and controls (CMC) information of a future therapeutic will need to be defined prior to production of an analogous human product. As examined here, the tissue engineering

methods optimized in the minipig costal chondrocyte source can inform the processes used for human costal chondrocytes toward defining CMC information for a future human TMJ disc therapeutic. Overall, the data produced in this dissertation can be applied to the translation of TMJ disc implants, but specific guidance from regulatory bodies, such as the FDA, will be crucial toward fully defining safety and efficacy for future TMJ disc therapeutics.

Ultimately, this work succeeded in meeting the proposed global objectives of 1) engineering neocartilage implants that can withstand the demanding environment of the TMJ disc, both mechanically and immunogenically, and 2) expanding treatable indications of tissue-engineered TMJ disc implants to perforation defects via preclinical investigations in the Yucatan minipig model. Through the four aims presented, 1) preclinical safety and efficacy of focal perforation defects were proven, 2) the tissue engineering processes used for self-assembled implants were examined and optimized toward generation of large neocartilage constructs, 3) the stiffness-mediated macrophage response resulted in minimal effects on the functional properties of robust, bioactive factor-treated constructs, and 4) implantation of TMJ disc neocartilages resulted in superior healing of large perforations, further bolstering the safety and efficacy of self-assembled neocartilage implants. This work is poised to affect the millions of patients suffering from intractable pain and dysfunction due to discal TMDs. Tissue-engineered, self-assembled TMJ disc implants are the next generation of treatments that will be able to heal discal defects, facilitate regeneration toward native tissue properties, and provide long-term relief to TMD patients.

References

1. Johansson, A., et al., *Gender difference in symptoms related to temporomandibular disorders in a population of 50-year-old subjects.* J Orofac Pain, 2003. **17**(1): p. 29-35.
2. Macfarlane, T.V., et al., *Oro-facial pain in the community: prevalence and associated impact.* Community Dent Oral Epidemiol, 2002. **30**(1): p. 52-60.
3. Pow, E.H., K.C. Leung, and A.S. McMillan, *Prevalence of symptoms associated with temporomandibular disorders in Hong Kong Chinese.* J Orofac Pain, 2001. **15**(3): p. 228-34.
4. Goulet, J.P., G.J. Lavigne, and J.P. Lund, *Jaw pain prevalence among French-speaking Canadians in Quebec and related symptoms of temporomandibular disorders.* J Dent Res, 1995. **74**(11): p. 1738-44.
5. Solberg, W.K., M.W. Woo, and J.B. Houston, *Prevalence of mandibular dysfunction in young adults.* J Am Dent Assoc, 1979. **98**(1): p. 25-34.
6. Schiffman, E., et al., *Diagnostic Criteria for Temporomandibular Disorders (DC/TMD) for Clinical and Research Applications: recommendations of the International RDC/TMD Consortium Network* and Orofacial Pain Special Interest Groupdagger.* J Oral Facial Pain Headache, 2014. **28**(1): p. 6-27.
7. Farrar, W.B. and W.L. McCarty, Jr., *The TMJ dilemma.* J Ala Dent Assoc, 1979. **63**(1): p. 19-26.
8. Katzberg, R.W. and P.-L. Westesson, *Diagnosis of the temporomandibular joint*. 1 ed. 1993: W.B. Saunders. 25-70.
9. Munoz-Guerra, M.F., et al., *Temporomandibular joint disc perforation: long-term results after operative arthroscopy.* J Oral Maxillofac Surg, 2013. **71**(4): p. 667-76.
10. Kuribayashi, A., et al., *MRI findings of temporomandibular joints with disk perforation.* Oral Surg Oral Med Oral Pathol Oral Radiol Endod, 2008. **106**(3): p. 419-25.
11. Bielajew, B.J., et al., *Knee orthopedics as a template for the temporomandibular joint.* Cell Rep Med, 2021. **2**(5): p. 100241.
12. Aryaei, A., et al., *Recent Tissue Engineering Advances for the Treatment of Temporomandibular Joint Disorders.* Curr Osteoporos Rep, 2016. **14**(6): p. 269-279.
13. Dolwick, M.F. and G. Dimitroulis, *Is there a role for temporomandibular joint surgery?* British Journal of Oral and Maxillofacial Surgery, 1994. **32**(5): p. 307-313.
14. Dimitroulis, G., *Management of temporomandibular joint disorders: A surgeon's perspective.* Aust Dent J, 2018. **63 Suppl 1**: p. S79-S90.
15. Donahue, R.P., et al., *Considerations for translation of tissue engineered fibrocartilage from bench to bedside.* J Biomech Eng, 2018.
16. Donahue, R.P., J.C. Hu, and K.A. Athanasiou, *Remaining Hurdles for Tissue-Engineering the Temporomandibular Joint Disc.* Trends Mol Med, 2019. **25**(3): p. 241-256.
17. Hu, J.C. and K.A. Athanasiou, *A self-assembling process in articular cartilage tissue engineering.* Tissue Eng, 2006. **12**(4): p. 969-79.
18. El-Sayed, K.M., *Temporomandibular joint reconstruction with costochondral graft using modified approach.* Int J Oral Maxillofac Surg, 2008. **37**(10): p. 897-902.
19. Huwe, L.W., et al., *Characterization of costal cartilage and its suitability as a cell source for articular cartilage tissue engineering.* J Tissue Eng Regen Med, 2018. **12**(5): p. 1163-1176.
20. Johns, D.E., M.E. Wong, and K.A. Athanasiou, *Clinically relevant cell sources for TMJ disc engineering.* J Dent Res, 2008. **87**(6): p. 548-52.
21. Anderson, D.E. and K.A. Athanasiou, *A comparison of primary and passaged chondrocytes for use in engineering the temporomandibular joint.* Arch Oral Biol, 2009. **54**(2): p. 138-45.

22. Johns, D.E. and K.A. Athanasiou, *Growth factor effects on costal chondrocytes for tissue engineering fibrocartilage.* Cell Tissue Res, 2008. **333**(3): p. 439-47.
23. Vapniarsky, N., et al., *Tissue engineering toward temporomandibular joint disc regeneration.* Sci Transl Med, 2018. **10**(446): p. 1-10.
24. Vapniarsky, N., et al., *The Yucatan Minipig Temporomandibular Joint Disc Structure-Function Relationships Support Its Suitability for Human Comparative Studies.* Tissue Engineering Part C: Methods, 2017. **23**(11): p. 700-709.
25. Kwon, H., et al., *Rejuvenation of extensively passaged human chondrocytes to engineer functional articular cartilage.* Biofabrication, 2021. **13**(3).
26. Arzi, B., et al., *Cartilage immunoprivilege depends on donor source and lesion location.* Acta Biomater, 2015. **23**: p. 72-81.
27. Koh, T.J. and L.A. DiPietro, *Inflammation and wound healing: the role of the macrophage.* Expert Rev Mol Med, 2011. **13**: p. e23.
28. Meli, V.S., et al., *Biophysical regulation of macrophages in health and disease.* J Leukoc Biol, 2019. **106**(2): p. 283-299.
29. Jansen, L.E., et al., *Zwitterionic PEG-PC Hydrogels Modulate the Foreign Body Response in a Modulus-Dependent Manner.* Biomacromolecules, 2018. **19**(7): p. 2880-2888.
30. Guerne, P.A., et al., *Growth factor responsiveness of human articular chondrocytes in aging and development.* Arthritis Rheum, 1995. **38**(7): p. 960-8.
31. Adkisson, H.D.t., et al., *The potential of human allogeneic juvenile chondrocytes for restoration of articular cartilage.* Am J Sports Med, 2010. **38**(7): p. 1324-33.
32. Li, Q., et al., *Effect of jaw opening on the stress pattern in a normal human articular disc: finite element analysis based on MRI images.* Head Face Med, 2014. **10**(1): p. 24.
33. Athanasiou, K.A., et al., *Articular Cartilage*. 2 ed. 2017: CRC Press.
34. Makris, E.A., P. Hadidi, and K.A. Athanasiou, *The knee meniscus: structure-function, pathophysiology, current repair techniques, and prospects for regeneration.* Biomaterials, 2011. **32**(30): p. 7411-31.
35. Detamore, M.S. and K.A. Athanasiou, *Structure and function of the temporomandibular joint disc: implications for tissue engineering.* J Oral Maxillofac Surg, 2003. **61**(4): p. 494-506.
36. Food and Drug Administration. *FDA Regulation of Human Cells, Tissues, and Cellular and Tissue-Based Products (HCT/P's) Product List*. 2018; Available from: https://www.fda.gov/biologicsbloodvaccines/tissuetissueproducts/regulationoftissues/ucm150485.htm.
37. Food and Drug Administration, *Guidance for Industry Preparation of IDEs and INDs for Products Intended to Repair or Replace Knee Cartilage*. 2011.
38. Cisternas, M.G., et al., *Trends in medical care expenditures of US adults with arthritis and other rheumatic conditions 1997 to 2005.* J Rheumatol, 2009. **36**(11): p. 2531-8.
39. Alomar, X., et al., *Anatomy of the temporomandibular joint.* Semin Ultrasound CT MR, 2007. **28**(3): p. 170-83.
40. Willard, V.P., L. Zhang, and K.A. Athanasiou, *Tissue Engineering of the Temporomandibular Joint*, in *Comprehensive Biomaterials*. 2011, Elsevier. p. 221-235.
41. Salata, M.J., A.E. Gibbs, and J.K. Sekiya, *A systematic review of clinical outcomes in patients undergoing meniscectomy.* Am J Sports Med, 2010. **38**(9): p. 1907-16.
42. Shetty, A., *U.S. Soft Tissue Repair Markets - Meniscus and Cartilage*. 2009, Frost & Sullivan. Available from: https://cds.frost.com/p/297836212#!/nts/c?id=N536-01-00-00-00&hq=meniscus.
43. Baker, B.E., et al., *Review of meniscal injury and associated sports.* Am J Sports Med, 1985. **13**(1): p. 1-4.

44. Hede, A., et al., *Epidemiology of meniscal lesions in the knee. 1,215 open operations in Copenhagen 1982-84.* Acta Orthop Scand, 1990. **61**(5): p. 435-7.
45. Hede, A., E. Larsen, and H. Sandberg, *The long term outcome of open total and partial meniscectomy related to the quantity and site of the meniscus removed.* Int Orthop, 1992. **16**(2): p. 122-5.
46. Hede, A., E. Larsen, and H. Sandberg, *Partial versus total meniscectomy. A prospective, randomised study with long-term follow-up.* J Bone Joint Surg Br, 1992. **74**(1): p. 118-21.
47. Englund, M., et al., *Incidental meniscal findings on knee MRI in middle-aged and elderly persons.* N Engl J Med, 2008. **359**(11): p. 1108-15.
48. Kim, S., et al., *Increase in outpatient knee arthroscopy in the United States: a comparison of National Surveys of Ambulatory Surgery, 1996 and 2006.* J Bone Joint Surg Am, 2011. **93**(11): p. 994-1000.
49. Fox, A.J., et al., *The human meniscus: a review of anatomy, function, injury, and advances in treatment.* Clin Anat, 2015. **28**(2): p. 269-87.
50. Greis, P.E., et al., *Meniscal injury: I. Basic science and evaluation.* J Am Acad Orthop Surg, 2002. **10**(3): p. 168-76.
51. Maffulli, N., et al., *Meniscal tears.* Open Access J Sports Med, 2010. **1**: p. 45-54.
52. Barber-Westin, S.D. and F.R. Noyes, *Clinical healing rates of meniscus repairs of tears in the central-third (red-white) zone.* Arthroscopy, 2014. **30**(1): p. 134-46.
53. Srinivasan, P., *Temporomandibular Disorders (TMD) and Use of Oral Appliance for Obstructive Sleep Apnea Syndrome in the United States*. 2015, Frost & Sullivan. Available from: https://cds.frost.com/p/297836212/#!/ppt/c?id=9AD2-00-02-00-00.
54. Halstead, J.M., et al., *Translation. An RNA biosensor for imaging the first round of translation from single cells to living animals.* Science, 2015. **347**(6228): p. 1367-671.
55. Warren, M.P. and J.L. Fried, *Temporomandibular disorders and hormones in women.* Cells Tissues Organs, 2001. **169**(3): p. 187-92.
56. Isong, U., S.A. Gansky, and O. Plesh, *Temporomandibular joint and muscle disorder-type pain in U.S. adults: the National Health Interview Survey.* J Orofac Pain, 2008. **22**(4): p. 317-22.
57. American Society of Temporomandibular Joint Surgeons, *Guidelines for diagnosis and management of disorders involving the temporomandibular joint and related musculoskeletal structures.* Cranio, 2003. **21**(1): p. 68-76.
58. Brooks, S.L., et al., *Prevalence of Osseous Changes in the Temporomandibular-Joint of Asymptomatic Persons without Internal Derangement.* Oral Surgery Oral Medicine Oral Pathology Oral Radiology and Endodontics, 1992. **73**(1): p. 118-122.
59. *Biomaterials for Tissue Engineering Applications: A Review of the Past and Future Trends*, ed. J.A. Burdick and R.L. Mauck. 2011, New York: Springer.
60. Xu, C. and J. Zhao, *A meta-analysis comparing meniscal repair with meniscectomy in the treatment of meniscal tears: the more meniscus, the better outcome?* Knee Surg Sports Traumatol Arthrosc, 2015. **23**(1): p. 164-70.
61. Rangger, C., et al., *Partial meniscectomy and osteoarthritis. Implications for treatment of athletes.* Sports Med, 1997. **23**(1): p. 61-8.
62. Herrlin, S., et al., *Arthroscopic or conservative treatment of degenerative medial meniscal tears: a prospective randomised trial.* Knee Surg Sports Traumatol Arthrosc, 2007. **15**(4): p. 393-401.
63. Katz, J.N., et al., *Surgery versus Physical Therapy for a Meniscal Tear and Osteoarthritis.* New England Journal of Medicine, 2013. **369**(7): p. 683-683.
64. Khan, M., et al., *Arthroscopic surgery for degenerative tears of the meniscus: a systematic review and meta-analysis.* CMAJ, 2014. **186**(14): p. 1057-64.

65. Dolwick, M.F., *The role of temporomandibular joint surgery in the treatment of patients with internal derangement.* Oral Surg Oral Med Oral Pathol Oral Radiol Endod, 1997. **83**(1): p. 150-5.
66. Wolford, L.M., *Factors to consider in joint prosthesis systems.* Proc (Bayl Univ Med Cent), 2006. **19**(3): p. 232-8.
67. McLeod, N.M., N.R. Saeed, and R. Hensher, *Internal derangement of the temporomandibular joint treated by discectomy and hemi-arthroplasty with a Christensen fossa-eminence prosthesis.* Br J Oral Maxillofac Surg, 2001. **39**(1): p. 63-6.
68. Bjornland, T. and T.A. Larheim, *Discectomy of the temporomandibular joint: 3-year follow-up as a predictor of the 10-year outcome.* J Oral Maxillofac Surg, 2003. **61**(1): p. 55-60.
69. Eriksson, L. and P.L. Westesson, *Discectomy as an effective treatment for painful temporomandibular joint internal derangement: a 5-year clinical and radiographic follow-up.* J Oral Maxillofac Surg, 2001. **59**(7): p. 750-8; discussion 758-9.
70. Henry, C.H. and L.M. Wolford, *Treatment outcomes for temporomandibular joint reconstruction after Proplast-Teflon implant failure.* J Oral Maxillofac Surg, 1993. **51**(4): p. 352-8; discussion 359-60.
71. Dimitroulis, G., *Condylar morphology after temporomandibular joint discectomy with interpositional abdominal dermis-fat graft.* J Oral Maxillofac Surg, 2011. **69**(2): p. 439-46.
72. Troulis, M.J., et al., *Condylectomy and costochondral graft reconstruction for treatment of active idiopathic condylar resorption.* J Oral Maxillofac Surg, 2008. **66**(1): p. 65-72.
73. Proffen, B.L., et al., *A comparative anatomical study of the human knee and six animal species.* Knee, 2012. **19**(4): p. 493-9.
74. Deponti, D., et al., *Animal models for meniscus repair and regeneration.* J Tissue Eng Regen Med, 2015. **9**(5): p. 512-27.
75. Helgeland, E., et al., *Scaffold-Based Temporomandibular Joint Tissue Regeneration in Experimental Animal Models: A Systematic Review.* Tissue Eng Part B Rev, 2018. **24**(4): p. 300-316.
76. Almarza, A.J., et al., *Preclinical Animal Models for Temporomandibular Joint Tissue Engineering.* Tissue Eng Part B Rev, 2018. **24**(3): p. 171-178.
77. Detamore, M.S., et al., *Cell type and distribution in the porcine temporomandibular joint disc.* J Oral Maxillofac Surg, 2006. **64**(2): p. 243-8.
78. Pauli, C., et al., *Macroscopic and histopathologic analysis of human knee menisci in aging and osteoarthritis.* Osteoarthritis Cartilage, 2011. **19**(9): p. 1132-41.
79. Zhao, J., et al., *Changes of rabbit meniscus influenced by hyaline cartilage injury of osteoarthritis.* Int J Clin Exp Med, 2014. **7**(9): p. 2948-56.
80. Kalpakci, K.N., et al., *An interspecies comparison of the temporomandibular joint disc.* J Dent Res, 2011. **90**(2): p. 193-8.
81. Huey, D.J. and K.A. Athanasiou, *Tension-compression loading with chemical stimulation results in additive increases to functional properties of anatomic meniscal constructs.* PLoS One, 2011. **6**(11): p. e27857.
82. Murphy, M.K., et al., *Characterization of degenerative changes in the temporomandibular joint of the bengal tiger (Panthera tigris tigris) and siberian tiger (Panthera tigris altaica).* J Comp Pathol, 2013. **149**(4): p. 495-502.
83. Makris, E.A., et al., *Combined use of chondroitinase-ABC, TGF-β1, and collagen crosslinking agent lysyl oxidase to engineer functional neotissues for fibrocartilage repair.* Biomaterials, 2014. **35**(25): p. 6787-6796.
84. Mardhiyah, A., M. Sha'Ban, and A. Azhim. *Evaluation of histological and biomechanical properties on engineered meniscus tissues using sonication decellularization*. in *2017 39th Annual International Conference of the IEEE Engineering in Medicine and Biology Society (EMBC)*. 2017. IEEE.

85. Milam, S.B., et al., *Characterization of the extracellular matrix of the primate temporomandibular joint.* J Oral Maxillofac Surg, 1991. **49**(4): p. 381-91.
86. Detamore, M.S., et al., *Quantitative analysis and comparative regional investigation of the extracellular matrix of the porcine temporomandibular joint disc.* Matrix Biol, 2005. **24**(1): p. 45-57.
87. Melrose, J., et al., *Comparative spatial and temporal localisation of perlecan, aggrecan and type I, II and IV collagen in the ovine meniscus: an ageing study.* Histochem Cell Biol, 2005. **124**(3-4): p. 225-35.
88. Sanchez-Adams, J. and K.A. Athanasiou, *The Knee Meniscus: A Complex Tissue of Diverse Cells.* Cellular and Molecular Bioengineering, 2009. **2**(3): p. 332-340.
89. Ribitsch, I., et al., *Structure-Function relationships of equine menisci.* PLoS One, 2018. **13**(3): p. e0194052.
90. Sweigart, M.A. and K.A. Athanasiou, *Tensile and compressive properties of the medial rabbit meniscus.* Proc Inst Mech Eng H, 2005. **219**(5): p. 337-47.
91. Gutman, S., et al., *Regionally variant collagen alignment correlates with viscoelastic properties of the disc of the human temporomandibular joint.* Arch Oral Biol, 2018. **86**: p. 1-6.
92. Hadidi, P. and K.A. Athanasiou, *Enhancing the mechanical properties of engineered tissue through matrix remodeling via the signaling phospholipid lysophosphatidic acid.* Biochem Biophys Res Commun, 2013. **433**(1): p. 133-8.
93. Cissell, D.D., et al., *A Modified Hydroxyproline Assay Based on Hydrochloric Acid in Ehrlich's Solution Accurately Measures Tissue Collagen Content.* Tissue Eng Part C Methods, 2017. **23**(4): p. 243-250.
94. Bank, R.A., et al., *Sensitive fluorimetric quantitation of pyridinium and pentosidine crosslinks in biological samples in a single high-performance liquid chromatographic run.* J Chromatogr B Biomed Sci Appl, 1997. **703**(1-2): p. 37-44.
95. Herwig, J., E. Egner, and E. Buddecke, *Chemical-Changes of Human Knee-Joint Menisci in Various Stages of Degeneration.* Annals of the Rheumatic Diseases, 1984. **43**(4): p. 635-640.
96. McDevitt, C.A. and R.J. Webber, *The ultrastructure and biochemistry of meniscal cartilage.* Clin Orthop Relat Res, 1990(252): p. 8-18.
97. Eyre, D.R. and J.J. Wu, *Collagen of fibrocartilage: a distinctive molecular phenotype in bovine meniscus.* FEBS Lett, 1983. **158**(2): p. 265-70.
98. Cheung, H.S., *Distribution of type I, II, III and V in the pepsin solubilized collagens in bovine menisci.* Connect Tissue Res, 1987. **16**(4): p. 343-56.
99. Nakano, T., J.R. Thompson, and F.X. Aherne, *Distribution of glycosaminoglycans and the nonreducible collagen crosslink, pyridinoline in porcine menisci.* Can J Vet Res, 1986. **50**(4): p. 532-6.
100. Almarza, A.J., et al., *Biochemical analysis of the porcine temporomandibular joint disc.* Br J Oral Maxillofac Surg, 2006. **44**(2): p. 124-8.
101. Tissakht, M. and A.M. Ahmed, *Tensile stress-strain characteristics of the human meniscal material.* J Biomech, 1995. **28**(4): p. 411-22.
102. Sweigart, M.A., et al. *Biomechanical properties of the medial meniscus in experimental animal models*. in *2002 IEEE Engineering in Medicine and Biology 24th Annual Conference and the 2002 Fall Meeting of the Biomedical Engineering Society (BMES / EMBS)*. 2002. IEEE.
103. Kim, K.W., et al., *Biomechanical tissue characterization of the superior joint space of the porcine temporomandibular joint.* Ann Biomed Eng, 2003. **31**(8): p. 924-30.
104. Sweigart, M.A., et al., *Intraspecies and interspecies comparison of the compressive properties of the medial meniscus.* Ann Biomed Eng, 2004. **32**(11): p. 1569-79.

105. Huey, D.J. and K.A. Athanasiou, *Maturational growth of self-assembled, functional menisci as a result of TGF-β1 and enzymatic chondroitinase-ABC stimulation.* Biomaterials, 2011. **32**(8): p. 2052-8.
106. Sweigart, M.A. and K.A. Athanasiou, *Biomechanical characteristics of the normal medial and lateral porcine knee menisci.* Proc Inst Mech Eng H, 2005. **219**(1): p. 53-62.
107. Mow, V.C., et al., *Biphasic creep and stress relaxation of articular cartilage in compression? Theory and experiments.* J Biomech Eng, 1980. **102**(1): p. 73-84.
108. Simon, B.R., J.S.S. Wu, and J.H. Evans. *Poroelastic mechanical models for the intervertebral disc*. in *Advances in Bioengineering: ASME Winter Annual Meeting*. 1983. Boston, MA, USA.
109. Mak, A.F., W.M. Lai, and V.C. Mow, *Biphasic indentation of articular cartilage--I. Theoretical analysis.* J Biomech, 1987. **20**(7): p. 703-14.
110. Mow, V.C., et al., *Biphasic indentation of articular cartilage--II. A numerical algorithm and an experimental study.* J Biomech, 1989. **22**(8-9): p. 853-61.
111. Athanasiou, K.A. and R.M. Natoli, *Introduction to Continuum Biomechanics*. 2008: Morgan & Claypool Publishers.
112. Lakes, E.H., et al., *Comparing the mechanical properties of the porcine knee meniscus when hydrated in saline versus synovial fluid.* J Biomech, 2015. **48**(16): p. 4333-8.
113. Joshi, M.D., et al., *Interspecies variation of compressive biomechanical properties of the meniscus.* J Biomed Mater Res, 1995. **29**(7): p. 823-8.
114. Hadidi, P., et al., *Critical seeding density improves the properties and translatability of self-assembling anatomically shaped knee menisci.* Acta Biomater, 2015. **11**(1): p. 173-82.
115. Thomas, M., D. Grande, and R.H. Haug, *Development of an in vitro temporomandibular joint cartilage analog.* J Oral Maxillofac Surg, 1991. **49**(8): p. 854-6; discussion 857.
116. Springer, I.N., et al., *Culture of cells gained from temporomandibular joint cartilage on non-absorbable scaffolds.* Biomaterials, 2001. **22**(18): p. 2569-77.
117. Allen, K.D. and K.A. Athanasiou, *Scaffold and growth factor selection in temporomandibular joint disc engineering.* J Dent Res, 2008. **87**(2): p. 180-5.
118. Wang, C.H., et al., *Layering Poly (lactic-co-glycolic acid)-based electrospun membranes and co-culture cell sheets for engineering temporomandibular joint disc.* J Biol Regul Homeost Agents, 2018. **32**(1): p. 55-61.
119. Almarza, A.J. and K.A. Athanasiou, *Seeding techniques and scaffolding choice for tissue engineering of the temporomandibular joint disk.* Tissue Eng, 2004. **10**(11-12): p. 1787-95.
120. Detamore, M.S. and K.A. Athanasiou, *Effects of growth factors on temporomandibular joint disc cells.* Arch Oral Biol, 2004. **49**(7): p. 577-83.
121. Detamore, M.S. and K.A. Athanasiou, *Evaluation of three growth factors for TMJ disc tissue engineering.* Ann Biomed Eng, 2005. **33**(3): p. 383-90.
122. Almarza, A.J. and K.A. Athanasiou, *Effects of initial cell seeding density for the tissue engineering of the temporomandibular joint disc.* Ann Biomed Eng, 2005. **33**(7): p. 943-50.
123. Detamore, M.S. and K.A. Athanasiou, *Use of a rotating bioreactor toward tissue engineering the temporomandibular joint disc.* Tissue Eng, 2005. **11**(7-8): p. 1188-97.
124. Almarza, A.J. and K.A. Athanasiou, *Evaluation of three growth factors in combinations of two for temporomandibular joint disc tissue engineering.* Arch Oral Biol, 2006. **51**(3): p. 215-21.
125. Bean, A.C., A.J. Almarza, and K.A. Athanasiou, *Effects of ascorbic acid concentration on the tissue engineering of the temporomandibular joint disc.* Proc Inst Mech Eng H, 2006. **220**(3): p. 439-47.

126. Almarza, A.J. and K.A. Athanasiou, *Effects of hydrostatic pressure on TMJ disc cells.* Tissue Eng, 2006. **12**(5): p. 1285-94.
127. Girdler, N.M., *In vitro synthesis and characterization of a cartilaginous meniscus grown from isolated temporomandibular chondroprogenitor cells.* Scand J Rheumatol, 1998. **27**(6): p. 446-53.
128. Anderson, D.E. and K.A. Athanasiou, *Passaged goat costal chondrocytes provide a feasible cell source for temporomandibular joint tissue engineering.* Ann Biomed Eng, 2008. **36**(12): p. 1992-2001.
129. Hagandora, C.K., et al., *Poly (glycerol sebacate): a novel scaffold material for temporomandibular joint disc engineering.* Tissue Eng Part A, 2013. **19**(5-6): p. 729-37.
130. Murphy, M.K., et al., *Neocartilage integration in temporomandibular joint discs: physical and enzymatic methods.* J R Soc Interface, 2015. **12**(103).
131. Puelacher, W.C., et al., *Temporomandibular-Joint Disc Replacement Made by Tissue-Engineered Growth of Cartilage.* Journal of Oral and Maxillofacial Surgery, 1994. **52**(11): p. 1172-1177.
132. Kalpakci, K.N., E.J. Kim, and K.A. Athanasiou, *Assessment of growth factor treatment on fibrochondrocyte and chondrocyte co-cultures for TMJ fibrocartilage engineering.* Acta Biomater, 2011. **7**(4): p. 1710-8.
133. MacBarb, R.F., et al., *Engineering functional anisotropy in fibrocartilage neotissues.* Biomaterials, 2013. **34**(38): p. 9980-9.
134. Kasemkijwattana, C., et al., *The use of growth factors, gene therapy and tissue engineering to improve meniscal healing.* Materials Science & Engineering C-Biomimetic and Supramolecular Systems, 2000. **13**(1-2): p. 19-28.
135. Eifler, R.L., et al., *Oscillatory fluid flow regulates glycosaminoglycan production via an intracellular calcium pathway in meniscal cells.* J Orthop Res, 2006. **24**(3): p. 375-84.
136. Aufderheide, A.C. and K.A. Athanasiou, *Assessment of a bovine co-culture, scaffold-free method for growing meniscus-shaped constructs.* Tissue Eng, 2007. **13**(9): p. 2195-205.
137. Gunja, N.J., R.K. Uthamanthil, and K.A. Athanasiou, *Effects of TGF-beta1 and hydrostatic pressure on meniscus cell-seeded scaffolds.* Biomaterials, 2009. **30**(4): p. 565-73.
138. Baker, B.M., et al., *Dynamic tensile loading improves the functional properties of mesenchymal stem cell-laden nanofiber-based fibrocartilage.* Tissue Eng Part A, 2011. **17**(9-10): p. 1445-55.
139. MacBarb, R.F., et al., *A chondroitinase-ABC and TGF-beta1 treatment regimen for enhancing the mechanical properties of tissue-engineered fibrocartilage.* Acta Biomater, 2013. **9**(1): p. 4626-34.
140. Ahtiainen, K., et al., *Autologous adipose stem cells and polylactide discs in the replacement of the rabbit temporomandibular joint disc.* J R Soc Interface, 2013. **10**(85): p. 20130287.
141. Moriguchi, Y., et al., *Repair of meniscal lesions using a scaffold-free tissue-engineered construct derived from allogenic synovial MSCs in a miniature swine model.* Biomaterials, 2013. **34**(9): p. 2185-93.
142. Higashioka, M.M., et al., *Building an anisotropic meniscus with zonal variations.* Tissue Eng Part A, 2014. **20**(1-2): p. 294-302.
143. MacBarb, R.F., et al., *Passive strain-induced matrix synthesis and organization in shape-specific, cartilaginous neotissues.* Tissue Eng Part A, 2014. **20**(23-24): p. 3290-302.
144. Murphy, M.K., et al., *Engineering a fibrocartilage spectrum through modulation of aggregate redifferentiation.* Cell Transplant, 2015. **24**(2): p. 235-45.
145. Legemate, K., et al., *Engineering Human TMJ Discs with Protein-Releasing 3D-Printed Scaffolds.* J Dent Res, 2016. **95**(7): p. 800-7.

146. Warren, P.B., et al., *Engineering 3D-Bioplotted scaffolds to induce aligned extracellular matrix deposition for musculoskeletal soft tissue replacement.* Connect Tissue Res, 2017. **58**(3-4): p. 342-354.
147. Wang, F., et al., *Scaffold-free cartilage cell sheet combined with bone-phase BMSCs-scaffold regenerate osteochondral construct in mini-pig model.* Am J Transl Res, 2018. **10**(10): p. 2997-3010.
148. Hadidi, P., et al., *Tendon and ligament as novel cell sources for engineering the knee meniscus.* Osteoarthritis Cartilage, 2016. **24**(12): p. 2126-2134.
149. Murphy, M.K., et al., *Enhancing post-expansion chondrogenic potential of costochondral cells in self-assembled neocartilage.* PLoS One, 2013. **8**(2): p. e56983.
150. Murphy, M.K., et al., *TGF-β1, GDF-5, and BMP-2 Stimulation Induces Chondrogenesis in Expanded Human Articular Chondrocytes and Marrow-Derived Stromal Cells.* Stem Cells, 2015. **33**(3): p. 762-73.
151. Hatsushika, D., et al., *Repetitive allogeneic intraarticular injections of synovial mesenchymal stem cells promote meniscus regeneration in a porcine massive meniscus defect model.* Osteoarthritis Cartilage, 2014. **22**(7): p. 941-50.
152. Nakagawa, Y., et al., *Synovial mesenchymal stem cells promote healing after meniscal repair in microminipigs.* Osteoarthritis Cartilage, 2015. **23**(6): p. 1007-17.
153. Suchorska, W.M., et al., *Comparison of Four Protocols to Generate Chondrocyte-Like Cells from Human Induced Pluripotent Stem Cells (hiPSCs).* Stem Cell Rev Rep, 2017. **13**(2): p. 299-308.
154. Brown, B.N., et al., *Inductive, scaffold-based, regenerative medicine approach to reconstruction of the temporomandibular joint disk.* J Oral Maxillofac Surg, 2012. **70**(11): p. 2656-68.
155. Lowe, J. and A.J. Almarza, *A review of in-vitro fibrocartilage tissue engineered therapies with a focus on the temporomandibular joint.* Arch Oral Biol, 2017. **83**: p. 193-201.
156. Athanasiou, K.A., et al., *Self-organization and the self-assembling process in tissue engineering.* Annu Rev Biomed Eng, 2013. **15**(1): p. 115-36.
157. Bhargava, M.M., et al., *The effect of cytokines on the proliferation and migration of bovine meniscal cells.* Am J Sports Med, 1999. **27**(5): p. 636-43.
158. Responte, D.J., et al., *Mechanisms underlying the synergistic enhancement of self-assembled neocartilage treated with chondroitinase-ABC and TGF-beta1.* Biomaterials, 2012. **33**(11): p. 3187-94.
159. Natoli, R.M., C.M. Revell, and K.A. Athanasiou, *Chondroitinase ABC treatment results in greater tensile properties of self-assembled tissue-engineered articular cartilage.* Tissue Eng Part A, 2009. **15**(10): p. 3119-28.
160. Makris, E.A., et al., *Developing functional musculoskeletal tissues through hypoxia and lysyl oxidase-induced collagen cross-linking.* Proc Natl Acad Sci U S A, 2014. **111**(45): p. E4832-41.
161. Shu, W., et al., *Tissue engineering of the temporomandibular joint disc: current status and future trends.* Int J Artif Organs, 2015. **38**(2): p. 55-68.
162. Chen, M., et al., *Biochemical Stimulus-Based Strategies for Meniscus Tissue Engineering and Regeneration.* Biomed Res Int, 2018. **2018**: p. 8472309.
163. Salinas, E.Y., J.C. Hu, and K. Athanasiou, *A Guide for Using Mechanical Stimulation to Enhance Tissue-Engineered Articular Cartilage Properties.* Tissue Eng Part B Rev, 2018. **24**(5): p. 345-358.
164. White, J.L., et al., *A Comparison of Bone Marrow and Cord Blood Mesenchymal Stem Cells for Cartilage Self-Assembly.* Tissue Eng Part A, 2018. **24**(15-16): p. 1262-1272.
165. Bansal, S., et al., *Large Animal Models of Meniscus Repair and Regeneration: A Systematic Review of the State of the Field.* Tissue Eng Part C Methods, 2017. **23**(11): p. 661-672.

166. Lu, L., et al., *Tissue engineered constructs: perspectives on clinical translation.* Ann Biomed Eng, 2015. **43**(3): p. 796-804.
167. Diehl, R., et al., *Immunosuppression for in vivo research: state-of-the-art protocols and experimental approaches.* Cell Mol Immunol, 2017. **14**(2): p. 146-179.
168. Brzezinski, A., et al., *(*) The Ovine Model for Meniscus Tissue Engineering: Considerations of Anatomy, Function, Implantation, and Evaluation.* Tissue Eng Part C Methods, 2017. **23**(12): p. 829-841.
169. Sindelar, B.J. and S.W. Herring, *Soft tissue mechanics of the temporomandibular joint.* Cells Tissues Organs, 2005. **180**(1): p. 36-43.
170. Arnett, G.W., S.B. Milam, and L. Gottesman, *Progressive mandibular retrusion-idiopathic condylar resorption. Part II.* Am J Orthod Dentofacial Orthop, 1996. **110**(2): p. 117-27.
171. Scrivani, S.J., D.A. Keith, and L.B. Kaban, *Temporomandibular disorders.* N Engl J Med, 2008. **359**(25): p. 2693-705.
172. Ohrbach, R. and S.F. Dworkin, *The Evolution of TMD Diagnosis: Past, Present, Future.* J Dent Res, 2016. **95**(10): p. 1093-101.
173. Slade, G.D., et al., *Painful Temporomandibular Disorder: Decade of Discovery from OPPERA Studies.* J Dent Res, 2016. **95**(10): p. 1084-92.
174. Wilkes, C.H., *Internal derangements of the temporomandibular joint. Pathological variations.* Arch Otolaryngol Head Neck Surg, 1989. **115**(4): p. 469-77.
175. Goncalves, D.A., et al., *Symptoms of temporomandibular disorders in the population: an epidemiological study.* J Orofac Pain, 2010. **24**(3): p. 270-8.
176. Martins-Junior, R.L., et al., *Temporomandibular disorders: a report of 124 patients.* J Contemp Dent Pract, 2010. **11**(5): p. 071-8.
177. Ballesteros, L.E. and S.F. Leon, *[Anatomical and pathological study of the temporomandibular joint disk in Colombian individuals].* Rev Med Chil, 1999. **127**(12): p. 1469-74.
178. Romero-Reyes, M. and J.M. Uyanik, *Orofacial pain management: current perspectives.* J Pain Res, 2014. **7**: p. 99-115.
179. Armijo-Olivo, S., et al., *Effectiveness of Manual Therapy and Therapeutic Exercise for Temporomandibular Disorders: Systematic Review and Meta-Analysis.* Phys Ther, 2016. **96**(1): p. 9-25.
180. Kuzmanovic Pficer, J., et al., *Occlusal stabilization splint for patients with temporomandibular disorders: Meta-analysis of short and long term effects.* PLoS One, 2017. **12**(2): p. e0171296.
181. Kurita Varoli, F., et al., *Analgesia evaluation of 2 NSAID drugs as adjuvant in management of chronic temporomandibular disorders.* ScientificWorldJournal, 2015. **2015**: p. 359152.
182. Mountziaris, P.M., P.R. Kramer, and A.G. Mikos, *Emerging intra-articular drug delivery systems for the temporomandibular joint.* Methods, 2009. **47**(2): p. 134-40.
183. De Riu, G., et al., *Arthrocentesis and temporomandibular joint disorders: clinical and radiological results of a prospective study.* Int J Dent, 2013. **2013**: p. 790648.
184. Sharma, H., et al., *Costochondral Graft as Interpositional material for TMJ Ankylosis in Children: A Clinical Study.* J Maxillofac Oral Surg, 2015. **14**(3): p. 565-72.
185. Wolford, L.M., et al., *Comparison of 2 temporomandibular joint total joint prosthesis systems.* J Oral Maxillofac Surg, 2003. **61**(6): p. 685-90; discussion 690.
186. Agerberg, G. and M. Lundberg, *Changes in the temporomandibular joint after surgical treatment. A radiologic follow-up study.* Oral Surg Oral Med Oral Pathol, 1971. **32**(6): p. 865-75.
187. Hinton, R.J., *Alterations in rat condylar cartilage following discectomy.* J Dent Res, 1992. **71**(6): p. 1292-7.

188. Mercuri, L.G., *The use of alloplastic prostheses for temporomandibular joint reconstruction.* Journal of Oral and Maxillofacial Surgery, 2000. **58**(1): p. 70-75.
189. Ingawale, S. and T. Goswami, *Temporomandibular joint: disorders, treatments, and biomechanics.* Ann Biomed Eng, 2009. **37**(5): p. 976-96.
190. Ronald, S. and D.K. Mills, *Fibrochondrocyte Growth and Functionality on TiO(2) Nanothin Films.* J Funct Biomater, 2016. **7**(2).
191. Tarafder, S., et al., *Micro-precise spatiotemporal delivery system embedded in 3D printing for complex tissue regeneration.* Biofabrication, 2016. **8**(2): p. 025003.
192. Wu, Y., et al., *The pilot study of fibrin with temporomandibular joint derived synovial stem cells in repairing TMJ disc perforation.* Biomed Res Int, 2014. **2014**: p. 454021.
193. Matuska, A.M., M.F. Dolwick, and P.S. McFetridge, *Approaches to improve integration and regeneration of an ex vivo derived temporomandibular joint disc scaffold with variable matrix composition.* J Mater Sci Mater Med, 2018. **29**(10): p. 152.
194. Bousnaki, M., et al., *Fibro/chondrogenic differentiation of dental stem cells into chitosan/alginate scaffolds towards temporomandibular joint disc regeneration.* J Mater Sci Mater Med, 2018. **29**(7): p. 97.
195. Juran, C.M., M.F. Dolwick, and P.S. McFetridge, *Engineered microporosity: enhancing the early regenerative potential of decellularized temporomandibular joint discs.* Tissue Eng Part A, 2015. **21**(3-4): p. 829-39.
196. Kommireddy, D.S., et al., *Stem cell attachment to layer-by-layer assembled TiO2 nanoparticle thin films.* Biomaterials, 2006. **27**(24): p. 4296-303.
197. Liu, X. and P.X. Ma, *Polymeric scaffolds for bone tissue engineering.* Ann Biomed Eng, 2004. **32**(3): p. 477-86.
198. Bryant, S.J., et al., *Crosslinking density influences the morphology of chondrocytes photoencapsulated in PEG hydrogels during the application of compressive strain.* J Orthop Res, 2004. **22**(5): p. 1143-9.
199. Lee, J.K., et al., *The Self-Assembling Process and Applications in Tissue Engineering.* Cold Spring Harb Perspect Med, 2017. **7**(11).
200. Kwon, H., et al., *Articular cartilage tissue engineering: the role of signaling molecules.* Cell Mol Life Sci, 2016. **73**(6): p. 1173-94.
201. Huwe, L.W., et al., *Using Costal Chondrocytes to Engineer Articular Cartilage with Applications of Passive Axial Compression and Bioactive Stimuli.* Tissue Eng Part A, 2018. **24**(5-6): p. 516-526.
202. Zhang, S., A.U. Yap, and W.S. Toh, *Stem Cells for Temporomandibular Joint Repair and Regeneration.* Stem Cell Rev Rep, 2015. **11**(5): p. 728-42.
203. Recklies, A.D., L. Baillargeon, and C. White, *Regulation of cartilage oligomeric matrix protein synthesis in human synovial cells and articular chondrocytes.* Arthritis Rheum, 1998. **41**(6): p. 997-1006.
204. Tanaka, E. and T. van Eijden, *Biomechanical behavior of the temporomandibular joint disc.* Crit Rev Oral Biol Med, 2003. **14**(2): p. 138-50.
205. Wu, Y., et al., *Viscoelastic shear properties of porcine temporomandibular joint disc.* Orthod Craniofac Res, 2015. **18 Suppl 1**(S1): p. 156-63.
206. Hodge, W.A., et al., *Contact pressures from an instrumented hip endoprosthesis.* J Bone Joint Surg Am, 1989. **71**(9): p. 1378-86.
207. Lee, J.K., et al., *Tension stimulation drives tissue formation in scaffold-free systems.* Nat Mater, 2017. **16**(8): p. 864-873.
208. Roveroni, R.C., et al., *Development of a behavioral model of TMJ pain in rats: the TMJ formalin test.* Pain, 2001. **94**(2): p. 185-191.
209. Nicoll, S.B., et al., *A rat model of temporomandibular joint pain with histopathologic modifications.* J Orofac Pain, 2010. **24**(3): p. 298-304.

210. Cledes, G., et al., *Validation of a chemical osteoarthritis model in rabbit temporomandibular joint: a compliment to biomechanical models.* Int J Oral Maxillofac Surg, 2006. **35**(11): p. 1026-33.
211. Guler, N., et al., *Sodium iodoacetate induced osteoarthrosis model in rabbit temporomandibular joint: CT and histological study (part I).* Int J Oral Maxillofac Surg, 2011. **40**(11): p. 1289-95.
212. Huang, B.J., et al., *Overcoming Challenges in Engineering Large, Scaffold-Free Neocartilage with Functional Properties.* Tissue Eng Part A, 2018. **24**(21-22): p. 1652-1662.
213. Miyamoto, H., et al., *A sheep model for temporomandibular joint ankylosis.* J Oral Maxillofac Surg, 1999. **57**(7): p. 812-7.
214. Li, L., et al., *Establishment and histological evaluation of a goat traumatic temporomandibular joint model.* J Oral Maxillofac Surg, 2015. **73**(5): p. 943-50.
215. Miyamoto, H., et al., *The effect of etodolac on experimental temporomandibular joint osteoarthritis in dogs.* J Craniomaxillofac Surg, 2007. **35**(8): p. 358-63.
216. Lowe, J., et al., *Properties of the Temporomandibular Joint in Growing Pigs.* J Biomech Eng, 2018. **140**(7).
217. Herring, S.W., *The dynamics of mastication in pigs.* Arch Oral Biol, 1976. **21**(8): p. 473-80.
218. Herring, S.W. and Z.J. Liu, *Loading of the temporomandibular joint: anatomic and in vivo evidence from the bones.* Cells, Tissues, Organs, 2001. **169**(1): p. 193-200.
219. Herring, S.W., et al., *Temporomandibular joint in miniature pigs: anatomy, cell replication, and relation to loading.* Anat Rec, 2002. **266**(3): p. 152-66.
220. Mosser, D.M. and J.P. Edwards, *Exploring the full spectrum of macrophage activation.* Nat Rev Immunol, 2008. **8**(12): p. 958-69.
221. Ogle, M.E., et al., *Monocytes and macrophages in tissue repair: Implications for immunoregenerative biomaterial design.* Exp Biol Med (Maywood), 2016. **241**(10): p. 1084-97.
222. Gaffney, L., et al., *Macrophages' Role in Tissue Disease and Regeneration.* Results Probl Cell Differ, 2017. **62**: p. 245-271.
223. Falah, M., et al., *Treatment of articular cartilage lesions of the knee.* Int Orthop, 2010. **34**(5): p. 621-30.
224. Basad, E., et al., *Matrix-induced autologous chondrocyte implantation (MACI) in the knee: clinical outcomes and challenges.* Knee Surg Sports Traumatol Arthrosc, 2015. **23**(12): p. 3729-35.
225. Salash, J.R., et al., *Potential Indications for Tissue Engineering in Temporomandibular Joint Surgery.* J Oral Maxillofac Surg, 2016. **74**(4): p. 705-11.
226. Berarducci, J.P., D.A. Thompson, and R.B. Scheffer, *Perforation into Middle Cranial Fossa as a Sequel to Use of a Proplast-Teflon Implant for Temporomandibular-Joint Reconstruction.* Journal of Oral and Maxillofacial Surgery, 1990. **48**(5): p. 496-498.
227. Chuong, R. and M.A. Piper, *Cerebrospinal fluid leak associated with proplast implant removal from the temporomandibular joint.* Oral Surg Oral Med Oral Pathol, 1992. **74**(4): p. 422-5.
228. Smith, R.M., M.S. Goldwasser, and S.R. Sabol, *Erosion of a Teflon-Proplast Implant into the Middle Cranial Fossa.* Journal of Oral and Maxillofacial Surgery, 1993. **51**(11): p. 1268-1271.
229. Bordoni, B. and M. Varacallo, *Anatomy, Head and Neck, Temporomandibular Joint*, in *StatPearls*. 2019, StatPearls Publishing: Treasure Island (FL).
230. Gupton, M., O. Imonugo, and R.R. Terreberry, *Anatomy, Bony Pelvis and Lower Limb, Knee*, in *StatPearls*. 2021: Treasure Island (FL).

231. Lee, Y.H., et al., *Emerging Potential of Exosomes in Regenerative Medicine for Temporomandibular Joint Osteoarthritis.* Int J Mol Sci, 2020. **21**(4).
232. Fryar, C.D., et al., *Mean Body Weight, Height, Waist Circumference, and Body Mass Index Among Adults: United States, 1999-2000 Through 2015-2016.* Natl Health Stat Report, 2018(122): p. 1-16.
233. D'Lima, D.D., et al., *Knee joint forces: prediction, measurement, and significance.* Proc Inst Mech Eng H, 2012. **226**(2): p. 95-102.
234. Pizolato, R.A., et al., *Maximal bite force in young adults with temporomandibular disorders and bruxism.* Braz Oral Res, 2007. **21**(3): p. 278-83.
235. Patel, J.M., et al., *A Systematic Review and Guide to Mechanical Testing for Articular Cartilage Tissue Engineering.* Tissue Eng Part C Methods, 2019. **25**(10): p. 593-608.
236. Allen, K.D. and K.A. Athanasiou, *A surface-regional and freeze-thaw characterization of the porcine temporomandibular joint disc.* Ann Biomed Eng, 2005. **33**(7): p. 951-62.
237. Bielajew, B.J., J.C. Hu, and K.A. Athanasiou, *Collagen: quantification, biomechanics and role of minor subtypes in cartilage.* Nature Reviews Materials, 2020. **5**(10): p. 730-747.
238. Singh, M. and M.S. Detamore, *Biomechanical properties of the mandibular condylar cartilage and their relevance to the TMJ disc.* J Biomech, 2009. **42**(4): p. 405-17.
239. Huey, D.J., J.C. Hu, and K.A. Athanasiou, *Unlike bone, cartilage regeneration remains elusive.* Science, 2012. **338**(6109): p. 917-21.
240. Lawrence, R.C., et al., *Estimates of the prevalence of arthritis and other rheumatic conditions in the United States. Part II.* Arthritis Rheum, 2008. **58**(1): p. 26-35.
241. Masini, B.D., et al., *Epidemiology of Isolated Meniscus Tears in Young Athletes.* Orthopaedic Journal of Sports Medicine, 2015. **3**(7_suppl2): p. 2325967115S0010.
242. Badlani, J.T., et al., *The effects of meniscus injury on the development of knee osteoarthritis: data from the osteoarthritis initiative.* Am J Sports Med, 2013. **41**(6): p. 1238-44.
243. Kalladka, M., et al., *Temporomandibular joint osteoarthritis: diagnosis and long-term conservative management: a topic review.* J Indian Prosthodont Soc, 2014. **14**(1): p. 6-15.
244. The TMJ Association. *TMD Basics*. 2017; Available from: http://www.tmj.org/Page/34/17.
245. American Academy of Orthopaedic Surgeons, *2019 Annual Report*. 2019. Available from: https://www.aaos.org/globalassets/about/annual-report---year-in-review/aaos-2019-annual-report.pdf.
246. American Association of Oral and Maxillofacial Surgeons. *About AAOMS*. 2020; Available from: https://www.aaoms.org/about.
247. Kwon, H., et al., *Surgical and tissue engineering strategies for articular cartilage and meniscus repair.* Nat Rev Rheumatol, 2019. **15**(9): p. 550-570.
248. Singh, J.A., et al., *Rates of Total Joint Replacement in the United States: Future Projections to 2020-2040 Using the National Inpatient Sample.* J Rheumatol, 2019. **46**(9): p. 1134-1140.
249. Onoriobe, U., et al., *How Many Temporomandibular Joint Total Joint Alloplastic Implants Will Be Placed in the United States in 2030?* J Oral Maxillofac Surg, 2016. **74**(8): p. 1531-8.
250. Glyn-Jones, S., et al., *Osteoarthritis.* Lancet, 2015. **386**(9991): p. 376-87.
251. Heidari, B., *Knee osteoarthritis prevalence, risk factors, pathogenesis and features: Part I.* Caspian J Intern Med, 2011. **2**(2): p. 205-12.
252. Braun, H.J. and G.E. Gold, *Diagnosis of osteoarthritis: imaging.* Bone, 2012. **51**(2): p. 278-88.
253. Im, Y.G., et al., *Diagnostic accuracy and reliability of panoramic temporomandibular joint (TMJ) radiography to detect bony lesions in patients with TMJ osteoarthritis.* J Dent Sci, 2018. **13**(4): p. 396-404.

254. Honey, O.B., et al., *Accuracy of cone-beam computed tomography imaging of the temporomandibular joint: comparisons with panoramic radiology and linear tomography.* Am J Orthod Dentofacial Orthop, 2007. **132**(4): p. 429-38.
255. Tomas, X., et al., *MR imaging of temporomandibular joint dysfunction: a pictorial review.* Radiographics, 2006. **26**(3): p. 765-81.
256. Daly, C. and R.Y. Kwong, *Cardiac MRI for myocardial ischemia.* Methodist Debakey Cardiovasc J, 2013. **9**(3): p. 123-31.
257. Maini, K. and A. Dua, *Temporomandibular Joint Syndrome*, in *StatPearls*. 2021: Treasure Island (FL).
258. Bakke, M., et al., *Bony deviations revealed by cone beam computed tomography of the temporomandibular joint in subjects without ongoing pain.* J Oral Facial Pain Headache, 2014. **28**(4): p. 331-7.
259. Talmaceanu, D., et al., *Imaging modalities for temporomandibular joint disorders: an update.* Clujul Med, 2018. **91**(3): p. 280-287.
260. Lee, J.W., et al., *Clinical utility of fluoride-18 positron emission tomography/CT in temporomandibular disorder with osteoarthritis: comparisons with 99mTc-MDP bone scan.* Dentomaxillofac Radiol, 2013. **42**(2): p. 29292350.
261. Monasterio, G., et al., *Osteoarthritis of the Temporomandibular Joint: Clinical and Imagenological Diagnosis, Pathogenic Role of the Immuno- Inflammatory Response, and Immunotherapeutic Strategies Based on T Regulatory Lymphocytes.* Temporomandibular Joint Pathology - Current Approaches and Understanding, 2018.
262. Glass, N., et al., *Examining sex differences in knee pain: the multicenter osteoarthritis study.* Osteoarthritis Cartilage, 2014. **22**(8): p. 1100-6.
263. Srikanth, V.K., et al., *A meta-analysis of sex differences prevalence, incidence and severity of osteoarthritis.* Osteoarthritis Cartilage, 2005. **13**(9): p. 769-81.
264. Boyan, B.D., et al., *Addressing the gaps: sex differences in osteoarthritis of the knee.* Biol Sex Differ, 2013. **4**(1): p. 4.
265. Poveda Roda, R., et al., *Review of temporomandibular joint pathology. Part I: classification, epidemiology and risk factors.* Med Oral Patol Oral Cir Bucal, 2007. **12**(4): p. E292-8.
266. Abubaker, A.O., W.F. Raslan, and G.C. Sotereanos, *Estrogen and progesterone receptors in temporomandibular joint discs of symptomatic and asymptomatic persons: a preliminary study.* J Oral Maxillofac Surg, 1993. **51**(10): p. 1096-100.
267. Berger, M., et al., *Association between estrogen levels and temporomandibular disorders: a systematic literature review.* Prz Menopauzalny, 2015. **14**(4): p. 260-70.
268. Stewart, C.L. and S.M. Standish, *Osteoarthritis of the TMJ in teenaged females: report of cases.* J Am Dent Assoc, 1983. **106**(5): p. 638-40.
269. Shan, L., et al., *Intermediate and long-term quality of life after total knee replacement: a systematic review and meta-analysis.* J Bone Joint Surg Am, 2015. **97**(2): p. 156-68.
270. Haskin, C.L., S.B. Milam, and I.L. Cameron, *Pathogenesis of degenerative joint disease in the human temporomandibular joint.* Crit Rev Oral Biol Med, 1995. **6**(3): p. 248-77.
271. Wolford, L.M., *Idiopathic condylar resorption of the temporomandibular joint in teenage girls (cheerleaders syndrome).* Proc (Bayl Univ Med Cent), 2001. **14**(3): p. 246-52.
272. Hatcher, D.C., *Cone beam computed tomography: craniofacial and airway analysis.* Dent Clin North Am, 2012. **56**(2): p. 343-57.
273. Detamore, M.S., K.A. Athanasiou, and J. Mao, *A call to action for bioengineers and dental professionals: directives for the future of TMJ bioengineering.* Ann Biomed Eng, 2007. **35**(8): p. 1301-11.
274. Tanaka, E., M.S. Detamore, and L.G. Mercuri, *Degenerative disorders of the temporomandibular joint: etiology, diagnosis, and treatment.* J Dent Res, 2008. **87**(4): p. 296-307.

275. Dupont, J.S., Jr., *The prevalence of trigeminal neuritis with TMD.* Cranio, 2003. **21**(3): p. 180-4.
276. Sims, A.B., V.P. Clark, and M.S. Cooper, *Suppression of movement disorders by jaw realignment.* Pain Med, 2012. **13**(5): p. 731-2.
277. Edvall, N.K., et al., *Impact of Temporomandibular Joint Complaints on Tinnitus-Related Distress.* Front Neurosci, 2019. **13**: p. 879.
278. Paparo, F., et al., *Anatomic relationship between trigeminal nerve and temporomandibular joint.* European Review for Medical and Pharmacological Sciences, 2008. **12**(1): p. 15-18.
279. Pedulla, E., et al., *Neuropathic pain in temporomandibular joint disorders: case-control analysis by MR imaging.* AJNR Am J Neuroradiol, 2009. **30**(7): p. 1414-8.
280. *Complications of Temporomandibular Joint Surgery*. 2017, New York: Springer International Publishing.
281. Brown, G.A., *AAOS clinical practice guideline: treatment of osteoarthritis of the knee: evidence-based guideline, 2nd edition.* J Am Acad Orthop Surg, 2013. **21**(9): p. 577-9.
282. Bouloux, G., et al., *Temporomandibular Joint Surgery.* J Oral Maxillofac Surg, 2017. **75**(8S): p. e195-e223.
283. Meneses, S.R., et al., *Clinical algorithms to aid osteoarthritis guideline dissemination.* Osteoarthritis Cartilage, 2016. **24**(9): p. 1487-99.
284. Dimitroulis, G., *The role of surgery in the management of disorders of the temporomandibular joint: a critical review of the literature. Part 2.* Int J Oral Maxillofac Surg, 2005. **34**(3): p. 231-7.
285. Inacio, M.C.S., et al., *Projected increase in total knee arthroplasty in the United States - an alternative projection model.* Osteoarthritis Cartilage, 2017. **25**(11): p. 1797-1803.
286. UnitedHealthcare Oxford. *Surgical and Non-Surgical Treatment of Temporomandibular Joint Disorders*. 2005; Available from: https://www.oxhp.com/providers/toolsResources/practicalResources/policy/tmd.html.
287. Zimmer Biomet, *Knee Systems Coding Reference Guide*. 2019. Available from: https://www.zimmerbiomet.com/content/dam/zimmer-biomet/medical-professionals/reimbursement/Coding-Guides/knee-systems-coding-reference-guide.pdf.
288. Kumar, S., *Training Pathways in Oral and Maxillofacial Surgery Across the Globe-A Mini Review.* J Maxillofac Oral Surg, 2017. **16**(3): p. 269-276.
289. American Association of Oral and Maxillofacial Surgeons, *OMS Residency Training Programs*. 2020.
290. Commission on Dental Accreditation, *Accreditation Standards for Advanced Dental Education Programs in Oral and Maxillofacial Surgery*. 2018.
291. Momin, M., et al., *Senior Oral and Maxillofacial Surgery Resident Confidence in Performing Invasive Temporomandibular Joint Procedures.* J Oral Maxillofac Surg, 2017. **75**(10): p. 2091 e1-2091 e10.
292. Accreditation Council for Graduate Medical Education, *ACGME Program Requirements for Graduate Medical Education in Orthopaedic Surgery*. 2019.
293. Baskies, M.A., et al., *Operative experience in an orthopaedic surgery residency program: the effect of work-hour restrictions.* J Bone Joint Surg Am, 2008. **90**(4): p. 924-7.
294. Accreditation Council for Graduate Medical Education, *Orthopaedic Surgery Case Logs National Data Report*. 2019.
295. Daniels, A.H. and C.W. DiGiovanni, *Is subspecialty fellowship training emerging as a necessary component of contemporary orthopaedic surgery education?* J Grad Med Educ, 2014. **6**(2): p. 218-21.
296. Commission on Dental Accreditation, *Accreditation Standards for Clinical Fellowship Training Programs in Oral and Maxillofacial Surgery*. 2017.

297. Fattahi, T. and R. Fernandes, *Fellowship training and academic careers.* Oral Maxillofac Surg Clin North Am, 2008. **20**(1): p. 11-5.
298. Perruccio, A.V., et al., *Sex-Modified Effects of Depression, Low Back Pain, and Comorbidities on Pain After Total Knee Arthroplasty for Osteoarthritis.* Arthritis Care Res (Hoboken), 2020. **72**(8): p. 1074-1080.
299. Haggman-Henrikson, B., et al., *Increasing gender differences in the prevalence and chronification of orofacial pain in the population.* Pain, 2020. **161**(8): p. 1768-1775.
300. Keogh, E. and M. Herdenfeldt, *Gender, coping and the perception of pain.* Pain, 2002. **97**(3): p. 195-201.
301. Edwards, R.R., et al., *Pain-related catastrophizing in healthy women is associated with greater temporal summation of and reduced habituation to thermal pain.* Clin J Pain, 2006. **22**(8): p. 730-7.
302. Pincus, T., et al., *A systematic review of psychological factors as predictors of chronicity/disability in prospective cohorts of low back pain.* Spine (Phila Pa 1976), 2002. **27**(5): p. E109-20.
303. Paller, C.J., et al., *Sex-based differences in pain perception and treatment.* Pain Med, 2009. **10**(2): p. 289-99.
304. Bartley, E.J. and R.B. Fillingim, *Sex differences in pain: a brief review of clinical and experimental findings.* Br J Anaesth, 2013. **111**(1): p. 52-8.
305. Chambers, C.C., et al., *Women in Orthopaedic Surgery: Population Trends in Trainees and Practicing Surgeons.* J Bone Joint Surg Am, 2018. **100**(17): p. e116.
306. Kolokythas, A. and M. Miloro, *Why Do Women Choose to Enter Academic Oral and Maxillofacial Surgery?* J Oral Maxillofac Surg, 2016. **74**(5): p. 881-8.
307. DeMaio, M. *Making the Case (Again) for Gender Equity*. 2019; Available from: https://www.aaos.org/aaosnow/2019/jun/youraaos/youraaos05.
308. Drew, S.J. *President's Editorial*. 2018 [cited 2020; Available from: https://www.acoms.org/news/407850/Presidents-Editorial.htm.
309. National Institutes of Health. *Consideration of Sex as a Biological Variable in NIH-funded Research*. 2015; Available from: https://orwh.od.nih.gov/sex-gender/nih-policy-sex-biological-variable.
310. Office of Research on Women's Health. *NIH Policy on Sex as a Biological Variable*. Available from: https://orwh.od.nih.gov/sex-gender/nih-policy-sex-biological-variable.
311. Nolan, M.R. and T.L. Nguyen, *Analysis and reporting of sex differences in phase III medical device clinical trials-how are we doing?* J Womens Health (Larchmt), 2013. **22**(5): p. 399-401.
312. McKeever, D.C., *Tibial Plateau Prosthesis.* Clin. Orthop. Relat. Res., 1960. **18**: p. 86-95.
313. Carr, B.C. and T. Goswami, *Knee implants - Review of models and biomechanics.* Materials & Design, 2009. **30**(2): p. 398-413.
314. Christensen, R.W., *The correction of mandibular ankylosis by arthroplasty and the insertion of a cast vitallium glenoid fossa: a new technique. A preliminary report of three cases.* Am J Orthop, 1963. **5**: p. 16-24.
315. Hamelynck, K.J., *The history of mobile-bearing total knee replacement systems.* Orthopedics, 2006. **29**(9 Suppl): p. S7-12.
316. Wen, J., *Patent Insight into Knee Replacement Prosthetics*, in *Orthopedic Design & Technology*. 2017.
317. Mercuri, L.G., *Temporomandibular joint replacement devices - dark past to challenging future.* Stomatological Disease and Science, 2019. **2019**.
318. Kulber, D.A., I. Davos, and J.A. Aronowitz, *Severe cutaneous foreign body giant cell reaction after temporomandibular joint reconstruction with Proplast-Teflon.* J Oral Maxillofac Surg, 1995. **53**(6): p. 719-22; discussion 722-3.

319. Cowley, T. *A delicate balance: The food and drug administration (FDA) and the reform of the medical device approval process*. 2011 2011/4/13; Available from: http://tmj.org/wp-content/uploads/2020/08/Senate-Special-Committee-on-Aging-Statement-by-Terrie-Cowley.pdf.
320. Food and Drug Administration. *Temporomandibular Joint (TMJ) Implants*. 2019; Available from: https://www.fda.gov/medical-devices/temporomandibular-disorders-tmd-devices/temporomandibular-joint-tmj-implants.
321. Thangavelu, A., et al., *Fate of Free Fat Dermis Graft in TMJ Interpositional Gap Arthroplasty: A Long Term MRI Study.* J Maxillofac Oral Surg, 2015. **14**(2): p. 321-6.
322. Evans, J.T., et al., *How long does a knee replacement last? A systematic review and meta-analysis of case series and national registry reports with more than 15 years of follow-up.* The Lancet, 2019. **393**(10172): p. 655-663.
323. Center for Devices and Radiological Health. *PS110004: 522 Postmarket Surveillance Studies*. 2016; Available from: https://www.accessdata.fda.gov/scripts/cdrh/cfdocs/cfPMA/pss.cfm?t_id=41&c_id=394.
324. Johnson, N.R., et al., *Total temporomandibular joint replacement prostheses: a systematic review and bias-adjusted meta-analysis.* Int J Oral Maxillofac Surg, 2017. **46**(1): p. 86-92.
325. Arias, E., *United States Life Tables, 2017.* Natl Vital Stat Rep, 2019. **68**(7): p. 1-66.
326. Food and Drug Administration. *FDA approves first autologous cellularized scaffold for the repair of cartilage defects of the knee*. 2016 2016/12/13; Available from: https://www.fda.gov/news-events/press-announcements/fda-approves-first-autologous-cellularized-scaffold-repair-cartilage-defects-knee.
327. McCormick, F., et al., *Treatment of Focal Cartilage Defects With a Juvenile Allogeneic 3-Dimensional Articular Cartilage Graft.* Operative Techniques in Sports Medicine, 2013. **21**(2): p. 95-99.
328. Faculdade de Medicina de Petrópolis Faculdade Arthur Sá Earp Neto. *Nasal Septum Autologous Chondrocytes Transplantation for Condylar Resorption After Orthognathic Surgery*. 2017; Available from: https://clinicaltrials.gov/ct2/show/study/NCT03137914.
329. The National Academies of Sciences, Engineering, and Medicine, *Temporomandibular Disorders: Priorities for Research and Care*. 2020.
330. Almarza, A., et al., *State of TMJ Bioengineering: Working Together Toward Improving Clinical Outcomes.* J Biomech Eng, 2019.
331. Li, D. and L. Agha, *Research funding. Big names or big ideas: do peer-review panels select the best science proposals?* Science, 2015. **348**(6233): p. 434-8.
332. National Institutes of Health, *Research Project Grants and Other Mechanisms: Competing applications, awards, success rates, and funding, by Institute/Center, mechanism/funding source, and activity code*. 2019. Available from: https://report.nih.gov/success_rates/index.aspx.
333. Laskin, D.M., *Temporomandibular Disorders: A Term Whose Time Has Passed!* J Oral Maxillofac Surg, 2020. **78**(4): p. 496-497.
334. American Academy of Orthopaedic Surgeons. *The AAOS American Joint Replacement Registry*. Available from: https://www.aaos.org/registries/registry-program/american-joint-replacement-registry.
335. Erickson, B.J., S.M. Strickland, and A.H. Gomoll, *Indications, Techniques, Outcomes for Matrix Induced Autologous Chondrocyte Implantation (MACI).* Operative Techniques in Sports Medicine, 2018. **26**(3): p. 175-182.
336. Chin, A.R., et al., *Regenerative Potential of Various Soft Polymeric Scaffolds in the Temporomandibular Joint Condyle.* J Oral Maxillofac Surg, 2018. **76**(9): p. 2019-2026.
337. Acri, T.M., et al., *Tissue Engineering for the Temporomandibular Joint.* Adv Healthc Mater, 2019. **8**(2): p. e1801236.

338. Donahue, R.P., et al., *The Effect of Neonatal, Juvenile, and Adult Donors on Rejuvenated Neocartilage Functional Properties.* Tissue Eng. Part A, 2022.
339. Kwon, H., et al., *Translating the application of transforming growth factor-β1, chondroitinase-ABC, and lysyl oxidase-like 2 for mechanically robust tissue-engineered human neocartilage.* Journal of Tissue Engineering and Regenerative Medicine, 2019. **13**(2): p. 283-294.
340. Hunziker, E.B. and A. Stahli, *Surgical suturing of articular cartilage induces osteoarthritis-like changes.* Osteoarthritis Cartilage, 2008. **16**(9): p. 1067-73.
341. Merkel, J.R., et al., *Type I and type III collagen content of healing wounds in fetal and adult rats.* Proc Soc Exp Biol Med, 1988. **187**(4): p. 493-7.
342. Corr, D.T. and D.A. Hart, *Biomechanics of Scar Tissue and Uninjured Skin.* Adv Wound Care (New Rochelle), 2013. **2**(2): p. 37-43.
343. Makris, E.A., J.C. Hu, and K.A. Athanasiou, *Hypoxia-induced collagen crosslinking as a mechanism for enhancing mechanical properties of engineered articular cartilage.* Osteoarthritis Cartilage, 2013. **21**(4): p. 634-41.
344. Chang, S.W., S.J. Shefelbine, and M.J. Buehler, *Structural and mechanical differences between collagen homo- and heterotrimers: relevance for the molecular origin of brittle bone disease.* Biophys J, 2012. **102**(3): p. 640-8.
345. Wang, S., et al., *Strain distribution of repaired articular cartilage defects by tissue engineering under compression loading.* J Orthop Surg Res, 2018. **13**(1): p. 19.
346. Bielajew, B.J., J.C. Hu, and K.A. Athanasiou, *Methodology to Quantify Collagen Subtypes and Crosslinks: Application in Minipig Cartilages.* Cartilage, 2021. **13**(2_suppl): p. 1742S-1754S.
347. Hance, A.J. and R.G. Crystal, *Rigid control of synthesis of collagen types I and III by cells in culture.* Nature, 1977. **268**(5616): p. 152-4.
348. Sisino, G., et al., *Diabetes during pregnancy influences Hofbauer cells, a subtype of placental macrophages, to acquire a pro-inflammatory phenotype.* Biochim Biophys Acta, 2013. **1832**(12): p. 1959-68.
349. Wijesundera, K.K., et al., *M1- and M2-macrophage polarization in thioacetamide (TAA)-induced rat liver lesions; a possible analysis for hepato-pathology.* Histol Histopathol, 2014. **29**(4): p. 497-511.
350. Krzyszczyk, P., et al., *The Role of Macrophages in Acute and Chronic Wound Healing and Interventions to Promote Pro-wound Healing Phenotypes.* Front Physiol, 2018. **9**: p. 419.
351. Hu, J.M., et al., *CD163 as a marker of M2 macrophage, contribute to predicte aggressiveness and prognosis of Kazakh esophageal squamous cell carcinoma.* Oncotarget, 2017. **8**(13): p. 21526-21538.
352. Donahue, R.P., et al., *Stiffness- and bioactive factor-mediated protection of self-assembled cartilage against macrophage challenge in a novel co-culture system* Cartilage. In press, 2022.
353. Brown, W.E., J.C. Hu, and K.A. Athanasiou, *Ammonium-Chloride-Potassium Lysing Buffer Treatment of Fully Differentiated Cells Increases Cell Purity and Resulting Neotissue Functional Properties.* Tissue Engineering Part C: Methods, 2016. **22**(9): p. 895-903.
354. Mehra, P. and L.M. Wolford, *Use of the Mitek anchor in temporomandibular joint disc-repositioning surgery.* Proc (Bayl Univ Med Cent), 2001. **14**(1): p. 22-6.
355. Link, J.M., J.C. Hu, and K.A. Athanasiou, *Chondroitinase ABC Enhances Integration of Self-Assembled Articular Cartilage, but Its Dosage Needs to Be Moderated Based on Neocartilage Maturity.* Cartilage, 2020: p. 1947603520918653.
356. Bankhead, P., et al., *QuPath: Open source software for digital pathology image analysis.* Sci Rep, 2017. **7**(1): p. 16878.

357. Cox, J. and M. Mann, *MaxQuant enables high peptide identification rates, individualized p.p.b.-range mass accuracies and proteome-wide protein quantification.* Nat Biotechnol, 2008. **26**(12): p. 1367-72.
358. Pritzker, K.P., et al., *Osteoarthritis cartilage histopathology: grading and staging.* Osteoarthritis Cartilage, 2006. **14**(1): p. 13-29.
359. Fernandes, T.L., et al., *Macrophage: A Potential Target on Cartilage Regeneration.* Frontiers in immunology, 2020. **11**: p. 111-111.
360. Camarero-Espinosa, S., et al., *Articular cartilage: from formation to tissue engineering.* Biomater Sci, 2016. **4**(5): p. 734-67.
361. Centers for Disease Control and Prevention. *Osteoarthritis*. 2020; Available from: https://www.cdc.gov/arthritis/basics/osteoarthritis.htm.
362. Centers for Disease Control and Prevention. *Arthritis-Related Statistics*. 2018; Available from: https://www.cdc.gov/arthritis/data_statistics/arthritis-related-stats.htm.
363. Dunkin, B.S. and C. Lattermann, *New and Emerging Techniques in Cartilage Repair: MACI.* Oper Tech Sports Med, 2013. **21**(2): p. 100-107.
364. Smeriglio, P., et al., *Comparative potential of juvenile and adult human articular chondrocytes for cartilage tissue formation in three-dimensional biomimetic hydrogels.* Tissue Eng Part A, 2015. **21**(1-2): p. 147-55.
365. Barbero, A., et al., *Age related changes in human articular chondrocyte yield, proliferation and post-expansion chondrogenic capacity.* Osteoarthritis Cartilage, 2004. **12**(6): p. 476-84.
366. Eckstein, F., et al., *Interindividual variability and correlation among morphological parameters of knee joint cartilage plates: analysis with three-dimensional MR imaging.* Osteoarthritis Cartilage, 2001. **9**(2): p. 101-11.
367. Hunziker, E.B., T.M. Quinn, and H.J. Hauselmann, *Quantitative structural organization of normal adult human articular cartilage.* Osteoarthritis Cartilage, 2002. **10**(7): p. 564-72.
368. Darling, E.M. and K.A. Athanasiou, *Rapid phenotypic changes in passaged articular chondrocyte subpopulations.* J Orthop Res, 2005. **23**(2): p. 425-32.
369. Murphy, M.K., et al., *Inducing articular cartilage phenotype in costochondral cells.* Arthritis Res Ther, 2013. **15**(6): p. R214.
370. Choi, W.R. and Y.J. Jang, *Reconstruction of a Severely Damaged Cartilaginous Septum with a Bypass L-Strut Graft using Costal Cartilage.* Facial Plast Surg, 2021. **37**(1): p. 92-97.
371. Lee, J., et al., *Comparison of articular cartilage with costal cartilage in initial cell yield, degree of dedifferentiation during expansion and redifferentiation capacity.* Biotechnol Appl Biochem, 2007. **48**(Pt 3): p. 149-58.
372. Cho, S.A., et al., *Effects of hesperidin loaded poly(lactic-co-glycolic acid) scaffolds on growth behavior of costal cartilage cells in vitro and in vivo.* J Biomater Sci Polym Ed, 2014. **25**(6): p. 625-40.
373. O'Sullivan, N.A., et al., *Adhesion and integration of tissue engineered cartilage to porous polyethylene for composite ear reconstruction.* J Biomed Mater Res B Appl Biomater, 2015. **103**(5): p. 983-91.
374. National Institute of Child Health and Human Development. *Puberty and Precocious Puberty*. 2021; Available from: https://www.nichd.nih.gov/health/topics/puberty.
375. Premier BioSource. *Swine Models*. Available from: http://www.premierbiosource.com/swine-models.
376. Cech, D.J. and S.T. Martin, *Chapter 6 - Skeletal System Changes*, in *Functional Movement Development Across the Life Span (Third Edition)*, D.J. Cech and S.T. Martin, Editors. 2012, W.B. Saunders: Saint Louis. p. 105-128.

377. Huang, B.J., et al., *Engineering biomechanically functional neocartilage derived from expanded articular chondrocytes through the manipulation of cell-seeding density and dexamethasone concentration.* J Tissue Eng Regen Med, 2017. **11**(8): p. 2323-2332.
378. Gonzalez-Leon, E.A., et al., *Engineering self-assembled neomenisci through combination of matrix augmentation and directional remodeling.* Acta Biomater, 2020. **109**: p. 73-81.
379. Bruckner, P. and M. van der Rest, *Structure and function of cartilage collagens.* Microsc Res Tech, 1994. **28**(5): p. 378-84.
380. Cremer, M.A., E.F. Rosloniec, and A.H. Kang, *The cartilage collagens: a review of their structure, organization, and role in the pathogenesis of experimental arthritis in animals and in human rheumatic disease.* J Mol Med (Berl), 1998. **76**(3-4): p. 275-88.
381. Eyre, D.R., J.J. Wu, and P.E. Woods, *The cartilage collagens: structural and metabolic studies.* J Rheumatol Suppl, 1991. **27**: p. 49-51.
382. Sugrue, S.P., et al., *Immunoidentification of type XII collagen in embryonic tissues.* J Cell Biol, 1989. **109**(2): p. 939-45.
383. Wessel, H., et al., *Type XII collagen contributes to diversities in human corneal and limbal extracellular matrices.* Invest Ophthalmol Vis Sci, 1997. **38**(11): p. 2408-22.
384. Oh, S.P., et al., *Tissue-specific expression of type XII collagen during mouse embryonic development.* Dev Dyn, 1993. **196**(1): p. 37-46.
385. Walchli, C., et al., *Tissue-specific expression of the fibril-associated collagens XII and XIV.* J Cell Sci, 1994. **107 (Pt 2)**: p. 669-81.
386. Gregory, K.E., et al., *Developmental distribution of collagen type XII in cartilage: association with articular cartilage and the growth plate.* J Bone Miner Res, 2001. **16**(11): p. 2005-16.
387. Andrzejewska, A., et al., *Multi-Parameter Analysis of Biobanked Human Bone Marrow Stromal Cells Shows Little Influence for Donor Age and Mild Comorbidities on Phenotypic and Functional Properties.* Front Immunol, 2019. **10**: p. 2474.
388. Martin, I., et al., *Mammalian chondrocytes expanded in the presence of fibroblast growth factor 2 maintain the ability to differentiate and regenerate three-dimensional cartilaginous tissue.* Exp Cell Res, 1999. **253**(2): p. 681-8.
389. Barbero, A., et al., *Plasticity of clonal populations of dedifferentiated adult human articular chondrocytes.* Arthritis Rheum, 2003. **48**(5): p. 1315-25.
390. Hsieh-Bonassera, N.D., et al., *Expansion and redifferentiation of chondrocytes from osteoarthritic cartilage: cells for human cartilage tissue engineering.* Tissue Eng Part A, 2009. **15**(11): p. 3513-23.
391. Chieppa, M.N., et al., *Modeling amyotrophic lateral sclerosis in hSOD1 transgenic swine.* Neurodegener Dis, 2014. **13**(4): p. 246-54.
392. Basad, E., et al., *Matrix-induced autologous chondrocyte implantation versus microfracture in the treatment of cartilage defects of the knee: a 2-year randomised study.* Knee Surg. Sports Traumatol. Arthrosc., 2010. **18**(4): p. 519-527.
393. Flanigan, D.C., et al., *Prevalence of chondral defects in athletes' knees: a systematic review.* Med. Sci. Sports Exerc., 2010. **42**(10): p. 1795-1801.
394. Kreuz, P.C., et al., *Results after microfracture of full-thickness chondral defects in different compartments in the knee.* Osteoarthritis Cartilage, 2006. **14**(11): p. 1119-25.
395. Venäläinen, M.S., et al., *Quantitative Evaluation of the Mechanical Risks Caused by Focal Cartilage Defects in the Knee.* Sci. Rep., 2016. **6**: p. 37538.
396. Makris, E.A., et al., *Repair and tissue engineering techniques for articular cartilage.* Nature Reviews Rheumatology, 2015. **11**(1): p. 21-34.
397. Armiento, A.R., et al., *Biomaterials for articular cartilage tissue engineering: Learning from biology.* Acta Biomater., 2018. **65**: p. 1-20.

398. Blein-Nicolas, M. and M. Zivy, *Thousand and one ways to quantify and compare protein abundances in label-free bottom-up proteomics.* Biochim. Biophys. Acta, 2016. **1864**(8): p. 883-895.
399. Ofek, G., et al., *Matrix development in self-assembly of articular cartilage.* PLoS One, 2008. **3**(7): p. e2795.
400. Natoli, R.M., et al., *Intracellular Na and Ca2 modulation increases the tensile properties of developing engineered articular cartilage.* Arthritis & Rheumatism, 2010. **62**(4): p. 1097-1107.
401. Little, C.J., N.K. Bawolin, and X. Chen, *Mechanical properties of natural cartilage and tissue-engineered constructs.* Tissue Eng Part B Rev, 2011. **17**(4): p. 213-27.
402. Yoon, K.H., et al., *Costal Chondrocyte-Derived Pellet-Type Autologous Chondrocyte Implantation for Treatment of Articular Cartilage Defect.* Am J Sports Med, 2020. **48**(5): p. 1236-1245.
403. Mao, Y., et al., *An Innovative Laboratory Procedure to Expand Chondrocytes with Reduced Dedifferentiation.* Cartilage, 2018. **9**(2): p. 202-211.
404. Lee, J., et al., *Fully Dedifferentiated Chondrocytes Expanded in Specific Mesenchymal Stem Cell Growth Medium with FGF2 Obtains Mesenchymal Stem Cell Phenotype In Vitro but Retains Chondrocyte Phenotype In Vivo.* Cell Transplant, 2017. **26**(10): p. 1673-1687.
405. Mao, Y., et al., *Extracellular matrix derived from chondrocytes promotes rapid expansion of human primary chondrocytes in vitro with reduced dedifferentiation.* Acta Biomater, 2019. **85**: p. 75-83.
406. Hall, A.C., *The Role of Chondrocyte Morphology and Volume in Controlling Phenotype-Implications for Osteoarthritis, Cartilage Repair, and Cartilage Engineering.* Curr Rheumatol Rep, 2019. **21**(8): p. 38.
407. Bielajew, B.J., et al., *Proteomic, Mechanical, and Biochemical Characterization of Cartilage Development.* Acta Biomaterialia, 2022.
408. Calabro, A., et al., *Fluorophore-assisted carbohydrate electrophoresis (FACE) of glycosaminoglycans.* Osteoarthritis Cartilage, 2001. **9 Suppl A**: p. S16-22.
409. Kagan, H.M. and W. Li, *Lysyl oxidase: properties, specificity, and biological roles inside and outside of the cell.* J Cell Biochem, 2003. **88**(4): p. 660-72.
410. Hasegawa, M., T. Yoshida, and A. Sudo, *Role of tenascin-C in articular cartilage.* Mod Rheumatol, 2018. **28**(2): p. 215-220.
411. Schmid, T.M. and T.F. Linsenmayer, *Immunohistochemical localization of short chain cartilage collagen (type X) in avian tissues.* J Cell Biol, 1985. **100**(2): p. 598-605.
412. Shen, G., *The role of type X collagen in facilitating and regulating endochondral ossification of articular cartilage.* Orthod Craniofac Res, 2005. **8**(1): p. 11-7.
413. Pacifici, M., et al., *Development of articular cartilage: what do we know about it and how may it occur?* Connect. Tissue Res., 2000. **41**(3): p. 175-184.
414. Morrison, E.H., et al., *The development of articular cartilage: I. The spatial and temporal patterns of collagen types.* J. Anat., 1996. **189 (Pt 1)**: p. 9-22.
415. Archer, C.W., et al., *The development of articular cartilage: II. The spatial and temporal patterns of glycosaminoglycans and small leucine-rich proteoglycans.* J. Anat., 1996. **189 (Pt 1)**: p. 23-35.
416. Kempson, G.E., *Relationship between the tensile properties of articular cartilage from the human knee and age.* Annals of the Rheumatic Diseases, 1982. **41**(5): p. 508-511.
417. Williamson, A.K., A.C. Chen, and R.L. Sah, *Compressive properties and function-composition relationships of developing bovine articular cartilage.* J. Orthop. Res., 2001. **19**(6): p. 1113-1121.

418. Williamson, A.K., et al., *Tensile mechanical properties of bovine articular cartilage: variations with growth and relationships to collagen network components.* J Orthop Res, 2003. **21**(5): p. 872-80.
419. Ding, M., et al., *Mechanical properties of the normal human tibial cartilage-bone complex in relation to age.* Clin. Biomech., 1998. **13**(4-5): p. 351-358.
420. Lotz, M. and R.F. Loeser, *Effects of aging on articular cartilage homeostasis.* Bone, 2012. **51**(2): p. 241-248.
421. Peters, A.E., et al., *The effect of ageing and osteoarthritis on the mechanical properties of cartilage and bone in the human knee joint.* Sci. Rep., 2018. **8**(1): p. 5931.
422. Barbour, K.E., et al., *Vital Signs: Prevalence of Doctor-Diagnosed Arthritis and Arthritis-Attributable Activity Limitation - United States, 2013-2015.* MMWR Morb Mortal Wkly Rep, 2017. **66**(9): p. 246-253.
423. Center for Biologics, E. and Research, *IDEs & INDs for Products to Repair or Place Knee Cartilage.* 2019.
424. Book, S.A. and L.K. Bustad, *The Fetal and Neonatal Pig in Biomedical Research.* Journal of Animal Science, 1974. **38**(5): p. 997-1002.
425. Cone, S.G., P.B. Warren, and M.B. Fisher, *Rise of the Pigs: Utilization of the Porcine Model to Study Musculoskeletal Biomechanics and Tissue Engineering During Skeletal Growth.* Tissue Eng Part C Methods, 2017. **23**(11): p. 763-780.
426. Pomin, V.H. and B. Mulloy, *Glycosaminoglycans and Proteoglycans.* Pharmaceuticals, 2018. **11**(1).
427. Sanchez-Adams, J., et al., *The mechanobiology of articular cartilage: bearing the burden of osteoarthritis.* Curr. Rheumatol. Rep., 2014. **16**(10): p. 451.
428. Tsukazaki, T., et al., *Growth hormone directly and indirectly stimulates articular chondrocyte cell growth.* Osteoarthritis Cartilage, 1994. **2**(4): p. 259-267.
429. Althen, T.G. and R.J. Gerrits, *Pituitary and serum growth hormone levels in Duroc and Yorkshire swine genetically selected for high and low backfat.* J. Anim. Sci., 1976. **42**(6): p. 1490-1497.
430. Macfadyen, M.A., et al., *The commercial pig as a model of spontaneously-occurring osteoarthritis.* BMC Musculoskelet. Disord., 2019. **20**(1): p. 70.
431. Reiland, S., *The effect of decreased growth rate on frequency and severity of osteochondrosis in pigs.* Acta Radiol. Suppl., 1978. **358**: p. 107-122.
432. Takroni, T., et al., *Anatomical study: comparing the human, sheep and pig knee meniscus.* J Exp Orthop, 2016. **3**(1): p. 35.
433. López-Álvarez, M., et al., *Quantitative evaluation of sulfation position prevalence in chondroitin sulphate by Raman spectroscopy.* Journal of Raman Spectroscopy, 2019. **50**(5): p. 656-664.
434. Volpi, N., *Disaccharide mapping of chondroitin sulfate of different origins by high-performance capillary electrophoresis and high-performance liquid chromatography.* Carbohydrate Polymers, 2004. **55**(3): p. 273-281.
435. Kulkarni, P., et al., *Glycosaminoglycan measured from synovial fluid serves as a useful indicator for progression of Osteoarthritis and complements Kellgren–Lawrence Score.* BBA Clinical, 2016. **6**: p. 1-4.
436. Lei, J., et al., *Proteomic analysis of knee cartilage reveals potential signaling pathways in pathological mechanism of Kashin-Beck disease compared with osteoarthritis.* Sci. Rep., 2020. **10**(1): p. 6824.
437. Önnerfjord, P., et al., *Quantitative proteomic analysis of eight cartilaginous tissues reveals characteristic differences as well as similarities between subgroups.* J. Biol. Chem., 2012. **287**(23): p. 18913-18924.

438. Wilson, R., et al., *Changes in the chondrocyte and extracellular matrix proteome during post-natal mouse cartilage development.* Mol Cell Proteomics, 2012. **11**(1): p. M111 014159.
439. Eyre, D., *Collagen of articular cartilage.* Arthritis Res., 2002. **4**(1): p. 30-35.
440. Ansorge, H.L., et al., *Type XIV Collagen Regulates Fibrillogenesis: Premature Collagen Fibril Growth and Tissue Dysfunction in Null Mice.* J. Biol. Chem., 2009. **284**(13): p. 8427-8438.
441. Heinemeier, K.M., et al., *Radiocarbon dating reveals minimal collagen turnover in both healthy and osteoarthritic human cartilage.* Sci. Transl. Med., 2016. **8**(346): p. 346ra90.
442. Roughley, P.J. and J.S. Mort, *The role of aggrecan in normal and osteoarthritic cartilage.* J Exp Orthop, 2014. **1**(1): p. 8.
443. Hernandez, P.A., et al., *Early-Onset Osteoarthritis originates at the chondrocyte level in Hip Dysplasia.* Scientific Reports, 2020. **10**(1).
444. Goetz, J.E., et al., *A clinically realistic large animal model of intra-articular fracture that progresses to post-traumatic osteoarthritis.* Osteoarthritis Cartilage, 2015. **23**(10): p. 1797-1805.
445. Frisbie, D.D., M.W. Cross, and C.W. McIlwraith, *A comparative study of articular cartilage thickness in the stifle of animal species used in human pre-clinical studies compared to articular cartilage thickness in the human knee.* Vet. Comp. Orthop. Traumatol., 2006. **19**(3): p. 142-146.
446. Athanasiou, K.A., et al., *Biomechanical Properties of Hip Cartilage in Experimental Animal Models.* Clinical Orthopaedics and Related Research®, 1995(316): p. 254-266.
447. Athanasiou, K.A., et al., *Biomechanical topography of human articular cartilage in the first metatarsophalangeal joint.* Clin Orthop Relat Res, 1998(348): p. 269-81.
448. Zimmerman, B.K., et al., *Role of interstitial fluid pressurization in TMJ lubrication.* J Dent Res, 2015. **94**(1): p. 85-92.
449. McCormick, F., et al., *Trends in the surgical treatment of articular cartilage lesions in the United States: an analysis of a large private-payer database over a period of 8 years.* Arthroscopy, 2014. **30**(2): p. 222-6.
450. Salinas, E.Y., et al., *Shear stress induced by fluid flow produces improvements in tissue-engineered cartilage.* Biofabrication, 2020. **12**(4): p. 045010.
451. Gemmiti, C.V. and R.E. Guldberg, *Shear stress magnitude and duration modulates matrix composition and tensile mechanical properties in engineered cartilaginous tissue.* Biotechnology and Bioengineering, 2009. **104**(4): p. 809-820.
452. Gemmiti, C.V. and R.E. Guldberg, *Fluid flow increases type II collagen deposition and tensile mechanical properties in bioreactor-grown tissue-engineered cartilage.* Tissue Engineering, 2006. **12**(3): p. 469-479.
453. Ruhlen, R. and K. Marberry, *The chondrocyte primary cilium.* Osteoarthritis and Cartilage, 2014. **22**(8): p. 1071-1076.
454. Wann, A.K., et al., *Primary cilia mediate mechanotransduction through control of ATP-induced Ca2+ signaling in compressed chondrocytes.* The FASEB Journal, 2012. **26**(4): p. 1663-1671.
455. Bastow, E.R., et al., *Selective activation of the MEK-ERK pathway is regulated by mechanical stimuli in forming joints and promotes pericellular matrix formation.* J Biol Chem, 2005. **280**(12): p. 11749-58.
456. Dowthwaite, G., et al., *A mechanism underlying the movement requirement for synovial joint cavitation.* Matrix Biology, 2003. **22**(4): p. 311-322.
457. Brama, P.A.J., et al., *Influence of development and joint pathology on stromelysin enzyme activity in equine synovial fluid.* Annals of the Rheumatic Diseases, 2000. **59**(2): p. 155.

458. Kim, I.G., et al., *Mesenchymal cells condensation-inducible mesh scaffolds for cartilage tissue engineering.* Biomaterials, 2016. **85**: p. 18-29.
459. Panepinto, L.M. and R.W. Phillips, *The Yucatan miniature pig: characterization and utilization in biomedical research.* Lab Anim Sci, 1986. **36**(4): p. 344-7.
460. Gutierrez, K., et al., *Efficacy of the porcine species in biomedical research.* Frontiers in genetics, 2015. **6**: p. 293-293.
461. Pfeifer, C.G., et al., *Age-Dependent Subchondral Bone Remodeling and Cartilage Repair in a Minipig Defect Model.* Tissue Eng Part C Methods, 2017. **23**(11): p. 745-753.
462. Gotterbarm, T., et al., *The minipig model for experimental chondral and osteochondral defect repair in tissue engineering: Retrospective analysis of 180 defects.* Laboratory Animals, 2008. **42**(1): p. 71-82.
463. Fisher, M.B., et al., *Cartilage repair and subchondral bone remodeling in response to focal lesions in a mini-pig model: implications for tissue engineering.* Tissue Eng Part A, 2015. **21**(3-4): p. 850-60.
464. Elder, B.D. and K.A. Athanasiou, *Systematic assessment of growth factor treatment on biochemical and biomechanical properties of engineered articular cartilage constructs.* Osteoarthritis Cartilage, 2009. **17**(1): p. 114-23.
465. Elder, B.D. and K.A. Athanasiou, *Synergistic and additive effects of hydrostatic pressure and growth factors on tissue formation.* PloS one, 2008. **3**(6): p. e2341.
466. van der Kraan, P.M., et al., *Interaction of chondrocytes, extracellular matrix and growth factors: relevance for articular cartilage tissue engineering.* Osteoarthritis and Cartilage, 2002. **10**(8): p. 631-637.
467. Madry, H., et al., *Transforming growth factor Beta-releasing scaffolds for cartilage tissue engineering.* Tissue Eng Part B Rev, 2014. **20**(2): p. 106-25.
468. Blunk, T., et al., *Differential effects of growth factors on tissue-engineered cartilage.* Tissue Eng, 2002. **8**(1): p. 73-84.
469. Moore, E.R. and C.R. Jacobs, *The primary cilium as a signaling nexus for growth plate function and subsequent skeletal development.* J Orthop Res, 2018. **36**(2): p. 533-545.
470. Elisseeff, J., et al., *Controlled-release of IGF-I and TGF-beta1 in a photopolymerizing hydrogel for cartilage tissue engineering.* J Orthop Res, 2001. **19**(6): p. 1098-104.
471. Berson, R.E., M.R. Purcell, and M.K. Sharp, *Computationally determined shear on cells grown in orbiting culture dishes*, in *Oxygen Transport to Tissue XXIX*. 2008, Springer. p. 189-198.
472. Chakraborty, A., et al., *Impact of bi-axial shear on atherogenic gene expression by endothelial cells.* Annals of Biomedical Engineering, 2016. **44**(10): p. 3032-3045.
473. Thomas, J.M.D., et al., *Validation of a CFD model of an orbiting culture dish with PIV and analytical solutions.* AIChE Journal, 2017. **63**(9): p. 4233-4242.
474. Thomas, J.M.D., et al., *Spatial and temporal resolution of shear in an orbiting petri dish.* Biotechnology Progress, 2011. **27**(2): p. 460-465.
475. Allen, K.D. and K.A. Athanasiou, *Viscoelastic characterization of the porcine temporomandibular joint disc under unconfined compression.* J Biomech, 2006. **39**(2): p. 312-22.
476. Makris, E.A., et al., *A copper sulfate and hydroxylysine treatment regimen for enhancing collagen cross-linking and biomechanical properties in engineered neocartilage.* FASEB J, 2013. **27**(6): p. 2421-30.
477. Eggenschwiler, J.T. and K.V. Anderson, *Cilia and Developmental Signaling.* Annual Review of Cell and Developmental Biology, 2007. **23**(1): p. 345-373.
478. Waller, K.A., et al., *Intra-articular Recombinant Human Proteoglycan 4 Mitigates Cartilage Damage After Destabilization of the Medial Meniscus in the Yucatan Minipig.* Am J Sports Med, 2017. **45**(7): p. 1512-1521.

479. Christensen, B.B., et al., *Experimental articular cartilage repair in the Göttingen minipig: the influence of multiple defects per knee.* J Exp Orthop, 2015. **2**(1): p. 13.
480. Otsuki, S., et al., *Evaluation of Meniscal Regeneration in a Mini Pig Model Treated With a Novel Polyglycolic Acid Meniscal Scaffold.* Am J Sports Med, 2019. **47**(8): p. 1804-1815.
481. Thompson, C.L., et al., *Chondrocyte expansion is associated with loss of primary cilia and disrupted hedgehog signalling.* Eur Cell Mater, 2017. **34**: p. 128-141.
482. Ikada, Y., *Challenges in tissue engineering.* J R Soc Interface, 2006. **3**(10): p. 589-601.
483. Murphy, M.K., et al., *Tensile characterization of porcine temporomandibular joint disc attachments.* J Dent Res, 2013. **92**(8): p. 753-8.
484. O'Leary, S.A., et al., *Characterization of facet joint cartilage properties in the human and interspecies comparisons.* Acta Biomater, 2017. **54**: p. 367-376.
485. Schook, L., et al., *Swine in biomedical research: creating the building blocks of animal models.* Anim Biotechnol, 2005. **16**(2): p. 183-90.
486. Summerfield, A., F. Meurens, and M.E. Ricklin, *The immunology of the porcine skin and its value as a model for human skin.* Mol Immunol, 2015. **66**(1): p. 14-21.
487. Anderson, J.M., *Biological responses to materials.* Annual review of materials research, 2001. **31**(1): p. 81-110.
488. Langer, R., *Perspectives and challenges in tissue engineering and regenerative medicine.* Adv Mater, 2009. **21**(32-33): p. 3235-6.
489. Sadtler, K., et al., *Design, clinical translation and immunological response of biomaterials in regenerative medicine.* Nature Reviews Materials, 2016. **1**(7): p. 1-17.
490. Lanza, R., *Principles of tissue engineering*. 2020, Waltham: Elsevier. pages cm.
491. Ma, M., et al., *Development of cationic polymer coatings to regulate foreign-body responses.* Adv Mater, 2011. **23**(24): p. H189-94.
492. Meli, V.S., et al., *YAP-mediated mechanotransduction tunes the macrophage inflammatory response.* Sci Adv, 2020. **6**(49).
493. Wang, T., et al., *Topographical modulation of macrophage phenotype by shrink-film multi-scale wrinkles.* Biomater Sci, 2016. **4**(6): p. 948-52.
494. Huynh, J., et al., *Age-related intimal stiffening enhances endothelial permeability and leukocyte transmigration.* Sci Transl Med, 2011. **3**(112): p. 112ra122.
495. Palombo, C. and M. Kozakova, *Arterial stiffness, atherosclerosis and cardiovascular risk: Pathophysiologic mechanisms and emerging clinical indications.* Vascul Pharmacol, 2016. **77**: p. 1-7.
496. Wynn, T.A. and T.R. Ramalingam, *Mechanisms of fibrosis: therapeutic translation for fibrotic disease.* Nat Med, 2012. **18**(7): p. 1028-40.
497. Pickup, M.W., J.K. Mouw, and V.M. Weaver, *The extracellular matrix modulates the hallmarks of cancer.* EMBO Rep, 2014. **15**(12): p. 1243-53.
498. Moshayedi, P., et al., *The relationship between glial cell mechanosensitivity and foreign body reactions in the central nervous system.* Biomaterials, 2014. **35**(13): p. 3919-25.
499. Anderson, J.M., A. Rodriguez, and D.T. Chang, *Foreign body reaction to biomaterials.* Semin Immunol, 2008. **20**(2): p. 86-100.
500. Hsieh, J.Y., et al., *Differential regulation of macrophage inflammatory activation by fibrin and fibrinogen.* Acta Biomater, 2017. **47**: p. 14-24.
501. Blakney, A.K., M.D. Swartzlander, and S.J. Bryant, *The effects of substrate stiffness on the in vitro activation of macrophages and in vivo host response to poly(ethylene glycol)-based hydrogels.* J Biomed Mater Res A, 2012. **100**(6): p. 1375-86.
502. Gao, J., et al., *A new and efficient culture method for porcine bone marrow-derived M1- and M2-polarized macrophages.* Vet Immunol Immunopathol, 2018. **200**: p. 7-15.

503. Kapetanovic, R., et al., *Pig bone marrow-derived macrophages resemble human macrophages in their response to bacterial lipopolysaccharide.* J Immunol, 2012. **188**(7): p. 3382-94.
504. Holness, C.L. and D.L. Simmons, *Molecular cloning of CD68, a human macrophage marker related to lysosomal glycoproteins.* Blood, 1993. **81**(6): p. 1607-13.
505. Chistiakov, D.A., et al., *CD68/macrosialin: not just a histochemical marker.* Lab Invest, 2017. **97**(1): p. 4-13.
506. Poulsen, C.B., et al., *Treatment with a human recombinant monoclonal IgG antibody against oxidized LDL in atherosclerosis-prone pigs reduces cathepsin S in coronary lesions.* Int J Cardiol, 2016. **215**: p. 506-15.
507. Waddell, L.A., et al., *ADGRE1 (EMR1, F4/80) Is a Rapidly-Evolving Gene Expressed in Mammalian Monocyte-Macrophages.* Front Immunol, 2018. **9**: p. 2246.
508. Choi, J.Y., et al., *Expression and cellular localization of inducible nitric oxide synthase in lipopolysaccharide-treated rat kidneys.* J Histochem Cytochem, 2012. **60**(4): p. 301-15.
509. Bernardini, C., et al., *Differential expression of nitric oxide synthases in porcine aortic endothelial cells during LPS-induced apoptosis.* J Inflamm (Lond), 2012. **9**(1): p. 47.
510. Liu, H., et al., *Heterogeneity and plasticity of porcine alveolar macrophage and pulmonary interstitial macrophage isolated from healthy pigs in vitro.* Biol Open, 2019. **8**(10).
511. Wang, L., et al., *Porcine alveolar macrophage polarization is involved in inhibition of porcine reproductive and respiratory syndrome virus (PRRSV) replication.* J Vet Med Sci, 2017. **79**(11): p. 1906-1915.
512. Tao, Y., et al., *Immunohistochemical localization of inducible and endothelial nitric oxide synthase in porcine ovaries and effects of NO on antrum formation and oocyte meiotic maturation.* Mol Cell Endocrinol, 2004. **222**(1-2): p. 93-103.
513. Villanueva, C. and C. Giulivi, *Subcellular and cellular locations of nitric oxide synthase isoforms as determinants of health and disease.* Free Radic Biol Med, 2010. **49**(3): p. 307-16.
514. Chmelikova, E., et al., *Nitric oxide synthase isoforms and the effect of their inhibition on meiotic maturation of porcine oocytes.* Zygote, 2010. **18**(3): p. 235-44.
515. Seaton, M., A. Hocking, and N.S. Gibran, *Porcine models of cutaneous wound healing.* ILAR J, 2015. **56**(1): p. 127-38.
516. Sullivan, T.P., et al., *The pig as a model for human wound healing.* Wound Repair Regen, 2001. **9**(2): p. 66-76.
517. Genovesi, E.V., et al., *Effect of macrophage-specific colony-stimulating factor (CSF-1) on swine monocyte/macrophage susceptibility to in vitro infection by African swine fever virus.* Vet Microbiol, 1990. **25**(2-3): p. 153-76.
518. Schneemann, M. and G. Schoedon, *Species differences in macrophage NO production are important.* Nat Immunol, 2002. **3**(2): p. 102.
519. Zelnickova, P., et al., *Quantitative nitric oxide production by rat, bovine and porcine macrophages.* Nitric Oxide, 2008. **19**(1): p. 36-41.
520. McNally, A.K. and J.M. Anderson, *Macrophage fusion and multinucleated giant cells of inflammation.* Adv Exp Med Biol, 2011. **713**: p. 97-111.
521. Pereira, M., et al., *Common signalling pathways in macrophage and osteoclast multinucleation.* J Cell Sci, 2018. **131**(11).
522. McNally, A.K. and J.M. Anderson, *Interleukin-4 induces foreign body giant cells from human monocytes/macrophages. Differential lymphokine regulation of macrophage fusion leads to morphological variants of multinucleated giant cells.* Am J Pathol, 1995. **147**(5): p. 1487-99.

523. Kyriakides, T.R., et al., *The CC chemokine ligand, CCL2/MCP1, participates in macrophage fusion and foreign body giant cell formation.* Am J Pathol, 2004. **165**(6): p. 2157-66.
524. Fang, J.Y., Z. Yang, and B. Han, *Switch of macrophage fusion competency by 3D matrices.* Sci Rep, 2020. **10**(1): p. 10348.
525. McWhorter, F.Y., C.T. Davis, and W.F. Liu, *Physical and mechanical regulation of macrophage phenotype and function.* Cell Mol Life Sci, 2015. **72**(7): p. 1303-16.
526. Yagi, M., et al., *DC-STAMP is essential for cell-cell fusion in osteoclasts and foreign body giant cells.* J Exp Med, 2005. **202**(3): p. 345-51.
527. Cui, W., et al., *The intracellular domain of CD44 promotes the fusion of macrophages.* Blood, 2006. **107**(2): p. 796-805.
528. Helming, L., J. Winter, and S. Gordon, *The scavenger receptor CD36 plays a role in cytokine-induced macrophage fusion.* J Cell Sci, 2009. **122**(Pt 4): p. 453-9.
529. McNally, A.K. and J.M. Anderson, *Beta1 and beta2 integrins mediate adhesion during macrophage fusion and multinucleated foreign body giant cell formation.* Am J Pathol, 2002. **160**(2): p. 621-30.
530. Wang, Y., et al., *Role of actin filaments in fusopod formation and osteoclastogenesis.* Biochim Biophys Acta, 2015. **1853**(7): p. 1715-24.
531. Goswami, R., et al., *Transient Receptor Potential Vanilloid 4 Is Required for Foreign Body Response and Giant Cell Formation.* Am J Pathol, 2019. **189**(8): p. 1505-1512.
532. Tse, J.R. and A.J. Engler, *Preparation of hydrogel substrates with tunable mechanical properties.* Curr Protoc Cell Biol, 2010. **Chapter 10**: p. Unit 10 16.
533. Kennedy, A., et al., *Macrophages in synovial inflammation.* Front Immunol, 2011. **2**: p. 52.
534. Chen, Y., et al., *Macrophages in osteoarthritis: pathophysiology and therapeutics.* Am J Transl Res, 2020. **12**(1): p. 261-268.
535. Wang, K.H., et al., *Effects of collagen matrix and bioreactor cultivation on cartilage regeneration of a full-thickness critical-size knee joint cartilage defects with subchondral bone damage in a rabbit model.* PLoS One, 2018. **13**(5): p. e0196779.
536. Kondo, M., et al., *Safety and efficacy of human juvenile chondrocyte-derived cell sheets for osteochondral defect treatment.* NPJ Regen Med, 2021. **6**(1): p. 65.
537. Mantovani, A., et al., *The chemokine system in diverse forms of macrophage activation and polarization.* Trends Immunol, 2004. **25**(12): p. 677-86.
538. Van Dyken, S.J. and R.M. Locksley, *Interleukin-4- and interleukin-13-mediated alternatively activated macrophages: roles in homeostasis and disease.* Annu Rev Immunol, 2013. **31**: p. 317-43.
539. Martinez, F.O. and S. Gordon, *The M1 and M2 paradigm of macrophage activation: time for reassessment.* F1000Prime Reports, 2014. **6**: p. 13.
540. Fang, H., et al., *Lipopolysaccharide-induced macrophage inflammatory response is regulated by SHIP.* J Immunol, 2004. **173**(1): p. 360-6.
541. Bogdan, C., Y. Vodovotz, and C. Nathan, *Macrophage deactivation by interleukin 10.* J Exp Med, 1991. **174**(6): p. 1549-55.
542. Utomo, L., et al., *Cartilage inflammation and degeneration is enhanced by pro-inflammatory (M1) macrophages in vitro, but not inhibited directly by anti-inflammatory (M2) macrophages.* Osteoarthritis and Cartilage, 2016. **24**(12): p. 2162-2170.
543. Müller, R.D., et al., *IL-10 overexpression differentially affects cartilage matrix gene expression in response to TNF-α in human articular chondrocytes in vitro.* Cytokine, 2008. **44**(3): p. 377-385.
544. Behrendt, P., et al., *IL-10 reduces apoptosis and extracellular matrix degradation after injurious compression of mature articular cartilage.* Osteoarthritis and Cartilage, 2016. **24**(11): p. 1981-1988.

545. Patel, N.R., et al., *Cell Elasticity Determines Macrophage Function.* PLoS ONE, 2012. **7**(9): p. e41024.
546. Sridharan, R., et al., *Material stiffness influences the polarization state, function and migration mode of macrophages.* Acta Biomaterialia, 2019. **89**: p. 47-59.
547. Atcha, H., et al., *Mechanically activated ion channel Piezo1 modulates macrophage polarization and stiffness sensing.* Nat Commun, 2021. **12**(1): p. 3256.
548. Previtera, M.L. and A. Sengupta, *Substrate Stiffness Regulates Proinflammatory Mediator Production through TLR4 Activity in Macrophages.* Plos One, 2015. **10**(12).
549. Perrier-Groult, E., et al., *Evaluation of the biocompatibility and stability of allogeneic tissue-engineered cartilage in humanized mice.* PloS one, 2019. **14**(5): p. e0217183-e0217183.
550. Kemble, S. and A.P. Croft, *Critical Role of Synovial Tissue-Resident Macrophage and Fibroblast Subsets in the Persistence of Joint Inflammation.* Front Immunol, 2021. **12**: p. 715894.
551. Han, D., et al., *The emerging role of fibroblast-like synoviocytes-mediated synovitis in osteoarthritis: An update.* J Cell Mol Med, 2020. **24**(17): p. 9518-9532.
552. Hsieh, J.Y., et al., *Matrix crosslinking enhances macrophage adhesion, migration, and inflammatory activation.* APL Bioeng, 2019. **3**(1): p. 016103.
553. Meli, V.S., et al., *Isolation and characterization of porcine macrophages and their inflammatory and fusion responses in different stiffness environments.* Biomater Sci, 2021. **9**: p. 7851-7861.
554. Kim, Y.K., et al., *Modification of biomaterials with a self-protein inhibits the macrophage response.* Adv Healthc Mater, 2014. **3**(7): p. 989-94.
555. Brown, W.E., et al., *Functional self-assembled neocartilage as part of a biphasic osteochondral construct.* PLoS One, 2018. **13**(4): p. e0195261.
556. Dąbrowska, A.M. and R. Słotwiński, *The immune response to surgery and infection.* Cent Eur J Immunol, 2014. **39**(4): p. 532-7.
557. Smith, T.D., et al., *Regulation of macrophage polarization and plasticity by complex activation signals.* Integr Biol (Camb), 2016. **8**(9): p. 946-55.
558. Nemir, S., H.N. Hayenga, and J.L. West, *PEGDA hydrogels with patterned elasticity: Novel tools for the study of cell response to substrate rigidity.* Biotechnol Bioeng, 2010. **105**(3): p. 636-44.
559. Han, P.F., et al., *Contribution of IL-1beta, 6 and TNF-alpha to the form of post-traumatic osteoarthritis induced by "idealized" anterior cruciate ligament reconstruction in a porcine model.* Int Immunopharmacol, 2018. **65**: p. 212-220.
560. Liacini, A., et al., *Induction of matrix metalloproteinase-13 gene expression by TNF-alpha is mediated by MAP kinases, AP-1, and NF-kappaB transcription factors in articular chondrocytes.* Exp Cell Res, 2003. **288**(1): p. 208-17.
561. Zhang, Y., et al., *Combined effects of tumor necrosis factor-alpha and interleukin-1beta on lysyl oxidase and matrix metalloproteinase expression in human knee synovial fibroblasts in vitro.* Exp Ther Med, 2017. **14**(6): p. 5258-5266.
562. Saudek, D.M. and J. Kay, *Advanced glycation endproducts and osteoarthritis.* Curr Rheumatol Rep, 2003. **5**(1): p. 33-40.
563. Nah, S.S., et al., *Advanced glycation end products increases matrix metalloproteinase-1, -3, and -13, and TNF-alpha in human osteoarthritic chondrocytes.* FEBS Lett, 2007. **581**(9): p. 1928-32.
564. Albro, Michael B., et al., *Accumulation of Exogenous Activated TGF-β in the Superficial Zone of Articular Cartilage.* Biophysical Journal, 2013. **104**(8): p. 1794-1804.
565. Zhang, F., et al., *TGF-β induces M2-like macrophage polarization via SNAIL-mediated suppression of a pro-inflammatory phenotype.* Oncotarget, 2016. **7**(32): p. 52294-52306.

566. Das, A., et al., *A Modified Collagen Dressing Induces Transition of Inflammatory to Reparative Phenotype of Wound Macrophages.* Scientific Reports, 2019. **9**(1): p. 14293.
567. Wrenshall, L.E., et al., *Modulation of macrophage and B cell function by glycosaminoglycans.* J Leukoc Biol, 1999. **66**(3): p. 391-400.
568. Helgeland, E., et al., *3D printed gelatin-genipin scaffolds for temporomandibular joint cartilage regeneration.* Biomed Phys Eng Express, 2021. **7**(5).
569. Ângelo, D.F., et al., *A randomized controlled preclinical trial on 3 interposal temporomandibular joint disc implants: TEMPOJIMS-Phase 2.* J. Tissue Eng. Regen. Med., 2021. **15**(10): p. 852-868.
570. Donahue, R.P., et al., *Long-term safety and efficacy of temporomandibular joint disc repair in the Yucatan minipig.* Nature Biomedical Engineering. In preparation.
571. Barzegar, H., et al., *Arthroscopically-assisted vs. open surgery in repairing anterior cruciate ligament avulsion.* Pak J Biol Sci, 2011. **14**(8): p. 496-501.
572. Walton, J.R. and G.A. Murrell, *A two-year clinical outcomes study of 400 patients, comparing open surgery and arthroscopy for rotator cuff repair.* Bone Joint Res, 2012. **1**(9): p. 210-7.
573. Food and Drug Administration, *Pharamacology/Toxicology Review - MACI*. 2016.